Exploring the Importance of PREX Proteins in Glucose Homeostasis and Insulin Signalling

Elpida Tsonou

Darwin College

July 2019

This dissertation is submitted to The University of Cambridge for the degree of Doctor of Philosophy

Welch Group

Signalling Programme

The Babraham Institute

Cambridge

United Kingdom

CB22 3AT

Declaration

This thesis is the result of my own work and includes nothing which is the outcome of work done in collaboration except as declared in the Preface and specified in the text. It is not substantially the same as any that I have submitted, or, is being concurrently submitted for a degree or diploma or other qualification at the University of Cambridge or any other University or similar institution except as declared in the Preface and specified in the text. I further state that no substantial part of my thesis has already been submitted, or, is being concurrently submitted for any such degree, diploma or other qualification at the University of Cambridge or any other University or similar institution except as declared in the Preface and specified in the text. It does not exceed the prescribed word limit for the Faculty of Biology Degree Committee.

Elpida Tsonou

July 2019

Exploring the Importance of PREX Proteins in Glucose Homeostasis and Insulin Signalling

Elpida Tsonou, Babraham Institute

PREX protein family (PREX1 and PREX2) guanine-nucleotide exchange factors (GEFs) activate the small G protein Rac. They are important in many physiological and pathophysiological processes, including inflammation, neuronal plasticity, cancer progression and metastasis, with an exciting new role in metabolic processes currently emerging. PREX1 was shown to regulate the thermogenic capacity and insulin-stimulated glucose uptake in adipocytes, whereas PREX2 was reported to mediate glucose tolerance, possibly through its adaptor function as an inhibitor of the tumour suppressor PTEN.

The aims of this project were to explore the importance of PREX proteins in glucose homeostasis and insulin signalling, and to assess the significance of PREX Rac-GEF activity in these processes.

Western blotting showed that both Prex proteins are expressed in brain, liver and brown adipose tissue, whereas Prex1 is also expressed white adipose tissue. Prex1 deficient mice had small livers, with reduced glycogen storage, eosinophilia in brown adipose tissue and reduced fasting plasma levels of adiponectin. Surprisingly, Prex1 deficiency lowered fasting blood glucose levels and protected mice from age-related glucose intolerance, in a diet- and sex-dependent manner. Bone marrow transplantation revealed that hematopoietic Prex1 deficiency was sufficient for the improved glucose tolerance. In contrast, Prex2 deficiency only affected glucose homeostasis in mice on high-fat diet, causing glucose intolerance and insulin resistance in old age. The phenotype of Prex1/Prex2 double-deficient mice suggested limited sex- and diet-dependent redundancy between both Prex proteins, as well as compensation by other regulators of glucose homeostasis.

Overexpression of wild type or catalytically-inactive PREX1 and PREX2 in HepG2 cells caused increased insulin-stimulated Akt activity, suggesting that both PREX proteins can mediate insulin signalling at least in part through adaptor functions. Therefore, catalytically-inactive Prex1 and Prex2 mouse strains were generated and the metabolic phenotype of the catalytically-inactive Prex2 strain was assessed. In contrast to the Prex2 KO mice, catalytically-inactive Prex2 mice had reduced fasting blood glucose levels and improved glucose tolerance, both on chow and high fat diet.

Taken together, these finding indicate that Prex1 and Prex2 have unexpected, important and divergent physiological roles in the regulation of glucose homeostasis, and that some of these roles are through adaptor functions. My work suggests that the development of therapeutics to target PREX activity may be a new avenue for the treatment of metabolic syndrome.

Dedicated to my family for their infinite patience and support.

Acknowledgements

First and foremost, I would like to acknowledge my supervisor Dr. Heidi Welch, who was always present to offer guidance and answer my million questions. No words can express my gratitude for her continuous support both professionally and personally. She has been a real inspiration and I could have never asked for a better mentor. I am also immensely grateful to my industrial supervisor Dr David Hornigold for his insight and expertise. Throughout this project, he has always been available to discuss ideas and provide valuable feedback both conceptual and technical.

I would like to acknowledge Dr Dominik Spensberger for all his help with the mouse gene targeting, Dr David Baker for sharing his deep knowledge in metabolism, Dr Chris Church for introducing me to the amazing world of adipose tissue, and Dr Barbara Musial for showing me the ropes in industry. I also owe my gratitude to Anna Roberts for kindly taking care of my mice, while I was on my maternity leave. Her excellent work provided me with peace of mind while I was away.

I am forever thankful to all the past and present members of the HW lab for making me feel part of the PREX family. Kirsti, Anna, Martin, Chiara, Loraine, Izzy, and Polly, thank you for all the great moments we shared in the lab. It was a pleasure working alongside you. Kirsti, thank you so much for sharing your scientific expertise with me and for all your life-saving tips. Chiara, thank you for been like a sister to me. Your understanding, support and encouragement worth more than I can express on paper. Izzy, thanks for all your help with the proof-reading, I promise to read your thesis cover-to-cover when time comes.

Away from work, special thanks go to Angie, Dimitris, Fiore and Ber for the wonderful times, and incredible food, we shared. You have made Cambridge feel like home. I would also like to thank Elena and Sevi for being great friends and never leaving me alone despite the distance.

I am extremely grateful to my parents and brother for their never-ending support, encouragement and love. Mum and Dad, thank you for coming to Cambridge to be my side when I needed it most. Giorgo, thank for being so pure and caring, you make me want to be a better person.

Finally, I would like to say a sweet thank you to my son, Nestor, for being the light of my life, and to my husband, Panos, for being strong, selfless, and always pushing me to grow. I am grateful to you both for making my life beautiful. Your belief in me far surpasses my own; I could not have done this without you by my side.

Acknowledgements of assistance

Initial training in techniques and laboratory practice and subsequent mentoring

General laboratory techniques: Dr Heidi Welch, Dr Kirsti Hornigold, Dr Anna-Karin Johnsson, Dr Martin Baker (Babraham Institute)
Mentoring: Dr Heidi Welch(Babraham Institute), Dr David Hornigold, Dr David Baker (CVRM team AstraZeneca)
Adipose tissue isolation, Seahorse analysis: Dr Cristopher Church (CVRM team AstraZeneca)
Mesoscale analysis: Dr Barbara Musial (CVRM team AstraZeneca)
qPCR: Dr Graeme Davis
Statistics: Dr Anne Segonds-Pichon (Babraham Institute Bioinformatics Service)
NMR spectroscopy: Dr Jules Griffin (Department of Biochemistry, University of Cambridge)

Data obtained from a technical service provider

Bioinformatics: Dr Simon Andrews (Babraham Institute Bioinformatics Service)
Genome Engineering: Dr Dominik Spensberger (Babraham Institute Gene Targeting facility)
Mouse breeding and maintenance: Babraham Institute Biological Support Unit
Mouse Body Composition analysis: Dr Lihuan Liang (AstraZeneca)
Veterinary Pathology: Dr Cheryl Scudamore (ExePathology)
DNA Sequencing: Genewiz
Mouse genotyping: Transnetyx

Data produced jointly (e.g. where it was necessary or desirable to have two people performing an experiment)

During maternity leave (15th of January 2018 to 5th of May 2018) the ageing mouse cohorts were kindly maintained by Masters' student Ms Anna Roberts. Data from her work are part of the following figures: 4.2.1, 4.2.4, 4.2.5, 4.2.7, 4.2.9, 4.2.15, 4.3.1, 4.3.5, 4.3.7, 4.3.13, 4.4.1, 4.4.3, 4.4.5, 4.4.7, 4.4.9, 4.4.11, 4.4.13, 4.4.15.

Materials provided by someone else

***Prex1*$^{-/-}$*;Prex2*$^{-/-}$, *Prex1*$^{-/-}$, and *Prex2*$^{-/-}$ mouse strains:** Dr Heidi Welch (Babraham Institute)
Wild Type PREX DNA constructs and baculovirus: Dr Kirsti Hornigold (Babraham Institute)
Seahorse plates and reagents: Dr Dr Cristopher Church (CVRM team AstraZeneca)
Mesoscale plates and reagents: Dr Barbara Musial (CVRM team AstraZeneca)

Table of Contents

List of Figures

List of Tables

Summary

The PREX protein family (PREX1 and PREX2) are guanine-nucleotide exchange factors (GEFs) that activate the small G protein Rac. They are important in many physiological and pathophysiological processes, including inflammation, neuronal plasticity, cancer progression and metastasis. However, an exciting new role in metabolic processes is currently emerging. PREX1 was shown to regulate the thermogenic capacity of adipocytes, as well as insulin-stimulated glucose uptake, whereas PREX2 was reported to mediate glucose tolerance, possibly through its adaptor function as an inhibitor of the tumour suppressor PTEN.

The aims of this project were to explore the importance of PREX proteins in glucose homeostasis and insulin signalling and to assess the significance of PREX Rac-GEF activity in these processes.

Western blot analysis of insulin-sensitive mouse tissues confirmed that both Prex proteins are expressed in brain, liver and brown adipose tissue, whereas Prex1 is also expressed white adipose tissue. Prex1 KO mice had small livers, reduced glycogen storage in the liver, and eosinophilia in brown adipose tissue. Moreover, Prex1 KO mice had reduced fasting plasma levels of adiponectin. However, Prex1 deficiency did not obviously affect insulin signalling pathway activity in liver, skeletal muscle or inguinal white adipose tissue.

Unexpectedly, Prex1 deficiency resulted in lower fasting blood glucose levels and improved glucose homeostasis during glucose tolerance tests throughout ageing. In addition, Prex1-deficient mice showed an altered response to insulin challenge. This phenotype was diet-dependent, as Prex1 KO males on high fat diet (HFD) became glucose intolerant similarly to wild type mice. It was also sex-dependent, as Prex1 KO females showed improved glucose homeostasis only on HFD. Importantly, bone marrow transplantation revealed that Prex1-deficiency in hematopoietic cells was sufficient to recapitulate the metabolic phenotype of Prex1-deficient mice, as wild type mice with a Prex1 KO hematopoietic system exhibited improved glucose tolerance. Taken together, these findings indicate that Prex1 has an important role in glucose homeostasis. Prex1 deficiency helps maintain low blood glucose levels and protects from age-related glucose intolerance. Although the

mechanisms through which Prex1 contributes to glucose regulation *in vivo* are still unclear, the bone marrow transplant experiments indicated that this could be through the regulation of inflammation.

To evaluate the importance of PREX Rac-GEF activity in insulin signalling, wild type PREX1 or PREX2 and catalytically-inactive mutants were overexpressed in HepG2 cells. All were found to cause increased Akt activity upon insulin stimulation, suggesting that both PREX proteins mediate insulin signalling at least in part through adaptor functions. Therefore, I generated mouse strains with catalytically-inactive Prex1 and Prex2, using CRISPR gene targeting to introduce point mutations into their catalytic DH domains. I succeeded in establishing the catalytically-inactive Prex2 mouse strain and compared its metabolic phenotype to Prex2 KO. Against expectations, Prex2 deficiency did not affect glucose homeostasis, except when mice were on HFD, where it caused glucose intolerance and insulin resistance in old age. In contrast, catalytically-inactive Prex2 mice had low fasting blood glucose levels and improved glucose tolerance, both on chow and HFD. These data suggest that Prex2 regulates glucose homeostasis both through its Rac-GEF activity and through adaptor functions.

Prex1/Prex2 double deficient mice had a metabolic phenotype which suggested that there was limited redundancy between the Prex proteins only under some sex- and diet-dependent conditions, and that other regulators of glucose homeostasis compensate for the loss of both Prex proteins.

In summary, this project has uncovered unexpected, important and distinct physiological roles of Prex1 and Prex2 in the regulation of glucose homeostasis that are in part due to their roles as Rac-GEFs and in part through adaptor functions. My work suggests that the development of therapeutics to target PREX Rac-GEF activity may be a new avenue for the treatment of metabolic syndrome**.**

Papers published as a result of the work presented in this thesis

P-Rex1

Hornigold K, Tsonou E, Pantarelli C, Welch HC.
Encyclopedia of Signaling Molecules, 2nd Edition, Editor S Choi. 2018

P-Rex2

Tsonou E, Pantarelli C, Hornigold K, Welch HC.
Encyclopedia of Signaling Molecules, 2nd Edition, Editor S Choi. 2018

List of Abbreviations

Hepes	4-(2-hydroxyethyl)-1-piperazineethanesulfonic acid
p60^{Dok}	60-kDa tyrosine phosphorylated protein
Arp2/3	Actin Related Protein-2/3
APS protein	Adapter protein with a PH and SH2 domain
ATP	Adenosine Triphosphate
AC	Adenylate Cyclase
ATGL	Adipose Triglyceride Lipase
Arf	ADP-Ribosylation Factor
AgRP	Agouti-Related Peptide
APS	Ammonium Persulphate
AMPK	AMP-activated protein Kinase
ANOVA	Analysis of Variance
AUC	Area Under the Curve
BSA	Bovine Serum Albumin solution
BAT	Brown Adipose Tissue
CaN	Calcium-Calcineurin
CH	Calponin Homology
CREB	cAMP Response Element Binding protein
CRTC2	cAMP-regulated Transcriptional Coactivator 2
Cbl	Casitas B-lineage Lymphoma
CDC25-HD	CDC25 Homology Domains
JNK	c-Jun N-terminal Protein Kinase
CRISPR	Clustered Regularly Interspaced Short Palindromic Repeats
CR	Conserved Regions
cAMP	cyclic Adenosine Monophosphate
DH	Dbl Homology
DOCK	Dedicator of Cytokinesis
DNA	Deoxyribonucleic Acid
dNTP	Deoxyribonucleotide Triphosphate
Dbl	Diffuse B-cell Lymphoma
DMSO	Dimethyl Sulfoxide
DEP	Dishevelled, Egl-10 and Pleckstrin
DTT	Dithiothreitol
DHR1	DOCK Homology Region 1
DHR2	DOCK Homology Region 2
DMEM	Dulbecco's Modified Eagle's Medium
DPBS	Dulbecco's Phosphate-Buffered Saline

EMSA	Electrophoretic Mobility Shift Assay
ES cells	Embryonic Stem cells
ER	Endoplasmic Reticulum
ELMO	Engulment and Motility
ECL	Enhanced Chemiluminescence
EDTA	Ethylenediaminetetraacetic Acid
EGTA	Ethyleneglycoltetraacetic Acid
FAF-BSA	Fatty Acid Free - Bovine Serum Albumin
FLII	Flightless-1 homolog
FBS	Foetal Bovine Serum
FoxO1	Forkhead Box Class O1
FFA	Free Fatty Acid
FBPase-1	Fructose-1,6-Bisphosphatase 1
Fru-2,6-BP	Fructose-2,6-Bisphosphate
GPCR	G Protein Coupled Receptor
GCGR	Glucagon Receptor
GLP-1	Glucagon-Like Peptide-1
GLUT2	Glucose Transporter-2
GLUT4	Glucose Transporter-4
G1P	Glucose-1-Phosphate
G6Pase	Glucose-6-Phosphatase
G6P	Glucose-6-Phosphate
GIP	Glucose-Dependent Insulinotropic Peptide
GSV	GLUT4 Storage Vesicle
PhK	Glycogen Phosphorylase Kinase
GSK3	Glycogen Synthase Kinase-3
Gab-1	Grb2-Associated-Binding protein 1
Grb10	Growth Factor Receptor-bound Protein 10
Grb2	Growth Factor Receptor-bound Protein 2
GAP	GTPase Activating Protein
GEF	Guanine Nucleotide Exchange Factor
G Proteins	Guanine-Nucleotide Binding Proteins
GTPγS	Guanosine 5'-O-[gamma-thio]triphosphate
GDP	Guanosine Nucleotide Diphosphate
GDI	Guanosine Nucleotide Dissociation Inhibitor
GTP	Guanosine Nucleotide Triphosphate
'large' G proteins	Heterotrimeric G protein complexes
HFD	High Fat Diet
HDAC	Histone Deacetylase

HDR	Homology-Directed Repair
HSL	Hormone-Sensitive Lipase
HepG2	Human Liver Hepatocellular Carcinoma cell line
HLMVEC	Human Lung Microvascular Endothelia Cells
HMEC	Human Microvascular Endothelia Cells
HUVEC	Human Umbilical Vein Endothelial Cells
PVDF	Immobilon-P Polyvinylidene Fluoride
IKKβ	Inhibitor of Nuclear Factor κ-B Kinase-β
IP4P	Inositol Polyphosphate 4-Phosphatase
IP3R	Inositol-1,4,5-Trisphosphate Receptor
IR	Insulin Receptor
IRS1	Insulin Receptor Substrate-1
IRS	Insulin/IGF-1 Receptor Substrate
INS-1 832/13	Insulinoma cell line
IL-6	Interleukin-6
IP	Intraperitoneal
IPGTT	Intraperitoneal Glucose Tolerance Test
i.p.	Intraperitoneally
i.v.	Intravenously
KO	Knockout
KO-DMEM	Knockout Dulbecco's Modified Medium
LIF	Leukemia Inhibitor Factor
LIMK1/2	LIM Kinase
L-PK	Liver-type Pyruvate Kinase
LTD	Long-Term Depression
LB	Luria Bertiani
MRI	Magnetic Resonance Imaging
mTOR	Mammalian Target of Rapamycin
mTORC1	Mammalian Target of Rapamycin Complexe 1
mTORC2	Mammalian Target of Rapamycin Complexe 2
miRNA	microRNA
NGF	Nerve Growth Factor
NPC	Neural Progenitor Cell
NPY	Neuropeptide Y
NMDAR	N-Methyl-D-Aspartate Receptor
NAFLD	Non-Alcoholic Fatty Liver Disease
NF-κB	Nuclear Factor-kappa-B
OE	Over Expression
PAK	p21-Activated Protein Kinase
p70S6K	p70 Ribosomal S6 Kinase

P/S	Penicillin/Streptomycin
PMSF	Phenylmethylsulfonyl Fluoride
PTEN	Phosphatase and Tensin Homolog Deleted from Chromosome 10 (Human)
Pten	Phosphatase and Tensin Homolog Deleted from Chromosome 10 (Mouse)
PBS	Phosphate-Buffered Saline
PC	Phosphatidylcholine
PI	Phosphatidylinositol
PIP_3	Phosphatidylinositol 3,4,5-triphosphate / PtdIns(3,4,5)P3
$PI(3,4)P_2$	Phosphatidylinositol *3,4*-bisphosphate
PIP_2	Phosphatidylinositol 4,5-bisphosphate / PtdIns(4,5)P_2
PREX1	Phosphatidylinositol-3,4,5-trisphosphate-Dependent Rac Exchange Factor 1 (Human)
Prex1	Phosphatidylinositol-3,4,5-trisphosphate-Dependent Rac Exchange Factor 1 (Mouse)
PREX2	Phosphatidylinositol-3,4,5-trisphosphate-Dependent Rac Exchange Factor 2 (Human)
Prex2	Phosphatidylinositol-3,4,5-trisphosphate-Dependent Rac Exchange Factor 2 (Mouse)
PS	Phosphatidylserine
PDE3B	Phosphodiesterase 3B
PEP	Phosphoenolpyruvate
PEPCK	Phosphoenolpyruvate Carboxykinase
PFK-1	Phosphofructo-1-kinase
PFK-2/FBPase-2	Phosphofructokinase-2/Fructose Bisphosphatase-2
PGM	Phosphoglucomutase
PI3K	Phosphoinositide 3 Kinase
PDK1	Phosphoinositide-Dependent Protein Kinase 1
PH	Pleckstrin Homology
PCR	Polymerase Chain Reaction
PDZ	Postsynaptic-Density Protein, Discs Large, Zona Occludens-1
PGC1α	PPARγ Coactivator-1α
P1	PREX1
P2	PREX2
P-rich	Proline rich
PKA	Protein Kinase A
PKB/Akt	Protein Kinase B
PKC	Protein Kinase C
PKCλ/ζ	Protein Kinase C λ/ζ
PKCδ	Protein Kinase Cδ

PP1	Protein Phosphatase 1
PP1α	Protein Phosphatase 1A
PP2A	Protein Phosphatase 2A
PTP1B	Protein Tyrosine Phosphatase 1B
PAM	Protospacer Adjacent Motif
PSGL-1	P-Selectin Glycoprotein Ligand-1
qPCR	Quantitative Polymerase Chain Reaction
RGC	RAL GAP Complex
RBD	Ras Binding Domain
REM	Ras Exchange Motif
Rho	Ras homologous
Ras	Ras Sarcoma
Ran	Ras-Like Nuclear Protein
Rab	Ras-Like Proteins in Brain
ROS	Reactive Oxygen Species
RTK	Receptor Tyrosine Kinase
RCC1	Regulator of Chromosome Condensation 1
RGS	Regulator of G Protein Signalling
RNA	Ribonucleic Acid
SIK2	Salt-Inducible Kinase 2
Shc	SH2-Domain Containing Protein
STAT3	Signal Transducer and Activator of Transcription 3
sgRNA	Single Guide RNA
SNP	Single Nucleotide Polymorphism
ssDNA	Single Stranded DNA
SM	Skeletal Muscle
SDS-PAGE	Sodium Dodecyl Sulphate-Polyacrylamide Gel Electrophoresis
SGLT2	Sodium–Glucose Cotransporter 2
Sos-1	Son of Sevenless
Sf9	Spodoptera frugiperda
SH2	Src Homology 2
SHIP2	Src Homology 2 Domain-Containing Inositol-5-Phosphatase 2
SH3	Src Homology 3
PTPN11	Src Homology Region 2 Domain-Containing Tyrosine Phosphatase-2
SHP2	Src Homology Region 2 Domain-Containing Tyrosine Phosphatase-2
SEM	Standard Error of the Mean
SDF1	Stromal Cell Derived Factor-1
ingWAT	Subcutaneous Inguinal White Adipose Tissue
SCITT	Subcutaneous Insulin Tolerance Test
intBAT	Subcutaneous Interscapular Brown Adipose Tissue

s.c.	Subcutaneously
SOCS3	Suppressor of Cytokine Signalling 3
PMEL-NRAS*	TERT-immortalised human melanocytes engineered to express NRAS(G12D)
TEMED	Tetra-Methyl-Ethylenediamine
TRB3	Tribbles Homolog 3
TBS	Tris Buffered Saline
TBS-T	Tris Buffered Saline - Tween-20
TBE	Tris/Borate/EDTA
TmG	Tubular maximum Glucose
TNF-α	Tumour Necrosis Factor-α
T1D	Type 1 Diabetes
T2DM	Type 2 Diabetes Mellitus
UCP1	Uncoupling Protein 1
UPR	Unfolded-Protein Response
v.o.	Vector Only
v/v	Volume/Volume
w/v	Weight/Volume
WAT	White Adipose Tissue
WT	Wild Type

Chapter 1 - Introduction

1.1 Guanine-nucleotide Binding Proteins

Guanine-nucleotide binding proteins (G Proteins) are binary molecular switches involved in cell signal transduction. There are two classes of G proteins, the heterotrimeric G protein complexes ('large' G proteins) and the monomeric G proteins, also known as small GTPases (small G proteins).

1.1.1 'Large' G Proteins

The heterotrimeric G protein complexes are composed of α, β, and γ subunits. They are mainly located in the plasma membrane and are activated by G protein coupled receptors (GPCRs). Upon activation, the receptors undergo a conformational change that enables the G protein to bind to the receptor and the Gα subunit to exchange GDP for GTP. GTP binding activates the G protein and promotes its dissociation into active Gα subunit and Gβγ dimer. The cycle is completed by the hydrolysis of Gα-bound GTP to GDP, which leads to the re-association of the Gα and Gβγ subunits and the formation of an inactive trimer (**Figure 1.1.1**). The Gα subunit has a weak intrinsic GTPase activity, which is often accelerated by GTPase activating proteins (GAPs) such as the Regulator of G protein Signalling proteins (RGS). Further regulation of G proteins is achieved by covalent modification that can affect the interaction with effector proteins, RGS proteins, and between the Gα subunit and Gβγ subunits (Chen and Manning, 2001; Oldham and Hamm, 2008).

G proteins are identified by their Gα subunits, which are grouped into four families ($G\alpha_s$, $G\alpha_i$, $G\alpha_q$, and $G\alpha_{12}$) on the bases of their sequence and function. Moreover, 5 Gβ and 12 Gγ genes have been identified in mammals. Different Gβ and Gγ isoforms form dimers, which directly interact with specific GPCRs creating a complex system of signal transduction. Among the effectors of G proteins are the PREX proteins, the primary focus of this study, and an isoform of phosphoinositide 3-kinase, PI3Kγ, which is an important regulator of PREX proteins.

G protein-mediated signalling is involved in many cell processes such as regulation of cell proliferation, growth, differentiation and migration, and

physiological functions such as perception of sensory information, modulation of synaptic transmission, hormone release and actions, blood vessel formation, bone homeostasis. Finally, G protein malfunctions have been involved in many diseases, including metabolic conditions such as diabetes, cardiovascular defects, and cancer (Syrovatkina and Huang, 2019; Wettschureck and Offermanns, 2005; Worzfeld et al., 2008).

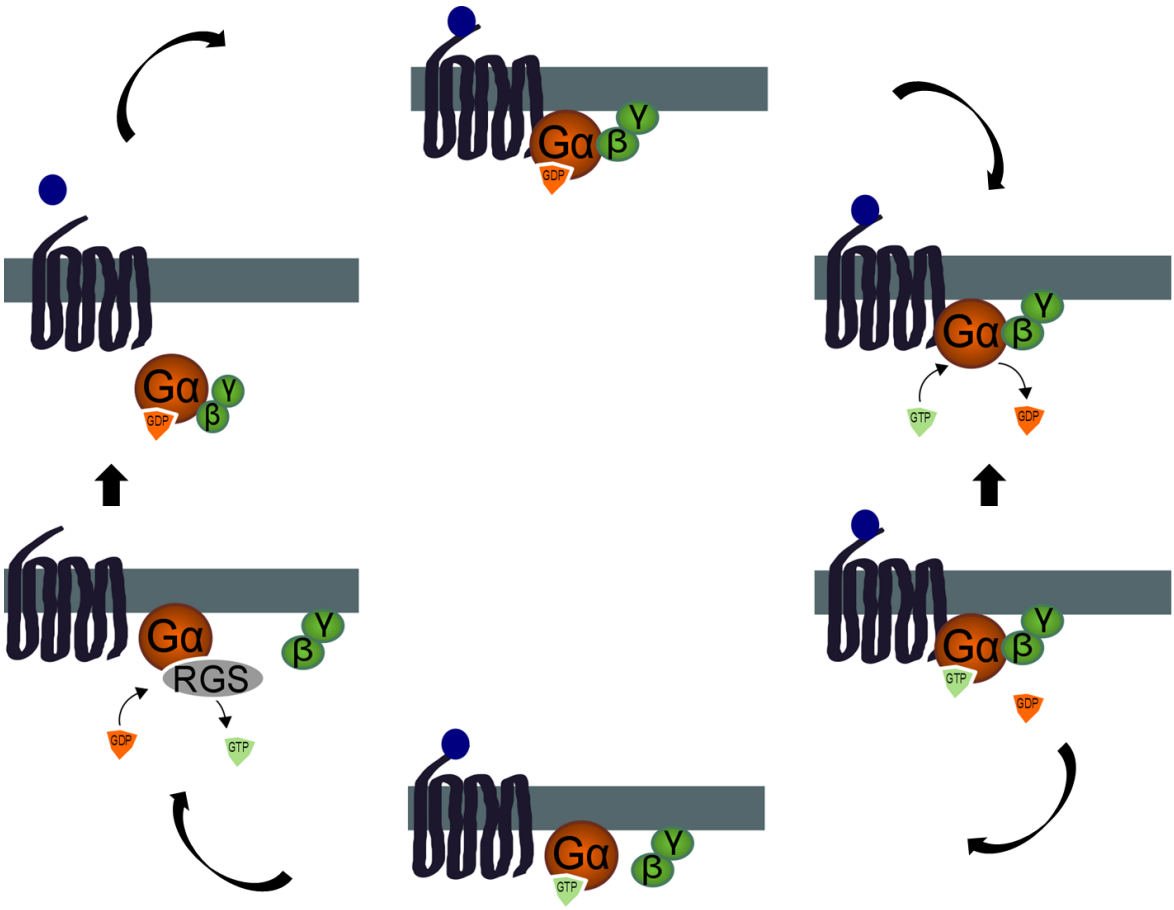

Figure 1.1.1: Regulation of 'Large' G protein activity
G protein-coupled receptors (GPCRs) are associated on the intracellular side with heterotrimeric G proteins. Ligand-binding to the extracellular side of the GPCRs results in conformational changes that enable the G protein to bind to the receptor and the Gα subunit to exchange GDP for GTP. GTP binding activates the G protein and promotes the dissociation of the Gα–GTP from the Gβγ subunit dimer and the initiation of downstream signalling events. The cycle is completed by the hydrolysis of Gα-bound GTP to GDP, which is facilitated by the intrinsic GTPase activity of the Gα subunit, but regulator of G protein signalling (RGS) proteins can enhance it. The GTP hydrolysis leads to the re-association of the Gα and Gβγ subunits and the formation of an inactive trimer. (Figure adapted from (Kamp et al., 2016))

1.1.2 Small G Proteins

The Ras family small G proteins were the first to be characterised, however many related proteins have subsequently been identified, forming the Ras superfamily of small G proteins. The human Ras superfamily consists of 166 members. Although most of them can be grouped into five different subfamilies (Ras, Rab, Arf, Ran and Rho) based upon their sequence and function, a few still remain unclassified.

Just like the 'Large' G proteins, the Small G proteins exist in two interconvertible forms: the active GTP-bound and the inactive GDP-bound form. The guanine-nucleotide binding domain consists of a single polypeptide chain (20-25 kDa) with six conserved motifs that are responsible for nucleotide binding and two flexible switch regions (Switch I and II), whose conformation is determined by the nucleotide state (GTP- or GDP-bound), and who are responsible for effector binding (**Figure 1.1.2**). Upon activation, small G proteins undergo conformational changes that enable them to interact with an array of downstream effector proteins and regulate a plethora of cellular events. The GDP/GTP cycling is tightly regulated by guanine-nucleotide-exchange factors (GEFs), which promote the release of the GDP to be replaced by the more abundant GTP, and by GAPs, which accelerate the weak intrinsic GTPase activity to promote formation of the inactive GDP-bound form (**Figure 1.1.3**) (Reiner and Lundquist, 2018; Wennerberg et al., 2005).

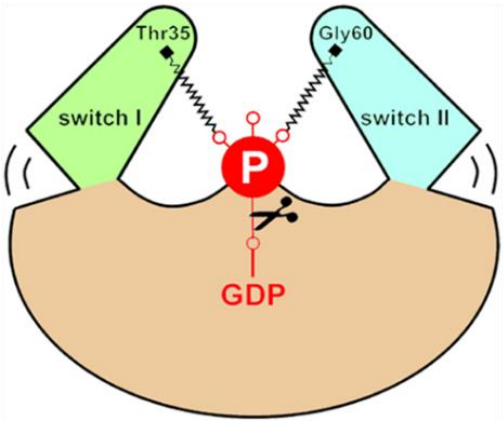

Figure 1.1.2: Schematic diagram of the small G protein switch mechanism.
At the GTP-bound state, two conserved residues, Thr35 (switch I) and Gly60 (switch II), form hydrogen bonds with the γ-phosphate of GTP, a mechanism known as 'loaded spring'. This contact of GTP with the switches I and II pulls the rest of the switch residues into a conformation that enables the interaction with effector proteins. (Figure taken from (Vetter and Wittinghofer, 2001))

The small G proteins, when active, are largely membrane associated. Their subcellular localisation and interaction with distinct membrane compartments is regulated through post-translational modification by lipids. Most of the Ras and Rho family proteins carry a CAAX C-terminal motif (C = cysteine, A = aliphatic amino acid and X = any amino acids), which is recognised for covalent addition of a farnesyl or geranylgeranyl isoprenoid to the cysteine residue of the tetrapeptide sequence by the farnesyltransferase and geranylgeranyltransferase I, respectively; this process is known as prenylation. Rab family proteins also undergo geranylgeranylation, whereas some members of the Arf family are targeted to their membrane compartments through the addition of myristate fatty acids to their N-terminus. No lipid modification has been described for Ran and it is not usually associated with cell membranes, instead it shuttles between nucleus and cytoplasm. Rho and Rab GTPases are also regulated by a third class of proteins, guanine nucleotide dissociation inhibitors (GDIs), which mask the prenyl modification and promote cytosolic localisation of these GTPases (**Figure 1.1.3**) (Reiner and Lundquist, 2018; Wennerberg et al., 2005). The localisation and regulation of small G proteins enables them to function as modulators in a plethora of cellular functions.

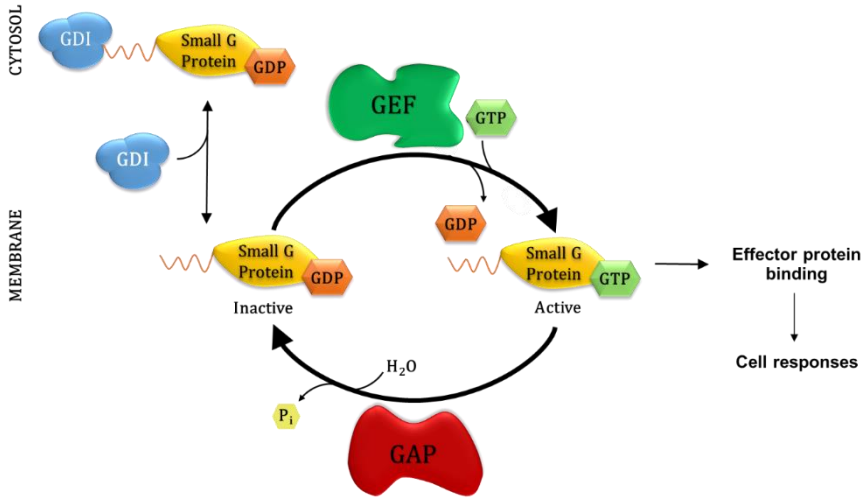

Figure 1.1.3: Regulation of small G protein activity
The activation of the small G protein is regulated by guanine-nucleotide-exchange factors (GEFs), which catalyse the exchange of GDP for GTP. On the other hand, the inactivation is mediated by GTPase-activating proteins (GAPs), which catalyse the hydrolysis of GTP to GDP. The active, GTP-bound form of the small G protein adopts a conformation that allows it to interact with effectors to mediate downstream signalling. In addition to this, guanine nucleotide dissociation inhibitors (GDIs) can sequester inactive Rho-family small G proteins by promoting their cytosolic localisation and inhibiting nucleotide dissociation. They do so by masking the hydrophobic prenyl modification of the small G protein.

The Ras sarcoma (Ras) protein subfamily consists of 36 members and regulate gene expression, cell survival, proliferation and differentiation (Wennerberg et al., 2005). The Ras proteins, and especially K-ras, are often mutated in cancer. According to the Sanger Centre, 30% of all human tumours carry *ras* mutations (Fernández-Medarde and Santos, 2011).

The Ras-like proteins in brain (Rab) family is the largest branch of the superfamily with more than 60 members. Rabs regulate intracellular vesicle formation and trafficking on actin and microtubule filaments, and membrane fusion. More recently, it has been shown that Rabs are also implicated in signal transduction and autophagy (Li and Marlin, 2015).

The ADP-ribosylation factor (Arf) family is divided in three classes based mainly on sequence homology (Class I, II, and III). Arfs mainly regulate protein and lipid trafficking by modulating vesicle budding and un-coating within the Golgi system. However, they also have roles in actin cytoskeleton remodelling, trafficking of the ciliary membrane, lipid droplet metabolism and mitosis (Jackson and Bouvet, 2014).

The Ras-like nuclear protein (Ran) is the only member of the Ran subfamily but is the most abundant small G protein in the cell. During the G1, S, and G2 phases of the cell cycle, Ran regulates nucleocytoplasmic transport, whereas during the M phase it is involved in the mitotic spindle assembly by regulating microtubule organisation, and in the nuclear envelope formation (Clarke and Zhang, 2008).

Finally, the Ras homologous (Rho) protein family consists of 20 mammalian proteins, which can be broadly separated into five different groups based upon sequence identity and known function. Relatively little is known about three of these proteins (RhoH, RhoD and RIF); however, the others can be divided into the Rho-like, Rac-like, Cdc42-like, Rnd or RhoBTB subfamilies. Overall, the Rho family is involved in actomyosin cytoskeletal reorganisation, gene expression, cell-cycle progression, and reactive oxygen species (ROS) production (Heasman and Ridley, 2008; Sadok and Marshall, 2014).

This thesis focuses on the role of PREX family Rac-GEFs in insulin signalling and glucose homeostasis. Therefore, the Rac subfamily is described in more detail

in the following section.

1.1.2.1 The Rac-like Subfamily

The Rac-like subfamily consists of four isoforms, Rac1, Rac2, Rac3 and RhoG. The Rac1, Rac2 and Rac3 isoforms share ≥89% amino acid identity, while RhoG is 72% identical to Rac1. There is also a splice variant of Rac1, Rac1b, which contains a 19 amino acid insertion near the switch II region. The members of the Rac-like subfamily are regulated as described in **Section 1.1.2** and demonstrate relatively high intrinsic GTPase activity (Wennerberg and Der, 2004). The only exception is Rac1b, which cannot bind to Rho-GDI and has reduced intrinsic GTPase activity, hence it is mainly bound to the plasma membrane and displays constitutive activity (Fiegen et al., 2004; Matos et al., 2003).

The Rac-like GTPases exhibit distinct tissue distribution. Rac1 and RhoG are both ubiquitously expressed, whereas Rac2 is restricted to haematopoietic cells (Wennerberg and Der, 2004) and Rac1b is preferentially expressed in breast and colon cancer (Jordan et al., 1999; Schnelzer et al., 2000). Rac3 is predominantly expressed in the nervous system with lower expression levels found in lung, liver, and pancreas, but it is absent from white blood cells (Haataja et al., 1997).

Although Rac proteins appear to have redundant functions when coexpressed, they also exhibit striking isoform specificity. For instance, genetic ablation of Rac1 results in embryonic lethality during gastrulation (Sugihara et al., 1998). Instead, Rac2 deficiency allows normal embryonic development, but it has been associated with severe neutrophilic, phagocytic and lymphocytic defects (Kasper et al., 2000; Li et al., 2000; Roberts et al., 1999; Williams et al., 2000). In neutrophils, for example, Rac1 deficiency merely impairs the directionality of migration, whereas Rac2 deficiency blocks cell migration altogether (Pantarelli and Welch, 2018). Rac3 knockout mice are also viable and do not demonstrate any obvious physical abnormality, suggesting that Rac3 is not strictly required for the embryonic development; however it is important during the late maturation of specific populations of neurons (Corbetta et al., 2005; Pennucci et al., 2016). Finally, RhoG deficiency produces a mild phenotype in leukocytes, where it is highly expressed, indicating a functional redundancy of RhoG with other Rac proteins in

these cells (Vigorito et al., 2004).

The Rac GTPases as intracellular signal transducers play a regulatory role in a wide variety of cellular functions. For instance, Racs are crucial for actin cytoskeleton rearrangements and they are fundamental in the regulation of cell adhesion and migration (Ridley et al., 1992). Moreover, the Rac-like subfamily are important for many cellular functions such as ROS production, cell proliferation and cell survival. To do so, they interact with a variety of downstream effector molecules in order to engage distinct signalling cascades (Bustelo et al., 2007; Mack et al., 2011). However, their involvement in these processes is also dependent on their ability to bind GEFs. Racs can be regulated by a large number of GEFs which also display signalling pathway and cell type specificities, thus contributing further to the functional diversity of Racs.

1.2 Guanine-nucleotide Exchange Factors (GEFs)

GEFs are large multi-domain proteins that respond to a diverse array of cellular inputs to regulate the spatiotemporal activation of small G proteins (Bos et al., 2007). Upon activation, GEFs interact with the switch I and switch II domains of small G proteins, causing a series of structural rearrangements, which increase the rate of GDP release by several orders of magnitude. Subsequently, the nucleotide is replaced by the highly abundant cytosolic GTP (Bos et al., 2007; Cherfils and Zeghouf, 2013; Vetter and Wittinghofer, 2001). GEFs are primarily defined by their catalytic domain, which is normally able to regulate individual members of only one of the five small G protein families. For instance, GEFs that activate Ras contain CDC25 homology domains (CDC25-HD), which are usually found in combination with a Ras exchange motif (REM). Similarly, GEFs involved in the regulation of the Rab family contain Vps9, Sec2 or Mss4 catalytic domains. The Arf family is regulated by GEFs bearing a Sec7 domain, whereas Ran is stimulated by the β-propeller GEF RCC1. Finally, GEFs that regulate members of the Rho family contain either a Dbl homology (DH) domain in tandem with a Pleckstrin homology (PH) domain, or a DOCK homology region 2 (DHR2) domain. These two domains are structurally unrelated and they are the basis of sorting the Rho GEFs into two

subtypes: the diffuse B-cell lymphoma (Dbl)-type Rho-GEFs and the dedicator of cytokinesis (DOCK)-type Rho-GEFs (Bos et al., 2007; Cherfils and Zeghouf, 2013). Despite GEFs being specific for one or more members of a single small G protein family, some can have catalytic domains for multiple small G proteins. Son of sevenless (Sos-1) for example carries catalytic domains for both the Ras and Rho family (Innocenti et al., 2002).

Apart from their catalytic domain, GEFs have multiple other domains, which are involved in the modulation of their localisation, activity or interaction with binding partners and effector proteins. This regulation includes intramolecular interactions, post-translational modifications, and/or control of subcellular localisation via protein-protein, protein-lipid, and/or protein-second messenger molecule (Bos et al., 2007; Cherfils and Zeghouf, 2013).

1.2.1 Rho-GEFs

The Rho-GEF family in humans comprises more than 80 members, of which over 70 are Dbl-type and 11 are DOCK-type GEFs. This vastly outnumbers the small G proteins upon which they act (20 Rho family members in humans) with individual small G proteins often being regulated by multiple GEFs. In addition, some GEFs will act on multiple Rho-subfamily members, all be it with different efficiencies, whilst some are specific for just one (Cook et al., 2014). Although GEF expression displays tissue specificity, in any given cell type there are multiple GEFs for each Rho family member. It is generally assumed that this allows the coupling of small G proteins to different upstream pathways as well as providing functional redundancy (Cook et al., 2014).

1.2.1.1 Dbl-Type Rho-GEFs

The Dbl-type Rho-GEF family owes its naming to the Dbl protein, the first identified Rho-GEF originally found as a transforming factor in diffuse B-cell lymphoma (Eva et al., 1988). Dbl is now known to be a GEF for the Rho-family small G protein Cdc42 (Hart et al., 1991). Dbl family Rho-GEFs share a catalytic DH domain, which stimulates the guanine nucleotide exchange and is usually in tandem with a PH domain. The PH domain often interacts with phosphoinositide lipids, contributing to the membrane localisation of the Rho-GEFs. Although the DH domain is sometimes

sufficient for GEF activity, in some Dbl-type GEFs the PH domain is also required for full catalytic activity through allosteric mechanisms (Rossman et al., 2005).

Crystal or NMR structures have been solved for the DH domains of several Dbl-type GEFs including Vav1, ITSN1, Sos1, Trio, Tiam1, LARG, Dbs, Asef, β-Pix, p115-RhoGEF and PREX1 (Aghazadeh et al., 1998; Ahmad and Lim, 2010; Cash et al., 2016; Chrencik et al., 2008; Kristelly et al., 2003; Liu et al., 1998; Lucato et al., 2015; Murayama et al., 2007; Rossman et al., 2002; Soisson et al., 1998; Worthylake et al., 2000). These studies have revealed that despite the low primary sequence homology among the members of the Dbl-type Rho-GEFs, their DH domains fold into similar 3D structures (**Figure 1.2.1**). They usually comprise of 6-15 α-helices and 3_{10}-helices, arranged along six main axes, forming an oblong helical bundle (Rossman et al., 2005). The core of the DH domain consists of three highly conserved regions (CR1, CR2 and CR3). Among these, the CR1 and CR3 interact with the switch I region of the small G protein, whereas the CR3 region and elements of the C-terminal helix interact with the switch II region (Rossman et al., 2005). Interactions with the conserved regions of the DH domain are thought to induce structural changes in small G proteins' switch I and II that obstruct the binding of the GDP and its essential cofactor Mg^{2+}, thus facilitating nucleotide exchange on the small G proteins (Rossman et al., 2005). Specifically for PREX1, the CR1 residues Glu56 and Gln197 were found to interact with the switch I region of Rac1, while the CR3 residues Lys201, Asn238, and Arg242 were found to mediate interactions with the switch II region of Rac1 (Lucato et al., 2015) (**Figure 1.2.1**). Importantly, mutation of these residues resulted in decreased GEF activity of the PREX1 DH/PH tandem *in vitro*, highlighting their importance not only in Rac1 binding but also in its activation (Lucato et al., 2015). The less well-conserved regions of the DH domain are considered essential for GEF selectivity, and they have been found to interact with contiguous patches within the GTPase interface that are also poorly conserved, indicating that both sets of proteins co-evolved such as to enable pairing specificity.

The DH domain is most commonly found with a PH domain immediately adjacent to the C-terminal side. However, there are cases like the Rho-GEF DEF6 where this domain motif is inverted with the PH domain on the N-terminal side of the

DH domain (Mavrakis et al., 2004), or the Cdc42-GEF Tuba in where the DH domain is adjacent to a BAR domain and there is no PH domain (Cestra et al., 2005). The PH domain was shown in several cases to contribute in the interaction of the GEF with the small G protein and participate in the nucleotide exchange. For example, the PH domain of Dbs is required for efficient activation of Rho family proteins (Rossman et al., 2003). In contrast, the PH domains of other Rho-GEFs, such as PREX1 and Tiam, do not contact the small G proteins and thereby are not involved in their activation (Lucato et al., 2015; Worthylake et al., 2000). The PH domain is not specific to Rho-GEFs, instead it is found in many intracellular signalling proteins where they promote plasma membrane localisation by binding phospholipids (Lemmon et al., 1995). However, the affinity of Dbl-like family PH domains for phosphoinositides is low and in most cases insufficient for the effective translocation of Rho-GEFs to the plasma membrane (Baumeister et al., 2006; Snyder et al., 2001). One such example is PREX1, where binding of the phosphoinositide 3-kinase (PI3K)-derived lipid second messenger phosphatidylinositol-3,4,5-trisphosphate (PtdIns(3,4,5)P_3, PIP_3) to the PH domain can only confer robust membrane translocation if membrane-bound Gβγ subunits of heterotrimeric G proteins are also present (Barber et al., 2007). Instead, phospholipid binding can modulate GEF-activity. Phosphoinositide binding to the PH domain of Vav1 was the first reported to promote GEF activity through weakening of the interaction between the DH and PH domains *in vitro* (Das et al., 2000), although this was a relatively weak effect that was not observed in some other studies. Other Rac-GEFs that are strongly activated by PIP_3 include PREX1 and Swap70 (Welch et al., 2002; Welch et al., 2003). In contrast, PIP_2 and PIP_3 binding to the PH domain of Dbl inhibited its GEF-activity towards Cdc42 (Russo et al., 2001).Therefore, the role of the PH domain in the DH/PH tandem is variable between GEF proteins.

Apart from the DH/PH tandem, Rho-GEFs usually contain several other domains with diverse functions. The roles of these domains can be broadly divided into the following three categories: protein interaction-mediating domains, such as the Src Homology 3 (SH3) domain, the Postsynaptic-density protein, Discs large, Zona occludens-1 (PDZ) domain, the Dishevelled, Egl-10 and Pleckstrin (DEP) domain and the Ras Binding Domain (RBD); second messenger-interacting domains, like the phorbol ester-/diacylglycerol-binding C1 domain; and subcellular

localisation-modulating domains, such as the Src Homology 2 (SH2) domain and the Calponin Homology actin binding (CH) domain. As previously outlined, these protein domains can modulate the GEF activity, localisation and effector interactions with different combinations of domains defining each GEF, giving it diverse roles and functions within the cell (Cook et al., 2014).

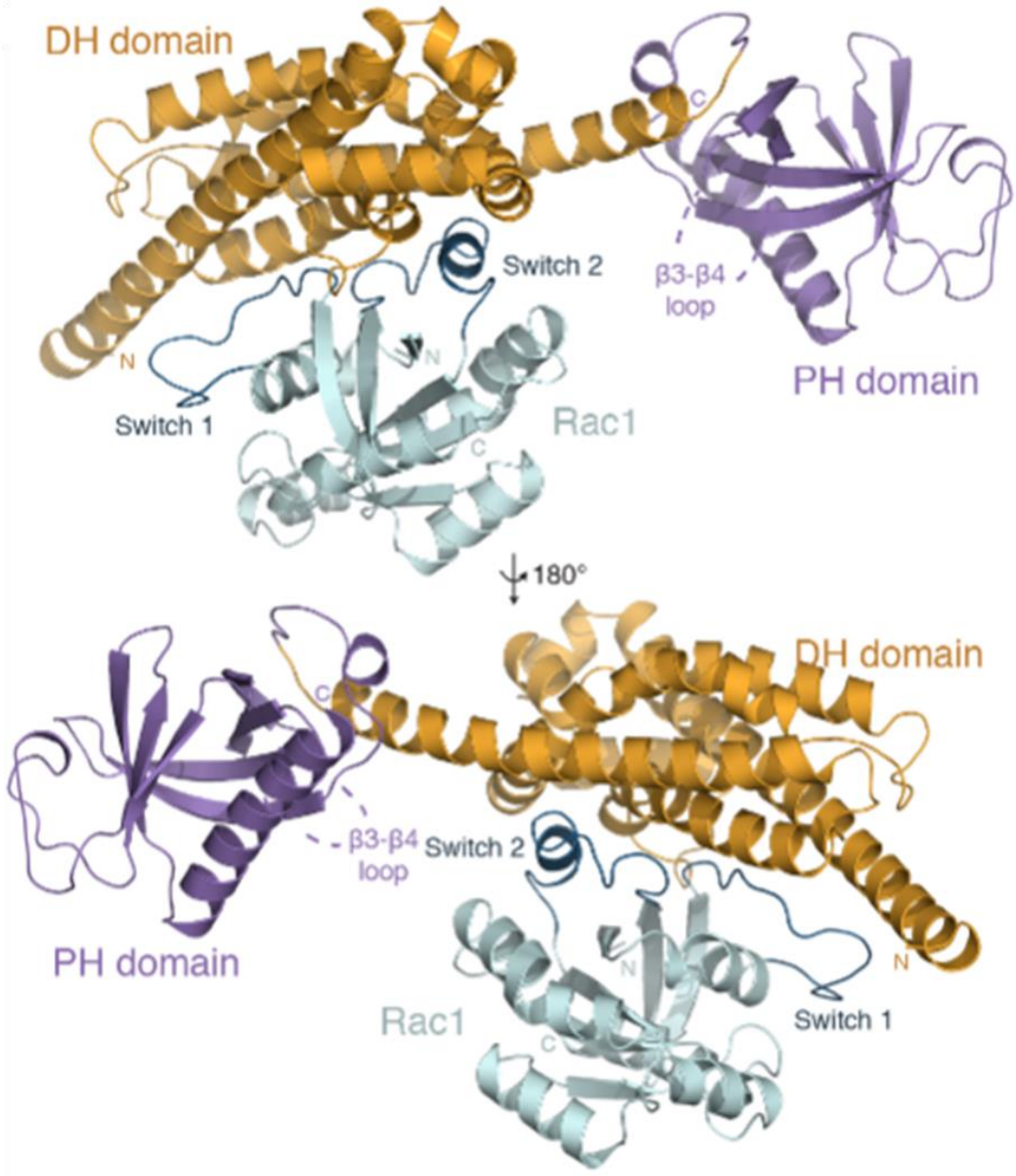

Figure 1.2.1: Structure of the PREX1:Rac1 complex.

Ribbon view of crystal structure of the DH (yellow) and PH (purple) domains of PREX1 in complex with Rac1 (teal). Interactions between the DH domain of PREX1 and Rac1 stabilise the two switch regions in a nucleotide-free conformation. Shown are the switch I and switch II regions (blue) of Rac1 which interact with the CR1 and CR3 regions of the PREX1 Dbl-type GEF. (Figure taken from (Lucato et al., 2015))

1.2.1.2 DOCK-Type Rho-GEFs

The DOCK-type GEFs are structurally unrelated to Dbl-type GEFs, yet capable of catalysing nucleotide exchange on Rho family small G proteins. The members of the DOCK family contain a catalytic DHR2 domain that is preceded by a regulatory DOCK homology region 1 (DHR1) domain, and they can subdivided into four groups according to sequence similarity. The DOCK-A subfamily (DOCK1, DOCK2, and DOCK5), as well as the DOCK-B subfamily (DOCK3 and DOCK4) are GEFs for Rac1 small G proteins. From the DOCK-C subfamily (DOCK6, DOCK7 and DOCK8), DOCK8 is capable of activating Cdc42, whilst DOCK6 and DOCK 7 can activate both. Finally, the DOCK-D subfamily (DOCK9, DOCK10, and DOCK11) are specific for Cdc42 (Gadea and Blangy, 2014; Laurin and Côté, 2014).

The DHR2 domain is responsible for the GEF activity of DOCK proteins. The crystal structures of the DHR2 domain of DOCK2, DOCK7, DOCK8 and DOCK9 have been solved in complex with their substrate GTPases and provided insight into the mechanism of DOCK-mediated nucleotide exchange and specificity for certain substrates (Hanawa-Suetsugu et al., 2012; Harada et al., 2012; Kukimoto-Niino et al., 2019; Kulkarni et al., 2011; Yang et al., 2009). The DHR2 domain is organised into three lobes (lobes A, B and C), with catalytic activity being conferred from lobes B and C. Lobe A shares multiple contacts with lobe B to stabilise the DHR2 domain and lobe C contains the most conserved region of DH2 domains that is interrupted by the loop known as the 'nucleotide sensor'. In DOCK9, it was shown that contrary to the DH domains interacting with both switches I and II of small G proteins, the DHR2 domain catalyses nucleotide exchange by interacting with only the switch I region of Cdc42. The 'nucleotide sensor' region within the DHR2 domain has been shown to maintain the switch I region of the small G protein in an open conformation. Subsequently, a conserved valine residue from the GEF, occludes the Mg^{2+} cofactor from the nucleotide-binding site, resulting in the release of GDP and Mg^{2+} from the small G protein and facilitating its replacement with GTP (Yang et al., 2009). Moreover, mutational analysis of DOCK proteins revealed that DHR2 domains specifically recognise the residue at position 56 of Rac1 or Cdc42 (Kulkarni et al., 2011; Zhou et al., 2013) and the rotation of lobe B relative to lobe C is important for dual substrate specificity (Kukimoto-Niino et al., 2019).

The DHR1 domain was shown to share weak sequence homology with C2 lipid binding domains and bind phosphoinositides, thus controlling the membrane localisation of DOCK proteins (Premkumar et al., 2010; Zhang and Aravind, 2010). DOCK1, DOCK4 and DOCK5 demonstrated specificity towards PIP_3 (Côté et al., 2005; Jungmichel et al., 2014), whereas DOCK6, DOCK7 and DOCK8 preferentially bind to PIP_2 (Jungmichel et al., 2014). In addition to the DHR2 and DHR1 domains, members of the DOCK-A and DOCK-B subfamily contain an N-terminal SH3 protein binding domain, which can interact with the adaptor protein Engulment and Motility (ELMO) that promotes the GEF activity of DOCK, and a proline rich (P-rich) region at the C-terminus, which binds Crk proteins. Instead, the DOCK-D subfamily proteins have an N-terminal PH lipid binding domain involved in membrane translocation (Gadea and Blangy, 2014; Laurin and Côté, 2014).

1.3 PREX Family Rac-GEFs

The PREX protein family consists of two members, the phosphatidylinositol-3,4,5-trisphosphate-dependent Rac exchange factor 1 (PREX1) and the phosphatidylinositol-3,4,5-trisphosphate-dependent Rac exchange factor 2 (PREX2). They are Dbl-type GEFs for the Rac subgroup of Rho family small GTP-binding proteins, and they are synergistically activated by the lipid second messenger PIP_3, which is generated by PI3K, and the Gβγ subunits of heterotrimeric G proteins (Donald et al., 2004; Welch et al., 2002) (**Figure 1.4.1**). The PREX proteins have been reported to play an important role in physiological functions such as inflammation (Herter et al., 2013; Welch et al., 2005), skin pigmentation (Lindsay et al., 2011) and neuronal development (Waters et al., 2008). However, numerous studies have also associated the PREX family with pathologies like cancer and there is an emerging role of the PREX proteins in metabolic disorders (Hornigold et al., 2018; Pandiella and Montero, 2013; Tsonou et al., 2018; Welch, 2015). Currently we have limited molecular insight into whether both PREX1 and PREX2 are important in metabolic disorders or how they are involved in insulin signalling and glucose homeostasis. Herein, it is considered important to further investigate how and to which extent the PREX proteins are involved in these processes.

1.4 PREX Genes and Proteins

In humans, the *PREX1* gene is located on chromosome 20 (20q13.13), near a region associated with type 2 diabetes (Bento et al., 2008). *PREX1* encodes for the 185 KDa cytoplasmic protein PREX1. The PREX2 is a 183 KDa protein encoded by the *PREX2* gene, which is located in chromosome 8 (8q13.2) close to a region linked to aggressive cancer and metastasis (Fejzo et al., 1998). Alternative splicing generates the 112 KDa splice variant PREX2b, which lacks the C-terminal half. The PREX1 and PREX2 proteins are conserved throughout vertebrates, are 56% identical in their amino-acid sequence, and share a common domain structure (Donald et al., 2004; Welch et al., 2002). As is characteristic for Dbl-type Rho-GEFs, the PREX proteins consist of an N-terminal DH domain which confers their catalytic Rac-GEF activity in tandem with a PH domain (Rossman et al., 2005). Following the DH/PH domains there are two DEP and two PDZ protein interaction domains.

Finally, in their C-terminal half there is a large inositol polyphosphate 4-phosphatase (IP4P) homology domain. Although the IP4P domain contains the minimal residues required for phosphatase activity, no catalytic phosphatase activity of the PREX proteins has been reported to date (Welch et al., 2002) (**Figure 1.4.1**).

Recently, the crystal structures of the PREX1 DH/PH domain tandem in complex with constitutively active Rac 1 (Lucato et al., 2015) or nucleotide-free Rac1 (Cash et al., 2016) were solved, which demonstrated that only the DH domain makes multiple contacts with and activates Rac1. Furthermore, it was revealed that the DH domain interacts with both switch I and switch II of Rac1, through its highly conserved regions CR1 and CR3. Moreover, the PREX1 residues Glu56 and Asn238 were confirmed as essential for Rac1 binding and catalytic activity (Lucato et al., 2015). These residues had previously been predicted to be important facilitators of PREX1-Rac1 interaction, and their mutation was shown early on to render the protein catalytically inactive (Hill et al., 2005), and thereafter Glu56/Asn238 mutants are in widespread use as catalytically inactive forms of PREX1 (Hornigold et al., 2018).

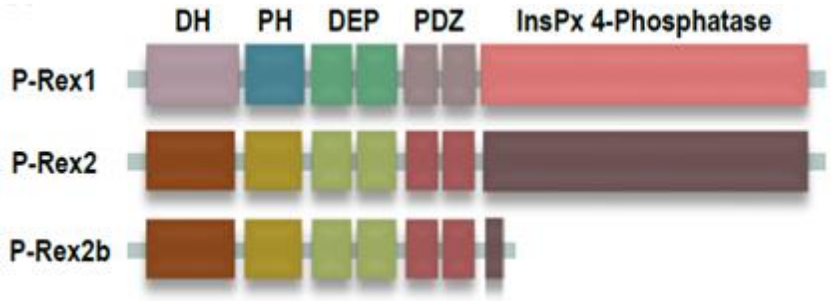

Figure 1.4.1: PREX domain structure and function.
PREX1 and PREX2 are Dbl-type Rho-GEFs and share an identical domain structure (Donald et al., 2004; Welch et al., 2002). At their N-terminus, they have a DH domain, which confers Rac-GEF activity, in tandem with the adjacent PH domain, which binds PIP_3. This is followed by two DEP and two PDZ protein interaction domains. Finally, in their C-terminal half there is an inositol polyphosphate 4-phosphatase (IP4P) domain that harbours no phosphatase activity and has weak homology between the PREX proteins. PREX2b is a splice variant of PREX2 (Welch et al., 2002).

1.5 Tissue Distribution of PREX Proteins

The PREX1 protein was initially purified from neutrophils, where it is strongly expressed and constitutes 0.1% of the cytosolic protein (Hill and Welch, 2006; Welch et al., 2002). Other cell types that highly express PREX1 include macrophages (Wang et al., 2008), platelets (Aslan et al., 2011; Qian et al., 2012), endothelial cells (Carretero-Ortega et al., 2010) and neurons (Yoshizawa et al., 2005). Northern-blot and western-blot studies on mouse tissues have found Prex1 to be most strongly expressed in brain, but it is also abundant in other tissues like bone marrow, thymus, spleen, lymph nodes and lung (Donald et al., 2008; Welch et al., 2002).

PREX2 mRNA expression has been detected in many mouse tissues (Donald et al., 2004), but the protein is not as widely expressed. Western-blot studies showed that Prex2 is abundant in brain, especially in the Purkinje neurons of the cerebellum, and in the lungs. At lower levels, Prex2 has been detected in liver, adipose tissue, thymus and spleen (Donald et al., 2008; Hodakoski et al., 2014). Notably, Prex2 protein is not present in peripheral blood leukocytes (Damoulakis et al., 2014; Lawson et al., 2011; Welch et al., 2005). It is currently unknown which mechanisms restrict the distribution of Prex2 protein to a few tissues despite the wider expression of its mRNA. Little is also known about Prex2b's expression. To date, Prex2b mRNA has been detected only in heart and endothelial cells, and the endogenous Prex2b protein has only be studied in the latter (Li et al., 2005; Rosenfeldt et al., 2004).

1.6 Regulation of PREX Expression

The molecular mechanisms underlying PREX proteins' expression have so far only been studied in the context of their deregulation in cancer. Work in prostate cancer cell lines has shown that the suppression of *PREX1* expression in normal prostate epithelial cells is due to histone deacetylation (Wong et al., 2011). Treatment of human prostate epithelial cells and prostate cancer cells with Histone deacetylase (HDAC) inhibitors or HDAC siRNAs results in the stimulation of *PREX1* expression, while HDAC overexpression represses *PREX1* gene expression. Dual luciferase

assay experiments identified a 92 bp region (-190/-98) upstream of *PREX1* as its minimal promoter, and electrophoretic mobility shift assay (EMSA) identified Sp1 transcription factor as an important regulator of *PREX1* gene promoter activity. It was proposed that Sp1 mediates HDAC binding to the *PREX1* promoter, which leads to histone deacetylation-mediated repression. In metastatic prostate cancer, the observed disassociation of HDACs from Sp1 might be a contributing reason for the aberrant *PREX1* up-regulation (Wong et al., 2011). Alongside regulation by HDACs, hypermethylation of CpG islands in the promoter and transcriptional start regions of PREX1 has been reported as a major mechanism to suppress *PREX1* expression in normal breast epithelial cells (Barrio-Real et al., 2014). *PREX1* promoter methylation was found to be reduced in luminal breast tumours and was associated with ER-positive status. Moreover, hypomethylation was correlated with high *PREX1* expression and with poor long-term survival of breast cancer patients (Barrio-Real et al., 2014). A further mechanism of *PREX1* expression linked PREX1 deregulation to drug resistance of prostate carcinoma cells. In drug resistant cells, the transcription factor Myc was upregulated and binding of Myc to a consensus site in the *PREX1* promoter induced *PREX1* transcription (Goel et al., 2016).

The expression of PREX2 has been found to be post-transcriptionally repressed by the microRNA (miRNA) miR-338-3p, which binds to the 3'-UTR of the *PREX2* gene at three sites and negatively regulates its expression (Chen et al., 2013; Guo et al., 2014). In metastatic neuroblastoma and in gastric cancer, miR-338-3p is significantly down-regulated. Work in human neuroblastoma cell lines demonstrated that downregulation of PREX2 by siRNA rescues miR-338-3p antisense oligonucleotide-induced cell growth and invasion (Chen et al., 2013). Comparably, miR-338-3p overexpression in a human gastric cell line (BGC-823) reduced PREX2 levels and inhibited cell proliferation, and *PREX2* down-regulation had the same effect (Guo et al., 2014). In the same way, blockade of the miR-338 promoter by the transcriptional suppressor MECP2, in gastric cancer cells, was sufficient to induce *PREX2* expression, cell growth, and proliferation (Tong et al., 2016).

1.7 Regulation of PREX Activity

1.7.1 PIP_3 and Gβγ

On matters of activity regulation, Prex1 was initially purified from neutrophils on the basis of its PIP_3-dependent activation (Welch et al., 2002). Work with recombinant human PREX1 demonstrated that its Rac-GEF activity can be directly stimulated by PIP_3 more than 30-fold (Hill et al., 2005; Welch et al., 2002). Interestingly, when different phosphoinositides were evaluated for their ability to bind and activate PREX1, it was shown that PREX1 can also bind to $PI(3,4)P_2$ (Cash et al., 2016; Welch et al., 2002), which however cannot activate its Rac-GEF activity *in vitro* (Welch et al., 2002). Furthermore, it was observed in neutrophils that the Gβγ subunits of heterotrimeric G proteins, which are released upon activation of GPCRs (see **Section 1.1.1**), can also promote Rac activity (**Figure 1.7.1**). Sf9 cell transduction with viruses encoding PREX1, p101/p110γ- PI3K, and $Gβ_1γ_2$ showed that Gβγ subunits can activate PREX1 and that PIP_3 and Gβγ act synergistically on PREX1 (Welch et al., 2002). The study of a panel of deletion and truncation mutants of human PREX1 revealed that the PH domain of the protein is necessary for the PIP_3 binding, and the DH/PH tandem is sufficient for the PIP_3-dependent activation of PREX1 Rac-GEF activity (**Figure 1.7.1**). In contrast, the basal and Gβγ-stimulated Rac-GEF activity of PREX1 appears to be mediated by its DH domain (Hill et al., 2005), although other PREX1 domains also contribute to Gβγ regulation at least *in vivo* (Urano et al., 2008). The DEP, PDZ and IP4P domains of the protein have been found to contribute to keeping the basal activity of PREX1 low, potentially through intramolecular interaction with the DH/PH tandem (Hill et al., 2005).

Similarly, PREX2 and PREX2b are also directly and synergistically activated by PIP_3 and Gβγ (Donald et al., 2004; Li et al., 2005; Rosenfeldt et al., 2004). Experiments in Sf9 cells expressing combinations of PREX2, p101/p110γ-PI3K and/or $Gβ_1γ_2$ subunits demonstrated that PI3K or Gβγ alone can activate PREX2 Rac-GEF activity but their synergistic interaction is required for full activation (Donald et al., 2004). Notably however, work in HEK293 cells has shown that inhibition of PI3K negatively affects the Gβγ-mediated activation of PREX2b, suggesting that PIP_3 might be required for the Gβγ/PREX2 interaction in a cellular context (Li et al., 2005).

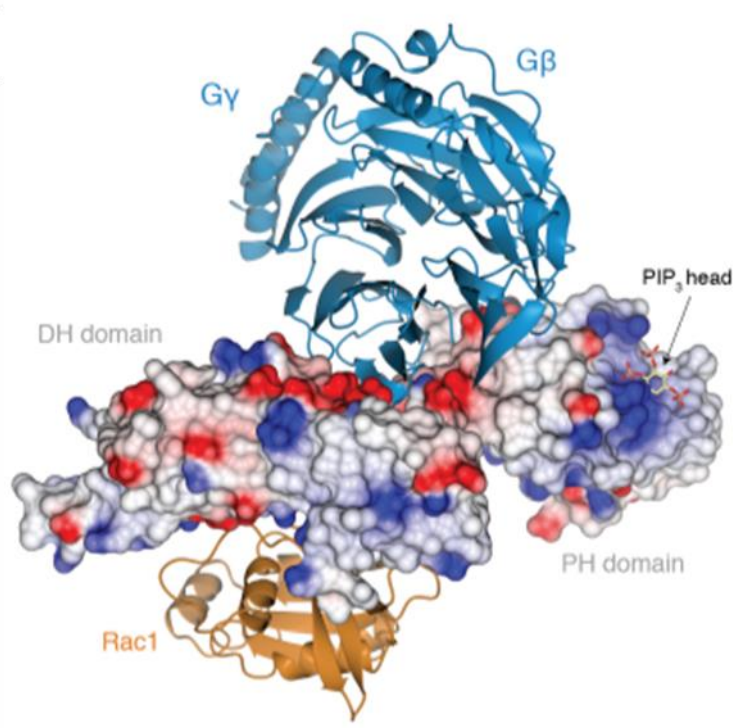

Figure 1.7.1: Crystal structure of the catalytic core of PREX1 in complex with Rac1, showing the PIP3 binding site and predicted Gβγ binding site.

Crystal structure of the DH/PH domain tandem of PREX1 (electrostatic surface view) in complex with Rac1, shown alongside modelling of Gβγ and PIP_3 binding. The crystal structure confirmed that residues Glu56 and Asn238 in the PREX1 DH domain are crucial for Rac1 binding, and that the DH domain is sufficient for catalysis. Furthermore, the modelling suggested that PIP_3 and Gβγ binding sites are likely situated away from the Rac1 binding site and that Gβγ might contact both the PREX1 DH and PH domains (Lucato et al., 2015). The PREX1 PH domain was also crystalized in complex with the soluble PIP_3 analogue IP_4, which revealed that Lys280, Arg289, and Lys368 in the PH domain are required for PIP_3 binding (Cash et al., 2016). (Figure taken from (Lucato et al., 2015))

1.7.2 Regulatory Partners

In addition to PIP_3 and Gβγ. PREX protein activity can be further regulated by phosphorylation or protein-protein interactions (**Figures 1.7.2** and **1.8.1**) (Hornigold et al., 2018; Tsonou et al., 2018).

1.7.2.1 PP1α

Both PREX1 and PREX2 have been found to directly bind protein phosphatase 1α (PP1α) *in vitro*, through a RVxF motif in their IP4P domains. Experiments with recombinant proteins and in HEK-293 cells have shown that PP1α (and to a less extent PP1β) stimulates PREX1 directly by dephosphorylating several residues in the C-terminal half, with Ser1165 being the major target (Barber et al., 2012). Study of hippocampal neurons has shown that stimulation through the ionotropic glutamate receptor NMDAR increases the binding of PP1α to PREX1, thereby contributing to PREX1-mediated synaptic plasticity (Li et al., 2015).

Likewise, PP1α (and to a less extent PP2A) can regulate the phosphorylation state of PREX2 by dephosphorylating Ser1107, although it remains to be investigated further how PP1a regulates the PREX2 activity (Barrows et al., 2015). Regarding the splice variant PREX2b, it is unlikely to be regulated by PP1a as it does not contain the consensus RVxF motif required for PP1a binding.

1.7.2.2 PAK

In contrast to PP1, the p21-activated protein kinases (PAKs) were identified to be negative regulators of PREX proteins. PAKs were shown to phosphorylate PREX1 in response to stimulation of receptor tyrosine kinases (RTKs); PAK2 could phosphorylate PREX1 directly *in vitro*, and phosphorylation by PAK1 reduced the PIP_3-stimulated Rac-GEF activity of PREX1 in a broken-cell assay (Barrows et al., 2016). As PAKs are activated by Rac1-GTP, a negative feedback loop to limit PREX1 activity was proposed (Barrows et al., 2016).

It has been shown *in vitro* that PAK2 can also phosphorylate PREX2 at Ser1107. Moreover, co-expression of PREX2 with wild type but not kinase-dead PAK1 inhibited its Rac-GEF activity in broken-cell assays (Barrows et al., 2015). Knowing that phosphorylation of Ser1107 depends on PIP_3 binding to PREX2, and

on its Rac-GEF activity, it was concluded that PREX2, similarly to PREX1, can catalyse its own inactivation through a Rac1/PAK-dependent negative feedback loop (Barrows et al., 2015). However, it is still unclear if phosphorylation of Ser1107 by PAK is sufficient to inhibit PREX2. Interestingly, phosphorylation of the equivalent residue in PREX1 (Ser1169) by unknown kinases is associated with increased Rac-GEF activity (Montero et al., 2013). It also remains to be seen whether other pathways affect the PAK-dependent inhibition of P-Rex2 during PI3K signalling.

1.7.2.3 PKC

Phosphorylation of PREX1 at Ser313 was found to limit its Rac-GEF activity (Montero et al., 2010). Interestingly, the crystal structure of the PREX1 DH/PH domain revealed that Ser313 lies within the β3/β4 loop of the PH domain, which is considered to be highly mobile. On this basis, Lucato et al suggested that phosphorylation of Ser313 may enable the β3/β4 loop to interact with the DH domain to sterically inhibit Rac1 binding (Lucato et al., 2015). More recently, the Pandiella lab showed that the PREX1 Ser313 could be directly phosphorylated by the protein kinase Cδ (PKCδ) isoform. Functional studies using overexpression of either wild type PREX1 or PREX1 S313A in several breast cancer cell lines with low intrinsic expression of PREX1 further confirmed that phosphorylation of PREX1 at Ser313 restricts Rac-GEF activity (Montero et al., 2016).

1.7.2.4 PKA

The protein kinase A (PKA) is another known inhibitor of PREX1 which completely blocks PREX1 activation by either PIP_3 or Gβγ (Mayeenuddin and Garrison, 2006; Urano et al., 2008). Work with HEK-293 cells has demonstrated that PKA can effectively inhibit PREX1, and that it does so by affecting the interaction between the second DEP/first PDZ domains and the IP4P domain of PREX1, which is important for Gβγ binding within cells (Urano et al., 2008). More recently, it was confirmed that the PKA regulatory subunit interacts with the PDZ1 domain of PREX1 while the PKA catalytic domain phosphorylates Ser436 in the PREX1 DEP domain (Chavez-Vargas et al., 2016). Pull-down assays showed that PKA-mediated phosphorylation of DEP1 at Ser436 promotes its interaction with the DH/PH domain tandem, which probably results in an inhibitory intramolecular conformation

(Chavez-Vargas et al., 2016). Similarly, PKA was found to mediate the inhibition of the DH/PH domain by the C-terminal half of PREX1. However, this was independent of its interaction with the DEP/PDZ1 domains, suggesting that PKA might also target residues within the PREX1 C-terminus (Chavez-Vargas et al., 2016). Interestingly, another recent study showed that PKA, downstream of chemotactic G_s-coupled receptors, can also activate PREX1 independently of its kinase activity (Adame-Garcia et al., 2019). It was proposed that upon cAMP production, the cAMP-bound regulatory subunits dissociate from the catalytic subunits of PKA and while the catalytic subunits phosphorylate and inhibit a fraction of the PREX1 protein pool, the regulatory subunits directly activate another fraction of PREX1 molecules. Eventually, the activity of the PKA catalytic subunits prevails and desensitises PREX1 signalling (Adame-Garcia et al., 2019). To this day, PKA has not been reported to regulate PREX2 phosphorylation.

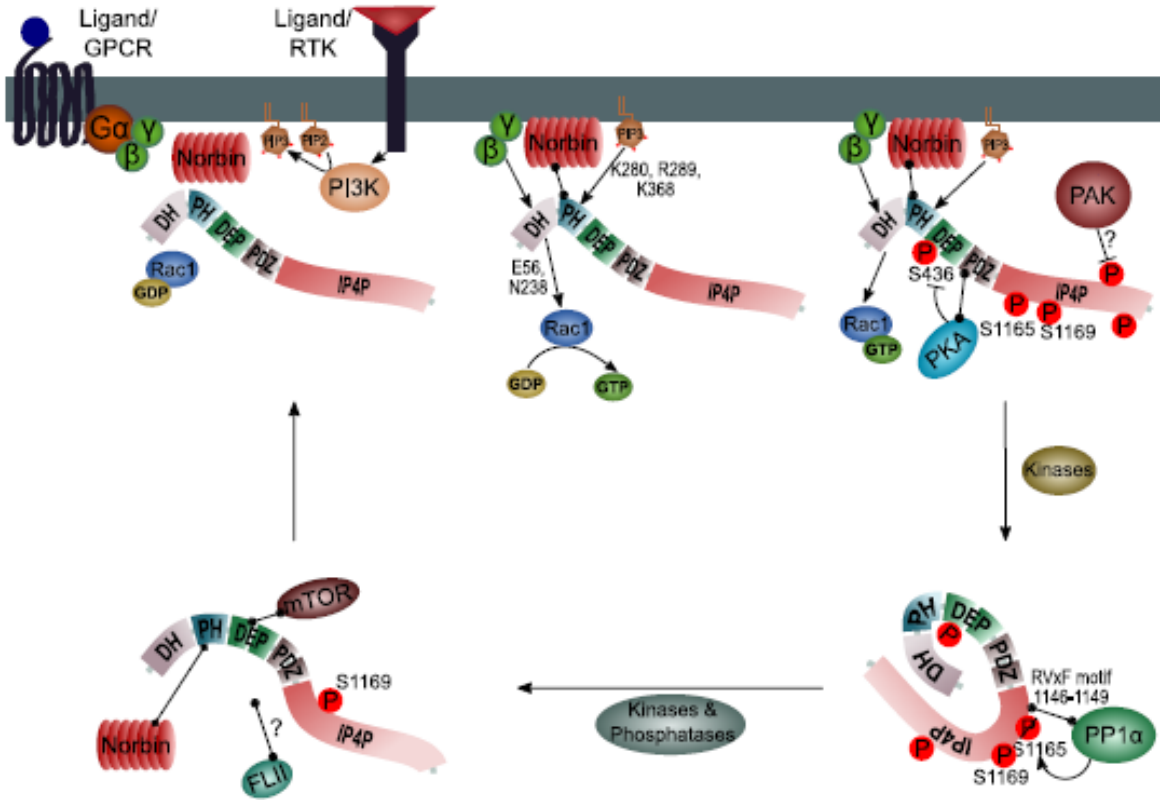

Figure 1.7.2: PREX1 regulation and binding partners.
Depicted are direct interactions of PREX1 with its regulators, substrate, and binding proteins. Arrows denote activation, blunt ends show inhibition, and bobble-ends show direct binding.

In basal cells: PREX1 is largely cytosolic and has low basal Rac-GEF activity, due to intramolecular inhibition. In the cytosol, PREX1 binds constitutively to the serine phosphatase PP1a, the GPCR adaptor protein Norbin, the protein kinases PKA and mTOR and the gelsolin superfamily adaptor protein FLII. PP1a binds to the RVXF motif (residues 1146–1149) of PREX1 and dephosphorylates Ser1165, which is sufficient to weakly stimulate PREX1 Rac-GEF activity. This interaction between PP1a and PREX1 in neurons increases upon NMDAR stimulation. Norbin binds to the PH domain, induces a robust membrane translocation of PREX1 and also weakly stimulates Rac-GEF activity. FLII binds PREX1 constitutively (at an unknown site), and PREX1 mediates an interaction of FLII with Rac1-GTP that promotes cell migration and contraction. In addition, PREX1 binds constitutively to mTOR through its DEP domains and forms part of TORC1 and TORC2. PREX1 affects mTOR responses (and likely also vice versa), but the underlying mechanisms remain to be elucidated. It also remains to be shown if the interactions of REX1 with Norbin, FLII and mTOR are affected by cell stimulation.

Upon cell stimulation: Both the membrane association and the catalytic activity of REX1 are increased upon cell stimulation, through various mechanisms that cause release of intramolecular inhibition. PREX1 is directly activated by the lipid second messenger PIP_3, which is generated by PI3K, and by the Gβγ subunits of heterotrimeric G proteins. PIP_3 binds to the PH domain, and activation by Gβγ occurs through the DH domain, although further domains are involved in Gβγ binding *in vivo*. PIP_3 and Gβγ can activate PREX1 independently, but also synergistically. This synergistic activation makes PREX1 a coincidence detector for the concomitant stimulation of PI3K-coupled receptors and GPCRs. As well as Rac-GEF activity, PIP_3, and Gβγ also synergistically stimulate the membrane localization of PREX1. Other mechanisms of PREX1 activation include Norbin binding and dephosphorylation by PP1a, as well as the phosphorylation of Ser1169 by unidentified serine kinases. Interestingly, the equivalent site in PREX2 (Ser1107) is phosphorylated by PAK, an inhibitor of PREX Rac-GEFs.

Negative regulation: PKA binds to the PDZ1 domain and inactivates PREX1 by phosphorylating Ser436 in the DEP1 domain, which promotes an inhibitory intramolecular interaction with the catalytic core. In addition, PKA also regulates (possibly indirectly) an intramolecular interaction of the C-terminal half with the catalytic core. The Rac1 GTP-dependent kinase PAK can also phosphorylate PREX1 directly (at unknown sites) and inhibits PREX1 activity (possibly indirectly) within cells, which led to the proposal of a negative feedback loop involving PREX1, Rac1, and PAK to limit PREX1 signalling.

1.7.2.5 Norbin

Norbin (Neurochondrin) is a leucine-rich cytoplasmic protein that is predominantly expressed in the nervous system where it is implicated in brain and neuron development, as well as the regulation of synaptic plasticity (Wang et al., 2010). Recently, our lab identified Norbin as a direct binding partner for PREX1, which promotes PREX1 membrane localisation and Rac-GEF activity (Pan et al., 2016).

1.7.2.6 PTEN

PREX2 binds directly to the tumour suppressor Phosphatase and Tensin Homolog Deleted from Chromosome 10 (PTEN) that blocks PI3K signalling by converting the PI3K product PIP_3 back to $PI(4,5)P_2$ (Fine et al., 2009). This interaction between PREX2 and PTEN is conferred by binding of the PREX2 PH domain to the catalytic and C2 domains of PTEN, and through additional contacts of the PREX2 IP4P domain with the C-terminal PDZ-binding domain of PTEN (Fine et al., 2009; Hodakoski et al., 2014). The interaction is specific to PREX2, as PREX1 does not bind PTEN. Importantly, PREX2 inhibits the phosphatase activity of PTEN, independently of its Rac-GEF activity. Consequently, PREX2 deficiency leads to increased PTEN activity and a suppression of PIP_3 levels and PI3K pathway activity (Hodakoski et al., 2014).

Intriguingly, PREX2 does not only inhibit PTEN, but inversely, PTEN also regulates PREX2 (Mense et al., 2015). PTEN attenuated the PREX2-dependent invasive migration of breast cancer cells, independently of its lipid- and protein-phosphatase activities. This suggested that PTEN has an adaptor role, which blocks PREX2 function. Indeed, PTEN reduced the Rac1-GEF activity of PREX2, both *in vitro* and upon expression in HEK293 cells, independently of its own catalytic activity. Mutational analysis identified furthermore that the most C-terminal amino acids of PTEN are required for the inhibition of PREX2-dependent invasive cell migration (Mense et al., 2015). Importantly, PREX2 mutants that are frequently present in cancer were able to escape the inhibition by PTEN, both *in vitro* and in assays of invasive cell migration (**Figure 1.7.2**). The PREX2 V432M and P948S mutants (which are seen in melanoma and pancreatic cancer, respectively) showed normal binding to PTEN, but the ability of PTEN to inhibit their Rac-GEF activity was

reduced. In contrast, the melanoma-associated PREX2 G844D mutant evaded PTEN inhibition through reduced binding (Mense et al., 2015). It remains to be shown why PTEN could not inhibit the former two PREX2 mutants. However, it appears that these mutants retained their ability to inhibit PTEN, as PTEN was unable to suppress Akt phosphorylation in glioblastoma cells expressing the mutants (Mense et al., 2015). In summary, PTEN is a negative regulator of PREX2 and loss of this inhibition in cancer cells promotes invasive migration. Future work will need to elucidate the effects of PTEN on physiological roles of PREX2.

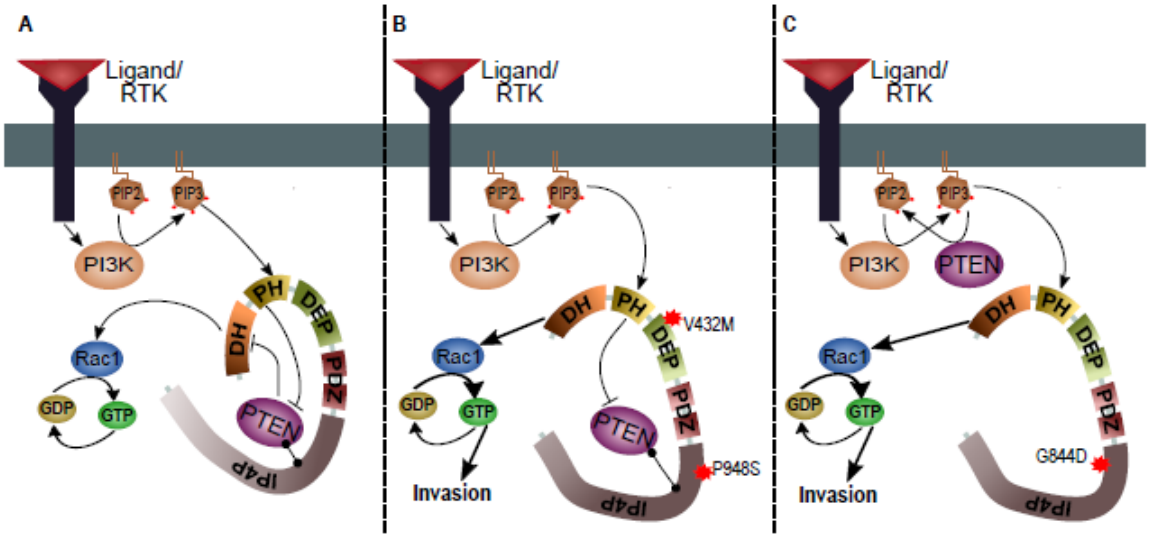

Figure 1.7.3: Cancer-associated PREX2 mutants escape negative regulation by PTEN.

(A) Wild type PREX2: PREX2 binds to the tumour suppressor PTEN through its PH and IP4P domains and inhibits PTEN phosphatase activity, independently of its Rac-GEF activity. This leads to increased PI3K pathway activity. Inversely, PTEN also inhibits PREX2 Rac-GEF activity, thus limiting cell migration. It remains to be investigated under which physiological conditions PTEN can inhibit PREX2, and vice versa. **(B) Cancer-associated PREX2 mutations V432M and P948S:** The melanoma-associated PREX2 mutant V432M and the pancreatic cancer-associated mutant P948S escape inhibition by PTEN. These mutants bind PTEN normally, but their Rac-GEF activity is less sensitive to PTEN. It is likely that these PREX2 mutants retain their ability to inhibit PTEN, however. Cancer cells carrying these PREX2 mutations show increased invasive migration. **(C) Cancer-associated PREX2 mutation G844D:** The melanoma-associated PREX2 mutant G844D escapes inhibition by PTEN through reduced PTEN binding. Cancer cells carrying this PREX2 mutation show increased invasive migration. Due to the reduced interaction, this PREX2 mutant should also not be able to inhibit PTEN. This may lead to a suppression of PI3K signalling in cells expressing PREX2 G844D, which requires further investigation.

1.8 PREX Binding Proteins

Apart from Rac and the regulators described above, few binding proteins have been identified to bind PREX1 and/or PREX2 directly (**Figures 1.7.2** and **1.8.1**) (Hornigold et al., 2018; Tsonou et al., 2018).

1.8.1 mTOR

The serine kinase mammalian target of rapamycin (mTOR), a key regulator of cell growth and of a plethora of other cell responses, was found to bind PREX1 directly through the DEP domains. PREX1 interacts with both mTOR-containing protein complexes, mTORC1, which is central in cell growth, and mTORC2 (also known as PDK2), which controls cell morphology and migration (Hernandez-Negrete et al., 2007). Although there is evidence suggesting that PREX1 can signal both upstream and downstream of mTOR (Hernandez-Negrete et al., 2007; Kim et al., 2011a), more research is required to elucidate whether PREX1 can regulate both TORC1- and TORC2-dependent cellular processes. Similarly, PREX2 and PREX2b also directly interact with the serine kinase mTOR (Hernandez-Negrete et al., 2007). However, it is unknown if PREX2 and PREX2b can modulate mTOR signalling or vice versa.

1.8.2 FLII

The Malliri lab performed a SILAC screen that identified proteins, which interact with Rac1 specifically in the presence of PREX1. This identified the actin remodelling protein flightless-1 homolog (FLII), a member of the gelsolin superfamily, as a PREX1 binding protein (Marei et al., 2016b). PREX1 bound directly to FLII, independently of its Rac-GEF activity. PREX1 interacted with the C-terminal GEL domain of FLII, whereas Rac1 bound to the N-terminal LRR domain of FLII. In addition, the actin capping protein TMOD3 was shown to bind Rac1 and FLII more strongly in the presence of PREX1 (Marei et al., 2016a). Importantly, PREX1 enabled the interaction between Rac1 and FLII in fibroblasts preferentially when Rac1 was GTP-loaded, and the ability of PREX1 to induce cell migration and myosin contractility required FLII. Based on these findings, a model was proposed where PREX1 activates Rac1 and acts as a scaffold that enables FLII to interact with this active Rac1, thus inducing cell responses that require both Rac1-GTP and FLII

(Marei et al., 2016b).

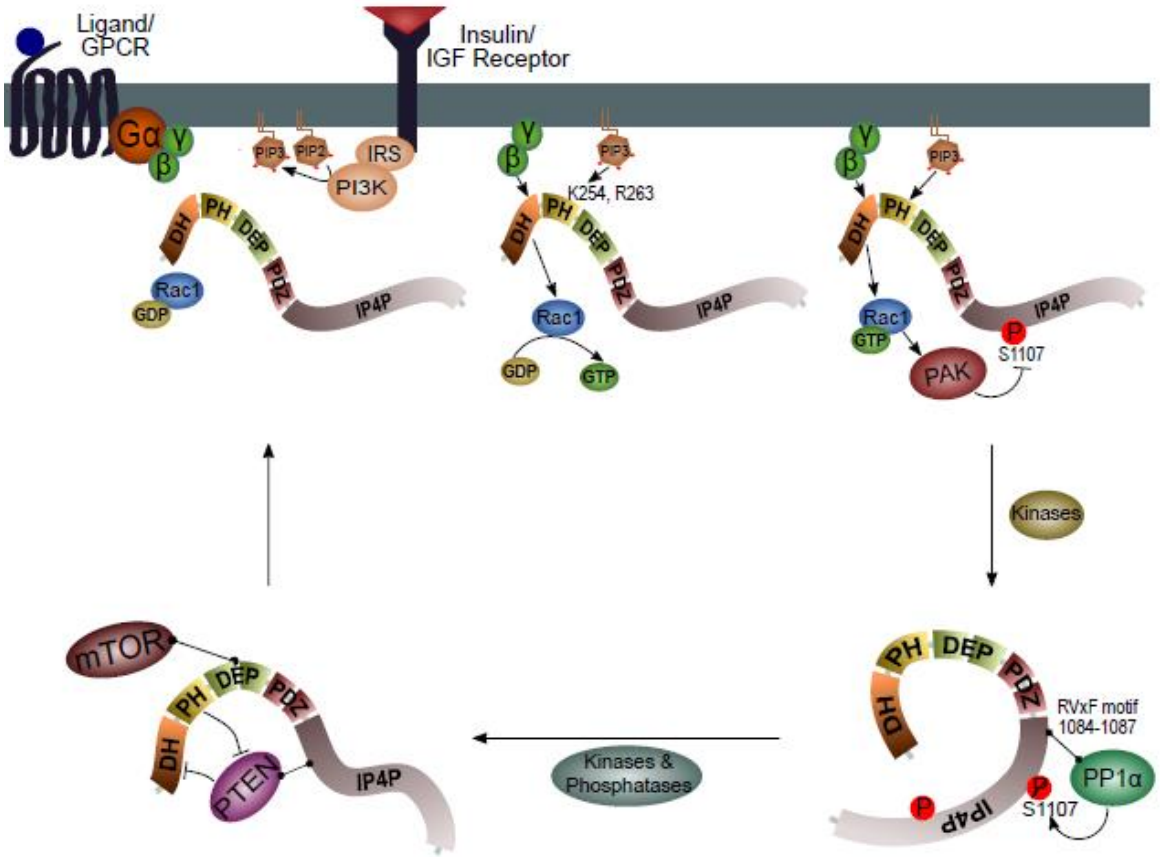

Figure 1.8.1: PREX2 regulation and interacting proteins.

In basal cells: PREX2 is largely cytosolic and has low basal Rac-GEF activity, through intramolecular inhibition. In the cytosol, PREX2 constitutively interacts with the tumour suppressor PTEN, the serine phosphatase PP1a, and the serine kinase mTOR. PREX2 and PTEN can inhibit each other, independently of their respective catalytic activities. PP1a binds to the RVxF motif (residues 1084–1087) and dephosphorylates Ser1107 of PREX2, and possibly other residues. It is likely that PP1a activates PREX2, similar to PREX1. The consequences of the interaction with mTOR are unknown.

Upon cell stimulation: PREX2 is activated by the lipid second messenger PIP_3, which is generated by PI3K, and by the Gβγ subunits of heterotrimeric G proteins, which are released upon stimulation of GPCRs. PIP_3 and Gβγ can activate PREX2 either individually or synergistically. The DH domain is sufficient for activation by Gβγ, whereas Lys254 and Arg263 in the PH domain are required for activation by PIP_3. In order to activate Rac1, PPEX2 must be recruited to the cell membrane. By analogy with PREX1, it seems likely that PIP_3 and Gβγ not only activate the Rac-GEF, but also induce its membrane translocation in a synergistic manner.

Negative regulation: One of the effector proteins of active Rac1 (Rac1-GTP) is the serine kinase PAK. Active PAK can phosphorylate PREX2 directly and inhibit PREX2 Rac-GEF activity in broken-cell assays. Thus, active PREX2 seems to be able to generate a negative feedback loop from PREX2/Rac1/PAK for PAK-mediated inhibition of its own Rac-GEF activity. PAK phosphorylates Ser1107 of PREX2, among other residues, but it is unknown if phosphorylation of Ser1107 is sufficient for inhibition.

1.9 Physiological and Pathophysiological Functions of PREX Proteins

1.9.1 Leukocytes, Platelets, and Inflammation

Work in neutrophils isolated from *Prex1* knockout mice has demonstrated that Prex1 acts downstream of GPCRs and is involved in Rac-dependent ROS production, actin polymerisation, polarisation and migration, whereas *in vivo* work has shown that Prex1 is important for neutrophil recruitment to inflammatory sites (Damoulakis et al., 2014; Welch et al., 2005). In addition to neutrophils, Prex1 is also expressed in platelets (Qian et al., 2012). *Prex1* knockout mice show mild defects in haemostasis, and Prex1 deficient platelets show a partial impairment in GPCR-dependant aggregation and dense granule secretion (Qian et al., 2012). However, in contrast to this minor role in haemostasis, Prex1/Vav expression in platelets was found to be important for the platelet-dependent vascular adhesion and tissue recruitment of neutrophils and eosinophils during inflammation (Pan et al., 2015). *Prex1*$^{-/-}$*;Vav1*$^{-/-}$ and *Prex1*$^{-/-}$*;Vav3*$^{-/-}$ platelets had low surface levels of the selectin ligand PSGL-1, and the mice showed a reduced occurrence of platelet-neutrophil adhesion in the circulation, which is prerequisite for the extravasation of these leukocytes (Pan et al., 2015). Finally, Prex1 has been shown to be required for pulmonary fibrosis, a late phase of pulmonary inflammation, which can result in loss of lung function. *Prex1* knockout mice exhibited reduced early leukocyte infiltration and fibrosis, which drastically increased survival in a bleomycin-induced model of pulmonary fibrosis (Liang et al., 2016).

1.9.2 Neurons and Behaviour

Another role of PREX proteins is regulation of neuronal development and behaviour. Prex1 was found to be localised in the leading processes and adjacent cytoplasmic regions of migrating neurons in the cortex (Yoshizawa et al., 2005). Activation of Prex1 in neuronal PC12 cells by stimulation with NGF resulted in increased Rac activity, lamellipodia formation, membrane ruffling, cell spreading and migration, whereas knockdown of endogenous Prex1 had the opposite effect (Yoshizawa et al., 2005). One study found single nucleotide polymorphisms (SNPs), copy number deletions and reduced mRNA levels of PREX1 in children with autism spectrum disorders (Li et al., 2015). Evaluation of *Prex1*$^{-/-}$ mice in behavioural models of

autism revealed deficits in social recognition, reversal learning and fear extinction. Acute knockdown of *Prex1* in the hippocampal CA1 region of young wild type mice resulted in similar behavioural defects as seen in *Prex1*$^{-/-}$ mice, suggesting that Prex1 expression in the hippocampus is required for social interaction and flexible behaviours (Li et al., 2015). Furthermore, NMDAR-induced long-term depression (LTD) was shown to be impaired in the hippocampal CA1 region of *Prex1*$^{-/-}$ mice. Remarkably, the impairments in NMDAR-dependent hippocampal LTD, social recognition and behavioural flexibility seen in *Prex1*$^{-/-}$ mice could be rescued by the overexpression of Prex1 in pyramidal neurons of the CA1 region of the hippocampus (Li et al., 2015). More recently, a deep learning approach of analysing GWAS data from Taiwanese population identified the SNP *rs4810894* adjacent to the *PREX1* gene as a putative modulator of the antidepressant treatment response (Lin et al., 2018). However, the functional relevance of the effects of this SNP on the antidepressant treatment response is yet to be investigated.

Prex2 is highly expressed in the cerebellum. Study of *Prex2* knockout mice revealed that they have impaired Purkinje cell morphology, and they exhibit a mild motor coordination defect, which gets worse with ageing, especially in females (Donald et al., 2008). *Prex1*$^{-/-}$*;Prex2*$^{-/-}$ mice showed an exacerbated phenotype, with a more severe impairment of motor activity, as well as posture and gait defects. These impairments were consistent with cerebellar dysfunction and were evident in both males and females from a young age (Donald et al., 2008). Furthermore, patch clamp electrophysiology showed that *Prex1*$^{-/-}$*;Prex2*$^{-/-}$ Purkinje neurons compensate well for the dendrite morphology defect, as their passive membrane properties and basal synaptic transmission were normal. However, these neurons had impaired synaptic plasticity, as they were unable to maintain long-term potentiation, which is required for learned motor coordination skills (Jackson et al., 2010).

1.9.3 Endothelial Cells and Vascular Biology

PREX proteins are also implicated in vascular biology. PREX1 deficiency in human microvascular endothelia cells (HMEC) inhibits stromal cell derived factor-1 (SDF1) stimulated Rac1 activity, chemotaxis and *in vitro* angiogenesis (Carretero-Ortega et al., 2010). Moreover, work in human lung microvascular endothelia cells (HLMVEC)

has demonstrated that PREX1 is involved in the tumour necrosis factor-α (TNF-α)-induced endothelial barrier disruption, via Rac activation, ROS production, c-Src activation, and VE-cadherin phosphorylation (Naikawadi Ram et al., 2012). These findings were further confirmed *in vivo*, as Prex1 deficient mice showed significantly decreased vascular endothelial permeability and oedema formation. Finally, endothelial Prex1 has also been associated with the promotion of leukocyte transendothelial migration (Naikawadi Ram et al., 2012). In addition, PREX1 was also shown to mediate Weibel-Palade body secretion in primary human umbilical vein endothelial cells (HUVECs), a process required for the upregulation of P-selectin on the endothelium and for the capture of leukocytes from the blood stream during inflammation (van Hooren et al., 2014).

The PREX2 isoforms are also expressed in endothelia cells. Knockdown of PREX2b in HUVECs showed that it is required for the sphingosine 1-phosphate stimulated migration of endothelial cells (Li et al., 2005). Moreover, a study that employed an shRNA knockdown screen in HUVECs, identified PREX2 as a potential regulator of mechanical-force-induced orientation of endothelial cells, a response which is relevant *in vivo* for the integrity of blood vessel walls (Abiko et al., 2015).

1.9.4 Cancer

Both *PREX1* and *PREX2* genes are located in genomic regions that are often amplified in cancer, and in particular melanoma, breast, prostate, and colorectal tumours (Berger et al., 2012; Pandiella and Montero, 2013).

Deregulated PREX1 expression was shown to be sufficient to drive the growth and the metastasis of melanoma, breast, and prostate cancer. It was demonstrated that overexpression of PREX1 can occur through amplification of the *PREX1* gene, as it is common in breast cancer (Sosa et al., 2010), or through the loss of epigenetic repression seen in prostate cancer (Wong et al., 2011) and in breast cancer subtypes (Barrio-Real et al., 2014). In contrast to overexpression, somatic mutations of *PREX1* in cancer are rare. They have only be reported to occur in lung carcinomas, with a frequency of 5% (Suzuki et al., 2013), and in 3.65% of breast cancers (Dillon et al., 2014). It remains to be shown if such mutations affect

the function of the PREX1 in a manner that could promote the growth or spread of lung cancer. Finally, a SNP in the third intron of *PREX1* (rs6066835) was identified in a GWAS study to be associated with multiple myeloma and with increased PREX1 expression in multiple myeloma plasma cells (Mitchell et al., 2016).

Apart from the mechanisms regulating *PREX1* gene expression, additionally the PREX1 signalling pathway has been extensively studied in cancer cells, especially in the context of breast cancer and melanoma. In breast cancer cells, it has been shown that PREX1 is activated downstream of the RTK receptor ErbB and the GPCR receptor CXCR4. Signalling through the CXCR4 receptor has been associated with cell growth and migration, whereas signalling through the ErbB receptor promotes cell motility (Liu et al., 2016; Lopez-Haber et al., 2016; Sosa et al., 2010). Interestingly, it was also shown that ErbB can transactivate CXCR4, and it has been proposed that signalling pathways downstream of these two receptors intersect at PREX1 (Kazanietz et al., 2018; Sosa et al., 2010). Moreover, in breast cancer, PREX1 has been reported to promote PI3K/AKT signalling, while itself being modulated by PI3K at the transcriptional and posttranslational levels (Dillon et al., 2014). Aberrant PREX1 signalling has been involved in the increased activation of the Raf/MEK/Erk pathway, in a Rac1 dependent way (Dillon et al., 2014; Liu et al., 2016). It was also suggested that PREX1 is involved in breast cancer cell proliferation through PREX1-dependent regulation of the cell cycle regulators Cyclin D1 and $p21^{Cip1}$ (Liu et al., 2016). However, a more recent study has argued that PREX1 is not required for the Erk-pathway dependent mitotic or survival responses of breast cancer cells (Barrio-Real et al., 2018).

Prex1 was also implicated in the melanoblast migration during the normal development in mice. *Prex1*$^{-/-}$ mice, on C57BL/6J genetic background, have white bellies, feet and tail tips. This migration defect becomes relevant in melanoma, where melanocytes are transformed into melanoma cells. Prex1 expression is deregulated in melanoma cells and is critical for melanoma metastasis, at least in part, in a Rac1 dependent way (Lindsay et al., 2011; Lindsay et al., 2015). PREX1 was shown to regulate cell proliferation, invasion and migration of cutaneous melanoma cells via PREX1/RAC1/PAK1/p38/MMP-2 pathway. It was also found that PREX1 knockdown in melanoma cell lines inhibits cell cycle by reducing

survivin and cyclin D1 expression (Wang et al., 2017). Furthermore, comparison of PREX1 expression in human cutaneous melanoma specimens with disease outcome revealed lower distant metastasis-free survival among AJCC stage I/II/III patients with high PREX1 expression compared to patients with low PREX1 expression (Wang et al., 2017).

The *PREX2* locus lies within a genomic region that is linked with aggressive cancers and metastasis (Berger et al., 2012). In melanoma, the locus also undergoes frequent chromosomal translocations and rearrangements (Berger et al., 2012). Hence, multiple mechanisms seem to contribute to the deregulation of PREX2 expression in cancer. Furthermore, although it is very unusual for Rho-GEFs to be mutated, *PREX2* mutations are frequently observed in cancer, particularly in melanoma, where the Rac-GEF is mutated in 14% of cases (Berger et al., 2012), and in pancreatic ductal adenocarcinomas (PDACs; 10%) (Waddell et al., 2015). Both the deregulated expression and mutations of PREX2 were shown to promote tumour growth.

In a follow up study, Lissanu Deribe and colleagues generated a genetically engineered conditional knockout mouse harbouring the *Prex2*^{E824*} mutation in an iNRAS background and observed that the *Prex2*^{E824*} mutation accelerated melanoma development compared to control mice (Lissanu Deribe et al., 2016). Biochemical analysis revealed that Prex2^{E824*} contributes to melanoma tumorigenesis both through increased Rac1 GEF activity and abolished PTEN binding (Lissanu Deribe et al., 2016). Interestingly, a replication study of the Berger et al. 2012 paper that repeated the tumour xenografts experiments, where TERT-immortalised human melanocytes engineered to express NRAS(G12D) (PMEL-NRAS*) and PREX2^{G844D} or PREX2^{Q1430*} isoforms were transplanted into immunodeficient mice, failed to observe the accelerated *in vivo* tumorigenesis that had been originally reported. This was largely attributed to different rates in tumour development in control mice between the two studies (Horrigan et al., 2017).

1.10 Glucose Homeostasis

Recent evidence suggests a role of PREX proteins in metabolic conditions. To date, however, there has been no detailed investigation into the importance of PREX proteins in glucose homeostasis and insulin signalling, or into the molecular mechanism underlying their involvement in these processes. The purpose of this project was to investigate the metabolic effects of Prex deficiency in mice. Therefore, the rest of this introduction is focused on the mechanisms that control glucose homeostasis, and what is known about the roles of Rho-GEFs, and PREX Rac-GEFs in particular, in metabolism.

1.11 Systems of Glucose Homeostasis

Glucose is an essential source of metabolic energy, required by most cells in the body. The brain accounts for approximately 50% of all glucose utilisation, another 25% of glucose is being used by organs of the splanchnic area such as the liver and the gastrointestinal tissue, and the remaining 25% of glucose uptake occurs in insulin-dependent tissues, like muscle and adipose tissue (Cersosimo et al., 2000). Glucose is provided either through release from endogenous glycogen stores, mainly the liver and kidneys, or through intestinal absorption of exogenous dietary glucose. Low blood glucose levels (hypoglycaemia) can trigger dizziness, seizures, and loss of consciousness, while profound and prolonged hypoglycaemia can result in death. In contrast, increased blood glucose levels (hyperglycaemia) can cause, among others, headache, blurred vision, and dehydration. Moreover, long-term hyperglycaemia has been associated with cardiovascular diseases, loss of vision, renal failure, and neuropathy. Hence, it is crucial to maintain the blood glucose within a relatively narrow range (Szablewski, 2011).

Glucose homeostasis is defined as the process of maintaining stable glucose levels in the blood. Glucose homeostasis is mainly achieved by the balanced actions of insulin and glucagon, two pancreas-released hormones with antagonistic effects. However, various other organs such as the brain, liver, kidneys, intestine, skeletal muscle and adipose tissue also contribute to the tight regulation of blood glucose levels by means of uptake, metabolism, storage, and excretion (Röder et al., 2016;

Triplitt, 2012) (**Figure 1.11.1**).

The mechanisms orchestrating the regulation of glucose homeostasis are considerably complex both at cellular and at systemic levels. The tight regulation of circulating glucose is a diverse process that requires the sophisticated coordination of many organs, which respond to multiple hormonal and physiological signals. Here, I will focus on summarising how insulin and glucagon regulate glucose disposal and production in various organs while also creating a system of inter-organ metabolic communication (**Figures 1.11.1** and **1.11.4**).

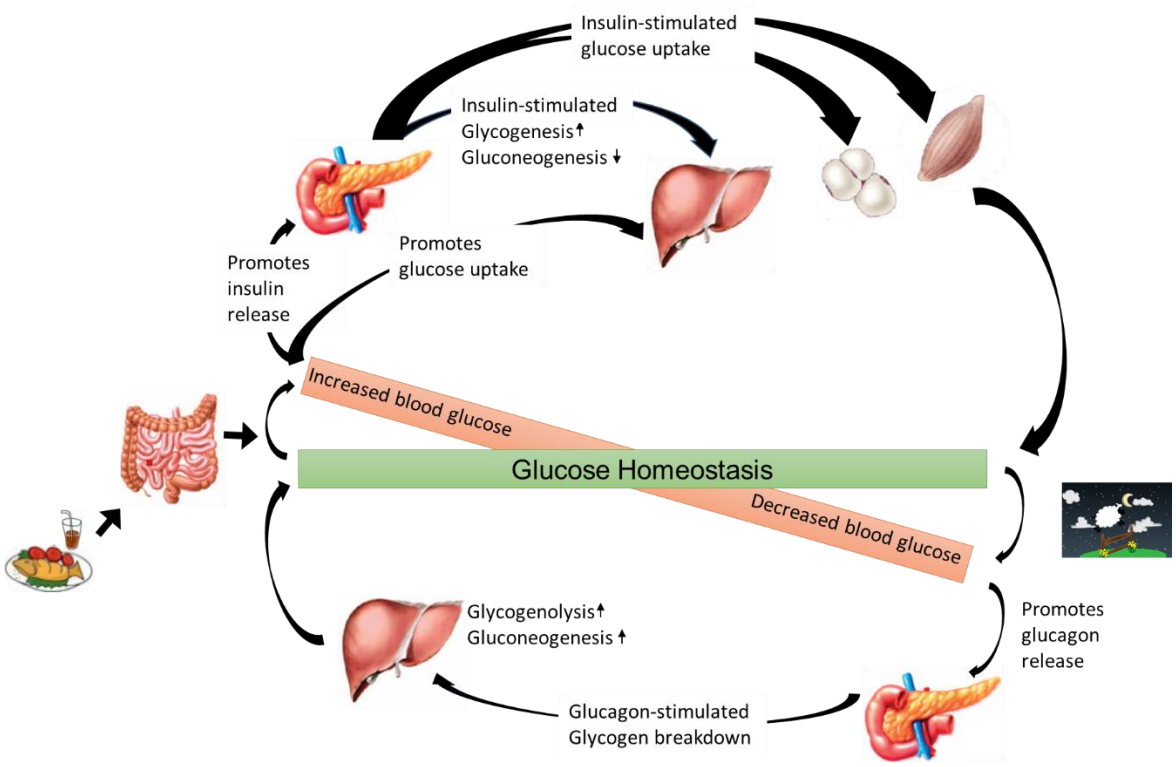

Figure 1.11.1: Maintenance of glucose homeostasis by insulin and glucagon.
Food consumption results in increased glucose levels in the blood stream that in turn promote insulin release from the pancreas. Insulin stimulates glucose uptake from the adipose tissue and skeletal muscle, as well as glycogenesis in the liver, which coordinate to return the blood glucose to normal levels. In contrast, low blood glucose levels promote glucagon release from the pancreas that increases blood glucose levels through glycogenolysis and gluconeogenesis in the liver. (Figure adapted from (Röder et al., 2016))

1.11.1 Pancreas

The pancreas is an exocrine and endocrine organ with a central role in glucose homeostasis. Its exocrine function involves the secretion of various digestive enzymes into the upper small intestine through the pancreatic ducts. In contrast, the pancreatic endocrine cells (α-, β-, γ-, δ-, and ε-cells) are clustered together in the islets of Langerhans and release hormones directly into the blood stream. As mentioned above, glucagon and insulin have key roles in glucose homeostasis. Glucagon is produced in the pancreatic α-cells and stimulates glucose production and release from the liver, when blood glucose levels are low during sleep or in between meals. On the other hand, insulin is produced in β-cells and is released when blood glucose levels are elevated, following a meal. Insulin promotes glucose uptake by adipose tissue and skeletal muscle, as well as glycogen formation in the liver (Röder et al., 2016; Triplitt, 2012).

However, the pancreas is not involved in glucose homeostasis only by coordinating the metabolic status of other organs. The existence of an islet-acinar axis has been proposed which underlines the communication of the endocrine and exocrine parts of the pancreas (Barreto et al., 2010; Pierzynowski et al., 2018). One such example is the regulation of pancreatic amylase, a digestive enzyme released from the exocrine pancreas under feeding conditions to promote digestion. Postprandial increased glucose levels lead to insulin release, which was found to regulate the production of amylase (Kanno and Saito, 1976; Trimble et al., 1986). Inversely, intravenous amylase infusion in pig was found to decrease insulin levels during postprandial hyperglycaemia (Pierzynowska et al., 2018). Moreover, there are evidence suggesting an intra-islet communication. Work on α-cell-specific insulin receptor conditional knockout mouse has shown that insulin inhibits glucagon secretion *in vivo* (Kawamori et al., 2009). In contrast, glucagon was found to stimulate insulin secretion, thus preventing uncontrolled increase of glucose levels (Song et al., 2017) (**Figure 1.11.4**).

1.11.2 Liver

Glycogen is a multibranched glucose polysaccharide that serves as a form of energy storage. Liver and skeletal muscle are the major sites for glycogen storage. However, while skeletal muscle mainly uses glycogen for energy purposes, the liver is able to accumulate glycogen or release glucose according to blood glucose availability. Hence, the liver is an important organ in systemic glucose homeostasis.

In the case of reduced blood glucose levels, pancreatic-released glucagon binds to the glucagon receptor (GCGR), a GPCR on the surface of hepatocytes and activates the adenylate cyclase (AC) that in turn increases the amount of intracellular cyclic adenosine monophosphate (cAMP). The increased cAMP levels stimulate PKA to inhibit glycogen synthesis (glycolysis and glycogenesis) while promoting glycogen breakdown and glucose release (glycogenolysis/gluconeogenesis) (Röder et al., 2016) (**Figure 1.11.2**).

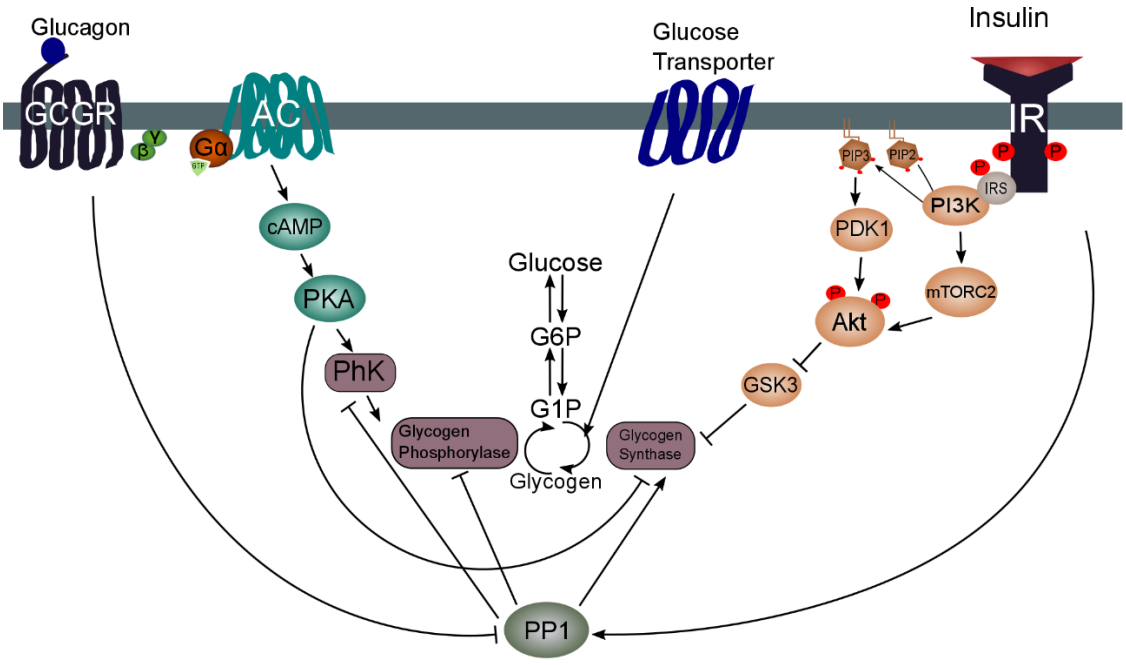

Figure 1.11.2: Regulation of glycogen metabolism in the liver.
When blood glucose levels are low, glucagon signals through GCGR to induce cAMP-dependent signalling cascades, which result in the activation of glycogen phosphorylase and therefore promote glycogenolysis. Through the same pathway, glucagon also inhibits glycogenesis. Conversely, high blood glucose levels trigger insulin-mediated signalling in the liver, resulting in the activation of the PI3K/Akt pathway and also PP1. In this way, insulin promotes increased glucose uptake into the liver cells and glycogen synthesis, while also inhibiting glycogen breakdown. (Figure adapted from (Han et al., 2016))

During glycogenolysis, PKA activates the glycogen phosphorylase kinase (PhK) (Ramachandran et al., 1987), which afterwards activates the glycogen phosphorylase, an enzyme that causes phosphoroclastic cleavage into glycogen to produce glucose-1-phosphate (G1P). Finally, G1P is converted by phosphoglucomutase (PGM) to glucose-6-phosphate (G6P) which in turn is hydrolysed by the glucose-6-phosphatase (G6Pase) to a phosphate residue and free glucose. Meanwhile, PKA also inhibits the enzyme glycogen synthase by phosphorylating it, which catalyses the production of glycogen from G1P (Feher, 2017; Koren and Palladino, 2016; Proud et al., 1977) (**Figure 1.11.2**).

Upon depletion of glycogen stores, the liver turns to gluconeogenesis to meet glucose demands. Gluconeogenesis is the process of synthesis of new glucose from lactate, pyruvate and amino acids. PKA was found to promote gluconeogenesis at multiple levels. PKA stimulates the phosphatase activity of the bifunctional enzyme phosphofructokinase-2/fructose bisphosphatase-2 (PFK-2/FBPase-2) which in turn reduces the levels of fructose-2,6-bisphosphate (Fru-2,6-BP), resulting in the activation of fructose-1,6-bisphosphatase 1 (FBPase-1) and promotion of G6P production. In addition, the PKA-mediated activation of FBPase-2 suppresses glycolysis (Pilkis et al., 1982; Rider et al., 2004). PKA is also involved in gluconeogenesis at a transcriptional level by phosphorylating the cAMP response element binding protein (CREB). CREB induces the expression of the transcriptional PPARγ coactivator-1α (PGC1α) and together potentiate the expression of the rate-limiting gluconeogenic enzymes phosphoenolpyruvate carboxykinase (PEPCK) and G6Pase (Herzig et al., 2001). Finally, PKA promotes the nuclear localisation of another CREB coactivator, the cAMP-regulated transcriptional coactivator 2 (CRTC2). PKA stimulates the nuclear translocation of CRTC2 by dephosphorylation through the inositol-1,4,5-trisphosphate receptor (IP3R)/calcium-calcineurin (CaN) pathway. Simultaneously, PKA further promotes the nuclear translocation of CRTC2 by phosphorylation of the salt-inducible kinase (SIK2), a negative regulator of CRTC2 (Altarejos et al., 2011; Wang et al., 2012) (**Figure 1.11.3**).

Under feeding conditions, blood glucose is taken up in the liver via the glucose transporter-2 (GLUT2), in an insulin-independent manner. The absorbed glucose is initially converted into glucose 6-phosphate, which in turn is mainly used

to either meet the energy needs of the liver or to produce glycogen (glycogenesis). Excess glucose 6-phosphate is utilised to form fatty acids, cholesterol, and bile salts (Berg JM, 2002). Insulin-dependent glycogenesis is promoted by the PI3K-Akt-mediated inactivation of the glycogen synthase kinase-3 (GSK3). This results in the activation of glycogen synthase, an enzyme that catalyses the formation and storage of glycogen (Akpan et al., 1974; Miller and Larner, 1973). Moreover, insulin regulates glycogen metabolism by activating PP1. PP1 acts both to promote glycogen synthesis by activation of glycogen synthase and to inhibit glycogen breakdown by the inactivation of the glycogen phosphorylase kinase and glycogen phosphorylase (Bollen et al., 1983a; Bollen et al., 1983b; Ceulemans and Bollen, 2004) (**Figure 1.11.2**). In addition, insulin was found to mediate the activation of the liver-type pyruvate kinase (L-PK), a rate-limiting enzyme in the glycolysis pathway that converts phosphoenolpyruvate (PEP) into pyruvate (Guo et al., 2012). Insulin and glucose, in an additive or synergistic manner, further promote glycolysis through PFK-2/FBPase-2 de-phosphorylation, which increases the kinase activity of PFK-2, leading to increased levels of fructose-2,6-bisphosphate (Fructose 2,6-BP) and elevated phosphofructo-1-kinase (PFK-1) activity (Guo et al., 2012). Finally, insulin signalling also leads to SIK2 kinase activation, thus promoting CRTC2 phosphorylation and nuclear exclusion. At the same time, upon insulin stimulation, Akt directly phosphorylates critical residues of the transcription factor FoxO1, turning off the transcription of hepatic gluconeogenesis (Oh et al., 2013) (**Figure 1.11.3**).

More recently, it was shown that the role of the liver in glucose homeostasis is not limited to the control of various pathways of glucose metabolism; it also contributes in the regulation of pancreas secretion. For instance, blocking of glucagon signalling to the liver results in elevated levels of circulating amino acids, especially L-glutamine, which in turn promote mouse and human pancreatic α-cell proliferation (Dean et al., 2017) (**Figure 1.11.4**).

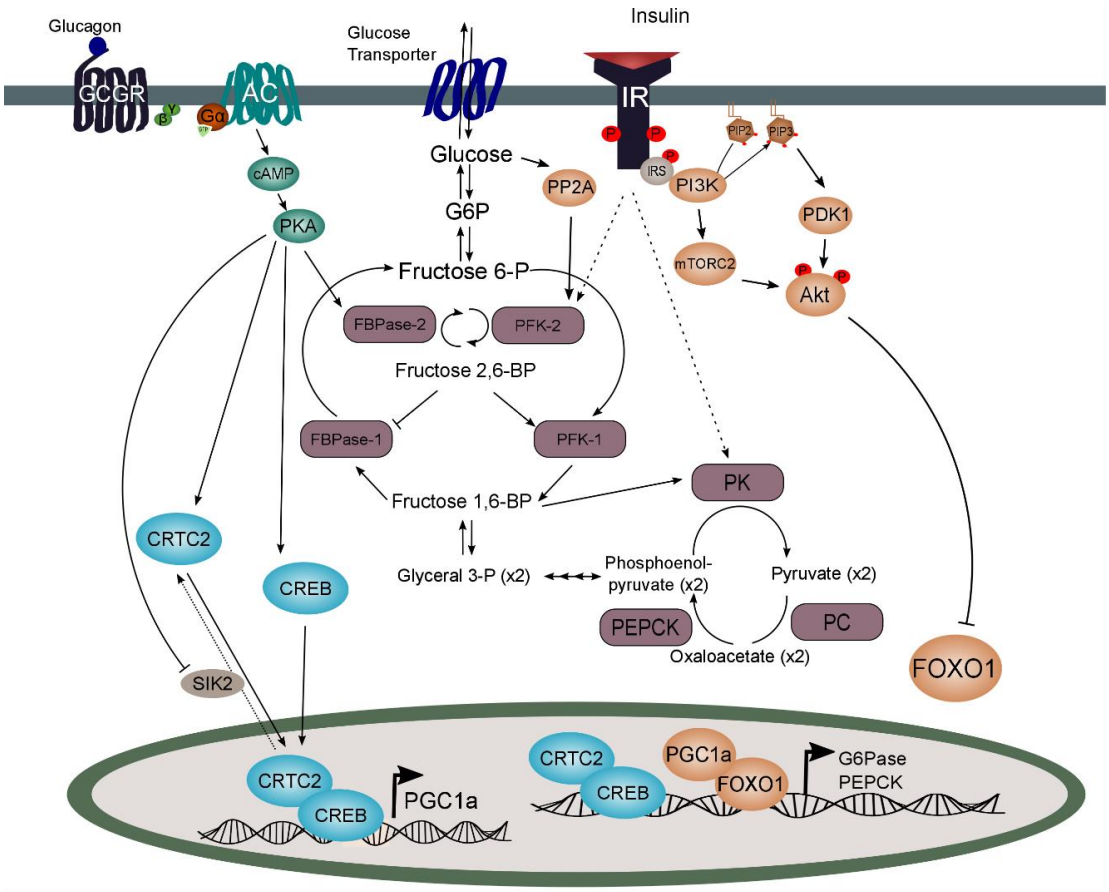

Figure 1.11.3: Regulation of hepatic gluconeogenesis.
Under fasting conditions, glucagon binding to GCGR promotes the activation of PKA, which in turn phosphorylates the serine 32 of the bifunctional enzyme PFK-2/FBPase-2, hence decreasing its kinase activity (PFK-2) and increasing its phosphatase activity (FBPase-2). Consequently, the levels of Fructose 2,6-BP are decreased, leading to reduction of PFK-1 activity and elevation of FBPase-1 activity. This results in a decrease in the rate of glycolysis and an increase in gluconeogenesis. At a transcriptional level, PKA also activates the transcription factor CREB. In addition, PKA promotes de-phosphorylation of CRTC2 by inactivating SIK2 kinase, leading to the nuclear localization and increased association of CRTC2 with chromatin-bound CREB. These events lead to the increased expression of gluconeogenic genes such as PEPCK and G6Pase, leading to the increases in hepatic gluconeogenesis during the early phase of fasting. At the same time, CREB/CRTC2 can enhance the expression of PGC1α, which is a key transcriptional regulators of hepatic gluconeogenesis during the later phase of fasting.
Under feeding conditions, the increased glucose levels lead to increased insulin release from the pancreas and insulin signalling in the liver. Glucose is taken up by the liver cells through the glucose transporter GLUT2, largely in an insulin-independent manner. Glucose signalling activates PP2A, while insulin signalling activates the pyruvate kinase (PK). In an additive or synergistic manner, glucose and insulin promote the de-phosphorylation (serine 32) of PFK2/FBPase2, hence increasing the kinase activity of PFK-2 and decreasing the phosphatase activity of FBPase-2. Consequently, the levels of Fructose 2,6-BP increase, leading to the elevation of PFK-1 activity and reduction of FBPase-1 activity. This results in an increase in the rate of glycolysis and decrease in gluconeogenesis. Insulin signalling also leads to the activation of SIK2 kinase, via Akt, thus promoting increased phosphorylation of CRTC2. At the same time, Akt directly phosphorylates critical residues of the transcription factor FoxO1, turning off the transcription of hepatic gluconeogenesis. (Figure adapted from (Guo et al., 2012; Liu and Zhang, 2018; Oh et al., 2013))

1.11.3 Skeletal Muscle

The skeletal muscle is another tissue with a central role in glucose homeostasis. In humans, it accounts for 85% of the total glucose uptake. As mentioned before, skeletal muscle, alongside liver, is a major site for glycogen storage. However, contrary to liver, insulin-stimulated glucose uptake in skeletal muscle is solely for local energy consumption. As skeletal muscle does not express the enzyme G6Pase, hence it cannot release glucose back into the blood stream. Instead, glycogen is readily converted into glucose 6-phosphate, which is used as a local energy source, especially during exercise (Berg JM, 2002; Carnagarin et al., 2015).

Following glucose ingestion, insulin stimulates skeletal muscle glucose uptake by promoting the translocation of the glucose transporter-4 (GLUT4) from intracellular vesicles to the plasma membrane (Bryant et al., 2002). Furthermore, insulin enhances glucose storage as glycogen. Insulin has been shown to stimulate the activation of glycogen synthase via the PI3K-Akt-mediated inactivation of GSK3. Inhibition of GSK3 through phosphorylation results in the dephosphorylation of glycogen synthase, which increases the enzyme's affinity for G6P and promotes full activation (Bouskila et al., 2010).

Apart from insulin, physical activity can also stimulate the AMP-activated protein kinase (AMPK)-mediated translocation of GLUT4 to the cell surface (Richter and Hargreaves, 2013). Moreover, exercise increases skeletal muscle insulin sensitivity and enhances glycemic control (Kjøbsted et al., 2017; Sjøberg et al., 2017). Correspondingly, physical inactivity has been shown to promote the development of insulin resistance, initially through reduced skeletal muscle insulin sensitivity (Hamburg et al., 2007; Krogh-Madsen et al., 2010).

Secretion of cytokines from contracting skeletal muscle (myokines) has been found to affect the function and physiology of the skeletal muscle itself but also of other organs, contributing further to the systemic glucose homeostasis. For instance, skeletal muscle derived interleukin-6 (IL-6) has been associated with improved glucose homeostasis during exercise in humans (Febbraio et al., 2004). Through a mechanism that remains unclear, contracting skeletal muscle promotes hepatic glucose production via IL-6 stimulation. Moreover, IL-6 may also increase

whole body glucose disposal independently of glucose production (Febbraio et al., 2004). Finally, exercise related IL-6 secretion has been involved in the activation of AMPK in the adipose tissue (Kelly et al., 2004). Taken together these findings show that skeletal muscle is able to modulate systemic glucose homeostasis and insulin sensitivity.

1.11.4 Adipose Tissue

Adipose tissue has a profound effect on energy balance and glucose homeostasis. Although it only accounts for 2-5% of total glucose uptake, adipose tissue regulates lipid metabolism and influences insulin sensitivity in the liver and skeletal muscle via hormone secretion.

In the postprandial phase, insulin stimulation of adipocytes promotes GLUT4 translocation from the cytoplasm to the cell surface. Despite the relatively small contribution of adipose tissue to glucose clearance, selective GLUT4 deletion in adipose tissue results in glucose intolerance and insulin resistance in mice (Abel et al., 2001). In contrast, overexpression of GLUT4 in adipose tissue can reverse fasting hyperglycemia and enhance whole body glucose clearance and insulin sensitivity in skeletal muscle GLUT4 knockout mice (Carvalho et al., 2005). These findings highlight the important role of GLUT4-mediated glucose uptake in adipocytes to systemic glucose homeostasis.

Moreover, insulin can regulate lipolysis in adipocytes directly via PI3K-dependent activation of the phosphodiesterase 3B (PDE3B), which in turn inhibits cAMP/PKA signalling via increased cAMP degradation. cAMP inactivation was shown to facilitate the inhibition of the adipose triglyceride lipase (ATGL), a rate-limiting enzyme of lipolysis, and the hormone-sensitive lipase (HSL), a neutral lipase that in the lipid droplet acts mainly as a diglyceride lipase (Choi et al., 2010). In addition, insulin supresses lipolysis indirectly through the lactate/ G protein–coupled receptor GPR81-dependent inhibition of cAMP. Work in GPR81 deficient mice has revealed that insulin-induced glucose uptake results in the production and release of lactate from adipocytes. This lactate then activates the adipocyte specific receptor GPR81 that in turn inhibits adenylyl cyclase, the enzyme which catalyses the cyclisation of adenosine triphosphate (ATP) into cAMP (Ahmed et al., 2010).

The contribution of adipose tissue to glucose homeostasis is not limited to glucose uptake and energy storage. Adipocytes also have a considerable effect on glycaemic control by secreting various factors, such as adipokines, that enable the communication of adipose tissue with other organs. One such adipokine is adiponectin, the most abundant adipose derived hormone in the plasma. Adiponectin was found to mainly stimulate liver insulin sensitivity. Moreover, adiponectin has been implicated in the promotion of β-cell survival and function while also stimulating insulin gene expression and release (Holland et al., 2011; Wijesekara et al., 2010) (**Figure 1.11.4**). Likewise, insulin stimulates both leptin biosynthesis and secretion from adipose tissue (Barr et al., 1997). Leptin serves as a major regulator of systemic glucose homeostasis by repressing food intake and increasing energy expenditure (Schwartz et al., 2000). In addition, leptin improves peripheral insulin sensitivity and modulates pancreatic β-cell function (D'Souza et al., 2017; Kieffer and Habener, 2000) (**Figure 1.11.4**). Finally, omentin-1 and visfatin are two more adipokines known to be regulated by insulin and by glucose levels that act as modulators of insulin expression and function (Brown et al., 2010; Haider et al., 2006; Tan et al., 2008; Yang et al., 2006). However, many more adipocyte-secreted proteins exist that demonstrate a variety of effects on glucose homeostasis.

1.11.5 Intestine

The gastrointestinal tract is an important player in the regulation of systemic glucose homeostasis in the postprandial phase. Starting from the stomach, the gastric emptying process ensures the steady delivery of nutrients and glucose into the duodenum. Afterwards, the digestion and absorption of nutrients from the small intestine stimulate the release of gastrointestinal peptide hormones (incretins) from the intestinal mucosa that can feed back to regulate subsequent gastric emptying as well as enhance hyperglycaemia-stimulated insulin release from the pancreas (Holst et al., 2016). Neatly, amylin, another pancreatic hormone that is co-secreted with insulin from β-cells, is involved in slowing down the rate of gastric emptying, while also regulating postprandial glucagon, and reducing food intake (Kiriyama and Nochi, 2018).

Among the best-characterised incretin hormones, glucose-dependent insulinotropic peptide (GIP) and glucagon-like peptide-1 (GLP-1) are most relevant to glucose homeostasis, through their involvement in the regulation of pancreatic hormone secretion. In response to nutrient absorption, K cells in the duodenum and proximal small intestine, as well as L cells in the jejunum, ileum, and colon produce and release GIP and GLP-1, respectively. Pancreatic β-cells have receptors for both GIP and GLP-1, which upon stimulation promote cAMP production and consequently PKA activation. Activation of this signalling pathway acts additively to signalling pathways stimulated by hyperglycaemia to facilitate insulin release (Nauck et al., 2002; Nauck and Meier, 2018; Parker et al., 2010) (**Figure 1.11.4**). Moreover, GLP-1 and GIP have been implicated in the regulation of glucagon and somatostatin release (**Figure 1.11.4**). Interestingly, in this context GLP-1 and GIP have opposing effects. GIP promotes glucagon secretion under basal glucose levels (Meier et al., 2003), while GLP-1 suppresses it during hyperglycaemia (Nauck et al., 1993). GLP-1 is also responsible for the reduction in appetite and food intake (Turton et al., 1996), influencing therefore the size of adipose tissue stores. In addition, GLP-1 was shown to directly regulate adipogenesis, thus having an important role in peripheral insulin sensitivity (Challa et al., 2012; El Bekay et al., 2016). Finally, insulin was found to promote GLP-1 secretion via Rho GTPase Cdc42-mediated activation of MEK/ERK1/2 pathway and actin remodelling (Lim et al., 2009).

1.11.6 Central Nervous System

The brain accounts for 60-70% of glucose utilisation in the resting state, since glucose is its only source of energy in the normal state. During prolonged starvation, only ketone bodies (not free fatty acids) can cross the blood-brain barrier and be partly used as an alternative fuel for the cells of the central nervous system. Despite its great need for energy, the brain does not store glucose and therefore relies on a continuous supply of glucose from the circulation (Berg JM, 2002). Consequently, glucose level monitoring and maintenance is of great importance for the brain. Specific subsets of hypothalamic neurons – as well as glial tanycytes and astrocytes – act as glucose sensors and are able to trigger counterregulatory responses during hypoglycaemia (Evans et al., 2004; Routh et al., 2014). The brain, similarly to the liver, does not require insulin for glucose uptake. It utilises the high affinity glucose

transporters GLUT1 and GLUT3 that allow efficient glucose uptake under normal glucose levels (Berg JM, 2002).

Despite brain glucose uptake not being insulin dependent, insulin can cross the blood–brain barrier via insulin-receptor-mediated active transport, and insulin signalling has many important functions in the brain. Work on neural progenitor cells (NPCs) isolated from neonatal rat telencephalons showed that insulin induces neuronal differentiation via the PI3K-Akt-mTOR pathway (Han et al., 2008). Moreover, studies in mouse hippocampal slices demonstrated that insulin modulates basal synaptic transmission and synaptic plasticity in a dose-dependent manner (Zhao et al., 2019). In regards to glucose homeostasis, insulin has been identified as a major contributor to the regulation of food intake and systemic glucose homeostasis. Insulin signalling in orexigenic acting neuropeptide Y (NPY) neurons inhibits food intake and increases energy expenditure (Loh et al., 2017). Furthermore, through the PI3K signalling pathway, insulin suppresses the ability of ventromedial hypothalamus glucose-excited neurons to sense physiological decreases in glucose (Cotero and Routh, 2009). Finally, insulin signalling in the hypothalamus has been associated, in mice and rats, with the inhibition of hepatic glucose production (Pocai et al., 2005), and with glucagon secretion from pancreatic α-cells (Paranjape et al., 2010) (**Figure 1.11.4**), as well as the promotion of lipogenesis in adipose tissue (Koch et al., 2008; Scherer et al., 2011) and glycogen synthesis in skeletal muscle (Perrin et al., 2004).

Overall, these studies suggest that the brain, and especially the hypothalamus, modulates peripheral glucose metabolism via insulin signalling. However, insulin is not the only hormone that exerts its actions through the CNS in order to promote systemic glucose homeostasis. The brain receives a plethora of metabolic information from the peripheral organs and tissues through humoral and neuronal pathways, which enable it to orchestrate appropriate systemic responses. Pancreatic insulin and glucagon, adipose tissue-derived leptin, and intestinal GLP-1 are only a few examples of hormones that exert CNS-dependent glucoregulatory effects. Glucagon, for instance, was found to signal through the mediobasal hypothalamus. Interestingly, central glucagon signalling inhibits hepatic glucose production, under glucagon-stimulated conditions, thus creating a self-regulatory

feedback loop that abates increased glucose production from raised peripheral glucagon concentrations (Mighiu et al., 2013). Moreover, the adipokine leptin binds receptors in the hypothalamus and stimulates multiple signalling cascades that modulate glucose homeostasis. For example, central leptin signalling has been associated with reduced food intake, improved hepatic metabolism and increased glucose uptake from the skeletal muscle (Friedman and Halaas, 1998; Fujikawa et al., 2013). Finally, the peptide hormone GLP-1 was shown to act through the vagal–brainstem–hypothalamic pathway to suppress food intake (Abbott et al., 2005). Moreover, GLP-1 was found to increase glucose-stimulated insulin secretion and reduce hepatic glucose production probably via receptors in the arcuate nucleus of the hypothalamus (Sandoval et al., 2008).

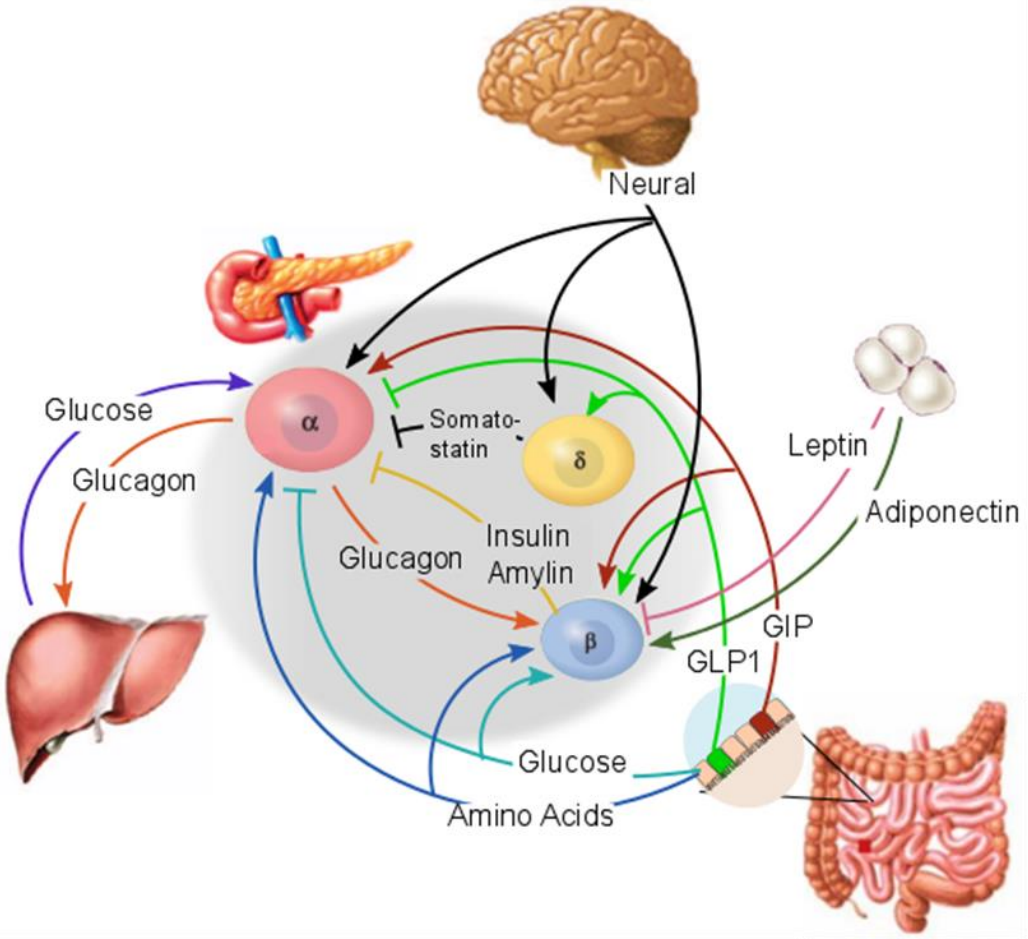

Figure 1.11.4: Neuronal and hormonal regulation of pancreatic hormone secretion. Glucose homeostasis requires the interaction of several organs. Neurotransmitters released from the brain play a central role in facilitating this inter-organ communication, for example by regulating the secretion of insulin and glucagon by the pancreas. Moreover, hormones secreted by the liver, intestine and adipose tissue are also important in modulating pancreatic function. (Figure adapted from (Röder et al., 2016))

1.11.7 Kidney

The kidney is increasingly recognised as an important contributor to systemic glucose homeostasis. Similarly to the liver, the kidney expresses the enzyme G6Pase, mainly in the renal cortex cells, which enables it to release glucose into the blood stream. Although under normal conditions, kidney's glucose release from the kidneys accounts only for a small portion of circulating glucose, during prolonged starvation, the contribution of the kidney may reach that of liver. This is due to the fact that all of the kidney-released glucose is the result of gluconeogenesis (Alsahli and Gerich, 2017). Gluconeogenesis was found to be suppressed, in the fed state, synergistically by activated insulin signalling on the basolateral side of the proximal tubules of the kidney and by increased glucose reabsorption through the sodium–glucose cotransporter 2 (SGLT2) on the luminal side of the proximal tubules (Sasaki et al., 2017).

Moreover, renal cells take up glucose to meet their own energy needs. Kidneys account for around 10% of the systemic glucose uptake, which is only in part directly insulin-dependent (Cersosimo et al., 1999; Meyer et al., 1998). However, targeted insulin receptor (IR) depletion from the proximal tubule, in mice, was found to result in increased fasting plasma glucose levels compared to wild type controls, suggesting that IR in proximal tubule has an important role in regulating systemic glucose levels (Tiwari et al., 2013).

In addition, kidneys contribute to glucose homeostasis by reabsorbing glucose from glomerular filtrate or by excreting it into the urine when glucose levels exceed the tubular maximum glucose reabsorptive capacity (TmG). In healthy individuals, ~180 g of D-glucose is filtered by the renal glomeruli per 24 h period. The ability of the proximal tubule to reabsorb glucose increases linearly with the increase in plasma glucose (Wilding, 2014). Interestingly, insulin receptor deficiency has been associated with renal glucosuria, in a mouse model of diet-induced obesity, hyperinsulinemia, and hyperaldosteronism through mineralocorticoid supplementation (Nizar et al., 2018).

Finally, kidneys are an important site of insulin degradation, hence contributing to the regulation of its levels in the circulation (Tokarz et al., 2018).

Consequently, renal insulin degradation contributes to the regulation of systemic glucose homeostasis.

1.12 Obesity, insulin resistance and Type 2 Diabetes

Overweight and obesity are fast becoming leading risk factors of collective health worldwide. In Britain alone, 60% of adults are overweight and 26% are obese (Statistics, 2018). Obesity is closely linked with a large number of health conditions including type 2 diabetes mellitus (T2DM), heart disease, stroke and cancer (Pi-Sunyer, 2009). Whereas type 1 diabetes (T1D) is a metabolic disorder which is characterised by impaired insulin secretion and glucose metabolism (Atkinson et al., 2014), T2DM develops in adulthood and starts from an insulin-resistant state which progresses to pancreatic β-cell failure (Muoio and Newgard, 2008). Long-term T2DM can cause heart and blood vessel disease, neuropathy, kidney and eye damage as well as Alzheimer's disease.

T2DM is a complex metabolic disease that results from the malfunction of many glucoseregulatory mechanisms, ultimately leading to hyperglycaemia. Aberrant insulin secretion and insulin resistance play a central role in the development of T2DM. One of the most prominent effects of insulin resistance is the decreased hepatic glucose uptake combined with increased hepatic glucose production. Moreover, adipose tissue insulin resistance promotes increased lipolysis that is subsequently associated with increased hepatic gluconeogenesis and impaired skeletal muscle insulin response. In addition, the excess of lipids in the bloodstream results in their accumulation in other organs, like pancreas, liver, and muscle, where they further augment the development of insulin resistance. As a response to the increasing systemic insulin resistance, pancreatic β-cells produce and secrete more insulin in order to compensate. Eventually insulin secretion reaches a maximum, β-cells become damaged and insulin secretion deteriorates leading to the development of T2DM. The defect of insulin secretion alongside α-cell insulin resistance results in excessive glucagon secretion. Moreover, established T2DM has been associated with reduced responsiveness of insulin secretion to gastrointestinal hormones, further deteriorating glycaemic control. In

addition, T2DM was shown to result in hypothalamic insulin resistance and abolished central regulation of hepatic glucose production. Finally, diabetic patients were found to have increased renal release of glucose due to increased gluconeogenesis as well as enhanced glucose reabsorption from glomerular filtrate, which enables further the development and maintenance of hyperglycaemia (Alsahli and Gerich, 2017; Cersosimo et al., 2000; Esterson et al., 2016; Girard, 2017; Nauck and Meier, 2018; Petersen and Shulman, 2018) (**Figure 1.12.1**).

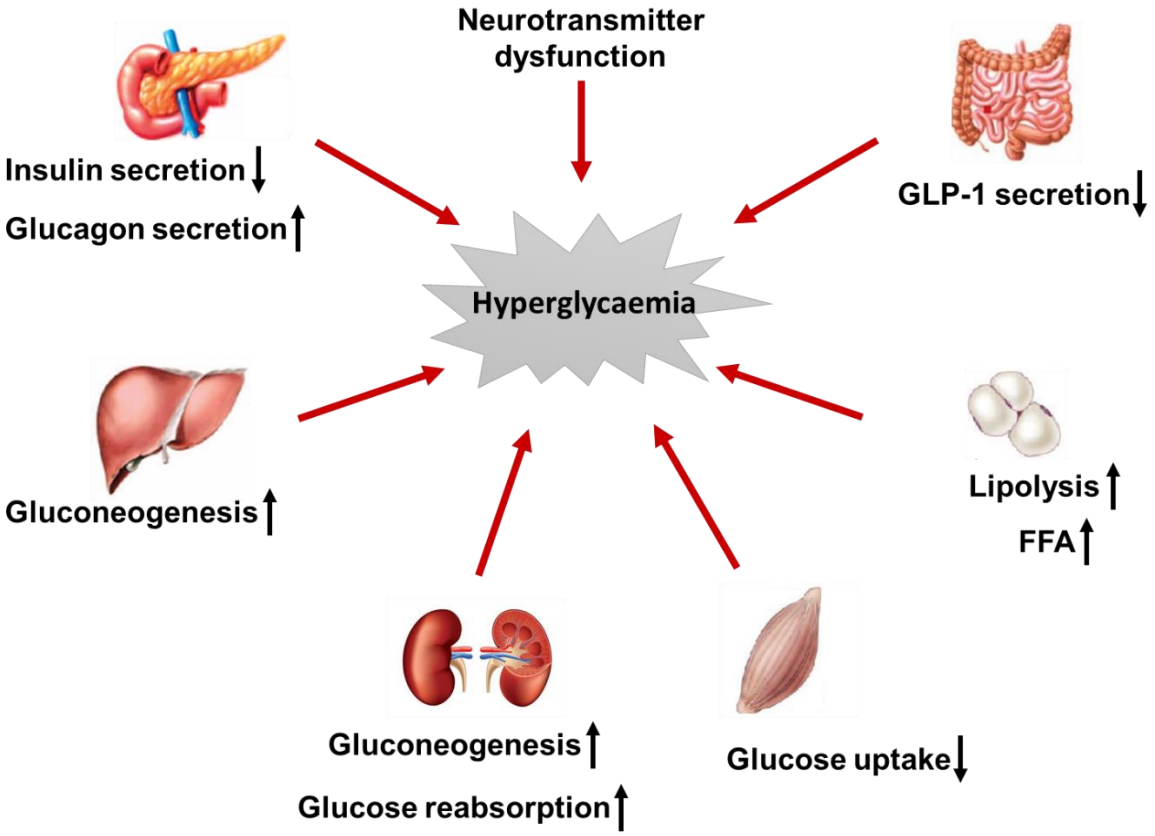

Figure 1.12.1: Pathophysiology of hyperglycaemia in type 2 diabetes
The main defects in T2DM include impaired insulin secretion by the pancreatic β-cells, and insulin resistance in muscle and liver, which leads decreased glucose uptake. Combination of decreased insulin secretion – due to β-cell resistance to the gastrointestinal hormone GLP-1 alongside β-cell failure – and increased glucagon levels result in excessive glucose production in the liver and the kidneys. Insulin resistance in adipose tissue enhances lipolysis and increases plasma FFA levels, both of which aggravate the insulin resistance in muscle and the liver and further deteriorate to β-cell function. Hypothalamic insulin resistance abolishes central regulation of hepatic glucose production and contributes to weight gain, exacerbating the insulin resistance. Finally, enhanced renal glucose reabsorption alongside the increased gluconeogenesis further augment the development and maintenance of hyperglycaemia.

Low-grade systemic inflammation is another underlying characteristic of obesity that can contribute to the pathogenesis of obesity-related metabolic disorders, by promoting insulin resistance and β-cell death. Excess of nutrients has been identified as the main drive of systemic inflammation. Free fatty acids (FFAs), alongside the hyperglycaemia, lead to stimulation of oxidative pathways ultimately resulting in mitochondrial dysfunction, increased ROS formation, and oxidative stress. Nutrient excess also triggers endoplasmic reticulum (ER) stress and unfolded-protein response (UPR). Under these conditions, transcription factors such as the nuclear factor-kappa-B (NF-κB) are activated, leading to the production and secretion of pro-inflammatory cytokines like TNF-α and IL-6, finally resulting to the establishment of inflammation (Gerst et al., 2019; Hotamisligil and Erbay, 2008; van Greevenbroek et al., 2013).

The increased adipose tissue mass observed in obesity is involved in the establishment of insulin resistance, by promoting a chronic activation of the innate immune system. Lean adipose tissue is populated by M2-anti-inflammatory macrophages and CD4+ regulatory T-cells which promote the production and secretion of anti-inflammatory adipokines such as adiponectin and interleukin 10 (IL-10). As adipose tissue expands, poor vascularisation results in the generation of hypoxic signals, which induce angiogenesis and trigger inflammation. Adipose tissue hypoxia stimulates the transcription factor NF-κB that promote the secretion of pro-inflammatory cytokines, while also reducing the secretion of anti-inflammatory adipokines. Moreover, adipose tissue hypoxia promotes the infiltration of CD8+ cytotoxic T cells and the conversion of macrophages to an M1 pro-inflammatory phenotype, which also secrete pro-inflammatory cytokines hence promoting the infiltration of additional macrophages from the circulation (Keane et al., 2017; van Greevenbroek et al., 2013; Ye, 2009).

Similarly, consumption of a high fat diet was shown to promote the conversion of hepatic macrophages, Kupffer cells, towards the M1 phenotype, which promotes the development of obesity-induced insulin resistance and fatty liver disease. TNF-α production by M1 Kupffer cells in the liver increases blood glucose levels by promoting hepatic gluconeogenesis and glycogenolysis. Moreover, TNF-α signalling inhibits intracellular lipases and provides intracellular fatty acids for triacylglycerol

synthesis, which enhances lipid production and storage in the liver, thus promoting fatty liver disease (Esser et al., 2014; Keane et al., 2015).

Overall, chronically elevated levels of IL-6 and TNF-α promote insulin resistance through the activation of serine kinases which suppress the IR mediated phosphorylation of insulin receptor substrate-1 (IRS1), an important effector in the insulin signalling pathway. TNF-α signalling leads to the activation of the inhibitor of nuclear factor κ-B kinase-β (IKKβ) and c-Jun N-terminal protein kinase (JNK) both of which inhibit IRS1. Similarly, IL-6 activates the signal transducer and activator of transcription 3 (STAT3) transcription factor, which drives the expression of suppressor of cytokine signalling 3 (SOCS3), a negative regulator of IL-6 signalling that also inhibits IRS1 (Kern et al., 2018).

1.13 Insulin Signalling Pathway in Glucose Homeostasis

As discussed above, insulin is a peptide hormone released from pancreatic β-cells in response to elevated glucose levels in the blood, following a meal, and controls critical energy functions such as glucose and lipid metabolism.

1.13.1 Signal Initiation

Insulin signals by activating the intrinsic tyrosine kinase of the IR, a tetrameric protein that consists of two α- and two β- subunits linked by disulphide bonds. The α-subunits are extracellular and contain the insulin-binding domain, whereas the β-subunits are transmembrane and act as a tyrosine kinase. In the inactive state, the α-subunits inhibit the β-subunits' kinase activity. Upon insulin binding, conformational changes in the extracellular domains promote the transphosphorylation of the β-subunits, allowing subsequent activation of the receptor's tyrosine kinase activity. Following insulin stimulation, the tyrosine kinase subunits of the IR phosphorylate key tyrosine residues on at least nine intracellular substrates. Out of these identified IR substrates, four are members of the family of insulin/IGF-1 receptor substrate (IRS) proteins (IRS1 to IRS4) while the others are: Casitas B-lineage lymphoma (Cbl), adapter protein with a PH and SH2 domain (APS), Grb2-associated-binding protein (Gab-1), 60-kDa tyrosine phosphorylated protein ($p60^{Dok}$), and isoforms of the SH2-domain containing proteins (Shc). Once phosphorylated the IRS proteins serve as recognition sites for proteins containing Src-homology 2 (SH2) domain such as PI3K and growth factor receptor-bound protein 2 (Grb2) (Saltiel and Kahn, 2001).

1.13.2 PI3K Pathway

Class IA PI3K consists of a p110 catalytic subunit in complex with a p85 regulatory subunit, which maintains the heterodimer in an inactive state in the cytosol. PI3Kα has mostly been implicated in insulin signalling and metabolic regulation. Upon recruitment to the plasma membrane and activation, PI3K produces the lipid second messenger PIP_3 by phosphorylation of the phosphatidylinositide 4,5-bisphosphate ($PtdIns(4,5)P_2$, PIP_2). PIP_3 recruits and activates a number of downstream effector proteins, by binding to their PH domain, including phosphoinositide-dependent

protein kinase 1 (PDK1). In turn, PDK1 phosphorylates serine/threonine protein kinase B (PKB/Akt) on T308 and PKCλ/ζ on T410. For the complete activation of Akt, phosphorylation of S473, mediated by mTORC2, is also required. Several substrates have been identified for Akt, implicating it in a plethora of cellular functions including cell survival, cell cycle progression, metabolism, transcription, protein synthesis, and apoptosis. There are three Akt isoforms (Akt1, 2, 3) of which Akt1 and Akt2 are ubiquitously expressed, but Akt2 shows an enrichment in insulin sensitive tissues such as liver, skeletal muscle and pancreas (Bilanges et al., 2019; Escribano et al., 2017; Saltiel, 2016) (**Figure 1.13.1**).

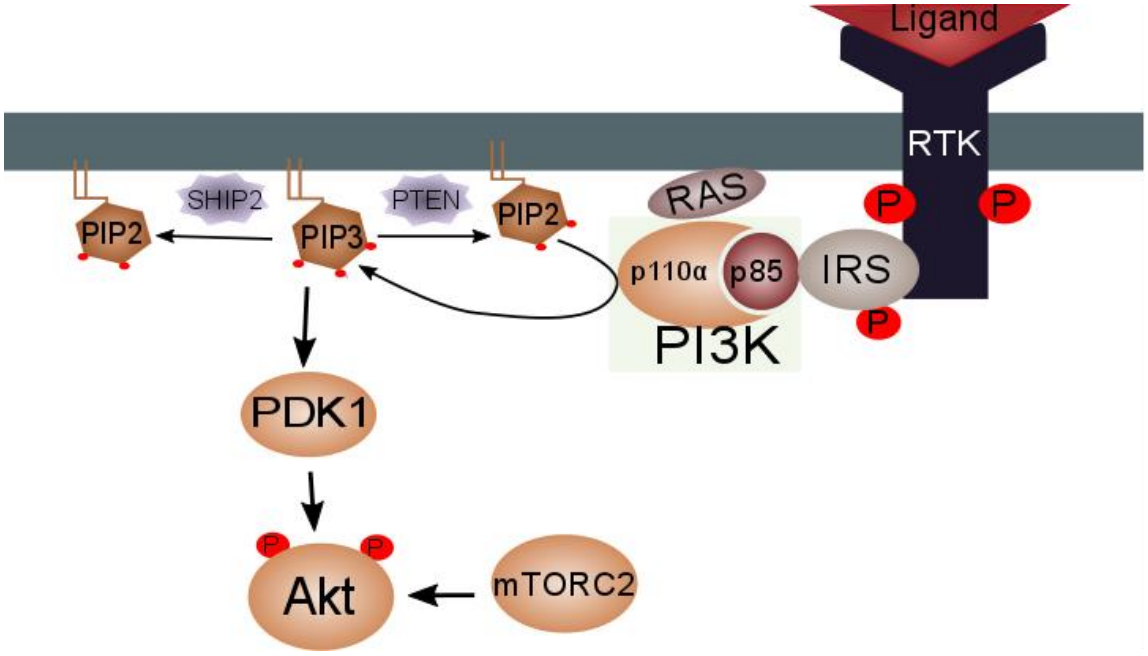

Figure 1.13.1: PI3K/Akt pathway initiation

Class PI3Ks are activated by cell surface receptors and phosphorylate the PtdIns(4,5)P_2 (PIP_2) to generate PtdIns(3,4,5)P_3 (PIP_3). PIP_3 promotes the translocation of PDK1 and Akt to the plasma membrane, through their PH domains. At the membrane, PDK1 phosphorylates Akt on Thr308. Additional phosphorylation of Akt on Ser473 by mTORC2 leads to its full activation. In turn, activated Akt phosphorylates many downstream protein targets, hence modulating a plethora of signalling pathways involved in cell growth, proliferation, survival, autophagy, and metabolism. The inositol phosphatases SHIP2 and PTEN hydrolyse PIP_3 back to PI(3,4)P_2 (PIP_2) or PtdIns(4,5)P_2, respectively. Thus, they limit the cellular pool of second messenger PIP_3 and tightly regulate the downstream pathways.

1.13.2.1 Metabolic Effects of the PI3K Pathway

A central effect of insulin on glucose homeostasis is its ability to promote glucose uptake in skeletal muscle and in adipose tissue. Insulin-dependent Akt activation results in GLUT4 storage vesicle (GSV) exocytosis through the phosphorylation and inactivation of two GAP proteins, AS160 and the RAL GAP complex (RGC). In turn, these GAPs regulate small GTPases such as Rab8, Rab10, Rab14, and RalA, which are involved in the trafficking of the glucose transporter GLUT4 from intracellular GSVs to the plasma membrane, thus allowing glucose to be transported into the cell (Leto and Saltiel, 2012). In addition to stimulating glucose uptake, insulin enhances glycogenesis in the liver and in skeletal muscle, and inhibits gluconeogenesis in the liver and kidneys. Insulin achieves these effects by directly regulating the expression of key metabolic enzymes, as well as controlling their phosphorylation state and hence their activity. Activated Akt was found to phosphorylate GSK3 and, at least in part, to contribute to the dephosphorylation of the enzyme glycogen synthase, thus promoting glycogen accumulation (Cross et al., 1995). Moreover, Akt-mediated phosphorylation of the Forkhead box class O 1 (FoxO1) transcription factor results in its nuclear exclusion, which subsequently decreases the transcription of the gluconeogenic enzymes G6Pase and PEPCK (Oh et al., 2013). Insulin also acts on the hypothalamus to suppress food intake. Akt signalling to FoxO1 suppresses food intake by transcriptional inhibition of the orexigenic peptides NPY and agouti-related peptide (AgRP) (Kim et al., 2006). Moreover, hypothalamic mTORC1 and p70 ribosomal S6 kinase (p70S6K) signalling also blocks NPY and AgRP production (Cota et al., 2006)(**Figure 1.13.2**).

As mentioned above, in addition to the IRSs, insulin receptors also phosphorylate other substrates. One such substrate is the adapter protein APS. Upon phosphorylation, APS is recruiting to the IR a protein complex consisting of the Cbl protooncogene product and the adapter protein CAP, thus facilitating the phosphorylation of Cbl by the IR. Subsequently, the Cbl/CAP complex moves into lipid rafts on the cell surface, guided by the interaction of CAP with the caveolar protein flotillin. There, Cbl recruits the adaptor protein CrkII in complex with the GEF C3G, resulting in the activation of TC10, a lipid raft-associated Rho family small GTPase that has been implicated in both insulin-dependent and osmotic shock-

induced GLUT4 translocation and glucose uptake (Baumann et al., 2000; Leto and Saltiel, 2012) (**Figure 1.13.2**).

The small GTPase Rac1 was also implicated in the insulin-stimulated translocation of GLUT4 transporter to the plasma membrane of skeletal muscle. Cytoskeletal remodelling is an important step for the transport of GSVs within the cytoplasm and for their retention beneath the plasma membrane. Rac1, as major regulator of actin rearrangement, has been associated with the GLUT4 translocation downstream of insulin signalling in L6 myotubes (JeBailey et al., 2004; Khayat et al., 2000) and in skeletal muscle (Sylow et al., 2013; Sylow et al., 2014). The mechanism still remains unclear but is likely to include the activation of Rac1 through Rac-GEFs that are known to signal within the insulin pathway, such as PREX1 and FLJ00068. Upon activation, Rac1 activates the WAVE protein, which in turn promotes the actin related protein-2/3 (Arp2/3) complex to generate branching networks of filaments and facilitate GSV movement to the plasma membrane (Chiu et al., 2010). Moreover, Rac1 stimulates the serine/threonine kinase PAK1, which inhibits the cofilin-mediated actin filament severing by promoting the function of LIM kinase (LIMK1/2) (Sylow et al., 2013; Tunduguru et al., 2014). More recently, it was also proposed that Rac1 can act as a downstream effector of Akt2 to regulate GLUT4 translocation through the small G protein RalA, a component of the GSV that interacts with the exocyst subunit Sec5 and the motor protein Myo1c (Takenaka et al., 2019).

1.13.3 Ras-MAPK Pathway

In addition to the PI3K pathway, insulin activation of the IR also stimulates the Ras-MAPK pathway, through the interaction of phosphorylated IRSs or Shc with the adaptor protein Grb2. Subsequently Grb2 recruits to the plasma membrane and activates the GEF SOS, which leads to the activation of the small GTPase Ras. Full Ras activation also requires stimulation from the protein Src homology region 2 domain-containing tyrosine phosphatase-2 (SHP2, also known as PTPN11), which also interacts with IRS proteins such as Gab-1 and IRS1/2. Upon activation, Ras triggers a signalling cascade that involves the stepwise activation of Raf, MEK1/2 and ERK1/2. Activated MAPK/ERK proteins can translocate into the nucleus to modulate gene expression of various proteins that promote cell proliferation

(Escribano et al., 2017; Saltiel, 2016). Finally, Ras is also a direct activator of class 1 PI3Ks, so this arm of the insulin pathway also feeds into PI3K signalling.

1.13.4 Inactivation of Insulin Pathway

Maintenance of glucose homeostasis requires the rapid activation and inactivation of the insulin pathway; therefore, the IR and its downstream effectors are subject to multiple regulatory controls. Once insulin dissociates from the receptor, the IR is dephosphorylated and inhibited by the protein tyrosine phosphatase 1B (PTP1B). Inversely, hydrogen peroxide produced through the IR signalling pathway inhibits PTP1B. Moreover, the activity of another IR inhibitor, the adaptor protein Grb10 that acts as a pseudo-substrate and obstructs IRS binding and activation, was shown to be enhanced through phosphorylation by mTORC1. Similarly, some members of the SOCS family attenuate insulin signalling by binding to the IR and obstructing its ability to bind and activate IRS. In addition to their inhibitory effect on the IR, SOCS proteins recruit a ubiquitin ligase, which targets IRS for proteasomal degradation. More recently, it has been proposed that the SHP2-MAPK pathway promotes IR endocytosis and thus creates a negative feedback regulation of insulin signalling (Choi et al., 2019).

The insulin pathway undergoes regulation also at the IRS level. In response to insulin, a number of serine/threonine kinases have been found to phosphorylate serine residues of IRS proteins. This leads to the inhibition of IRS activity by decreasing their activating tyrosine phosphorylation. An example of such inhibitory feedback loop is the phosphorylation of IRS1 by mTORC1 and p70S6K. Other stimuli also activate serine kinases in insulin-sensitive cells. Pro-inflammatory cytokines and free fatty acids, for instance, activate JNK1 that also inhibits IRS1.

Insulin signalling inhibition also extends to downstream effectors. For instance, PTEN and the Src homology 2 domain-containing inositol-5-phosphatase 2 (SHIP2) facilitate the degradation of PIP_3 (Fukui et al., 2005; Ogg and Ruvkun, 1998). Furthermore, the putative protein kinase tribbles homolog 3 (TRB3) and protein phosphatase 2A (PP2A) inhibit insulin signalling by deactivation of Akt (Du et al., 2003; Ugi et al., 2004).

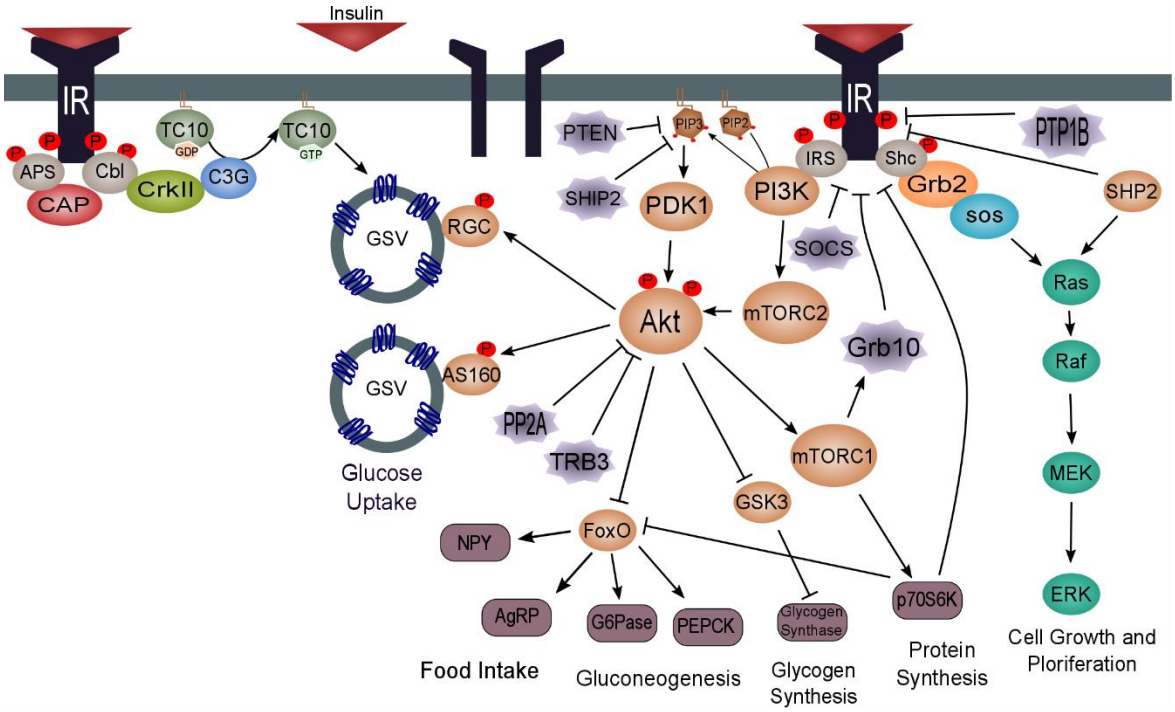

Figure 1.13.2: Insulin signalling pathway in glucose homeostasis

Schematic illustration of insulin signalling pathway involvement in glucose homeostasis. Insulin binding to the insulin receptor (IR) leads to conformational changes in the receptor that enable autophosphorylation, which in turn augments its intrinsic tyrosine kinase activity. Upon receptor activation, the next step in the signal transduction is the phosphorylation of insulin receptor substrate (IRS) proteins that facilitate the docking, apposition, interaction, and activation of other downstream effectors. Different IRS propagate the activation of different signal transduction pathways such as the metabolic PI3K and CAP/Cbl/TC10 pathways and the mitogenic Ras/MAPK pathway. The insulin signalling pathway is subject to an extensive array of inhibitory mechanisms that safeguard its physiological dynamic functioning.

1.14 Role of Rho-GEFs in Glucose Homeostasis and Diabetes

Rho-GEFs have a key role in the regulation of glucose homeostasis. It was found that deficiency of the Rho-GEF Vav3, in mice, results in the development of metabolic syndrome, non-alcoholic fatty liver disease (NAFLD), and T2DM, but not increased adiposity under chow diet. By contrast, Vav3 knockout also protected from obesity and metabolic syndrome in mice on high fat diet (HFD) (Menacho-Márquez et al., 2013). It was shown that depletion of Vav3 resulted in a diet-dependent abnormal regulation of the sympathetic nervous system, leading to enhanced trans-differentiation of white adipose tissue (WAT) into brown adipose tissue (BAT) (Menacho-Márquez et al., 2013). In a recent review from the same lab, it was reported that Vav2 is also important regulator of insulin signalling in skeletal muscle. Mice expressing catalytically inactive Vav2 were reported to exhibit reduced skeletal muscle mass and insulin sensitivity resulting in the development of a metabolic syndrome-like condition. The inversed phenotype was observed in mice expressing a catalytically hyperactive Vav2 (unpublished manuscript, findings reported in this review by the authors (Rodríguez-Fdez and Bustelo, 2019)). Moreover, experiments in the rat insulinoma cell line (INS-1 832/13) and primary rodent islets demonstrated that Vav2 is involved in the glucose-stimulated insulin secretion from pancreatic β-cells. Vav2 was found to facilitate glucose-stimulated Rac1 activation, thus promoting F-actin depolymerisation and insulin secretion (Veluthakal et al., 2015).

In addition, the Rac1-GEF Tiam1 was identified as a mediator of metformin-induced glucose uptake (You et al., 2013). Metformin is a medicine used to treat type 2 diabetes, particularly in obese patients, which promotes normal insulin responses, decreases liver glucose production and release, and reduces glucose absorbance by the intestines. Experiments in the mouse skeletal muscle cell line C2C12 showed that Tiam1 is required for metformin-mediated GLUT4 translocation to the plasma membrane (You et al., 2013). It was suggested that metformin signalling stimulates the formation of an AMPK2/14-3-3/Tiam1 complex that could influence Rac1 activation and hence modulate actin cytoskeletal dynamics and GLUT4 trafficking (You et al., 2013).

The PDZ-RhoGEF, which specifically activates the RhoA small GTPase was also implicated in glucose homeostasis. PDZ-RhoGEF deficiency in mice resulted in reduced body weight and fat mass, as well as in increased energy expenditure. In addition, depletion of PDZ-RhoGEF protected mice from diet-dependent development of obesity and T2DM (Chang et al., 2015). It was proposed that under normal dietary conditions, PDZ-RhoGEF supports insulin signalling in WAT through the regulation of ROCK-dependent phosphorylation of IRS-1. Under conditions of excess nutrients, elevated levels of PDZ-RhoGEF increased signalling to p70S6K created an inhibitory feedback loop towards the IRS-1 (Chang et al., 2015).

1.15 Role of PREX Proteins in Glucose Homeostasis and Diabetes

PREX1 is a modulator of insulin signalling in a range of cell types (Balamatsias et al., 2011; Ghalali et al., 2014; Kim et al., 2012; Montero et al., 2013). As has been previously stated, the human *PREX1* gene is mapped to a genetic locus highly associated with type 2 diabetes (Bento et al., 2008). Moreover, SNPs genotyping in the *PREX1* perigenic region suggested that PREX1 may contribute to the susceptibility of obese people to type 2 diabetes (Lewis et al., 2010). However, it remains to be seen if these SNPs affect PREX1 expression or function.

A study in 3T3-L1 adipocytes has demonstrated that the PREX1 protein is involved in the insulin-dependent translocation of the glucose transporter GLUT4 to the plasma membrane through its Rac-GEF activity (Balamatsias et al., 2011). It was shown that the disruption of Prex1-dependent Rac1 activation, by overexpression of a PREX1 mutant that lacks its DH domain, results in an inhibition of insulin-induced GLUT4 trafficking in 3T3-L1 adipocyte cells. It also negatively affected insulin-stimulated glucose uptake by these cells (Balamatsias et al., 2011) (**Figure 1.15.1**).

PREX1 has also recently been identified as a biomarker of the thermogenic potential of human brown adipocytes (Xue et al., 2015). Immortalised pre-adipocytes were established from human brown and WAT, and were screened by microarray profiling for molecular determinants of thermogenic potential. This identified that PREX1 expression in preadipocytes correlates with the presence of

the brown fat marker UCP1 in differentiated cells. Clustered Regularly Interspaced Short Palindromic Repeats (CRISPR)-mediated knockout of PREX1 in brown adipose precursors showed that the GEF had no effect on the ability of preadipocytes to differentiate into adipocytes. However, PREX1 deficiency significantly decreased the expression of UCP1 and other brown fat markers, as well as reducing the basal respiration, proton leak and maximal respiration capacity of differentiated adipocytes. Therefore, PREX1 is required for the development of the thermogenic potential of brown adipose cells (Xue et al. 2015). The mechanism, through which PREX1 regulates gene expression in adipocytes, and its significance for the function of BAT *in vivo*, remain to be investigated.

The Parsons lab reported that PREX2 also plays an important role in insulin signalling. Studies in *Prex2* knockout mice have shown that deficiency of Prex2 can significantly affect glucose homeostasis and insulin sensitivity *in vivo*. Upon glucose challenge, *Prex2* knockout mice - despite having the same baseline glucose levels as wild type *Prex2* mice - exhibited higher peak and more sustained blood glucose levels, suggesting impaired glucose tolerance. Moreover, insulin tolerance tests showed that the sustained response of *Prex2* knockout mice to insulin injection was reduced, suggesting insulin resistance (Hodakoski et al., 2014). Moreover, PIP_3 levels and the activities of several insulin pathway components were suppressed in the adipose tissue and liver of *Prex2* knockout mice, whereas PTEN activity was elevated (Hodakoski et al., 2014) (**Figure 1.15.1**). Therefore, PREX2 has been suggested to be involved in insulin signalling, not through its Rac-GEF activity, but by inhibiting PTEN. However, the relative contribution of GEF-dependent and -independent functions of PREX2 to insulin signalling and glucose homeostasis remains to be elucidated. These results seem to be relevant in humans, as analysis of PREX2 protein levels in adipocyte tissue from insulin-resistant and insulin-sensitive humans revealed that insulin-resistant people have lower PREX2 levels (Hodakoski et al., 2014). As insulin resistance can develop into type 2 diabetes, it seems possible that reduced PREX2 expression may be involved in the development of metabolic syndrome, although this remains to be investigated.

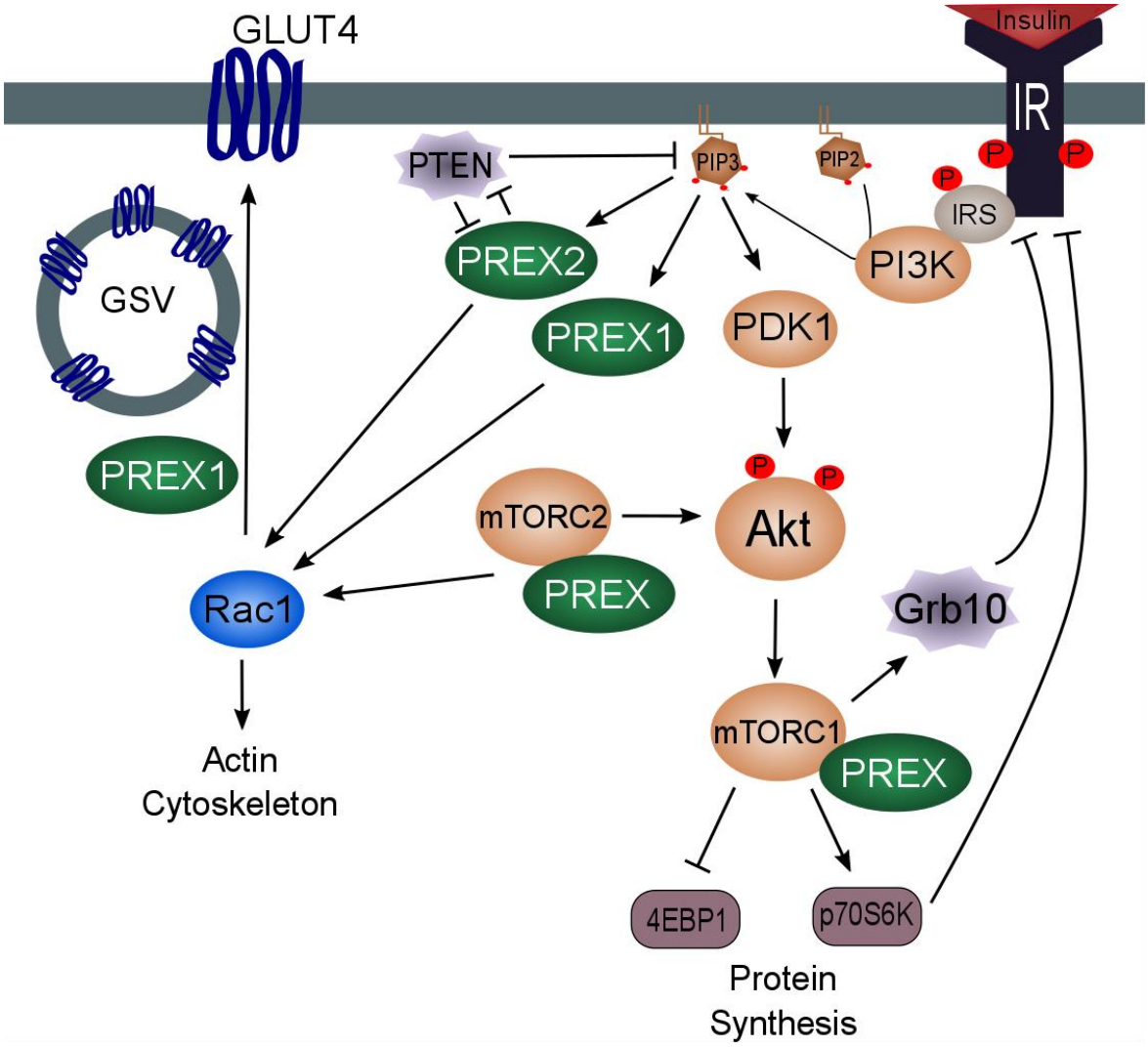

Figure 1.15.1: PREX proteins in insulin signalling.
Both PREX1 and PREX2 have been identified as direct binding partners of the two mTOR-containing protein complexes mTORC1 and mTORC2, which are important effectors of the insulin signalling pathway. Moreover, both PREX proteins activate Rac1, and specifically PREX1 has been associated with the insulin-dependent translocation of the glucose transporter GLUT4 to the plasma membrane of adipocytes. Finally, PREX2 (but not PREX1) was shown to inhibit PTEN and therefore contribute to the regulation of PIP_3 levels, in a GEF-activity independent manner. The inhibition is reciprocal, as PTEN also inhibits the Rac-GEF activity of PREX2.

Chapter 2 - Aims and Hypothesis

The importance of PREX proteins in physiological and pathophysiological processes such as inflammation, neuronal plasticity, cancer progression and metastasis is well established. However, less is known regarding their role in metabolic processes. Despite this, there is some evidence to suggest that PREX proteins may have a role in insulin signalling and glucose homeostasis. PREX1 was shown to regulate the thermogenic capacity of adipocytes, as well as insulin-stimulated glucose uptake, whereas PREX2 was reported to mediate glucose tolerance, possibly through its adaptor function as an inhibitor of the tumour suppressor PTEN.

I therefore aimed to investigate the contribution of PREX proteins to glucose homeostasis *in vivo* by measuring fasting blood glucose levels, glucose tolerance and response to insulin challenge in genetically-modified mouse strains (Prex1 knockout, Prex2 knockout and Prex null mice). I followed up *in vivo* phenotypic observations with *ex vivo* assessment of insulin signalling in liver, inguinal white adipose tissue and skeletal muscle.

Based on the proposal that the role of PREX2 in glucose homeostasis may depend on its adaptor role as an inhibitor of PTEN, rather than its Rac-GEF catalytic activity, an additional aim of the project was to assess the significance of the Rac-GEF activity of PREX1 and PREX2 in glucose homeostasis and insulin signalling. To this end, I aimed to generate and evaluate mouse strains with catalytically inactive forms of Prex1 or Prex2 (Prex GEF-Dead).

Chapter 3 - Materials and Methods

3.1 Molecular Biology Techniques

3.1.1 Polymerase Chain Reaction (PCR)

PCR was performed according to guidelines provided by the manufacturer of the Pfu DNA polymerase (Promega, M774A). Amplifications were carried out in 50 μl reaction volumes containing 100 ng template DNA, 0.5 μM forward and reverse primers (Sigma), 0.2 mM dNTPs (Bioline), 1 unit Pfu Polymerase in the manufacturer's supplied buffer and, when necessary, 5% DMSO. Reaction conditions for standard PCRs were: initial denaturing step at 95°C for 5 min, followed by 30 cycles of denaturing at 95°C for 30 s, re-annealing for 30 s at 60°C (or the optimal temperature for the primer pair as stated by the manufacturer; Sigma), extension at 74°C for 2 min/kb of DNA and completion with a final extension at 74°C for 5 min. The relevant DNA was isolated by agarose gel electrophoresis (see **Section 3.1.5**), and either the appropriate bands were extracted from the gel and purified using QIAquick Gel Extraction kit (Qiagen), or the whole PCR product was purified using QIAquick PCR purification kit (Qiagen) according to the manufacturer's instructions. PCR-derived constructs were verified by sequencing prior to use (GENEWIZ).

For the genotyping of the *Prex1* knockout, *Prex2* knockout and *Prex1;Prex2* double knockout mouse strains, PCR was performed according to guidelines provided by the manufacturer of the HotStartTaq DNA polymerase (Qiagen, 203203). Amplifications were carried out in 20 μl reaction volumes containing ~500 ng template DNA, 0.25 μM forward and reverse primers (Sigma), 0.2 mM dNTPs (Bioline) and 2.5 units HotStartTaq DNA polymerase in the manufacturer's supplied buffer. Reaction conditions for standard PCRs were: initial denaturing step at 95°C for 15 min, followed by 30 cycles of denaturing at 94°C for 1 min, re-annealing for 30 s at 64°C, extension at 74°C for 1 min and completion with a final extension at 74°C for 5 min. The relevant DNA was analysed by agarose gel electrophoresis (see **Section 3.1.5**).

For the genotyping of the newly generated catalytically inactive *Prex1*

E51A/N233A and *Prex2 E22A/N204A* mouse strains (see Result **Sections 4.5.5,** and **4.5.6**), PCR was performed using Pfu DNA polymerase, as described above. Reaction conditions for touch-down PCRs were: initial denaturing step at 95ºC for 5 min, followed by 3 cycles of denaturing at 95ºC for 30 s, re-annealing for 30 s at 68ºC, extension at 74°C for 2 min/kb of DNA, then 3 cycles of denaturing at 95ºC for 30 s, re-annealing for 30 s at 65ºC, extension at 74°C for 2 min/kb of DNA, then 3 cycles of denaturing at 95ºC for 30 s, re-annealing for 30 s at 62ºC, extension at 74°C for 2 min/kb of DNA, and 35 cycles of denaturing at 95ºC for 30 s, re-annealing for 30 s at 59ºC, extension at 74°C for 2 min/kb of DNA and completion with a final extension at 74ºC for 5 min. The relevant DNA was isolated by agarose gel electrophoresis (see **Section 3.1.5**), and the PCR product was purified using QIAquick PCR purification kit (Qiagen) according to the manufacturer's instructions. PCR-product sequence was verified by Sanger sequencing (GENEWIZ).

3.1.2 Site-directed mutagenesis

To generate the catalytically inactive human PREX2 E30A/N212A construct, that was used for the generation of recombinant proteins, site-directed mutagenesis was performed using the Site-Directed Mutagenesis Kit (New England Biolabs, E0554) and following the manufacturer's instructions. Briefly, 1-25 ng of wild type PREX2 cDNA in the pENTR3C vector was PCR amplified using the Q5 Hot Start High-Fidelity DNA Polymerase and the primers listed below in **Table 3.1**. The substitutions were created by incorporating the desired nucleotide change in the centre of the forward primer, including 19 complementary nucleotides on the 3' side of the mutation. The reverse primer was designed so that the 5' ends of the two primers anneal back-to-back. Then, the PCR product was treated with a provided enzyme mix containing a kinase, a ligase and DpnI for circularisation of the PCR product and digestion of the template DNA. Finally, the treated mix was used to transform supplied high-efficiency NEB 5-alpha Competent *E. coli* cells.

Table 3.1: List of primers used for site-directed mutagenesis of PREX2 cDNA. With bold are annotated the mutated nucleotides.

Substitution	Forward Primer	Reverse primer
***PREX2* Exon 1 E30A**	CGCGTGTGCGTGCTCAGCG **C**GCTCCAGAAGACCGAGCGG	CAGGCGAAGCTGCTTCTC CAGGTCCTTGGCGCTCTCGGC
***PREX2* Exon 6 N212A**	GCTGTCTGTTCCAACATA **GC**CGAGGCCAAGAGACAGATG	TTTCATGGCTTGGAGGG CTTCCATCACTGCTGCATAGTC

3.1.3 Analytical restriction digestion of DNA

Plasmid DNA (200-400 ng) or PCR products were digested by incubation for 1-2 h, with 5 units of the appropriate restriction enzyme. The reaction was set up in the manufacturer's recommended buffer, at the recommended temperature and in a final volume of 20 µl containing 0.1 mg/ml BSA.

3.1.4 Preparative restriction digestion of DNA

Plasmid DNA (5 µg) or PCR products were digested by incubation for 3 h with 5 units/μg^{-1} DNA of the appropriate restriction enzyme. The reaction was set up in the manufacturer's recommended buffer at the recommended temperature in a final volume of 100 µl containing 0.1 mg/ml BSA.

3.1.5 Analysis of DNA by agarose gel electrophoresis

DNA fragments were routinely resolved in TBE (40 mM Tris-borate, 1 mM EDTA) agarose gels (1-2% (w/v), Helena Biosciences) stained with ethidium bromide (0.5 µg/ml, BioRad). The size and quantity of DNA was estimated by comparison with the DNA marker Hyperladder I or IV (Bioline). When required, the desired molecular weight band was cut from the agarose gel using a clean razor blade. The DNA was purified from the gel slice using the QIAquick Gel Extraction Kit (Qiagen) according to the manufacturer's instructions.

3.1.6 Ligation of DNA fragments

All ligation reactions were carried out in a volume of 10-20 µl containing 20-200 ng of DNA fragments, 1-2 µl of the manufacturer's 10x ligation buffer and 1-2 µl of T4 DNA ligase (Promega). Typically, 50 ng of vector DNA was ligated with the appropriate amount of insert DNA to give a 3:1 molar ratio of insert:vector. The

reaction mixture was incubated at 16ºC overnight and then stored at -20ºC prior to DNA introduction into competent *E. coli* (DH5α) cells as described below.

3.1.7 Expression vectors

Human PREX1 cDNA constructs in pCMV3(EE) and pCMV3(MYC) vectors for mammalian expression were described previously (Barber et al., 2012; Hill et al., 2005; Welch et al., 1998; Welch et al., 2002), as was the human PREX2 cDNA construct in pCMV3(MYC) vector for mammalian expression (Donald et al., 2004).

3.1.8 Introduction of plasmid DNA into DH5α

Transformation of subcloning efficiency competent *E. coli* DH5α (Invitrogen, 18265-017) was performed using the manufacturer's protocol. Briefly, an aliquot of 50 µl DH5α was thawed on ice and mixed with 1-10 ng of plasmid DNA followed by 30 min incubation on ice. Cells were heat shocked for 20 s using a water bath at 42°C and placed on ice for 2 min. 900 µl of super optimal broth with catabolite repression (SOC) (2% tryptone, 0.5% yeast extract, 10 mM NaCl, 2.5 mM KCl, 10 mM $MgCl_2$, 10 mM $MgSO_4$, 10 mM glucose), was added and cells were incubated for 1 h at 37°C in an orbital shaker at 225 rpm to recover from the transformation. The bacteria cells were then spread onto selective Luria-Bertani (LB) (10 g/L tryptone, 5 g/L yeast extract, 5 g/L NaCl) agar plates containing antibiotics (100 µg/ml ampicillin or 50 µg/ml kanamycin, as appropriate) and cultured at 37°C overnight.

3.1.9 Purification of plasmid DNA

Single colonies were picked and cultured for the isolation of plasmid DNA. For small scale purifications, 5 ml LB containing the appropriate antibiotics (100 µg/ml ampicillin, or 50 µg/ml kanamycin) were grown overnight at 37°C in an orbital shaker. Plasmid DNA was purified from cultures using the GeneJET miniprep kit (Life Technologies, K0503) according to the manufacturer's instructions. For large-scale purifications, a 1 ml starter culture was added to 100 ml of LB with the appropriate antibiotic and incubated overnight at 37°C in an orbital shaker. Cells were pelleted, and plasmid DNA was purified using the plasmid maxiprep plus kit with vacuum manifold (Qiagen, 12965) according to the manufacturer's instructions.

3.1.10 Purification of genomic DNA

Isolation of genomic DNA from tissue culture cells was performed using the Wizard Genomic DNA Purification Kit (Promega, A1120) according to the manufacturer's instructions. Briefly, cells were harvested using a 0.25% (w/v) Trypsin 0.53 mM EDTA solution, collected into a 1.5 ml micro-centrifuge tube and pelleted by a 10 s centrifugation at 16000 x g. The supernatant was removed, and the cell pellet was washed with PBS prior to being centrifuged again. PBS was removed, leaving behind the cell pellet with residual liquid to resuspend cells by vortexing. Cells were then lysed with the provided Nuclei Lysis Solution, treated with RNase Solution and incubated at 37ºC for 30 min. Afterwards, Protein Precipitation Solution was added, and samples were kept on ice for 5 min prior to being centrifuged at 16000 x g for 4 min to pellet the proteins. DNA precipitation was performed by transferring the supernatant to a new tube containing isopropanol, centrifuging at 16000 x g for 1 min, washing the DNA pellet with 70% ethanol and air-drying it. The dry DNA pellet was then rehydrated with nuclease-free water at 65ºC for 1 h.

To isolate genomic DNA from tissue biopsies, ear or tissue biopsies were collected in 1.5 ml micro-centrifuge tubes. Tissues were lysed with 500 µl of tissue lysis buffer (100 mM Tris-HCl, pH 8.5, 200 mM NaCl, 5 mM EDTA, 0,2% SDS) supplemented with 10 mg/ml proteinase K in 10 mM Tris, pH 8.1, 1 mM EDTA, 50% glycerol. Samples were then incubated at 55ºC for 4 h, and DNA was precipitated by adding 350 µl of isopropanol, mixing by inversion and centrifuging at 17000 x g for 10 min. The supernatant was removed, and the DNA pellet was washed with 70% ethanol. Following that, samples were centrifuged again at 17000 x g for 5 min, the supernatant was removed, and the DNA pellet was left to air-dry. The dry DNA pellet was then rehydrated with 30 µl of TE buffer (10 mM Tris, pH 8.0, 1 mM EDTA) at 37ºC for 1 h.

3.1.11 RNA isolation

To isolate RNA from frozen tissues, less than 50 mg of tissue were used for extraction – typically 2 biopsy punches of 2 mm length (KAI Disposable Biopsy Punch, BP-20F). Tissue was homogenised in TRI Reagent (ZYMO RESEARCH, R2050-1-200), using the TissueLyser II (Qiagen) at a frequency of 300/s for 1.5 min, and particulates were removed by centrifugation at 12000 x g for 1 min. RNA

purification was performed using the Direct-zol RNA MiniPrep (ZYMO RESEARCH, R2053) following the manufacturer's protocol, including the *in-column* DNase I digestion. Purified RNA, eluted in 25 µl of nuclease free water, was stored at -80^{o}C.

3.1.12 Determination of DNA and RNA purity and quantity

To determine the quantity and purity of DNA and RNA preparations, the UV absorbance at 230, 260 and 280 nm was measured using a NanoDrop ND-100 Spectrophotometer. The amount of DNA or RNA was determined using the absorbance at 260 nm with the appropriate constant for each sample (50 for DNA and 40 for RNA). Guanidinium salt and protein contaminations were detected at 230 and 280 nm, respectively. The ratios of UV absorbance at 260/280 and 260/230 were used to determine purity of the DNA and were considered acceptable when at least 1.85 and 2.15, respectively.

3.1.13 cDNA synthesis and qPCR

To quantify the expression levels of *PEPCK* and *G6P*, equal amounts of cDNA were synthesised using the High-Capacity RNA-to-cDNA Kit (Applied Biosystems, 4388950) following the manufacturer's protocol. qPCR was performed using the TaqMan Fast Advanced Master Mix according to the manufacturer's guidelines. The reaction was performed using the QuantStudio 12K Flex Real-Time PCR System following the manufacturer's instructions.

3.2 Cell Culture Techniques

All mammalian cell lines were obtained from ATCC at the beginning of this project. For long-term stock preparation, aliquots of the cells were prepared at early passages and stored in liquid nitrogen. All mammalian cell lines were used between passages 4 and 25.

3.2.1 Human Liver Hepatocellular Carcinoma cell line (HepG2)

The Human Liver Hepatocellular Carcinoma cell line (HepG2) (ATCC, HB-8065) was cultured in cell culture flasks (Nunc) using Dulbecco's Modified Eagle's Medium

(DMEM) (Invitrogen, 41965-039) supplemented with heat-inactivated Foetal Bovine Serum (FBS) (Invitrogen, 10270-106) to a final concentration of 10%. Cells were maintained at 37°C in a humidified atmosphere with 5% CO_2. HepG2 cells were subcultured twice per week, using a 0.25% (w/v) Trypsin-0.53 mM EDTA solution, to a subcultivation ratio of 1:4 to 1:6.

3.2.2 Mouse Embryonic Fibroblast cell line NIH/3T3

The Mouse Embryonic Fibroblast cell line NIH/3T3 (ATCC, CRL-1658) was cultured in cell culture flasks (Nunc) using the ATCC-formulated DMEM, (ATCC, 30-2002) supplemented with bovine calf serum (ATCC, 30-2030). Cells were maintained at 37°C in a humidified atmosphere with 5% CO_2. The NIH/3T3 cells were subcultured twice per week, using a 0.25% (w/v) Trypsin-0.53 mM EDTA solution, to a subcultivation ratio of 1:6 to 1:8.

3.2.3 Mouse Embryonic Stem cells (ES cells)

Mouse ES cells used for CRISPR targeting were kindly maintained, frozen and stored by Dr Dominik Spensberger at the Babraham Institute Gene Targeting facility. The ES cells were maintained in knockout Dulbecco's Modified Medium (KO-DMEM) (GIBCO, 10829-018) supplemented with 2 mM GlutaMAX/Glutamate (Invitrogen, 35050061), 1x 2-mercaptoethanol (Sigma, M7522), 3 ml Penicillin/Streptomycin at final concentration of 50 U/ml (Invitrogen, 15140-122), 300 µl leukemia inhibitor factor (LIF) at 2000 U/ml (Miltenyi Biotech, 130-095-772), and 15% FBS. Gelatin was prepared with 0.1% w/v gelatin (Sigma, 9391) in cell culture grade water or 1x PBS and was autoclaved to dissolve and sterilise prior to being stored at 4^{o}C.

3.2.4 Transfection of HepG2 and NIH/3T3 cells with expression vectors

Transfection of both HepG2 and NIH/3T3 cell lines was achieved by JetPEI (Polyplus, 101-10N) transfection following the manufacturer's protocol. Briefly, cells were collected by tryptic digest, counted on a hematocytometer, and diluted to the required concentration (**Table 3.2**) in complete medium before being seeded onto Nunc tissue-culture grade plastic ware. For immunofluorescence imaging experiments, cells were seeded onto 20 mm sterile glass coverslips. The following

day, mammalian expression vectors were diluted in sterile NaCl solution (150 mM) and vortexed briefly. JetPEI reagent, diluted in sterile NaCl (150 mM), was then mixed with the DNA solution before being vortexed again and incubated at room temperature for 20 min. Mixtures were added drop-wise onto the pre-seeded cells. NIH/3T3 cells were incubated in transfection medium for 24 h prior to experiments, while HepG2 were incubated for 48 h.

Table 3.2: Number of cells, amount of mammalian expression vectors, and volume of JetPEI used for transient transfections.

Cell line	Plastic-ware	Cells per ml	Volume per well	Amount of expression vectors/NaCl (150 mM)	Volume of JetPEI/NaCl (150 mM)
HepG2	6 well plate	$5x10^5$	2 ml	3 µg / 100 µl	6 µl / 100 µl
	T75 flask	$1.88x10^6$	10 ml	18 µg / 250 µl	36 µl / 250 µl
NIH/3T3	6 well plate	$1x10^5$	2 ml	3 µg / 100 µl	6 µl / 100 µl

3.3 Protein Detection Techniques

3.3.1 Sodium dodecyl sulphate-polyacrylamide gel electrophoresis (SDS-PAGE)

To separate proteins by size for further Coomassie staining or western-blotting, the BioRad Mini Protean II gel electrophoresis system was used to perform SDS-PAGE. Gels of 1.5 mm thickness were prepared. The resolving parts were cast first, followed by the stacking gels, using 2x buffer stocks. The amounts of acrylamide (37.5:1, 30% stock, BioRad) and water used for both the stacking and resolving gels and the final concentrations of the resolving gels are listed in the table below (**Table 3.3**). Gels were polymerised with 0.1% Tetra-methyl-ethylenediamine (TEMED) (BioRad) and 0.05% ammonium persulphate (APS), from a freshly prepared 10% stock. Full Range (12-225 kDa) molecular weight markers from GE Healthcare were used as standards. Electrophoresis was performed at 120 volts through the stacking gel and 180 volts through the resolving gel in 1x running buffer (10x running buffer stock: 0.25 M Tris, 1.92 M glycine, 1% SDS). Boiling SDS-PAGE sample buffer

(Laemmli buffer, 4x: 0.4 M DTT, 160 mM Tris pH 6.8, 8% SDS, 50% glycerol, 0.012% bromophenol blue) was added to samples to a final 1.3x concentration, and samples were boiled for least 5 min prior to loading.

Table 3.3: The volume of resolving and stacking buffer, bis-acrylamide, water, 10% aps and temed required for making up two 1.5 mm thick gels.

Separating/Resolving gel		Stacking gel	
2x Separation Buffer (0.75 M Tris, 0.2% SDS, pH 8.8)	7.5 ml	2x Stacking Buffer (0.25 M Tris, 0.2% SDS, pH 6.8)	7.5 ml
30% Acrylamide 37.5:1	3 ml	30% Acrylamide 37.5:1	2.5 ml
Water	4.5 ml	Water	5 ml
10% APS	75 µl	Bromophenol Blue	35 µl
TEMED	15 µl	10% APS	75 µl
		TEMED	15 µl

3.3.2 Transfer of proteins onto PVDF membrane

Following SDS-PAGE, proteins were transferred onto Immobilon-P Polyvinylidene fluoride (PVDF) membrane (Millipore) using a standard wet transfer protocol. Transfer buffer contained 24 mM Tris, 193 mM glycine and methanol (5% methanol for proteins between 120-200 kDa, 10% for all other proteins). Transfers were done using a cooling-block in the tank, usually at 100 volts for 120 min, with the mini Protean II electrophoresis system, all with constant stirring.

3.3.3 Detection of proteins by western-blot

As a standard protocol, following the transfer step, the membrane was blocked for 1 h in 1x Tris buffered saline (TBS: 20 mM Tris, 0.15 M NaCl, pH 8), 0.05% (v/v) Tween-20, 5% non-fat milk powder at room temperature with constant gentle shaking. For anti-P-Rex1 6F12 western-blots, an additional 20 min blocking step with 0.1% (v/v) BSA in TBS-T was carried out. Primary antibodies were diluted in fresh blocking buffer and incubated with the membrane for 1–2 h at room temperature (**Table 3.4**). This was followed by two washes in blocking buffer and two additional washes in TBS-T (1x TBS, 0.05% Tween-20) for a total of 30 min

before addition of the secondary antibody (goat anti-mouse IgG-Horseradish Peroxidase [HRP] conjugate, BioRad, 1:3000; or goat anti-rabbit IgG Horseradish Peroxidase [HRP] conjugate, BioRad, 1:3000, as appropriate) in blocking buffer. The incubation was carried out for 1 h and the membrane was again washed twice in blocking buffer and twice with TBS-T for a total of 40 min. Proteins were detected by Amersham Enhanced Chemiluminescence reagents (ECL or ECL+) according to the manufacturer's instructions and were visualised by exposure to X-ray film (Fuji) for an appropriate time and then developed using an X-ray film processor (Xograph Imaging Systems).

Table 3.4: Antibodies used for protein detection.

Antibody target	Dilution	Source	Type	Cross-reactivity
Human PREX1 6F12	1:30	Marcus Thelen Laboratory, Bellinzona, Switzerland (Welch et al., 2005)	Mouse monoclonal	Human, Mouse
Human PREX2	1:20000	Welch Laboratory, Cambridge, UK (Donald et al., 2008)	Rabbit polyclonal, affinity purified	Human, Mouse

3.3.4 Stripping and re-blotting of the membrane

If required, bound antibodies on western-blotting membranes were stripped off in stripping buffer (25 mM glycine, pH 2.0, 1% SDS) for 30 min at room temperature. Membranes were then washed in several changes of TBS-T before blocking and re-probing with a different primary antibody.

3.3.5 Coomassie-staining of proteins

To determine the presence of proteins and assess the quantity and purity of protein preparations, gels or western-blots were Coomassie stained. Gels were incubated in the Coomassie staining solution (0.1% Coomassie brilliant blue R-250, 50% methanol, 10% acetic acid) for 1 h, followed by several washes in gel de-staining solution (10% methanol, 7% acetic acid). Western-blots were stained with the same staining solution for 5 min, followed by several changes of blot de-staining solution (50% methanol, 7% acetic acid).

3.3.6 Prex1 and Prex2 expression profile analysis

To assess the expression of Prex1 and Prex2 in different mouse tissues, western-blotting with antibodies against PREX1 and PREX2 was carried out with whole tissue lysate samples from *Prex1*$^{+/+}$;*Prex2*$^{+/+}$ (wild type), *Prex1*$^{-/-}$;*Prex2*$^{-/-}$ (double knockout), *Prex1*$^{-/-}$ (*Prex1* knockout) and Prex2$^{-/-}$ (*Prex2* knockout) mice. Brain, subcutaneous interscapular brown adipose tissue (intBAT), subcutaneous inguinal white adipose tissue (ingWAT), anterior thigh skeletal muscle, and liver were retrieved from mice, snap-frozen in liquid N_2, and stored at -80^{o}C. For the preparation of total lysates frozen tissues (except adipose) were wrapped in cling film and homogenised with the use of a hammer. Lysates were prepared with 9 ml/g RIPA buffer (30 mM Hepes pH 7.4, 150 mM NaCl, 1% Nonidet P-40, 0.5% deoxycholate, 0.1% SDS, 5 mM EGTA, 4 mM EDTA, supplemented with 1 mM DTT, 1 µg/ml leupeptin, 1 µg/ml pepstatin A, 1 µg/ml aprotinin and 1 mM PMSF). Lysates were sonicated in a Misonix S-3000 sonicator, using the 1/8" probe at 8.5-power and with 15 cycles of 1 s on / 1 s off pulses while kept on ice. Finally, samples were centrifuged for 5 min at 800 x g and 4^{o}C, the supernatant was collected, and proteins from equal volumes of tissue lysates were denatured by the addition of boiling 4x SDS-PAGE sample buffer to a final concentration of 1.3x and by boiling for 5 min prior to snap freezing in liquid N_2. To prepare total lysates from adipose tissue, the frozen tissue was homogenised with a hammer and treated with 500 µl of isolation medium (50 mM Tris, 150 mM NaCl, 0.2 mM EDTA and protease inhibitors). 500 µl of the homogenised adipose tissue were then transferred into a 5 ml polypropylene round-bottom tube carrying 1875 µl of chloroform/methanol (1:2) mixture and mixed sporadically while being kept on ice for 15 min. Following this, the homogenate was diluted with 625 µl water to change the water/chloroform/methanol ratio from 0.8:1:2 to 1.8:2:2. Then the mixture was centrifuged at 800 x g and 4^{o}C for 5 min, and the protein disk between the two phases was collected and resolved with 1 ml of boiling 1.3x SDS-PAGE sample buffer. Finally, the mixture was incubated at 105^{o}C for 10 min and mixed regularly to solubilise the proteins. Thereafter, the protein concentration among tissue lysates from each condition was evaluated by Coomassie staining of protein gels as described above, and lysates were diluted appropriately to accomplish equal concentrations among all samples.

3.4 Production of Recombinant Proteins from Sf9 cells

3.4.1 Insect Sf9 cells

Sf9 (*Spodoptera frugiperda*) cells were obtained from ThermoFisher, and aliquots were stored in liquid nitrogen. Sf9 cells were maintained at 27^{o}C without gassing, in suspension at a density of 0.5-2.0 x 10^6 cells/ml in 500 ml or 1-litre spinner flasks (Techne). TNM-FH insect medium (Sigma 1 litre powder aliquots, T1032-1L, 1.75 g $NaHCO_3$, 87.5 ml 1M NaOH, pH 6.3, 0.2 µm filtered and stored in the dark) was used for routine culture, supplemented with 10% FBS (Invitrogen, 10270-106) and 1% penicillin/streptomycin solution (P/S) (Invitrogen, 15140-122). Cells were used for protein production between 1 and 10 weeks in culture. When required, cells were grown as adherent monolayers in tissue culture flasks.

3.4.2 Lipofection of Sf9 cells

Escort™ IV is a liposome suspension composed of a polycationic lipid and a neutral, non-transfecting lipid compound. For the lipofection of Sf9 cells, the Escort™ IV Transfection Reagent (Sigma-Aldrich, L3287) was used following the manufacturer's protocol. Briefly, 9 x 10^5 cells were seeded per well into a six-well plate, and left in the incubator for an hour to adhere. Baculovirus DNA was diluted in serum-free Grace's insect medium (ThermoFisher Scientific, 11605-045). Escort™ IV reagent, also diluted in serum-free Grace's insect medium, was mixed with the DNA solution and incubated at room temperature for 30 min to allow complexes to form. After settling, cells were washed twice with serum-free Grace's insect medium, and 1 ml of serum-free Grace's insect medium was added in each well. Mixtures were added drop-wise onto the pre-seeded cells, and plates were incubated at 27^{o}C for five hours. Afterwards, transfection medium was removed and replaced with complete TMN-FH medium. Plates were incubated for four days at 27^{o}C to allow for the expansion of viral particles in the cells. After four days, the supernatant was removed from the cells, centrifuged at 433 x g for 15 min, and the resulting viral suspension was stored at 4^{o}C in the dark (Low-titre supernatant).

3.4.3 Amplification of viral particles

Viral suspensions were amplified twice prior to protein production to produce medium- and high-titre supernatant. For the first round of amplification, 0.75 ml of low-titre supernatant was used to infect 1.5 x 10^7 cells in T75 tissue culture flasks for 48 hours. At this point, cells were analysed for protein expression. To do this, the supernatant was removed from the cells, centrifuged at 433 x g for 15 min and stored at 4^{o}C in the dark (medium titre supernatant). The cells were washed with 1 ml of Sf9 wash solution (0.7% KCl, 2.66% sucrose, 7 mM NaH_2PO_4 pH 6.2 RT, 20 mM $MgCl_2$), were scraped off (large cell scrapers, Sigma) and were centrifuged at 1500 x g for 10 min. The supernatant was discarded, and the pellets were snap frozen and analysed for protein expression by chemical isolation (see **Section 3.4.5**). For the second round of amplification, 1.2 ml of medium-titre supernatant was used to infect 3.5x10^7 cells in T175 tissue culture flasks for 48 hours, after which time the supernatant was removed and centrifuged at 433 x g for 15 min and stored at 4^{o}C in the dark (high-titre supernatant).

3.4.4 Establishing optimal protein production conditions in Sf9 cells

Optimal infection times and viral titres for highest protein production were identified for each protein. 75 ml of cells at a density of 1 x 10^6 cells/ml were put into 250 ml spinner flasks and were infected with 0.8% or 2.5% (v/v) of high-titre supernatant. 15 ml of cells were then harvested on days 0, 1, 2, 3 and 4 post infection, centrifuged at 3901 x g for 10 min at RT, and the pellets were snap frozen. Protein production was analysed by chemical isolation (see **Section 3.4.5**). Once optimal infection times were established for each protein, 1 litre of cells at 1 x 10^6 were put into a 2 litre spinner flask and were infected with high-titre supernatant at the required concentration for the required time. Cells were harvested by centrifugation at 433 x g for 30 min at 4^{o}C. The supernatant was discarded, and the cells were resuspended in 40 ml of Grace's insect medium and transferred into a 50 ml falcon tube. A second centrifugation followed at 433 x g for 10 min at 4^{o}C, and again the supernatant was discarded while the cells were resuspended in Grace's insect medium, at a volume equal to the size of the pellet. The cells were then pipetted drop-wise into liquid nitrogen, and the resulting Sf9 cell beads were stored at -80^{o}C, ready for protein

purification.

3.4.5 Small scale chemical isolation from Sf9 cells

In order to identify the optimal viral infection times and viral titres for optimal protein production, small-scale chemical isolation of His-tagged proteins were performed using Ni-NTA (nickel-nitrilotriacetic acid) agarose beads (QIAGEN, 30210). Fresh or frozen Sf9 cells pellets were vortexed into 1 ml of ice-cold lysis buffer (1% Triton X-100, 150 mM NaCl, 5 mM $MgCl_2$, 40 mM Hepes pH 7.5 4^{o}C) until resuspended and were incubated for 5 min on ice. Lysates were centrifuged at 13225 x g for 12 min at 4^{o}C to pellet insoluble material. Ni-NTA Agarose beads, typically 100 µl for each sample, were washed 3x in 1 ml water and 3x in 1 ml lysis buffer before cytosolic fractions were added to aliquoted agarose beads. These were left to immunoprecipitate at 4^{o}C with end-over-end rotation for 60-90 min. Ni-NTA Agarose beads were then washed 4x in lysis buffer. Aspirated beads were boiled in 1.3x SDS sample buffer before being analysed using 6% SDS-PAGE gel electrophoresis. Proteins were visualised by Coomassie staining of the gel.

3.4.6 Purification of recombinant PREX2 proteins from Sf9 cells

His-tagged proteins were purified from Sf9 cells by chemical isolation with Ni-NTA Agarose beads. Frozen Sf9 cell beads (the equivalent of approximately 400 ml of culture), infected with the appropriate protein-producing baculovirus, were thawed on ice. 25 ml of ice-cold lysis buffer (1% PBS, 1% Triton X-100, 25 mM NaF, 20 mM β-Glycerophosphate, 1 mM DTT, 0.1 mM PMSF and 10 µg/ml each of antipain, pepstatin A, leupeptin, aprotinin) were used to resuspend the pellet, and the solution was left on ice for 5 min. The cytosolic fraction was obtained by ultracentrifugation (Optima L-100XP ultracentrifuge, rotor T70 Ti) for 1 h at 215577 x g at 4^{o}C. After centrifugation, the supernatant was added to 1 ml of packed Ni-NTA Agarose beads (pre-washed 3x in water and 3x in lysis buffer) and was left to precipitate with end-over-end rotation for 90-120 min at 4^{o}C. After precipitation, the beads were washed 3x in cold wash buffer (2x PBS and 1% Triton X-100) followed by 4 washes in wash/elution buffer (1x PBS, 10% glycerol, 1 mM DTT, 0.01% azide and 20 mM imidazole). After the final wash, the supernatant was aspirated close to the pellet, and the volume of the beads was estimated. To elute the His-tagged proteins from

the Ni-NTA Agarose beads, the equivalent volume of wash/elution buffer containing 600 mM imidazole was added to the beads, and they were incubated on ice for 10 min. The supernatant was obtained by centrifugation at 800 x g for 1 min at 4^{o}C. The Ni-NTA Agarose beads were then eluted with wash/elution buffer containing 300 mM imidazole, and the supernatants were pooled. A final centrifugation was performed to remove any contaminating Ni-NTA Agarose beads. In order to wash the PREX2 proteins free of imidazole, PD-10 Desalting Columns (GE Healthcare Life Sciences, 52130800) were used according to the manufacturer's instructions. Briefly, PD-10 Desalting Columns, containing Sephadex G-25 resin, were equilibrated with equilibration buffer (1x PBS, 10% glycerol, 1 mM DTT, 1 mM EGTA, 0.01% azide)**.** Then, a maximal volume of 2.5 ml of sample was added onto the column and was left to enter the packed bed completely. The flow-through was discarded, collection tubes were placed under the columns, and proteins were eluted by adding 3.5 ml elution buffer (1x PBS, 10% glycerol, 1 mM DTT, 0.01% azide) through the column. To concentrate the eluted proteins, the Amicon® Ultra-2 mL Centrifugal Filter (Merck, UCF210024) was used. Following the instructions provided by the manufacturer, 2 ml of each sample were added to filter devices and spun at 7500 x g in JA14.5 rotor for 20 min, initially. Then, the samples were centrifuged further with briefer spins to reduce the volume to approximately 100 µl. To further reduce the imidazole concentration, 2 ml of equilibration buffer (1x PBS, 10% glycerol, 1 mM DTT, 1 mM EGTA, 0.01% azide) were added onto the columns, and the samples were concentrated again to 100 µl through centrifugation. Once concentrated, the protein was in wash/elution buffer which was supplemented with 2 mg/ml FAF-BSA and adjusted to contain 50% glycerol (some protein was also stored without BSA). The protein was aliquoted, snap frozen in liquid N_2 and stored at -80^{o}C. Aliquots of all purified proteins were analysed using SDS-PAGE gel electrophoresis, and the gels were stained with Coomassie to assess the purity of the individual proteins. Proteins used in GEF activity assays were freeze-thawed a maximum of three times.

3.4.7 Rac GEF activity assay for recombinant PREX2 proteins

This *in vitro* assay measured the activation (GTP-loading) of recombinant Rac by recombinant PREX proteins in the presence of liposomes that either contained the PREX activator PIP_3 or not. In order to prevent the de-activation of Rac during or

after the assay, GTP was presented in the form of the non-hydrolysable analogue GTPγS. EDTA, which enables the maximal GTP-loading of Rac, was used as a positive control. The final concentrations of assay components were liposomes composed of 200 µM each of the lipids phosphatidylcholine (PC), phosphatidylserine (PS), and phosphatidylinositol (PI), plus 100 nM EE-Rac1, 50 nM wild type or GEF-dead His-PREX2 and 5 µM GTPγS, including 1 µCi [35S]GTPγS per sample. The final concentration of PIP3 varied as specified for each assay and the concentration of EDTA in the positive control was 2 mM.

The assay was carried out in a volume of 10 µl by incubation for 10 min at 30ºC, followed by the isolation and quantification of GTPγS-loaded Rac. In the assay, the liposomes, Rac and GTPγS were combined from 5x stocks (see below, 2 µl/sample) and PREX proteins added from 2.5x stocks (4 µl/sample). First, 2 µl of 5x liposomes that either contained or not PIP_3 were mixed with 2 µl of 5x stock GDP-loaded (inactive) EE-Rac1 and incubated on ice for 10 min. Then, 4 µl of 2.5x wild type or mutated PREX2 were added, followed by 2 µl of 5x GTPγS. Samples were mixed and incubated for 10 min at 30ºC. The reaction was stopped by the addition of 400 µl ice-cold lysis buffer (1x PBS, 1 mM EGTA, 10 mM MgCl2, 1% Triton X-100, 0.1 mM GTP). EE-Rac1 was immunoprecipitated using anti-EE antibody coupled to prewashed protein G Sepharose beads (‘anti-EE beads’, Onyx Pharmaceuticals) by end-over-end rotation for 60 min on ice. The anti-EE beads were washed four times with 400 µl of ice-cold lysis buffer. After the last wash, any remaining liquid was carefully aspirated and 400 µl of Ultima Gold scintillation fluid (PerkinElmer, 6013329) added to the samples and tubes vortexed well. The tubes were transferred into scintillation vials (PerkinElmer, 6000292), 5 ml of scintillation fluid added, and the [35S]GTPγS-loading of Rac detected by scintillation γ-counting.

The 5x and 2.5x stocks of all assay components were prepared freshly on the day of each assay, as follows: For the preparation of 5x liposomes, a mixture of PC, PS and PI (all from Sigma, stored at 12.5 mM each in $CHCl_3$) was dried down to form a thin film in a 0.5 ml tube with or without synthetic D,D-Stearoyl-arachidonyl-PtdIns(3,4,5)P_3 (D,D-(S/A)-PIP_3), and was then bath sonicated into lipid buffer (20 mM Hepes pH 7.5 at 4ºC, 100 mM NaCl, 1 mM EGTA) to give a concentration of 1 mM for each lipid (with PIP_3 as indicated). For the 5x positive EDTA control, PC, PS

and PI were dried down and bath sonicated into lipid buffer supplemented with 10 mM EDTA. For the preparation of 5x Rac stocks, purified, GDP-loaded, recombinant, lipid modified EE-Rac1 (from laboratory stocks, (Hill and Welch, 2006), stored at -80°C) was diluted to 500 nM in 20 mM Hepes (pH 7.5 at 4ºC), 0.1 M NaCl, 1 mM EGTA, 5 mM $MgCl_2$, 50 mg/ml FAF BSA and 5 mM DTT. For the preparation of 2.5x PREX protein stocks, purified recombinant His-PREX2 or mutated GEF-dead His-PREX2 (prepared as described in **Section 3.4.6**, stored at -80°C) were diluted to 125 nM in 20 mM Hepes (pH 7.0 at 4ºC), 1% betaine, 0.01% Na azide, 0.5 mM EGTA pH 7.3 RT, 200 mM KCl, 10% ethylene glycol. For the preparation of the 5x GTPγS, pH-adjusted GTPγS (in 20 mM Hepes (pH 7.5, 4ºC), 0.1 M NaCl; stored at -20°C) was diluted to 25 µM in lipid buffer and [35S]GTPγS added to this mix to give 1 µCi/2 µl.

3.5 Mouse Strains

Prex1$^{-/-}$;*Prex2*$^{-/-}$ (double knockout, Prex1/2 DKO), *Prex1*$^{-/-}$ (*Prex1* knockout, Prex1 KO), *Prex2*$^{-/-}$ (*Prex2* knockout, Prex2 KO) and *Prex1*$^{+/+}$;*Prex2*$^{+/+}$ (wild type, Prex WT) mice were generated by the Welch laboratory. The mice were initially on a C57Bl6/129Ola mixed genetic background and were previously described (Donald et al., 2008; Welch et al., 2005). The mice were group-housed (up to five) in individually ventilated cages in the Babraham Small Animal Unit. Mice were kept at a 12 h light/12 h dark cycle with dawn/dusk settings. Mice were fed either chow diet (CRM (P), SDS, 801722) or 45% high fat diet (RM AFE 45% Fat (P), SDS, 826161) *ad libitum*. Experiments were carried out in accordance with the British Home Office, PPL 70-9018, and with the approval of the local Animal Welfare and Ethical Review Body.

To minimise genetic drift, the double knockout and wild type strains were crossed with each other and single and double mutant mice were derived from these crosses at least once every two years. For this study, recrossing of the *Prex1*$^{-/-}$;*Prex2*$^{-/-}$ strain with *Prex1*$^{+/+}$;*Prex2*$^{+/+}$ wild type mice was used to rederive *Prex1*$^{-/-}$ and *Prex2*$^{-/-}$ single deficient as well as *Prex1*$^{-/-}$;*Prex2*$^{-/-}$ double deficient mouse strains immediately prior to the start of the experiments. The Babraham Breading

Unit provided C57BL/6J mice for the generation of the PREX catalytically inactive mice (*Prex1*$^{E51A/N233A}$ and *Prex2*$^{E22A/N204A}$) as described in **Sections 4.5.5**, and **4.5.6** of the results chapter.

3.5.1 Mouse genotyping

Mouse genotyping of the *Prex1* knockout, *Prex2* knockout and *Prex1;Prex2* double knockout mouse strains was routinely performed in the laboratory by research assistant Laraine Crossland. Genomic DNA was isolated from mouse ear or tail biopsies as described in **Section 3.1.10**, and the genotyping was done through PCR following the protocol described in **Section 3.1.1**. The sequences of the primers used are detailed in the **table 3.5**.

Towards the end of this project, genotyping of these strains was outsourced to Transnetyx who developed proprietary real-time PCR protocols using the probes detailed in **table 3.6**.

Table 3.5: List of primer pairs used for the genotyping of genetically modified mouse strains.

Target	Forward primer	Reverse primer	PCR product size
Prex1 Knockout allele	GGACCAGAGTTTGA CCCCTGAACCTGTGTG	CCAAATTAAGGGCC AGCTCATTCCTCCCAC	436 bp
Prex1 Wild Type allele	GACCTGAGGTTTTT TTCTGGCCTCCGTGGC	GAAAGAGGCAGAAG CTGGGCACGCCTGGCC	1 kb
Prex2 Knockout allele	TCACTGAAGCGG GAAGGGACTGGCTGC	GTTTCAGGTTCAGG GGGAGGTGTGGGAGG	800 bp
Prex2 Wild Type allele	GATGCACTTTCAAA AGGGCCTAGTCCTGCC	CCCACTGGTCTTGG TTAATGATGGGTGTCC	800 bp

Table 3.6: List of probes used for the genotyping of genetically modified mouse strains from Transnetyx.

Target	Forward primer	Reverse primer	Reporter
Prex1 Knockout allele	TGTTTTGCCAAGTTC TAATTCCATCAGA	GGGCCCTTAATCCTA GACTTTGG	CTCTAGTGCAATGCCC
Prex1 Wild Type allele	TGAAACTCTGCAGAA ACCTTTATGGT	ACACCGGCTATGGCA TGG	CCCAGGCCCCAGCATG
Prex2 Knockout allele	CCTGCTAGCTCTATA AGTTAAGTGGGATA	CCAAAGGGCAAACCC AAAAGG	ACATCCGGGCACTTTT
Prex2 Wild Type allele	CCCCTTTTTTCCTGC TAGCTCTATA	CATAGCTTGAGTTTG CTTCTTTTATTGCT	ACTTTTGAATTAGAG GAAATAAA

For the genotyping of the catalytically inactive *Prex1*$^{E51A/N233A}$ ES cells, genomic DNA was isolated from ES cells as described in **Section 3.1.10**, and the genotyping was done by PCR using the primers listed in the **Table 3.7** and following the PCR protocol described in **Section 3.1.1**.

For the genotyping of the catalytically inactive *Prex1*$^{E51A/N233A}$ and *Prex2*$^{E22A/N204A}$ mouse strains, genomic DNA was isolated from mouse ear or tail biopsies as described in **Section 3.1.10**, and the genotyping was done through Sanger sequencing (GENEWIZ) of PCR products, produced following the protocol described in **Section 3.1.1**. The sequences of the primers used are detailed in the **Table 3.8**.

Once the *Prex2*$^{E22A/N204A}$ mouse strain had been established as homozygous mice, Transnetyx also developed an assay for their genotyping, as detailed in the **Table 3.9**, and we outsourced their genotyping.

Table 3.7: List of primers used for genotyping of catalytically inactive Prex1 ES cells. Annotated with red are the nucleotides that are specific for either the wild type or the mutated allele.

Target	Forward primer	Reverse primer	PCR product size
Prex1 E51A allele (1st set)	GTACTCAAC**GCC**ATCCT AGG	TGACTGTGCAATTCGAG CTG	279
Prex1 E51A allele (2nd set)	TGAATGGGTCTTGGCCT ACA	GCTCGGTGCCTAGGATG **GC**G	643
Prex1 E51 WT allele (1st set)	GTACTCAAC**GAG**ATCCT GGG	TGACTGTGCAATTCGAG CTG	279
Prex1 E51 WT allele (2nd set)	TGAATGGGTCTTGGCCT ACA	GCTCGGTGCCCAGGATC **TC**G	652
Prex1 N233A allele (1st set)	**GCG**GAGACCAAGCGACA AAT	AGTTACTGAGGGGAGTT GGC	328
Prex1 N233A allele (2nd set)	CTGGGAAGACTGACACT CGT	TTGTCGCTTGGTCTC**CG C**GA	255
Prex1 N233 WT allele (1st set)	**AAT**GAGACTAAGAGGCA GAT	AGTTACTGAGGGGAGTT GGC	328
Prex1 N233 WT allele (2nd set)	CTGGGAAGACTGACACT CGT	CTGCCTCTTAGTCTC**AT T**GA	256

Table 3.8: List of primers used for genotyping of catalytically inactive Prex1 and Prex2 mouse strains.

Target	Forward Primer	Reverse primer	PCR product size
Prex1 Exon 1	TTCTACAAAGATCCC CGCCCAC	TGACTGTGCAATTCGA GCTG	893
Prex1 Exon 6	CTGGGAAGACTGAC ACTCGT	AGTTACTGAGGGGAG TTGGC	566
Prex2 Exon 1	GACTGTCCCGTTCTG AGTCC	AATTTGCCCTGGGAG ATGGA	571
Prex2 Exon 6	TGCTCACTCATGGAT TTGACC	TCCATCACACATGTC TCAGGT	536

Table 3.9: List of probes used for genotyping of catalytically inactive Prex2 mouse strain by Transnetyx.

Target	Forward primer	Reverse primer	Reporter 1	Reporter 2
Prex2 Exon 1	CCGAGCGCGACT ACGTG	GACTTGGTGCCG TGCG	CACGCTGGAG TTCCTG	TACCCTAGAGT TCCTGGT
Prex2 Exon 6	CTGTACCGGAGC ACTGGAGATCA	GCCTGCCACTCT TCTAAAACTTCCA	TCTCCATCTGT CTCTTGG	TCTCCATTTGC CGCTTG

3.5.2 *In vivo* testing of mice

Cohorts were selected for age- and sex-match between wild type and genetically modified mice (*Prex1*$^{-/-}$, *Prex2*$^{-/-}$, double mutant *Prex1*$^{-/-}$;*Prex2*$^{-/-}$, or *Prex2*^{E22A} mice), and were additionally weight-matched at the onset of the study. Cohorts were followed for one year of their life, from young adult to old age. Glucose tolerance tests were performed at 10, 15, 25, 39 and 52 weeks of age. Insulin tolerance tests were done at 25 and 43 weeks of age on the same mice, and the mice were also tested in metabolic cages at the age of 11 months. At the end of the study, at 12 months of age, the mice were culled humanely by CO_2 inhalation and pithing. The carcasses were kept in the -80^{o}C freezer for body composition analysis by EchoMRI.

3.5.3 Mouse intraperitoneal glucose tolerance test (IPGTT)

For IPGTT, mice were habituated to being handled by tail marking with permanent marker pen, weighing and scruffing for at least two days preceding the experiment. On the day of the glucose challenge, the mice were fasted for 6 h starting at 8.30 AM, water remaining available *ad libitum* throughout. 15 min prior to glucose

injection, the mice were weighed and their baseline blood glucose level tested by tail prick and glucometer reading, using the AlphaTRAK 2 blood glucose monitoring system (Abbott) with the 'dog' code as indicated on the test strips. 2 g/kg of glucose (20% glucose at 10 ml/kg) was then given intraperitoneally (i.p.) at time 0. Tail bleeds were performed at 15, 30, 45, 60, 75 and 90 min after glucose injection and the blood glucose level was determined by glucometer.

3.5.4 Mouse subcutaneous insulin tolerance test (SCITT)

For SCITT, the mice were fasted for 4 h on the day of the insulin challenge, starting at 8.30 AM, water remaining available *ad libitum* throughout. 15 min prior to insulin injection, the mice were weighed and their baseline blood glucose level were tested as described above. 0.75 IU/kg of sterile human recombinant insulin (Actrapid) diluted in DPBS (5 ml/kg at 0.15 IU/ml) was then given subcutaneously (s.c.) at time 0. Tail bleeds were performed at 15, 30, 45, 60, 90, 120 and 180 min after insulin injection and blood glucose level was determined by glucometer. In rare cases, animals reached dangerously low blood glucose levels of around 2-3 mM. These mice were injected intraperitoneally with 100 µl 20% glucose in order to avoid hypoglycemic shock and were excluded from the rest of the experiment. During experimental optimisation, a lower concentration of insulin (0.5 IU/kg) was tested for female mice on HFD, where sterile human recombinant insulin, diluted in DPBS, was given subcutaneously (5 ml/kg at 0.10 IU/ml). However, this did not trigger a sufficient response, so the higher dose of 0.75 IU/kg was selected for the majority of experiments (see supplementary **Figure S15**).

3.5.5 Mouse metabolic cages

To monitor food and water consumption and the production of urine and faeces, mice were group-housed in metabolic cages (up to 3 mice/cage), usually at the age of 11 months, unless otherwise indicated. Mice were habituated to metabolic cages for 1 h on a Friday and for 3 h on the following Monday. Then, mice were housed in metabolic cages for 16 h, overnight, for 3 subsequent nights with pre-weighed food and water available *ad libitum* throughout. During daytime, the mice were returned into their individually ventilated cages. The remaining food and water, as well as the produced urine and faeces, were weighed and recorded for each night. The metabolic cages were cleaned and fresh collection tubes were used for each of the

3 testing nights.

3.5.6 Mouse body composition and organ weight

To analyse the overall body composition of the mice that had undergone metabolic assessment, mice were culled after the end of the experiment at 12 months of age, and the mouse carcasses kept in the -80^{o}C freezer. The bodies were thawed and scanned by EchoMRI to determine the whole body fat and lean mass.

For organ weighing, young mice (10 week-old males and females), as well as middle-aged mice (25 week-old males and 30 week-old females, mostly ex-breeders) were culled by CO_2 and exsanguination, weighed and dissected for organ collection. The weights of thirteen organs (brain, intBAT, ingWAT, anterior thigh skeletal muscle, pancreas, kidneys, spleen, liver, thymus, heart, lung, salivary gland, and when applicable testes) were measured and data were normalised to total body weight.

3.5.7 Ex vivo insulin signalling using mesoscale

For *ex vivo* insulin signalling studies, mice were challenged with insulin prior to sacrifice and tissue retrieval. For these experiments, mice were fasted for 4 h from 8.30 AM and tested for their basal blood glucose level by tail prick and glucometer reading as described in **Section 3.5.4**. The mice were subcutaneously injected with sterile DPBS at 500 ml/kg or with sterile 0.75 IU/kg human recombinant insulin, diluted in DPBS, (5 ml/kg at 0.15 IU/ml). 14 min post injection, the blood glucose level was measured again to confirm a response to insulin. At 15 min post injection, the mice were sacrificed humanely by cervical dislocation and pithing. Immediately thereafter, tissues (liver, anterior thigh skeletal muscle and ingWAT) were collected, snap frozen in liquid nitrogen and stored at -80^{o}C.

Tissue lysates were prepared from less than 50 mg of tissue – typically 2 biopsy punches of 2 mm length (KAI Disposable Biopsy Punch, BP-20F). Tissue was homogenised in Tris lysis buffer (150 mM NaCl, 20 mM Tris, pH 7.5, 1 mM EDTA, 1 mM EGTA, 1% Triton-X-100), supplemented with 1% Protease Inhibitor Solution, 1% Phosphatase Inhibitor Solution I, 1% Phosphatase Inhibitor Solution II, and 0.4% PMSF in DMSO (MSD, R60TX-2), using the TissueLyser II (Qiagen) at a frequency of 300/s for 1.5 min. Samples were then incubated on ice for 30 min with

frequent vortexing. Finally, samples were centrifuged for 10 min at 1000 x g and 4^{o}C, and the supernatant was collected and stored at -80^{o}C. For the skeletal muscle there was an additional step of tissue homogenisation using the TissueLyser II prior to the addition of Tris lysis buffer, and for the adipose tissue there was a delipidation step after the centrifugation. Sample concentration was determined using the Pierce BCA Protein Assay Kit (ThermoScientific, 23227) following guidelines provided by the manufacturer. The Mesoscale Multi-Spot assay system was used to measure the phospho-protein and total levels of Akt, p70S6K, and GSK3β (Akt Signaling Panel Whole Cell Lysate, K15115D-2, MSD and Akt Signaling (Total Protein) Panel Whole Cell Lysates, K15133D, MSD, respectively), following manufacturer's guidelines. Briefly, plates were blocked by the addition of 150 µl/well blocking solution and incubation for 1 h with shaking at 700 rpm, RT. After blocking, the plates were washed 3 times with 300 µl/well of Tris wash buffer, and 25 µl of sample (liver at 2125 µg/ml, skeletal muscle at 1500 µg/ml, ingWAT at 800 µg/ml) was added per well. Plates were incubated at RT for 1 h with shaking at 700 rpm, prior to being washed, as previously. Finally, plates were incubated with 25 µl/well of detection antibody solution for 1 h at RT with shaking, 700 rpm, they were washed, as previously, and 150 µl/well of 1x read buffer T were added directly before imaging each plate using the SECTOR Imager.

3.5.8 ELISA

For ELISA 14 weeks old mice were fasted for 6 h from 8.30 AM and were anaesthetised by rising concentration of CO_2 followed by pithing. Whole blood was collected by cardiac puncture, taking advantage of the atrial fibrillation and placed in EDTA treated Microvette (Microvette CB 300 K2E, SARSTEDT, 16.444.100). Samples were centrifuged at RT for 5 min at 2000 x g and the resulting supernatant was transferred into a clean polypropylene tube. Samples were centrifuged for a second time at RT for 5 min at 2000 x g, the supernatant (plasma) was apportioned into 0.5 ml aliquots and stored at -80^{o}C.

For the quantitative determination of adiponectin, glucagon, and insulin in mouse plasma the Mouse Adiponectin ELISA kit (Crystal Chem, 80569), Mercodia Glucagon ELISA kit (Mercodia, 10-1281-01), and Ultra Sensitive Mouse Insulin ELISA kit (Crystal Chem, 90080) were used, respectively, following manufacturer's

guidelines.

3.5.9 Bone marrow transplant

6-8 week old bone marrow recipient mice were γ-irradiated with two doses of 500 rads (5 Gy) of ^{137}Cs, separated over 3 hours. From this day onwards to 2 weeks, their drinking water was supplemented with 2 mg/mL neomycin to minimise chances of infections during the critical period of bone marrow reconstitution. On the day after the irradiation, bone marrow cells were prepared from 12 week-old donor mice, using sterile techniques and solutions throughout. Bone marrow was flushed from isolated femurs, tibia and pelvises with PBS-FBS (Dulbecco's PBS, 10% FBS) using a 25G needle, and cells were gently triturated. Cells were counted using a haemocytometer and resuspended at 5×10^7 cells/mL in PBS-FBS before passing them through a sterile 40 μm cell strainer. One hundred microliter of the cell suspension (5×10^6 cells) was then injected intravenously (i.v.) into the irradiated recipient mice through the tail vein. The irradiation and i.v. injections were performed by senior animal technicians. Animals were housed in individually ventilated caging for the next 10 weeks to allow the reconstitution of the hematopoietic system. The efficiency of the reconstitution was assessed at the end of the experiments, by western blotting of total lysates of cells recovered from the bone marrow for the expression of Prex1.

3.6 Generation of GEF-Dead Prex Mouse Strains

Mouse strains with catalytically inactive versions of Prex1 or Prex2 were generated using CRISPR technology by introducing mutations in the genomic DNA which result in two amino acid substitutions at critical residues in the catalytic DH domain of the mouse Prex1 and Prex2 proteins.

3.6.1 Single guide RNA (sgRNA) selection and design

sgRNAs were designed such that they would direct Cas9 nuclease-mediated double-strand cleavage to exon 1 and exon 6 of the *Prex1* and *Prex2* genomic sequences, close to the residues of interest. sgRNAs were designed to be 20 nucleotides long, positioned directly upstream of a requisite 5'-NGG protospacer

adjacent motif (PAM) and to not have highly homologous sites elsewhere in the mouse genome, to reduce the risk of off-target cleavage. Off-target potential was assessed and scored using several CRISPR sgRNA bioinformatic design tools, including the software provided by the Feng Zhang laboratory (http://crispr.mit.edu/), the Broad Institute (http://www.broadinstitute.org/rnai/public/analysis-tools/sgrna-design), and the E-CRISPR (http://www.e-crisp.org/E-CRISP/). Three sgRNAs were selected for each target based on their score in these web-based tools, their position relevant to the region in which we aimed to introduce the point mutation and the DNA strand they were targeting. To clone the guide sequence into the sgRNA expression plasmid, two oligonucleotides of the following form were synthesized, with the 5'-NGG motif not being included in the 20-nt guide sequence:

5' – CACCGNNNNNNNNNNNNNNNNN – 3'
3' – CNNNNNNNNNNNNNNNNNNCAAA – 5'

Since a 5' guanine is required for transcription from the U6 promoter that is used to express the sgRNAs, any sgRNAs that lacked this feature were extended in the 5' direction by the addition of a single guanine. The sequences of the guide RNAs designed are detailed in the results **Table 4.4**.

3.6.2 Guide-it sgRNA *in vitro* transcription and screening system

sgRNAs were produced and the assessment of their targeting efficiency *in vitro* done using the Guide-it kit (Clontech, 631439), following the manufacturer's protocol. Briefly, DNA template that contained the sgRNA encoding sequence under the control of a T7 promoter was generated by a PCR reaction according to guidelines provided by the manufacturer. 100 ng of sgRNA-encoding template was then transcribed *in vitro* to create the sgRNA, using the T7 polymerase and transcription buffer provided. A cleavage template for screening the sgRNAs was also created by amplifying a ~2 kb fragment of mouse genomic DNA, containing the target sequence in an asymmetric position that produces two cleavage fragments of unequal size – primers are listed in **Table 4.5**. Thereafter, the DNA template was cleaved *in vitro* using a sgRNA in combination with the Guide-it Recombinant Cas9 Nuclease in the manufacturer's recommended buffer. The reaction was incubated at 37^{o}C for 1 h and then stopped by a 10 min incubation at 70^{o}C. Finally, the whole

reaction volume was analysed on a 1% TBE agarose gel.

3.6.3 Surveyor assay

To assess the ability of sgRNAs to guide the Cas9 nuclease to the right genomic site within cells, the Surveyor Assay was performed on DNA extracts of NIH/3T3 cells transfected with sgRNA-expressing pSpCas9(BB)-2A-GFP plasmid. The Surveyor Assay was performed using the IDT Surveyor Mutation Detection Kit following the manufacturer's instructions. Briefly, touch-down PCR amplicons of the DNA regions of interest from mutant and wild type cells were prepared using Pfu polymerase as described in **Section 3.1.1** and the primers listed in **Table 4.5**. Equal amounts of mutant and wild type DNA were mixed and hybridized to form hetero/homoduplexes. The hetero/homoduplex formation was performed by heating the mixture at 95^{o}C for 10 min and then letting it cool down to 25^{o}C by 2.5^{o}C/min. Wild type DNA underwent the same procedure to serve as homoduplex negative control. The annealed test hetero/homoduplex and reference homoduplex mixtures were digested with Surveyor Nuclease S following the manufacturer's protocol. The reaction was incubated at 42^{o}C for 1 h and then analysed on a 1% TBE agarose gel.

3.6.4 Single stranded DNA (ssDNA) repair template design

To promote homology-directed repair (HDR), ssDNA repair templates were designed such that they were around 200 bp long and, apart from the desired point mutation, carried at least one silent mutation, which created restriction digest site for screening purposes. When possible, silent mutations that destroyed the PAM sides were also introduced. The sequences of the ssDNA designed are detailed in the **Table 4.6**. The repair templates were ordered from Dharmacon as PAGE-purified Ultramer ssDNA.

3.6.5 Mouse strain generation by HDR-mediated gene targeting of mouse ES cells

To generate knock-in mouse ES cell clones, Freestyle MAX reagent (Thermofisher, 16447100) was used following the manufacturer's instructions. ES cells (15 × 10^5 cells), maintained as described in **Section 3.2.3**, were transfected with 500 ng sgRNA targeting Prex1 E51A in the pSpCas9(BB)-2A-GFP (PX458) vector, 500 ng

of sgRNA targeting Prex1 N233A in the pCas-Guide-EF1a-CD4 vector, 200 ng of donor ssDNA for Prex1 E51A, and 200 ng of donor ssDNA for Prex1 N233A. The sequences of the guide RNAs designed are detailed in the results **Table 4.4**, while the sequences of the ssDNA designed are detailed in the **Table 4.6**. The cells were cultured for 10 days prior to being trypsinised and diluted to single cells. Expanded colonies were then split into two 96-well plates. One plate of ES cells was frozen at -80°C, and another plate was used to prepare genomic DNA for PCR screening and confirmation by Sanger sequencing. Positive colonies were taken forward by Dr Dominik Spensberger to the Babraham Small Animal Unit for implantation into mouse White-C57BL/6J blastocysts. Mice were screened for chimerism by coat colour, and biopsies of promising chimeras were screened as described in **Section 3.5.1**. Targeted chimeras were bred with wild type C57BL/6J mice and all offspring were genotyped to test for germline transmission.

3.6.6 Mouse strain generation by zygote microinjection

In order to generate $Prex2^{E22A}$ mice, Dr Dominik Spensberger performed zygote microinjection. Briefly, the microinjection solution consisted of annealed crRNA (20 ng/µl; IDT), tracrRNA (20 ng/µl; Dharmacon), Cas9 mRNA (50 ng/µl; Dharmacon) and ssDNA donor (15 ng/µl; Dharmacon), which were suspended in nuclease-free water. The sequences of the guide RNAs designed are detailed in the results **Table 4.4**, while the sequences of the ssDNA designed are detailed in the **Table 4.6**. The injection solution was microinjected into the pronucleus of C57BL/6J mouse zygotes. All pups were genotyped as described in **Section 3.5.1**, and heterozygous $Prex2^{E22A/+}$ mice were bred together to generate homozygous $Prex2^{E22A/E22A}$ animals. Once this strain was established, females were super-ovulated for zygote production, and were re-targeted by a further round of pronuclear injections to target the second site, $Prex2^{N204A}$. $Prex2^{E22A/E22A;N204A/+}$ mice were bred together to generate homozygous double knock-in $Prex2^{E22A/E22A;N204A/N204A}$ mice.

3.7 Statistical Analysis

Results are given as mean ± standard error of the mean (SEM). For the analysis of IPGTT and SCITT, data were normalised by subtracting the basal blood glucose

level – as measured 15 min before the injection – of each individual mouse from the blood glucose level measured at each time point. The total glucose response was calculated as the area under the curve (AUC) of the normalised data. For comparison between two groups, unpaired Student's *t*-test was used, whereas for comparison among multiple groups, ordinary one-way ANOVA followed by post-hoc tests with Tukey's multiple comparisons correction. Longitudinally observed parameters in different groups were compared by 2-way ANOVA with repeated measures followed by post-hoc tests with Sidak multiple comparisons correction. Parameters with values $p<0.05$ were considered to differ significantly.

Chapter 4 - Results

4.1 Expression of endogenous Prex1 and Prex2 in insulin-responsive mouse tissues

To begin the study of the roles of endogenous Prex1 and Prex2 in glucose metabolism, the expression levels of these proteins in insulin-responsive tissues needed to be assessed. The main insulin-sensitive tissues are the liver, adipose tissue and skeletal muscle. Furthermore, as the brain is the overall controller of metabolic processes, brain samples were also included.

Published data from our lab showed that both Prex proteins are expressed in brain and, at lower levels, in liver. Here, brain, liver, skeletal muscle, subcutaneous inguinal and visceral epididymal (gonadal) white adipose tissue as well as interscapular brown adipose tissue (intBAT) from *Prex1*$^{+/+}$;*Prex2*$^{+/+}$ (Prex WT), *Prex1*$^{-/-}$ *(Prex1 KO), Prex2*$^{-/-}$ *(Prex2 KO)* and *Prex1*$^{-/-}$;*Prex2*$^{-/-}$ (Prex DKO) were tested by western-blotting for the endogenous expression levels of the Prex proteins. Total tissue lysates from each genotype were blotted with the 6F12 mouse monoclonal antibody against PREX1. Total protein extracts from HepG2 cells transiently overexpressing PREX2 or PREX1, as described in **Section 3.2.4**, were used as controls. As shown in **Figure 4.1.1A**, clear Prex1 bands were detected in brain and liver tissue extracts, but skeletal muscle showed no expression of Prex1 protein. Prex1 was also detected in the subcutaneous inguinal and visceral epididymal (gonadal) white adipose tissue as well as in inBAT. The same membranes were also blotted with rabbit polyclonal antibody against PREX2. Prex2 protein was found to be expressed at low but detectable levels in total brain but not in liver. Like Prex1, Prex2 was undetectable in skeletal muscle, but unlike Prex1, its expression in adipose tissue was restricted to intBAT (**Figure 4.1.1B**). After blotting for both PREX proteins the membranes were stained with coomassie to confirm even protein loading (**Figure 4.1.1C**). No global up-regulation of Prex2 was seen in Prex1-deficient insulin-sensitive tissues, and vice versa, suggesting that Prex proteins do not compensate for the loss of the other isoform on a gross protein level scale.

Taken together, the results indicate that Prex proteins are expressed in all major insulin sensitive tissues except skeletal muscle, and therefore could potentially play a role in glucose homeostasis *in vivo*.

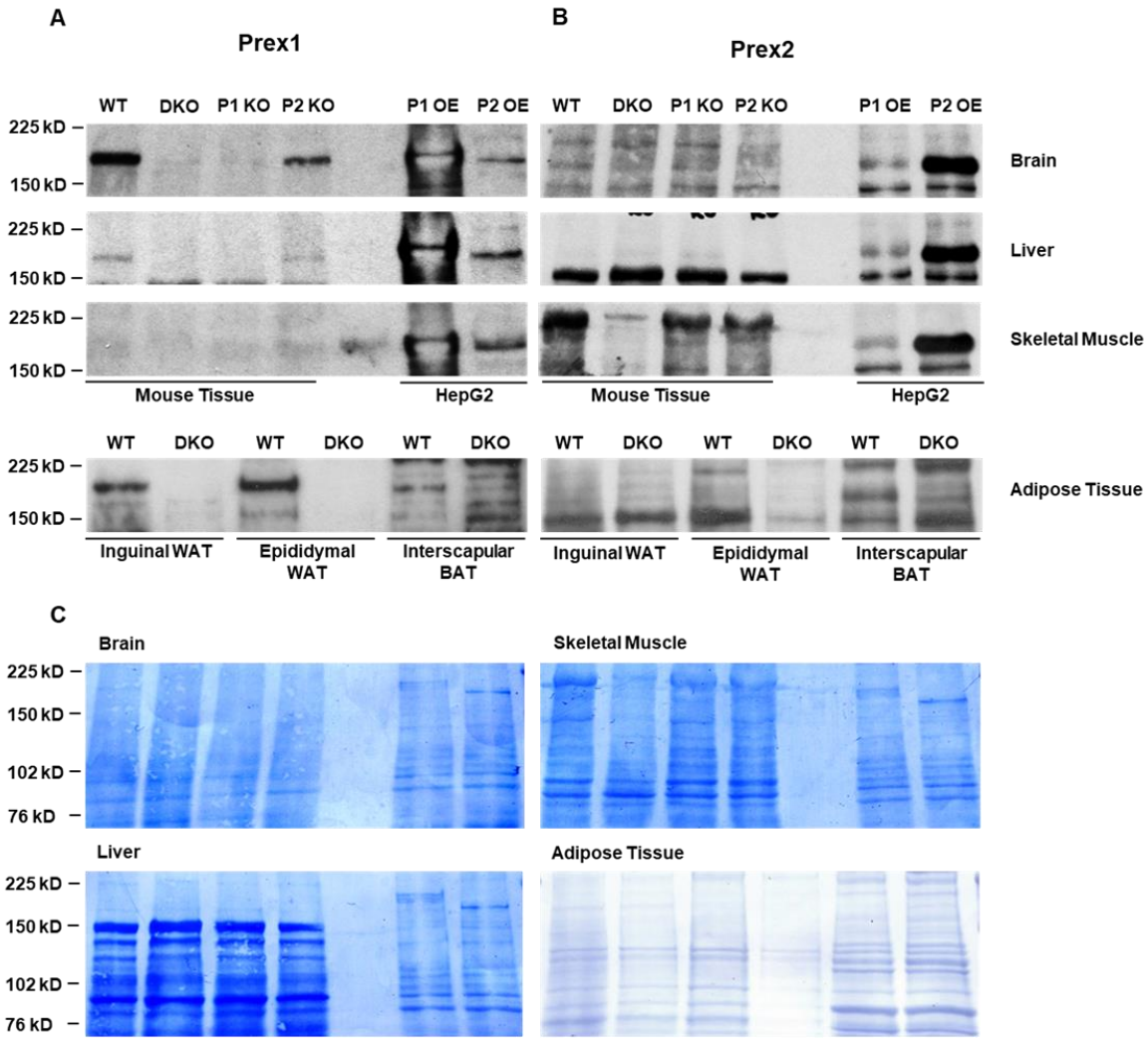

Figure 4.1.1: Expression of endogenous Prex1 and Prex2 in insulin-responsive mouse tissues.

(A,B) Brain, liver, skeletal muscle, white adipose tissues (WAT) and brown adipose tissue (BAT) were collected from *Prex1*$^{+/+}$;*Prex2*$^{+/+}$ wild type (WT), *Prex1*$^{-/-}$;*Prex2*$^{-/-}$ (DKO), *Prex1*$^{-/-}$ (P1 KO) and *Prex2*$^{-/-}$ (P2 KO) mice. Total lysates were prepared at 2% w/v and western-blotted for **(A)** Prex1 and **(B)** Prex2. Total lysates from HepG2 cells overexpressing either PREX1 (PREX1 OE) or PREX2 (PREX2 OE) were used as positive and negative controls, respectively. **(C)** Coomassie stain of blots to show that equal amounts of lysate were loaded per lane. Representative blots from 3 preparations are shown.

4.2 Metabolic phenotype of Prex1 KO mice

To understand the role of Prex1 in glucose metabolism in vivo, the metabolic phenotype of Prex1–/– (Prex1 KO) mice was studied. Briefly, the mice were tested for fasting blood glucose levels, response to glucose tolerance test and response to insulin tolerance test, throughout ageing. Glucose tolerance tests (IPGTT) were performed at 10 and 15 weeks, and at 6, 9 and 12 months of age by i.p. administration of 2 g/kg glucose (20% glucose at 10 ml/kg) after 6 h of fasting, unless otherwise indicated. Insulin sensitivity tests (SCITT) tests were done at 5 and 10 months of age by s.c. administration of 0.75 IU/kg of human recombinant insulin at 0.15 IU/ml after 4 h of fasting, unless otherwise indicated. Both sexes were tested, and two diets were compared, normal chow diet and 45% HFD. In addition, mice were assessed for body weight throughout ageing, tested in metabolic cages at 11 months of age, and their body composition was analysed post mortem at one year. Prex1 KO and Prex1+/+;Prex2+/+ (Prex WT) mice of same age and sex were tested in parallel under the same conditions for direct comparison.

4.2.1 Male Prex1 KO mice on chow diet show lower fasting blood glucose levels and better glucose tolerance than Prex WT mice

Two independent cohorts, set up almost a year apart, were used to characterise the metabolic phenotype of male Prex1 KO mice on chow diet. The Prex WT mice in these cohorts responded as expected throughout ageing (see Supplemental Data, **Section 6**), except for an elevated basal blood glucose level at 10 weeks of age, 14 mM instead of the 12 mM average for Prex WT mice.

As seen in **Figures 4.2.1A** and **4.2.2A**, the fasting blood glucose level was around 11 mM in Prex1 KO males and remained stable throughout ageing, contrary to Prex WT males whose blood glucose steadily rose within the year, as expected from our analysis of multiple Prex WT cohorts shown in **Section 6.1**. During IPGTT (2 g/kg), the blood glucose levels of Prex1 KO mice peaked lower, at 21-24 mM, compared to Prex WT males, 15 min after the glucose challenge, and also decreased back to basal level faster and more rapidly (**Figure 4.2.1A**). Moreover, Prex1 KO males did not exhibit the mild glucose intolerance observed in Prex WT mice from the age of 6 months onwards (**Figure 4.2.1B**). Overall, Prex1 KO had

better glucose tolerance than Prex WT males throughout ageing (**Figures 4.2.1C** and **4.2.1B**), despite gaining weight at a comparable rate and having similar body composition (**Figure 4.2.2C-D**). Therefore, Prex1 KO males show lower fasting blood glucose and better glucose clearance compared to Prex WT controls.

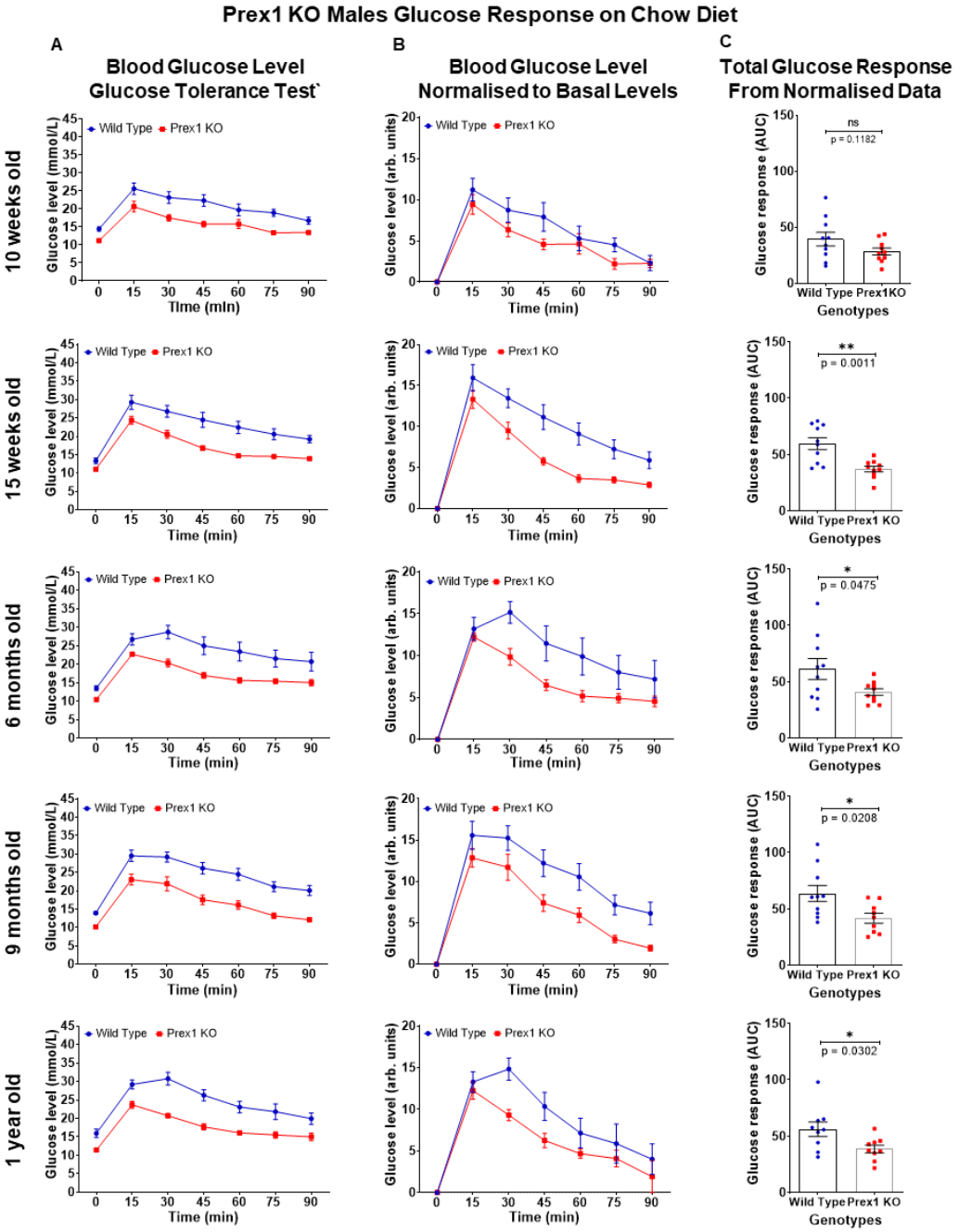

Figure 4.2.1: Male Prex1 KO mice on chow diet show lower fasting blood glucose levels and better glucose tolerance than Prex WT mice.

Male *Prex1*$^{-/-}$ (Prex1 KO, red) and *Prex1*$^{+/+}$;*Prex2*$^{+/+}$ (Prex WT, blue) mice on chow diet were subjected to i.p. glucose tolerance test (IPGTT) at the ages of 10 and 15 weeks, 6, 9 and 12 months. Food was withdrawn 6 h prior to i.p. injection of 20% glucose at 10 ml/kg (final concentration 2 g/kg). Blood glucose levels were tested by tail bleed 15 min prior to the i.p. injection to determine the basal fasted blood glucose levels, and every 15 min after the glucose injection for 90 min, as indicated, to assess the response to glucose challenge.**(A)** Blood glucose concentration during IPGTT. **(B)** Blood glucose levels during IPGTT, normalised by subtracting the basal blood glucose level. **(C)** Total glucose response (AUC of normalised data). Data are pooled from 2 independent cohorts (Prex WT n=10; Prex1 KO n=10), and are presented as mean ± SEM. 2-way ANOVA with repeated measures and Sidak's multiple comparisons correction was used to compare genotypes during IPGTT. Unpaired Student's *t*-test was used to analyse the total glucose response.

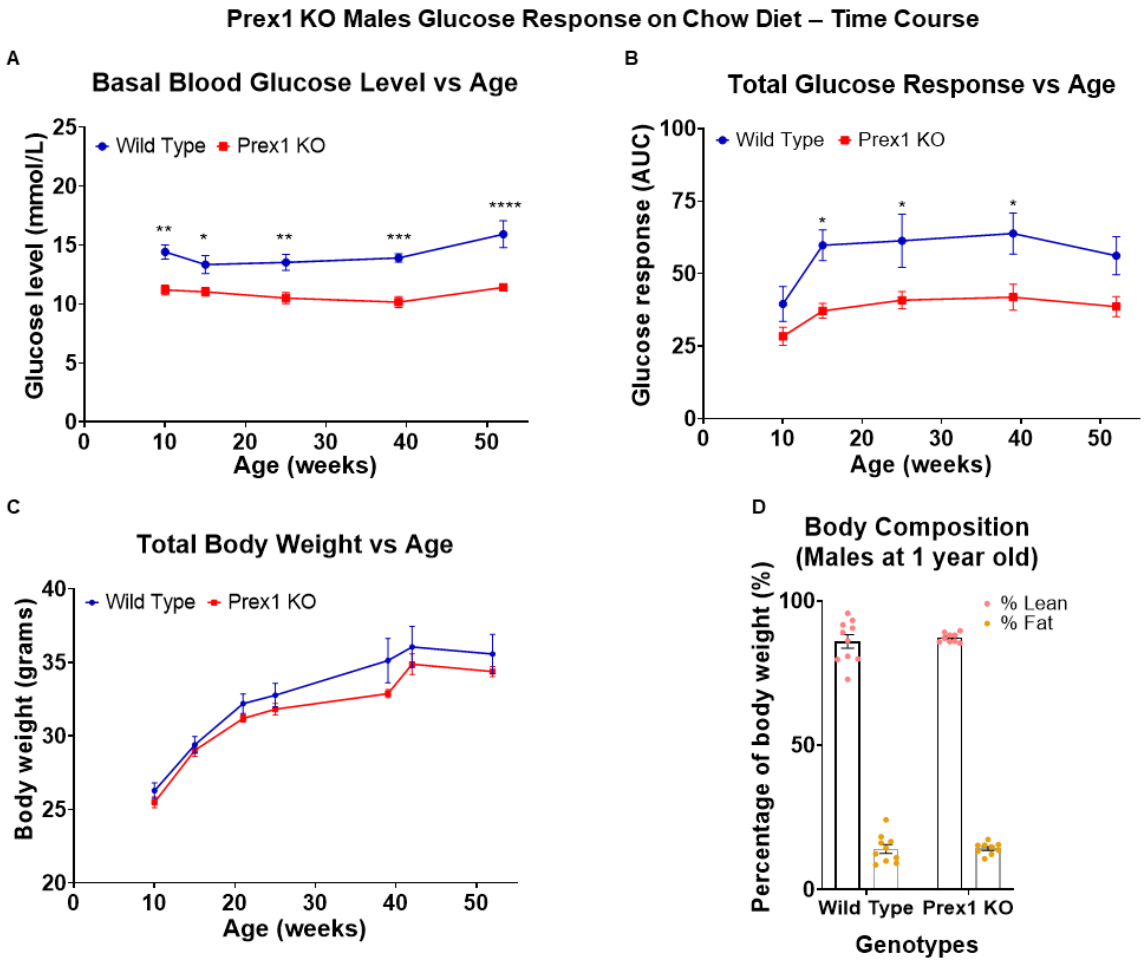

Figure 4.2.2: The low fasting blood glucose levels and improved glucose tolerance of male Prex1 KO mice on chow diet persist throughout ageing.

The fasting blood glucose levels, response to glucose challenge, and body weight of the male Prex1 KO (red) and Prex WT (blue) mice from **Figure 4.2.1** are expressed as a function of age. **(A)** Fasting blood glucose levels; data from column A in **Figure 4.2.1**. **(B)** Response to IPGTT; normalised data from columns B and C in **Figure 4.2.1**. **(C)** Body weight, measured after 6 and 4 h fasting, prior to glucose and insulin challenges, respectively. **(D)** Body composition at 1 year of age. The mice in (**A-C**) were culled at 1 year of age and the cadavers were scanned by Echo MRI for lean mass and body fat. Data are pooled from 2 independent cohorts (Prex WT n=10; Prex1 KO n=10) and presented as mean ± SEM. 2-way ANOVA with repeated measures and Sidak's multiple comparisons correction was used to compare genotypes during ageing. Unpaired Student's *t*-test was used to analyse the body composition.

Upon insulin challenge, the blood glucose levels of Prex1 KO males dropped to their lowest level at 45 min post injection, showing a drop of 5 mM, and returned to around 10 mM at 180 min (**Figure 4.2.3A,C**), similarly to the Prex WT controls. At 10 months of age however, Prex1 KO males showed a reduced response to insulin challenge compared to their Prex WT counterparts (**Figure 4.2.3E-H**). The fasting blood glucose levels were significantly lower in the Prex1 KO than the Prex WT males (**Figure 4.2.3E-F**), and their response to insulin was smaller and shorter-lasting (**Figure 4.2.3G**). In Prex1 KO males, the glucose levels dropped only by 3 mM, instead of the 5 mM seen in Prex WT, and returned to basal levels at 120 min instead of persisting for the duration of the test (**Figure 4.2.3G**). This would suggest that Prex1 KO mice became insulin resistant at old age. However, **Figure 4.2.3E** shows that this may be consequence of the reduced fasting blood glucose level of these mice. In absolute terms, the blood glucose level of the Prex1 KO mice actually dropped lower than that of Prex WT mice in response to the insulin challenge and in both genotypes glucose returned to around 10 mM at 150 min. It is difficult, therefore, to conclude whether the ageing Prex1 KO males are truly insulin resistant or if their lower fasting blood glucose levels mean they simply need to respond less to insulin in order to maintain a similar level of glucose homeostasis. In any event, their response to insulin is less at 10 months of age and this is an effect of ageing, as the Prex1 KO males responded normally to the insulin challenge at 5 months of age.

To begin to investigate the cause of the lower fasting blood glucose level and improved glucose tolerance, the mice were housed in metabolic cages at 12 weeks and 11 months of age. In both ages, the water and food consumption as well as the urine and faeces production of Prex1 KO male mice were normal (**Figure 4.2.4A-H**). The only parameter that showed a tendency towards differences between genotypes was the water consumption, which was slightly increased in Prex1 KO males, although this did not reach statistical significance.

In summary, Prex1 KO males on chow diet show lower fasting blood glucose levels and improved glucose homeostasis compared to Prex WT mice throughout ageing, and apparently, they become insulin-resistant in old age.

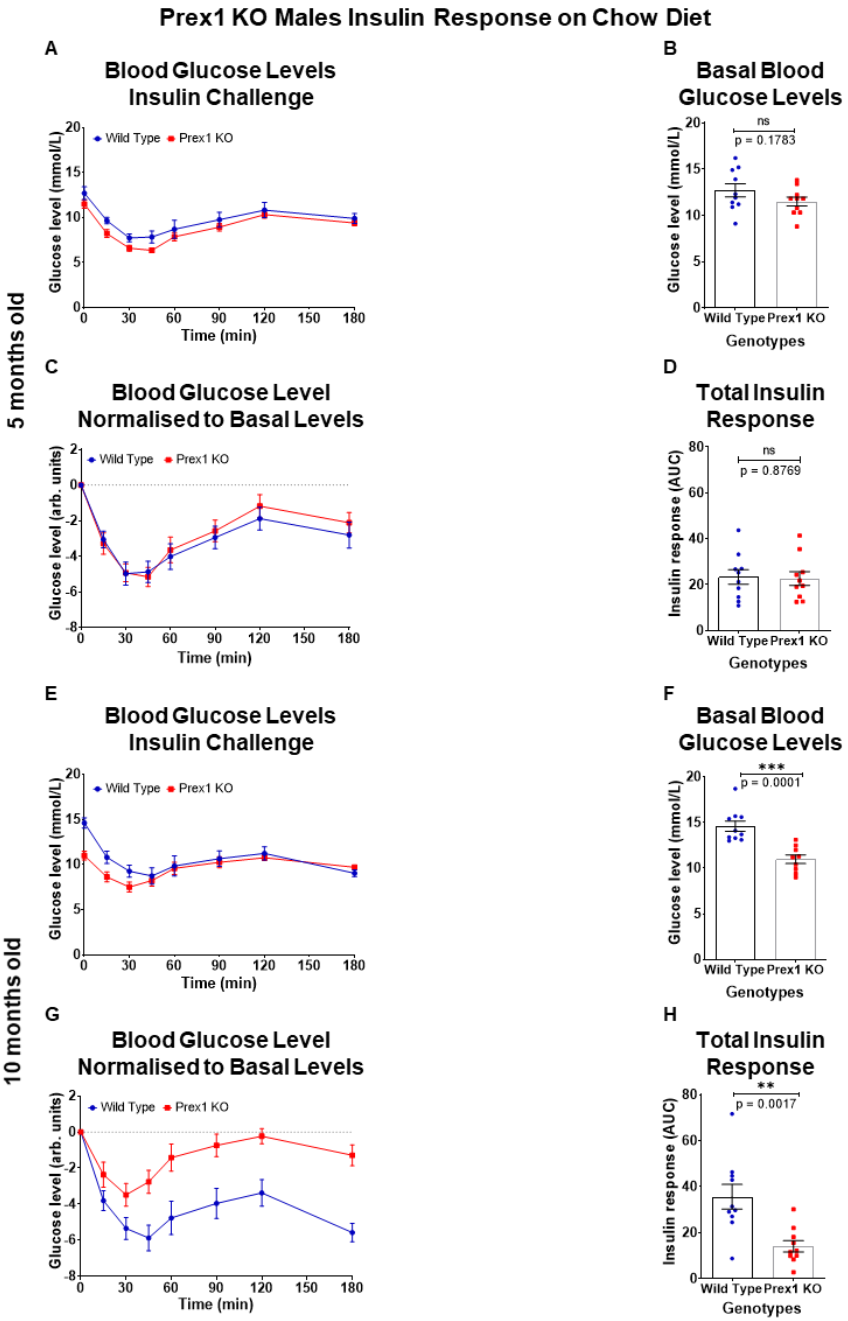

Figure 4.2.3: Prex1 KO male mice on chow diet show apparent insulin resistance in old age.

The male Prex1 KO (red) and Prex WT (blue) mice on chow diet shown in **Figure 4.2.1** were subjected to s.c. insulin tolerance test (SCITT) at the ages of **(A-D)** 5 and **(E-H)** 10 months. Food was withdrawn 4 h prior to s.c. injection of 0.75 IU/kg of human recombinant insulin at 0.15 IU/ml. Blood glucose levels were tested by tail bleed 15 min prior to the s.c. injection to determine basal blood glucose levels, as well as after the insulin injection at 15, 30, 45, 60, 90,120 and 180 min to assess the response to insulin. **(A,E)** Blood glucose concentration during SCITT. **(B,F)** Fasting blood glucose levels after 4 h fasting. **(C,G)** Blood glucose levels during SCITT, normalised by subtracting the fasting blood glucose level from each mouse individually. **(D,H)** Total insulin response (AUC of normalised data). Data are pooled from 2 independent cohorts (Prex WT n=10; Prex1 KO n=10) and are presented as mean ± SEM. 2-way ANOVA with repeated measures and Sidak's multiple comparisons correction was used to compare genotypes during SCITT. Unpaired Student's *t*-test was used to analyse the basal blood glucose levels and total insulin response.

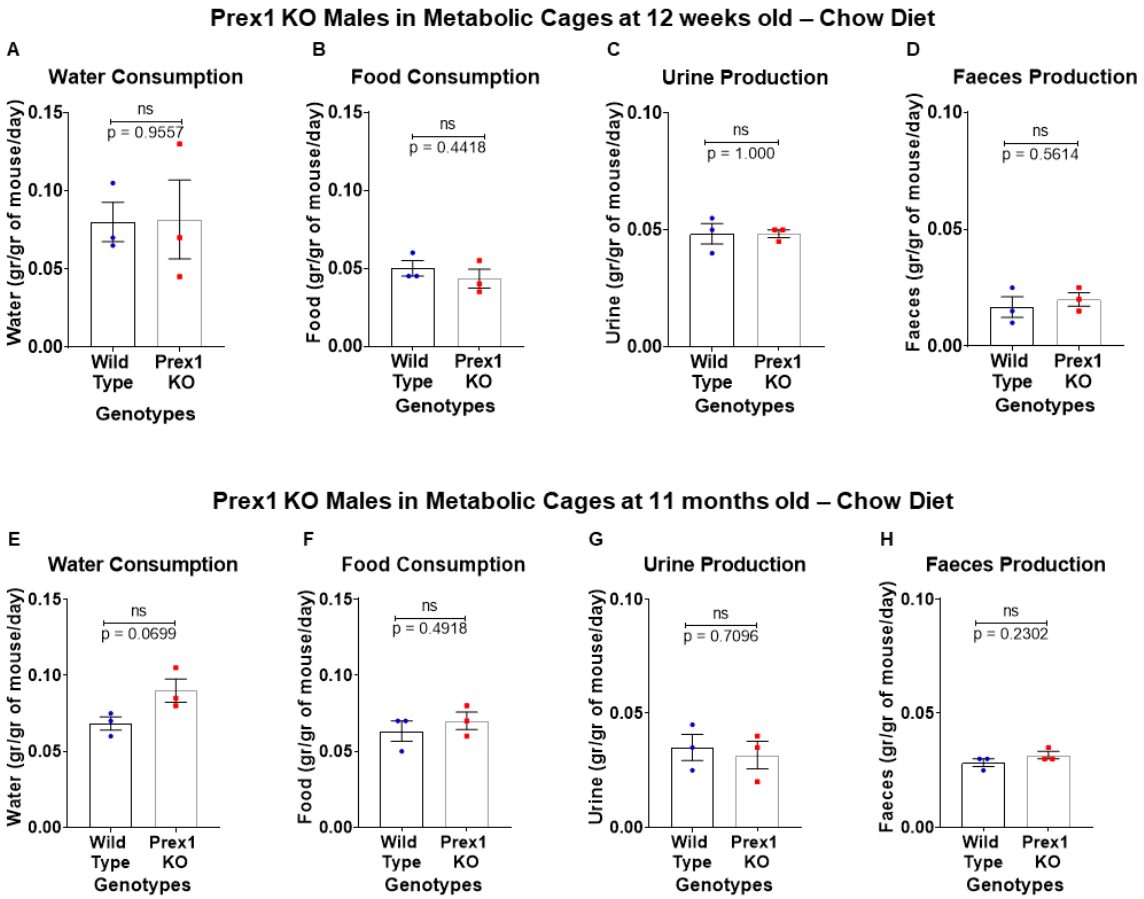

Figure 4.2.4: Male Prex1 KO mice on chow diet perform normally in metabolic cages.

Male Prex1 KO (red) and Prex WT (blue) mice were habituated to metabolic cages, as detailed in Materials and Methods, weighed and group-housed (up to 3) in metabolic cages overnight for 16 h on 3 subsequent nights with food and water provided *ad libitum*. Their **(A,E)** water consumption, **(B,F)** food consumption, **(C,G)** urine production, and **(D,H)** faeces production were measured after each night and were normalised to the combined body weights of the mice housed in each cage. **(A-D)** Data are pooled from 2 independent cohorts of 12 week-old males (WT n=9; Prex1 KO n=9). **(E-H)** Data pooled from 2 independent cohorts of male Prex1 KO and Prex WT mice in **Figure 4.2.1** at 11 months of age (Prex WT n=10; Prex1 KO n=10). Data are presented as the mean ± SEM of each night (n=3), with unpaired Student's *t*-test for comparison between genotypes.

4.2.2 Male Prex1 KO mice on HFD have low fasting blood glucose levels, but a normal glucose tolerance

Next, male Prex1 KO mice were introduced to 45% HFD, after a “reference” glucose challenge at 10 weeks of age, and remained on this HFD throughout their life. Data here are pooled from two independent cohorts, set up almost 5 months apart. The Prex WT control mice in these cohorts responded as expected throughout ageing.

As shown in **Figure 4.2.5A**, Prex1 KO male mice on HFD maintained their lower fasting blood glucose levels up to the age of 6 months. Similarly to Prex WT mice, HFD caused a rapid onset of glucose intolerance in Prex1 deficient mice (**Figure 4.2.5A**). During glucose tolerance tests (performed as for mice on chow diet) , the blood glucose levels of HFD-fed Prex1 mice kept increasing beyond the 15 min time point, reaching 42 mM at 60 min, and remaining around 40 mM within the 90 min of the test. Normalisation of the glucose response showed that Prex1 KO mice had slightly worse glucose tolerance than the Prex WT mice after only one month of HFD (**Figure 4.2.5B-C**). As one month of HFD was sufficient to render the mice of both genotypes severely glucose intolerant, we reduced the dosage of glucose in IPGTTs at later ages to one quarter of the original dose (0.5 g/kg, data in ochre box). As well as preventing mice from going into hyperglycaemic shock, it was reasoned that submaximal doses of glucose might unravel subtle differences between the genotypes. The graphs within the ochre box show that, under these conditions, glucose only triggered a mild response (**Figure 4.2.5C**). Although it still took longer for blood glucose levels to return to normal (**Figure 4.2.5B**), there was no difference between the genotypes. Hence, in contrast to mice on chow diet, Prex1 KO males on HFD were not protected from developing glucose intolerance.

The effects of ageing are summarised in **Figure 4.2.6**. As mentioned above, the HFD induced an increase in the fasting blood glucose levels of male Prex1 KO mice. However, this increase was not as sharp as for their Prex WT counterparts, meaning that the fasting blood glucose levels of the Prex1 KO males remained lower than those of the Prex WT controls until 9 months of age (**Figure 4.2.6A**). On the other hand, the response to glucose challenge in Prex1 KO mice on HFD was slightly worse at 15 weeks of age that that or WT controls, but comparable to the response of Prex WT males at all other ages tested (**Figure 4.2.6B**).

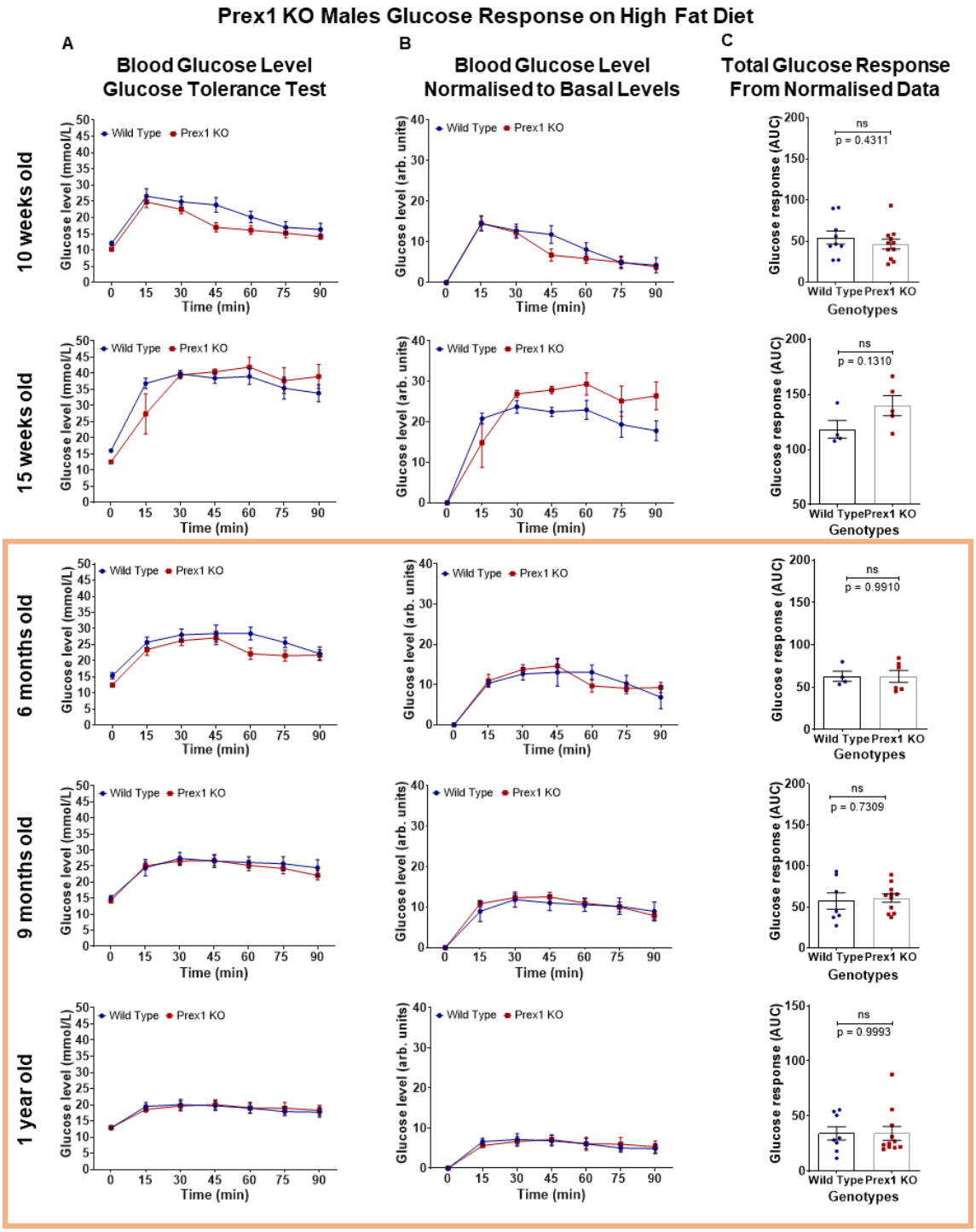

Figure 4.2.5: Male Prex1 KO mice on HFD have low fasting blood glucose levels, but exhibit a normal response to glucose challenge.

The fasting blood glucose levels and response to IPGTT were measured in male Prex1 KO (red) and Prex WT (blue) mice on 45% HFD at the ages of 10 and 15 weeks, 6, 9 and 12 months, as described in the legend to **Figure 4.2.1**. Glucose was injected at 2 g/kg at 10 and 15 weeks of age, and at 0.5 g/kg at later ages (ochre box). **(A)** Blood glucose concentration during IPGTT. **(B)** Blood glucose levels during IPGTT, normalised by subtracting the basal blood glucose level. **(C)** Total glucose response (AUC of normalised data). Data are pooled from 2 independent cohorts (Prex WT n=10; Prex1 KO n=10), and are presented as mean ± SEM. 2-way ANOVA with repeated measures and Sidak's multiple comparisons correction was used to compare genotypes during IPGTT. Unpaired Student's *t*-test was used to analyse the total glucose response.

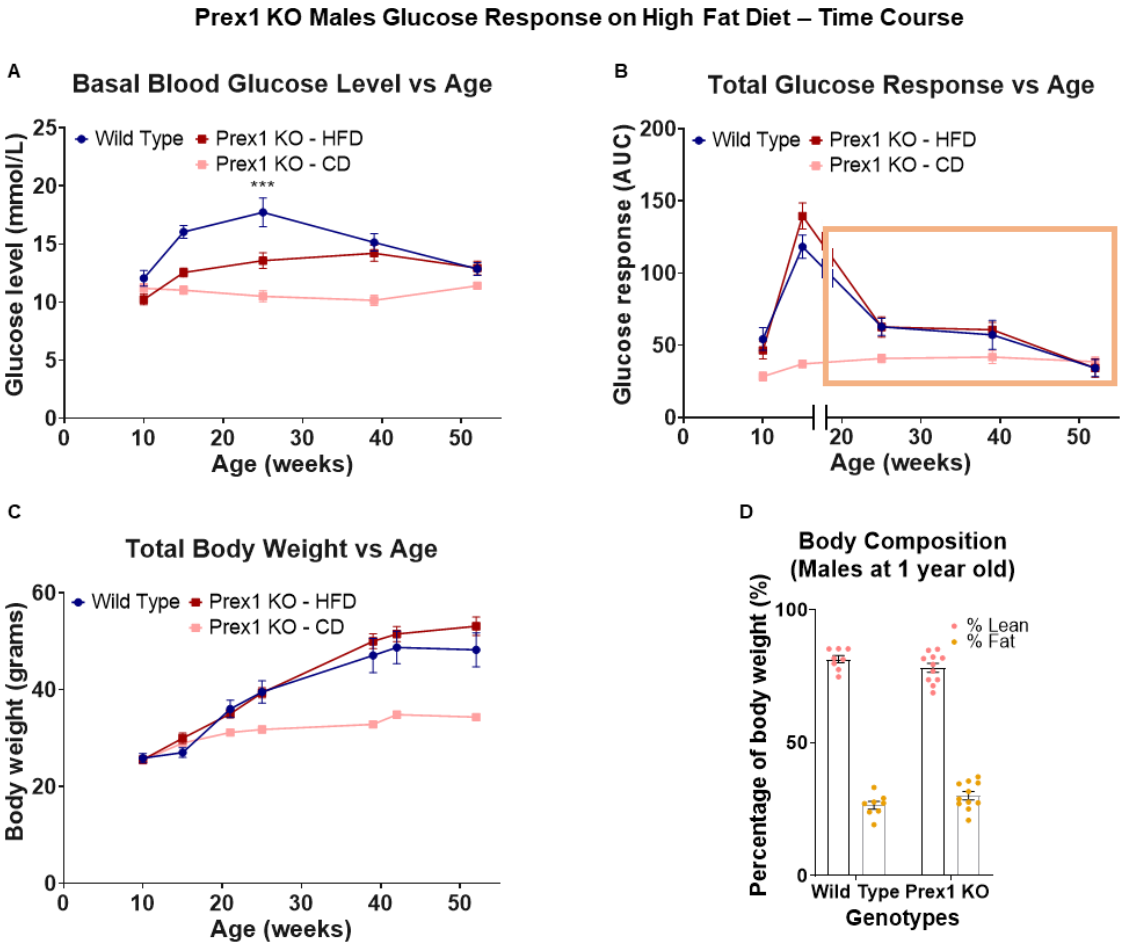

Figure 4.2.6: Prex1 KO males on HFD are not protected from developing glucose intolerance.

The fasting blood glucose levels, response to glucose challenge, and body weight of the male Prex1 KO (red) and Prex WT (blue) mice on HFD from **Figure 4.2.5** are expressed as a function of age. Note that the dose of glucose was reduced from 2 g/kg to 0.5 g/kg from the age of 6 months onwards (data in ochre box). In faded red are represented the Prex1 KO male mice on chow diet from **Figure 4.2.1** for visual comparison, but no statistical analysis was performed, as the animals were not directly compared experimentally. **(A)** Fasting blood glucose levels; data from column A in **Figure 4.2.5**. **(B)** Response to IPGTT; normalised data from columns B and C in **Figure 4.2.5**. **(C)** Body weight, measured after 6 and 4 h fasting, prior to glucose and insulin challenges, respectively. **(D)** Body composition at 1 year of age. The mice in (**A-C**) were culled at 1 year of age and the cadavers were scanned by Echo MRI for lean mass and body fat. Data are pooled from 2 independent cohorts (Prex WT n=10; Prex1 KO n=10), and are presented as mean ± SEM. 2-way ANOVA with repeated measures and Sidak's multiple comparisons correction was used to compare genotypes during ageing. Unpaired Student's *t*-test was used to analyse the body composition.

Both at 5 and 10 months of age, the response of male Prex1 KO mice on HFD to insulin challenge was similar to that of Prex WT mice (**Figure 4.2.7A-D, E-H**), despite differences in their basal blood glucose levels (**Figure 4.2.7B, F**). Interestingly the response of both genotypes to insulin was greater in mice on HFD compared to chow diet. Moreover, the insulin response of HFD-fed mice was reduced at 10 months compared to 5 months of age in a similar manner for both genotypes (**Figure 4.2.7D, H**), indicating that HFD did render Prex1 KO males insulin intolerant with age, but to a similar extent to Prex WT mice.

The mice from both genotypes gained weight in a similar way, and their body composition at one year of age was identical (**Figure 4.2.6C-D**). Finally, no difference was found in their water and food consumption or urine and faeces production in the metabolic cages (**Figure 4.2.8A-D**).

In summary, Prex1 deficiency did not prevent mice on HFD from becoming glucose intolerant, although it helped maintain low fasting blood glucose levels, and neither did it affect their insulin sensitivity. Hence, the absence of Prex1 improves glucose tolerance, but only during healthy ageing and not in mice with metabolic syndrome.

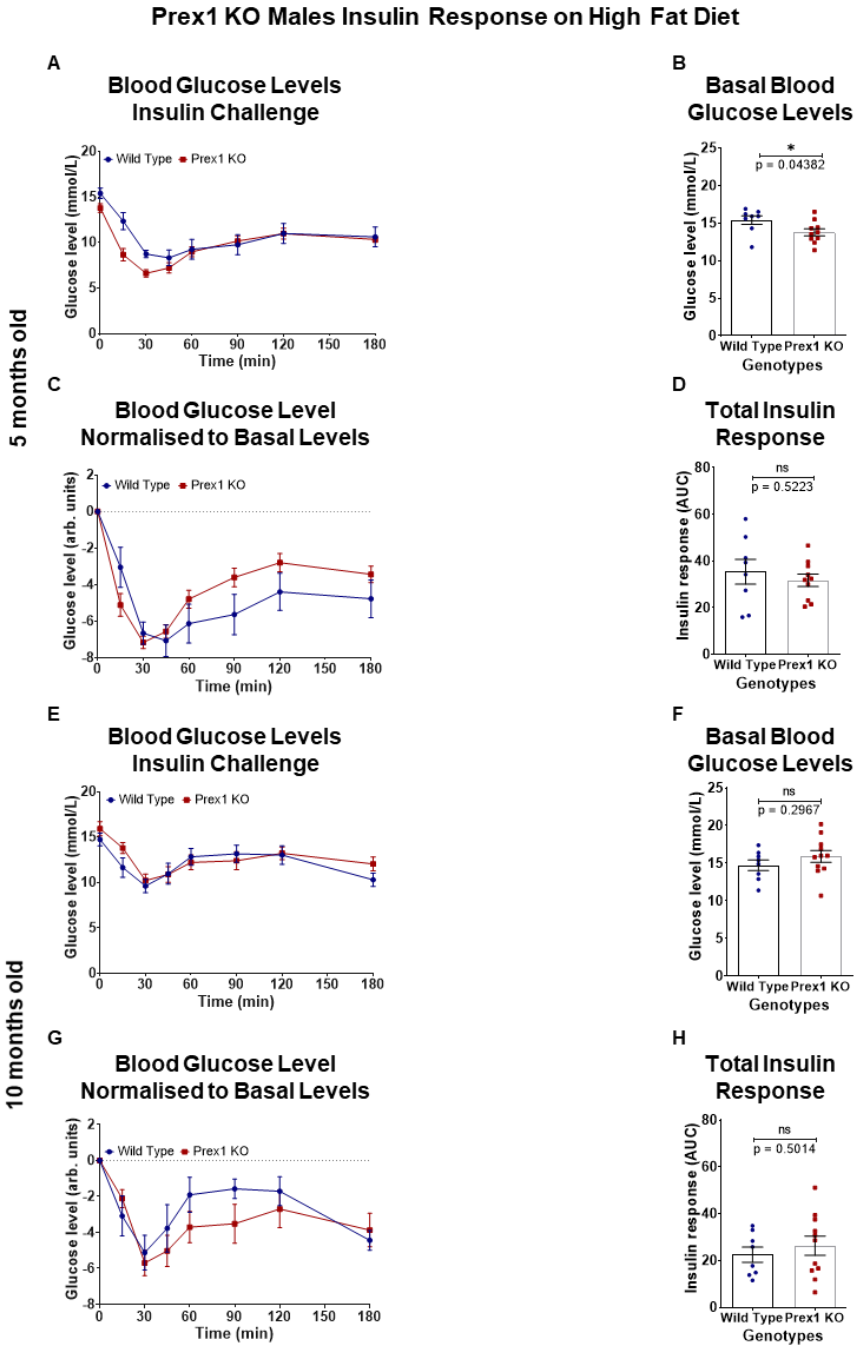

Figure 4.2.7: Male Prex1 KO mice on HFD show a normal response to insulin challenge.

The fasting blood glucose levels and response to SCITT were measured in the male Prex1 KO (red) and Prex WT (blue) mice on 45% HFD from **Figure 4.2.5** at the ages of **(A-D)** 5 and **(E-H)** 10 months, as described in the legend to **Figure 4.2.3**. **(A,E)** Blood glucose concentration during SCITT. **(B,F)** Fasting blood glucose levels. **(C,G)** Blood glucose levels during SCITT, normalised by subtracting the fasting basal blood glucose level from each mouse individually. **(D,H)** Total insulin response (AUC of normalised data). Data are pooled from 2 independent cohorts (Prex WT n=10; Prex1 KO n=10) and are presented as mean ± SEM. 2-way ANOVA with repeated measures and Sidak's multiple comparisons correction was used to compare genotypes during SCITT. Unpaired Student's *t*-test was used to analyse the basal blood glucose level and total insulin response.

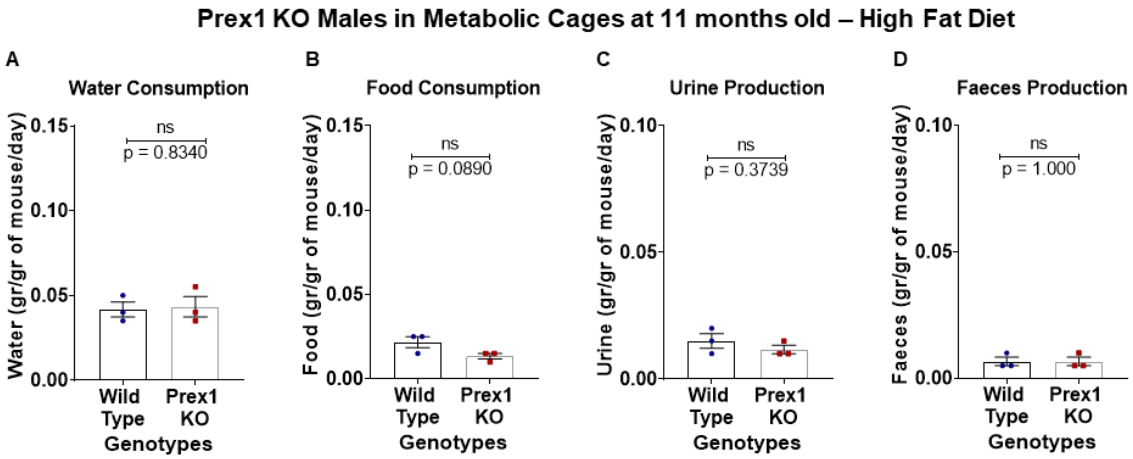

Figure 4.2.8: Male Prex1 KO mice performed normally in metabolic cages.
The male Prex1 KO (red) and Prex WT (blue) mice from **Figure 4.2.5** were habituated to metabolic cages at 11 months of age, as detailed in Materials and Methods, weighed and group-housed (up to 3) in metabolic cages overnight for 16 h on 3 subsequent nights with food and water provided *ad libitum*. Their **(A)** water consumption, **(B)** food consumption, **(C)** urine production, and **(D)** faeces production were measured after each night and were normalised to the combined body weights of the mice housed in each cage. Data are pooled from 2 independent cohorts (Prex WT n=10; Prex1 KO n=10). Data are presented as the mean ± SEM of each night (n=3), and unpaired Student's *t*-test was used for the comparison between the genotypes.

4.2.3 Female Prex1 KO mice on chow diet show similar glucose response to Prex WT mice throughout ageing

Similar to males, Prex1 KO females had lower fasting blood glucose levels than Prex WT females, throughout ageing (**Figures 4.2.9A** and **4.2.10A**). However, this phenotype of females was not as pronounced as that of males, presumably because females have lower fasting glucose levels than males anyway. It is worth mentioning that the Prex WT females in this cohort had slightly higher fasting blood glucose levels compared to most other Prex WT females tested under the same conditions (see Supplementary Data, **Section 3**). Regarding the response to glucose challenge, Prex1 KO females also showed a trend towards improved glucose tolerance compared to Prex WT controls (**Figure 4.2.9B-C**). However, this did not persist at all tested ages and was not statistically significant, unlike in males, presumably again because the glucose tolerance of females is better than that of males (**Figure 4.2.10B**). The response of Prex1 KO females to insulin challenge, at 10 months of age, was identical to that of their Prex WT controls (**Figure 4.2.11A-E**).

The rate of body weight gain and the body composition of Prex1 KO females were also identical to that of Prex WT female mice (**Figure 4.2.10C, D**). Interestingly, the Prex1 deficient females had a tendency to increased water consumption, and produced significantly more urine compared to their Prex WT counterparts at 11 months of age (**Figure 4.2.12A, C**), whereas food consumption and faeces production, were similar between the groups (**Figure 4.2.12B, D**).

Overall, therefore, there was a sex dependence in the metabolic phenotype of Prex1 KO mice. Only Prex1 KO males showed significantly lower basal blood glucose levels and improved glucose tolerance throughout ageing compared to Prex WT controls. However, females showed a similar trend. It should be kept in mind that only one cohort of Prex1 KO females was tested, and bigger n-numbers would be required to further investigate the extent and possible causes of this sex dependency.

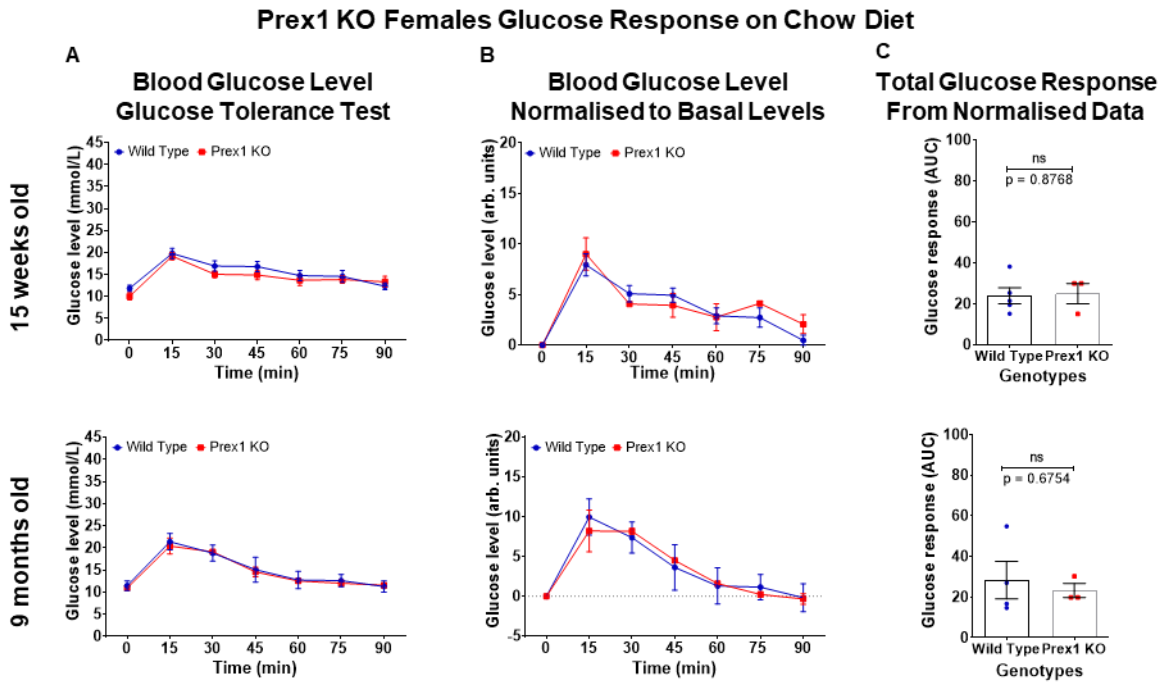

Figure 4.2.9: Female Prex1 KO mice on chow diet show a normal response to glucose challenge.

The fasting blood glucose levels and response to IPGTT were measured in female Prex1 KO (red) and Prex WT (blue) mice on chow diet, as described in the legend to **Figure 4.2.1**. Only data from 15 weeks and 9 months of age are shown, for brevity, although mice of all ages up to one year were tested. **(A)** Blood glucose concentration during IPGTT. **(B)** Blood glucose levels during IPGTT, normalised by subtracting the basal blood glucose level. **(C)** Total glucose response (AUC of normalised data). Data are from 1 cohort (Prex WT n=4; Prex1 KO n=3) and presented as mean ± SEM. 2-way ANOVA with repeated measure and Sidak's multiple comparisons correction was used to compare genotypes during IPGTT. Unpaired Student's *t*-test was used to analyse the total glucose response.

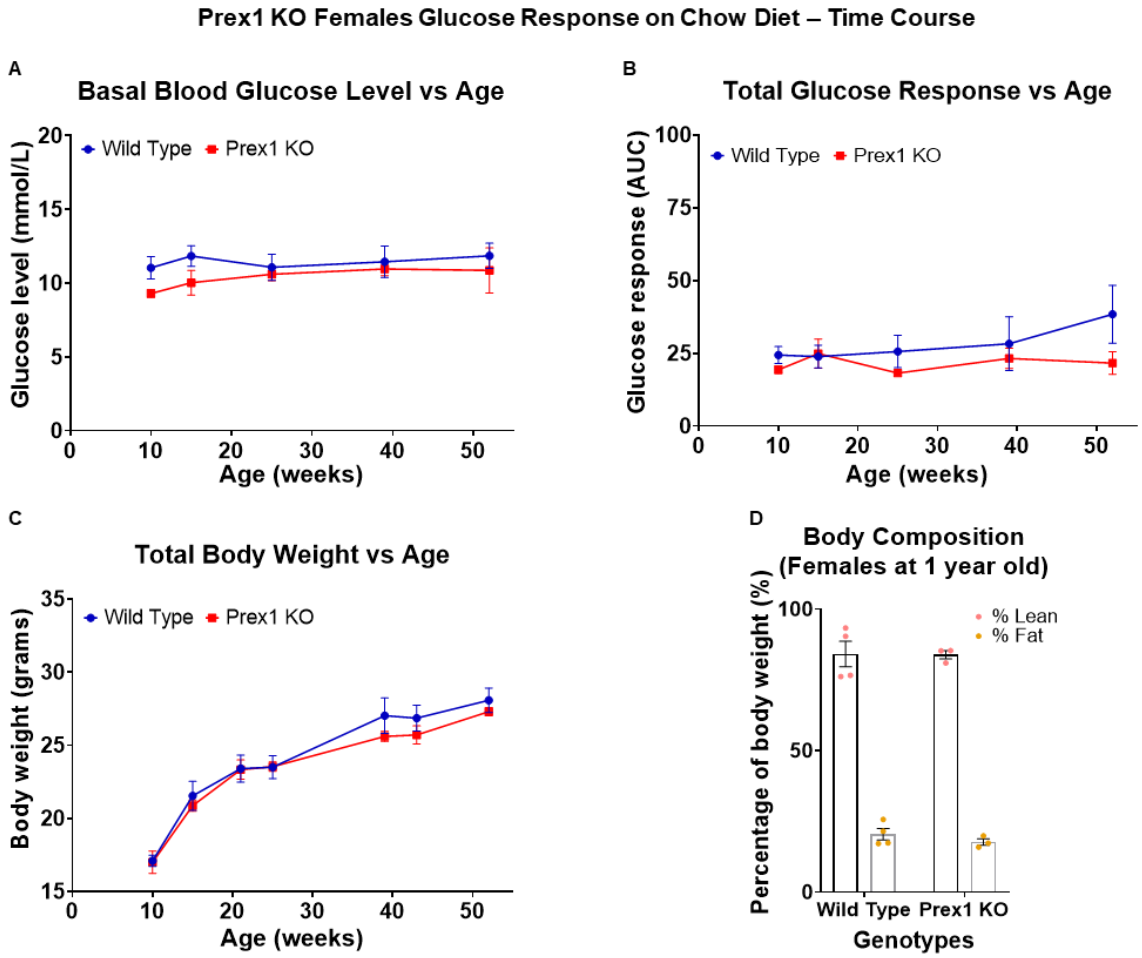

Figure 4.2.10: Prex1 KO females on chow diet show a tendency for improved glucose tolerance during ageing, although the phenotype is milder than in males. The fasting blood glucose levels, response to glucose challenge, and body weight of the female Prex1 KO (red) and Prex WT (blue) mice in **Figure 4.2.9** are expressed as a function of age. **(A)** Fasting blood glucose levels; data from column A in **Figure 4.2.9**. **(B)** Response to IPGTT; normalised data from columns B and C in **Figure 4.2.9**. **(C)** Body weight, measured after 6 and 4 h fasting, prior to glucose and insulin challenges, respectively. **(D)** Body composition at 1 year of age. The mice in (**A-C**) were culled at 1 year of age and the cadavers were scanned by Echo MRI for lean mass and body fat. Data are from 1 cohort (Prex WT n=4; Prex1 KO n=3) and presented as mean ± SEM. 2-way ANOVA with repeated measures and Sidak's multiple comparisons correction was used to compare genotypes during ageing. Unpaired Student's *t*-test was used to analyse the body composition.

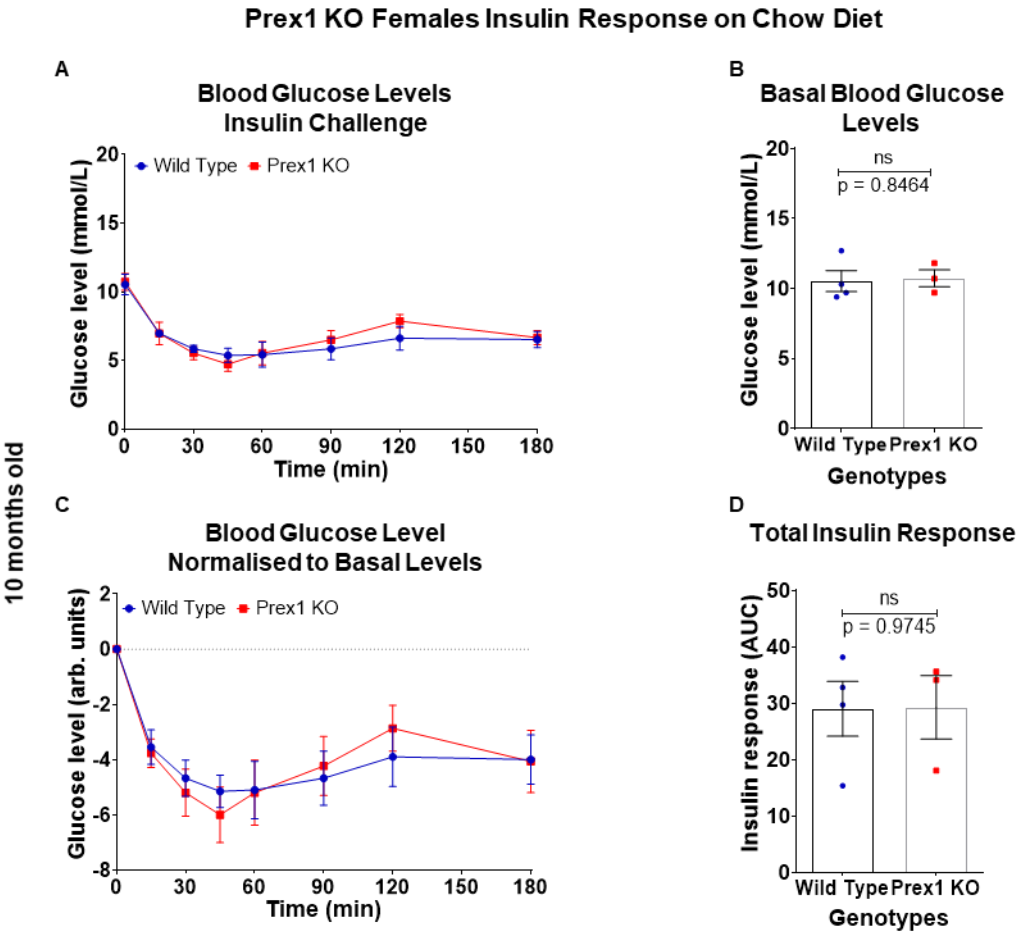

Figure 4.2.11: Female Prex1 KO mice on chow diet show a normal response to insulin challenge.

The fasting blood glucose levels and response to SCITT were measured in the female Prex1 KO (red) and Prex WT (blue) mice from **Figure 4.2.9** on chow diet at 10 months of age, as described in the legend to **Figure 4.2.3. (A)** Blood glucose concentration during SCITT. **(B)** Fasting blood glucose levels. **(C)** Blood glucose levels during SCITT, normalised by subtracting the fasting basal blood glucose level from each mouse individually. **(D)** Total insulin response (AUC of normalised data). Data from 1 cohort (Prex WT n=4; Prex1 KO n=3) and presented as mean ± SEM. 2-way ANOVA with repeated measures and Sidak's multiple comparisons correction was used to compare genotypes during SCITT. Unpaired Student's *t*-test was used to analyse the fasting basal blood glucose levels and total insulin response.

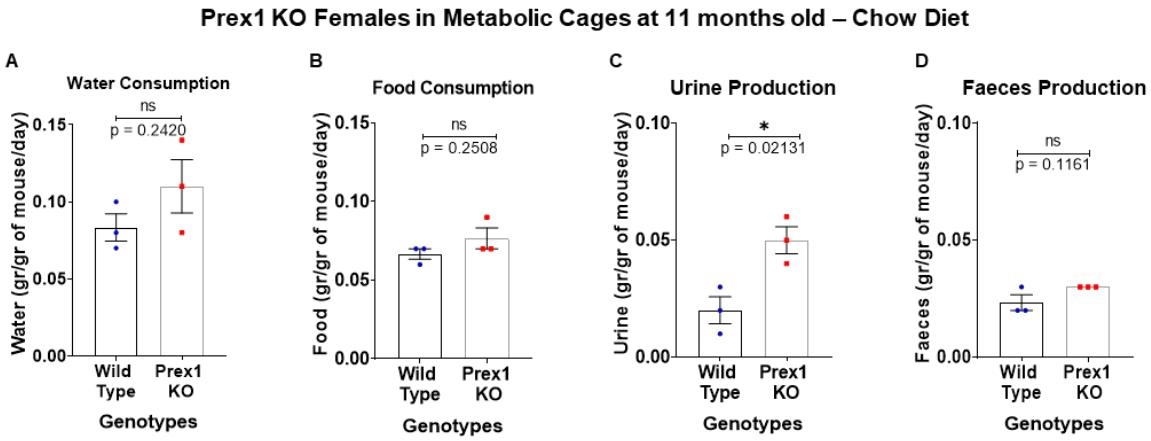

Figure 4.2.12: Female Prex1 KO mice produce more urine than Prex WT mice.
The female Prex1 KO (red) and Prex WT (blue) mice in **Figure 4.2.9** were habituated to metabolic cages at 11 months of age, as detailed in Materials and Methods, weighed and group-housed (up to 3) in metabolic cages overnight for 16 h on 3 subsequent nights with food and water provided *ad libitum*. Their **(A)** water consumption, **(B)** food consumption, **(C)** urine production, and **(D)** faeces production were measured after each night and were normalised to the combined body weights of the mice housed in each cage. **(A-D)** Data are from 1 cohort (Prex WT n=4; Prex1 KO n=3) and presented as the mean ± SEM of each night (n=3). Unpaired Student's *t*-test was used for comparison between genotypes.

4.2.4 Female Prex1 KO mice on HFD exhibit improved glucose tolerance compared to Prex WT mice at 6 months of age

Having seen that diet affected the metabolic phenotype of Prex1 KO males, Prex1 KO females were also introduced to 45% HFD. Throughout ageing, HFD did not affect the fasting blood glucose levels of Prex1 KO females or Prex WT controls (**Figures 4.2.13A** and **4.2.14A**). Yet, HFD rapidly induced a worse response to glucose challenge in both genotypes. At 15 weeks, there was no difference between the genotypes in their response to glucose challenge. However, interestingly, at 6 months, when the glucose intolerance of Prex WT females worsened yet further, the Prex1 KO mice showed significantly better glucose tolerance, maintaining the level of response seen at 15 weeks' time point. Nevertheless, at 9 months the glucose tolerance of Prex1 KO females worsened and became comparable again to that of Prex WT mice (**Figures 4.2.13B-C** and **4.2.14B**). For the 12-month time point, therefore, a lowered dose of glucose was used during the IPGTT, in order to reveal any subtle protection that might be afforded by the Prex1 deficiency, and this is indeed what was observed. This protection from glucose intolerance was seen despite both genotypes starting from identical body weight and gaining weight at the same rate throughout ageing (**Figure 4.2.14C**). Hence, Prex1 deficiency affords some protection from glucose intolerance to female mice on HFD. This was in contrast to Prex1 KO males, who showed improved glucose tolerance only on chow diet, but not on HFD.

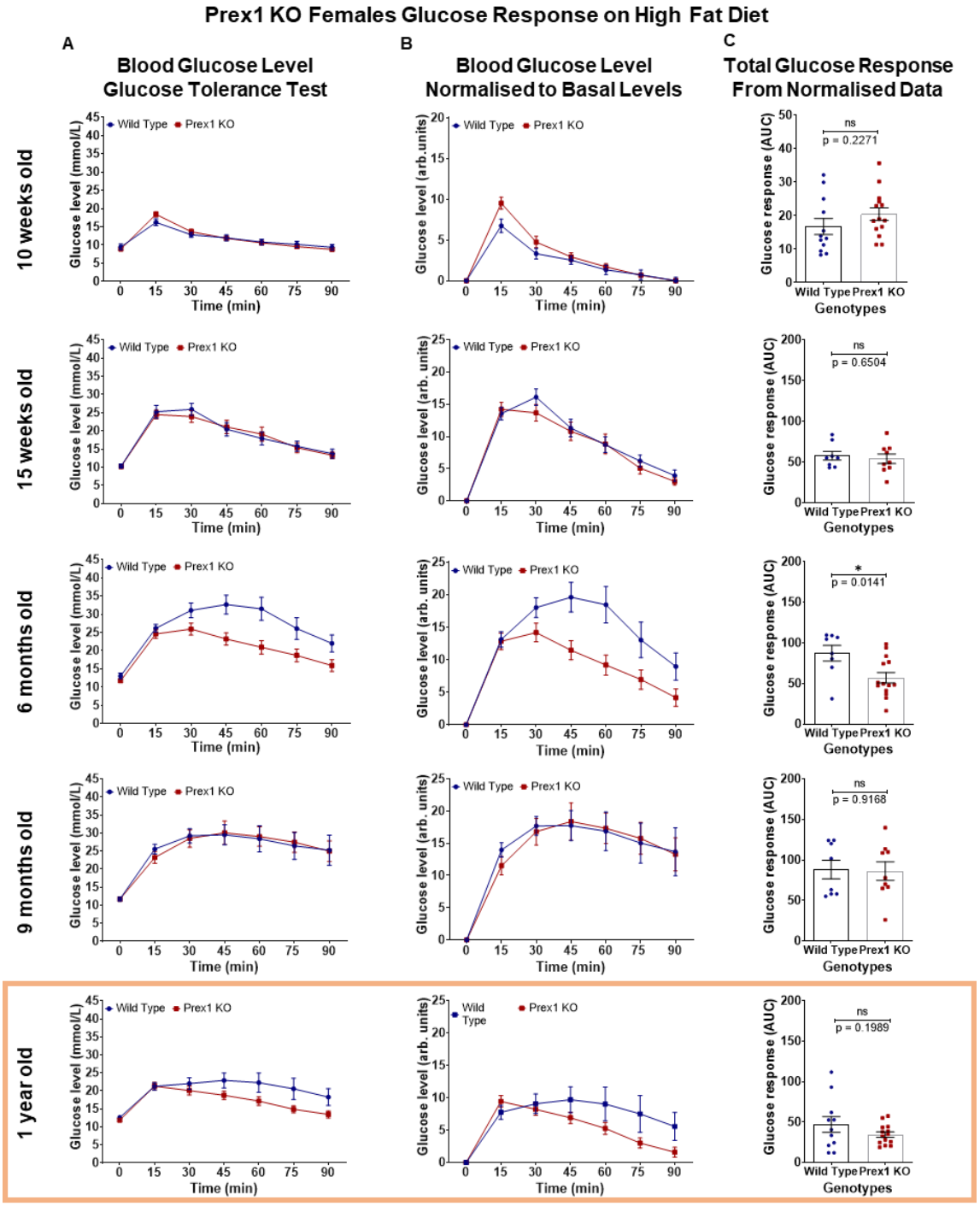

Figure 4.2.13: Female Prex1 KO mice on HFD are less glucose intolerant than Prex WT mice at 6 months of age.

The fasting blood glucose levels and response to IPGTT were measured in female Prex1 KO (red) and Prex WT (blue) mice on 45% HFD at the ages of 10 and 15 weeks, 6, 9 and 12 months, as described in the legend to **Figure 4.2.1**. The ochre box denotes glucose challenge at the reduced dose of 1 g/kg instead of 2 g/kg **(A)** Blood glucose concentration during IPGTT. **(B)** Blood glucose levels during IPGTT, normalised by subtracting the basal blood glucose level. **(C)** Total glucose response (AUC of normalised data). Data are pooled from 3 independent cohorts (Prex WT n=12; Prex1 KO n=14), and are presented as mean ± SEM. 2-way ANOVA with repeated measures and Sidak's multiple comparisons correction was used to compare genotypes during IPGTT. Unpaired Student's *t*-test was used to analyse the total glucose response.

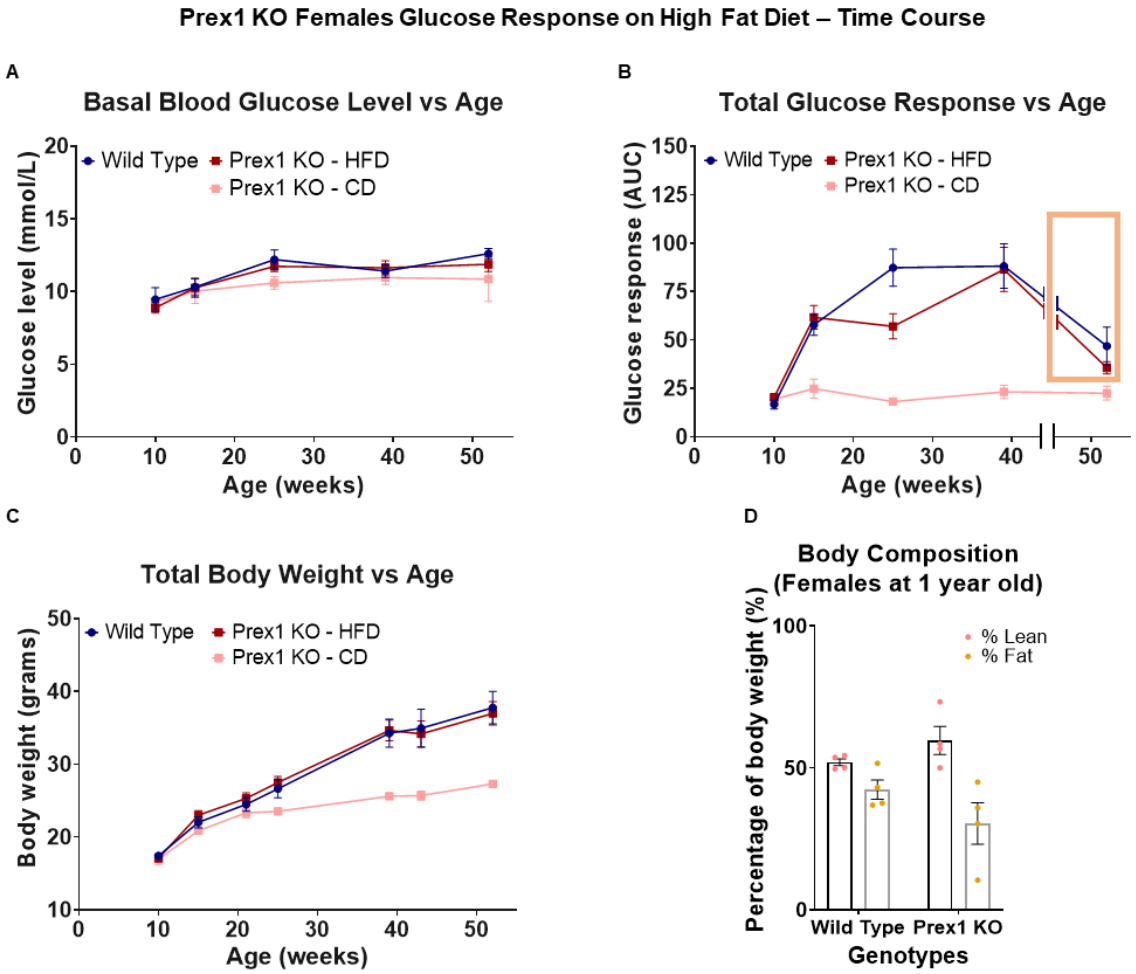

Figure 4.2.14: Female Prex1 KO mice show some protection from HFD-induced glucose intolerance.

The fasting blood glucose levels, response to glucose challenge, and body weight of the female Prex1 KO (red) and Prex WT (blue) mice on 45% HFD from **Figure 4.2.13** are expressed as a function of age. In faded red are represented the female Prex1 KO mice on chow diet from **Figure 4.2.9** for visual comparison, but no statistical analysis was performed, as these animals were not directly compared experimentally. **(A)** Response to IPGTT; normalised data from columns B and C in **Figure 4.2.13**. **(B)** Fasting blood glucose levels; data from column A in **Figure 4.2.13**. The ochre box denotes glucose challenge at the reduced dose of 1 g/kg instead of 2 g/kg. **(C)** Body weight, measured after 6 and 4 h fasting, prior to glucose and insulin challenges, respectively. **(D)** Body composition at 1 year of age. The mice in **(A-C)** were culled at 1 year of age and the cadavers were scanned by Echo MRI for lean mass and body fat. Data are pooled from 3 independent cohorts (Prex WT n=12; Prex1 KO n=14), and are presented as mean ± SEM. 2-way ANOVA with repeated measures and Sidak's multiple comparisons correction was used to compare genotypes during ageing. Unpaired Student's *t*-test was used to analyse the body composition.

Due to the increased response of HFD-fed males to insulin (compared to mice on chow diet), it was expected that females might also be more sensitive to insulin. In order to avoid causing hypoglycaemic shock, considering the low basal blood glucose levels of HFD-fed females, the females were therefore challenged with a lower dose of insulin (0.5 IU/kg compared to the 0.75 IU/kg routinely used) at the 5 months time point. **Figure 4.2.15A-E** shows that the glucose levels of Prex1 KO females dropped by 6 mM after 45 min, to 5 mM. Under these conditions, a smaller drop by 4 mM was observed in the Prex WT mice, before steadily returning to ~8 mM at 120 min and remaining there until the end of the test. This was seen despite normal fasting blood glucose levels (**Figure 4.2.15D**). However, this increased insulin sensitivity was subtle, and overall the response to insulin was not significantly different in Prex1 KO females than WT controls (**Figure 4.2.15B-C**). Using the normal insulin dose (0.75 IU/kg) for the 10 months challenge (**Figure 4.2.15F-J**), the Prex1 KO females were again found to be slightly more sensitive to insulin compare to Prex WT controls, in a similar way to what was observed at 5 months, but again this did not reach statistical significance.

Housing of females on HFD in metabolic cages at the age of 11 months did not reveal any significant differences in their water and food consumption or urine and faeces production (**Figure 4.2.16A-D**). However, interestingly, the post mortem body composition analysis at the age of one year revealed that Prex1 KO females had slightly less fat percentage compared to Prex WT mice (**Figure 4.2.14D**). This reduced fat level might be a consequence of the improved glucose tolerance; perhaps an increased glucose metabolism throughout the life-course meant that less fat deposits needed to be laid down to store excess energy.

Overall, it can be concluded that Prex1 deficiency protects females on HFD from glucose intolerance to some degree, and that it also affords a tendency towards increased sensitivity to insulin. Hence, it affords the mice some metabolic advantage.

To summarise the metabolic phenotype of Prex1 deficient mice overall (see **Table 4.1**), Prex1 deficiency results in low fasting blood glucose levels in males and in improved glucose tolerance both in males on chow diet and in females on HFD. Hence, Prex1 deficiency affords improved glucose homeostasis to mice. This

phenotype was diet dependent, as Prex1 KO males showed improved glucose tolerance only on chow diet throughout ageing, but were not protected from HFD-diet induced glucose intolerance. This was despite lower fasting blood glucose levels in Prex1 KO than Prex WT mice on both diets, suggesting that low fasting glucose levels are either not causally related or insufficient to afford the protection against glucose intolerance. Moreover, the metabolic phenotype of Prex1 KO mice also showed sex-dependence. Prex1 KO females on chow diet showed a tendency to improved glucose tolerance throughout ageing, but this phenotype was not as strong as in males. This could possibly be a reflection of the fact that females had much better glucose tolerance than males anyway, so the Prex1 KO made relatively less of a difference in females. However, intriguingly, Prex1 deficient females on HFD exhibited significantly improved glucose tolerance compared to Prex WT controls, although this was obvious only at 6 months of age, and seen at later ages merely when the dose of glucose in challenges was reduced. Hence, Prex1 deficiency affords some protection from glucose intolerance in females but not males on HFD. Perhaps this sex difference is again a reflection of the fact that WT females on HFD were less glucose intolerant than males, so the mild protection afforded by Prex1 deficiency became more evident in the females. On both chow and HFD, Prex1 KO females had normal fasting blood glucose levels, throughout ageing, which again suggests that the improved glucose tolerance of these mice is uncoupled mechanistically from their fasting blood glucose levels. During insulin challenge, Prex1 deficient males showed an accelerated recovery phase, suggesting that Prex1 deficiency might alter the counter-regulatory response to hypoglycaemia.

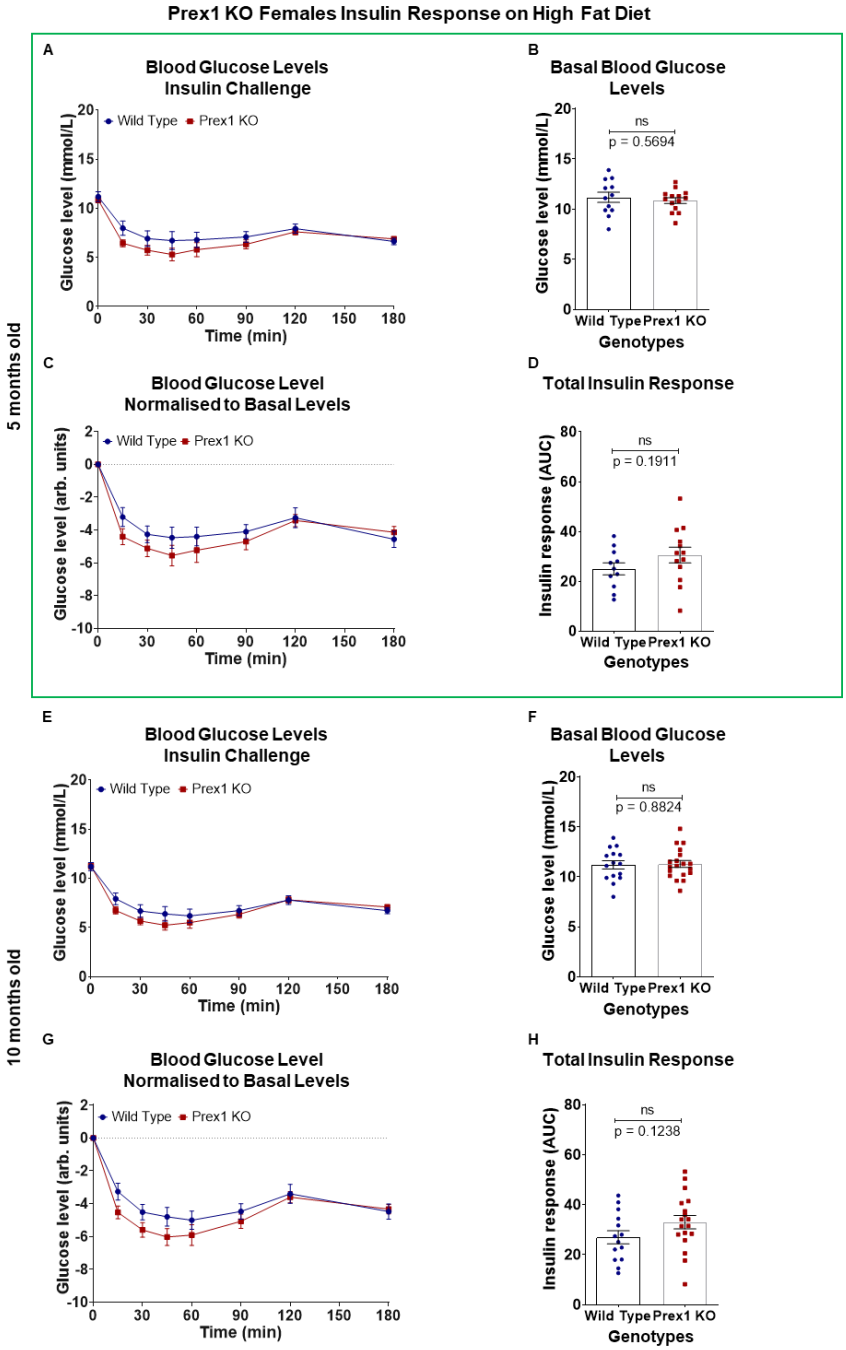

Figure 4.2.15: Female Prex1 KO mice on HFD show a normal response to insulin challenge.

The female Prex1 KO (red) and Prex WT (blue) mice on 45% HFD from **Figure 4.2.13** were subjected to SCITT at the ages of (**A-D**) 5 and (**E-H**) 10 months, as described in the legend **to Figure 4.2.3**. At 5 months mice were injected with 0.5 IU/kg of human recombinant insulin whereas at 10 months with 0.75 IU/kg **(A,E)** Blood glucose concentration during SCITT. **(B,F)** Fasting blood glucose levels. **(C,G)** Blood glucose levels during SCITT, normalised by subtracting the fasting basal blood glucose level from each mouse individually. **(D,H)** Total insulin response (AUC of normalised data). Data are pooled from 3 independent cohorts (Prex WT n=12; Prex1 KO n=14) and are presented as mean ± SEM. 2-way ANOVA with repeated measures and Sidak's multiple comparisons correction was used to compare genotypes during SCITT. Unpaired Student's *t*-test was used to analyse the basal blood glucose level and total insulin response.

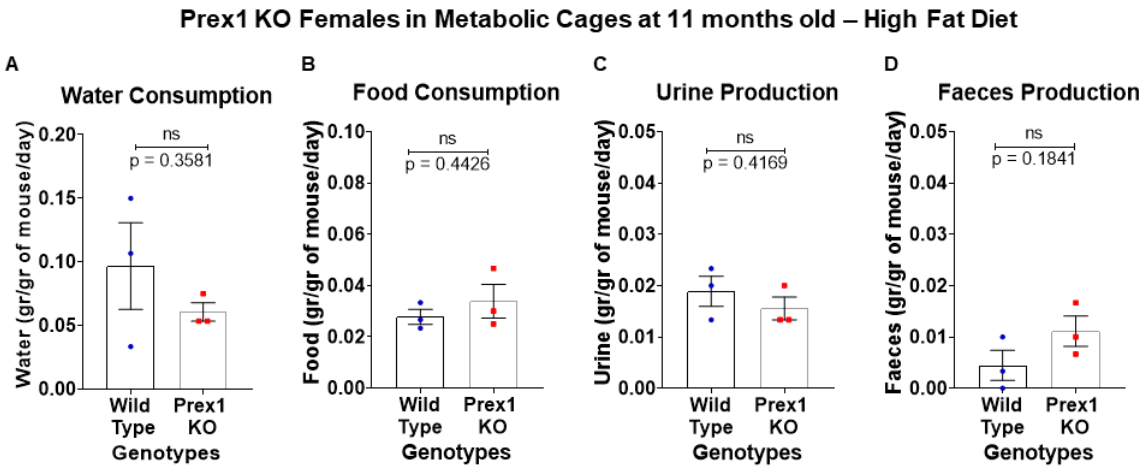

Figure 4.2.16: Female Prex1 KO mice perform normally in metabolic cages.
The female Prex1 KO (red) and Prex WT (blue) mice from **Figure 4.2.13** were habituated to metabolic cages at the age of 11 months, as detailed in Materials and Methods, weighed and group-housed (up to 3) in metabolic cages overnight for 16 h on 3 subsequent nights with food and water provided *ad libitum*. Their **(A)** water consumption, **(B)** food consumption, **(C)** urine production, and **(D)** faeces production were measured after each night and were normalised to the combined body weights of the mice housed in each cage. Data pooled from 3 independent cohorts (Prex WT n=12; Prex1 KO n=14) and are presented as the mean ± SEM of each night (n=3). Unpaired Student's *t*-test was used for the comparison between the genotypes.

Table 4.1: Summary table of metabolic phenotype of Prex1 KO mice on chow or high fat diet. Bold font was used to annotate findings that reached statistical significance in most time points tested, while bold and italic font was used to indicate strong trends that show statistical significance in only one or two time points tested.

		Prex1 KO		Prex2 KO		Prex1/2 DKO	
		Male	**Female**	**Male**	**Female**	**Male**	**Female**
Chow Diet	**Fasting Blood Glucose**	**Low fasting blood glucose**	Tendency to low fasting blood glucose				
	Glucose Tolerance	**Improved glucose tolerance throughout ageing**	Tendency to improved glucose tolerance in old age				
	Insulin Response	Apparent insulin resistance in old age	Normal				
High Fat Diet	**Fasting Blood Glucose**	***Low fasting blood glucose***	Normal				
	Glucose Tolerance	Normal	***Improved glucose tolerance (some ages)***				
	Insulin Response	Normal	Normal				

4.2.5 *Ex vivo* characterisation of Prex1 KO metabolic phenotype

In order to begin to understand the possible mechanism for the metabolic phenotype of Prex1 KO mice, mice from all genotypes were dissected and the weight of their organs at young adult (10 weeks old) and middle age (24 weeks old for males, 30 weeks old for females) were compared.

Figure 4.2.17 shows that the liver of Prex1 KO mice was consistently smaller than of Prex WT across all groups tested. Young Prex1 KO males also had smaller inguinal WAT (ingWAT), skeletal muscle and testes compared to Prex WT controls, which persisted tendentially to 24 weeks of age but only the liver and ingWAT reached statistical significance in these middle-aged mice. Young Prex2 KO mice also had smaller ingWAT and skeletal muscle than Prex WT mice but larger kidneys and livers. Both male and female Prex1/2 DKO mice had smaller livers compared to the Prex WT controls, to a similar level as seen in Prex1 KO. Overall, the reduced liver size in Prex1 KO and Prex1/2 DKO mice was the most consistent difference in both sexes and ages.

Organ weight of animals on HFD was not systematically measured. However, in light of the findings presented above, the liver and intBAT of some HFD-fed mice were weighed, after their cadavers had been screened by the Echo MRI at 1 year of age. Under these conditions, only the Prex1/2 DKO males, but not Prex1 KO males were found to have smaller liver, and no difference was observed in the weight of the intBAT (**Figure 4.2.18**). It should be noted, however, that the condition of the cadavers at this stage was less than ideal, as they had been thawed for more than a day, so these results should be interpreted with caution.

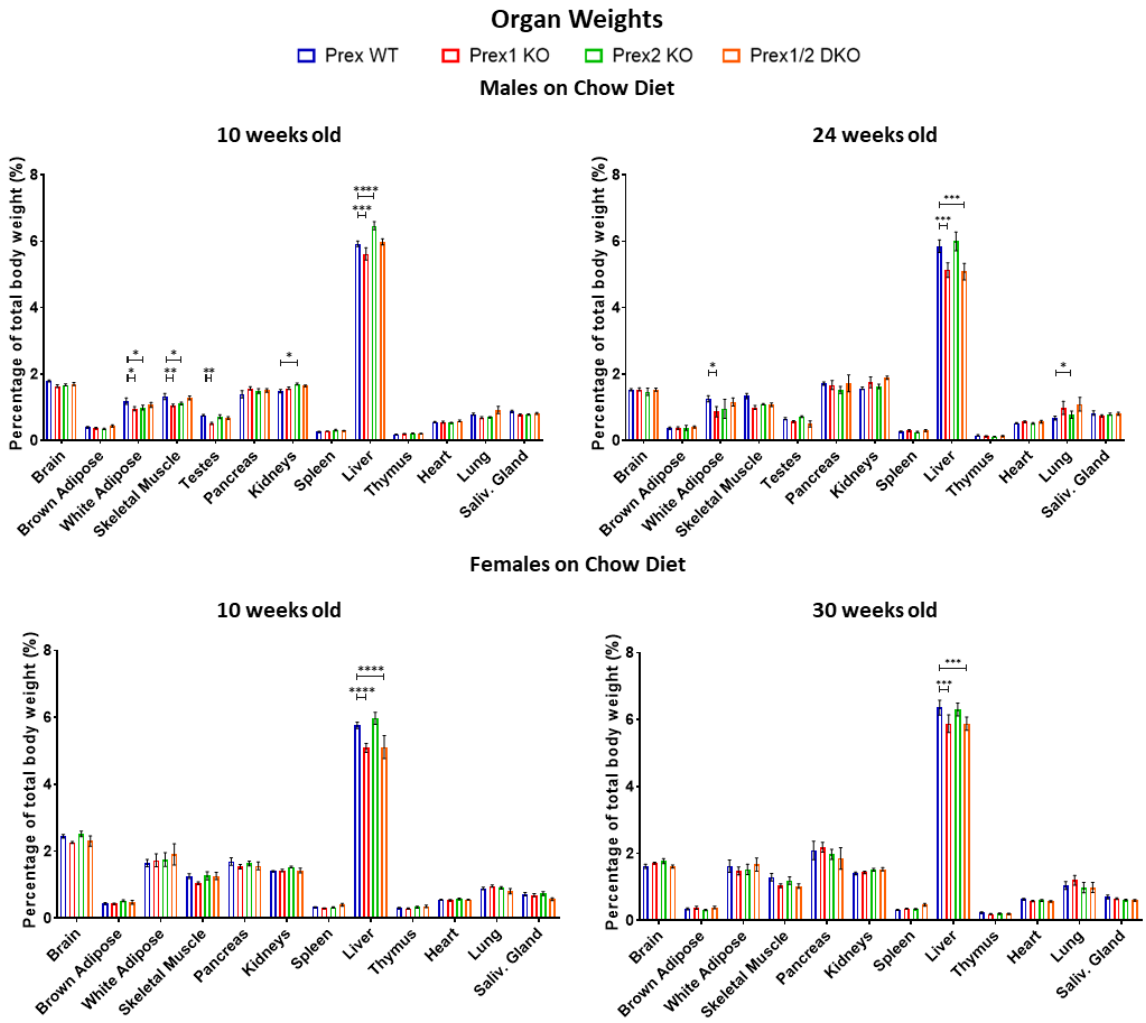

Figure 4.2.17: Prex1 KO mice have smaller livers.

Prex WT, Prex1 KO, Prex2 KO and Prex1/2 DKO male and female mice (symbol colours as indicated in the chart legend) were culled by CO_2 asphyxiation followed by severance of the femoral artery at the ages indicated and were dissected for organ collection. The weights of thirteen organs (brain, interscapular brown adipose, inguinal white adipose, skeletal muscle, pancreas, kidneys, spleen, liver, thymus, heart, lung, salivary gland, and when applicable testes) were measured, and data were normalised by total body weight. Data are presented as mean ± SEM. 2-way ANOVA with Sidak's multiple comparisons correction was used to compare the genotypes. (10 week-old males : Prex WT n=10, Prex1 KO n=10, Prex2 KO n=10 and Prex1/2 DKO n=9; 10 week-old females : Prex WT n=14, Prex1 KO n=12, Prex2 KO n=11 and Prex1/2 DKO n=4; 24 week-old males old: Prex WT n=8, Prex1 KO n=6, Prex2 KO n=6 and Prex1/2 DKO n=5; 30 week-old females old: Prex WT n=10, Prex1 KO n=12, Prex2 KO n=11 and Prex1/2 DKO n=10)

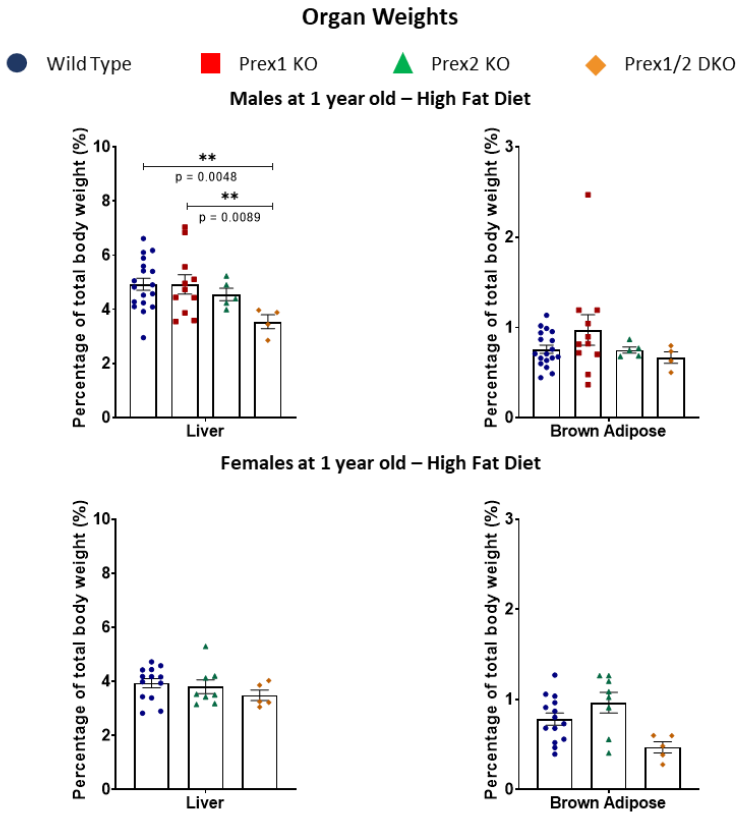

Figure 4.2.18: Male Prex1/2 DKO mice on HFD have smaller livers at 1 year of age. Prex WT, Prex1 KO, Prex2 KO and Prex1/2 DKO male and female mice on HFD (symbol colours as indicated in the chart legend) were dissected for organ collection at 1 year of age, after their cadavers had been thawed and scanned by Echo MRI. The weights of two organs (liver and interscapular brown adipose) were measured, and data were normalised to total body weight before dissection. Data are presented as mean ± SEM. 2-way ANOVA with Sidak's multiple comparisons correction was used to compare the genotypes. (1 year-old males at: Prex WT n=18, Prex1 KO n=11, Prex2 KO n=5 and Prex1/2 DKO n=4; 1 year-old females: Prex WT n=13, Prex2 KO n=8 and Prex1/2 DKO n=5).

Following up on the tissue size differences observed in younger Prex1 KO mice, the freshly dissected liver, skeletal muscle, ingWAT and intBAT of 10 week-old males were fixed in formalin and sent to Abbey Veterinary Services for preparation of standard H&E sections which were analysed by pathologist Dr Cheryl Scudamore. The histological analysis revealed that glycogen storage was reduced in Prex1 KO livers compared to Prex WT control livers, while increased eosinophilia was found in Prex1 KO intBAT (**Figure 4.2.19**). No obvious morphological changes between the two genotypes were observed in skeletal muscle and ingWAT. Given that I had identified sex difference in the low fasting blood glucose levels of Prex1 KO mice, which were only observed in males but not females, as well as in the improved glucose tolerance, which was more pronounced in males than females, at least on chow diet, tissues from female Prex1 KO and Prex WT mice were also sent for analysis. The histological analysis failed to uncover any morphological changes in the tissues of Prex1 KO females, despite these females having reduced liver size, just like their male counterparts. By correlation, these results suggest that reduced liver glycogen storage and/or BAT eosinophilia could be linked to the low fasting blood glucose or improved glucose tolerance of male Prex1 KO mice.

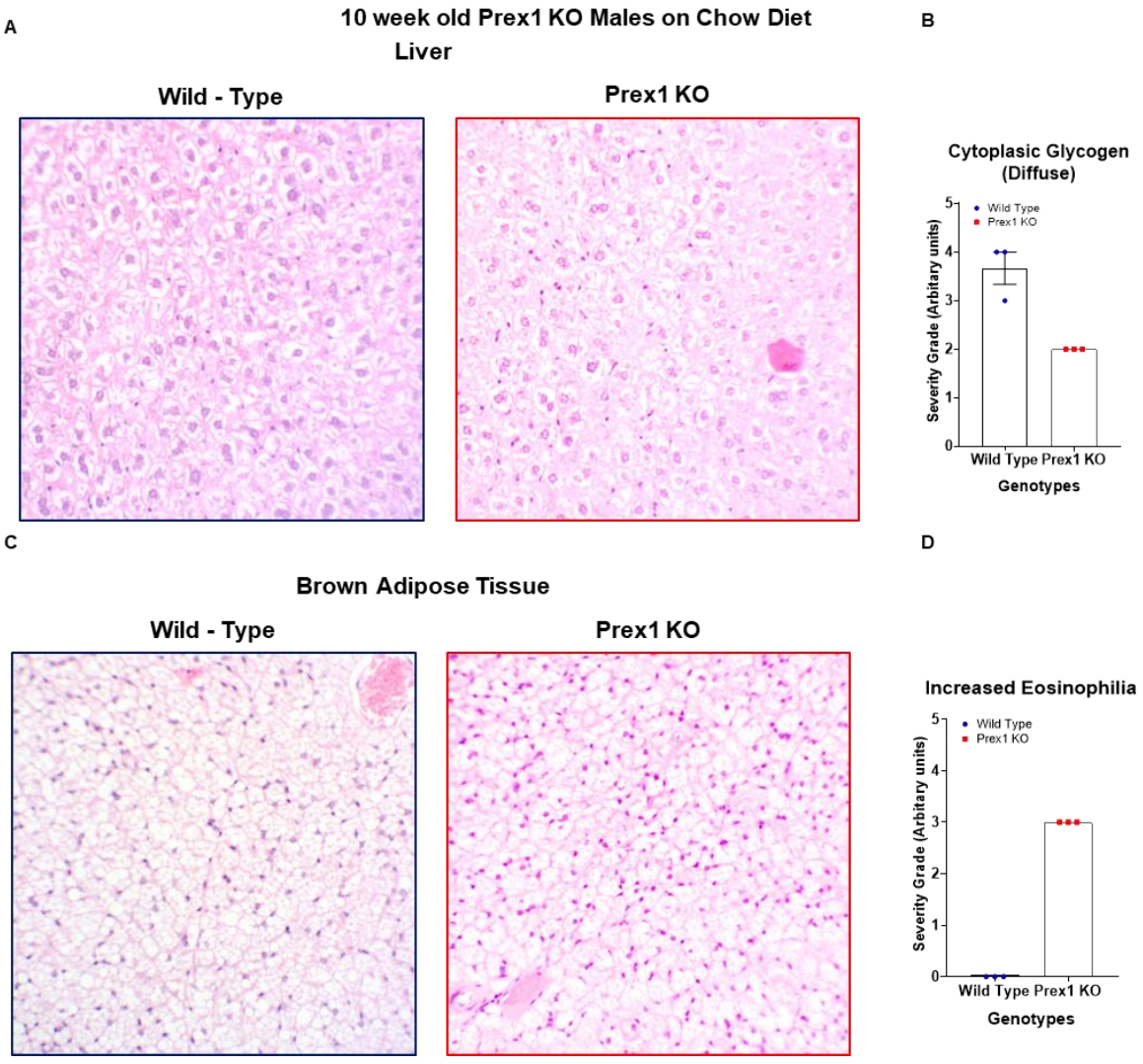

Figure 4.2.19: Prex1 KO mice have reduced glycogen storage in the liver and eosinophilia in the brown adipose tissue.

Haematoxylin-eosin staining of formalin-fixed **(A)** liver and **(C)** interscapular brown adipose tissue from 10 week-old Prex WT (blue) and Prex1 KO (red) mice on chow diet was performed and analysed by professional pathologists at Abbey Veterinary Services. Images shown are representative of three mice per group. **(B, D)** Findings in the tissues were scored by the pathologist using a non-linear semi-quantitative grading system from 0 to 5, where 0 = no significant change and 5 = whole organ or tissue affected. **(B)** Grading of clear cytoplasm in liver cells, consistent with glycogen storage. **(D)** Grading of eosinophilia in brow adipose tissue. Data are from 1 cohort (WT n=3; Prex1 KO n=3) and are presented as mean ± SEM.

In order to explore the possibility of low fasting blood glucose levels in Prex1 KO males being a result of altered insulin signalling, this pathway was investigated in 10 week-old Prex1 KO and Prex WT males on chow diet by *ex vivo* analysis. The mice were injected s.c. with either DPBS or insulin at 0.75 IU/kg, culled 15 min thereafter by cervical dislocation (with pithing as secondary method), and ingWAT, skeletal muscle, and liver were collected and snap-frozen in liquid nitrogen within 2 min of the animal's death. Total tissue lysates were prepared in the presence of 1% TX100, protease inhibitors and phosphatase inhibitors. Mesoscale analysis was performed on these total lysates for the phosphorylated and total levels of the insulin pathway components Akt, p70S6K and GSK3β. The activity of these enzymes (judged by the phosphorylation status of regulatory sites) increased with insulin treatment, as expected, in the Prex WT tissues. Insulin stimulation increased the levels of phospho-Akt most, in all tissues, whereas phospho-p70S6K was mainly increased in the ingWAT and phospho-GSK3β in the liver. However, no differences were found in the insulin pathway activity between Prex1 KO and control tissues (**Figure 4.2.20**), except for an apparent increase in GSK3β activity in insulin-treated Prex1 KO ingWAT that was not observed in Prex WT tissue. Dissection of the possible origin of this signal showed that the phospho-GSK3β level in these samples was normal, but total GSK3β levels had significantly decreased, leading to a relative increase in phosphorylated GSK3β per amount of total protein expressed. It is not impossible, but unlikely, that the total level of GSK3β should have declined within 15 min of insulin stimulation specifically in Prex1 KO tissue. Hence, this result must be interpreted with caution until it can be confirmed by repeats of the experiment. Overall, therefore, it seems that Prex1 deficiency has no obvious effects on the insulin pathway activity under the conditions tested.

The liver samples from insulin- and control-treated animals were also used for mRNA extraction, and the expression levels of *Pepck* and *G6p* were analysed by qPCR as a measure of the hepatic reaction to insulin stimulation. Although Pepck levels were slightly increased in the mock-treated Prex1 KO mice compared to the Prex WT controls, this did not reach statistical significance. Moreover, no difference was observed in the *Pepck* levels after insulin stimulation between the two genotypes (**Figure 4.2.21**). Hence, Prex1 KO has no obvious effects on the expression levels of these two liver enzymes, but more experiments would be

needed to investigate the possibility of a constitutive increase in *Pepck* levels.

Another avenue explored were the plasma levels of hormones relevant to glucose homeostasis. To this end, the levels of adiponectin, glucagon, and insulin were measured in the plasma of fasted 14 week-old Prex1 KO and Prex WT males. Surprisingly, adiponectin was found to be significantly reduced in the Prex1 KO mice, although glucagon and insulin levels were normal (**Figure 4.2.22**). This was surprising given that low adiponectin levels are usually associated with poor rather than good glucose tolerance.

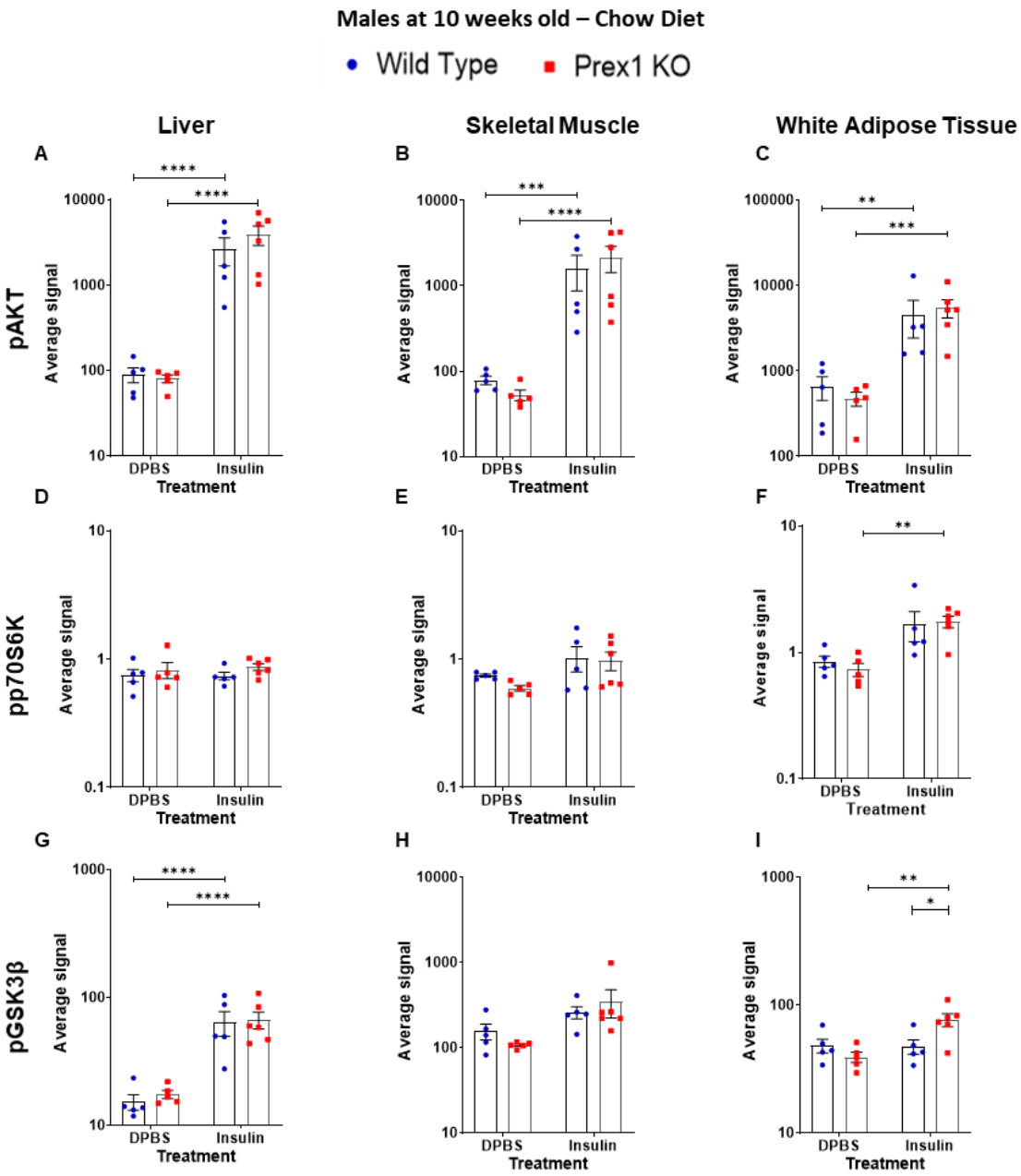

Figure 4.2.20: Insulin signalling is apparently unaffected in Prex1 KO liver, skeletal muscle and white adipose tissue.

10 week-old male Prex WT (blue) and Prex1 KO (red) mice on chow diet were fasted 4 h prior to s.c. injection of either DPBS or insulin at 0.75 IU/kg. Blood glucose levels were tested by tail bleed 15 min prior to the s.c. injection to determine basal blood glucose levels, as well as 14 min after the insulin injection to assess the response to insulin. At 15 min, mice were culled and tissues – inguinal white adipose tissue, skeletal muscle and liver – were collected and snap-frozen in liquid nitrogen within 2 min. Total lysates were prepared and samples were tested for regulatory phosphorylation and total levels of Akt, p70S6K and GSK3β using mesoscale multiplex plates. Data are pooled form 3 independent cohorts (Prex WT DPBS n=5; Prex WT Insulin n=5; Prex1 KO DPBS n=5; Prex1 KO Insulin n=6), and are presented as mean ± SEM of the phosphorylated protein divided by the total level of that protein for each sample. Statistical analysis was done by 2-way ANOVA with Sidak's multiple comparisons correction.

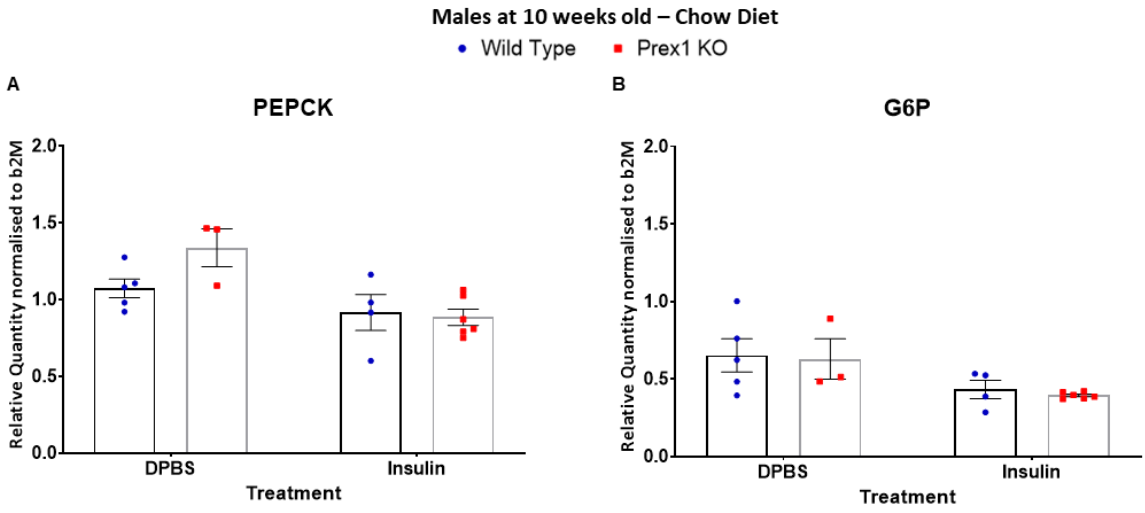

Figure 4.2.21: Prex1 KO males show a normal hepatic reaction to insulin challenge.
A) *Pepck* and **(B)** *G6p* transcripts were analysed by qPCR of RNA from the livers of same insulin- or mock-treated Prex WT (blue) and Prex1 KO (red) mice as in **Figure 4.2.20**. Transcript levels were normalized to the housekeeping gene b2M. Data are pooled form 3 independent cohorts (Prex WT DPBS n=5; Prex WT Insulin n=5; Prex1 KO DPBS n=5; Prex1 KO Insulin n=6), and are presented as mean ± SEM. Statistical analysis was done by 2-way ANOVA with Sidak's multiple comparisons correction.

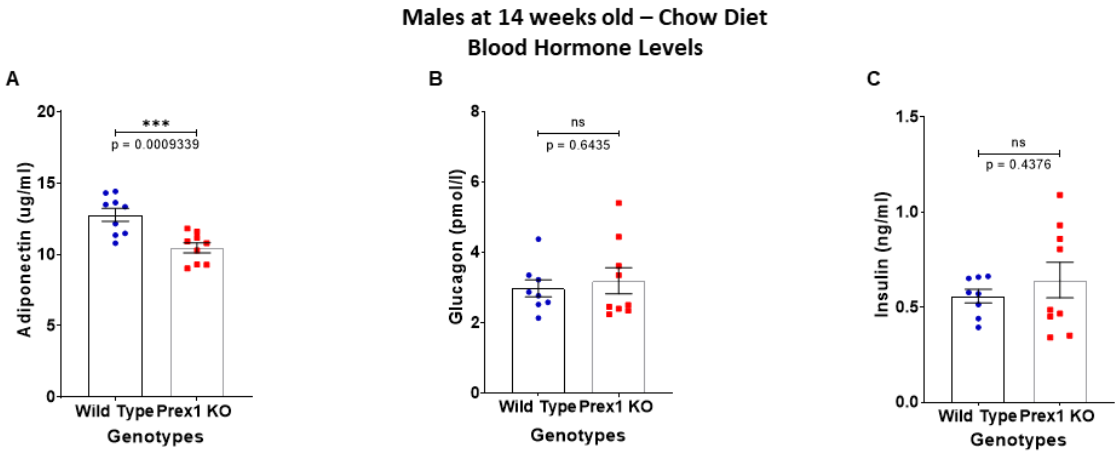

Figure 4.2.22: Prex1 KO males have reduced plasma levels of adiponectin levels under fasting conditions.
14 week-old male Prex WT (blue) and Prex1 KO (red) mice on chow diet were fasted for 6 h prior to the collection of peripheral blood and preparation of blood plasma. The plasma levels of **(A)** adiponectin, **(B)** glucagon and **(C)** insulin were quantified by ELISA. Data are pooled from 2 independent cohorts (Prex WT n=9; Prex1 KO n=9). Statistical analysis was done by unpaired Student's *t*-test.

Finally, given that Prex1 is widely expressed in cells of the hematopoietic system and known to mediate neutrophil-, macrophage-, and platelet-dependent inflammatory responses (Pantarelli and Welch, 2018; Pitchford et al., 2017) combined with the fact that inflammation is a key player in metabolic syndrome (Saltiel and Olefsky, 2017), we wanted to investigate a possible contribution of the immune system to the phenotype of low fasting blood glucose levels and improved glucose tolerance observed in Prex1 KO mice. Therefore, 7 week-old mice were lethally irradiated, and their hematopoietic system was reconstituted with bone marrow cells from 12 week-old donor mice that were either Prex WT or Prex1 KO. After bone marrow transplantation, the mice were kept on chow diet for 10 weeks in order to let their haematopoietic system reconstitute with that of the donor mice, and then they were subjected to IPGTT. **Figure 4.2.23A-C** shows that Prex1 KO males with a Prex1 KO hematopoietic system had improved glucose tolerance compared to irradiated Prex WT with either a Prex WT- or Prex1 KO-derived hematopoietic system. Hence, the improved glucose tolerance of Prex1 KO mice persisted through the bone marrow transplantation process. However, at that stage, a Prex1 KO haematopoietic system was insufficient to afford improved glucose tolerance to mice that were otherwise wild type. Moreover, this was seen despite the fact that the Prex WT mice, which had undergone bone marrow transplantation, had lower fasting blood glucose levels than wild type mice have usually. This might be taken as a further indication that the improved glucose tolerance of Prex1 KO mice is not a direct consequence of their low fasting blood glucose levels (**Figure 4.2.23D**). It is also worth noting that, on the day of the experiment, all tested mice had comparable weight (**Figure 4.2.23E**).

Importantly, the glucose tolerance of the same mice was tested again 10 weeks later, at 20 weeks after the bone marrow transplant. At that age, Prex WT mice with Prex WT hematopoietic system had developed considerable glucose intolerance, whereas the Prex1 KO mice with Prex1 KO hematopoietic system had maintained their significantly improved glucose tolerance. Surprisingly however, the Prex WT mice that had been reconstituted with a Prex1 KO hematopoietic system also exhibited improved glucose tolerance (**Figure 4.2.23F-H**).

It is worth pointing out that, at this time point, the Prex WT controls had again somewhat lower basal blood glucose than other WT groups (**Figure 4.2.23I**), and all mice gained weight at comparable rates (**Figure 4.2.23J**), hence it is unlikely that fasting blood glucose levels or body weight had any crucial influence on the observed improved glucose tolerance.

Overall, the results from the bone marrow transplantation experiment show that a Prex1 KO hematopoietic system is sufficient to protect otherwise wild type mice from developing age-related glucose intolerance, provided that the haematopoietic system is given ample time to establish itself.

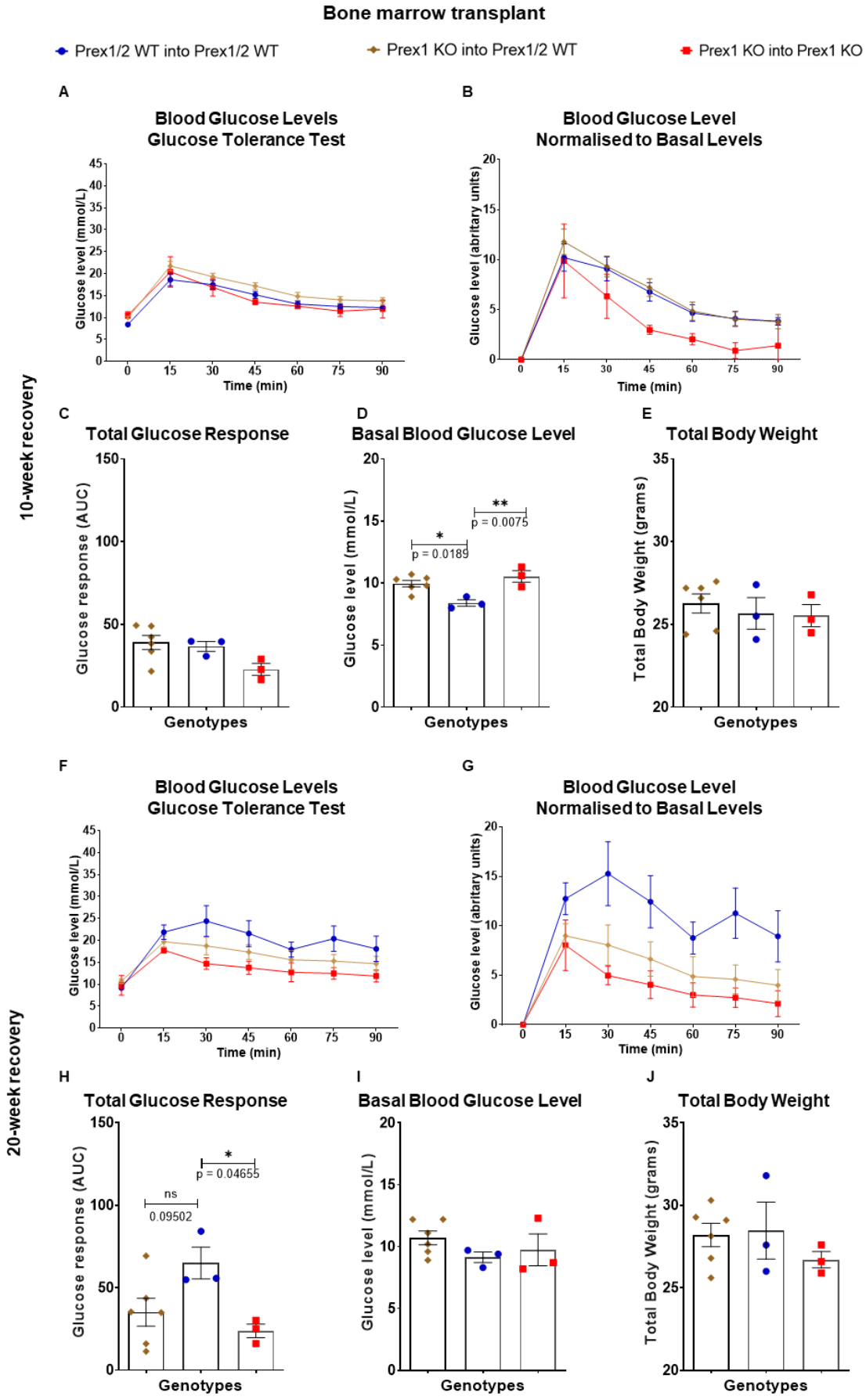
Bone marrow transplant
Prex1/2 WT into Prex1/2 WT
Prex1 KO into Prex1/2 WT
Prex1 KO into Prex1 KO
10-week recovery
20-week recovery
A
Blood Glucose Levels
Glucose Tolerance Test
Glucose level (mmol/L)
Time (min)
B
Blood Glucose Level
Normalised to Basal Levels
Glucose level (abritary units)
Time (min)
C
Total Glucose Response
Glucose response (AUC)
Genotypes
D
Basal Blood Glucose Level
Glucose level (mmol/L)
p = 0.0189
p = 0.0075
Genotypes
E
Total Body Weight
Total Body Weight (grams)
Genotypes
F
Blood Glucose Levels
Glucose Tolerance Test
Glucose level (mmol/L)
Time (min)
G
Blood Glucose Level
Normalised to Basal Levels
Glucose level (abritary units)
Time (min)
H
Total Glucose Response
Glucose response (AUC)
ns
0.09502
p = 0.04655
Genotypes
I
Basal Blood Glucose Level
Glucose level (mmol/L)
Genotypes
J
Total Body Weight
Total Body Weight (grams)
Genotypes

Figure 4.2.23: Hematopoietic cells contribute to the metabolic phenotype observed in Prex1 KO mice.

7 week-old Prex WT or Prex1 KO recipient mice were lethally irradiated and their hematopoietic system reconstituted with bone marrow from 12 week-old Prex WT or Prex1 KO donor mice, as indicated (symbol colours as indicated in the chart legend). Irradiated mice were kept on chow diet and their water was supplemented with neomycin (2 mg/ml) for 2 weeks post irradiation. At (**A-E**) 10 weeks and (**F-J**) 20 weeks after the bone marrow transplantation, mice were subjected to IPGTT, as described in the legend to **Figure 4.2.1**. **(A,F)** Blood glucose concentration during IPGTT. **(B,G)** Blood glucose levels during IPGTT, normalised by subtracting the fasting basal blood glucose level from each mouse individually. **(C,H)** Total glucose response (AUC of normalised data). **(D,I)** Fasting blood glucose levels. **(E,J)** Total body weight as measured after 6 h fasting. Data are from 1 cohort (Prex1 KO bone marrow transplanted into Prex WT mice n=9; Prex WT bone marrow transplanted into Prex WT mice n=3; Prex1 KO bone marrow transplanted into Prex1 KO mice n=3) and are presented as mean ± SEM. 2-way ANOVA with repeated measures and Sidak's multiple comparisons correction was used to compare genotypes during IPGTT. 1-way ANOVA was used to analyse the total glucose response, basal blood glucose level and total body weight.

4.3 Metabolic phenotype of Prex2 KO mice

In order to understand the role of Prex2 in glucose metabolism *in vivo*, the metabolic phenotype of *Prex2*$^{-/-}$ (Prex2 KO) mice was studied, as previously described for the Prex1 KO mice. Prex2 KO and Prex WT mice of same age and sex were tested in parallel under the same conditions for direct comparison.

4.3.1 Male Prex2 KO mice on chow diet show similar fasting blood glucose levels and glucose tolerance to Prex WT mice

As can be seen from the representative graphs in **Figure 4.3.1** (which only show the 15-week and 9-month time points, for brevity), Prex2 KO males on chow diet had normal basal blood glucose levels and response to glucose challenge compared to Prex WT mice at both ages. The overview of all time-points tested showed that Prex2 KO males had identical basal blood glucose levels to the Prex WT controls throughout ageing (**Figure 4.3.2A**). In contrast, the response to glucose challenge fluctuated with age between the two genotypes. It started similar at 10 weeks, but then the Prex2 KO mice had slightly better glucose tolerance then Prex WT controls at 15 weeks and 6 months of age and worse at one year of age (**Figure 4.3.2B**). Overall, although the total glucose response of the Prex2 KO males showed a tendency to improved glucose tolerance in young age and worse in old age, it did not differ significantly from the response of control males. The fluctuations in the response to glucose challenge could be a reflection of the uneven weight gain of the Prex2 KO cohorts throughout the ageing process, which was significantly different from WT at those ages (15 weeks and 1 year, **Figure 4.3.2C**), where the largest differences in glucose tolerance were observed. The body composition of the mice at one year of age was normal (**Figure 4.3.2D**).

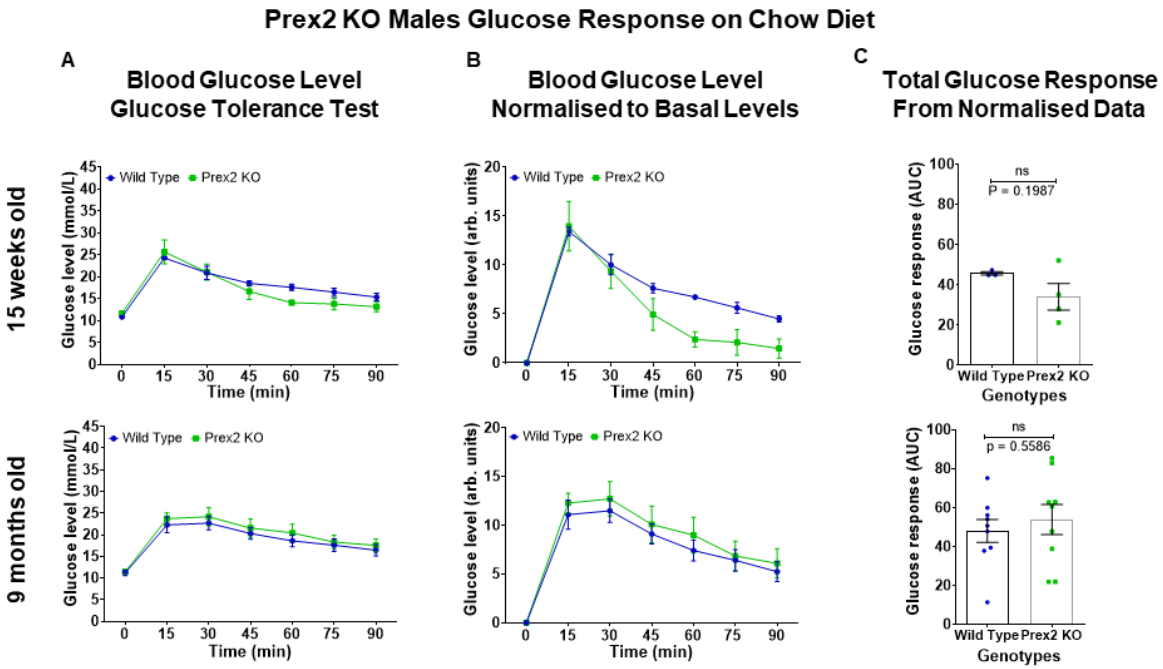

Figure 4.3.1: Male Prex2 KO mice on chow diet show similar fasting blood glucose levels and glucose tolerance to Prex WT mice.

The fasting blood glucose levels and response to IPGTT were measured in male *Prex2*$^{-/-}$ (Prex2 KO, green) and Prex WT (blue) mice on chow diet, as described in the legend to **Figure 4.2.1**. Only data from 15 weeks and 9 months of age are shown for brevity, although mice of all ages up to one year were tested. **(A)** Blood glucose concentration during IPGTT. **(B)** Blood glucose levels during IPGTT, normalised by subtracting the basal blood glucose level. **(C)** Total glucose response (AUC of normalised data). Data are pooled from 2 independent cohorts (Prex WT n=9; Prex2 KO n=9), and are presented as mean ± SEM. 2-way ANOVA with repeated measures and Sidak's multiple comparisons correction was used to compare genotypes during IPGTT. Unpaired Student's *t*-test was used to analyse the total glucose response.

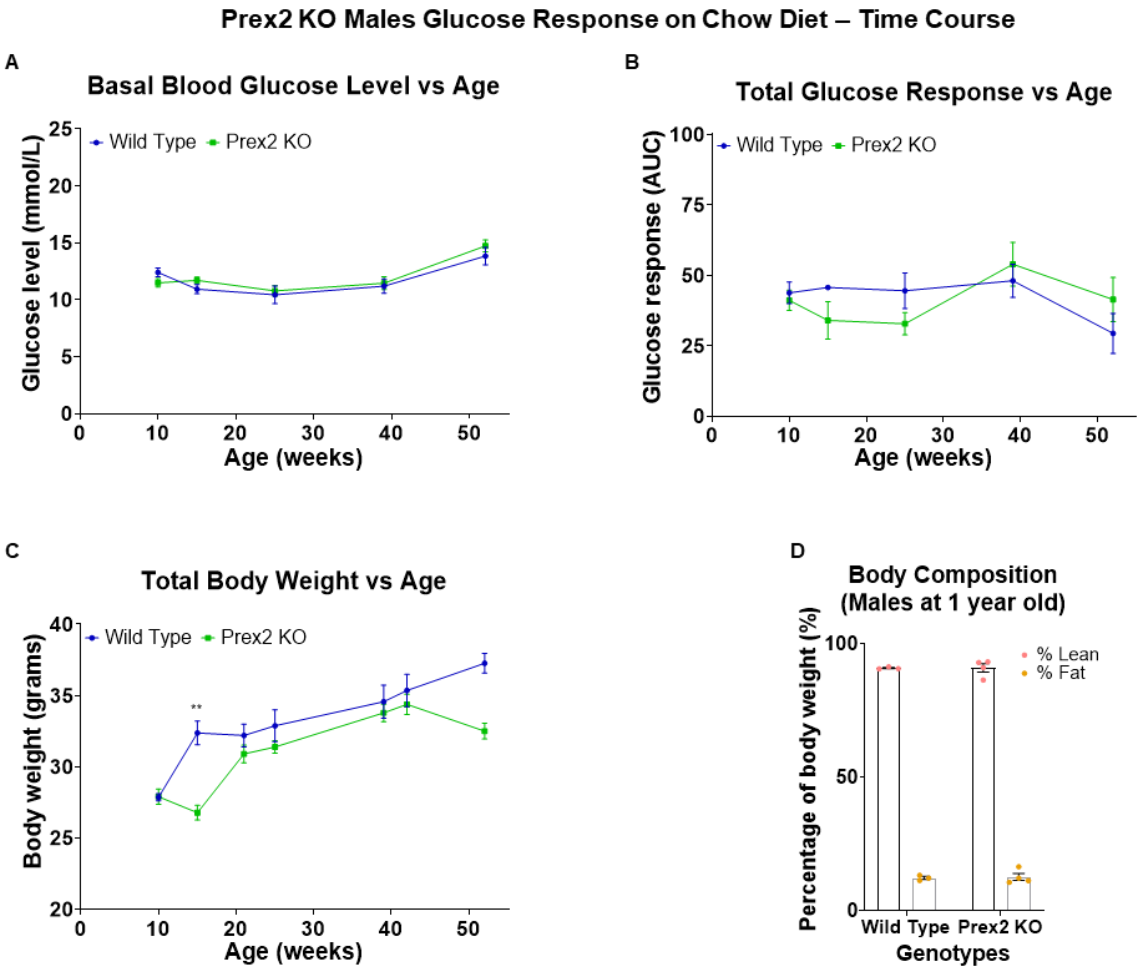

Figure 4.3.2: Male Prex2 KO mice on chow diet overall have a normal response to glucose challenge, with some age-related fluctuations.

The fasting blood glucose levels, response to glucose challenge, and body weight of the male Prex2 KO (green) and Prex WT (blue) mice in **Figure 4.3.1** are expressed as a function of age. **(A)** Fasting blood glucose levels; data from column A in **Figure 4.3.1**. **(B)** Response to IPGTT; normalised data from columns B and C in **Figure 4.3.1**. **(C)** Body weight, measured after 6 and 4 h fasting, prior to glucose and insulin challenges, respectively. **(D)** Body composition at 1 year of age. The mice in (**A-C**) were culled at 1 year of age and the cadavers were scanned by Echo MRI for lean mass and body fat. Data are pooled from 2 independent cohorts (Prex WT n=9; Prex2 KO n=9), and are presented as mean ± SEM. 2-way ANOVA with repeated measures and Sidak's multiple comparisons correction was used to compare genotypes during ageing. Unpaired Student's *t*-test was used to analyse the body composition.

Upon insulin challenge in 5 month-old mice, the blood glucose levels of Prex2 KO males dropped to their lowest level at 45 min post injection, by 5 mM, and returned to around 8 mM at 120 min (**Figure 4.3.3A,C**), similar to the response of the Prex WT controls. At 10 months however, Prex2 KO males showed increased insulin sensitivity compared to their Prex WT counterparts (**Figure 4.3.3G-H**), as their response to insulin was the same as at the young age (5 mM drop in blood glucose). In contrast, the Prex WT controls had developed insulin resistance, as their glucose levels only dropped by 3 mM, and returned to basal levels within 120 min (**Figure 4.3.3G**) Yet, the fasting blood glucose level of Prex2 KO mice was higher, and the absolute level of blood glucose, at the peak of the response, was similar between genotypes. As discussed previously for Prex1 KO mice, where a similar effect was observed, it seems possible that the counter-regulatory mechanisms to insulin were elicited more weakly in Prex WT than Prex2 KO mice in order to achieve similar homeostasis (**Figure 4.3.3E-F**).

It is worth pointing out that the Prex WT males in this cohort had lower basal glucose levels, a smaller response to glucose challenge from the age of 15 weeks onwards, and a reduced response to insulin at the age of 10 months compared to most male Prex WT cohorts on chow diet (see Supplementary Data, **Section 1**). Hence, there is a possibility that Prex2 KO deficiency actually leads to somewhat improved glucose tolerance and insulin sensitivity. In any event, it is clear that Prex2 KO mice on chow diet are not glucose intolerant or insulin resistant.

To complete the assessment of the metabolic phenotype of Prex2 KO males, the same cohort of mice was tested in the metabolic cages at 11 months of age, and no difference was found between Prex2 KO and Prex WT mice (**Figure 4.3.4F-I**). Interestingly, a separate cohort of 12 week-old mice was also tested in the metabolic cages, and these young Prex2 KO males showed significantly reduced water and food consumption, as well as reduced urine production, compared to Prex WT controls (**Figure 4.3.4B-E**) despite being heavier (**Figure 4.3.4A**). It may be useful to repeat the latter experiment with a different cohort of young mice for confirmation.

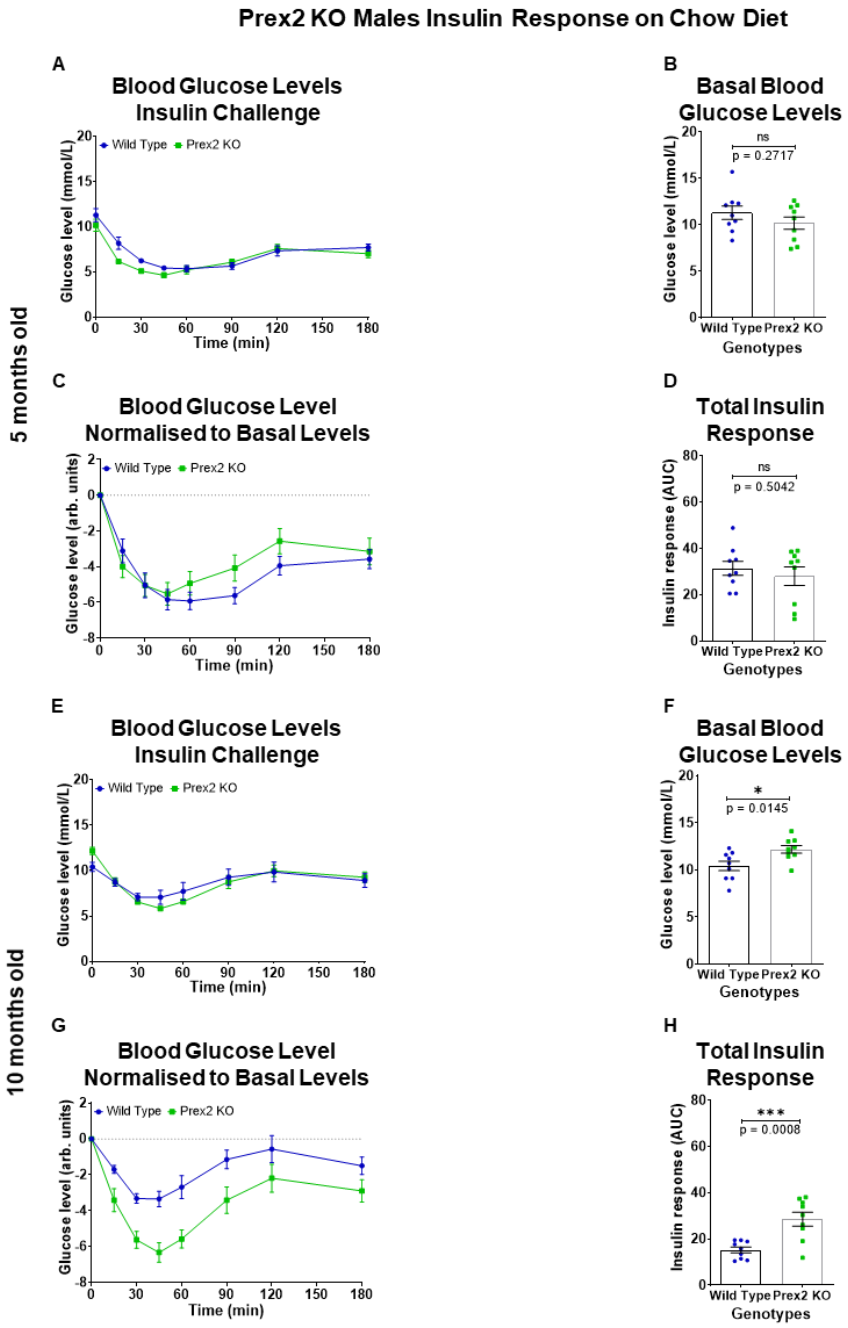

Figure 4.3.3: Prex2 KO male mice on chow diet show an apparent increase in insulin sensitivity in old age.

The fasting blood glucose levels and response to SCITT were measured in the male Prex2 KO (green) and Prex WT (blue) mice on chow diet from **Figure 4.3.1** at the ages of **(A-D)** 5 and **(E-H)** 10 months, as described in the legend to **Figure 4.2.3**. **(A,E)** Blood glucose concentration during SCITT. **(B,F)** Fasting blood glucose levels. **(C,G)** Blood glucose levels during SCITT, normalised by subtracting the fasting basal blood glucose level from each mouse individually. **(D,H)** Total insulin response (AUC of normalised data). Data are pooled from 2 independent cohorts (Prex WT n=9; Prex1 KO n=9) and are presented as mean ± SEM. 2-way ANOVA with repeated measures and Sidak's multiple comparisons correction was used to compare genotypes during SCITT. Unpaired Student's *t*-test was used to analyse the basal blood glucose level and total insulin response.

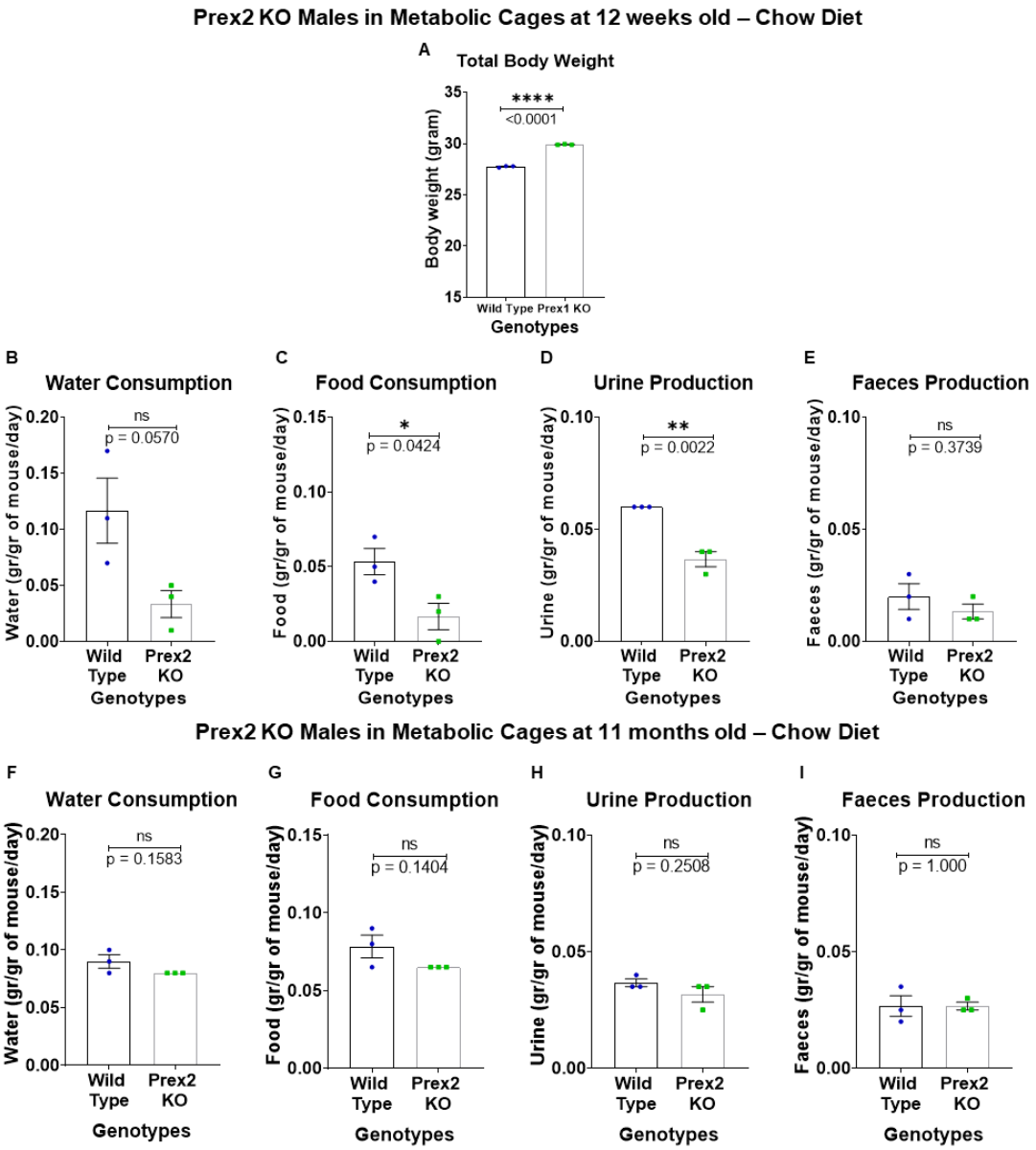

Figure 4.3.4: Young, but not old, male Prex2 KO mice are less active in metabolic cages than Prex WT mice.

Male Prex2 KO (green) and Prex2 WT (blue) mice were habituated to metabolic cages at the age of 12 weeks **(A-E)** and 11 months **(F-I)** as detailed in Materials and Methods, weighed and group-housed (up to 3) in metabolic cages overnight for 16 h on 3 subsequent nights with food and water provided *ad libitum*. Their **(B,F)** water consumption, **(C,G)** food consumption, **(D,H)** urine production, and **(E,I)** faeces production were measured after each night and were normalised to the combined body weights of the mice housed in each cage. **(A)** Body weight of 12 weeks old males on chow diet. **(A-E)** Data are from 1 cohort of 12 week-old males on chow diet (Prex WT n=6; Prex2 KO n=6). **(F-I)** Data are pooled from the 2 independent cohorts of male Prex2 KO and Prex WT mice on chow diet in **Figure 4.3.1**, tested at the age of 11 months (Prex WT n=9; Prex2 KO n=9). Data are presented as the mean ± SEM of each night (n=3), and unpaired Student's *t*-test was used for the comparison between genotypes.

4.3.2 Male Prex2 KO mice on HFD have lower fasting blood glucose levels but worse glucose tolerance than Prex WT mice

Prex2 KO males were introduced to 45% HFD at 10 weeks of age. As shown in **Figure 4.3.5A**, although they had similar basal blood glucose levels to their Prex WT counterparts at 10 weeks, they then maintained lower fasted blood glucose levels up to 9 months of age. However, Prex2 deficiency was not enough to protect them from glucose intolerance. Similarly to Prex WT, HFD caused a rapid onset of glucose intolerance in Prex2 KO males (**Figure 4.3.5A**). During glucose challenge, the blood glucose levels kept increasing beyond the 15 min time point, reaching 41 mM at 30 min and remaining around 40 mM within the 90 min of the test. Normalisation of the glucose response revealed that Prex2 KO mice had slightly worse glucose tolerance than Prex WT mice throughout ageing (**Figure 4.3.5B-C**). As described before, the dosage of glucose in IPGTTs was reduced from 6 months onwards to one quarter of the original dose (0.5 g/kg, data in ochre box). The graphs within the ochre box show that, under these conditions, glucose triggered a milder response in both genotypes (**Figure 4.3.5C**), but it still took longer for blood glucose levels to return to normal (**Figure 4.3.5B**), and importantly Prex2 KO males were more glucose intolerant under these conditions than the WT controls.

The effects of ageing are summarised in **Figure 4.3.6**. As mentioned above, the HFD-induced increase in fasting blood glucose levels was delayed in male Prex2 KO mice, remaining significantly lower than in Prex WT controls until the age of 9 months (**Figure 4.3.6A**). Furthermore, the glucose tolerance of Prex2 KO mice on HFD was worse than that of Prex WT males at most ages, and this reached significance at the age of 9 months (**Figure 4.3.6B**).

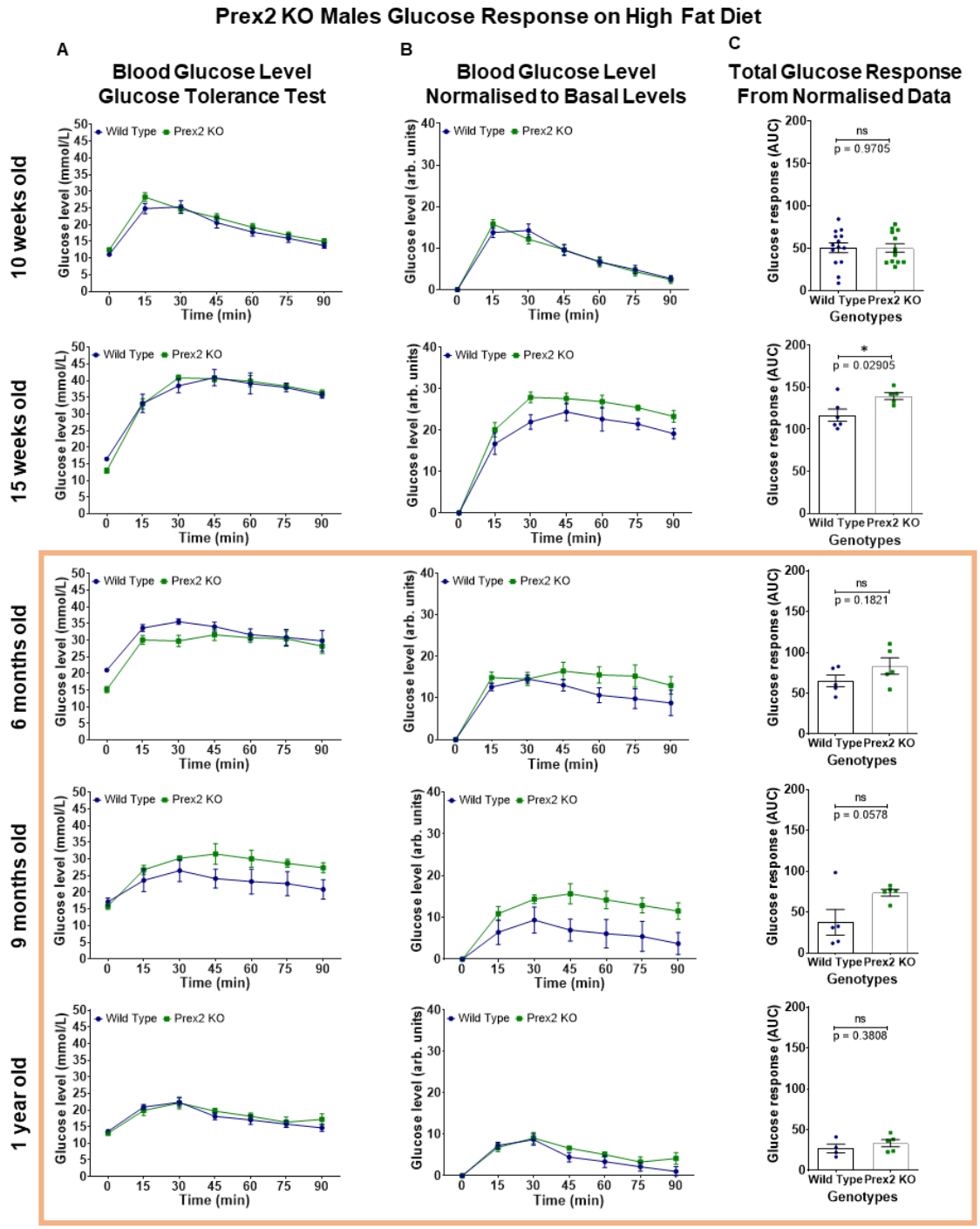

Figure 4.3.5: Male Prex2 KO mice on HFD show reduced glucose tolerance.
The fasting blood glucose levels and response to IPGTT were measured in male Prex2 KO (green) and Prex WT (blue) mice on 45% HFD at the ages of 10 and 15 weeks, 6, 9 and 12 months, as described in the legend to **Figure 4.2.1**. **(A)** Blood glucose concentration during IPGTT. The dose of glucose used in the IPGTT was 2 g/kg at the ages of 10 and 15 weeks, and 0.5 g/kg thereafter (data in ochre box) **(B)** Blood glucose levels during IPGTT, normalised by subtracting the basal blood glucose level. **(C)** Total glucose response (AUC of normalised data). Data are pooled from 1-2 independent cohorts with 4-5 mice per genotype each, and are presented as mean ± SEM. 2-way ANOVA with repeated measures and Sidak's multiple comparisons correction was used to compare genotypes during IPGTT. Unpaired Student's *t*-test was used to analyse the total glucose response.

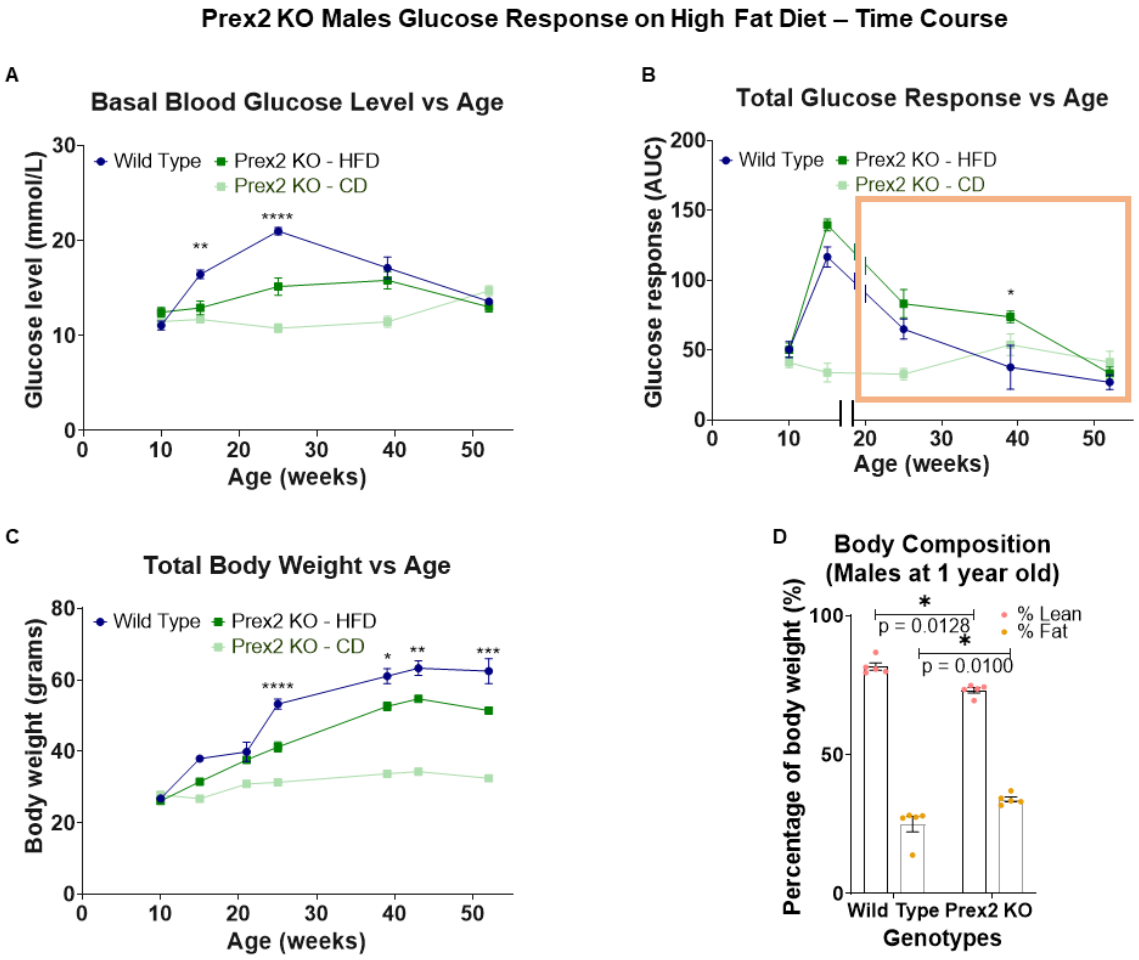

Figure 4.3.6: Male Prex2 KO mice on HFD weigh less and have lower fasting blood glucose levels than WTs, but are glucose intolerant throughout most of their lives. The fasting blood glucose levels, response to glucose challenge, and body weight of the male Prex2 KO (green) and Prex WT (blue) mice in **Figure 4.3.5** are expressed as a function of age. Note that the dose of glucose was reduced from 2 g/kg to 0.5 g/kg from the age of 6 months onwards (data in ochre box). In pale green are represented the Prex2 KO male mice on chow diet from **Figure 4.3.1** for comparison, but these mice were not included in the statistical analysis as they were not directly compared experimentally. **(A)** Fasting blood glucose levels; data from column A in **Figure 4.3.5**. **(B)** Response to IPGTT; normalised data from columns B and C in **Figure 4.3.5**. **(C)** Body weight, measured after 6 and 4 h fasting, prior to glucose and insulin challenges, respectively. Data are pooled from 1-2 independent cohorts with 4-5 mice per genotype each, and are presented as mean ± SEM. 2-way ANOVA with repeated measures and Sidak's multiple comparisons correction was used to compare genotypes during ageing. **(D)** Body composition at 1 year of age. The mice in (**A-C**) were culled at 1 year of age and the cadavers were scanned by Echo MRI for lean mass and body fat. Data from 1 cohort (Prex WT n=5; Prex1 KO n=5) and presented as mean ± SEM. Unpaired Student's *t*-test was used to analyse the body composition.

At 5 months of age, the overall response of Prex2 KO males on HFD to insulin challenge was similar to that of Prex WT mice. Although they had an accelerated counter-regulatory response, meaning their blood glucose returned towards fasting levels slightly more rapidly (**Figure 4.3.7A-D**). In contrast, at 10 months of age, Prex2 KO males demonstrated a pronounced reduction in insulin sensitivity. Their total response to insulin being half that of Prex WT mice (**Figure 4.3.7 E-H**), indicating that Prex2 KO males on HFD develop age-related insulin resistance which is more severe than in Prex WT mice.

Although the two genotypes had identical body weight at the onset of the study, Prex2 KO males gained weight more slowly and were significantly lighter than Prex WT mice from 6 months of age onwards (**Figure 4.3.6C**). Surprisingly, the body composition analysis, at 1 year, revealed that Prex2 KO males on HFD had increased body fat percentage compared to the heavier Prex WT controls (**Figure 4.3.6D**). Their lower body weight would argue against their having worse glucose tolerance than WTs, but the increased body fat of Prex2 KO males on HFD could be a contributing factor to their glucose intolerant and insulin resistant phenotype. Finally, no difference was found in the water and food consumption, or urine and faeces production of Prex2 KO mice on HFD in metabolic cages (**Figure 4.3.8A-D**).

To summarise the metabolic phenotype of Prex2 KO males, Prex2 deficiency did not obviously affect the fasting blood glucose levels, glucose tolerance or insulin sensitivity of mice on chow diet, in contrast to an earlier report by the Parsons lab (Hodakoski et al., 2014). Importantly, however, Prex2 deficiency rendered mice on HFD glucose intolerant and insulin resistant in old age.

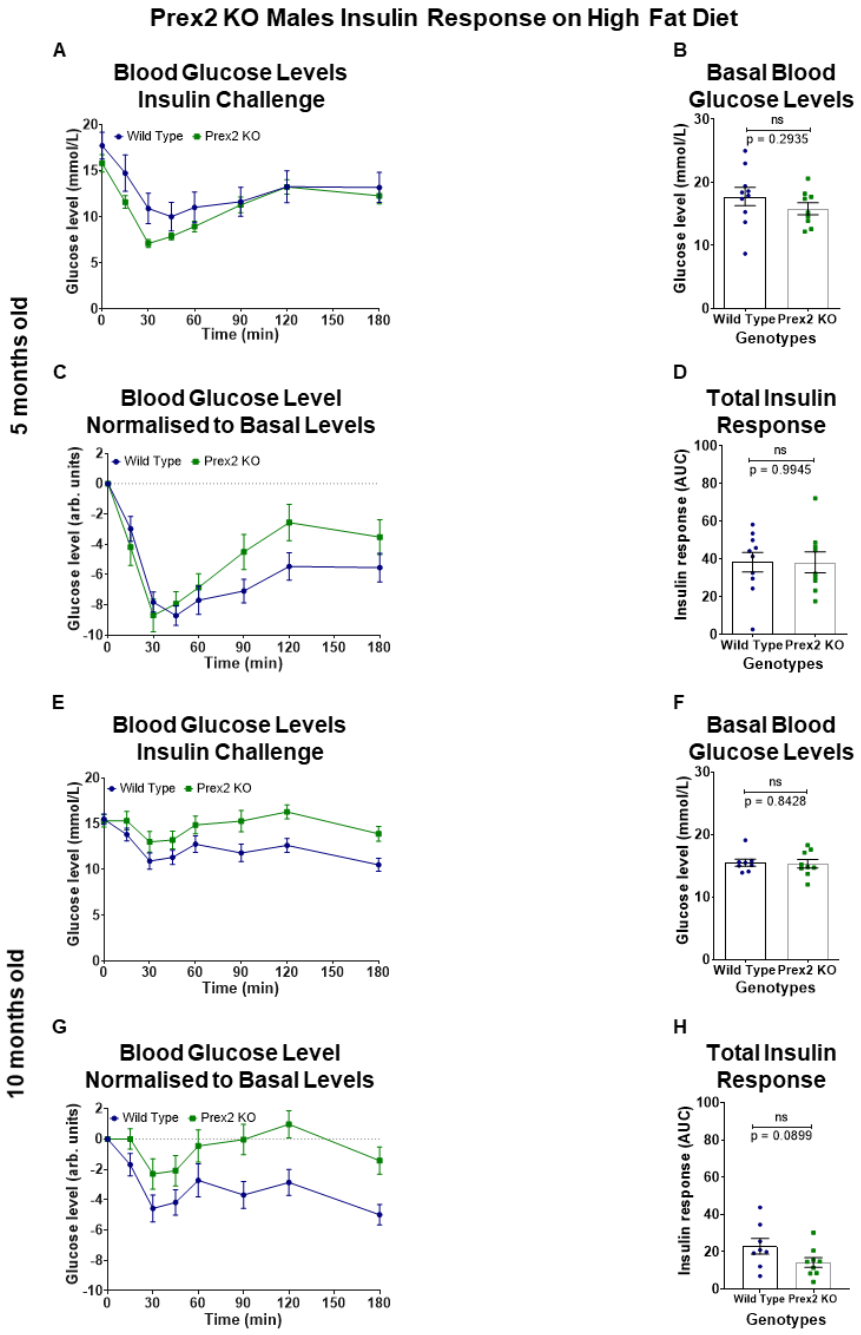

Figure 4.3.7: Male Prex2 KO mice on HFD become insulin resistant in old age.
The fasting blood glucose levels and response to SCITT were measured in the male Prex2 KO (green) and Prex WT (blue) mice on 45% HFD from **Figure 4.3.5** at the age of **(A-D)** 5 and **(E-H)** 10 months, as described in the legend to **Figure 4.2.3**. **(A,E)** Blood glucose concentration during SCITT. **(B,F)** Fasting blood glucose levels. **(C,G)** Blood glucose levels during SCITT, normalised by subtracting the fasting basal blood glucose level from each mouse individually. **(D,H)** Total insulin response (AUC of normalised data). Data are pooled from 2 independent (Prex WT n=8; Prex2 KO n=9), and are presented as mean ± SEM. 2-way ANOVA with repeated measures and Sidak's multiple comparisons correction was used to compare genotypes during SCITT. Unpaired Student's *t*-test was used to analyse the basal blood glucose level and total insulin response.

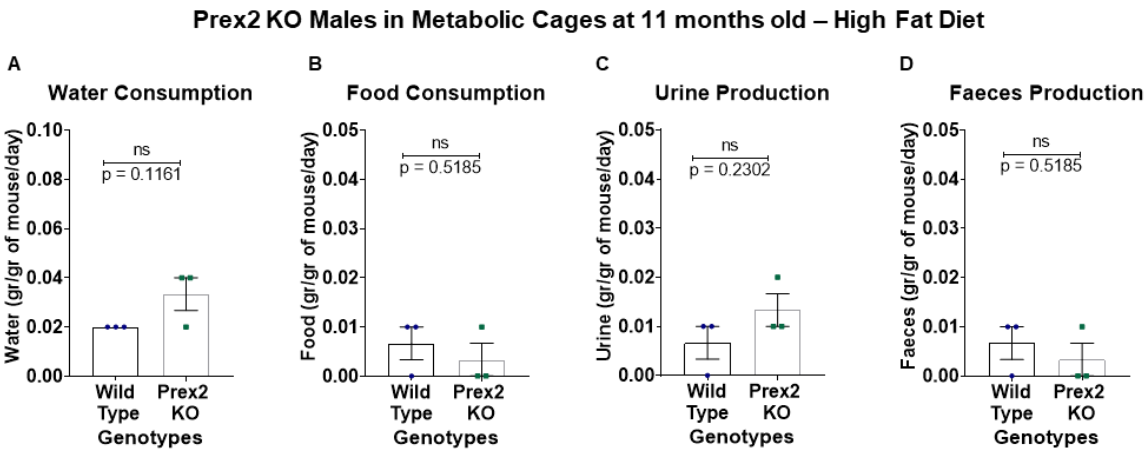

Figure 4.3.8: Male Prex2 KO mice perform normally in metabolic cages.
The male Prex2 KO (green) and Prex WT (blue) mice from **Figure 4.3.5** were habituated to metabolic cages at 11 months of age, as detailed in Materials and Methods, weighed and group-housed (up to 3) in metabolic cages overnight for 16 h on 3 subsequent nights with food and water provided *ad libitum*. Their **(A)** water consumption, **(B)** food consumption, **(C)** urine production, and **(D)** faeces production were measured after each night and were normalised to the combined body weights of the mice housed in each cage. Data are from 1 cohort (Prex WT n=5; Prex1 KO n=5). Data are presented as the mean ± SEM of each night (n=3), and unpaired Student's *t*-test was used for the comparison between genotypes.

4.3.3 Ageing female Prex2 KO mice on HFD show age-related fluctuations in their glucose tolerance

To investigate sex differences, the metabolic phenotype of female Prex2 KO mice was also tested. As can be seen from the representative graphs in **Figure 4.3.9**, and the ageing overview graphs in **Figure 4.3.10**, Prex2 females had normal fasting blood glucose levels (**Figures 4.3.9A** and **4.3.10A**) and a normal response to glucose challenge throughout ageing (**Figure 4.3.10B**). However, there was an interesting tendency for improved glucose tolerance at young age, and worse glucose tolerance at old age, similar to what was previously observed in the male Prex2 KO mice. However, neither the improved glucose tolerance at young age (up to 6 months) nor the reduced glucose tolerance at old age reached statistical significance. Furthermore, the apparently improved glucose tolerance at young age (up to 6 months) could be a reflection of the fact that the Prex WT controls in this cohort had a bigger glucose response than expected for Prex WT females (see Supplemental Data in **Section 6**). In addition, Prex2 KO females had normal responses to insulin both at 5 months and at 10 months of age (**Figure 4.3.11A-B**).

Despite Prex2 KO females being slightly heavier than their Prex WT counterparts, mice of both genotypes gained weight at a similar rate, and the body composition at one year of age was comparable between the two genotypes (**Figure 4.3.10C-D**). Furthermore, housing of the same mice in metabolic cages at 11 months of age did not reveal any differences either in their water and food intake or urine and faeces excretion (**Figure 4.3.12A-D**).

Hence, overall Prex2 deficiency did not have any significant effects on the metabolic phenotype of female mice on chow diet, although it did induce an interesting tendency to improved glucose tolerance in the young and worsened glucose tolerance in the old female mice.

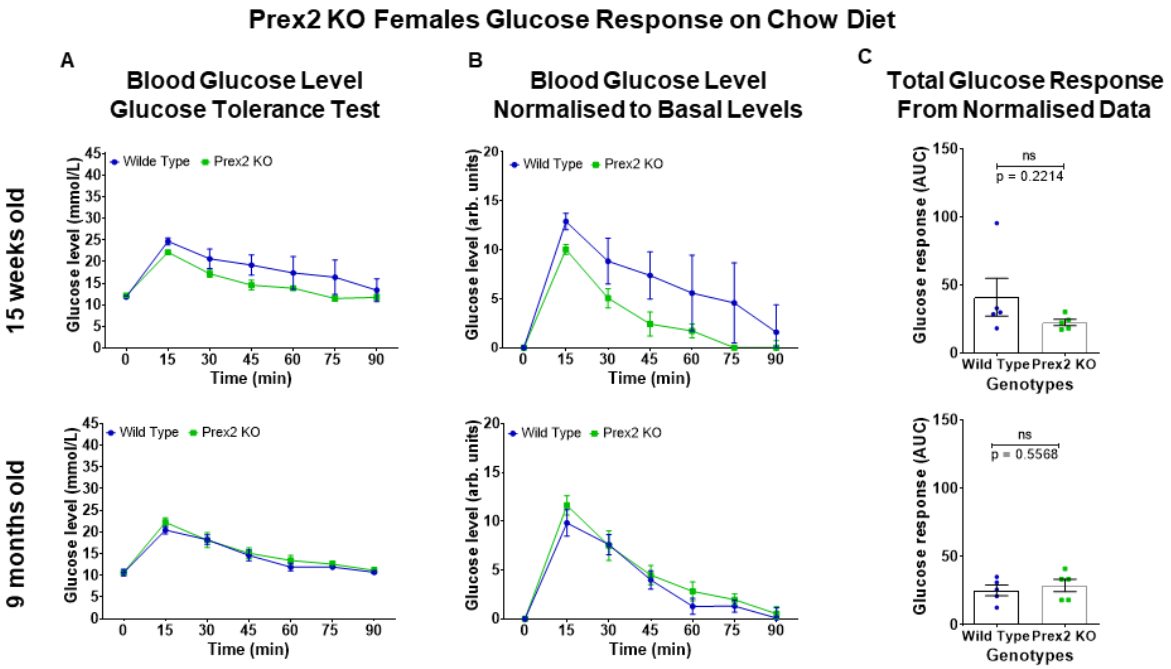

Figure 4.3.9: Female Prex2 KO mice on chow diet show similar fasting blood glucose levels and glucose tolerance to Prex WT mice.

The fasting blood glucose levels and response to IPGTT were measured in female Prex2 KO (green) and Prex WT (blue) mice on chow diet, as described in the legend to **Figure 4.2.1**. Only data from 15 weeks and 9 months of age are shown, for brevity, although mice of all ages up to one year were tested. **(A)** Blood glucose concentration during IPGTT. **(B)** Blood glucose levels during IPGTT, normalised by subtracting the basal blood glucose level. **(C)** Total glucose response (AUC of normalised data). Data are from 1 cohort (Prex WT n=5; Prex2 KO n=5), and are presented as mean ± SEM. 2-way ANOVA with repeated measures and Sidak's multiple comparisons correction was used to compare genotypes during IPGTT. Unpaired Student's *t*-test was used to analyse the total glucose response.

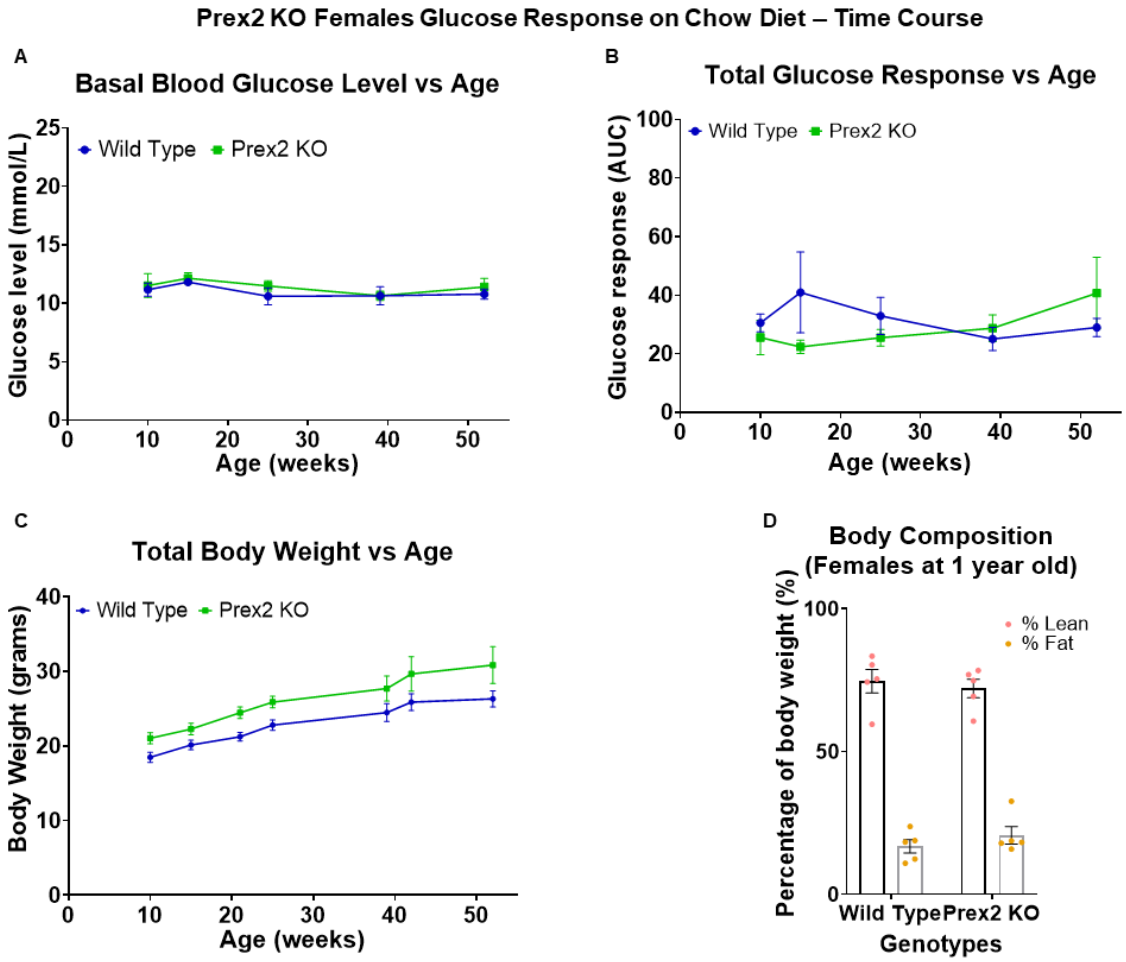

Figure 4.3.10: Female Prex2 KO mice on chow diet overall have a normal response to glucose challenge, with some age-related fluctuations.

The fasting blood glucose levels, response to glucose challenge, and body weight of the female Prex2 KO (green) and Prex WT (blue) mice in **Figure 4.3.9** are expressed as a function of age. **(A)** Fasting blood glucose levels; data from column A in **Figure 4.3.9**. **(B)** Response to IPGTT; normalised data from columns B and C in **Figure 4.3.9**. **(C)** Body weight, measured after 6 and 4 h fasting, prior to glucose and insulin challenges, respectively. **(D)** Body composition at 1 year of age. The mice in (**A-C**) were culled at 1 year of age and the cadavers were scanned by Echo MRI for lean mass and body fat. Data are from 1 cohort (Prex WT n=5; Prex2 KO n=5), and are presented as mean ± SEM. 2-way ANOVA with repeated measures and Sidak's multiple comparisons correction was used to compare genotypes during ageing. Unpaired Student's *t*-test was used to analyse the body composition.

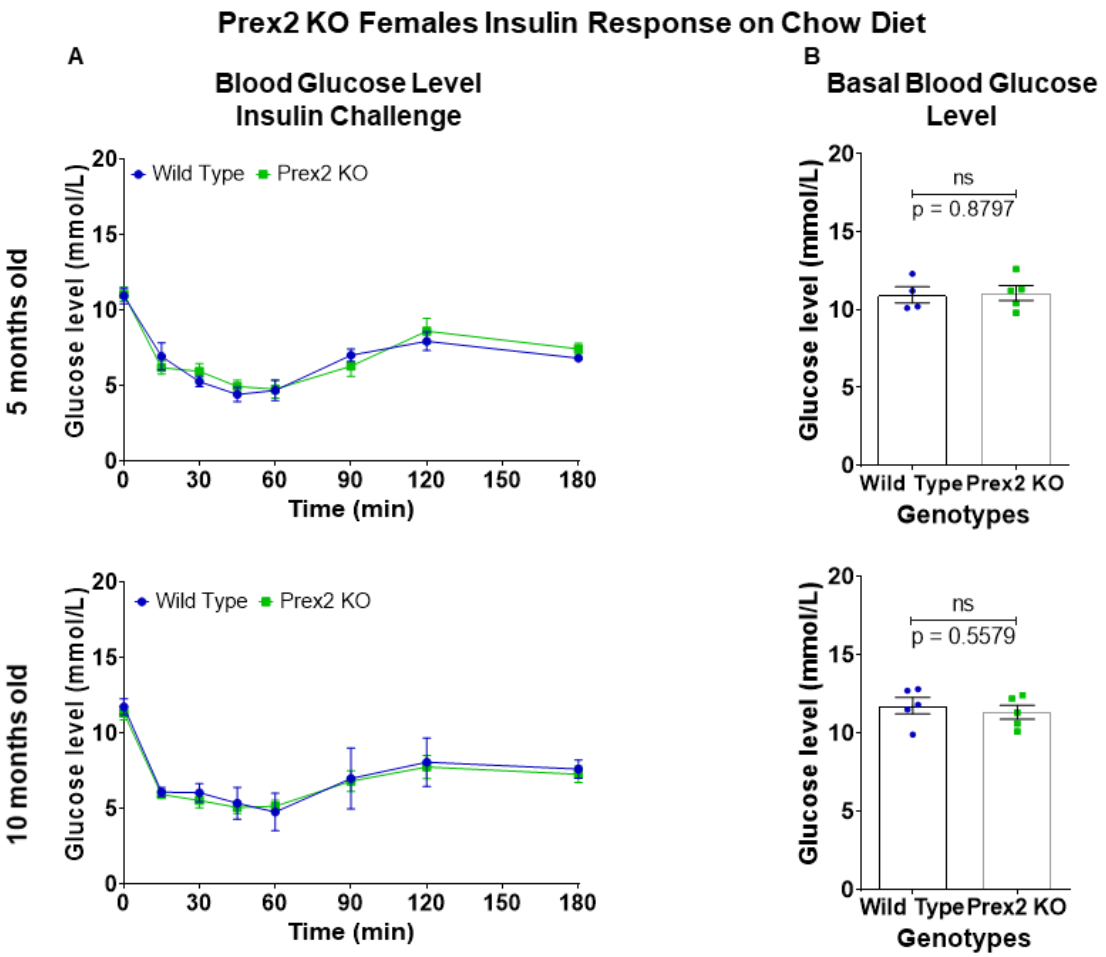

Figure 4.3.11: Female Prex2 KO mice on chow diet show a normal response to insulin challenge.

The fasting blood glucose levels and response to SCITT were measured in the female Prex2 KO (green) and Prex WT (blue) mice from **Figure 4.3.9** on chow diet at the ages of 5 and 10 months, as described in the legend to **Figure 4.2.3**. **(A)** Blood glucose concentration during SCITT. **(B)** Fasting blood glucose levels. Data are from 1 cohort (Prex WT n=5; Prex2 KO n=5), and are presented as mean ± SEM. 2-way ANOVA with repeated measures and Sidak's multiple comparisons correction was used to compare genotypes during SCITT. Unpaired Student's *t*-test was used to analyse the basal blood glucose levels.

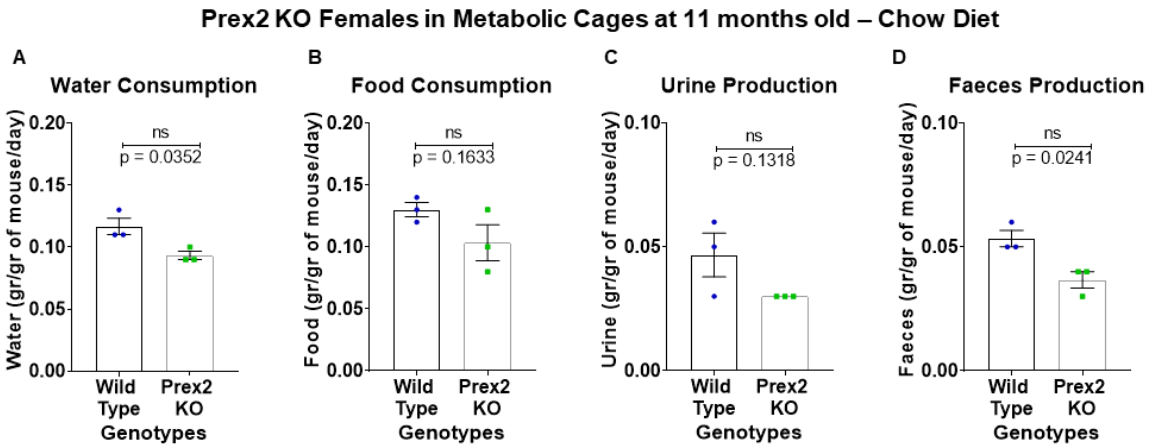

Figure 4.3.12: Female Prex2 KO mice performed normally in metabolic cages.
The female Prex2 KO (green) and Prex WT (blue) mice from **Figure 4.3.9** were habituated to metabolic cages at 11 months of age, as detailed in Materials and Methods, weighed and group-housed (up to 3) in metabolic cages overnight for 16 h on 3 subsequent nights with food and water provided *ad libitum*. Their **(A)** water consumption, **(B)** food consumption, **(C)** urine production, and **(D)** faeces production were measured after each night and were normalised to the combined body weights of the mice housed in each cage. Data are from 1 cohort (Prex WT n=5; Prex1 KO n=5) and are presented as the mean ± SEM of each night (n=3). Unpaired Student's *t*-test was used for comparison between genotypes.

Despite the lack of effect of Prex2 deficiency on the metabolic phenotype of female mice on chow diet, we were still interested in investigating whether introduction of the mice to HFD could unveil a role of Prex2 in glucose homeostasis, especially considering that a diet-dependent phenotype was seen in Prex2 KO males. To this end, Prex2 KO and Prex WT control female mice were fed HFD from 10 weeks of age until the end of the experiment at 1 year. Under these conditions, the fasting blood glucose levels of Prex2 KO mice remained identical to those of Prex WT controls (**Figure 4.3.13A** and **Figure 4.3.14A**). Interestingly, at 15 weeks and 6 months, when Prex WT mice started becoming glucose intolerant, the Prex2 KO females demonstrated a tendency to improved glucose clearance during IPGTT (**Figure 4.3.13A-C**), which was reversed to poorer glucose tolerance at later ages (**Figure 4.3.13A-C** and **Figure 4.3.14B**). This repeated the pattern of age-related effects on glucose tolerance that was previously observed in both male and female Prex2 KO mice on chow diet. The insulin sensitivity of Prex2-deficient females on HFD was normal (**Figure 4.3.15A-D**).

A possible reason for the apparent age-related switch from improved to worsened glucose tolerance could be that the Prex2 KO females on HFD were significantly heavier than the Prex WT controls from 9 months onwards (**Figure 4.3.14C**). **Figure 4.3.16** shows furthermore that Prex2 KO females also produced less faeces and urine than the Prex WT controls, although no significant difference was detected in their water and food intake, which might imply that these mice converted more energy into fat. Indeed, this was confirmed at 1 year of age by body composition analysis, when Prex2 KO females were found to have a higher body fat percentage (**Figure 4.3.14D**). Hence, whereas Prex2 KO males on HFD showed multiple signs of metabolic syndrome in their old age, the females put on more weight (and body fat) than WT controls, but did not develop metabolic syndrome.

In summary, Prex2 KO females did not show significant abnormalities in their glucose and insulin responses, except for a tendency to improved glucose tolerance at young age and worsened glucose intolerance at older age, both on chow and HFD.

Taken together, the results on the metabolic phenotype of Prex2 KO mice show that ageing male Prex2 KO mice on HFD develop significant glucose intolerance and insulin resistance. Ageing Prex2 KO males on chow diet, as well as Prex2 KO females on chow or HFD, also show a tendency to worsened glucose tolerance in old age, in spite of better glucose tolerance at young age and either normal or increased insulin sensitivity (**Table 4.2**).

Compared to Prex1 KO mice (**Section 4.2**), Prex2 KO mice showed almost the opposite metabolic phenotype. Where Prex1 deficiency improved glucose tolerance overall, Prex2 deficiency worsened it. Furthermore, only Prex2 deficiency but not Prex1 deficiency induced insulin resistance (**Table 4.2**).

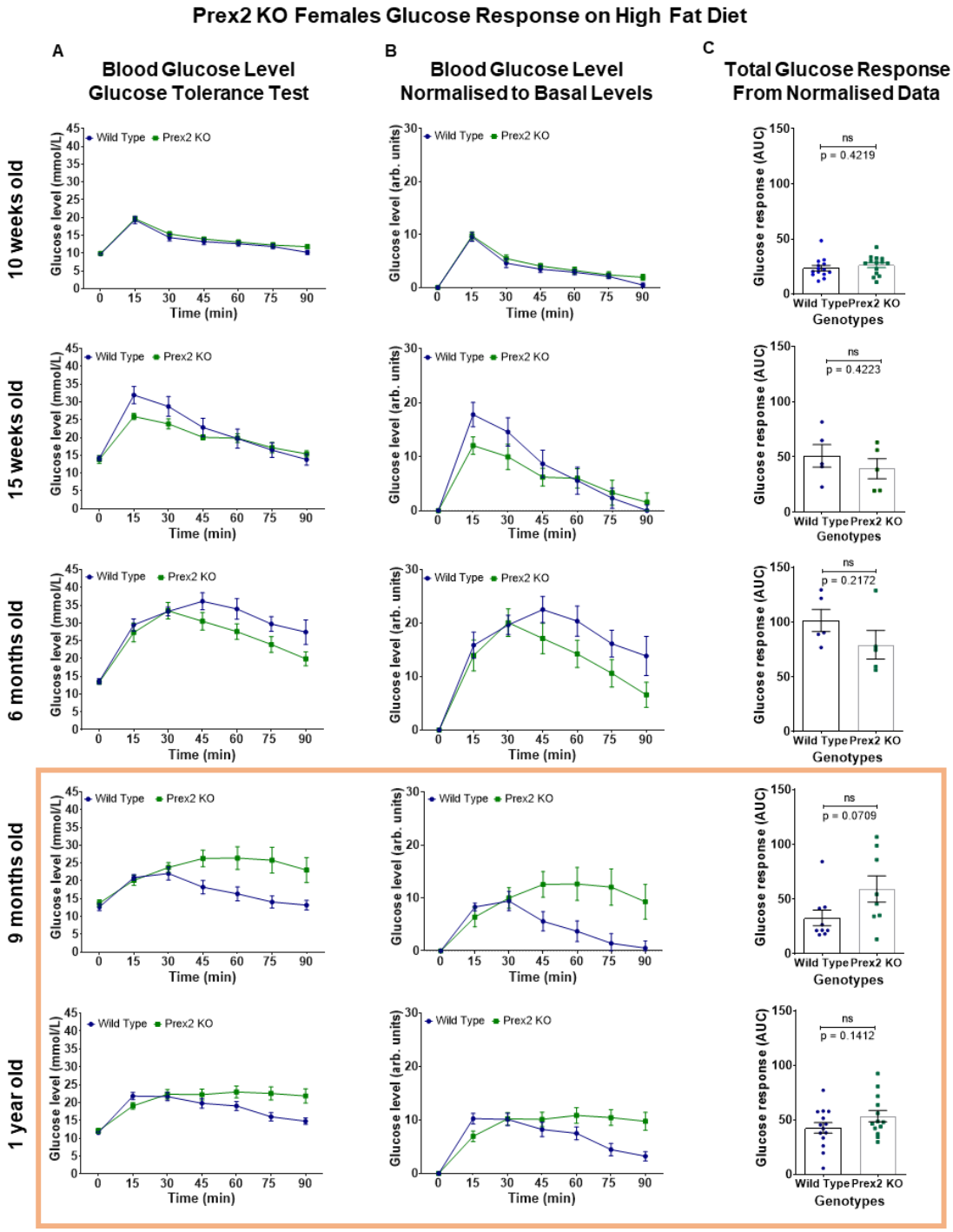

Figure 4.3.13: Female Prex2 KO mice on HFD show a tendency to age-dependent changes in glucose tolerance.

The fasting blood glucose levels and response to IPGTT were measured in female Prex2 KO (green) and Prex WT (blue) mice on 45% HFD at the ages of 10 and 15 weeks, 6, 9 and 12 months, as described in the legend to **Figure 4.2.1**. The ochre box denotes glucose challenge at the reduced dose of 1 g/kg instead of 2 g/kg. **(A)** Blood glucose concentration during IPGTT. **(B)** Blood glucose levels during IPGTT, normalised by subtracting the basal blood glucose level. **(C)** Total glucose response (AUC of normalised data). Data are pooled from 3 independent cohorts (Prex WT n=13; Prex2 KO n=15), and are presented as mean ± SEM. 2-way ANOVA with repeated measures and Sidak's multiple comparisons correction was used to compare genotypes during IPGTT. Unpaired Student's *t*-test was used to analyse the total glucose response.

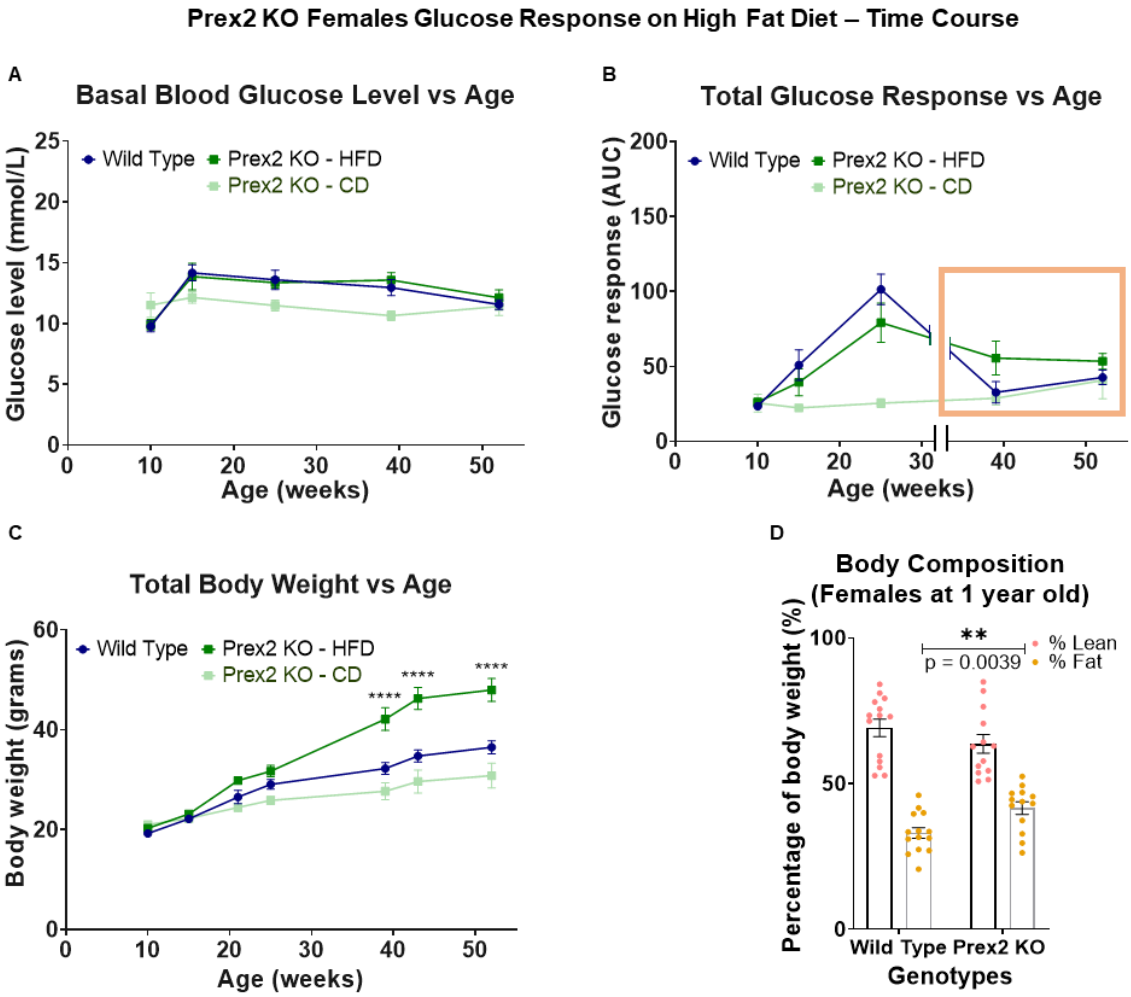

Figure 4.3.14: Ageing female Prex2 KO mice on HFD overall show normal glucose tolerance, with some age-related fluctuation.

The fasting blood glucose levels, response to glucose challenge, and body weight of the female Prex2 KO (green) and Prex WT (blue) mice on 45% HFD from **Figure 4.3.13** are expressed as a function of age. In pale green are represented the Prex2 KO female mice on chow diet from **Figure 4.3.9** for visual comparison, but were not included in the statistical analysis, as these animals were not directly compared experimentally. **(A)** Fasting blood glucose levels; data from column A in **Figure 4.3.13**. **(B)** Response to IPGTT; normalised data from columns B and C in **Figure 4.3.13**. **(C)** Body weight, measured after 6 and 4 h fasting, prior to glucose and insulin challenges, respectively. **(D)** Body composition at 1 year of age. The mice in (**A-C**) were culled at 1 year of age and the cadavers were scanned by Echo MRI for lean mass and body fat. Data are pooled from 3 independent cohorts (Prex WT n=13; Prex2 KO n=15), and are presented as mean ± SEM. 2-way ANOVA with repeated measures and Sidak's multiple comparisons correction was used to compare genotypes during ageing. Unpaired Student's *t*-test was used to analyse the body composition.

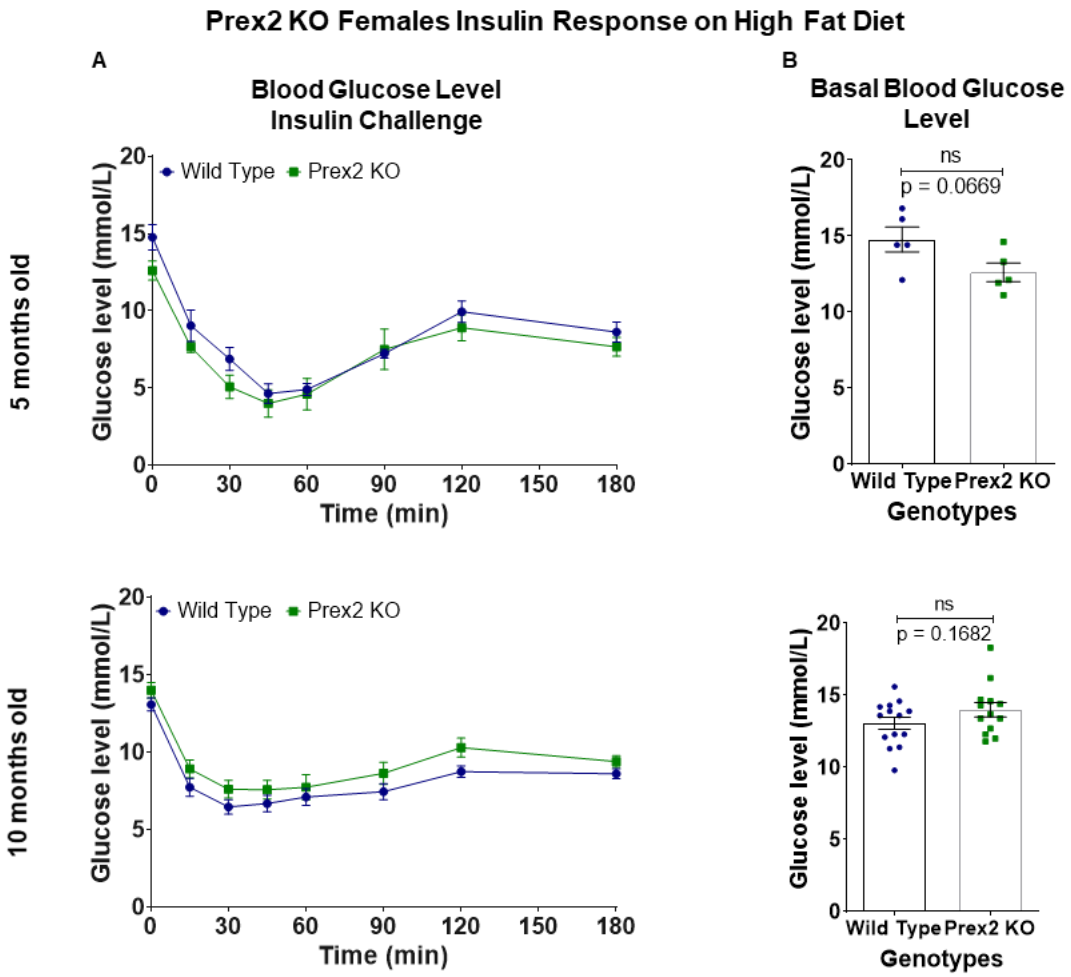

Figure 4.3.15: Female Prex2 KO mice on HFD show a normal response to insulin challenge.

The fasting blood glucose levels and response to SCITT were measured in the female Prex2 KO (green) and Prex WT (blue) mice on 45% HFD from **Figure 4.3.13** at the age of 5 and 10 months, as described in the legend to **Figure 4.2.3**. **(A)** Blood glucose concentration during SCITT. **(B)** Fasting blood glucose levels. Data from 1 cohort (Prex WT n=5; Prex2 KO n=5), and are presented as mean ± SEM. 2-way ANOVA with repeated measures and Sidak's multiple comparisons correction was used to compare genotypes during SCITT. Unpaired Student's *t*-test was used to analyse the basal blood glucose levels.

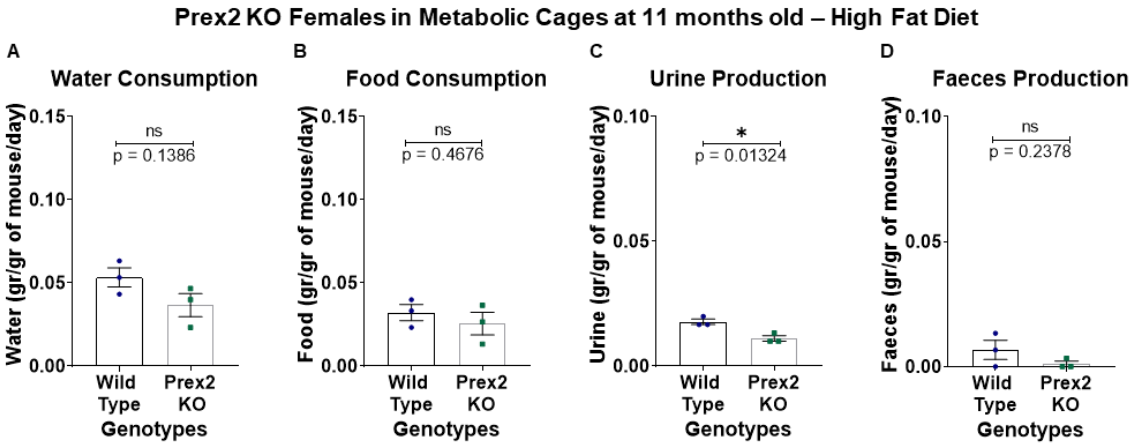

Figure 4.3.16: Female Prex2 KO mice on HFD produce less urine than Prex WT mice.

The female Prex2 KO (green) and Prex WT (blue) mice from **Figure 4.3.13** were habituated to metabolic cages at 11 months of age, as detailed in Materials and Methods, weighed and group-housed (up to 3) in metabolic cages overnight for 16 h on 3 subsequent nights with food and water provided *ad libitum*. Their **(A)** water consumption, **(B)** food consumption, **(C)** urine production, and **(D)** faeces production were measured after each night and were normalised to the combined body weights of the mice housed in each cage. Data are pooled from 3 independent cohorts (Prex WT n=13; Prex2 KO n=15), and are presented as the mean ± SEM of each night (n=3). Unpaired Student's *t*-test was used for the comparison between the genotypes.

Table 4.2: Summary table of metabolic phenotype of Prex1 KO, and Prex2 KO mice on chow or high fat diet. Bold font was used to annotate findings that reached statistical significance in most time points tested, while bold and italic font was used to indicate strong trends that show statistical significance in only one or two time points tested.

		Prex1 KO		Prex2 KO		Prex1/2 DKO	
		Male	**Female**	**Male**	**Female**	**Male**	**Female**
Chow Diet	**Fasting Blood Glucose**	**Low fasting blood glucose**	Tendency to low fasting blood glucose	Normal	Normal		
	Glucose Tolerance	**Improved glucose tolerance throughout ageing**	Tendency to improved glucose tolerance in old age	Tendency to improved glucose tolerance in young and worse in old age	Tendency to improved glucose tolerance in young and worse in old age		
	Insulin Response	Apparent insulin resistance in old age	Normal	Apparent increase in insulin sensitivity in old age	Normal		
High Fat Diet	**Fasting Blood Glucose**	***Low fasting blood glucose***	Normal	***Low fasting blood glucose***	Normal		
	Glucose Tolerance	Normal	***Improved glucose tolerance (some ages)***	***Glucose intolerance***	Tendency to improved glucose tolerance in young and worse in old age		
	Insulin Response	Normal	Normal	***Insulin resistance in old age***	Normal		

4.4 Metabolic phenotype of Prex1/2 DKO mice

Given that Prex1 and Prex2 deficiencies had almost opposing effects on the metabolic phenotype of mice, we wanted to explore how the absence of both Prex proteins would affect mouse glucose homeostasis. Therefore *Prex1*$^{-/-}$;*Prex2*$^{-/-}$ (Prex1/2 DKO) mice were studied, as described previously for the single KO mice. Prex1/2 DKO and Prex WT mice of same age and sex were tested in parallel under the same conditions for direct comparison.

4.4.1 Male Prex1/2 DKO mice on chow diet have normal homeostasis throughout ageing

Prex1/2 DKO males on chow diet had similar fasting blood glucose levels to Prex WT controls throughout ageing, with a tendency to lower levels than controls in old age (**Figures 4.4.1A** and **4.4.2A**). Moreover, although the two genotypes had an identical glucose response at most ages, the Prex1/2 DKO appeared to have better glucose tolerance at 6 months (**Figures 4.4.1B-C** and **4.4.2B**). This is more reminiscent of the Prex1 KO phenotype than the Prex2 KO phenotype, although it was less pronounced. Furthermore, it should be pointed out that the Prex WT controls tested here in parallel had an overall bigger response to glucose challenge than average Prex WT males, and therefore it is possible that the increased glucose tolerance at 6 months of age might not stand if further cohorts were tested.

Upon insulin challenge, the blood glucose levels of Prex1/2 DKO males dropped to their lowest level at 45 min post injection and returned to around 8 mM at 120 min, similar to their Prex WT controls, and as typical for these conditions (**Figure 4.4.3A**). However, as seen previously in Prex1 KO males, this was confounded by the fact that the fasting blood glucose levels of Prex1/2 DKO males were slightly lower than that of Prex WT controls. Normalisation of the data revealed that the blood glucose of Prex1/2 DKO mice dropped by 3 mM, contrary to the Prex WT controls whose glucose levels dropped by 5 mM (**Figure 4.4.3B-D**). As discussed for the single KO mice above, it is suspected that the different levels of fasting blood glucose cause homeostatic mechanisms to be engaged to a different extent in order to achieve similar glucose homeostasis overall. At 10 months of age, the Prex1/2 DKO males showed a slightly increased and longer-lived response to insulin compared to the Prex WT mice, but not significantly so, which again

suggested that the insulin sensitivity of Prex1/2 DKO mice on chow diet is normal (**Figure 4.4.3E-H**).

Prex1/2 KO mice were leaner than their Prex WT counterparts throughout ageing, and from 10 months this reached statistical significance (**Figure 4.4.2C**), although there was no difference in the body composition between Prex1/2 DKO and Prex WT mice at 1 year (**Figure 4.4.2D**). What is more, no difference was found in the water and food intake or the urine and faeces production between Prex1/2 DKO males and controls when they were housed in metabolic cages at 11 months of age (**Figure 4.4.4A-D**).

Overall, it seems that on chow diet, deficiency in both Prex proteins causes a phenotype that is similar to the Prex1 KO phenotype, but milder. As the phenotype of the DKO mice is not worse than either of the single KOs', there is no obvious redundancy between the Prex proteins in the control of glucose homeostasis under chow diet conditions. Furthermore, as the phenotype of the DKO mice is milder than that of Prex1 KO mice, it can be hypothesised that currently unidentified regulators of glucose homeostasis compensate for the absence of both Prex proteins, which is not required when only one Prex protein is deleted.

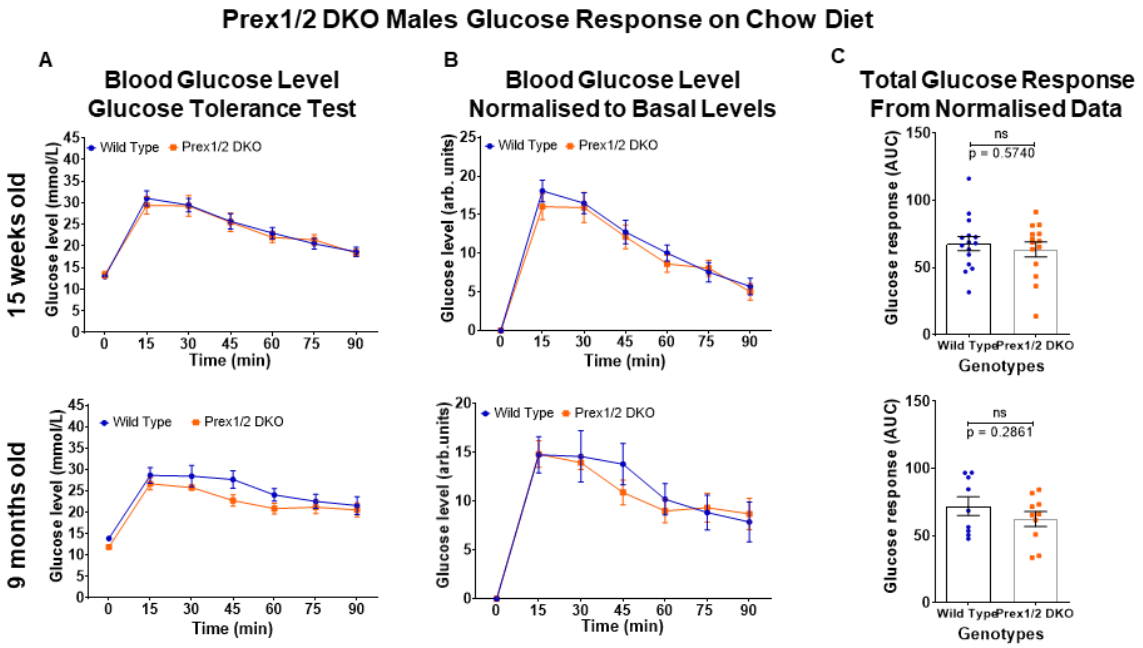

Figure 4.4.1: Male Prex1/2 DKO mice on chow diet show similar fasting blood glucose levels and glucose tolerance to Prex WT mice.

The fasting blood glucose levels and response to IPGTT were measured in male *Prex1*$^{-/-}$;*Prex2*$^{-/-}$ (Prex1/2 DKO, orange) and Prex WT (blue) mice on chow diet, as described in the legend to **Figure 4.2.1**. Only data from 15 weeks and 9 months of age are shown, for brevity, although mice of all ages up to one year were tested. **(A)** Blood glucose concentration during IPGTT. **(B)** Blood glucose levels during IPGTT, normalised by subtracting the basal blood glucose level. **(C)** Total glucose response (AUC of normalised data). Data are pooled from 2-3 independent cohorts with 4-5 mice per genotype, and are presented as mean ± SEM. 2-way ANOVA with repeated measures and Sidak's multiple comparisons correction was used to compare genotypes during IPGTT. Unpaired Student's *t*-test was used to analyse the total glucose response.

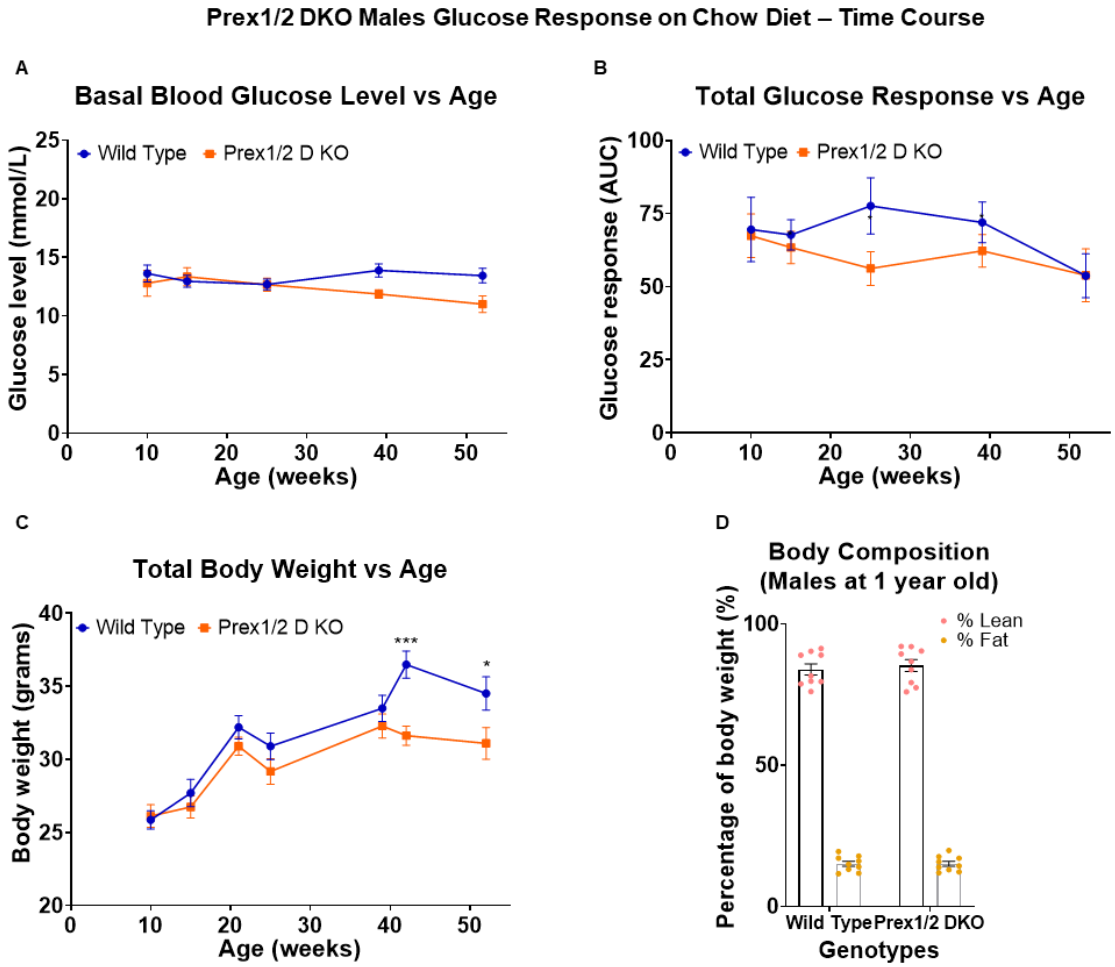

Figure 4.4.2: Old male Prex1/2 DKO mice on chow diet have a tendency to low fasting blood glucose levels and middle-aged mice appear to have somewhat improved glucose tolerance.

The fasting blood glucose levels, response to glucose challenge, and body weight of the male Prex1/2 DKO (orange) and Prex WT (blue) mice in **Figure 4.4.1** are expressed as a function of age. **(A)** Fasting blood glucose levels; data from column A in **Figure 4.4.1**. **(B)** Response to glucose challenge (IPGTT); normalised data from columns B and C in **Figure 4.4.1**. **(C)** Body weight, measured after 6 and 4 h fasting, prior to glucose and insulin challenges, respectively. Data are pooled from 2-3 independent cohorts with 4-5 mice per genotype, and are presented as mean ± SEM. 2-way ANOVA with repeated measures and Sidak's multiple comparisons correction was used to compare genotypes during ageing. **(D)** Body composition at 1 year of age. The mice in (**A-C**) were culled at 1 year of age and the cadavers were scanned by Echo MRI for lean mass and body fat. Data are pooled from 2 independent cohorts (Prex WT n=9; Prex1/2 DKO n=9) and presented as mean ± SEM. Unpaired Student's *t*-test was used to analyse the body composition.

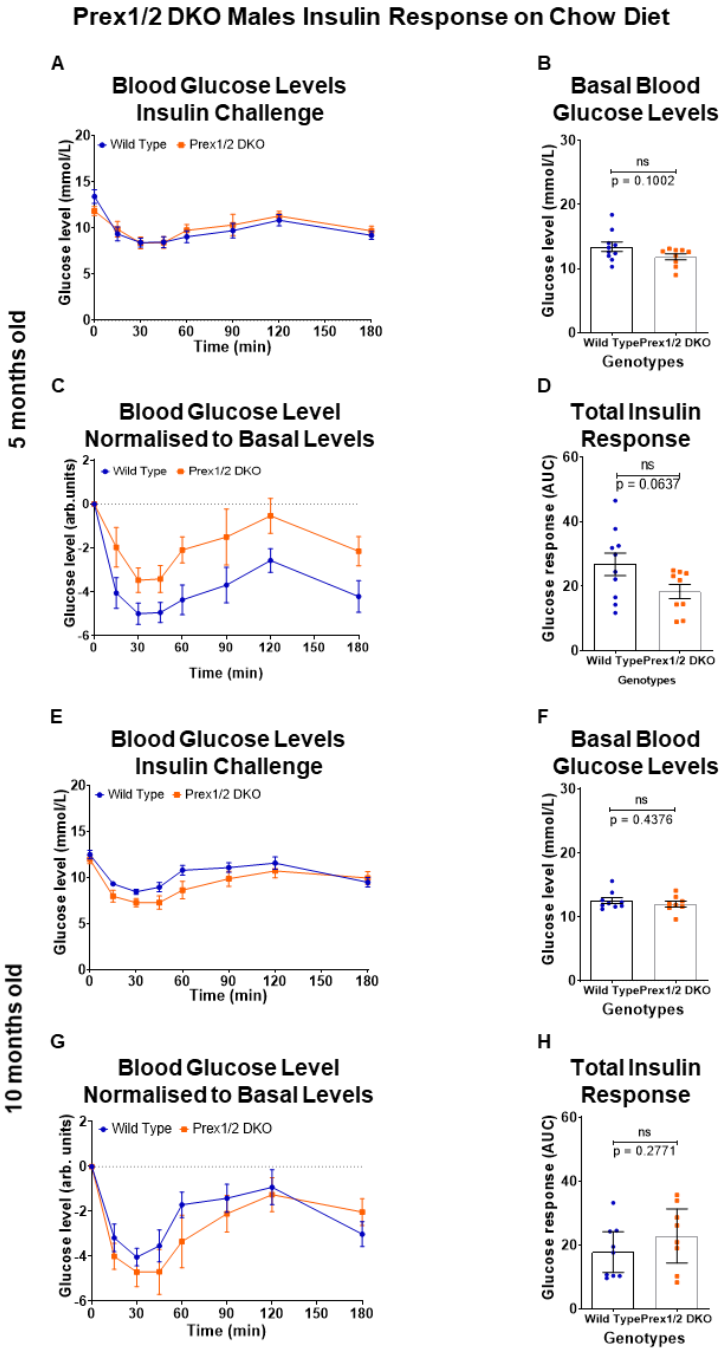

Figure 4.4.3: Male Prex1/2 DKO mice on chow diet apparently show a reduced response to insulin challenge in middle age.

The fasting blood glucose levels and response to SCITT were measured in the male Prex1/2 DKO (orange) and Prex WT (blue) mice on chow diet from **Figure 4.4.1** at the ages of **(A-D)** 5 and **(E-H)** 10 months, as described in the legend to **Figure 4.2.3**. **(A,E)** Blood glucose concentration during SCIT. **(B,F)** Fasting blood glucose levels. **(C,G)** Blood glucose levels during SCITT, normalised by subtracting the fasting basal blood glucose level from each mouse individually. **(D,H)** Total insulin response (AUC of normalised data). Data are pooled from 2 independent cohorts (Prex WT n=9; Prex1/2 DKO n=9), and are presented as mean ± SEM. 2-way ANOVA with repeated measures and Sidak's multiple comparisons correction was used to compare genotypes during SCIT. Unpaired Student's *t*-test was used to analyse the basal blood glucose level and total insulin response.

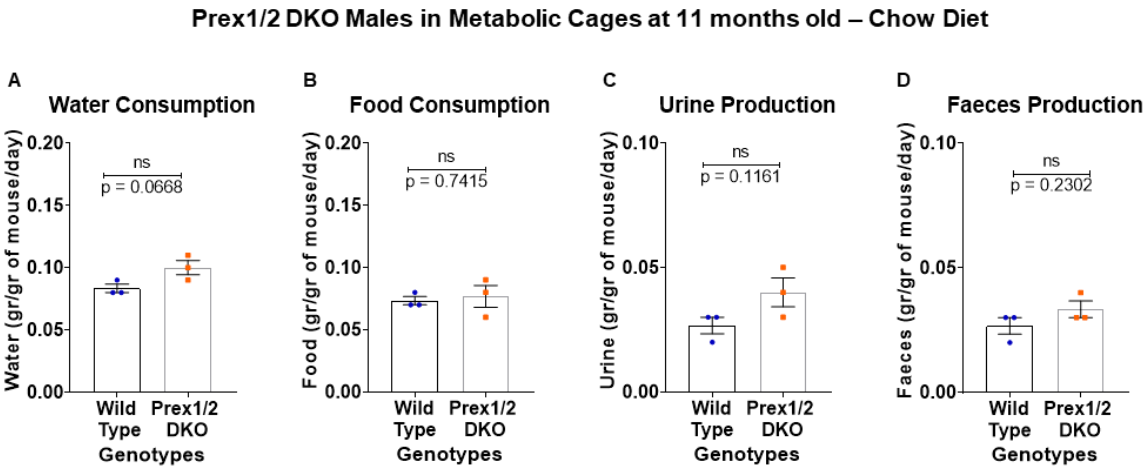

Figure 4.4.4: Male Prex1/2 DKO mice perform normally in metabolic cages.
The male Prex1/2 DKO (orange) and Prex WT (blue) mice in **Figure 4.4.1** were habituated to metabolic cages at 11 months of age, as detailed in Materials and Methods, weighed and group-housed (up to 3) in metabolic cages overnight for 16 h on 3 subsequent nights with food and water provided *ad libitum*. Their **(A)** water consumption, **(B)** food consumption, **(C)** urine production, and **(D)** faeces production were measured after each night and were normalised to the combined body weights of the mice housed in each cage. **(A-D)** Data are pooled from 2 independent cohorts (WT n=9; Prex1/2 DKO n=9) and presented as the mean ± SEM of each night (n=3). Unpaired Student's *t*-test for comparison between genotypes.

To test for the effect of diet, Prex1/2 DKO males were introduced to 45% HFD at the age of 10 weeks. As seen before in Prex1 KO and Prex2 KO males, Prex1/2 DKO males on HFD had lower basal blood glucose levels than Prex WT controls (**Figures 4.4.5A** and **4.4.6A**). Surprisingly though, HFD only induced an increase in the fasting blood glucose levels of Prex WT controls, whereas Prex1/2 DKO mice maintained their fasting blood glucose at a level comparable to that of their chow diet-fed counterparts (**Figure 4.4.6A**). In spite of this protection, HFD rendered the mice glucose intolerant over time, to the same extent as in Prex WT controls (**Figures 4.4.5B-C** and **4.4.6B**). Again, this was more reminiscent of the Prex1 KO than the Prex2 KO phenotype, as Prex1 KO males also showed an improved glucose tolerance on chow diet that was lost on HFD.

Both at 5 and 10 months of age, insulin challenge caused the blood glucose of male Prex1/2 DKO on HFD to drop to levels similar to that in Prex WT controls (**Figure 4.4.7A, E**). However, as seen previously with other cohorts, likely due to their lower fasting blood glucose levels (**Figure 4.4.7B, F**), the overall response was smaller in Prex1/2 DKO males compared to Prex WT mice (**Figure 4.4.7C-D, G-H**). Moreover, the insulin response of HFD-fed mice was reduced at 10 months compared to 5 months of age, for both genotypes (**Figure 4.4.7D, H**), indicating that HFD rendered Prex1/2 DKO males insulin resistant with age in a similar manner to Prex WT mice. It should be kept in mind though that the Prex WT males here responded to insulin a little stronger than expected from the analysis of multiple cohorts (see Supplementary Data, **Section 2**).

Unlike Prex1/2 DKO mice on chow diet, which gained weight more slowly than WT controls, mice from both genotypes gained weight in an identical way on HFD. Surprisingly, however, the Prex1/2 DKO males had higher fat percentage compare to the controls at their post mortem examination (**Figure 4.4.6C-D**), similarly to what was previously observed with Prex2 KO males on HFD. Finally, no difference was found in the water and food consumption or urine and faeces production of Prex1/2 DKO males on HFD housed in the metabolic cages (**Figure 4.4.8A-D**).

In conclusion, similarly to Prex single knockout strains, Prex1/2 double deficiency helped males on HFD maintain low fasting blood glucose levels , but did

not prevent them from becoming glucose intolerant, nor did it affect their insulin sensitivity.

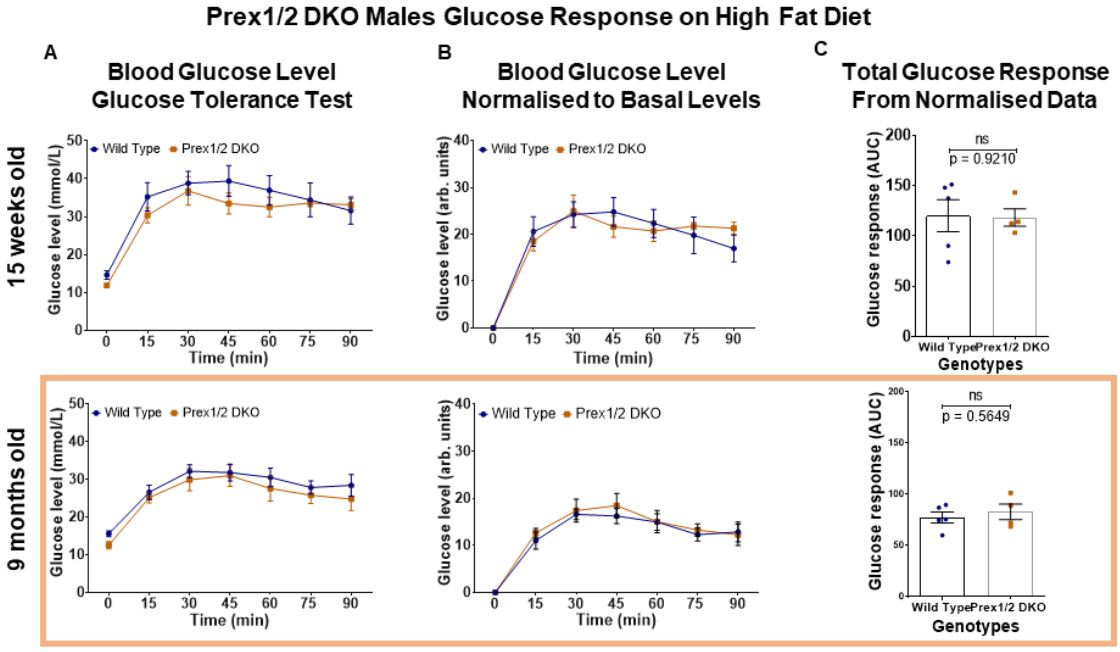

Figure 4.4.5: Male Prex1/2 DKO mice on HFD show similar glucose tolerance to Prex WT mice.

The fasting blood glucose levels and response to IPGTT were measured in male Prex1/2 DKO (orange) and Prex WT (blue) mice on 45% HFD at the ages, as described in the legend to **Figure 4.2.1**. Only data from 15 weeks and 9 months of age are shown for brevity, although mice of all ages up to one year were tested. **(A)** Blood glucose concentration during IPGTT. The dose of glucose used in the IPGTT was 2 g/kg at the ages of 10 and 15 weeks, and 0.5 g/kg thereafter (data in ochre box). **(B)** Blood glucose levels during IPGTT, normalised by subtracting the basal blood glucose level. **(C)** Total glucose response (AUC of normalised data). Data from 1 cohort (Prex WT n=4; Prex1/2 DKO n=5) and are presented as mean ± SEM. 2-way ANOVA with repeated measures and Sidak's multiple comparisons correction was used to compare genotypes during IPGTT. Unpaired Student's *t*-test was used to analyse the total glucose response.

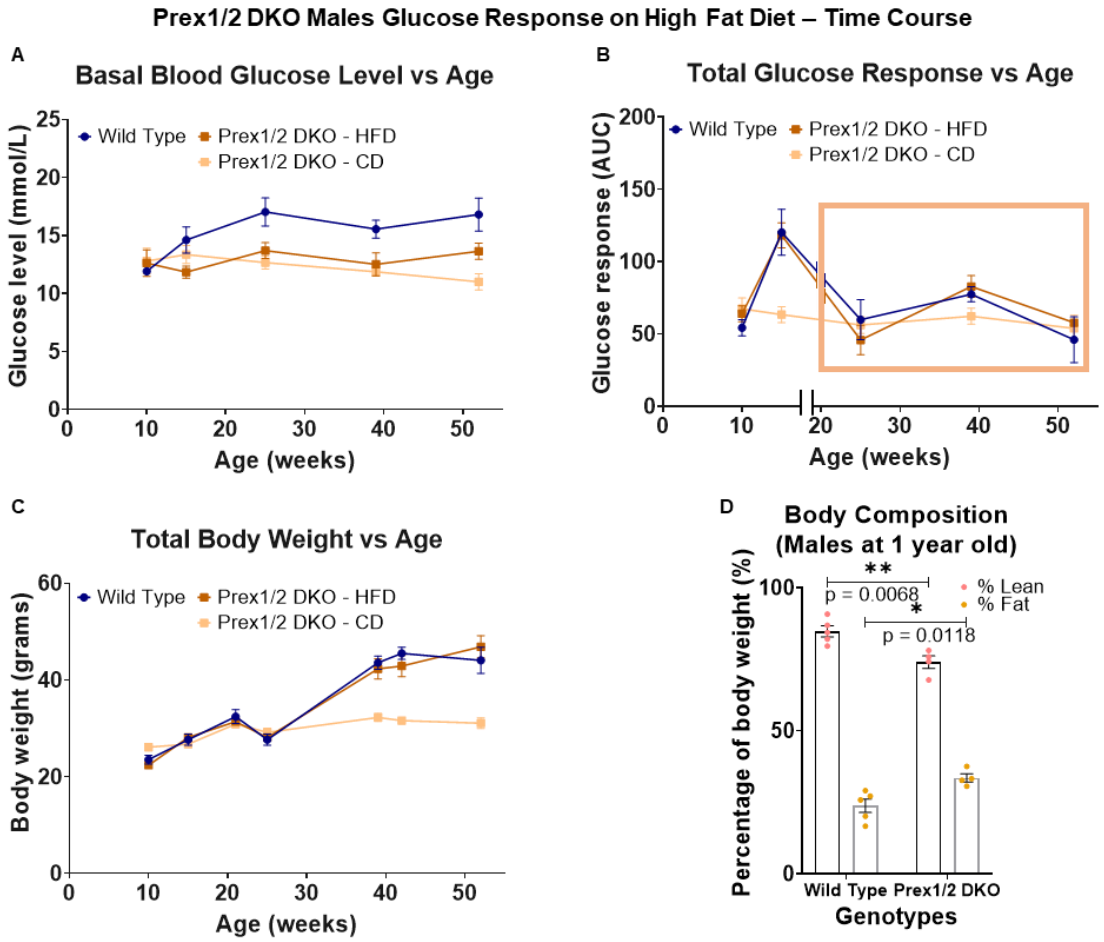

Figure 4.4.6: Male Prex1/2 DKO mice on HFD have low fasting blood glucose levels but a normal response to glucose challenge throughout ageing.

The fasting blood glucose levels, response to glucose challenge, and body weight of the male Prex1/2 DKO (orange) and Prex WT (blue) mice in **Figure 4.4.5** are expressed as a function of age. Note that the dose of glucose was reduced from 2 g/kg to 0.5 g/kg from the age of 6 months onwards (data in ochre box). In faded orange are represented the Prex1/2 DKO male mice on chow diet from **Figure 4.4.1** for visual comparison, but these mice were not included in the statistical analysis as they were not directly compared experimentally. **(A)** Fasting blood glucose levels; data from column A in **Figure 4.4.5**. **(B)** Response to IPGTT; normalised data from columns B and C in **Figure 4.4.5**. **(C)** Body weight, measured after 6 and 4 h fasting, prior to glucose and insulin challenges, respectively. **(D)** Body composition at 1 year of age. The mice in (**A-C**) were culled at 1 year of age and the cadavers were scanned by Echo MRI for lean mass and body fat. Data are from 1 cohort (Prex WT n=4; Prex1/2 DKO n=5) and presented as mean ± SEM. 2-way ANOVA with repeated measures and Sidak's multiple comparisons correction was used to compare genotypes during ageing. Unpaired Student's *t*-test was used to analyse the body composition.

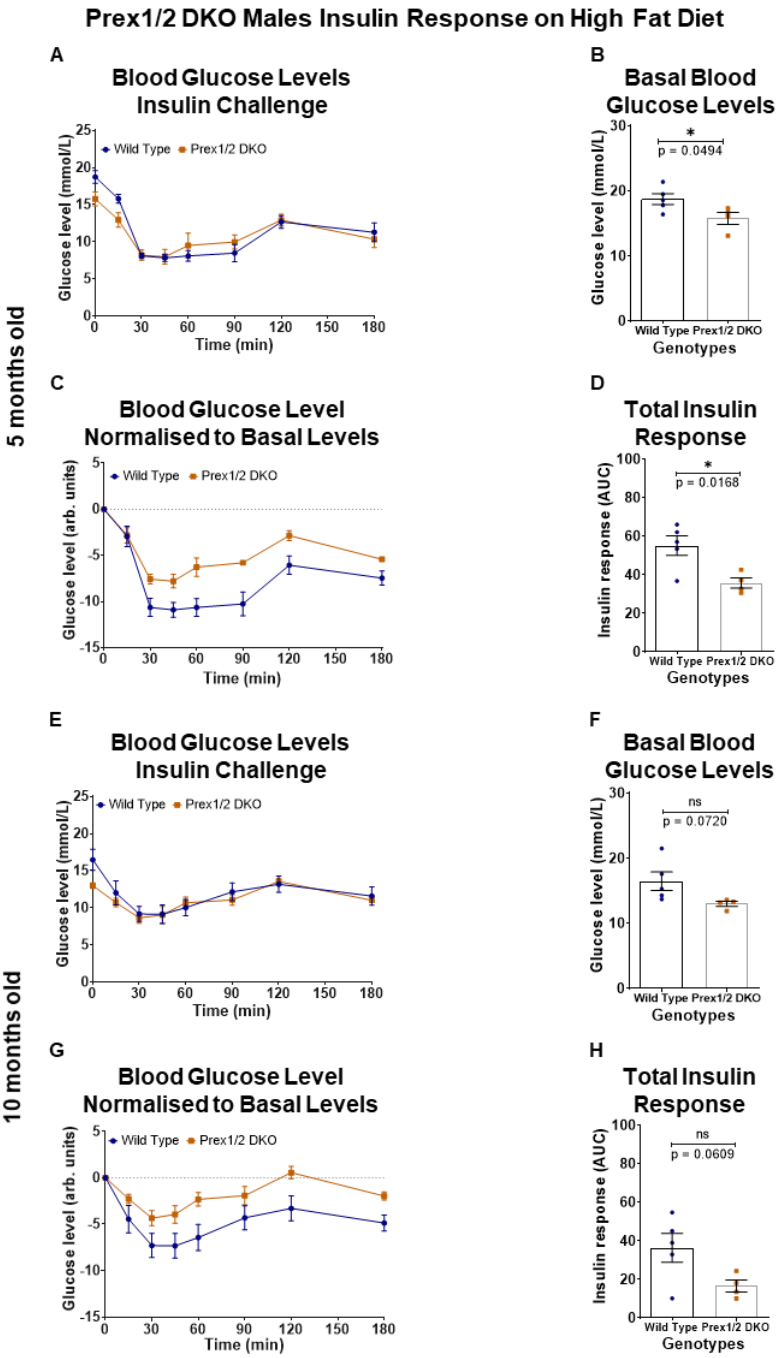

Figure 4.4.7: Male Prex1/2 DKO mice on HFD show apparent insulin resistance throughout ageing.

The fasting blood glucose levels and response to SCITT were measured in the male Prex1/2 DKO (orange) and Prex WT (blue) mice on 45% HFD from **Figure 4.4.5** at the age of **(A-D)** 5 and **(E-H)** 10 months, as described in the legend to **Figure 4.2.3**. **(A,E)** Blood glucose concentration during SCITT. **(B,F)** Fasting blood glucose levels. **(C,G)** Blood glucose levels during SCITT, normalised by subtracting the fasting basal blood glucose level from each mouse individually. **(D,H)** Total insulin response (AUC of normalised data). Data from 1 cohort (Prex WT n=4; Prex1/2 DKO n=5) and presented as mean ± SEM. 2-way ANOVA with repeated measures and Sidak's multiple comparisons correction was used to compare genotypes during SCITT. Unpaired Student's *t*-test was used to analyse the basal blood glucose level and total insulin response.

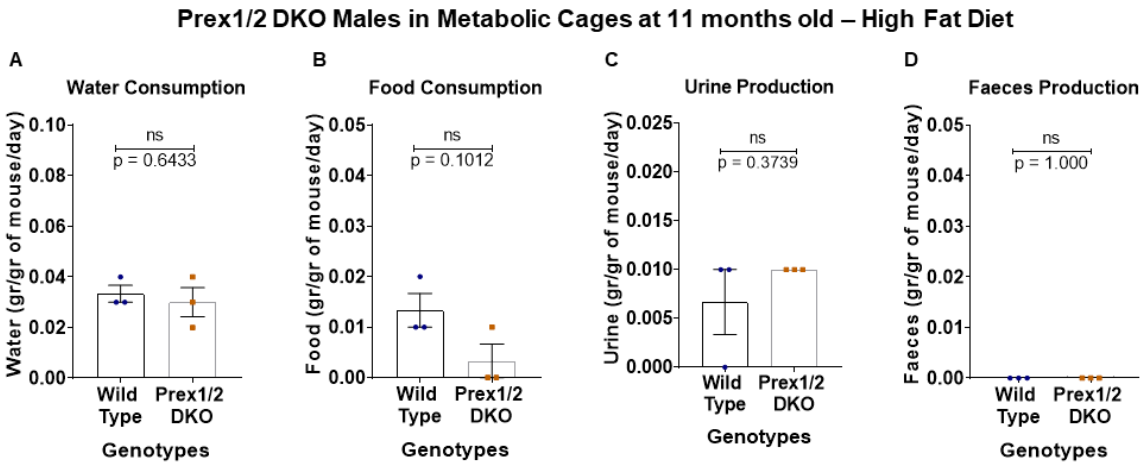

Figure 4.4.8: Male Prex1/2 DKO mice perform normally in metabolic cages.
The male Prex1/2 DKO (orange) and Prex WT (blue) mice from **Figure 4.4.5** were habituated to metabolic cages at 11 months of age, as detailed in Materials and Methods, weighed and group-housed (up to 3) in metabolic cages overnight for 16 h on 3 subsequent nights with food and water provided *ad libitum*. Their **(A)** water consumption, **(B)** food consumption, **(C)** urine production, and **(D)** faeces production were measured after each night and were normalised to the combined body weights of the mice housed in each cage. Data are from 1 cohort (Prex WT n=4; Prex1/2 DKO n=5) and are presented as the mean ± SEM of each night (n=3). Unpaired Student's *t*-test for comparison between genotypes.

4.4.2 Female Prex1/2 DKO mice have a tendency to worsened glucose response throughout ageing

Lastly, the metabolic phenotype of the Prex1/2 DKO females on chow and HFD was investigated. The representative graphs in **Figure 4.4.9** and the ageing overview graphs in **Figure 4.4.10** show that Prex1/2 DKO females on chow diet had identical fasting blood glucose levels to the Prex WT controls (**Figures 4.4.9A** and **4.4.10A**). Moreover, Prex1/2 deficiency did not alter significantly the response to glucose challenge in females on chow diet, although there was a tendency to worse glucose tolerance (**Figures 4.4.9B-C** and **4.4.10A**). Similarly, Prex1/2 DKO females on chow diet had normal insulin responses both at 5 months and at 10 months' time points, except for a slightly altered counter-regulatory response in old age (**Figure 4.4.11 A-B**). Finally, Prex1/2 DKO and Prex WT females on chow diet gained weight at a comparable rate and had similar body composition at one year of age (**Figure 4.4.10C-D**), despite Prex1/2 DKO consuming less water and food and producing less urine and faeces (**Figure 4.4.12 C-D**). Overall, therefore, the absence of both Prex proteins did not have any significant effect on the metabolic phenotype of female mice on chow diet.

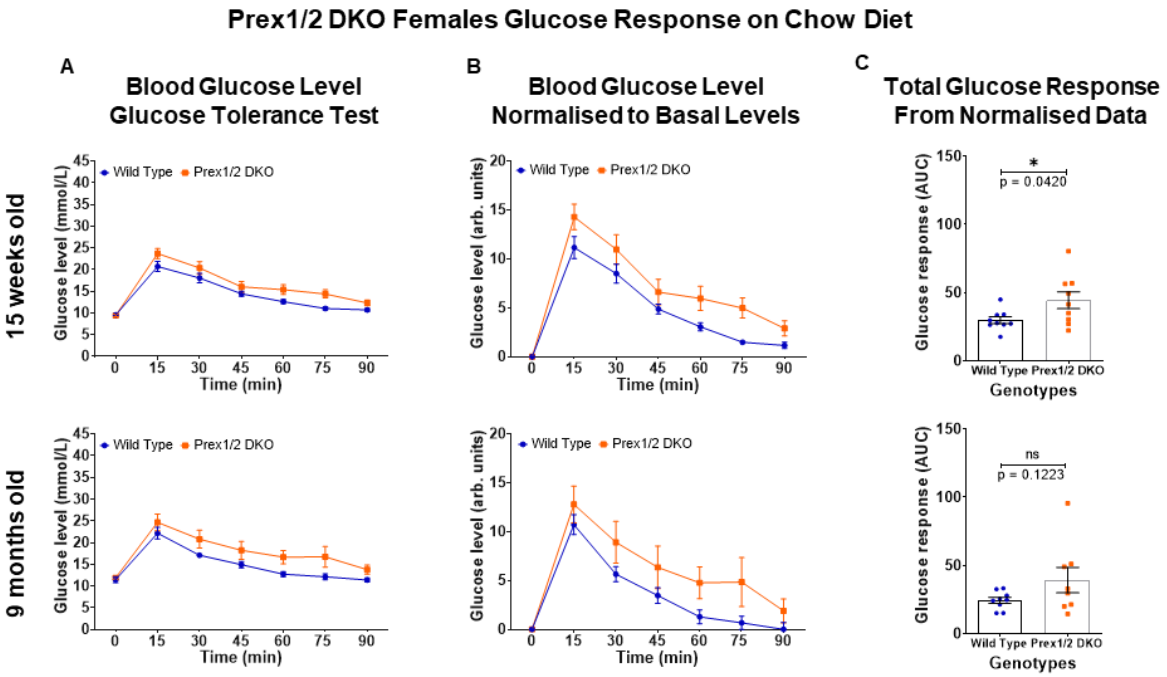

Figure 4.4.9: Female Prex1/2 DKO mice on chow diet show similar fasting blood glucose levels but a tendency towards worsened glucose tolerance compared to Prex WT mice.

The fasting blood glucose levels and response to IPGTT were measured in female Prex1/2 DKO (orange) and Prex WT (blue) mice on chow diet, as described in the legend to **Figure 4.2.1**. Only data from 15 weeks and 9 months of age are shown, for brevity, although mice of all ages up to one year were tested. **(A)** Blood glucose concentration during IPGTT. **(B)** Blood glucose levels during IPGTT, normalised by subtracting the basal blood glucose level. **(C)** Total glucose response (AUC of normalised data). Data are pooled from 2 independent cohorts (Prex WT n=9; Prex1/2 DKO n=8) and presented as mean ± SEM. 2-way ANOVA with repeated measures and Sidak's multiple comparisons correction was used to compare genotypes during IPGTT. Unpaired Student's *t*-test was used to analyse the total glucose response.

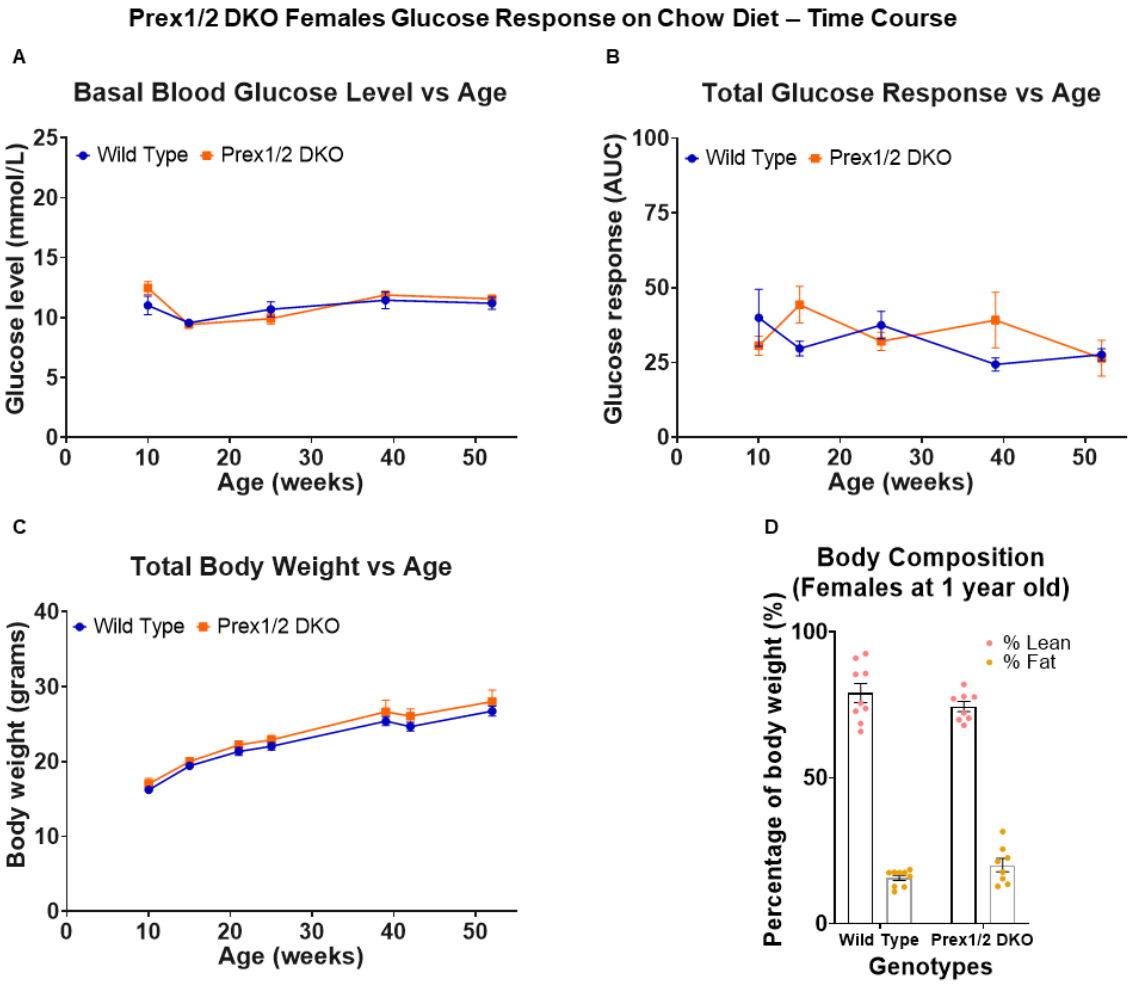

Figure 4.4.10: Female Prex1/2 DKO mice on chow diet have a tendency to worsened glucose tolerance throughout ageing.

The fasting blood glucose levels, response to glucose challenge, and body weight of the female Prex1/2 DKO (orange) and Prex WT (blue) mice in **Figure 4.4.9** are expressed as a function of age. **(A)** Fasting blood glucose levels; data from column A in **Figure 4.4.9**. **(B)** Response to IPGTT; normalised data from columns B and C in **Figure 4.4.9**. **(C)** Body weight, measured after 6 and 4 h fasting, prior to glucose and insulin challenges, respectively. **(D)** Body composition at 1 year of age. The mice in (**A-C**) were culled at 1 year of age and the cadavers were scanned by Echo MRI for lean mass and body fat. Data are pooled from 2 independent cohorts (WT n=9; Prex1/2 DKO n=8) and are presented as mean ± SEM. 2-way ANOVA with repeated measures and Sidak's multiple comparisons correction was used to compare genotypes during ageing. Unpaired Student's *t*-test was used to analyse the body composition.

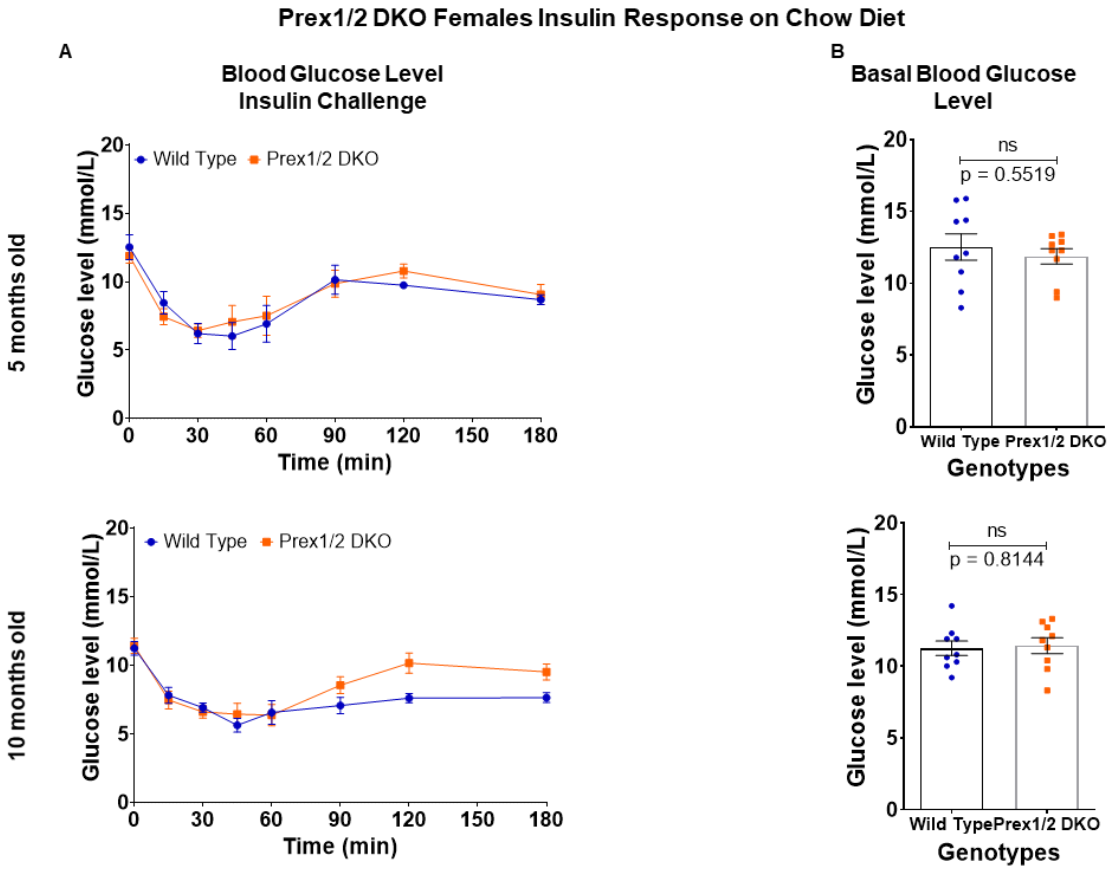

Figure 4.4.11: Female Prex1/2 DKO mice on chow diet show an altered late-phase response to insulin challenge in old age.

The fasting blood glucose levels and response to SCITT were measured in female Prex1/2 DKO (orange) and Prex WT (blue) mice from **Figure 4.4.9** on chow diet at the ages of 5 and 10 months, as described in the legend to **Figure 4.2.3**. **(A)** Blood glucose concentration during SCITT. **(B)** Fasting blood glucose levels. Data are pooled from 2 independent cohorts (Prex WT n=9; Prex1/2 DKO n=8) and are presented as mean ± SEM. 2-way ANOVA with repeated measures and Sidak's multiple comparisons correction was used to compare genotypes during SCITT. Unpaired Student's *t*-test was used to analyse the basal blood glucose levels.

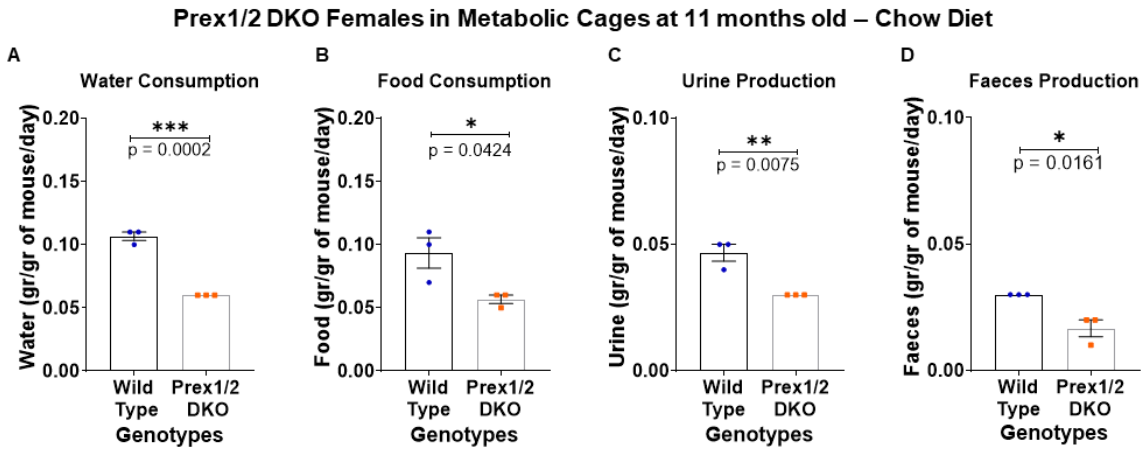

Figure 4.4.12: Female Prex1/2 DKO mice consume less water and food and produce less urine and faeces compared to Prex WT mice in metabolic cages.

The female Prex1/2 DKO (orange) and Prex WT (blue) mice from **Figure 4.4.9** were habituated to metabolic cages at 11 months of age, as detailed in Materials and Methods, weighed and group-housed (up to 3) in metabolic cages overnight for 16 h on 3 subsequent nights with food and water provided *ad libitum*. Their **(A)** water consumption, **(B)** food consumption, **(C)** urine production, and **(D)** faeces production were measured after each night and were normalised to the combined body weights of the mice housed in each cage. Data are pooled from 2 independent cohorts (Prex WT n=9; Prex1/2 DKO n=8) and are presented as the mean ± SEM of each night (n=3). Unpaired Student's *t*-test was used for comparison between genotypes.

On HFD, the basal blood glucose levels of Prex1/2 DKO females did not change compared to Prex WT controls, similarly to what had been seen in Prex1/2 DKO males (**Figures 4.4.13A** and **4.4.14A**). However, from 15 weeks of age, after just one month on HFD, Prex1/2 DKO females demonstrated reduced glucose clearance during IPGTT, compared to Prex WT mice, and this glucose intolerance persisted until the age of one year (**Figures 4.4.13B-C** and **4.4.14B**). This phenotype was contrary to what was previously seen with the Prex1 and Prex2 KO females on HFD, which had shown either improved glucose tolerance (Prex1 KO) or, at most, a tendency to worsened glucose tolerance in old age (Prex2 KO). This would suggest that the two Prex proteins can compensate, or even over-compensate, for each other to provide glucose tolerance in female mice on HFD, and this redundancy is lost when both proteins are deleted. This was a sex-specific phenotype, as Prex1/2 DKO males on HFD showed normal glucose tolerance.

The insulin sensitivity of the Prex1/2 deficient females on HFD was normal overall, except for the exaggerated counter-regulatory response in both middle-aged and old animals (**Figure 4.4.15A-B**). A similar phenotype had also been seen in old females on chow diet.

Finally, the Prex1/2 DKO and the Prex WT females gained weight at a comparable rate and had similar body composition at one year of age (**Figure 4.4.14C-D**). Moreover, as can be seen in **Figure 4.4.16**, Prex1/2 DKO females also had normal water and food intake as well as urine and faeces production.

Taken together these data suggest that, in the absence of both Prex proteins, females on HFD are glucose intolerant, unlike Prex WT females or females with Prex single KO under the same conditions.

To summarise this section (see also **Table 4.3**), deficiency of both Prex1 and Prex2 in chow diet fed males has no major effects, except causing a tendency to improved glucose tolerance in middle-aged animals. On HFD, Prex1/2 DKO males showed low fasting blood glucose levels throughout ageing, but normal glucose tolerance. Their apparent insulin resistance is likely to be a reflection of their low fasting blood glucose levels, rather than true insulin resistance, as normal absolute levels of blood glucose are achieved upon insulin challenge. In contrast to the

Prex1/2 DKO males and to singlePrex1 or Prex2 KO females, Prex1/2 DKO females showed a tendency to reduced glucose tolerance on chow diet and actual glucose intolerance on HFD. This phenotype of the DKO mice overall shows that there is sex- and diet-dependent redundancy between Prex proteins in the control of glucose tolerance (in females on HFD), as well as compensation from other regulators of glucose homeostasis that engages when both Prex proteins are deleted.

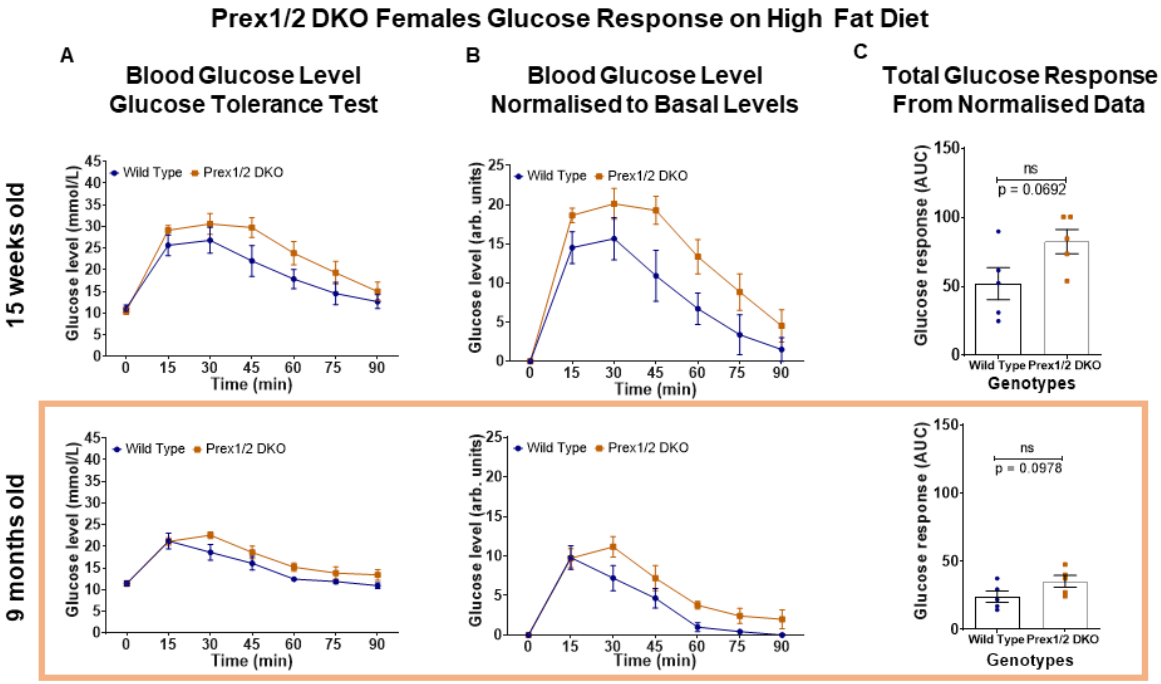

Figure 4.4.13: Female Prex1/2 DKO mice on HFD show normal fasting blood glucose levels but a trend to reduced glucose tolerance.

The fasting blood glucose levels and response to IPGTT were measured in female Prex1/2 DKO (orange) and Prex WT (blue) mice on 45% HFD, as described in the legend to **Figure 4.2.1**. Only data from 15 weeks and 9 months of age are shown, for brevity, although mice of all ages up to one year were tested. The ochre box denotes glucose challenge at the reduced dose of 1 g/kg instead of 2 g/kg. **(A)** Blood glucose concentration during IPGTT. **(B)** Blood glucose levels during IPGTT, normalised by subtracting the basal blood glucose level. **(C)** Total glucose response (AUC of normalised data). Data are from 1 cohort (Prex WT n=5; Prex1/2 DKO n=5) and are presented as mean ± SEM. 2-way ANOVA with repeated measures and Sidak's multiple comparisons correction was used to compare genotypes during IPGTT. Unpaired Student's *t*-test was used to analyse the total glucose response.

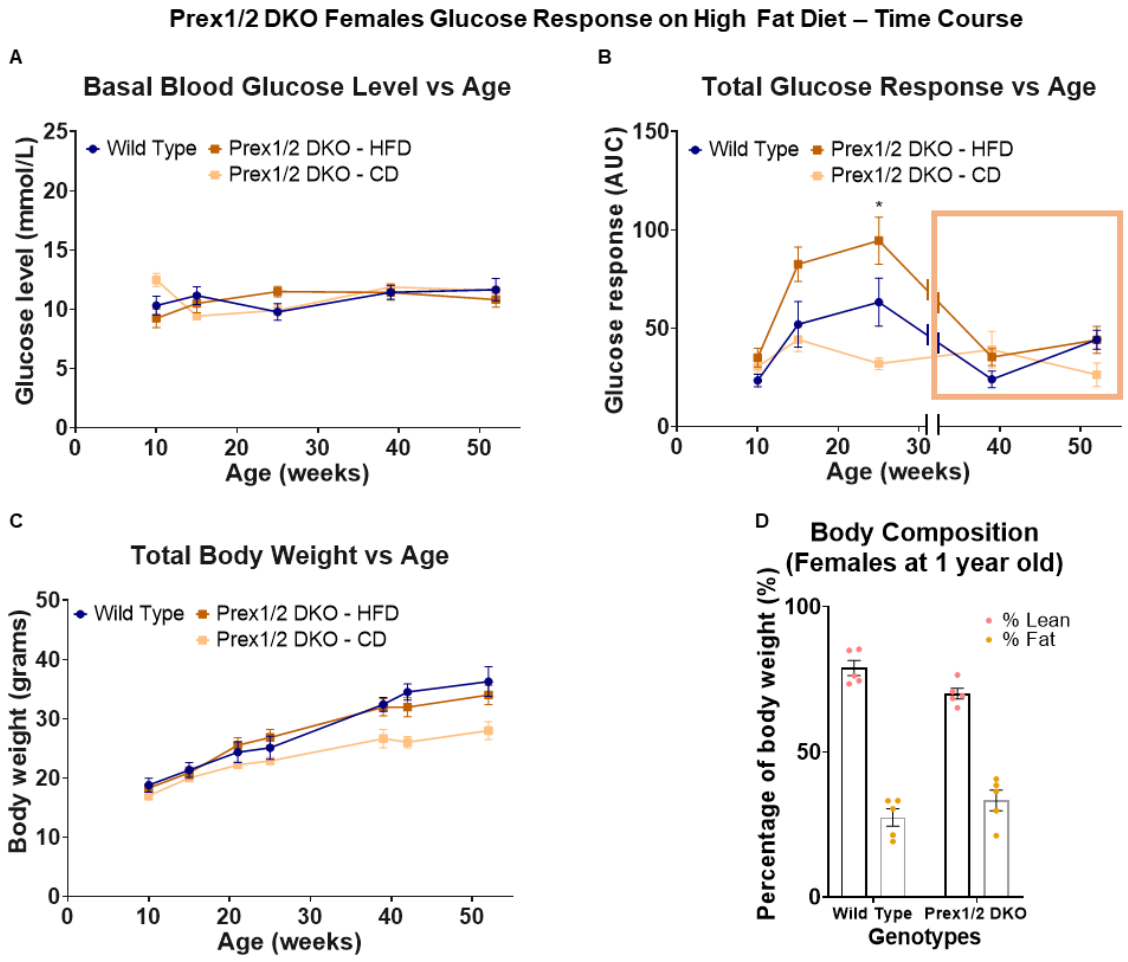

Figure 4.4.14: Middle-aged female Prex1/2 DKO mice on HFD are glucose intolerant. The fasting blood glucose levels, response to glucose challenge, and body weight of the female Prex1/2 DKO (orange) and Prex WT (blue) mice on 45% HFD from **Figure 4.4.13** are expressed as a function of age. The ochre box denotes glucose challenge at the reduced dose of 1 g/kg instead of 2 g/kg. In faded orange are represented the Prex1/2 DKO female mice on chow diet from **Figure 4.4.9** for visual comparison, but were not included in the statistical analysis, as these animals were not directly compared experimentally. **(A)** Fasting blood glucose levels; data from column A in **Figure 4.4.13**. **(B)** Response to IPGTT; normalised data from columns B and C in **Figure 4.4.13**. **(C)** Body weight, measured after 6 and 4 h fasting, prior to glucose and insulin challenges, respectively. **(D)** Body composition at 1 year of age. The mice in (**A-C**) were culled at 1 year of age and the cadavers were scanned by Echo MRI for lean mass and body fat. Data are from 1 cohort (Prex WT n=5; Prex1/2 DKO n=5) and are presented as mean ± SEM. 2-way ANOVA with repeated measures and Sidak's multiple comparisons correction was used to compare genotypes during ageing. Unpaired Student's *t*-test was used to analyse the body composition.

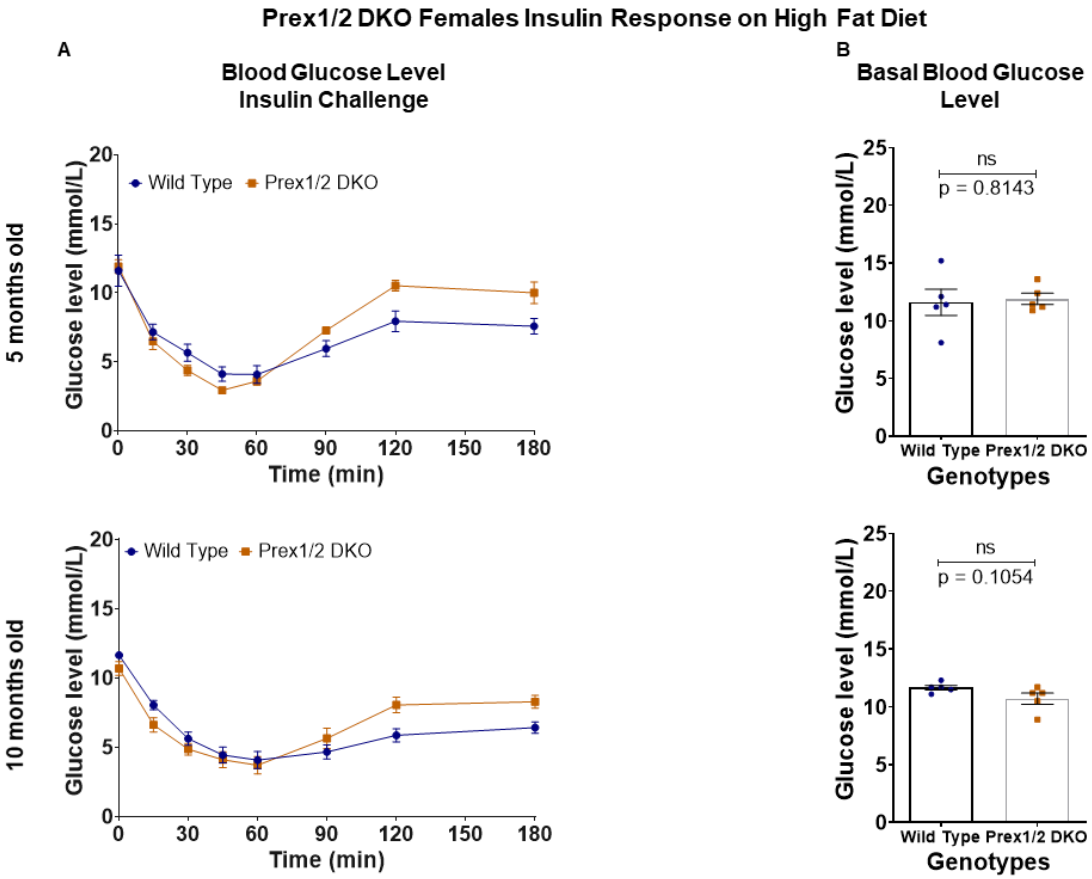

Figure 4.4.15: Female Prex1/2 DKO mice on HFD show normal fasting blood glucose levels but an altered late-phase response to insulin challenge.

The fasting blood glucose levels and response to SCITT were measured in the female Prex1/2 DKO (orange) and Prex WT (blue) mice on 45% HFD from **Figure 4.4.13** at the ages of 5 and 10 months, as described in the legend to **Figure 4.2.3**. **(A)** Blood glucose concentration during SCITT. **(B)** Fasting blood glucose levels. Data are from 1 cohort (Prex WT n=5; Prex1/2 DKO n=5) and are presented as mean ± SEM. Unpaired Student's *t*-test was used to analyse the total glucose response.

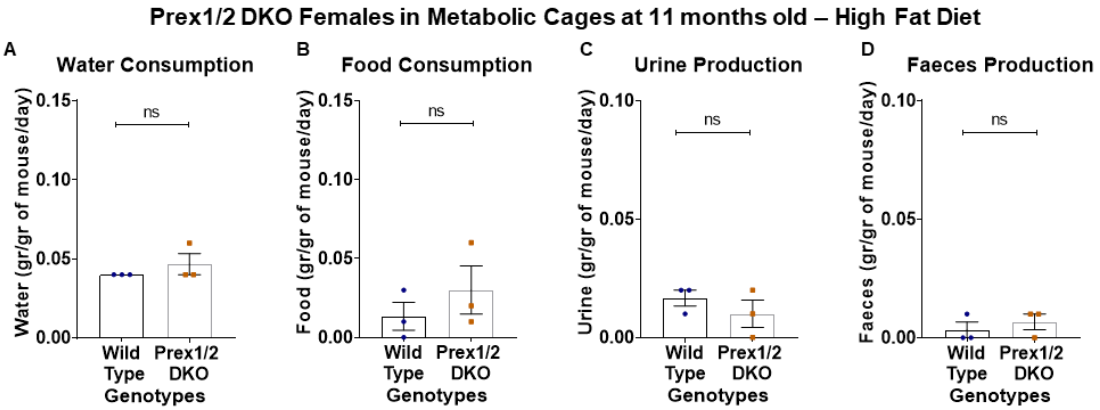

Figure 4.4.16: Female Prex1/2 DKO mice perform normally in metabolic cages.
The female Prex1/2 DKO (orange) and Prex WT (blue) mice from **Figure 4.4.13** were habituated to metabolic cages at 11 months of age, as detailed in Materials and Methods, weighed and group-housed (up to 3) in metabolic cages overnight for 16 h on 3 subsequent nights with food and water provided *ad libitum*. Their **(A)** water consumption, **(B)** food consumption, **(C)** urine production, and **(D)** faeces production were measured after each night and were normalised to the combined body weights of the mice housed in each cage. Data are from 1 cohort (Prex WT n=5; Prex1/2 DKO n=5) and are presented as the mean ± SEM of each night (n=3). Unpaired Student's *t*-test was used for comparison between genotypes.

Table 4.3: Summary table of metabolic phenotype of Prex1 KO, Prex2 KO, and Prex1/2 DKO mice on chow or high fat diet. Bold font was used to annotate findings that reached statistical significance in most time points tested, while bold and italic font was used to indicate strong trends that show statistical significance in only one or two time points tested.

		Prex1 KO		Prex2 KO		Prex1/2 DKO	
		Male	**Female**	**Male**	**Female**	**Male**	**Female**
Chow Diet	**Fasting Blood Glucose**	**Low fasting blood glucose**	Tendency to low fasting blood glucose	Normal	Normal	Tendency to low fasting blood glucose in old age	Normal
	Glucose Tolerance	**Improved glucose tolerance throughout ageing**	Tendency to improved glucose tolerance in old age	Tendency to improved glucose tolerance in young and worse in old age	Tendency to improved glucose tolerance in young and worse in old age	Tendency to improved glucose tolerance in middle-aged	Tendency to reduced glucose tolerance
	Insulin Response	Apparent insulin resistance in old age	Normal	Apparent increase in insulin sensitivity in old age	Normal	Apparent insulin resistance in middle-aged	Altered counter-regulatory response in old age
High Fat Diet	**Fasting Blood Glucose**	***Low fasting blood glucose***	Normal	***Low fasting blood glucose***	Normal	***Low fasting blood glucose***	Normal
	Glucose Tolerance	Normal	***Improved glucose tolerance (some ages)***	***Glucose intolerance***	Tendency to improved glucose tolerance in young and worse in old age	Normal	***Glucose intolerance***
	Insulin Response	Normal	Normal	***Insulin resistance in old age***	Normal	Apparent insulin resistance	Altered counter-regulatory response

4.5 Adaptor functions of PREX proteins in glucose homeostasis and insulin signalling

In order to study functions of PREX proteins that are independent of their catalytic Rac-GEF activity, I generated and studied GEF-dead proteins and mice. Recombinant protein was generated to confirm catalytic inactivity *in vitro*. Mammalian expression constructs were used for overexpression of GEF-dead proteins and analysis of their effects on the insulin signalling pathway. GEF-dead mouse strains were generated to test glucose homeostasis in the same manner as previously in the KO mice. Recombinant WT PREX1 and GEF-dead PREX1 proteins, as well as constructs for the expression of WT PREX1, WT PREX2 and GEF-dead PREX1 in mammalian cells were already available in the laboratory, but all other tools were generated in the frame of this PhD.

4.5.1 Design of human recombinant catalytically inactive PREX2

To generate catalytically inactive PREX2 protein, residues whose mutation would render the human PREX2 protein catalytically inactive were identified based on the literature. Mutation of the residues Glu^{56} and Asn^{238} within the catalytic DH domain of human PREX1 was previously shown to render the protein GEF-Dead both *in vitro* and in cells (Hill et al., 2005). Similarly, mutation of the Leu^{334} and Lys^{335} residues within the catalytic DH domain of the mouse GEF protein Vav1 resulted in inactivation of its GEF activity (Saveliev et al., 2009). Furthermore, these mutations in both GEFs had been reported to not affect the normal folding of the proteins, or their interaction with other proteins (**Figure 4.5.1A**). I annotated these target residues on the crystal structural of the DH domain of the Rac-GEF protein Tiam1 in complex with Rac1 (**Figure 4.5.1B**), which confirmed that all these amino acids present their side chains towards Rac1, hence their mutation was expected to specifically disrupt the Rac-GEF activity.

As presented in **Figure 4.5.1C**, alignment of the amino acid sequence of the Rac-GEFs Tiam1, Prex1 and Prex2 showed that the equivalent to Vav1 residue Leu^{334} was not conserved throughout Rac-GEFs. Therefore, it was decided to mutate the PREX2 residues that are equivalent to those in GEF-Dead PREX1 for the generation of catalytically inactive PREX2. These residues are Glu^{30} and Asn^{212}.

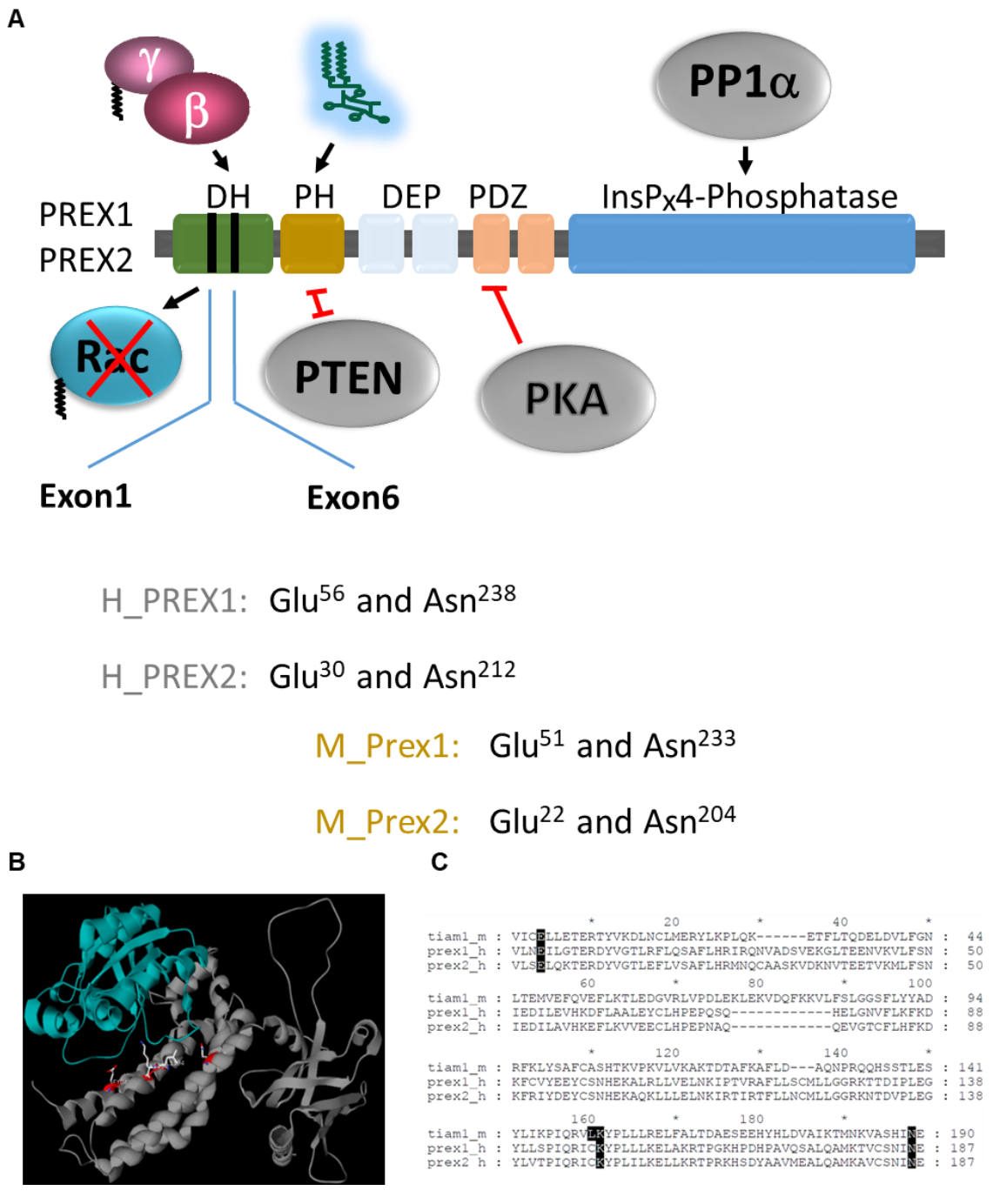

Figure 4.5.1: Strategy for the generation of atalytically inactive human PREX2 protein and catalytically inactive Prex1 and Prex2 mice.

(A) Graphical representation of PREX protein binding partners and intended point mutations in their DH domain. **(B)** Crystal structure of the DH domain of mouse GEF protein Tiam1 in complex with Rac1, with the equivalent residues highlighted in red that are known to produce GEF-dead PREX1 and Vav1 proteins when mutated to alanine. The two outer residues have been mutated in PREX1, the middle ones in Vav1 (Provided by Simon R. Andrews, Babraham Bioinformatics Facility). **(C)** Alignment of the mouse Tiam1 and the human PREX1 and PREX2 protein sequences. Black highlights annotate the equivalent residues of PREX1 Glu^{56} and Asn^{238} and Vav1 Leu^{334} and Lys^{335} that were reported to render PREX1 and Vav1 GEF-Dead (alignment provided by Simon R. Andrews).

4.5.2 Production and characterisation of catalytically inactive human PREX2 protein

To confirm that the mutation of Glu^{30} and Asn^{212} in the catalytic DH domain of PREX2 indeed rendered the protein catalytically inactive, recombinant human PREX2-E30A/N212A protein was produced and purified from Sf9 cells. Recombinant human wild type PREX2 (PREX2 WT) was produced at the same time as a control (**Figure 4.5.2A-B**). The purified proteins were tested in a liposome-based *in vitro* Rac-GEF activity assay, using human recombinant EE-Rac1-GDP as substrate, with increasing doses of PIP_3 as stimulus, and EDTA as a positive control. Rac-GEF activity was measured as the PREX2-stimulated ^{35}S-GTPγS loading of EE-Rac1. This confirmed that the introduction of mutations E30A and N212A into the DH domain of PREX2 inhibited it from acting as a PIP_3-regulated Rac-GEF (**Figure 4.5.2C**). Its basal (PIP_3-independent) Rac-GEF activity was also lower than that of the WT protein, hardly detectable over the no-GEF basal control that contained only EE-Rac1. Hence, the mutations chosen were effective at rendering PREX2 protein catalytically inactive.

4.5.3 Overexpression of GEF-dead PREX1 and GEF-dead PREX2 in HepG2 cells increases insulin pathway activity to a similar extent as overexpression of the wild type proteins.

To assess the importance of the Rac-GEF activity of PREX proteins in insulin signalling, an expression vector for the overexpression of human $Glu^{30} \rightarrow Ala^{30}$; $Asn^{212} \rightarrow Ala^{212}$ catalytically inactive PREX2 in mammalian cells was also generated. Expression constructs for catalytically inactive PREX1 as well as wild type PREX1 and PREX2 were already available in the lab and were used in parallel. HepG2 human liver carcinoma cells were transfected to overexpress wild type (WT) PREX1 or PREX2 or catalytically inactive PREX1 E56A/N238A or PREX2 E30A/N212A proteins, and mock-transfected cells with vector only constructs (v.o. control) were tested in parallel. The cells were serum-starved for 8 h in serum-free medium containing 0.1% BSA, prior to stimulation with 25 nM insulin for various lengths of time. Total cell lysates were prepared and analysed by western blot for the phosphorylation of Akt on the mTORC2 target site S473 that confers full activation, as a measure of insulin pathway activity, by western blot. As shown in

Figure 4.5.3A, overexpression of either wild type PREX1 or PREX1 E56A/N238A in insulin-stimulated HepG2 human liver cells caused increased Akt phosphorylation. Similar results were obtained upon overexpression of wild type PREX2 or PREX2 E30A/N212A (**Figure 4.5.3B**). The level of Akt phosphorylation on S473 increased in a time-dependent manner in cells that expressed either WT or GEF-dead PREX proteins, from 10 s of insulin stimulation onwards, and it remained elevated until the longest time-point tested, 2 hours. Under the same conditions, vector-control treated cells responded to insulin stimulation at a much lower level. The extent of Akt phosphorylation was very similar between wild type and GEF-dead PREX proteins, at comparable levels of overexpression. Quantification by ImageJ densitometric analysis confirmed that our observation reached statistical significance between v.o. control and PREX expressing cells, and that there was no statistically significant difference between WT and GEF-dead proteins, except that fewer time points reached significance with the PREX2 GEF-dead protein than the equivalent PREX2 WT protein (**Figure 4.5.3C-D**). These results suggest that both PREX proteins can promote insulin signalling not only through their Rac-GEF activity, but also in a GEF-activity independent manner as adaptor proteins, at least in this overexpression system.

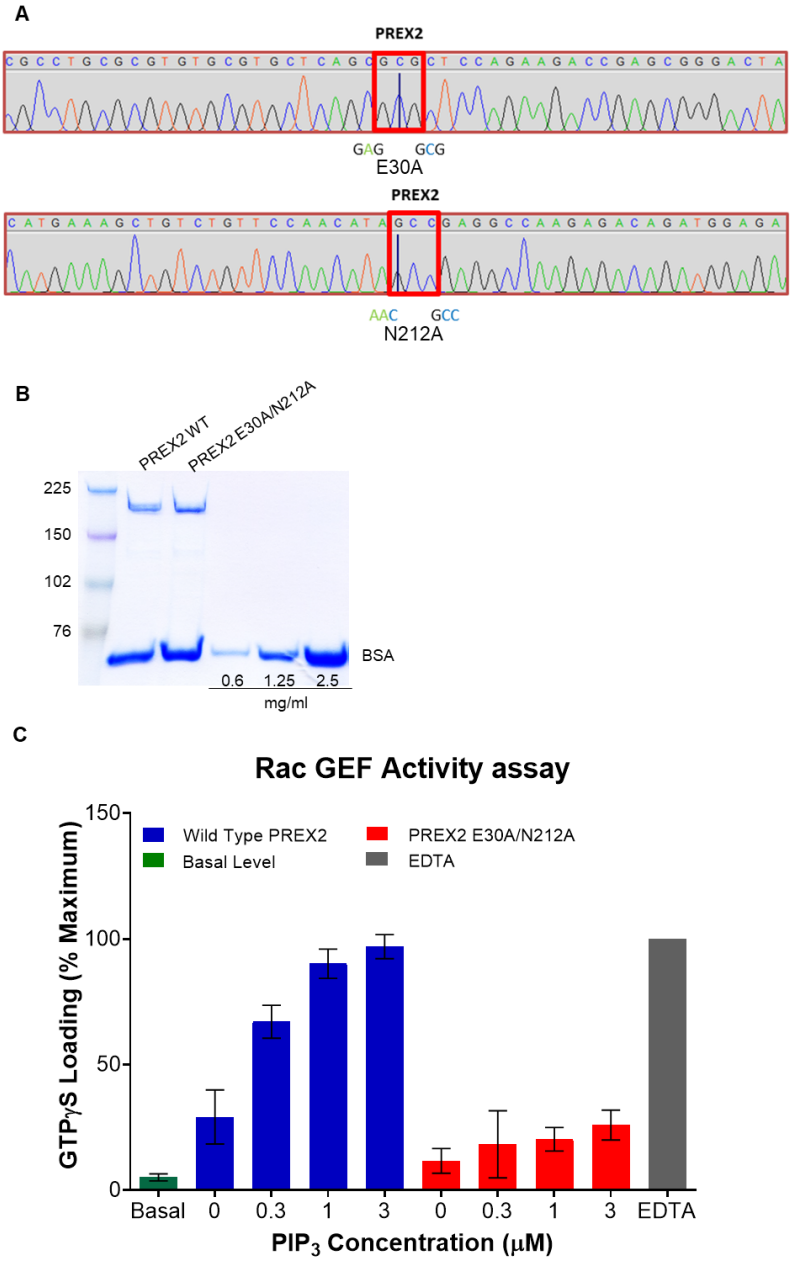

Figure 4.5.2: Generation of purified human recombinant catalytically inactive EE-PREX2$^{E30A/N212A}$ protein in Sf9 cells.

(A) Sequencing trace of human EE-PREX2$^{E30A/N212A}$ DNA construct, assembled with Gap4 software, showing the mutated residues in red boxes. This construct was used for lentivirus production, transduction of Sf9 insect cells, and expression of human recombinant catalytically inactive EE-PREX2$^{E30A/N212A}$ protein. Human recombinant wild type EE-PREX2 (blue bars) and mutated EE-PREX2$^{E30A/N212A}$ (red bars) were produced in Sf9 cells and purified to >90% purity using anti-EE antibody coupled protein A sepharose as detailed in Materials and Methods. **(B)** Protein gel of the purified protein. **(C)** The purified proteins were tested in a liposome-based *in vitro* GEF activity assay, using EE-Rac1-GDP as substrate and increasing doses of PIP3 as stimulus, together with either Sf9 cell derived purified recombinant PREX2 protein, either WT or GEF-dead, as indicated. 35S-GTPγS loading of EE-Rac1 was measured to determine Rac-GEF activity. EDTA was used as a positive control. Data are pooled from 3 independent experiments and presented at mean ± SEM.

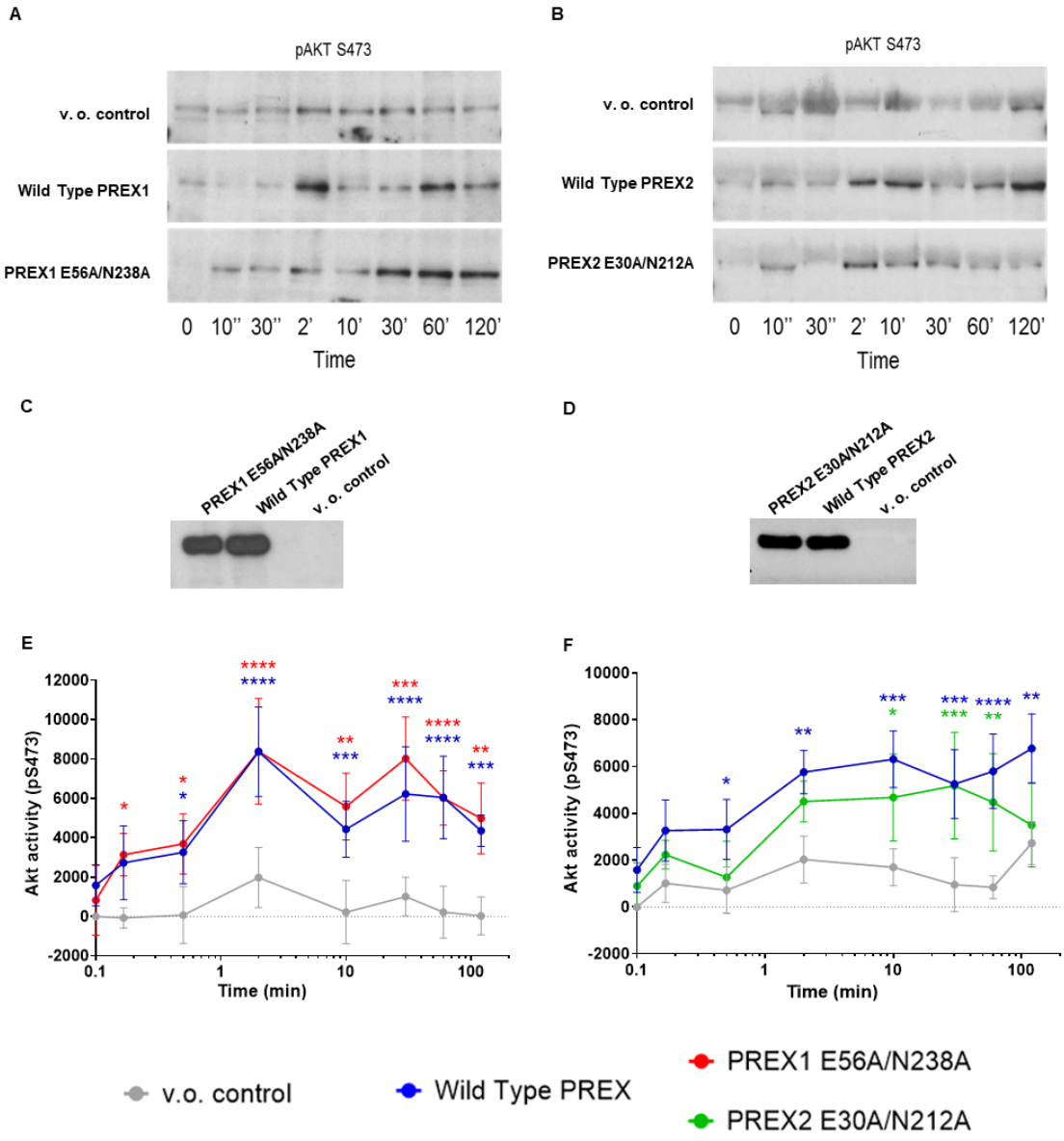

Figure 4.5.3: Overexpression of wild type and GEF-dead PREX1 or PREX2 in HepG2 cells increases AKT activity to a similar level in response to insulin stimulation.
HepG2 human liver carcinoma cells were transfected to overexpress WT PREX, or catalytically inactive PREX (PREX1 E56A/N238A, PREX2 E30A/N212A), or mock-transfected with vector only (v.o. control), and were serum-starved for 8 h in serum-free medium containing 0.1% BSA, prior to stimulation with 25 nM insulin for the indicated periods of time. Total cell lysates were western blotted for active Akt (phospho-S473). **(A,B)** Representative Western blots, **(C,D)** overexpression controls western blotted for EE tag and **(E,F)** quantification by ImageJ densitometric analysis of HepG2 with **(A,E)** PREX1 or PREX1 E56A/N238A, **(B,F)** PREX2 or PREX2 E30A/N212A. Data are mean ± SEM of 3-6 independent experiments, normalized to the v.o. 0-time point. Statistics are 2-way ANOVA repeated measures and Dunnett's multiple comparisons correction.

4.5.4 Targeting strategy of catalytically inactive Prex mouse strains

On the basis of my data that showed the effects of overexpressed human GEF-dead PREX1 E56A/N238A and PREX2 E30A/N212A on insulin signalling in HepG2 cells, together with the literature on the adaptor function of PREX2 as an inhibitor of PTEN, led me to generate knock-in mice. In these mice, point mutations were introduced in the genomic loci that turn wild type Prex1 and Prex2 into catalytically inactive Prex1 or Prex2 proteins, with the aim of studying adaptor functions of the Prex proteins in glucose homeostasis *in vivo*.

To generate catalytically inactive Prex1 and Prex2 mouse strains, the equivalent residues in the murine DH domain to those described above for the work in the HepG2 cell line and with human recombinant protein were targeted and mutated to alanine in the mouse genome. For mouse Prex1, these residues are Glu^{51} and Asn^{233}, and for mouse Prex2 they are Glu^{22} and Asn^{204}. Within the mouse genomic sequence, the two target residues in each gene are located ~ 90 kb apart, too far apart to be targeted through a single homologous recombination event, and too close to enable the generation of mice by crossing strains with a single mutation. Therefore, CRISPR technology was selected to be used. The principle of CRISPR technology is to design single guide RNAs (sgRNAs) that direct the *Streptococcus pyogenes*-derived wild type Cas9 nuclease to introduce a double-strand cleavage at a specific sequence within the genome and thus enable genome editing (Qi et al., 2013; Ran et al., 2013a; Ran et al., 2013b) (**Figure 4.5.4**).

For this project, the following targeting plans were considered. The first was to employ wild type Cas9, which mediates site-specific double-strand DNA brakes 3 bp 5’ of the PAM sequence, to target both exons of Prex1 or Prex2 at the same time, using two different repair templates. However, there were concerns about off-target effects and losing parts of the genomic sequence due to the introduction of double-strand brakes. Therefore, the alternative of using the Cas9D10A (Cas9 nickase), which cleaves only one DNA strand, was considered. Cas9D10A allows increased specificity when loci are targeted by paired Cas9 complexes designed to generate adjacent DNA nicks. The thought was that each locus would be targeted with a pair of Cas9D10A and the relevant repair template for the introduction of the

desired mutation. The drawbacks of this approach were the amount of components that needed to be microinjected into the zygote and the remaining fear of losing parts of the genomic sequence. A third option was to introduce one Cas9 nickase for each target locus, one aiming at the transcribed strand and one aiming at the non-transcribing strand, which would decrease the zygote loading and keep the genome stable. However, there were concerns about the efficiency with which the repair template would be incorporated. Taking everything into consideration, it was decided to opt for the first strategy, but the sgRNAs were selected in a way that would keep viable the third option as well.

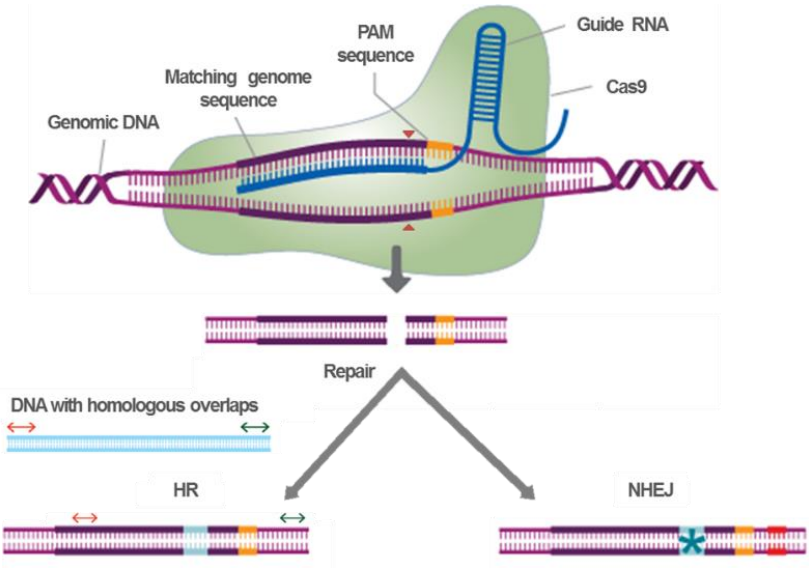

Figure 4.5.4: Principle of CRISPR-Cas9 gene editing technology
The Clustered Regularly Interspaced Short Palindromic Repeats (CRISPR) Type II system consists of the Cas9 nuclease from *S. pyogenes* (green) and the Guide RNA (blue), comprising a scaffold which binds to the Cas9 nuclease and a 20-nt guide sequence which pairs with the DNA target, directly upstream of a requisite 5′-NGG adjacent motif (PAM; yellow). Cas9 mediates a DSB ~3bp upstream of the PAM (red arrows). The double-strand brakes can be repaired either through the error-prone non-homologous end joining (NHEJ) mechanism which results in random indel mutations or through the homology directed (HD) repair by the introduction of a repair template (Ran et al., 2013b). (Diagram adapted from (transOMIC technologies, 2012)).

4.5.4.1 Design of the single guide RNAs

Having decided on a targeting strategy, the next step was to design sgRNAs for *Prex1* and *Prex2*. The genomic sequences of interest were analysed by web-based bioinformatic tools developed to identify suitable target sites and computationally predict off-target sites for each target. I chose the following databases: the Feng Zhang laboratory's CRISPR Design Tool, the Broad Institute's sgRNA Designer, and E-CRISPR. The intended target sites that were identified by all softwares as most specific were further evaluated as suitable sgRNAs for each specific genomic site to be targeted. The sgRNAs were selected to be into close proximity with the targeted residues which would enable the design of a smaller repair template. Moreover, sgRNAs for both DNA strands were selected to be tested for their efficiency (**Table 4.4**).

Table 4.4: sgRNA sequences tested for each intended point mutation in the mouse *prex1* and *prex2* genes. In green are annotated the requisite PAM sequences, which are not part of the sgRNA sequences themselves.

Mutation on Prex1 Exon 1, nt265-267, GAG -> GCG		
Name	**sgRNA Oligo Sequence**	**Target Strand**
mwt 1.1	GTGCGTACTCAACGAGATCC-TGG	sense
mwt 1.2	GGGCACCGAGCGCGACTACG-TGG	sense
mwt 1.3	GCGTTGAGTACGCACAGACGG-AGG	antisense
Mutation on *Prex1* Exon 6, nt92590-92592, AAT -> GCT		
Name	**sgRNA Oligo Sequence**	**Target Strand**
mmt 1B.2	GCAATGAGACTAAGAGGCAGA-TGG	sense
mwt 1.5	GCCAACATCAATGAGACTAAG-AGG	sense
mwt 1.6	GTTGGAGCAGACAGTCTTCA-TGG	antisense
Mutation on *Prex2* Exon 1, nt392-394, GAG -> GCG		
Name	**sgRNA Oligo Sequence**	**Target Strand**
mmt 2A.1	GCGCTGAGCACGCACACGCGC-AGG	antisense
mmt 2B.1	GAAGACCGAGCGCGACTACG-TGG	sense
mwt 2.3	GCGCGACTACGTGGGCACGC-TGG	sense
Mutation on *Prex2* Exon 6, nt96342-96344, AAT -> GCG		
Name	**sgRNA Oligo Sequence**	**Target Strand**
mwt 2.4	GCGTGTGTTCCAACATTAATG-AGG	sense
mmt 2A.2	GTTGGAACACACGGCTTTCA-TGG	antisense
mmt 2B.2	GTAATGAGGCCAAGAGACAGA-TGG	sense

4.5.4.2 *In Vitro* assessment of sgRNA efficiency

To assess the efficiency with which the designed sgRNAs guided the Cas9 nuclease to cleave at the right site in the *Prex1* and *Prex2* genomic sequence, the Guide-it sgRNA *In vitro* Transcription and Screening System was used initially. In this system, an sgRNA construct was produced by *in vitro* transcription, and it was subsequently used in combination with recombinant Cas9 nuclease *in vitro* to cleave PCR amplified *Prex1* or *Prex2* genomic target sequences, respectively (**Table 4.5**). DNA template and sgRNA provided by the kit manufacturer were used as positive controls, whereas negative controls were PCR amplified target sequences digested with recombinant Cas9 only, without any sgRNA.

After the *in vitro* cleavage reaction, the DNA products were resolved by gel electrophoresis. As can be seen in **Figure 4.5.5A**, all the designed sgRNAs managed to guide the Cas9 nuclease correctly to the intended *Prex1* or *Prex2* target sequence, and facilitated the introduction of a double-strand brake. For each target site, the upper band (labelled as Band A; **Figure 4.5.5A**) was the un-cleaved DNA sequence, whereas the two bands below, labelled Band B, where the cleavage products. Given that the produced DNA fragments were of the predicted size, it was concluded that the sgRNAs had indeed guided the Cas9 nuclease to the intended target sites. However, the presence of remaining un-cleaved DNA template also demonstrated that the sgRNAs resulted in a partial rather than total digest of the targeted sequence. In order to evaluate the efficiency of the sgRNAs therefore, lane profile analysis of the gel images was performed using Image Lab Software to quantify the band densities (**Figure 4.5.5B**). The efficiency of each sgRNA for each locus was defined as the percentage of un-cleaved template. The sgRNA that left the lowest percentage of un-cleaved targeting template was considered to be the best for that locus (**Figure 4.5.5B**).

For exon 1 of *Prex1,* the most efficient sgRNA was Mwt 1.2, with 26.4% of un-cleaved DNA template left, while for exon 6, Mmt 1B.2 (7.3%) was the best. Regarding the targeting of *Prex2*, the most efficient sgRNA for exon 1 was Mmt 2B.1 with only 9.7% of un-cleaved DNA template left, and for exon 6 Mmt 2B.2 (12.1%). In addition to the best sgRNA for each locus, the second best was also selected for further assessing of their efficiency in the NIH/3T3 mouse cell line. The selected

sgRNAs were the following: for the targeting of *Prex1* exon 1 - sgRNAs Mwt 1.1 and Mwt 1.2; for the targeting of *Prex1* exon 6 - sgRNAs Mmt 1B.2 and Mwt 1.6; for the targeting of *Prex2* exon1 - sgRNAs Mmt 2A.1 and Mmt 2B.1; and finally for the targeting of *Prex2* exon6 - sgRNAs Mwt 2.4 and Mmt 2B.2.

Table 4.5: List of primer pairs used for the amplification of ~2 kb DNA fragments containing the region of interest to be tasted in the guide-it sgRNA *in vitro* transcription and screening system and the surveyor assay.

#	gRNA Target	Forward Primer	Reverse Primer	Product size	gRNA Tested	Distance from F primer	Distance from R primer
1	Prex1 Exon1	TGAATGGGTCT TGGCCTACA	AAAACCGCAGT CAACCTAGC	1916	mwt 1.1	627	1289
					mwt 1.2	649	1268
					mwt 1.3	607	1309
2	Prex1 Exon6	GGCACCCACAG AACGAATTA	CAATGCCCCTT CCAAAGTCC	1978	mwt 1.5	617	1362
					mwt 1.6	587	1391
					mmt1B.2	623	1355
3	Prex2 Exon1	GGTCAGTGGTG TGGTTGTTT	CCACCAAGTCC AGCTCAAAT	2151	mmt2A.1	677	1474
					mwt 2.1	719	1432
					mwt 2.3	727	1424
4	Prex2 Exon6	TCAGTTTTGAA ATTGTGGTGCA	GCTGAGGGACA TTCAAGACC	2039	mwt 2.4	494	1545
					mmt2A.2	473	1566
					mmt2B.2	509	1530

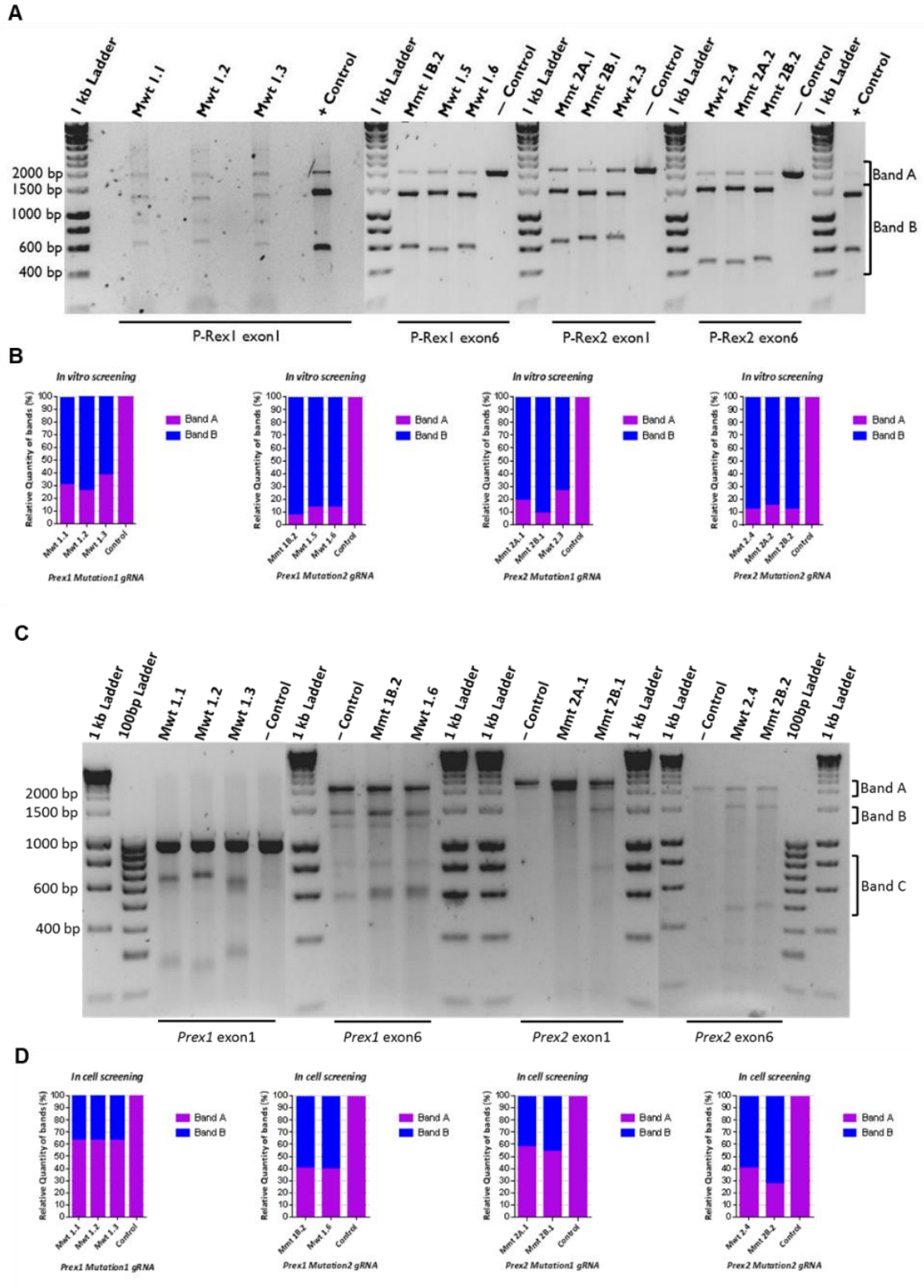
A
1 kb Ladder
Mwt 1.1
Mwt 1.2
Mwt 1.3
+ Control
1 kb Ladder
Mmt 1B.2
Mwt 1.5
Mwt 1.6
– Control
1 kb Ladder
Mmt 2A.1
Mmt 2B.1
Mwt 2.3
– Control
1 kb Ladder
Mwt 2.4
Mmt 2A.2
Mmt 2B.2
– Control
1 kb Ladder
+ Control
2000 bp
1500 bp
1000 bp
600 bp
400 bp
Band A
Band B
P-Rex1 exon1
P-Rex1 exon6
P-Rex2 exon1
P-Rex2 exon6
B
In vitro screening
Relative Quantity of bands (%)
Band A
Band B
Mwt 1.1
Mwt 1.2
Mwt 1.3
Control
Prex1 Mutation1 gRNA
In vitro screening
Mmt 1B.2
Mwt 1.5
Mwt 1.6
Control
Prex1 Mutation2 gRNA
In vitro screening
Mmt 2A.1
Mmt 2B.1
Mwt 2.3
Control
Prex2 Mutation1 gRNA
In vitro screening
Mwt 2.4
Mmt 2A.2
Mmt 2B.2
Control
Prex2 Mutation2 gRNA
C
1 kb Ladder
100bp Ladder
Mwt 1.1
Mwt 1.2
Mwt 1.3
– Control
1 kb Ladder
– Control
Mmt 1B.2
Mwt 1.6
1 kb Ladder
1 kb Ladder
– Control
Mmt 2A.1
Mmt 2B.1
1 kb Ladder
1 kb Ladder
– Control
Mwt 2.4
Mmt 2B.2
100bp Ladder
1 kb Ladder
2000 bp
1500 bp
1000 bp
600 bp
400 bp
Band A
Band B
Band C
Prex1 exon1
Prex1 exon6
Prex2 exon1
Prex2 exon6
D
In cell screening
Relative Quantity of bands (%)
Band A
Band B
Mwt 1.1
Mwt 1.2
Mwt 1.3
Control
Prex1 Mutation1 gRNA
In cell screening
Mmt 1B.2
Mwt 1.6
Control
Prex1 Mutation2 gRNA
In cell screening
Mmt 2A.1
Mmt 2B.1
Control
Prex2 Mutation1 gRNA
In cell screening
Mwt 2.4
Mmt 2B.2
Control
Prex2 Mutation2 gRNA

Figure 4.5.5: *In Vitro* and Surveyor DNA cleavage assays revealed the efficiency of sgRNAs and Cas9 nuclease for the generation of catalytically inactive Prex1 and Prex2 mice.

(A) PCR fragment of *Prex1* or *Prex2* mouse genomic sequence containing the sgRNA target sites were incubated with candidate sgRNAs and recombinant Cas9 nuclease and cleavage products resolved by gel electrophoresis. As a positive control (+ Control), a 2kb control fragment and control sgRNA were used as provided with the kit. As negative controls (– Control), DNA fragments were incubated with Cas9 in absence of sgRNA. **(B)** Image Lab Software was used to quantify the efficiency of the sgRNAs. In each lane, band A denotes the un-cleaved DNA template, and bands B and C the cleaved products. The quantity of un-cleaved DNA template remaining in band A was used to determine the cleavage efficiency of each sgRNA (low un-cleaved DNA template = high sgRNA efficiency). **(C)** DNA was extracted from NIH/3T3 cells transfected with pSpCas9(BB)-2A-GFP plasmid expressing sgRNA for exon 1 and exon 6 of *Prex1* and *Prex2*, respectively. The sgRNA target sites were PCR amplified from genomic DNA extracted from wild type and transfected cells. The PCR product of the mutated cells was combined with equal amounts of the corresponding PCR product from wild type cells, and the Surveyor Nuclease was used to cleave the mismatched sites. The cleavage products were resolved by gel electrophoresis. Homoduplexes from wild type DNA fragments were used as negative controls (– control). **(D)** Quantification of sgRNA efficiency as in (B). Cleavage products present in the negative control were considered to be due to the exonuclease activity of the Surveyor Nuclease, and were not taken into consideration.

4.5.4.3 Assessment of sgRNA efficiency in cells

To assess if the sgRNAs could perform as well in cells as they did in the *in vitro* system, the NIH/3T3 mouse cell line was chosen as the test system, and a Surveyor Assay was used that is based on the ability of Surveyor Nuclease to introduce double-strand brakes on the 3'-side of mismatched sites. For these experiments, NIH/3T3 cells were co-transfected with an sgRNA-expressing pSpCas9(BB)-2A-GFP plasmid and a puromycin-expressing plasmid. GFP fluorescence was used as a rough indicator of transfection efficiency. Puromycin resistance was used for antibiotic selection. After recovery, the cells were harvested and lysed for DNA extraction. Thereafter, the relevant genomic regions of Prex1 and Prex2 were amplified by PCR, and the DNA PCR products of wild type and transfected cells were mixed in equal quantities to enable heteroduplex formation. The heteroduplexes were then treated with Surveyor Nuclease. As a negative control, homoduplexes of wild type DNA samples were used.

As can be seen in **Figure 4.5.5C**, the Surveyor Nuclease treatment led to the cleavage of the heteroduplex DNA molecules into two smaller molecules, labelled Band B and Band C, respectively. Besides these products, there remained un-cleaved wild type or mutant homoduplexes (top bands: Band A), indicating that the cleavage sides were specific for mismatched DNA sequences, as desired. Furthermore, there were also some digestion products in the negative controls, likely due to the exonucleolytic activity of the Surveyor Nuclease. Although these bands were considered to be background, they were included in the lane profiling used for the quantification of the sgRNAs efficiency in order to provide conservative estimates of cleavage efficiency (**Figure 4.5.5D**). As with the previous *in vitro* analysis step, the efficiency of each sgRNA for each genomic locus was again defined as the percentage of un-cleaved template. The sgRNA that left the lowest percentage of un-cleaved targeting template was considered the best for that locus.

The results obtained by the Surveyor Assay reinforced our conclusion from the *in vitro* assay that the designed sgRNAs were of sufficiently high efficacy and specificity, and confirmed furthermore that they work in cells as well as *in vitro*. This result allowed progression to the next step in the targeting process, the design of appropriate repair template DNAs that carry the desired point mutations.

4.5.4.4 Design of the single-stranded DNA repair template

In order to introduce the desired point mutations in the *Prex1* or *Prex2* mouse genome by HDR, ssDNA donor oligo nucleotides were designed for each targeted genomic site. Following recommendation from the Head of our Gene Targeting Facility, Dr Dominik Spensberger, the repair templates were designed to be around ~200 nt long and have symmetric homology arms of at least 90 nt. Apart from the desired point mutation, the possibility of having additional "silent" point mutations that would destroy the PAM site and/or significantly change the sequence of the sgRNA was also explored. This was necessary in order to avoid Cas9 cleavage of the HDR-edited sites. Finally, to facilitate detection of successful targeting by PCR-based detection assay, silent nucleotide changes that would create restriction enzyme sites without affecting the amino acid sequence of the proteins were introduced (**Figure 4.5.6**).

Therefore, the final selection of the sgRNAs was done on the basis that it enabled the repair template to meet all the aforementioned criteria. The sequence of the designed templates is shown in **Table 4.6**

Table 4.6: ssDNA repair template sequence designed for each intended point mutation in the mouse Prex1 and Prex2 genes. In bold red are annotated the desired point mutations, whereas in plain red are highlighted the silent mutations. The nucleotide changes in Prex1 exon 1 will result in the E51A mutation and exon 6 in N233A. The equivalent changes in Prex2 will result in the E22A and N204A mutations, respectively

Mutation on Prex1 Exon 1, nt265-267, GAG -> GCG	
Name	**ssDNA Oligo Sequence**
P1M1	GGTGCGCATCCCGATGCTCGCGGCCCCGTCTCCGGGCCGTGCGCGGCC GCCCGCGACTCGGAGCGCCAGCTGCGCCTCCGTCTGTGCGTACTCAAC**G CC**ATCCTAGGCACCGAGCGCGACTACGTGGGCACCTTGCGTTTCCTGCA GTCGGTGAGCTCCCGCCACCTGTGGCCGGCCGGCCCGCGTTGCGCTTTT GTC
Mutation on *Prex1* Exon 6, nt92590-92592, AAT -> GCT	
Name	**ssDNA Oligo Sequence**
P1M2	ACTAGGAGTTGGCCAAGAGGACCCCCGGCAAGCACCCTGACCACACCGC GGTACAGAGTGCCCTGCAGGCCATGAAGACTGTCTGCTCCAACATC**GCG** GAGACCAAGCGACAAATGGAGAAGCTGGAGGCCCTGGAGCAGCTGCAGT CTCACATTGAAGGCTGGGAGGTGCGTGGTCAGGGTCCTCTGCTGAGGGG GCT
Mutation on *Prex2* Exon 1, nt392-394, GAG -> GCG	
Name	**ssDNA Oligo Sequence**
P2M1	CTTGCCCCCAGCTCCGCGCCCCGCCGGCCACCATGAGCGACGAAAGCG CCAGGGAAGTAGACAAGCAGCTTCGCCTGCGCGTGTGCGTGCTCAGC**GC TC**TTCAGAAGACCGAGCGCGACTACGTGGGTACCCTAGAGTTCCTGGTGT CGGTGAGTAGCCGGCCCCGCGCACGGCACCAAGTCTGGAGCATTGTCTG C
Mutation on *Prex2* Exon 6, nt96342-96344, AAT -> GCG	
Name	**ssDNA Oligo Sequence**
P2M2	TCTCCACAGGAATTACTGAAGCGGACTCCACGGAGACATAGTGACTACAC AGCAGTGATGGAAGCACTCCAAGCCATGAAAGCCGTGTGTTCCAATATT**G CT**GAGGCCAAGCGGCAAATGGAGAAACTGGAAGTTTTAGAAGAGTGGCA GGCACACATTGAAGGCTGGGAGGTACGTGTCCTTTGCTCAGCTCTT

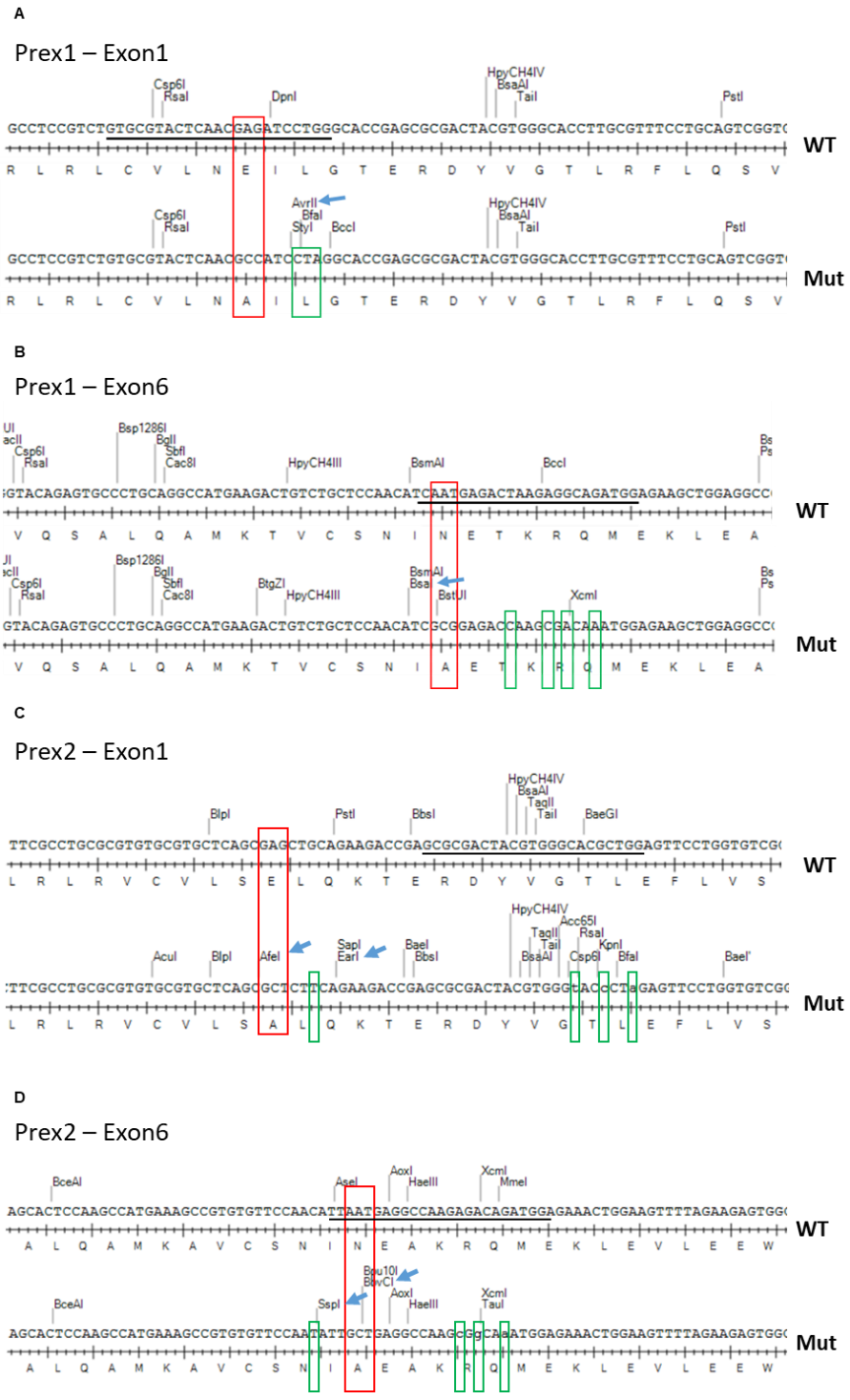

Figure 4.5.6: Design of DNA repair templates.

Part of the DNA repair templates used for the introduction of point mutations in Prex1 **(A)** exon 1 and **(B)** exon 6, and Prex2 **(C)** exon 1 and **(D)** exon 6. The top line represents the wild type sequence whereas the bottom line shows the sequence of the repair template. In red boxes are annotated the nucleotide changes introduced to render the protein catalytically inactive. In green boxes are highlighted the silent mutations introduced to create restriction enzyme sites and/or change the sgRNA sequence. Blue arrows show the unique restriction enzyme sites which could help in genotyping. The nucleotide changes in Prex1 exon 1 will result in the E51A mutation and exon 6 in N233A. The equivalent changes in Prex2 will result in the E22A and N204A mutations, respectively.

4.5.5 Generation of catalytically inactive Prex1 mouse strain

Once the CRISPR targeting components were designed and validated, the materials were given to Dr Dominik Spensberger from the Babraham gene Targeting Facility for injection into mouse zygotes. However, given that CRISPR zygote injections had not been performed previously at the Babraham Institute, it was decided to perform ES cell targeting in parallel as a backup strategy. For this approach, Dr Spensberger targeted White C57BL/6J ES cells (black-6 background cells with mutations in fur colour genes that produce white-coated animals), using the same strategy and materials.

The genotyping methods considered so far included PCR amplification of the two *Prex1* loci of interest, analysis by gel electrophoresis, purification of the PCR products and either analytical restriction enzyme digest or Sanger sequencing. Due to the large number of ES clones that resulted from the targeting for the two *Prex1* mutations, it was concluded that the aforementioned approach would not be cost- and time-effective for a big scale screening. Hence, primers specific for the desired mutations were designed and validated in order to develop a PCR-only based screening (see Materials and Methods **Table 3.7**).

Through this method, out of two 96 well plates, one ES clone was found to be positive for mutation E51A in exon 1 of Prex1, and this ES cell clone was retargeted for mutation N233A on exon 6. After the second round of targeting, out of two 96 well plates, one ES clone was found to be positive for mutation N233A on exon 6 by PCR. This finding was further confirmed by Sanger sequencing which showed that this ES colony was positive for both mutations in *Prex1* (**Figure 4.5.7A**)**.** This ES colony was used for injection into mouse C57BL/6J blastocysts. The blastocysts were then transferred into the ovaries of pseudopregnant C57BL/6J recipients and chimeric pups were born. The coat colour was used to estimate the contribution of targeted ES cells to the chimeric mice. Mice with agouti coats (**Figure 4.5.7B**) were genotyped by PCR to assess the extent of incorporation of the two *Prex1* mutations. Mice that were found to be heterozygous for the mutations were set up for breeding with wild type C57BL/6J mice. From this breeding, germline transmission was achieved, but only one mouse that was heterozygous for mutation on exon 6 of *Prex1* but wild type for E51A was born (**Figure 4.5.7C**). (Presumably,

this mouse was only mutated for N233A because the ES cell clone was not properly clonal after the initial E51A targeting event). In any event, the resulting heterozygous Prex1$^{E51A/+}$ mouse unfortunately died without giving birth to any heterozygous pups, and this first targeting attempt was therefore unsuccessful in establishing the mouse strain.

In our second attempt to generate mice with catalytically inactive Prex1, Dr Spensberger used the same targeting strategy but microinjected the material into zygotes instead of transfecting it into ES cells. Microinjected zygotes were then implanted into female recipients, and all resulting pups were genotyped by PCR and Sanger sequencing. Dr Spensberger trialled several options, and found the simultaneous injection of the targeting material for both mutations to be unfavourable, whereas targeting of E51A alone was successful and produced one heterozygous *Prex1*$^{E51A/+}$ animal. Unfortunately, this heterozugous female died while giving birth to her first litter, and all her pups perished, so this second attempt at generating a GEF-dead Prex1 mouse strain also failed. Further attempts are currently ongoing.

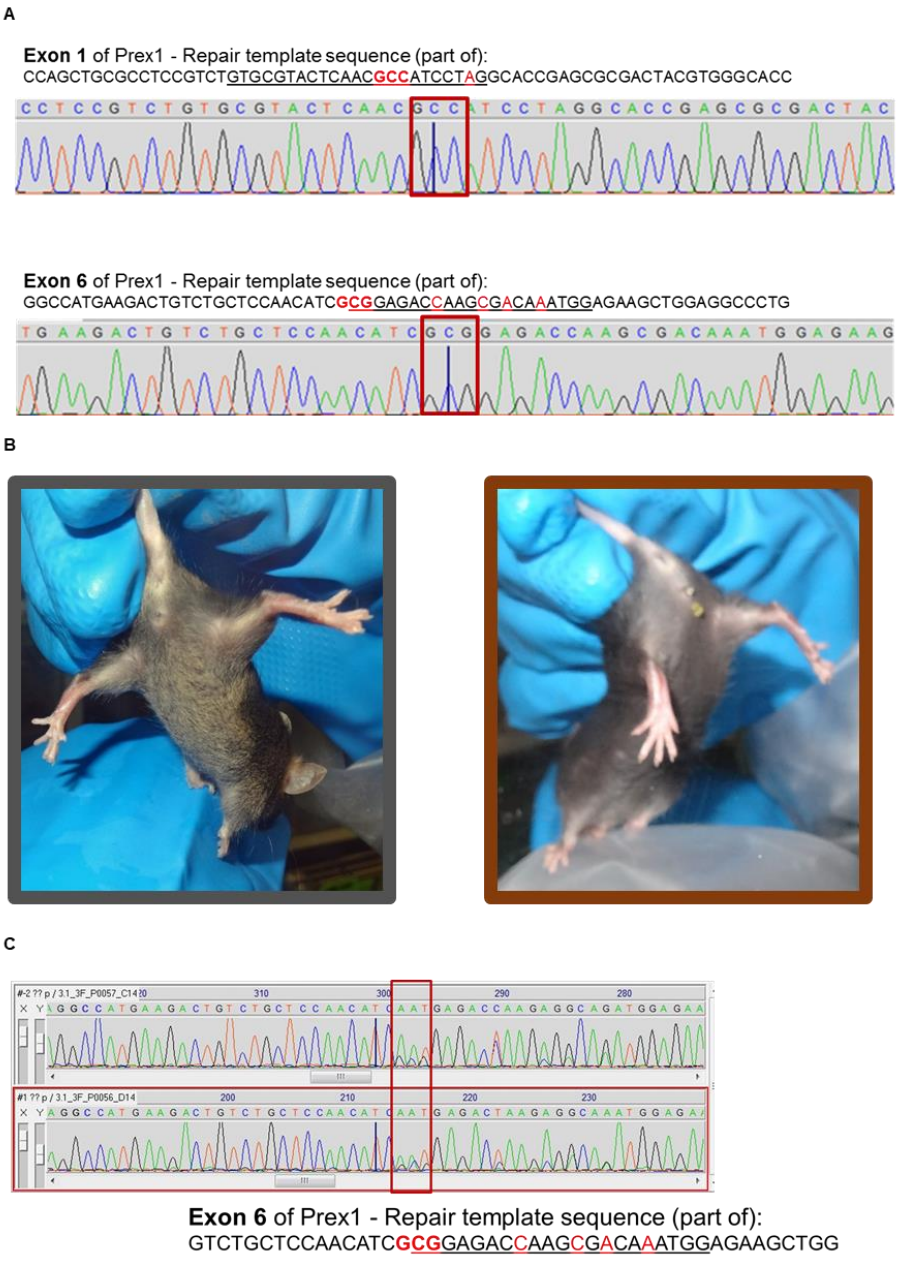

Figure 4.5.7: Generation of catalytically inactive Prex1 mouse strain.

(A) Positively targeted ES cells. One sgRNA for each mutation was cloned into the pCas-Guide-EF1a-CD4 vector. The CRISPR plasmids were transfected into mouse ES cells. To determine the overall editing efficiency of the CRISPR, DNA was extracted from the pool of transfected cells and pools containing recombinant alleles identified via PCR screening. To obtain monoclonal genome-edited colonies, positive pools were plated onto a P100 cell culture plate to form single-cell colonies. The individual ES cell clones were subjected to a second round of PCR screening to identify the clones containing the desired knock-in allele and positive clones were also confirmed by Sanger sequencing. Positively targeted ES cells were injected into C57BL/6J blastocysts to produce chimeras. **(B)** Representative images of positive and negative chimeric mice. **(C)** Germline transmission.

4.5.6 Generation of catalytically inactive Prex2 mouse strain

The experience from targeting the Prex1 strain allowed Dr Spensberger to optimise the protocol for direct zygote injection, and he used this for the generation of the catalytically inactive Prex2 mouse strain. Initially, mice positive for the mutation on exon 1 of Prex2 (E22A) were generated and bred together until the mutation was established at homozygous state. Zygotes from these homozygous mice were then re-targeted for the second mutation on exon 6 (N204A) (**Figure 4.5.8**). In this manner, both the *Prex2*$^{E22A/E22A}$ and the *Prex2*$^{E22A/E22A;\ N204A/N204A}$ strains were established successfully. These homozygous strains were called Prex2 E22A and Prex2 E22A/N204A, for brevity. The homozygous mice were born at the expected Mendelian rate, were fertile, bred well and appeared healthy.

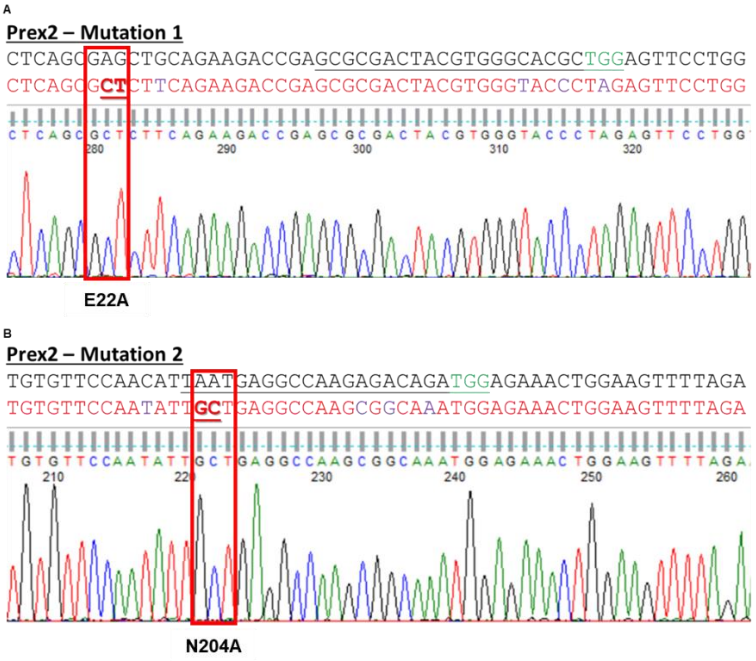

Figure 4.5.8: Generation of catalytically inactive Prex2 mouse strain.
Genomic sequence from the homozygous Prex2 E22A/N204A mouse. Prex2 **(A)** exon 1 and **(B)** exon 6. The top line (black) represents the wild type sequence whereas the bottom line (red) shows the sequence of the repair template. In bold and underlined red and in red boxes are annotated the nucleotide changes introduced to render the protein catalytically inactive. In purple are the silent point mutations introduced to create restriction enzyme sites and/or change the sgRNA sequence. In underlined black is the sgRNA sequence whereas in underlined green is the PAM sequence.

4.5.7 Metabolic phenotype characterisation of Prex2 E22A mice

According to the literature, introduction of just one of the intended mutations in the DH domain of Prex2 should be sufficient to render the protein catalytically inactive (Lucato et al., 2015). Therefore, the *Prex2*$^{E22A/E22A}$ (Prex2 E22A) mouse strain was used to investigate the importance of the Rac-GEF activity in glucose homeostasis while the *Prex2*$^{E22A/N204A}$ strain was still being bred to homozygosity. The metabolic phenotype of Prex2 E22A mice was studied in the same manner as described previously for the Prex KO mice. Wild type C57BL/6J (C57BL/6J WT) mice of same age and sex were tested in parallel under the same conditions for direct comparison.

4.5.7.1 Metabolic phenotype of male Prex2 E22A mice on chow diet

Figures 4.5.9A and **4.5.10A** show that, on chow diet, Prex2 E22A males had lower fasting blood glucose levels compared to controls throughout ageing. What is more, from 15 weeks of age onwards, the Prex2 E22A mice also had a significantly improved response to IPGTT (**Figures 4.5.9C** and **4.5.10B**). Although their glucose levels peaked at 15 min post glucose injection, similarly to their C57BL/6J WT counterparts, their blood glucose levels decreased faster than in WT controls, and were almost back to basal levels at 90 min (**Figure 4.5.9A-B**). In contrast, C57BL/6J WT males showed signs of glucose intolerance from 15 weeks of age onwards. This was despite both genotypes having similar body weight, which increased at a comparable rate during ageing (**Figure 4.5.10C**). This increased glucose tolerance in Prex2 E22A mice was a striking effect, and proves that Prex2 has adaptor functions in the control of glucose homeostasis. Furthermore, the phenotype of these mice is stronger and different to the phenotype previously observed in the Prex2 KO males, which showed at best a tendency to improved glucose tolerance at young age and to glucose intolerance in old age. Hence, in the Prex2 KO mouse, another regulator of glucose homeostasis is likely to compensate for the loss of Prex2, which does not do in the Prex2 E22A mouse, as the Prex2 protein is still expressed in these mice to fulfil important adaptor roles.

To assess insulin sensitivity, Prex2 E22A mice were challenged with 0.75 IU/kg human insulin as described previously. At 5 months of age, the overall insulin response was slightly reduced in the Prex2 E22A mice compared to the C57BL/6J

WT controls (**Figure 4.5.11A, D**). The blood glucose levels of Prex2 E22A males dropped to their lowest level at 45 min post injection, showing a drop of 5 mM from basal, and returned to around 8 mM at 120 min (**Figure 4.5.11A, C**), contrary to the 6.5 mM drop observed in the C57BL/6J WT males. However, as discussed for the various Prex KO strains above, this observation could be due to an altered counter-regulatory response to critically low blood glucose levels at the peak of the response, as a result of the low fasting blood glucose levels (**Figure 4.5.11B**). At 10 months of age, the Prex2 E22A males showed a longer lasting response to insulin compared to their WT counterparts (**Figure 4.5.11E, G**). Although both genotypes had become somewhat insulin resistant at that age (their blood glucose levels having dropped by only 3.5 mM), the WT males showed a sharp rise back to the basal glucose levels at 120 min, while the Prex2 E22A followed a more steady increase (**Figure 4.5.11G**).

Interestingly, from the housing of mice in the metabolic cages it was observed, that Prex2 E22A mice produce more urine, compared to their C57BL/6J WT counterparts, despite their average water intake being almost identical. The food consumption and faeces production were similar between the two genotypes (**Figure 4.5.12**).

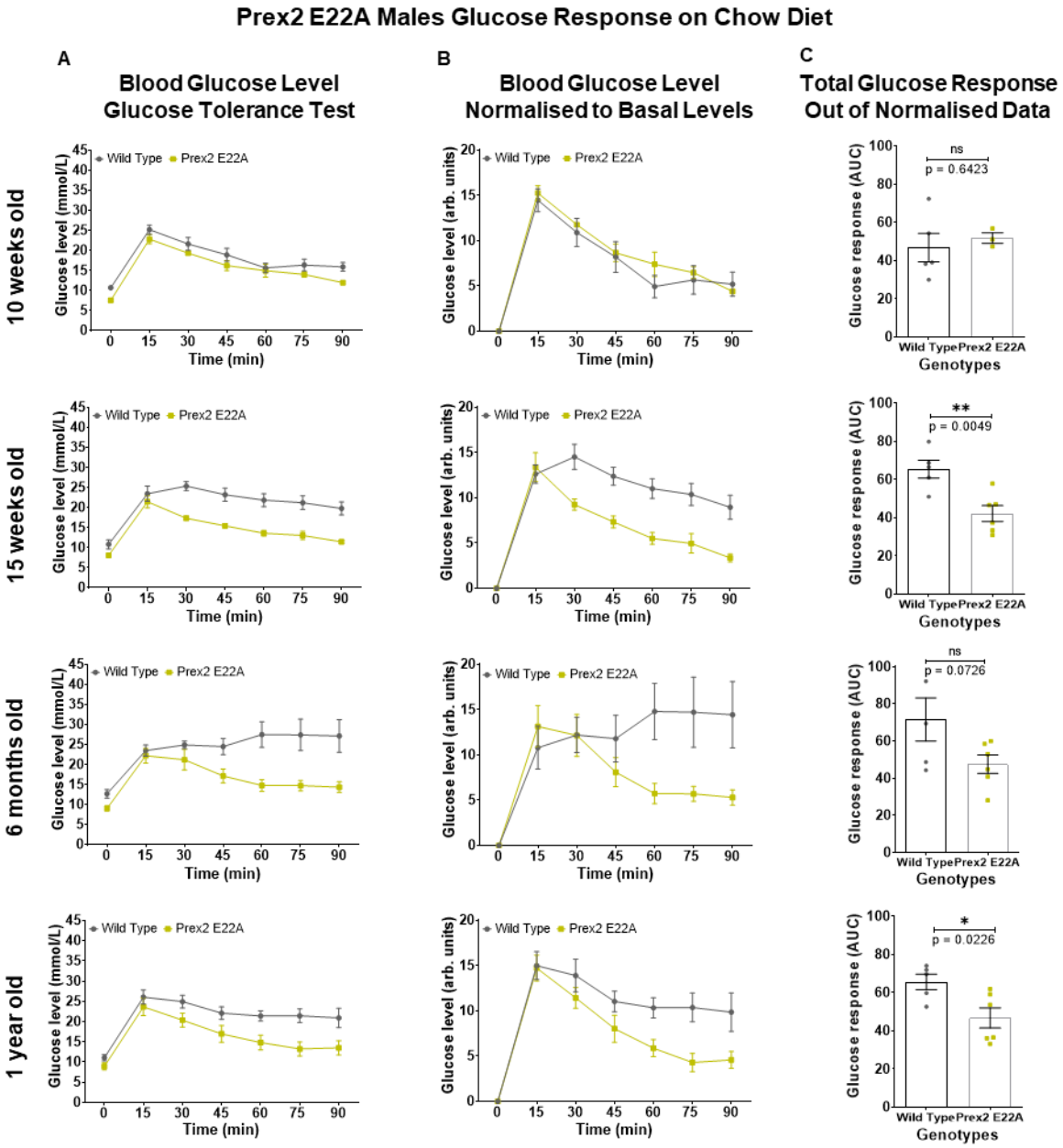

Figure 4.5.9: Male Prex2 E22A mice on chow diet show lower fasting blood glucose levels and better glucose tolerance than C57BL/6J WT mice.

The fasting blood glucose levels and response to IPGTT were measured in male *Prex2* $^{E22A/E22A}$ (Prex2 E22A, yellow) and C57BL/6J WT (grey) mice on chow diet at the ages of 10 and 15 weeks, 6, and 12 months, as described in the legend to **Figure 4.2.1**. **(A)** Blood glucose concentration during IPGTT. **(B)** Blood glucose levels during IPGTT, normalised by subtracting the basal blood glucose level. **(C)** Total glucose response (AUC of normalised data). Data are from 1 cohort (C57BL/6J WT n=4; Prex2 E22A n=5), and presented as mean ± SEM. 2-way ANOVA with repeated measures and Sidak's multiple comparisons correction was used to compare genotypes during IPGTT. Unpaired Student's *t*-test was used to analyse the total glucose response.

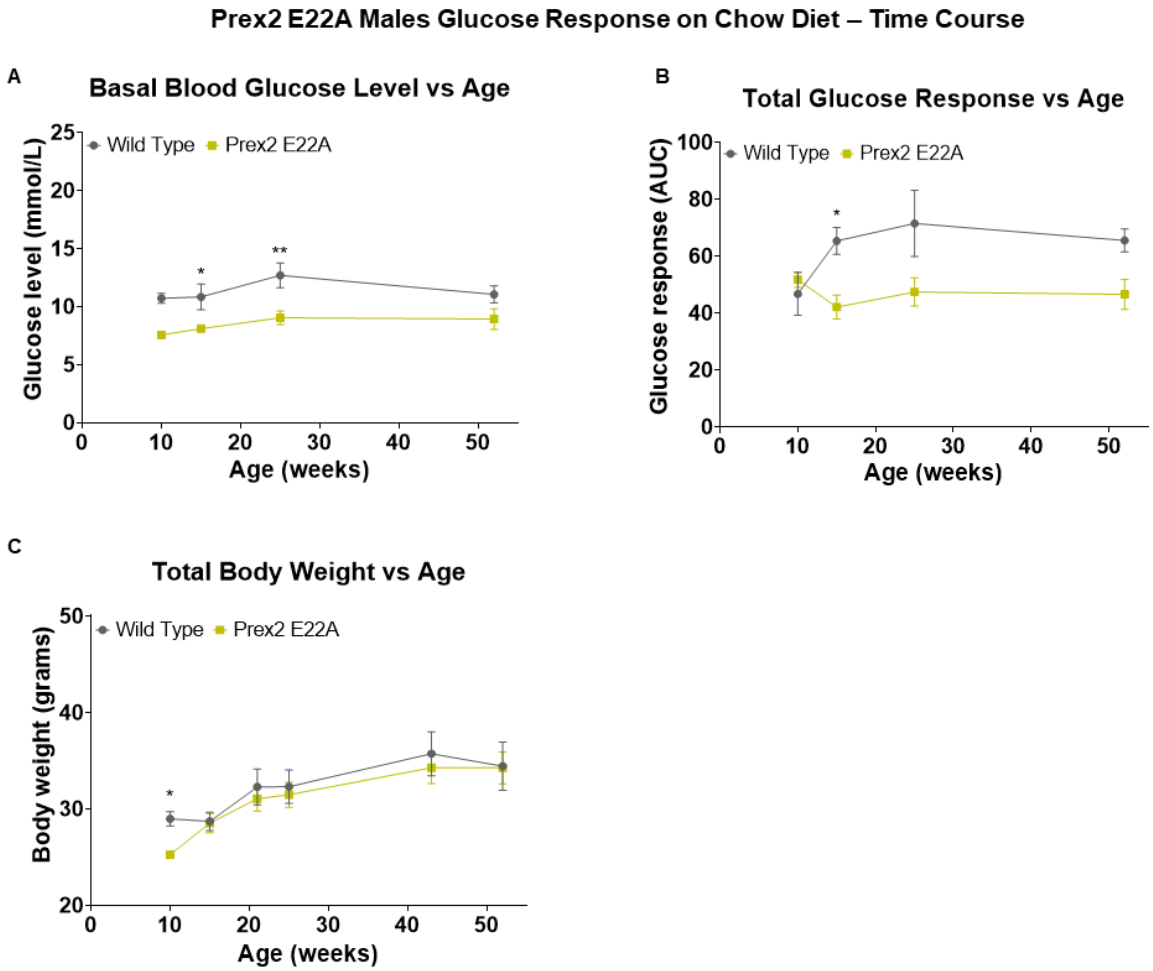

Figure 4.5.10: The low fasting blood glucose levels and improved glucose tolerance of male Prex2 E22A mice on chow diet persist throughout ageing.

The fasting blood glucose levels, response to glucose challenge, and body weight of the male Prex2 E22A (yellow) and C57BL/6J WT (grey) mice from **Figure 4.5.9** are expressed as a function of age. **(A)** Fasting blood glucose levels; data from column A in **Figure 4.5.9**. **(B)** Response to IPGTT; normalised data from columns B and C in **Figure 4.5.9**. **(C)** Body weight, measured after 6 and 4 h fasting, prior to glucose and insulin challenges, respectively. Data are from 1 cohort (C57BL/6J WT n=4; Prex2 E22A n=5), and are presented as mean ± SEM. 2-way ANOVA with repeated measures and Sidak's multiple comparisons correction was used to compare genotypes during ageing.

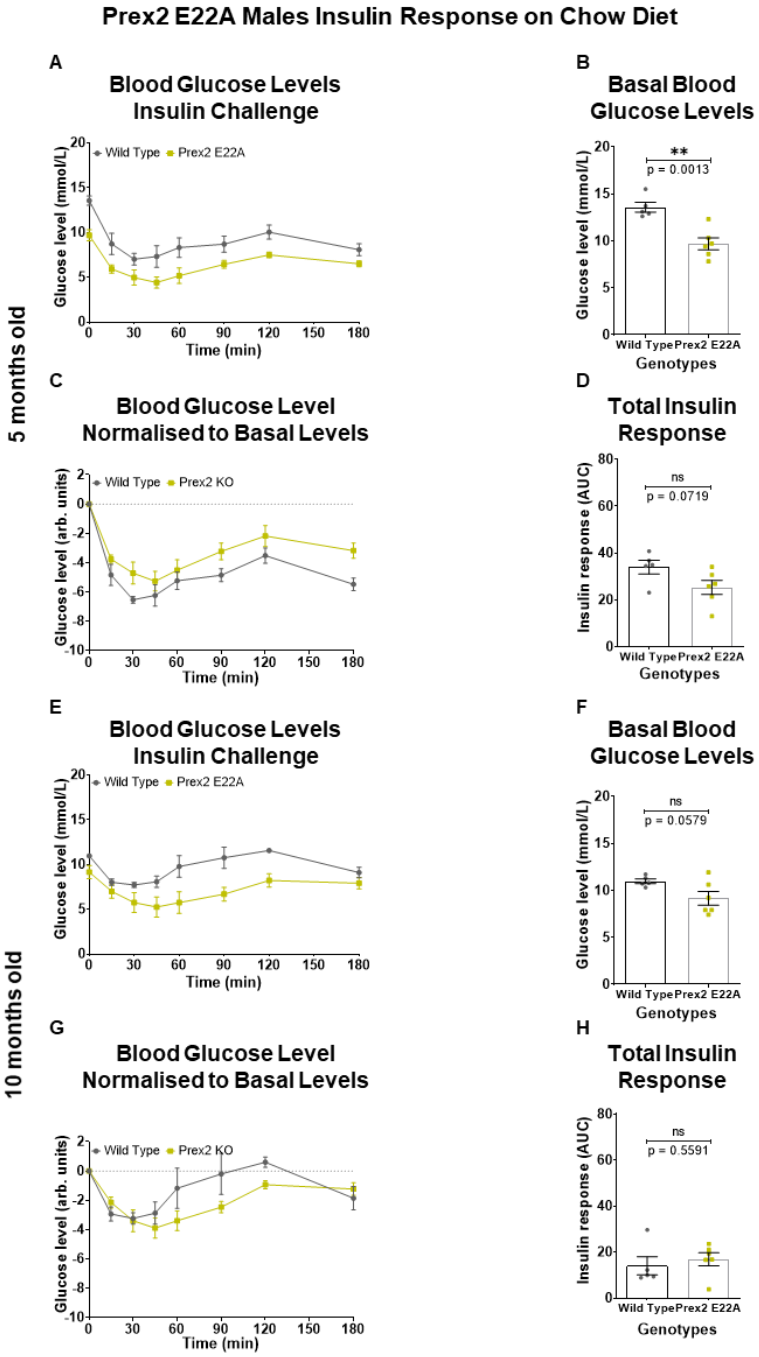

Figure 4.5.11: Male Prex2 E22A mice on chow diet show an altered response to insulin challenge compared to C57BL/6J WT mice.

The fasting blood glucose levels and response to SCITT were measured in male Prex2 E22A (yellow) and C57BL/6J WT (grey) mice on chow diet from **Figure 4.5.9** at the ages of **(A-D)** 5 and **(E-H)** 10 months, as described in the legend to **Figure 4.2.3**. **(A,E)** Blood glucose concentration during SCITT. **(B,F)** Fasting blood glucose levels. **(C,G)** Blood glucose levels during SCITT, normalised by subtracting the fasting basal blood glucose level from each mouse individually. **(D,H)** Total insulin response (AUC of normalised data). Data are from 1 cohort (C57BL/6J WT n=4; Prex2 E22A n=5), and are presented as mean ± SEM. 2-way ANOVA with repeated measures and Sidak's multiple comparisons correction was used to compare genotypes during SCITT. Unpaired Student's *t*-test was used to analyse the basal blood glucose levels and total insulin response.

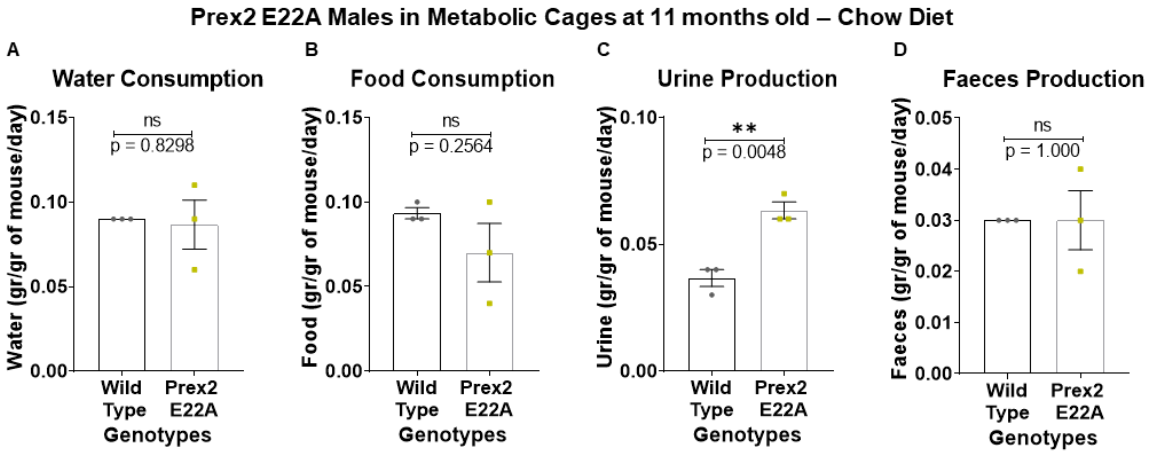

Figure 4.5.12: Male Prex2 E22A mice have increased urine production.
The male Prex2 E22A (yellow) and C57BL/6J WT (grey) mice from **Figure 4.5.9** were habituated to metabolic cages at 11 months of age, as detailed in Materials and Methods, weighed and group-housed (up to 3) in metabolic cages overnight for 16 h on 3 subsequent nights with food and water provided *ad libitum*. Their **(A)** water consumption, **(B)** food consumption, **(C)** urine production, and **(D)** faeces production were measured after each night and were normalised to the combined body weights of the mice housed in each cage. Data are from 1 cohort (C57BL/6J WT n=4; Prex2 E22A n=5), and are presented as the mean ± SEM of each night (n=3). Unpaired Student's *t*-test was used for the comparison between the genotypes.

4.5.7.2 Metabolic phenotype of male Prex2 E22A mice on HFD

To test the effects of diet on the metabolic phenotype of the Prex2 E22A mice, males were introduced to 45% HFD at the age of 10 weeks, after their "baseline" glucose challenge. As shown in **Figures 4.5.13A** and **4.5.14A**, male Prex2 E22A mice on HFD maintained low fasting blood glucose levels throughout ageing, similarly to what was observed previously in the Prex2 KO males on HFD. Surprisingly though, the Prex2 E22A mice also maintained their improved glucose tolerance throughout ageing (**Figures 4.5.132B-C and 4.5.14B**). Both the Prex2 E22A and their C57BL/6J WT controls developed some glucose intolerance due to the HFD. **Figure 4.5.13B** shows that it became difficult for mice to clear the glucose from their blood stream after glucose challenge, even though the dosage was reduced from 6 months onwards (to 0.5 g/kg, data in ochre box), similarly to what was previously observed in the Prex2 KO mice. However, the blood glucose levels in the Prex2

E22A males did not rise nearly as much as in the C57BL/6J WT controls and returned back to basal within the time frame of the experiment (**Figure 4.5.13B**). Again, this phenotype was more striking and distinct from that of Prex2 KO mice, which had been glucose intolerant under the same conditions. Hence, it seems that the Rac-GEF activity of Prex2 limits glucose tolerance, both on chow and HFD.

Both at 5 and 10 months of age, the insulin response of Prex2 E22A males on HFD was similar to that of C57BL/6J WT mice, despite their lower basal blood glucose levels (**Figure 4.5.15A-D, E-H**), which suggests that Prex2 does not have important adaptor functions in insulin sensitivity. This was again very different to the phenotype of the Prex2 KO mice on HFD, which were insulin resistant in old age. Hence, it seems that the Rac-GEF activity of Prex2 plays a role in maintaining the insulin sensitivity of old mice.

Although the two genotypes started from identical body weight, the Prex2 E22A mice gained weight at a slightly slower rate than the C57BL/6J WT mice (**Figure 4.4.14C**). Consequently, the body composition analysis, at 1 year, revealed that Prex2 E22A males on HFD had lower fat percentage compared to the heavier C57BL/6J WT controls (**Figure 4.4.14D**). This difference in the body fat percentage could be, at least in part, the reason for the improved glucose tolerance seen in Prex2 E22A mice. Finally, no difference was found in their water and food consumption or urine and faeces production in the metabolic cages (**Figure 4.5.16A-D**).

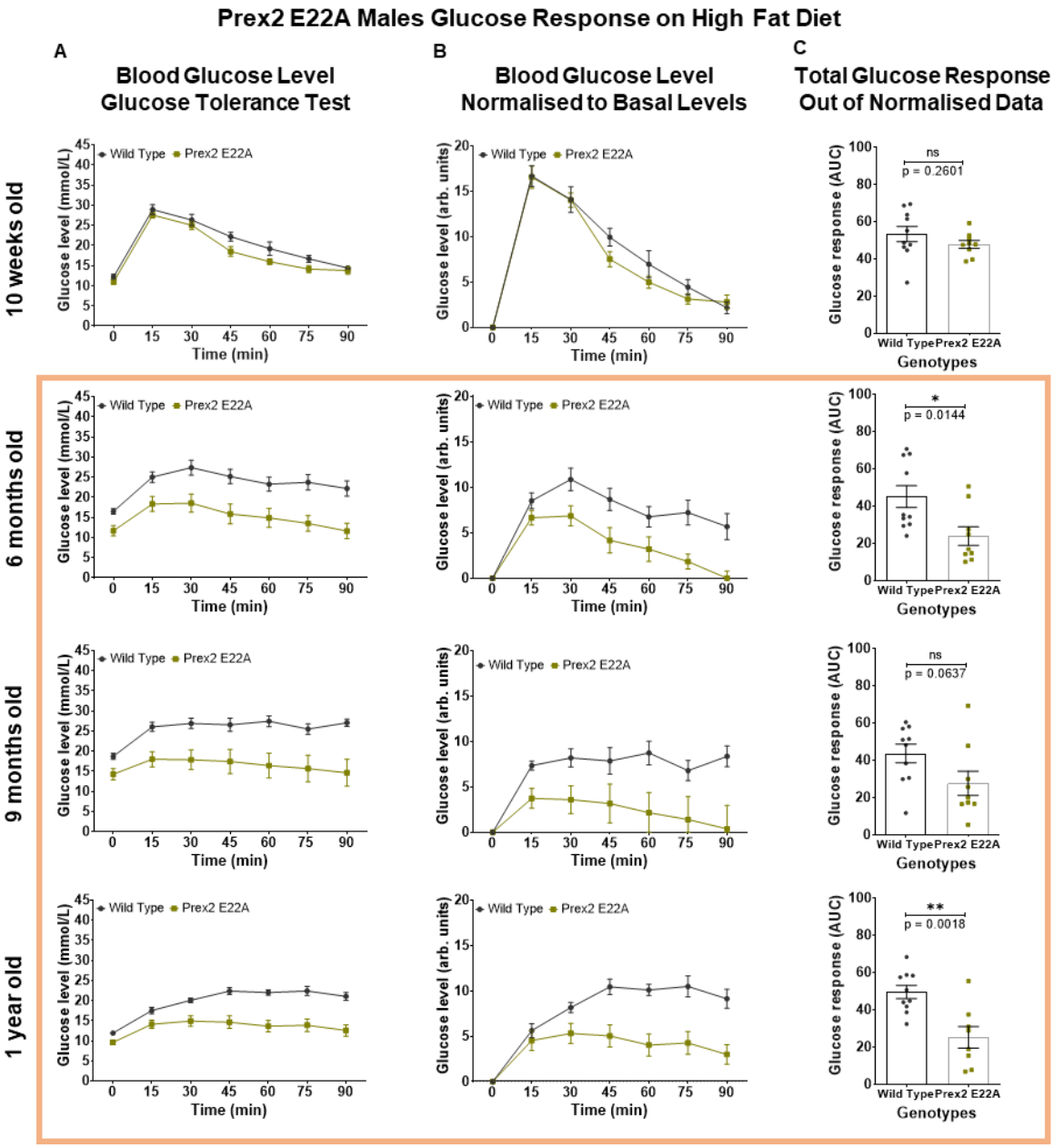

Figure 4.5.13: Male Prex2 E22A mice on HFD show lower fasting blood glucose levels and better glucose tolerance than C57BL/6J WT mice.

The fasting blood glucose levels and response to IPGTT were measured in male Prex2 E22A (yellow) and C57BL/6J WT (blue) mice on chow diet at the ages of 10 weeks, 6, 9, and 12 months, as described in the legend to **Figure 4.2.1**. Glucose was injected at 2 g/kg at 10 weeks of age, and at 0.5 g/kg at later ages (ochre box). **(A)** Blood glucose concentration during IPGTT. **(B)** Blood glucose levels during IPGTT, normalised by subtracting the basal blood glucose level. **(C)** Total glucose response (AUC of normalised data). Data are pooled from 2 independent cohorts (C57BL/6J WT n=10; Prex2 E22A n=9), and are presented as mean ± SEM. 2-way ANOVA with repeated measures and Sidak's multiple comparisons correction was used to compare genotypes during IPGTT. Unpaired Student's *t*-test was used to analyse the total glucose response.

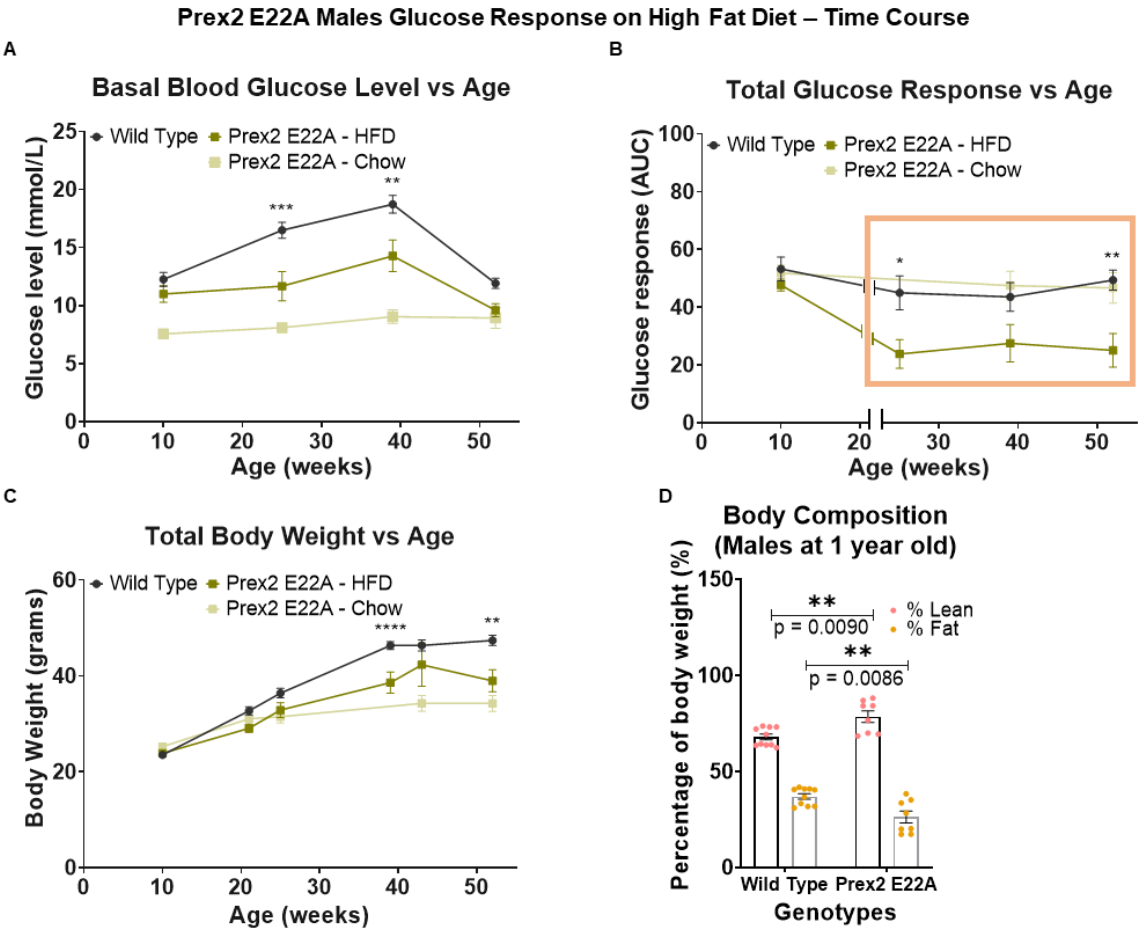

Figure 4.5.14: The low fasting blood glucose levels and improved glucose tolerance of male Prex2 E22A mice on HFD persist throughout ageing.

The fasting blood glucose levels, response to glucose challenge, and body weight of the male Prex2 E22A (yellow) and C57BL/6J WT (grey) mice on HFD from **Figure 4.5.13** are expressed as a function of age. In faded yellow are represented the Prex1 KO male mice on chow diet from **Figure 4.5.9** for visual comparison, but no statistical analysis was performed, as the animals were not directly compared experimentally. **(A)** Fasting blood glucose levels; data from column A in **Figure 4.5.13**. **(B)** Response to IPGTT; normalised data from columns B and C in **Figure 4.5.13**. **(C)** Body weight, measured after 6 and 4 h fasting, prior to glucose and insulin challenges, respectively. **(D)** Body composition at 1 year of age. The mice in (**A-C**) were culled at 1 year of age and the cadavers were scanned by Echo MRI for lean mass and body fat. Data are pooled from 2 independent cohorts (C57BL/6J WT n=10; Prex2 E22A n=9), and are presented as mean ± SEM. 2-way ANOVA with repeated measures and Sidak's multiple comparisons correction was used to compare genotypes during ageing. Unpaired Student's *t*-test was used to analyse the body composition.

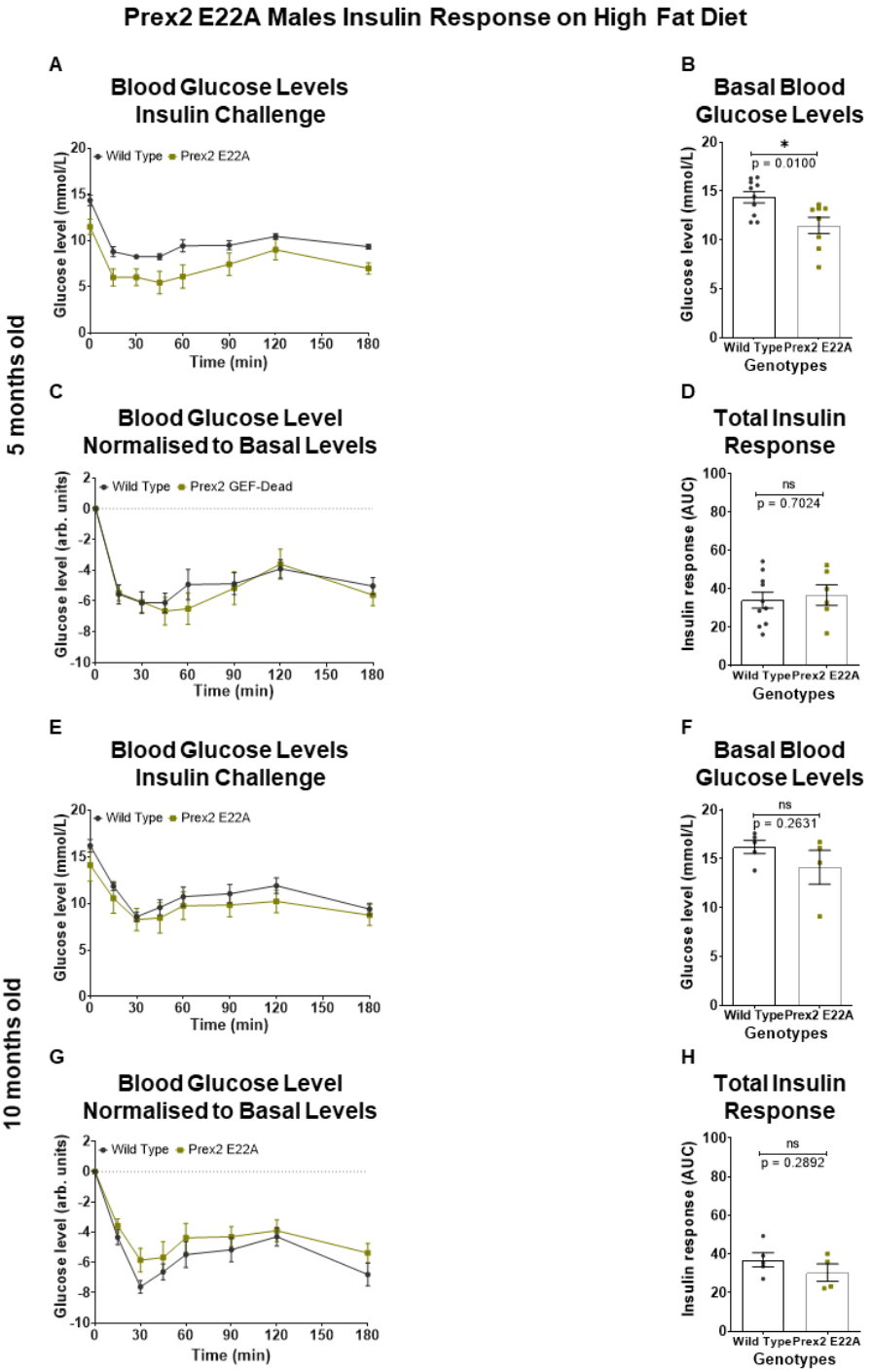

Figure 4.5.15: Male Prex2 E22A mice on HFD show a normal response to insulin challenge throughout ageing.

The fasting blood glucose levels and response to SCITT were measured in male Prex2 E22A (yellow) and C57BL/6J WT (grey) mice on 45% HFD from **Figure 4.5.13** at the ages of **(A-D)** 5 and **(E-H)** 10 months, as described in the legend to **Figure 4.2.3**. **(A,E)** Blood glucose concentration during SCITT. **(B,F)** Fasting blood glucose levels. **(C,G)** Blood glucose levels during SCITT, normalised by subtracting the fasting basal blood glucose level from each mouse individually. **(D,H)** Total insulin response (AUC of normalised data). Data are pooled from 2

independent cohorts (C57BL/6J WT n=10; Prex2 E22A n=9), and are presented as mean ± SEM. 2-way ANOVA with repeated measures and Sidak's multiple comparisons correction was used to compare genotypes during SCITT. Unpaired Student's *t*-test was used to analyse the basal blood glucose level and total insulin response.

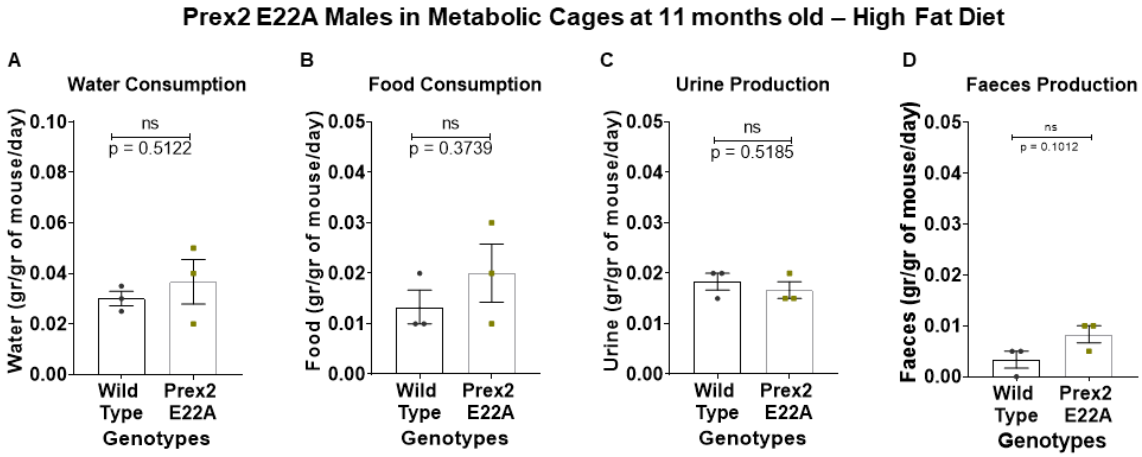

Figure 4.5.16: Male Prex2 E22A mice on HFD perform normally in metabolic cages. The male Prex2 E22A (yellow) and C57BL/6J WT (blue) mice on 45% HFD from **Figure 4.5.13** were habituated to metabolic cages at 11 months of age as detailed in Materials and Methods, weighed and group-housed (up to 3) in metabolic cages overnight for 16 h on 3 subsequent nights with food and water provided *ad libitum*. Their **(A)** water consumption, **(B)** food consumption, **(C)** urine production, and **(D)** faeces production were measured after each night and were normalised to the combined body weights of the mice housed in each cage. Data are pooled from 2 independent cohorts (C57BL/6J WT n=10; Prex2 E22A n=9), and are presented as the mean ± SEM of each night (n=3). Unpaired Student's *t*-test was used for the comparison between the genotypes.

4.5.7.3 Metabolic phenotype of female Prex2 E22A mice

To investigate sex differences in Prex2 E22A mice, females were also tested on HFD. As can be seen in **Figure 4.5.17A** and in the ageing overview graphs in **Figure 4.4.18A**, Prex2 E22A females had lower fasting blood glucose levels than C57BL/6J WT controls. However, contrary to their male counterparts, they did not exhibit improved glucose tolerance (**Figures 4.5.17B-C** and **4.45.18B**). Moreover, Prex2 E22A females were found to have normal insulin responses both at 5 months' and at 10 months' time point (**Figure 4.5.19A-B**). Females of both genotypes also gained weight at a similar rate (**Figure 4.5.18C**) and had identical body composition (**Figure 4.5.18D**). Housing of the mice in metabolic cages at 11 months of age also did not reveal any differences to the controls (**Figure 4.4.20A-D**). Hence, the phenotype of the Prex2 E22A mice is highly sex-dependent, more so than the phenotypes previously observed in the various Prex KO strains. As the phenotype is seen in the males but not the females, it seems likely that male sex hormones play a role in the underlying mechanism. It must be noted, however, the results of the Prex2 E22A females are from a single cohort, so they need to be confirmed in the future through at least a second, independent cohort, and females need also to be tested on chow diet.

Having seen previously in the Prex deficient mice that there were differences in the weight of some of their organs, 10 week-old and 1 year-old male Prex2 E22A mice on chow diet were dissected and organ weight was compared to C57BL/6J WT controls of the same sex and age. Interestingly, Prex2 E22A males had smaller livers compared to their C57BL/6J WT counterparts at both ages tested, similar to what was previously found in the Prex1 KO mice (**Figure 4.5.21A-B**). Moreover, the liver was found to be significantly smaller in 1 year-old HFD-fed males compared to controls (**Figure 4.5.21C**). Finally, 1 year-old females on HFD were found to have smaller intBAT than their C57BL/6J counterparts (**Figure 4.5.21D**). These data highlight the liver as a possible key organ for further study, at least in males, in order to unravel the molecular mechanism underlying the improved glucose tolerance of Prex2 E22A mice.

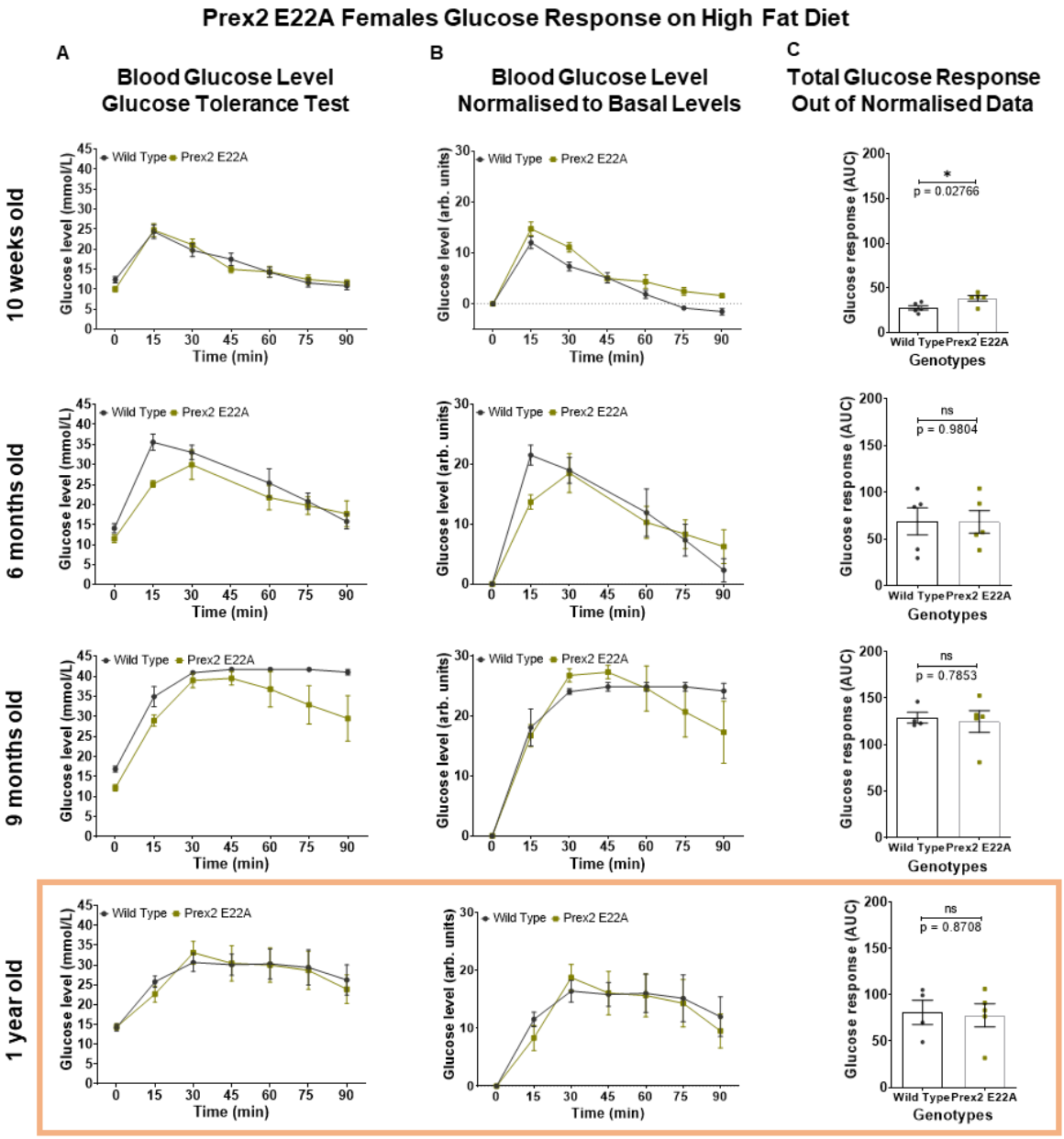

Figure 4.5.17: Female Prex2 E22A mice on HFD have low fasting blood glucose levels, but normal glucose tolerance.

The fasting blood glucose levels and response to IPGTT were measured in female Prex2 E22A (yellow) and C57BL/6J WT (grey) mice on 45% HFD at the ages of 10 weeks, 6, 9, and 12 months, as described in the legend to **Figure 4.2.1**. The ochre box denotes glucose challenge at the reduced dose of 1 g/kg instead of 2 g/kg. **(A)** Blood glucose concentration during IPGTT. **(B)** Blood glucose levels during IPGTT, normalised by subtracting the basal blood glucose level. **(C)** Total glucose response (AUC of normalised data). Data are from 1 cohort (C57BL/6J WT n=5; Prex2 E22A n=5), and are presented as mean ± SEM. 2-way ANOVA with repeated measures and Sidak's multiple comparisons correction was used to compare genotypes during IPGTT. Unpaired Student's *t*-test was used to analyse the total glucose response.

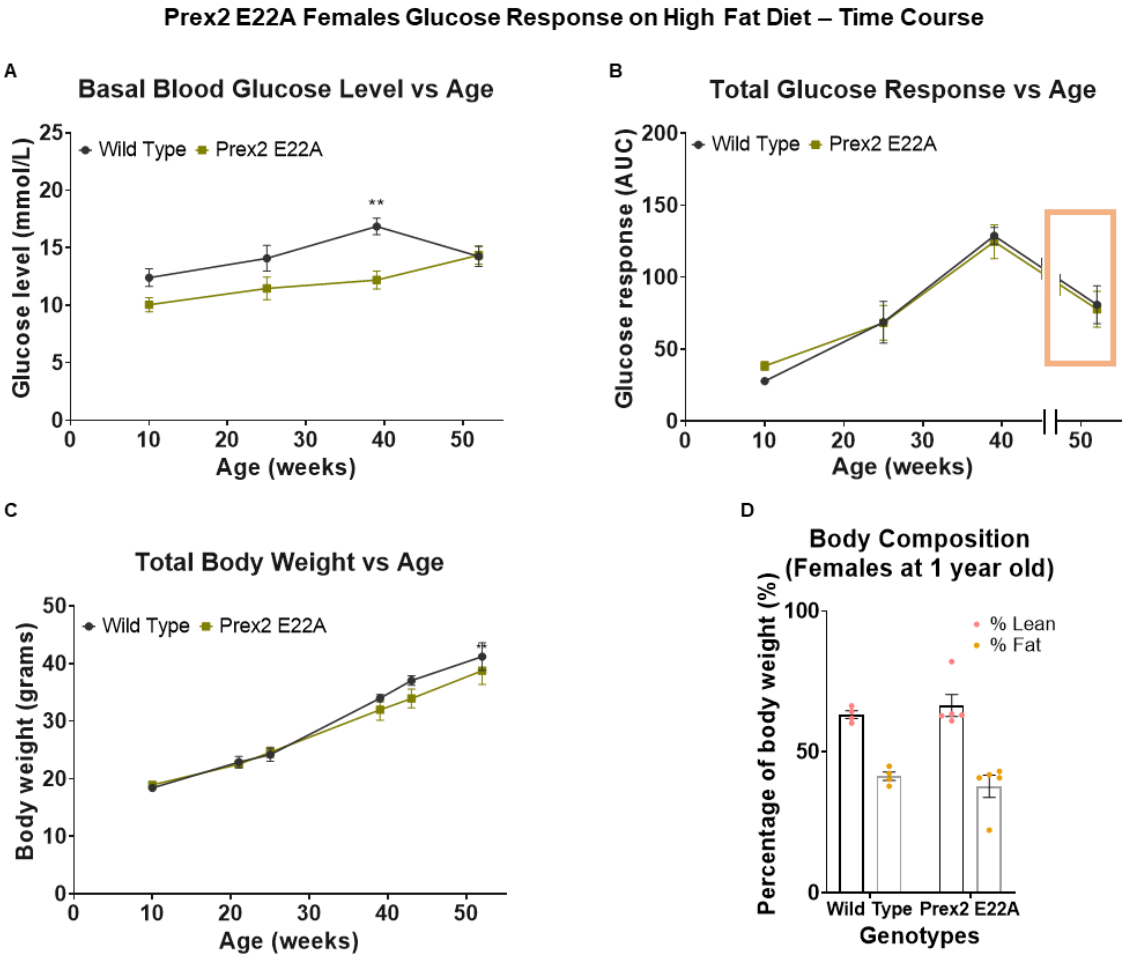

Figure 4.5.18: Female Prex2 E22A mice on HFD have normal glucose tolerance throughout ageing.

The fasting blood glucose levels, response to glucose challenge, and body weight of the female Prex2 E22A (yellow) and C57BL/6J WT (grey) mice on 455 HFD from **Figure 4.5.17** are expressed as a function of age. **(A)** Fasting blood glucose levels; data from column A in **Figure 4.5.17**. **(B)** Response to IPGTT; normalised data from columns B and C in **Figure 4.5.17**. **(C)** Body weight, measured after 6 and 4 h fasting, prior to glucose and insulin challenges, respectively. **(D)** Body composition at 1 year of age. The mice in (**A-C**) were culled at 1 year of age and the cadavers were scanned by Echo MRI for lean mass and body fat. Data are from 1 cohort (C57BL/6J WT n=5; Prex2 E22A n=5), and are presented as mean ± SEM. 2-way ANOVA with repeated measures and Sidak's multiple comparisons correction was used to compare genotypes during ageing. Unpaired Student's *t*-test was used to analyse the body composition.

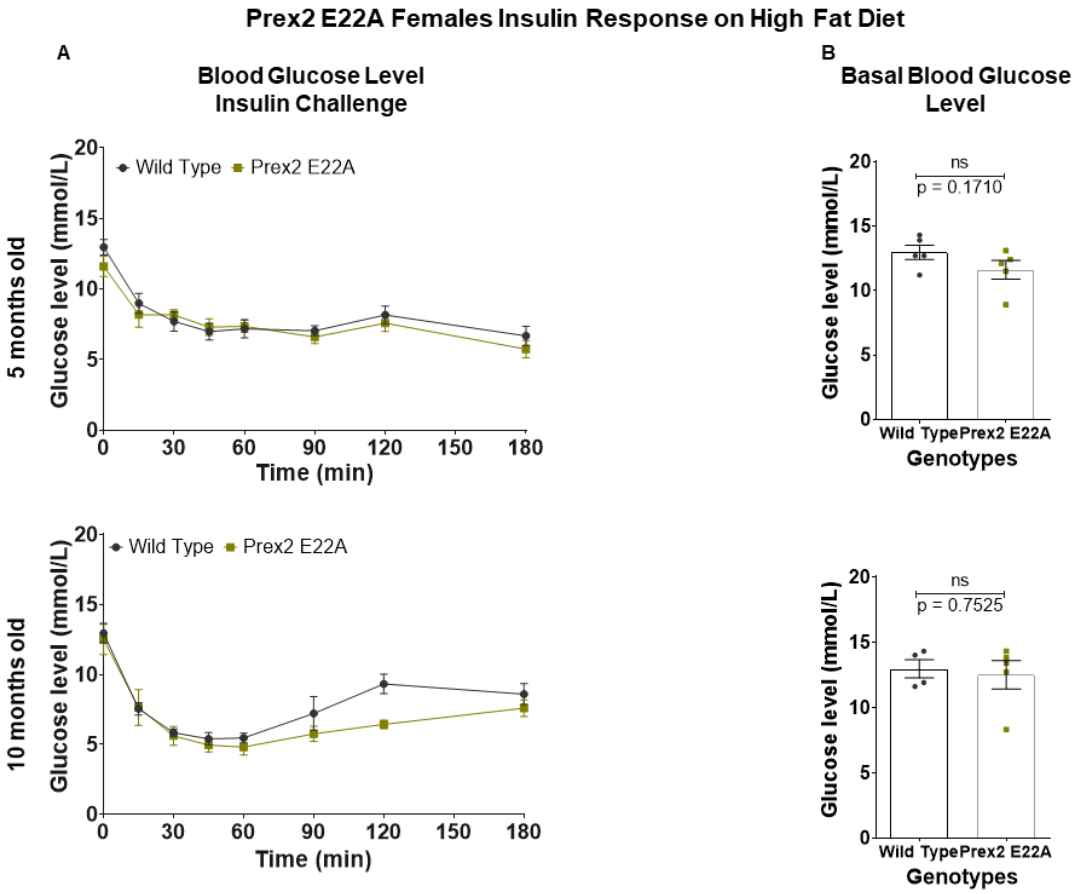

Figure 4.5.19: Female Prex2 E22A mice on HFD show similar fasting blood glucose levels and insulin response to C57BL/6J WT mice.

The fasting blood glucose levels and response to SCITT were measured in female Prex2 E22A (yellow) and C57BL/6J WT (grey) mice on 45% HFD from **Figure 4.5.17** at the ages of 5 and 10 months, as described in the legend to **Figure 4.2.3**. **(A)** Blood glucose concentration during SCITT. **(B)** Fasting blood glucose levels. Data are from 1 cohort (C57BL/6J WT n=5; Prex2 E22A n=5), and are presented as mean ± SEM. 2-way ANOVA with repeated measures and Sidak's multiple comparisons correction was used to compare genotypes during SCITT. Unpaired Student's *t*-test was used to analyse the basal blood glucose level.

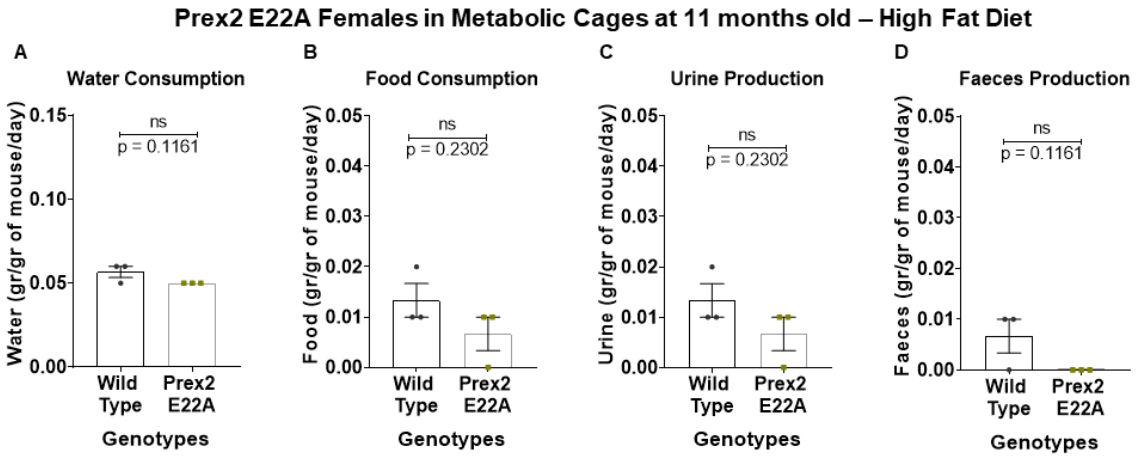

Figure 4.5.20: Female Prex2 E22A mice perform similarly to C57BL/6J WT mice in metabolic cages.

The female Prex2 E22A (yellow) and C57BL/6J WT (grey) mice from **Figure 4.5.17** were habituated to metabolic cages at 11 months of age, as detailed in Materials and Methods, weighed and group-housed (up to 3) in metabolic cages overnight for 16 h on 3 subsequent nights with food and water provided *ad libitum*. Their **(A)** water consumption, **(B)** food consumption, **(C)** urine production, and **(D)** faeces production were measured after each night and were normalised to the combined body weights of the mice housed in each cage. Data are from 1 cohort (C57BL/6J WT n=5; Prex2 E22A n=5) and are presented as the mean ± SEM of each night (n=3). Unpaired Student's *t*-test was used for the comparison between the genotypes.

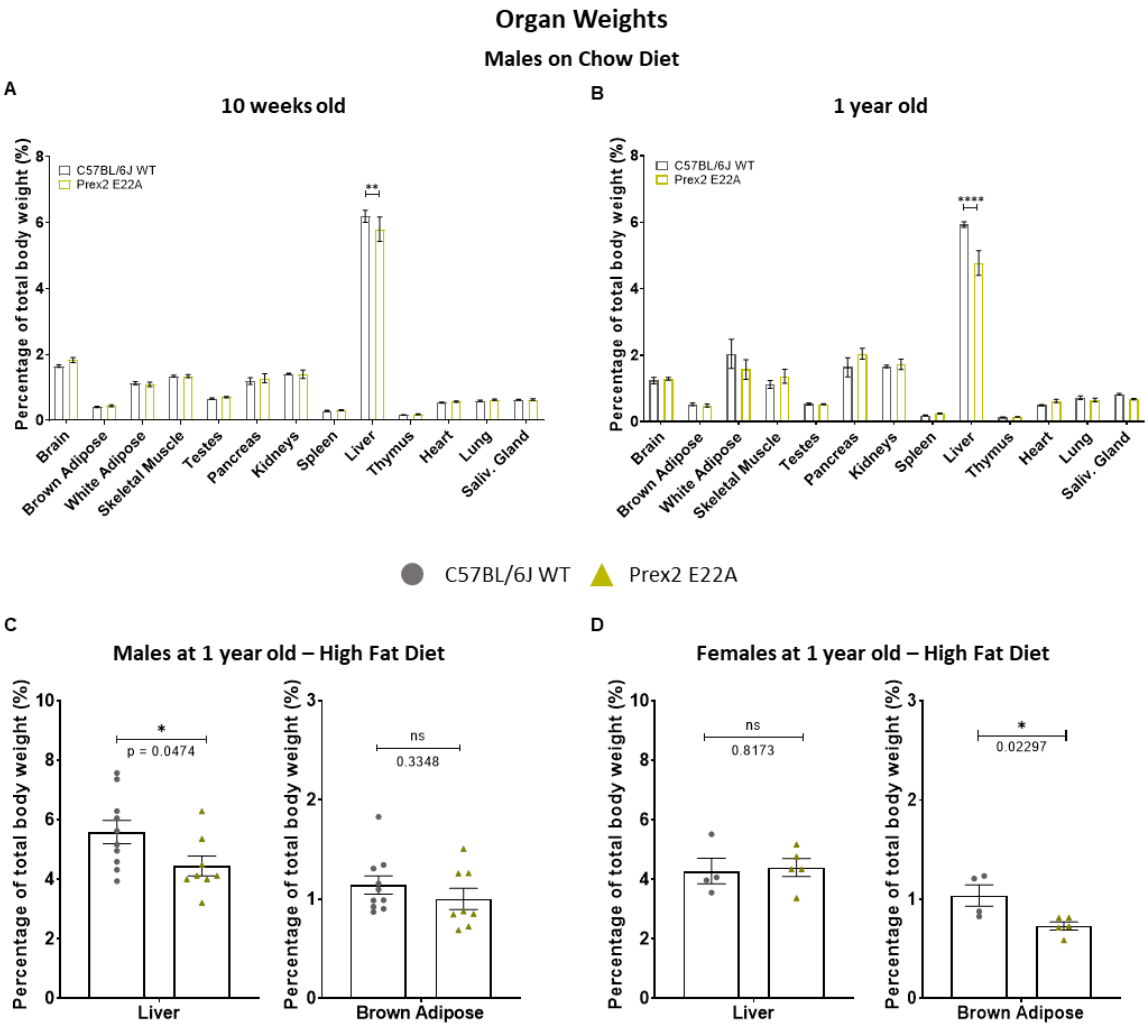

Figure 4.5.21: Male Prex2 E22A mice have smaller livers.

Male Prex2 E22A (yellow) and C57BL/6J WT (grey) mice on chow diet were culled by CO_2 asphyxiation followed by severance of the femoral artery and were dissected for organ collection at the ages **(A)** 10 weeks and **(B)** 1 year old. The weights of thirteen organs (brain, interscapular brown adipose, inguinal white adipose, skeletal muscle, pancreas, kidneys, spleen, liver, thymus, heart, lung, salivary gland, and testes) were measured and data were normalised by total body weight after culling. Data are presented as mean ± SEM. Statistics are 2-way ANOVA with Sidak's multiple comparisons correction. Prex2 E22A (yellow) and C57BL/6J WT (grey) **(C)** male and **(D)** female mice on 45% HFD were dissected for organ collection at 1 year of age, after their cadavers had been thawed and scanned by Echo MRI. The weights of two organs (liver and brown adipose) were measured and data were normalised to total body weight before dissection. Data are presented as mean ± SEM. Unpaired Student's *t*-test was used for the comparison between the genotypes. **(A)** Data from 2 cohorts (C57BL/6J WT n=11, and Prex2 E22A n=11). **(B)** Data from 1 cohort (C57BL/6J WT n=5, and Prex2 E22A n=6). **(C)** Data are from 2 cohorts (C57BL/6J WT n=10, and Prex2 E22A n=8). **(D)** Data from 1 cohort (C57BL/6J WT n=4, and Prex2 E22A n=5).

Table 4.7: Summary table of metabolic phenotype of Prex2 KO and Prex2 E22A mice on chow or high fat diet. Bold font was used to annotate findings that reached statistical significance in most time points tested.

		Prex2 KO		Prex2 E22A	
		Male	**Female**	**Male**	**Female**
Chow Diet	**Fasting Blood Glucose**	Normal	Normal	**Low fasting blood glucose**	
	Glucose Tolerance	Tendency to improved glucose tolerance in young and worse in old age	Tendency to improved glucose tolerance in young and worse in old age	**Improved glucose tolerance from 15 weeks**	
	Insulin Response	Apparent increase in insulin sensitivity in old age	Normal	Altered insulin response	
High Fat Diet	**Fasting Blood Glucose**	**Low fasting blood glucose**	Normal	**Low fasting blood glucose**	Low fasting blood glucose
	Glucose Tolerance	**Glucose intolerance**	Tendency to improved glucose tolerance in young and worse in old age	**Improved glucose tolerance from 15 weeks**	Normal
	Insulin Response	**Insulin resistance in old age**	Normal	Normal	Normal

Chapter 5 - Discussion

PREX proteins have been identified as instrumental contributors in many physiological and pathological processes such as inflammation, neuronal plasticity, cancer progression and metastasis. However, their importance in metabolic processes has only recently started to emerge. The main objectives of this project were to determine the functional roles of PREX proteins in glucose homeostasis and development of metabolic syndrome as well as to assess the importance of their Rac-GEF activity in these processes.

To briefly summarise the main findings of my project: Prex deficiency in mice has isoform-, sex-, diet-, age- and catalytic activity-dependent effects on glucose homeostasis. Prex1 KO caused low fasting blood glucose and improved glucose clearance in males on chow diet throughout ageing, whereas Prex1 KO males on HFD showed only low fasting blood glucose. In females Prex1 deficiency improved glucose tolerance in middle-aged mice on HFD. Bone marrow transplantation suggested that Prex1 contributes to the regulation of glucose homeostasis largely through the haematopoietic system. Prex2 KO also caused low fasting blood glucose, but unlike Prex1 KO, produced glucose intolerance and age-related insulin resistance in males on HFD. In females, Prex2 deficiency was associated with a tendency to improved glucose clearance in young age that worsened in old age. Hence, both Prex1 and Prex2 play significant roles in glucose homeostasis, but have nearly opposite effects, especially regarding glucose tolerance. Prex1/2 DKO males showed a phenotype that resembled Prex1 KO mice, although milder, on both chow and HFD. Instead, Prex1/2 DKO females displayed an overall worse phenotype than their single KO counterparts. These results suggest some redundancy between Prex Rac-GEFs in glucose homeostasis as well as compensation by other Rac-GEFs. Overexpression of catalytically inactive mutants of Prex1 and Prex2 in HepG2 cells revealed that both proteins can mediate insulin signalling in a Rac-GEF activity independent manner, and hence GEF-dead mice were generated to investigate the adaptor functions of Prex proteins in glucose homeostasis. Prex2 E22A GEF-dead mice had low fasting blood glucose levels, and males showed much improved glucose tolerance throughout ageing, both on chow

and HFD. Hence, Prex2 regulates glucose homeostasis both through its Rac-GEF activity and through adaptor functions; its Rac-GEF activity limits glucose homeostasis, whereas its adaptor functions improve it. My data suggest that it may be beneficial to develop inhibitors of Prex Rac-GEF activity for the treatment of hyperglycemia and glucose intolerance.

5.1 Prex expression in insulin-sensitive tissues

I began by investigating Prex1 and Prex2 expression in insulin-sensitive mouse tissues through western blotting of total lysates. Prex1 was strongly expressed in brain, at lower level in the liver, in white (inguinal and epididymal) and in brown adipose tissue, but there was no expression in skeletal muscle. These findings confirm and extend previous studies which showed that Prex1 is expressed in brain, thymus, spleen, lung, bone marrow and peripheral blood leukocytes, but absent from skeletal muscle on both the protein and mRNA level (Welch et al., 2002). Prex1 protein expression in liver and adipose tissue had not been reported before, but low levels of Prex1 mRNA had previously been observed (Uhlén et al., 2015; Welch et al., 2002).

Prex2 was expressed at low levels in brain and intBAT, but not detected in skeletal muscle, liver and white adipose tissue depots tested in this study. Prex2 expression in brain (cerebellum) and liver was previously reported, but these studies used immunoprecipitation to concentrate the protein prior to blotting, suggesting that Prex2 levels in brain and liver are low overall (Donald et al., 2004; Hodakoski et al., 2014). In addition, PREX2 expression was previously detected in human white adipose tissue, both on the mRNA (Uhlén et al., 2015) and protein (Hodakoski et al., 2014) level, but the protein was described as a low molecular weight form of PREX2 that could be a proteolytic fragment (Hodakoski et al., 2014). It is well known that while Prex2 mRNA is expressed in multiple mouse tissues, the protein is not as widely expressed (Donald et al., 2004). Although the mechanism through which Prex2 protein is suppressed in these cases is still unknown, the apparent lack of Prex2 in white adipose tissue in my study could either be real or be a limitation of the sensitivity of our antibody. This might be investigated further by immunoprecipitation before blotting, but as Prex2 was readily detectable in intBAT, its level in white adipose tissue will be low at best.

In this study, the expression of Prex proteins was not evaluated in pancreas. However, we have unpublished results from MSc student Anna Roberts, whom I tutored, which suggest that both Prex1 and Prex2 are expressed in mouse pancreas (data not shown). Moreover, expression of PREX2, was previously reported in human pancreatic epithelial cell line (Uhlén et al., 2015; Yang et al., 2016).

Therefore, Prex1 and Prex2 are expressed in all major organs that control glucose homeostasis, with the notable exception of the skeletal muscle. This lack of expression in skeletal muscle is surprising in light of my findings that several mouse strains in this study have improved glucose clearance, especially considering that skeletal muscle is the tissue that accounts for the majority of glucose uptake from the blood. It is of course entirely possible that Prex proteins affect glucose uptake by skeletal muscle without being expressed in that tissue.

This study only superficially investigated the possibility that a single knockout would lead to a deregulation of the other Prex protein, and no obvious compensatory upregulation was found. However, given that Prex1/2 DKO males have phenotype that resembles that observed with the Prex1 KO males, whereas Prex1/2 DKO females showed worse phenotype than both single KO females. It would be of interest to evaluate more systematically how knockout of one Prex protein affects the expression levels of the other, for example in sub-sections of tissues and within cell types, as well as to assess whether there are sex differences.

5.2 Role of Prex1 in glucose homeostasis

Once it was established that PREX proteins are indeed present in insulin sensitive organs, the aim was to investigate their role in glucose homeostasis *in vivo*. It was expected that Prex1-deficient mice would have reduced glucose tolerance. This hypothesis was based upon considerable body of evidence showing that Prex1 mediates insulin signalling in a range of cell types (Dillon et al., 2014), that Rac1 is involved in the insulin-stimulated translocation of GLUT4 transporter to the plasma membrane (JeBailey et al., 2004; Sylow et al., 2014; Takenaka et al., 2019), that PREX1 is modulating this process in adipocytes (Balamatsias et al., 2011), and that PREX1 knockout in brown adipocytes reduces their thermogenic capacity (Xue et al., 2015). From these findings, it was predicted that Prex1 KO

would lead to reduced glucose uptake by white adipocytes and reduced energy usage by brown adipocytes, and thus to elevated blood glucose levels and impaired glucose clearance *in vivo*. In contrast, male Prex1 KO mice on chow diet exhibited reduced fasting blood glucose levels which persisted throughout ageing and improved glucose tolerance from 15 weeks of age onwards. These observations were not due to obvious differences in the total body weight or body composition, as both Prex1 KO mice and their Prex WT counterparts put on weight at a similar rate and had identical lean and fat mass percentages.

The fact that the Prex1 KO phenotype differed so profoundly from the hypothesis formed on the basis of studies performed in cell lines highlights the importance of investigating *in vivo* the physiological relevance of observations made *in vitro*. Inter-organ crosstalk and the activation of compensatory mechanisms for the maintenance of systemic homeostasis cannot be taken into account when working in cell lines. In addition, some of the *in vitro* work, for example the experiments suggesting that PREX1 mediates GLUT4 translocation to the plasma membrane in 3T3-L1 adipocytes (Balamatsias et al., 2011), were done using overexpression systems. Therefore, some of these observations could be due to overexpression side effects like activation and overloading of specific biological pathways over other, promiscuous interactions, or disruption of regulation (Moriya, 2015).

One consideration when interpreting the fasting blood glucose levels is the stress of the mice during handling and sampling. The low fasting blood glucose levels observed in the Prex1 KO mice and several other strains used in this study could reflect that these mice were less stressed than their WT counterparts. All mice were handled repeatedly in the days before any procedure, in order to familiarise them with the process and reduce the stress level to a certain extent. Moreover, at least two blood samples were taken from each mouse, both to measure fasting blood glucose and to assess the response to glucose or insulin challenge, and the lower reading was used for plotting the response curve. In addition to these efforts to keep stress levels low, it could be of interest to also determine basal blood glucose levels by measuring glycated haemoglobin (HbA1c) (Carson et al., 2010; Sacks, 2011). HbA1c is formed by the non-enzymatic attachment of glucose to

haemoglobin and is considered to reflect a longer-term glycaemic status than measurement of fasting blood glucose levels by glucometer. Similarly, it would be of interest to test the levels of stress hormones, such as adrenaline, cortisol, and norepinephrine, in the plasma of Prex1 KO mice and other strains with low fasting blood glucose.

As outlined in the introduction, skeletal muscle is the main organ for glucose clearance from the blood stream and the insulin-regulated GLUT4 transporter is the main mechanism for glucose clearance by uptake into cells, both in skeletal muscle and adipose tissue. Hence, one of the attempts I made to find a mechanism for the increased glucose clearance in Prex1 KO mice was to analyse skeletal muscle and adipose tissue isolated from 10-week old male Prex1 KO and Prex WT animals, 15 min after s.c. insulin stimulation or mock treatment, for total Glut4 levels (data not shown). No difference was detected between the genotypes, which suggests it is unlikely that Prex1 KO caused an overall change in Glut4 levels. However, it would be beneficial to follow further the expression pattern of Glut4 by alternative methods, like qPCR. Moreover, I made a first attempt at fractionating dissociated skeletal muscle and ingWAT cells (from the experiment described here-above, using a commercially available kit Mem-PER Plus, 89842), in order to determine whether Prex1 KO affects the insulin-stimulated membrane translocation of Glut4 into the plasma membrane enriched fraction. However, that experimental protocol needs to be optimised further before conclusions can be drawn. Such *ex vivo* investigation of Glut4 trafficking will be useful to determine whether the Prex1 KO phenotype is due to aberrant presence of Glut4 transporter in the plasma membrane. Considering that, many mouse strains showed low fasting blood glucose levels, it could be worth to extend this line of work to other glucose transporters like the insulin-independent Glut1, Glut2, and Glut3.

Another approach that I trialled in order to determine the mechanisms that underlie the low fasting blood glucose and increased glucose clearance in Prex1 KO mice was a glucose uptake experiment performed using heavy glucose combined with NMR analysis, in collaboration with Professor Jules Griffin from the University of Cambridge Biochemistry Department (data not shown). In this experiment, skeletal muscle, ingWAT and liver were rapidly isolated from 15 week-

old male Prex1 KO and Prex WT mice 30 min after the i.p. injection of heavy [U-^{13}C6]D-glucose, and tissue lysates were examined by NMR for [U-^{13}C6]-containing metabolites. Unfortunately, [U-^{13}C6]-metabolites were undetectable in skeletal muscle and ingWAT. [U-^{13}C6]-lactate was discovered in the liver, but without any significant differences between genotypes, suggesting that glucose metabolism in the liver of Prex1 KO animals may be normal, although this would need to be corroborated by more work. The likely reason for the low levels of [U-^{13}C6] metabolite recovery is that the mice were injected with 0.15 g/kg of glucose rather than the 2 g/kg that I routinely used during glucose challenges. This dose was obviously insufficient to unravel differences in the relative contribution of various organs to glucose uptake between the genotypes. Due to time restrictions, the protocol could not be optimised further within the frame of this study. Adaptation of the route of administration or a different time for tissue collection would be appropriate factors to try in future experiments. Finally, injection of 2-Deoxy-D-glucose could be a better option, since it is phosphorylated by hexokinase to 2-DG-P but cannot be further metabolized in the glycolytic pathway, and therefore accumulates in cells and is more readily detectable. I trialled an i.p. challenge with a fluorescent variant of 2-Deoxy-D-glucose in Prex WT and Prex1 KO mice, followed by flow cytometric analysis of cell suspensions from isolated tissues, but no fluorescence was detected within cells under the conditions tested.

Another possible explanation for the phenotype observed could be enhanced energy expenditure, for example by increased locomotor activity or production of heat. Locomotor activity is unlikely to be the cause, as it is well documented that Prex1 KO mice have normal locomotor activity (Donald et al., 2008; Li et al., 2015). Moreover, housing of the mice in metabolic cages did not reveal any significant differences in water and food intake or urine and faeces production. It is however possible that the urine of Prex1 KO mice contains more glucose, which remains to be tested. Increased heat production is an interesting option, in view of PREX1 having been identified as a biomarker for BAT thermogenic capacity (Xue et al., 2015). The study showed that knockout of PREX1 in human brown adipose precursor cells significantly decreased the expression of the thermogenicity marker UCP1, as well as the basal respiration, proton leak and maximal respiration capacity of differentiated adipocytes (Xue et al., 2015). On the basis of this study, one would

predict that Prex1 KO mice have lower thermogenicity, lower energy expenditure and therefore increased blood glucose levels and reduced glucose clearance, rather than the low blood glucose and increased glucose clearance we observed. In addition to this, I found that Prex1 KO males have eosinophilia in intBAT, and according to the recent literature, this is indicative of beige-to-brown remodelling, as an attempt to increase the thermogenicity of adipose tissue (Lee and Tontonoz, 2014; Villarroya et al., 2018). In view of these results, one could speculate that brown adipose mass would increase due to accumulation of unused fat. However, no difference was found between the weights of intBAT obtained from Prex1 KO or Prex WT mice. It would be of interest to investigate the Ucp1 levels in the BAT and the body temperature of the mice in order to evaluate the effects of Prex1 deficiency on thermogenicity *in vivo*. Moreover, *ex vivo* Seahorse analysis of oxygen consumption rate and extracellular acidification rate in primary adipose cells could further interrogate the effect of Prex1 deficiency on the cellular metabolic function of these cells. Such Seahorse analysis was attempted in collaboration with Dr Chris Church at AstraZeneca, using isolated adipose cells from the white and brown adipose tissue of Prex WT and various Prex deficient strains, which had been cultured and differentiated *in vitro*. I obtained preliminary data on Prex1/2 DKO mice which suggested some changes in energy expenditure (data not shown), but it was concluded that these changes likely reflected differences in the level of differentiation into mature adipocytes achieved in this experiment, rather than true defects in thermogenicity. More optimisation of this protocol would be required to investigate thermogenicity further. If Prex1 deficiency was indeed found to impair the Ucp1 mediated heat-generating system, this in turn could force the utilisation of other, less efficient and metabolically costly thermogenic mechanisms such as the glycerol phosphate cycle (Newsholme and Stanley, 1987). Employment of such alternative mechanisms, due to reduced BAT thermogenic capacity, could be a possible explanation for the reduced fasting blood glucose levels observed in Prex1 KO mice. However, it seems overall unlikely that Ucp1-dependent mechanisms are grossly affected by the Prex1 KO, as a main phenotypical characteristic of UCP1 deficient mice is their resistance to developing diet-induced obesity (Liu et al., 2003). In contrast, the rate of body weight gain between Prex1 KO and Prex WT male mice on HFD was indistinguishable.

Measurement of the weight of individual organs revealed that Prex1 KO mice had smaller ingWAT compared to their Prex WT counterparts. However, histological analysis of this tissue did not reveal any differences, other than size, between Prex deficient mice and controls. Several studies have demonstrated that visceral white fat produces adverse metabolic effects, whereas increased subcutaneous adipose tissue is associated with improved insulin sensitivity and lower metabolic risk (Kwon et al., 2017; Neeland et al., 2013; Rosen and Spiegelman, 2014). Accordingly, fat distribution rather than the total fat mass seem to be important for homeostasis (Fox et al., 2007; Kim et al., 2011b; Tchkonia et al., 2013). Therefore, it would be important to investigate other white adipose tissue depots such as the gonadal, epicardial, retroperitoneal, peri-renal, omental, and mesenteric fat, in order to better understand the relative contribution of white adipose tissue to the metabolic phenotype observed of Prex1 KO mice.

In addition to reduced ingWAT mass, Prex1 deficient mice also had smaller livers. Histology and gene expression analysis revealed furthermore that their livers exhibit reduced glycogen storage and slightly increased Pepck expression (it should be noted that organ weight measurement and histological analysis were performed in fed mice whereas Pepck levels were assessed in 4 h-fasted mice). The trend towards increased Pepck could point to increased *de novo* glucose synthesis in the liver, maybe due to impaired hepatic glycogenolysis and as an attempt to counteract the low fasting blood glucose levels. More experiments are required to determine the significance of this trend, but if it stands, an evaluation of gluconeogenesis in Prex1 KO mice could be of interest. The reduced glycogen storage might account for the decreased liver size. It could also indicate that the low fasting blood glucose levels observed in Prex1 KO mice were a cause or consequence of the limited liver glycogen availability. However, at this point it is worth keeping in mind that Prex1 KO females also had reduced liver size but did not exhibit reduced glycogen storage (data not shown), and only showed a trend to reduced fasting blood glucose and improved glucose homeostasis on chow diet. Therefore, impaired glycogen accumulation is unlikely to be the only cause of reduced liver size. Systematic monitoring of blood glucose levels and histological analysis during fasting might help to elucidate whether low blood glucose levels correlate with hepatic glycogen stores. Such assessment would also help explain the improved glucose tolerance observed

in Prex1 KO mice. It has been shown that prolonged periods of fasting results in glycogen depletion-enhanced insulin-stimulated glucose utilisation in mice (Ayala et al., 2006; Heijboer et al., 2005). Therefore, it could be hypothesised that the 6-hour fasting to which mice were subjected to prior to glucose challenges induced a metabolic state of enhanced insulin sensitivity. Histological analysis of skeletal muscle, another major site of glycogen storage, revealed no difference between genotypes, suggesting that reduced hepatic glycogen storage does not elicit compensatory accumulation of glycogen in skeletal muscle. Together with the results from the heavy glucose tracking experiment discussed above, which had revealed no obvious differences in hepatic glucose metabolism, these findings could lead one to speculate that Prex1 deficiency reduces glycogen synthesis in the liver. One other possibility to assess the contribution of Prex1 expression in different tissues to the metabolic phenotype would be to make tissue-specific KO mice, for example using liver or adipose tissue specific deletion. However, for this, floxed Prex1 mice would first need to be generated.

Prex1 KO males had reduced fasting plasma levels of the insulin-sensitising hormone adiponectin. This was surprising because low adiponectin levels are heavily associated with adverse metabolic phenotype in mice and humans (Dridi and Taouis, 2009; Kadowaki and Yamauchi, 2005). A possible explanation for this finding, given the reduced fasting blood glucose levels in Prex1 KO mice, could be that less adiponectin signalling is required for the maintenance of homeostasis. Leptin is another important insulin-sensitising hormone; it could be of significance to determine its levels in Prex1 deficient mice. Interestingly the fasting plasma levels of glucagon and insulin levels were no different between genotypes. A bigger n-number would greatly benefit this set of experiments. Moreover, it could be useful to assess the levels of these hormones under fed conditions as well as during glucose challenge.

The immune system has recently emerged to be a key player in the maintenance of glucose homeostasis (Zmora et al., 2017). The development of metabolic syndrome is intricately entwined with chronic inflammation, and is now widely regarded as an inflammatory disease. For example, increased numbers and activity of pro-inflammatory tissue macrophages contribute to the development of

insulin resistance (Zmora et al., 2017). As Prex1 is widely expressed in cells of the hematopoietic system, contributing to the regulation of neutrophil-, macrophage-, and platelet-dependent inflammatory responses (Hornigold et al., 2018), the possible contribution of the immune system to the metabolic phenotype of Prex1 KO mice was investigated. Bone marrow transplantation surprisingly revealed that a Prex1 KO hematopoietic system is sufficient to protect otherwise wild type mice from developing age-related glucose intolerance. Hence, the increased glucose tolerance observed in Prex1 KO mice seems to be largely conferred by Prex1 deficiency in the haematopoietic system. Given that Prex1 is known to be required for inflammatory responses, this could be due to a reduction in inflammation in the Prex1 KO mice. It would be useful to investigate the expression of different inflammatory cytokines in plasma and further explore leukocyte tissue infiltrates by histology, especially in view of the increased eosinophilia observed in intBAT. It would also be interesting to trial a long-term treatment of Prex WT and Prex1 KO mice with non-steroid anti-inflammatory veterinary medicines, in order to assess if reduction in inflammation would have a larger effect on the glucose tolerance of Prex1 KO and Prex WT mice.

Another interesting finding of the bone marrow transplant experiment was that it uncoupled the low fasting blood glucose from improved glucose tolerance. Beforehand, several of the Prex deficient mouse strains showed low fasting blood glucose without having altered glucose tolerance, but in the bone marrow transplant experiment all animals had similar levels of fasting blood glucose levels, yet the mice with Prex1 KO hematopoietic systems had better glucose tolerance. This indicates that the improved glucose tolerance is not a consequence of low fasting blood glucose levels, and therefore the two observations probably have different aetiologies. Given that there is no obvious correlation between fasting blood glucose levels and glucose tolerance, these observations are likely due to deregulation of different pathways in different organs/tissues.

One interesting feature of the Prex1 KO mouse phenotype was the diet dependence. HFD induces obesity, insulin resistance and glucose tolerance, in mice as well as humans. Prex1 KO mice on HFD retained their lower fasting blood glucose levels throughout ageing, but not their improved glucose tolerance which

showed that their phenotype is diet-dependent. This was seen despite the fact that the diet did not induce any differences in the total body weight gain rate or body composition between Prex1 KO and Prex WT mice. The fact that the improved glucose tolerance was seen on chow but was lost on HFD (at least in males) suggests that Prex1 KO is beneficial for males during healthy ageing, but not robust enough to protect them from developing diet-induced metabolic syndrome. It is also possible, that another Rac-GEF compensates for the loss of Prex1 in a diet dependent manner. This could be investigated in the future through expression analysis, as discussed above, with the additional comparison of tissues from mice on HFD with mice on chow diet.

Loss of insulin sensitivity is a key factor in the development of age-related and diet-induced metabolic syndrome. Prex1 deficient mice on chow diet had a normal response to insulin challenge when middle-aged (5 months), but an altered response at old age (10 months). Although they did respond to insulin, their blood glucose levels did not drop as much, percent-wise, as in Prex WT mice, and returned to fasting levels within 2 hours after the insulin challenge, contrary to control mice whose blood glucose levels remained low. One obvious interpretation of this finding could be that Prex1 KO males developed insulin resistance with age. Although this might be true, it is worth considering that they did exhibit some response to insulin in the first phase of the challenge. The most significant deviation from the response of Prex WT mice was from 30 min after the insulin injection onwards. Given that insulin has a half-life of ~10 min in the blood stream, it is generally accepted that glucose excursions at later time points mostly depend on the counter-regulatory response to hypoglycaemia rather than direct effects of insulin (Alquier and Poitout, 2018; Hughey et al., 2014). This indicates that Prex1 deficiency might affect mainly counter-regulatory responses to low blood glucose levels and not insulin sensitivity. It could also be speculated that their low fasting blood glucose levels made these mice more capable to maintain glucose homeostasis by shifting the glycaemic threshold to higher glucose concentrations. Hence, counter-regulatory responses would be triggered more easily in Prex1 KO mice during insulin challenge. In the literature, counter-regulatory mechanisms to hypoglycaemia were reported to be initiated at elevated plasma glucose concentrations in subjects with T2DM (Burge et al., 2001; Cryer et al., 2003), which is not the case in the Prex1 KO mice. To

investigate this further, it would be of interest to follow the plasma levels of insulin, as well as of counter-regulatory factors such as glucagon, epinephrine, and norepinephrine during insulin challenge.

Another interesting aspect of the Prex1 KO mouse phenotype was its sex-dependence. Differences in the metabolic phenotypes of males and females are well documented in the literature (Mauvais-Jarvis et al., 2013; Reynolds et al., 2019). In the present study, comparison of wild type males and females showed the expected sex-differences, with lower fasting blood glucose as well as better glucose tolerance and insulin sensitivity in females than in males and thus overall better glucose homeostasis in females. The metabolic phenotype of both female and male Prex1 KO mice was tested in order to investigate the role of Prex1 in these sex differences. Females on chow diet had a tendency to low fasting blood glucose levels and improved glucose tolerance during ageing, but normal responses to insulin challenge. This result showed that there is indeed a sex-dependency of the Prex1 KO phenotype, with the phenotype of the females being milder than that of Prex1 KO males on chow diet. One could speculate that the phenotype of the females was milder because females had much better glucose homeostasis than males, and hence less protection was required. Interestingly, when the female Prex1 KO mice were introduced to HFD, they showed markedly improved glucose tolerance at 6 months of age, consistently across all three individually tested cohorts, and a tendency for improved glucose tolerance also at one year. This phenotype was not seen in males, so was again sex-dependent, but this time stronger in females than males. The HFD induced a stronger decline in glucose tolerance in males than females, even in wild type mice, and hence it is conceivable that the increase in glucose tolerance afforded by the Prex1 deficiency was too small to have an effect in males but sufficient to protect females from diet-induced glucose intolerance to some extent. I tried to address this possibility by titrating down the dose of glucose used when challenging mice on HFD, but this, while successful in females, failed to reveal a difference in the males.

The sex-dependency of the Prex1 KO phenotype seems likely to be due to sex hormones. Sex hormones affect a multitude of factors in the mouse, including size; muscle mass, stress levels and aggression, and all of these factors are known

to affect glucose homeostasis. The finding that Prex1 deficient females on HFD showed improved glucose tolerance particularly at 6 months of age is intriguing, as 6 months is the end of the reproductive age for females. Therefore, the improved glucose tolerance at that age could be associated with hormonal changes during menopause. Hormone treatment and/or gonadectomy could be employed to try and unravel the relevant contribution of sex hormones to the metabolic phenotype observed in Prex1 KO mice.

5.3 Role of Prex2 KO in glucose tolerance and insulin sensitivity

As described in the introduction, Prex2 has also been implicated in insulin signalling and metabolic syndrome. The Parsons lab described their Prex2$^{-/-}$ male mice to have reduced glucose tolerance and develop insulin resistance at young age (6-8 weeks old), on chow diet (Hodakoski et al., 2014). Moreover, the PREX2 protein was found to be down-regulated in the adipose tissue of insulin-resistant human patients (Hodakoski et al., 2014). Surprisingly, the Prex2 KO mouse findings were not reproduced in this study. Our male Prex2 KO mice were found to have an overall normal metabolic phenotype when on chow diet, with normal fasting blood glucose levels, overall normal glucose tolerance despite some age-related fluctuations, and if at all, somewhat improved insulin sensitivity in old age. This controversy between the report by the Parsons lab and my own findings could be a result of differences in many aspects of the experimental protocol. First, the two Prex2 KO mouse strains were produced independently by the two laboratories and different targeting strategies had been used. As both strains are on a C57BL/6 genetic background, it seemed unlikely that background plays a role. However, the number of times that mice were backcrossed could be different, and even the C57BL/6 strain is known to be highly divergent between institutions and thus not necessarily comparable. To account for this possibility, I compared our usual Prex2 KO mice (and Prex WT controls) that had been backcrossed five times to C57BL/6J background with Prex2 KO mice from the same strain that had been backcrossed more than 10 times to C57BL/6J (and C57BL/6J controls). The phenotype of normal fasting blood glucose levels and glucose tolerance was the same, both at the age tested by the Parsons lab (6 weeks) and at the age that we usually tested our mice (10 weeks) (data not shown). In addition to the mouse strains, experimental

conditions were slightly different, although the same dosage of glucose and insulin was applied. The Parsons lab they performed overnight starvation prior to glucose tolerance test, and insulin challenge at fed state. In contrast, in this study, a 6- or 4-hour fasting was performed prior to glucose and insulin tolerance tests, respectively. Such differences in the level of fasting are likely to affect the subsequent responses to glucose and insulin challenges (Andrikopoulos et al., 2008). Here, a 6-hour fasting period was selected, as it most closely resembles the human response to overnight starvation. Prolonged starvation in the mouse results in body weight loss and considerable metabolic stress, which promotes insulin-stimulated glucose utilisation. This is in contrast to the situation in humans, where prolonged fasting impairs insulin-mediated glucose transport (Alquier and Poitout, 2018). Moreover, the time of the day that the experiments are performed and the housing temperature have been reported to modify the metabolic phenotype of mice (Ayala et al., 2010). Another consideration was the dose in relation to the body weight. In the present study, the Prex2 KO mice put on weight more slowly during ageing than their Prex WT counterparts, and the dosage of both glucose and insulin was adjusted to total body weight rather than lean mass, as recommended (McGuinness et al., 2009). However, the body composition analysis at the end of the experiment showed that the lean mass percentage was comparable between the genotypes. Therefore, the doses used should not have been disproportionally larger for the Prex WT mice, which could have resulted in misleading results. Hence, categorically Prex2 KO mice on chow diet do not develop glucose intolerance and insulin resistance in our hands.

When the Prex2 KO males were introduced to HFD, they maintained their low fasting blood glucose levels throughout ageing, indicating that Prex2 KO mice are protected from diet-induced hyperglycaemia. However, this was not enough to protect them from developing diet-induced glucose intolerance and insulin resistance worse than their Prex WT counterparts. Prex2 KO mice on HFD showed a tendency to reduced glucose tolerance throughout their lifetime, and significant glucose intolerance at 9 months of age. In addition, middle-aged Prex2 KO males on HFD showed an exaggerated counter-regulatory response to insulin challenge and significant insulin resistance in old age. Interestingly, although the Prex2 KO mice tested in this study put on less body weight during ageing than the Prex WT

controls, they had increased fat mass percentage. Thereby, it is conceivable that the reduced glucose tolerance and insulin sensitivity could be due to these animals being dosed with disproportionally large amounts of glucose, when standardised to their lean mass. However, as previously discussed for mice on chow diet, the difference in lean mass was less than 10%, so the dosage would not have differed significantly when calculated to lean mass, and can therefore be discounted.

Importantly, unlike the phenotype of Prex2 KO mice on chow diet, that of Prex2 KO males on HFD resembles closely the findings reported by the Parsons lab for their Prex2 KO mice on chow diet (Hodakoski et al., 2014). Therefore, it appears that, overall, the phenotype of these mice is robust enough to be reproduced in independent mouse strains and by different labs, although certainly not under comparable experimental conditions. It would be interesting to determine the PIP3/PIP2 levels in insulin sensitive tissues of Prex2 KO mice on HFD, in order to investigate whether the glucose intolerance and insulin resistance seen here are associated with increased Pten activity. Such de-inhibited Pten activity would presumably lead to reduced PIP3 levels, and thus reduced insulin signalling and glucose clearance, which might eventually result in the glucose intolerance and insulin resistance observed in these mice. However, the mechanism is probably not that straightforward. In fact, it seems unlikely that the loss of Prex2-mediated Pten inhibition in the Prex2 KO is the only mechanism underlying the observed phenotype, as two-fold increase of Pten expression levels has been reported to result in improved insulin sensitivity and protection from diet-dependent metabolic defects (Ortega-Molina et al., 2012), the opposite phenotype to what was expected.

Important mechanistic insight into the origins of the metabolic phenotype was gained through the study of Prex2 catalytically-inactive mice, which evaluated the relative contribution of Prex2 Rac-GEF activity and Prex2 adaptor functions to glucose homeostasis. This is going to be discussed in **Section 5.7**.

In contrast to Prex1 KO mice, young male Prex2 KO mice exhibited increased liver and kidney size, as well as reduced ingWAT, and skeletal muscle size. Nevertheless, these findings did not persist into middle age; and their significance is presently unclear. Furthermore, histological analysis of the liver, ingWAT, and skeletal muscle in 10-week old Prex2 KO mice did not reveal any differences (data

not shown).

As previously with the Prex1 KO mice, it would be of interest to test the distribution of white adipose tissue, as increased subcutaneous adipose tissue might account for the maintenance of low fasting blood glucose levels in Prex2 KO males on HFD. Overall, a similar analysis of the underlying mechanisms would be useful, as were previously proposed for the Prex1 KO mouse strain, with the exception of the bone marrow transplantation, as Prex2 is not thought to be expressed in the haematopoietic system.

Like Prex1 KO mice, there was a sex-dependence on the Prex2 KO phenotype. On chow diet, both Prex2 KO males and females showed normal fasting blood glucose levels throughout ageing, and overall normal glucose tolerance, with some age-related fluctuations, as well as normal insulin sensitivity. However, where Prex2 KO males on HFD were glucose intolerant and insulin resistant, females were not. As proposed previously for Prex1 KO mice, gonadectomy and/or hormone treatment could be performed to analyse the causes of this observed sex difference in Prex2 KO mice.

5.4 Glucose homeostasis in Prex1/2 DKO mice

Male Prex1/2 DKO mice on chow diet showed low fasting blood glucose levels in old age, followed by somewhat improved glucose tolerance, and apparent insulin resistance in middle-age. Thus, their phenotype overall resembled that of Prex1 KO males, although it was not as strong. The fact that, in males, the double KO did not exacerbate the phenotype of either single KO suggests that in the absence of both Prex proteins, another Rac-GEF (or glucose homeostasis mechanism) compensates to some extent.

Prex1/2 DKO mice on HFD had low fasting blood glucose levels, similarly to what was observed in both single knockout strains, but their glucose tolerance was similar to that of Prex WT mice. Moreover, Prex1/2 DKO males on HFD exhibited altered insulin responses compared to Prex WT controls and had increased fat mass percentage, as it was seen with the Prex2 KO mice under the same conditions. However, similarly to what was discussed previously for the single KO mice, the apparent insulin resistance of Prex1/2 DKO mice could be a reflection of the

difference in fasting blood glucose levels rather than true insulin resistance.

More importantly, there was a definite sex-difference in Prex1/2 DKO mice. Whereas the phenotype of Prex1/2 DKO males overall was no worse than that of single KO strains, Prex1/2 DKO females were worse than their single KO counterparts on both diets. This implies that there is significant redundancy between Prex proteins specifically in females, which is an astonishing finding. Having repeatedly seen sexual dimorphism in the metabolic phenotype of Prex knockout mice, it seems that these sex-dependent differences even affect the signalling pathways through which the Prex proteins signal, largely non-redundant pathways in males and some redundant signalling in females. Therefore, it seems likely that gonadal hormones impact Prex signalling in a much more profound manner than could have been expected from studying the single KO strains alone.

Overall, the results obtained from Prex1/2 DKO males appear to resemble more the Prex1 KO phenotype on both diets, despite the single knockouts demonstrating almost opposing phenotypes on HFD. Instead, the results obtained from Prex1/2 DKO females were worse than the phenotype of the single KO mice. This demonstrates that the roles of Prex1 and Prex2 in glucose homeostasis are not simply interchangeable, except in some situations specifically in females, as discussed here above; it seems likely that this overall low redundancy triggers different compensatory responses. The most obvious difference is that the two Prex proteins show distinct tissue distribution; and even within organs where both proteins are expressed they might be present in different cell types. As discussed above, one major difference on the cellular level is that hematopoietic Prex1 was shown to be involved in regulating glucose tolerance, whereas Prex2 is not expressed in the haematopoietic system. On a molecular level, only Prex2 interacts with Pten and contributes to the regulation of PIP_3 levels, therefore modulating PI3K/Akt downstream signalling through at least one mechanism in which Prex1 is not involved.

It would be interesting to investigate which Rac-GEF, if any, compensates for the loss of Prex1 and Prex2 in male double KO mice, to produce a phenotype that is weaker than in the single KOs. As Vav and Tiam1 Rac-GEFs have previously been implicated in glucose homeostasis, they might be obvious candidates. This

could be tested in the future by expression analysis, searching for upregulation of Rac-GEFs on the mRNA or protein level in insulin-sensitive Prex1/2 DKO tissues. One could also measure Rac activity in DKO compared to single KO tissues, either by Pak-CRIB pull down assay, or better yet, by *in vivo* or *ex vivo* FLIM-Fret analysis using the Rac activity reporter strain that is already available in our laboratory. This may help elucidate if Rac activity levels are reduced in single KO tissues but rescued by upregulation of another Rac-GEF in double KO tissues. Finally, one could also employ genetic means, through the generation and testing of mice deficient in multiple Rac-GEFs, although this would likely have complex consequences for multiple organ systems.

5.5 Roles of Prex proteins in insulin signalling

As described in the introduction, both PREX1 and PREX2 are known to mediate IR signalling, although most of that literature is on PREX2. In this study, I investigated the role of Prex1 in insulin signalling *ex vivo*, and I tested the roles of both Prex proteins, and of their catalytic activities, in insulin signalling in an overexpression system in HepG2 cells.

The literature that previously investigated the role of PREX1 in IR signalling had shown that PREX1 knockdown in breast cancer cells reduces IGF-1 stimulated IR signalling to Rac1 (Dillon et al., 2014; Montero et al., 2013), and knockdown in ovarian cancer cells reduces the IGF-1 stimulated activation of both the mTORC2 substrate Akt-S473 and Rac1 (Kim et al., 2012). Surprisingly, high levels of Prex1 expression in human breast cancer are associated with decreased PI3K/Akt/mTOR/GSK3 pathway activity markers, possibly through a negative feedback loop where PI3K inhibits PREX1 expression. However, PREX1 overexpression in breast cancer cell lines enhanced the IGF-1 stimulated activating phosphorylation of the IGF-1R/IR, Akt (T308 and S473) and MEK via Rac, suggesting that PREX1 acts both downstream and upstream of PI3K to create a positive feedback loop (Dillon et al., 2014).

In the present study, I used Mesoscale analysis to evaluate insulin pathway activity in the liver, skeletal muscle and ingWAT of mock- and insulin-treated Prex1 KO and Prex WT mice. While I could readily detect the insulin-stimulated activation

of Akt in all tissues, of p70S6K in ingWAT and of GSK3β and in liver, there were no obvious differences between the genotypes under the conditions tested. One possible difference was an insulin-dependent increase in GSK3β activity in the ingWAT of Prex1 KO mice, but this was due to an apparent decrease in total GSK3β levels, which needs to be confirmed by further experiments. Considering that these *ex vivo* results were derived from a small n-number of mice and without much protocol optimisation, it is possible that the experimental parameters were not ideal for insulin pathway interrogation. For instance, a time course or dose response would give better insight into the pathway activation profile, but the scope for such optimisation is necessarily limited for *ex vivo* experiments. It seems likely that further optimisation would reveal a role for Prex1 in insulin signalling also *in vivo,* considering the importance seen *in vitro*.

Within the insulin signalling pathway, the importance of the interaction of Prex1 with mTOR is particularly intriguing. As described in the introduction, it was shown that both PREX1 and PREX2 bind directly to mTOR, and thus both mTOR complexes, mTORC1 and mTORC2. Furthermore, Prex1 knockdown was shown to reduce activation of the mTORC1 substrate p70S6K, although so far only studied in response to amino acid stimulation and not insulin (Hernandez-Negrete et al., 2007). The findings discussed above, which showed that Prex1 knockdown reduced the IGF-1 stimulated phosphorylation of the mTORC2 substrate Akt-S473 (Kim et al., 2012), suggest that Prex1 is able to mediate IR signalling through mTOR, although it is currently unknown whether any of this occurs through the direct interaction of Prex1 with mTOR. Hence, it could be of importance to work further towards understanding the significance of this interaction for the insulin signalling pathway.

In order to assess the importance of PREX Rac-GEF activity in insulin signalling, the generation of a catalytically inactive mutant of PREX2 was first required. For this purpose two residues, Glu30 and Asn212 within the PREX2 DH catalytic domain were mutated to alanine. Purified recombinant human $PREX2^{E30A/N212A}$ protein was produced, and tested in a liposome-based *in vitro* Rac-GEF activity assay, which confirmed that the E30A and N212A mutations successfully inhibited both the basal and PIP_3-stimulated Rac-GEF activity of PREX2. This was in line with recent analysis of the crystal structure of PREX1 in

complex with Rac1, which demonstrated that the equivalent residues to both of these are important for the PREX1:Rac1 interaction (Lucato et al., 2015). Moreover, the mutation of the equivalent residues in PREX1 to alanine rendered the PREX1 protein GEF-dead both *in vitro* and in cells without affecting its normal folding (Hill et al., 2005; Welch, 2015).

Overexpression of either wild type or catalytically inactive PREX1 and PREX2 in HepG2 cells resulted in increased Akt activity in response to insulin stimulation. These data suggest that both PREX proteins can mediate insulin signalling not only through their Rac-GEF activity, but also as adaptor proteins, at least in this overexpression system. In regards to PREX2, a GEF-independent role was to be expected, based upon the studies by the Parsons lab, which had shown that Prex2 binding inhibits Pten activity in a GEF-independent manner (Hodakoski et al., 2014). The Parsons lab had furthermore suggested that Prex2 KO might affect the insulin pathway activity also *in vivo* through relief of inhibition of Pten by Prex2 (Hodakoski et al., 2014). In contrast to Prex2, the GEF-activity independent role of PREX1 in insulin signalling came as a surprise. The only other GEF-independent role of PREX1 is in the regulation of agonist-induced GPCR trafficking, which was recently discovered in our lab and is as yet unpublished. Unlike PREX2, PREX1 does not interact with PTEN, and therefore it would be very interesting to investigate in the future through which adaptor function PREX1 regulates the insulin signalling pathway. It is possible that the interaction of PREX1 and PREX2 with mTOR is important in this regard.

5.6 Generation of catalytically inactive Prex mouse strains

On the basis of my *in vitro* results which suggested that both PREX1 and PREX2 have adaptor functions in insulin signaling, combined with the phenotypes of the Prex KO mice, it was considered useful to generate catalytically inactive Prex mouse strains. To achieve this goal, I targeted residues in the mouse genome that are equivalent to those in the human recombinant catalytically inactive PREX1 and PREX2 proteins, namely Glu51 and Asn233 for Prex1, and Glu22 and Asn204 for Prex2. The relevant nucleotides are located on exon 1 and exon 6, respectively, of each Prex gene, and in the mouse genome these exons are around 90 kb apart in

both genes. Hence, traditional gene targeting by homologous recombination would have been impossible, as this distance is too large for a single targeting vector yet too small for crossover to occur and allow crossing of single-mutant strains. Therefore, a CRISPR targeting approach was designed instead. The principle of CRISPR technology is to design sgRNAs that direct the Cas9 nuclease to cleave a specific sequence, and in the case of knock-in mice, introduce a repair template that encodes for the desired mutation.

The selected strategy was to target both exons 1 and 6 of the Prex1 or Prex2 genes at the same time, using wild type Cas9 and a repair template for each site to introduce the desired mutations. Although there were concerns regarding off-target effects due to Cas9-mediated un-specific double-strand brakes, the alternative of employing a pair of Cas9D10A nickases for higher specificity was rejected as it would have increased the amount of components needed to be microinjected into the zygote and reduce targeting efficiency. Moreover, it had been reported in the literature that off-target effects are rare in mouse zygotes microinjected with Cas9 mRNA, possibly due to the transient nature of the expression of Cas9 protein from mRNA compared to the relatively extended expression from a plasmid in cell line transfection experiments (Singh et al., 2015). Another concern regarding the simultaneous targeting of both exons with the wild-type Cas9 nuclease was the theoretical potential for deletion of parts of the genomic sequence. However, it was previously seen that two Cas9-mediated cleavage events ~700 bp apart in the mouse genome resulted in detrimental deletions only in 35% of the obtained mice (Yang et al., 2013). It was concluded that the risk of losing part or the whole 90 kb genomic sequence between the cut sites in the Prex genes was considerably lower.

The sgRNAs were designed using online available databases for each targeting locus and were all tested for their targeting efficiency *in vitro*. However, there was scepticism on how efficient these sgRNAs would be in cells. Therefore, the sgRNAs were also assessed for their efficiency in the NIH/3T3 mouse cell line using SURVEYOR nuclease assay. Comparable results were obtained with both methods, which confirmed that for future projects the *in vitro* assessment would likely be sufficient. Another important component of the CRISPR approach, when introducing point mutations, was the design of ssDNA that acts as a repair template,

promoting HDR. This repair template was designed in a way that it would not only introduce the desired point mutations, but also silent mutations that generated unique restriction sites, providing an efficient and robust screening method. In the end, I did not utilise these restriction sites in my genotyping, but rather developed a PCR protocol with primers specific for the mutated or the wild type sequence, as this method was deemed less time-consuming. However, that PCR protocol yielded many false positive results, so to be absolutely certain of the genotype, I resorted to Sanger sequencing of the PCR products, which was the most time consuming but yielded incontrovertible results.

Although catalytically inactive Prex1 mouse strain was not established within the time of this project, there were two successful targeting events that yielded one heterozygous Prex1 GEF-dead female each; both survived into adulthood but died before they could give birth to heterozygous pups. This should be regarded as very unfortunate rather than related to any detrimental effects of the genotype on breeding or viability, as the phenotype would not be expected to be severer than that of the Prex1 KO mouse, and thus further targeting efforts are currently ongoing. In contrast, the catalytically inactive Prex2 mouse strain was successfully established. As Dr Spensberger had learned that microinjection of too much targeting material into zygotes was detrimental, initially mice positive for the mutation on exon 1 of Prex2 were generated and bred together until the mutation was homozygous (E22A). Zygotes from these homozygous mice were subsequently retargeted for mutation N204A on exon 6 (N204A).

5.7 Metabolic phenotype of the GEF-dead Prex2 E22A mouse

While the re-targeting of the $Prex2^{E22A/E22A}$ (Prex2 E22A) mouse strain to $Prex2^{E22A/E22A;N204A/N204A}$ was ongoing, I decided to investigate the metabolic phenotype of the Prex2 E22A mouse. This strain was considered to be a “nearly GEF-dead” mouse, based on the documented low level of GEF-activity that remained in the equivalent human PREX1 G56A protein (Lucato et al., 2015). Glu56 of PREX1 forms high-density hydrogen bonds with residues within the switch 1 of Rac1, whereas Asn 238 (the equivalent of N204 in mouse Prex2) forms hydrogen bonds with residues in switch 2. Mutation of either of these residues alone was

sufficient to reduce the level of Rac1 binding and GDP-exchange activity of PREX1 in vitro to maximally 5% of residual activity (Lucato et al., 2015). Given the high homology between the Prex1 and Prex2 DH domains, it was concluded that this finding would extend to Prex2, and the *Prex2*$^{E22A/E22A}$ mouse would show a similar >95% loss of GEF activity, although formal verification is outstanding.

Prex2$^{E22A/E22A}$ (Prex2 E22A) males on chow diet had lower fasting blood glucose levels than controls throughout ageing, and exhibited improved glucose tolerance from 15 weeks of age onwards, despite an overall normal response to insulin challenge. Prex2 E22A males on HFD retained both their low fasting blood glucose levels and their improved glucose tolerance throughout ageing. Female Prex2 E22A mice also demonstrated reduced fasting blood glucose levels on HFD, but their glucose response was normal throughout ageing. Therefore, the phenotype of the Prex2 E22A mouse resembled much more that of Prex1 KO than Prex2 KO mice, except it was more pronounced and less diet-dependent, but just as sex-dependent. Overall, the Prex2 E22A mouse showed much improved glucose homeostasis. These results demonstrate that Prex2 has important Rac-GEF activity independent functions in the control of blood glucose levels.

In contrast to the Prex2 E22A mouse, the Prex2 KO mice had an overall normal metabolic phenotype on chow diet, but reduced glucose tolerance and age-related insulin resistance on HFD. Hence, the absence of Prex2 protein and the absence of Prex2 catalytic activity affect glucose homeostasis in almost opposite ways, with the GEF activity apparently limiting glucose tolerance and the adaptor functions promoting it. One mechanism that is lost in the Prex2 KO mouse that is likely intact in the Prex2 E22A mouse is the inhibition of Pten, although this needs to be corroborated by measurements of PIP3 levels. Additional differences in phenotype between Prex2 KO and E22A mice could be due to compensatory mechanisms (such as upregulation of other GEFs) being triggered in the absence of the Prex2 protein that are not triggered when the protein is expressed but catalytically inactive. In that case, one might presume that the adverse metabolic phenotype of the Prex2 KO mouse is in fact a ‘side-effect’ of such compensatory mechanisms.

Due to time-limitations, I could obtain body composition data for Prex2 E22A

mice only on HFD, which showed that they had reduced fat percentage compared to their WT counterparts. Moreover, both at 10 weeks and 1 year of age, Prex2 E22A mice had significantly smaller livers compared to their WT counterparts, on both chow diet and HFD, in contrast to young Prex2 KO mice, which had larger livers than controls. The reduced liver size suggests that the liver might be an important contributor to the observed phenotype in Prex2 E22A mice. Therefore, it would be of interest to measure the PIP_3/PIP_2 levels and Rac activity particularly in the liver (as well as other insulin sensitive tissues) of the Prex2 E22A mouse, and to interrogate the insulin signalling pathway in these tissues to determine whether the metabolic phenotype of Prex2 KO and Prex2 E22A mice are related to the Prex2/Pten interaction.

5.8 Comparison of the Prex mouse to other Rac-GEF and PI3K mutant strains

We need to consider how the metabolic phenotypes of Prex mice compare to those of related mouse strains, namely mice deficient in other Rho-GEFs or in the Prex regulator PI3K.

Like Prex proteins, PDZ-RhoGEF is a GEF that signals downstream of GPCRs, as it is regulated by the Gα subunits of heterotrimeric G proteins. Moreover, like Prex proteins, PDZ-RhoGEF regulates metabolism, specifically by governing susceptibility to diet-induced obesity and type 2 diabetes. PDZ-RhoGEF deficiency resulted in reduced body weight and fat mass as well as increased energy expenditure on chow-fed mice (Chang et al., 2015). Similarly, Prex1 deficiency resulted in reduced adipose tissue mass at both young and middle age. However, Prex1 KO mice were not significantly thinner than their Prex WT counterparts, and the percentage of fat mass was normal. Likewise, although Prex2 KO mice on chow diet were lighter than the Prex WT control mice, they had normal body composition. Therefore, it seems unlikely that there is any redundancy between Prex proteins and PDZ-RhoGEF in glucose homeostasis. This is unsurprising, as PDZ-Rho-GEF is a Rho-specific GEF, and not a Rac-GEF.

Vav-family GEFs, which activate Rac, and possibly also Cdc42 and RhoA *in vivo*, are also important regulators of metabolism. Vav3 deficient mice on chow diet

developed metabolic syndrome, NAFLD, and T2DM without increased adiposity (Menacho-Márquez et al., 2013), whereas, Prex deficiency either improved the metabolic phenotype of mice (Prex1 KO and Prex2 E22A) or had no significant effect (Prex2 KO). Moreover, mice expressing catalytically inactive Vav2 exhibit reduced skeletal muscle mass and insulin sensitivity, resulting in metabolic syndrome (Rodríguez-Fdez and Bustelo, 2019), whereas neither Prex1 nor Prex2 significantly affected the insulin sensitivity of mice on chow diet. As discussed before, the apparent insulin resistance observed under some conditions was probably due to low fasting blood glucose levels or altered counter-regulatory responses.

Both PDZ-RhoGEF and Vav3 depletion protected mice from diet-dependent development of obesity and metabolic syndrome (Chang et al., 2015; Menacho-Márquez et al., 2013). In the present study, Prex1 and Prex2 single knockout males on HFD were not protected from diet-induced obesity and glucose intolerance, despite their low fasting blood glucose levels. Only HFD-fed Prex2 E22A males showed reduced body weight and fat mass, as well as low fasting blood glucose levels and improved glucose tolerance. Therefore, it seems unlikely that Vav3 and Prex1 or Prex2 have redundant functions in metabolism, which was perhaps again unsurprising, because vav proteins are regulated by tyrosine phosphorylation and mostly signal downstream of different receptors to Prex. However, we previously demonstrated redundancy between Prex1 and Vav1 in neutrophils, and between Prex1 and either Vav1 or Vav3 in platelets (Pantarelli and Welch, 2018), so it would makes sense to explore possibility of redundancy with Vav in metabolism in the future.

Overall, Prex deficiency or GEF-activity deficiency revealed roles in glucose homeostasis that are both comparable, to an extent, and non-redundant to those of other Rho-GEFs, highlighting the complexity and crucial importance of tight Rho-GTPase regulation by multiple GEFs.

As Prex proteins mediate insulin signalling, we should consider the Prex KO phenotypes in relation to other mouse strains related to the insulin/PI3K signalling pathway. Systemic insulin receptor knockout in mice led to slightly reduced prenatal growth, as well as neonatal diabetic ketoacidosis due to hyperglycaemia and

hyperinsulinemia, ultimately resulting in early postnatal death (Accili et al., 1996; Joshi et al., 1996). In contrast, adipose tissue specific knockout of the insulin receptor surprisingly protected against diet- and age-related metabolic syndrome, despite glucose intolerance and insulin resistance at young age (Friesen et al., 2016). Analysis of whole-body IRS KO mice revealed that from the IRS tested, IRS1 and IRS2 are more relevant in insulin signalling-mediated glucose homeostasis. Knockout of IRS1 resulted in insulin resistance with compensatory IRS2-dependent hyperinsulinemia and β cell hyperplasia, which afforded normal glucose tolerance (Araki et al., 1994; Tamemoto et al., 1994). Instead, IRS2 deficiency was associated with peripheral insulin resistance but impaired compensatory insulin secretion, which led to hyperglycaemia and development of T2DM (Kubota et al., 2000; Withers et al., 1998). Considering the differences in phenotype, it seems unlikely that the effects of Prex KO on glucose homeostasis derive from altered IRS function. For example, the fasting insulin and glucagon levels of Prex1 KO mice were normal, whereas pancreatic function was strongly affected in the IRS KO mice. However, given that PREX1 overexpression in breast cancer cell lines enhanced the IGF-1 stimulated activation of the IGF-1R and IR (Dillon et al., 2014), it would be interesting to evaluate the phosphorylation state of IR in Prex1 KO mice upon insulin stimulation.

Insulin signalling downstream of IRS1 and IRS2, promotes the activation of the PI3K/Akt pathway. As described in the introduction, Class IA PI3Ks are heterodimeric molecules composed of p85 regulatory and p110 catalytic subunits. Knockout of *Pik3r1,* which codes for the p85α, p55α, and p50α isoforms of the regulatory subunit, resulted in perinatal death associated with liver necrosis (Fruman et al., 2000). Interestingly, these mice showed hypoglycaemia and improved glucose clearance, similarly to the Prex1 KO and Prex2 E22A mice here. Moreover, like Prex1 KO, *Pik3r1* deficiency did not reduce Akt activation in liver and skeletal muscle, and neither did it affect Glut1 and Glut4 expression in skeletal muscle (Fruman et al., 2000). However, contrary to Prex1 KO, Pik3r1 KO mice showed reduced insulin levels, both in fasting and fed state. Knockout of the p85α isoform specifically also led to hypoglycaemia and increased insulin sensitivity in mice, as well as upregulation of p55α and p50α which promoted insulin-mediated PIP_3 generation and Glut4 translocation to the plasma membrane in p85α KO mice

(Terauchi et al., 1999). Moreover, mutations in the C-terminal SH2 domain of human *PIK3R1* have been associated with insulin resistance, reduced subcutaneous fat in humans (Huang-Doran et al., 2016).

Systemic deficiency of the catalytic p110α or p110β subunits of PI3K is embryonic lethal. However, expression of a kinase-dead p110α knock-in ($p110\alpha^{D933A/WT}$) at heterozygous state resulted in hyperphagia, increased adiposity, glucose intolerance, hyperinsulinemia, and insulin resistance (Foukas et al., 2006). Interestingly, $p110\alpha^{D933A/WT}$ mice displayed an impaired insulin response that resembles the response of 10 months old Prex1 KO male mice (reduced glucose drop in the initial phase of the insulin challenge followed by quick recovery back to basal levels during the later phase). Nevertheless, $p110\alpha^{D933A/WT}$ mice had normal glucose levels (Foukas et al., 2006). Intriguingly, ageing $p110\alpha^{D933A/WT}$ mice were protected from age-related fat accumulation and demonstrated improved insulin sensitivity and glucose tolerance (Foukas et al., 2013). In contrast, male Prex2 KO mice showed apparent increased insulin sensitivity in old age, but both male and female Prex2 KO mice exhibited a tendency to improved glucose tolerance in young age, which worsened in old age. More recently, adipose tissue specific inactivation of p110α was reported to result in increased β-adrenergic signalling which promoted glucose uptake by BAT, and these mice maintained normal glucose homeostasis despite age-related insulin resistance (Araiz et al., 2019).

Overall, therefore, there is no obvious straightforward correlation between the phenotypes of mice with deficiencies in the insulin/PI3K signalling pathway and mice with Prex deficiency, suggesting that the effects in the Prex deficient mice derive from a complex combination of mechanisms, that may include but are not restricted to the insulin/PI3K signalling pathway.

5.9 Conclusion and Future Perspective

In conclusion, this study demonstrated that both Prex1 and Prex2 proteins have important and unexpected physiological roles in the regulation of glucose homeostasis. Prex1 deficiency helps maintain low glucose levels and protects from age-related glucose intolerance. Although the mechanisms through which Prex1 controls glucose homeostasis are still unclear, bone marrow transplant experiments

indicated this could be through the regulation of inflammation. Prex2 deficiency resulted in glucose intolerance in mice on HFD, whereas catalytically-inactive Prex2 mice had improved glucose tolerance both on chow and high fat diet. These data suggested that Prex2 regulates glucose homeostasis both through its Rac-GEF activity and through adaptor functions, with its Rac-GEF activity limiting glucose homeostasis and its adaptor functions promoting it. Following on from my work, the Prex1-GEF-Dead mouse will show the Rac-GEF activity or the adaptor functions of Prex1 regulate glucose homeostasis, and the Prex2 E22A/N204A mouse will show if total inhibition of Prex2 Rac-GEF activity would afford even more benefit than Prex2 E22A.

My work suggests that the development of therapeutics to target PREX1 and PREX2 may be a new avenue for the treatment hyperglycaemia and glucose intolerance associated with metabolic syndrome. For PREX1, work on the Prex1-GEF-Dead mouse will reveal whether drugs should target protein stability or Rac-GEF activity, and for PREX2, my results suggest that targeting the Rac-GEF activity should be beneficial, whereas targeting stability would be detrimental. Depending on the phenotypes of the Prex1-GEF-Dead and Prex2 E22A/N204A mice, it may be useful to generate and evaluate crosses that are GEF-dead for both Prex proteins. This would elucidate whether prospective PREX inhibitors would need to be isoform specific. In any event, more investigation is required to identify the molecular mechanism through which PREX proteins regulate glucose homeostasis, in order to facilitate the design of PREX-directed therapeutic approaches.

Although the selective targeting of PREX catalytic activity has proven challenging, as for other GEFs, the recent reports of the PREX1 crystal structure (Cash et al., 2016; Lucato et al., 2015) may facilitate the design of small molecule inhibitors. Drugs that target the level and/or stability of PREX1 could include epigenetic regulators (e.g. micro-RNAs), as PREX1 protein levels are known to be controlled by these processes. The development of such drugs is being trialled for other types proteins, but has not yet reached the clinic, usually due to lack of efficacy and specificity. Examples of small molecule inhibitors that affect the catalytic activity of other GEFs with high efficacy and specificity do exist, although mainly as laboratory tools and only for GEFs that activate quite distantly related GTPases,

such as the Arf-GEF inhibitor Brefeldin A (Cherfils and Zeghouf, 2013). Nevertheless, efforts are currently ongoing worldwide, both in academia and in industry, to target the activity of GEFs and small GTPases, such as the Ras-GEF SOS and K-Ras in human cancers (Evelyn et al., 2014; Simanshu et al., 2017). Therefore, it seems likely that the development of PREX Rac-GEF inhibitors for the treatment of hyperglycemia and glucose intolerance should be feasible in the future.

Chapter 6 - Bibliography

Abbott, C.R., Monteiro, M., Small, C.J., Sajedi, A., Smith, K.L., Parkinson, J.R.C., Ghatei, M.A., and Bloom, S.R. (2005). The inhibitory effects of peripheral administration of peptide YY3–36 and glucagon-like peptide-1 on food intake are attenuated by ablation of the vagal–brainstem–hypothalamic pathway. Brain Research *1044*, 127-131.

Abel, E.D., Peroni, O., Kim, J.K., Kim, Y.-B., Boss, O., Hadro, E., Minnemann, T., Shulman, G.I., and Kahn, B.B. (2001). Adipose-selective targeting of the GLUT4 gene impairs insulin action in muscle and liver. Nature *409*, 729-733.

Abiko, H., Fujiwara, S., Ohashi, K., Hiatari, R., Mashiko, T., Sakamoto, N., Sato, M., and Mizuno, K. (2015). Rho guanine nucleotide exchange factors involved in cyclic-stretch-induced reorientation of vascular endothelial cells. Journal of Cell Science *128*, 1683-1695.

Accili, D., Drago, J., Lee, E.J., Johnson, M.D., Cool, M.H., Salvatore, P., Asico, L.D., José, P.A., Taylor, S.I., and Westphal, H. (1996). Early neonatal death in mice homozygous for a null allele of the insulin receptor gene. Nature Genetics *12*, 106-109.

Adame-Garcia, S.R., Cervantes-Villagrana, R.D., Orduna-Castillo, L.B., del Rio, J.C., Gutkind, J.S., Reyes-Cruz, G., Taylor, S.S., and Vazquez-Prado, J. (2019). cAMP-dependent activation of the Rac guanine exchange factor P-REX1 by type I protein kinase A (PKA) regulatory subunits. The Journal of Biological Chemistry *294*, 2232-2246.

Aghazadeh, B., Zhu, K., Kubiseski, T.J., Liu, G.A., Pawson, T., Zheng, Y., and Rosen, M.K. (1998). Structure and mutagenesis of the Dbl homology domain. Nature Structural & Molecular Biology *5*, 1098-1107.

Ahmad, K.F., and Lim, W.A. (2010). The Minimal Autoinhibited Unit of the Guanine Nucleotide Exchange Factor Intersectin. PLOS One *5*, e11291.

Ahmed, K., Tunaru, S., Tang, C., Müller, M., Gille, A., Sassmann, A., Hanson, J., and Offermanns, S. (2010). An Autocrine Lactate Loop Mediates Insulin-Dependent Inhibition of Lipolysis through GPR81. Cell Metabolism *11*, 311-319.

Akpan, J.O., Gardner, R., and Wagle, S.R. (1974). Studies on the effects of insulin and acetylcholine on activation of glycogen synthase and on glycogenesis in hepatocytes. Biochemical and Biophysical Research Communications *61*, 222-229.

Alquier, T., and Poitout, V. (2018). Considerations and guidelines for mouse metabolic phenotyping in diabetes research. Diabetologia *61*, 526-538.

Alsahli, M., and Gerich, J.E. (2017). Renal glucose metabolism in normal physiological conditions and in diabetes. Diabetes Research and Clinical Practice *133*, 1-9.

Altarejos, J., Montminy, M., Altarejos, J., and Montminy, M. (2011). CREB and the CRTC co-activators: sensors for hormonal and metabolic signals. Nature Reviews Molecular Cell Biology *12*, 141-151.

Andrikopoulos, S., Blair, A.R., Deluca, N., Fam, B.C., and Proietto, J. (2008). Evaluating the glucose tolerance test in mice. American Journal of Physiology-Endocrinology and Metabolism *295*, E1323-E1332.

Araiz, C., Yan, A., Bettedi, L., Samuelson, I., Virtue, S., McGavigan, A.K., Dani, C., Vidal-Puig, A., and Foukas, L.C. (2019). Enhanced β-adrenergic signalling underlies an age-dependent beneficial metabolic effect of PI3K p110α inactivation in adipose tissue. Nature Communications *10*, 1546.

Araki, E., Lipes, M.A., Patti, M.-E., Brüning, J.C., Haag Iii, B., Johnson, R.S., and Kahn, C.R. (1994). Alternative pathway of insulin signalling in mice with targeted disruption of the IRS-1 gene. Nature *372*, 186-190.

Aslan, J.E., Spencer, A.M., Loren, C.P., Pang, J., Welch, H.C., Greenberg, D.L., and McCarty, O.J. (2011). Characterization of the Rac guanine nucleotide exchange factor P-Rex1 in platelets. Journal of Molecular Signaling *6*, 11.

Atkinson, M.A., Eisenbarth, G.S., and Michels, A.W. (2014). Type 1 diabetes. Lancet *383*, 69-82.

Ayala, J.E., Bracy, D.P., McGuinness, O.P., and Wasserman, D.H. (2006). Considerations in the Design of Hyperinsulinemic-Euglycemic Clamps in the Conscious Mouse. Diabetes *55*, 390-397.

Ayala, J.E., Samuel, V.T., Morton, G.J., Obici, S., Croniger, C.M., Shulman, G.I., Wasserman, D.H., McGuinness, O.P., and Consortium, N.I.H.M.M.P.C. (2010). Standard operating procedures for describing and performing metabolic tests of glucose homeostasis in mice. Dis Model Mech *3*, 525-534.

Balamatsias, D., Kong, A.M., Waters, J.E., Sriratana, A., Gurung, R., Bailey, C.G., Rasko, J.E., Tiganis, T., Macaulay, S.L., and Mitchell, C.A. (2011). Identification of P-Rex1 as a novel Rac1-guanine nucleotide exchange factor (GEF) that promotes actin remodeling and GLUT4 protein trafficking in adipocytes. The Journal of Biological Chemistry *286*, 43229-43240.

Barber, M.A., Donald, S., Thelen, S., Anderson, K.E., Thelen, M., and Welch, H.C. (2007). Membrane translocation of P-Rex1 is mediated by G protein betagamma subunits and phosphoinositide 3-kinase. The Journal of Biological Chemistry *282*, 29967-29976.

Barber, M.A., Hendrickx, A., Beullens, M., Ceulemans, H., Oxley, D., Thelen, S., Thelen, M., Bollen, M., and Welch, H.C. (2012). The guanine-nucleotide-exchange factor P-Rex1 is activated by protein phosphatase 1alpha. Biochemical Journal *443*, 173-183.

Barr, V.A., Malide, D., Zarnowski, M.J., Taylor, S.I., and Cushman, S.W. (1997). Insulin Stimulates Both Leptin Secretion and Production by Rat White Adipose Tissue. Endocrinology *138*, 4463-4472.

Barreto, S.G., Carati, C.J., Toouli, J., and Saccone, G.T.P. (2010). The islet-acinar axis of the pancreas: more than just insulin. American Journal of Physiology-Gastrointestinal and Liver Physiology *299*, G10-G22.

Barrio-Real, L., Benedetti, L.G., Engel, N., Tu, Y., Cho, S., Sukumar, S., and Kazanietz, M.G. (2014). Subtype-specific overexpression of the Rac-GEF P-REX1 in breast cancer is associated with promoter hypomethylation. Breast Cancer Research *16*, 441.

Barrio-Real, L., Lopez-Haber, C., Casado-Medrano, V., Goglia, A.G., Toettcher, J.E., Caloca, M.J., and Kazanietz, M.G. (2018). P-Rex1 is dispensable for Erk activation and mitogenesis in breast cancer. Oncotarget *9*, 28612-28624.

Barrows, D., He, J.Z., and Parsons, R. (2016). PREX1 Protein Function Is Negatively Regulated Downstream of Receptor Tyrosine Kinase Activation by p21-activated Kinases (PAKs). The Journal of Biological Chemistry *291*, 20042-20054.

Barrows, D., Schoenfeld, S.M., Hodakoski, C., Silkov, A., Honig, B., Couvillon, A., Shymanets, A., Nurnberg, B., Asara, J.M., and Parsons, R. (2015). p21-activated Kinases (PAKs) Mediate the Phosphorylation of PREX2 Protein to Initiate Feedback Inhibition of Rac1 GTPase. The Journal of Biological Chemistry *290*, 28915-28931.

Baumann, C.A., Ribon, V., Kanzaki, M., Thurmond, D.C., Mora, S., Shigematsu, S., Bickel, P.E., Pessin, J.E., and Saltiel, A.R. (2000). CAP defines a second signalling pathway required for insulin-stimulated glucose transport. Nature *407*, 202-207.

Baumeister, M.A., Rossman, K.L., Sondek, J., and Lemmon, M.A. (2006). The Dbs PH domain contributes independently to membrane targeting and regulation of guanine nucleotide-exchange activity. The Biochemical Journal *400*, 563-572.

Bento, J.L., Palmer, N.D., Zhong, M., Roh, B., Lewis, J.P., Wing, M.R., Pandya, H., Freedman, B.I., Langefeld, C.D., Rich, S.S.*, et al.* (2008). Heterogeneity in gene loci associated with type 2 diabetes on human chromosome 20q13.1. Genomics *92*, 226-234.

Berg JM, T.J., Stryer L. (2002). Biochemistry, 5th edition edn (New York: W.H.Freeman & Co Ltd).

Berger, M.F., Hodis, E., Heffernan, T.P., Deribe, Y.L., Lawrence, M.S., Protopopov, A., Ivanova, E., Watson, I.R., Nickerson, E., Ghosh, P.*, et al.* (2012). Melanoma genome sequencing reveals frequent PREX2 mutations. Nature *485*, 502-506.

Bilanges, B., Posor, Y., and Vanhaesebroeck, B. (2019). PI3K isoforms in cell signalling and vesicle trafficking. Nature Reviews Molecular Cell Biology.

Bollen, M., Gevers, G., and Stalmans, W. (1983a). The activity of glycogen synthase phosphatase limits hepatic glycogen deposition in the adrenalectomized starved rat. Biochemical Journal *214*, 539-545.

Bollen, M., Hue, L., and Stalmans, W. (1983b). Effects of glucose on phosphorylase and glycogen synthase in hepatocytes from diabetic rats. Biochemical Journal *210*, 783-787.

Bos, J.L., Rehmann, H., and Wittinghofer, A. (2007). GEFs and GAPs: critical elements in the control of small G proteins. Cell *129*, 865-877.

Bouskila, M., Hunter, R.W., Ibrahim, A.F.M., Delattre, L., Peggie, M., van Diepen, J.A., Voshol, P.J., Jensen, J., and Sakamoto, K. (2010). Allosteric Regulation of Glycogen Synthase Controls Glycogen Synthesis in Muscle. Cell Metabolism *12*, 456-466.

Brown, J.E., Onyango, D.J., Ramanjaneya, M., Conner, A.C., Patel, S.T., Dunmore, S.J., and Randeva, H.S. (2010). Visfatin regulates insulin secretion, insulin receptor signalling and mRNA expression of diabetes-related genes in mouse pancreatic beta-cells. Journal of Molecular Endocrinology *44*, 171-178.

Bryant, N.J., Govers, R., and James, D.E. (2002). Regulated transport of the glucose transporter GLUT4. Nature Reviews Molecular Cell Biology *3*, 267-277.

Burge, M.R., Sobhy, T.A., Qualls, C.R., and Schade, D.S. (2001). Effect of Short-Term Glucose Control on Glycemic Thresholds for Epinephrine and Hypoglycemic Symptoms. The Journal of Clinical Endocrinology & Metabolism *86*, 5471-5478.

Bustelo, X.R., Sauzeau, V., and Berenjeno, I.M. (2007). GTP-binding proteins of the Rho/Rac family: regulation, effectors and functions in vivo. Bioessays *29*, 356-370.

Carnagarin, R., Dharmarajan, A.M., and Dass, C.R. (2015). Molecular aspects of glucose homeostasis in skeletal muscle – A focus on the molecular mechanisms of insulin resistance. Molecular and Cellular Endocrinology *417*, 52-62.

Carretero-Ortega, J., Walsh, C.T., Hernandez-Garcia, R., Reyes-Cruz, G., Brown, J.H., and Vazquez-Prado, J. (2010). Phosphatidylinositol 3,4,5-triphosphate-dependent Rac exchanger 1 (P-Rex-1), a guanine nucleotide exchange factor for Rac, mediates angiogenic responses to stromal cell-derived factor-1/chemokine stromal cell derived factor-1 (SDF-1/CXCL-12) linked to Rac activation, endothelial cell migration, and in vitro angiogenesis. Molecular Pharmacology *77*, 435-442.

Carson, A.P., Reynolds, K., Fonseca, V.A., and Muntner, P. (2010). Comparison of A1C and Fasting Glucose Criteria to Diagnose Diabetes Among U.S. Adults. Diabetes Care *33*, 95-97.

Carvalho, E., Kotani, K., Peroni, O.D., and Kahn, B.B. (2005). Adipose-specific overexpression of GLUT4 reverses insulin resistance and diabetes in mice lacking GLUT4 selectively in muscle. American Journal of Physiology-Endocrinology and Metabolism *289*, E551-E561.

Cash, J.N., Davis, E.M., and Tesmer, J.J.G. (2016). Structural and Biochemical Characterization of the Catalytic Core of the Metastatic Factor P-Rex1 and Its Regulation by PtdIns(3,4,5)P3. Structure *24*, 730-740.

Cersosimo, E., Garlick, P., and Ferretti, J. (1999). Insulin regulation of renal glucose metabolism in humans. American Journal of Physiology-Endocrinology and Metabolism *276*, E78-E84.

Cersosimo, E., Triplitt, C., Solis-Herrera, C., Mandarino, L.J., and DeFronzo, R.A. (2000). Pathogenesis of Type 2 Diabetes Mellitus. In Endotext, K.R. Feingold, B. Anawalt, A. Boyce, G. Chrousos, K. Dungan, A. Grossman, J.M. Hershman, G. Kaltsas, C. Koch, P. Kopp*, et al.*, eds. (South Dartmouth (MA): MDText.com, Inc.).

Cestra, G., Kwiatkowski, A., Salazar, M., Gertler, F., and De Camilli, P. (2005). Tuba, a GEF for CDC42, links dynamin to actin regulatory proteins. Methods in Enzymology *404*, 537-545.

Ceulemans, H., and Bollen, M. (2004). Functional Diversity of Protein Phosphatase-1, a Cellular Economizer and Reset Button. Physiol Rev *84*, 1-39.

Challa, T.D., Beaton, N., Arnold, M., Rudofsky, G., Langhans, W., and Wolfrum, C. (2012). Regulation of adipocyte formation by GLP-1/GLP-1R signaling. The Journal of Biological Chemistry *287*, 6421-6430.

Chang, Y.-J., Pownall, S., Jensen, T.E., Mouaaz, S., Foltz, W., Zhou, L., Liadis, N., Woo, M., Hao, Z., Dutt, P.*, et al.* (2015). The Rho-guanine nucleotide exchange factor PDZ-RhoGEF governs susceptibility to diet-induced obesity and type 2 diabetes. Elife *4*, e06011.

Chavez-Vargas, L., Adame-Garcia, S.R., Cervantes-Villagrana, R.D., Castillo-Kauil, A., Bruystens, J.G., Fukuhara, S., Taylor, S.S., Mochizuki, N., Reyes-Cruz, G., and Vazquez-Prado, J. (2016). Protein Kinase A (PKA) Type I Interacts with P-Rex1, a Rac Guanine Nucleotide Exchange Factor: Effect on PKA Localization and P-Rex1 Signaling. The Journal of Biological Chemistry *291*, 6182-6199.

Chen, C.A., and Manning, D.R. (2001). Regulation of G proteins by covalent modification. Oncogene *20*, 1643-1652.

Chen, X., Pan, M., Han, L., Lu, H., Hao, X., and Dong, Q. (2013). miR-338-3p suppresses neuroblastoma proliferation, invasion and migration through targeting PREX2a. FEBS letters *587*, 3729-3737.

Cherfils, J., and Zeghouf, M. (2013). Regulation of Small GTPases by GEFs, GAPs, and GDIs. Physiol Rev *93*, 269-309.

Chiu, T.T., Patel, N., Shaw, A.E., Bamburg, J.R., and Klip, A. (2010). Arp2/3- and Cofilin-coordinated Actin Dynamics Is Required for Insulin-mediated GLUT4 Translocation to the Surface of Muscle Cells. Molecular biology of the cell *21*, 3529-3539.

Choi, E., Kikuchi, S., Gao, H., Brodzik, K., Nassour, I., Yopp, A., Singal, A.G., Zhu, H., and Yu, H. (2019). Mitotic regulators and the SHP2-MAPK pathway promote IR endocytosis and feedback regulation of insulin signaling. Nature Communications *10*, 1473.

Choi, S.M., Tucker, D.F., Gross, D.N., Easton, R.M., DiPilato, L.M., Dean, A.S., Monks, B.R., and Birnbaum, M.J. (2010). Insulin Regulates Adipocyte Lipolysis via an Akt-Independent Signaling Pathway. Molecular and Cellular Biology *30*, 5009-5020.

Chrencik, J.E., Brooun, A., Zhang, H., Mathews, I.I., Hura, G.L., Foster, S.A., Perry, J.J.P., Streiff, M., Ramage, P., Widmer, H*., et al.* (2008). Structural basis of guanine nucleotide exchange mediated by the T-cell essential Vav1. Journal of Molecular Biology *380*, 828-843.

Clarke, P.R., and Zhang, C. (2008). Spatial and temporal coordination of mitosis by Ran GTPase. Nature Reviews Molecular Cell Biology *9*, 464.

Cook, D.R., Rossman, K.L., and Der, C.J. (2014). Rho guanine nucleotide exchange factors: regulators of Rho GTPase activity in development and disease. Oncogene *33*, 4021-4035.

Corbetta, S., Gualdoni, S., Albertinazzi, C., Paris, S., Croci, L., Consalez, G.G., and de Curtis, I. (2005). Generation and Characterization of Rac3 Knockout Mice. Molecular and Cellular Biology *25*, 5763-5776.

Cota, D., Proulx, K., Smith, K.A.B., Kozma, S.C., Thomas, G., Woods, S.C., and Seeley, R.J. (2006). Hypothalamic mTOR Signaling Regulates Food Intake. Science *312*, 927-930.

Côté, J.-F., Motoyama, A.B., Bush, J.A., and Vuori, K. (2005). A novel and evolutionarily conserved PtdIns(3,4,5)P3-binding domain is necessary for DOCK180 signalling. Nature Cell Biology *7*, 797-807.

Cotero, V.E., and Routh, V.H. (2009). Insulin blunts the response of glucose-excited neurons in the ventrolateral-ventromedial hypothalamic nucleus to decreased glucose. American Journal of Physiology-Endocrinology and Metabolism *296*, E1101-E1109.

Cross, D.A.E., Alessi, D.R., Cohen, P., Andjelkovich, M., and Hemmings, B.A. (1995). Inhibition of glycogen synthase kinase-3 by insulin mediated by protein kinase B. Nature *378*, 785-789.

Cryer, P.E., Davis, S.N., and Shamoon, H. (2003). Hypoglycemia in Diabetes. Diabetes Care *26*, 1902-1912.

D'Souza, A.M., Neumann, U.H., Glavas, M.M., and Kieffer, T.J. (2017). The glucoregulatory actions of leptin. Molecular Metabolism *6*, 1052-1065.

Damoulakis, G., Gambardella, L., Rossman, K.L., Lawson, C.D., Anderson, K.E., Fukui, Y., Welch, H.C., Der, C.J., Stephens, L.R., and Hawkins, P.T. (2014). P-Rex1 directly activates RhoG to regulate GPCR-driven Rac signalling and actin polarity in neutrophils. Journal of Cell Science *127*, 2589-2600.

Das, B., Shu, X., Day, G.-J., Han, J., Krishna, U.M., Falck, J.R., and Broek, D. (2000). Control of Intramolecular Interactions between the Pleckstrin Homology and Dbl Homology Domains of

Vav and Sos1 Regulates Rac Binding. The Journal of Biological Chemistry *275*, 15074-15081.

Dean, E.D., Li, M., Prasad, N., Wisniewski, S.N., Von Deylen, A., Spaeth, J., Maddison, L., Botros, A., Sedgeman, L.R., Bozadjieva, N.*, et al.* (2017). Interrupted Glucagon Signaling Reveals Hepatic α Cell Axis and Role for L-Glutamine in α Cell Proliferation. Cell Metabolism *25*, 1362-1373.e1365.

Dillon, L.M., Bean, J.R., Yang, W., Shee, K., Symonds, L.K., Balko, J.M., McDonald, W.H., Liu, S., Gonzalez-Angulo, A.M., Mills, G.B.*, et al.* (2014). P-REX1 creates a positive feedback loop to activate growth factor receptor, PI3K/AKT and MEK/ERK signaling in breast cancer. Oncogene *34*, 3968.

Donald, S., Hill, K., Lecureuil, C., Barnouin, R., Krugmann, S., John Coadwell, W., Andrews, S.R., Walker, S.A., Hawkins, P.T., Stephens, L.R.*, et al.* (2004). P-Rex2, a new guanine-nucleotide exchange factor for Rac. FEBS letters *572*, 172-176.

Donald, S., Humby, T., Fyfe, I., Segonds-Pichon, A., Walker, S.A., Andrews, S.R., Coadwell, W.J., Emson, P., Wilkinson, L.S., and Welch, H.C. (2008). P-Rex2 regulates Purkinje cell dendrite morphology and motor coordination. Proceedings of the National Academy of Sciences of the United States of America *105*, 4483-4488.

Dridi, S., and Taouis, M. (2009). Adiponectin and energy homeostasis: consensus and controversy. The Journal of Nutritional Biochemistry *20*, 831-839.

Du, K., Herzig, S., Kulkarni, R.N., and Montminy, M. (2003). TRB3: A tribbles Homolog That Inhibits Akt/PKB Activation by Insulin in Liver. Science *300*, 1574-1577.

El Bekay, R., Coín-Aragüez, L., Fernández-García, D., Oliva-Olivera, W., Bernal-López, R., Clemente-Postigo, M., Delgado-Lista, J., Diaz-Ruiz, A., Guzman-Ruiz, R., Vázquez-Martínez, R.*, et al.* (2016). Effects of glucagon-like peptide-1 on the differentiation and metabolism of human adipocytes. British Journal of Pharmacology *173*, 1820-1834.

Escribano, O., Beneit, N., Rubio-Longás, C., López-Pastor, A.R., and Gómez-Hernández, A. (2017). The Role of Insulin Receptor Isoforms in Diabetes and Its Metabolic and Vascular Complications. Journal of Diabetes Research *2017*, 1403206-1403206.

Esser, N., Legrand-Poels, S., Piette, J., Scheen, A.J., and Paquot, N. (2014). Inflammation as a link between obesity, metabolic syndrome and type 2 diabetes. Diabetes Research and Clinical Practice *105*, 141-150.

Esterson, Y.B., Carey, M., Boucai, L., Goyal, A., Raghavan, P., Zhang, K., Mehta, D., Feng, D., Wu, L., Kehlenbrink, S.*, et al.* (2016). Central Regulation of Glucose Production May Be Impaired in Type 2 Diabetes. Diabetes *65*, 2569-2579.

Eva, A., Vecchio, G., Rao, C.D., Tronick, S.R., and Aaronson, S.A. (1988). The predicted DBL oncogene product defines a distinct class of transforming proteins. Proceedings of the National Academy of Sciences of the United States of America *85*, 2061-2065.

Evans, M.L., McCrimmon, R.J., Flanagan, D.E., Keshavarz, T., Fan, X., McNay, E.C., Jacob, R.J., and Sherwin, R.S. (2004). Hypothalamic ATP-sensitive K ⁺ Channels Play a Key Role in Sensing Hypoglycemia and Triggering Counterregulatory Epinephrine and Glucagon Responses. Diabetes *53*, 2542-2551.

Evelyn, C.R., Duan, X., Biesiada, J., Seibel, W.L., Meller, J., and Zheng, Y. (2014). Rational design of small molecule inhibitors targeting the Ras GEF, SOS1. Chemistry & Biology *21*, 1618-1628.

Febbraio, M.A., Hiscock, N., Sacchetti, M., Fischer, C.P., and Pedersen, B.K. (2004). Interleukin-6 Is a Novel Factor Mediating Glucose Homeostasis During Skeletal Muscle Contraction. Diabetes *53*, 1643-1648.

Feher, J. (2017). 2.9 - ATP Production I: Glycolysis. In Quantitative Human Physiology (Second Edition), J. Feher, ed. (Boston: Academic Press), pp. 218-226.

Fejzo, M.S., Godfrey, T., Chen, C., Waldman, F., and Gray, J.W. (1998). Molecular cytogenetic analysis of consistent abnormalities at 8q12-q22 in breast cancer. Genes, Chromosomes & Cancer *22*, 105-113.

Fernández-Medarde, A., and Santos, E. (2011). Ras in cancer and developmental diseases. Genes Cancer *2*, 344-358.

Fiegen, D., Haeusler, L.-C., Blumenstein, L., Herbrand, U., Dvorsky, R., Vetter, I.R., and Ahmadian, M.R. (2004). Alternative Splicing of Rac1 Generates Rac1b, a Self-activating GTPase. The Journal of Biological Chemistry *279*, 4743-4749.

Fine, B., Hodakoski, C., Koujak, S., Su, T., Saal, L.H., Maurer, M., Hopkins, B., Keniry, M., Sulis, M.L., Mense, S.*, et al.* (2009). Activation of the PI3K pathway in cancer through inhibition of PTEN by exchange factor P-REX2a. Science *325*, 1261-1265.

Foukas, L.C., Bilanges, B., Bettedi, L., Pearce, W., Ali, K., Sancho, S., Withers, D.J., and Vanhaesebroeck, B. (2013). Long-term p110α PI3K inactivation exerts a beneficial effect on metabolism. EMBO Molecular Medicine *5*, 563-571.

Foukas, L.C., Claret, M., Pearce, W., Okkenhaug, K., Meek, S., Peskett, E., Sancho, S., Smith, A.J.H., Withers, D.J., and Vanhaesebroeck, B. (2006). Critical role for the p110α phosphoinositide-3-OH kinase in growth and metabolic regulation. Nature *441*, 366-370.

Fox, C.S., Massaro, J.M., Hoffmann, U., Pou, K.M., Maurovich-Horvat, P., Liu, C.Y., Vasan, R.S., Murabito, J.M., Meigs, J.B., Cupples, L.A.*, et al.* (2007). Abdominal visceral and subcutaneous adipose tissue compartments: association with metabolic risk factors in the Framingham Heart Study. Circulation *116*, 39-48.

Friedman, J.M., and Halaas, J.L. (1998). Leptin and the regulation of body weight in mammals. Nature *395*, 763-770.

Friesen, M., Hudak, C.S., Warren, C.R., Xia, F., and Cowan, C.A. (2016). Adipocyte insulin receptor activity maintains adipose tissue mass and lifespan. Biochemical and Biophysical Research Communications *476*, 487-492.

Fruman, D.A., Mauvais-Jarvis, F., Pollard, D.A., Yballe, C.M., Brazil, D., Bronson, R.T., Kahn, C.R., and Cantley, L.C. (2000). Hypoglycaemia, liver necrosis and perinatal death in mice lacking all isoforms of phosphoinositide 3-kinase p85α. Nature Genetics *26*, 379-382.

Fujikawa, T., Berglund, Eric D., Patel, Vishal R., Ramadori, G., Vianna, Claudia R., Vong, L., Thorel, F., Chera, S., Herrera, Pedro L., Lowell, Bradford B.*, et al.* (2013). Leptin Engages a Hypothalamic Neurocircuitry to Permit Survival in the Absence of Insulin. Cell Metabolism *18*, 431-444.

Fukui, K., Wada, T., Kagawa, S., Nagira, K., Ikubo, M., Ishihara, H., Kobayashi, M., and Sasaoka, T. (2005). Impact of the liver-specific expression of SHIP2 (SH2-containing inositol 5'-phosphatase 2) on insulin signaling and glucose metabolism in mice. Diabetes *54*, 1958-1967.

Gadea, G., and Blangy, A. (2014). Dock-family exchange factors in cell migration and disease. European Journal of Cell Biology *93*, 466-477.

Gerst, F., Wagner, R., Oquendo, M.B., Siegel-Axel, D., Fritsche, A., Heni, M., Staiger, H., Häring, H.-U., and Ullrich, S. (2019). What role do fat cells play in pancreatic tissue? Molecular Metabolism 25, 1-10.

Ghalali, A., Wiklund, F., Zheng, H., Stenius, U., and Hogberg, J. (2014). Atorvastatin prevents ATP-driven invasiveness via P2X7 and EHBP1 signaling in PTEN-expressing prostate cancer cells. Carcinogenesis *35*, 1547-1555.

Girard, J. (2017). Glucagon, a key factor in the pathophysiology of type 2 diabetes. Biochimie *143*, 33-36.

Goel, H.L., Pursell, B., Shultz, L.D., Greiner, D.L., Brekken, R.A., Vander Kooi, C.W., and Mercurio, A.M. (2016). P-Rex1 Promotes Resistance to VEGF/VEGFR-Targeted Therapy in Prostate Cancer. Cell Reports *14*, 2193-2208.

Guo, B., Liu, L., Yao, J., Ma, R., Chang, D., Li, Z., Song, T., and Huang, C. (2014). miR-338-3p suppresses gastric cancer progression through a PTEN-AKT axis by targeting P-REX2a. Molecular Cancer Research *12*, 313-321.

Guo, X., Li, H., Xu, H., Woo, S., Dong, H., Lu, F., Lange, A.J., and Wu, C. (2012). Glycolysis in the control of blood glucose homeostasis. Acta Pharmaceutica Sinica B *2*, 358-367.

Haataja, L., Groffen, J., and Heisterkamp, N. (1997). Characterization of RAC3, a novel member of the Rho family. Journal of Biological Chemistry *272*, 20384-20388.

Haider, D.G., Schaller, G., Kapiotis, S., Maier, C., Luger, A., and Wolzt, M. (2006). The release of the adipocytokine visfatin is regulated by glucose and insulin. Diabetologia *49*, 1909-1914.

Hamburg, N.M., McMackin, C.J., Huang, A.L., Shenouda, S.M., Widlansky, M.E., Schulz, E., Gokce, N., Ruderman, N.B., Keaney, J.F., and Vita, J.A. (2007). Physical Inactivity Rapidly Induces Insulin Resistance and Microvascular Dysfunction in Healthy Volunteers. Arteriosclerosis, Thrombosis, and Vascular Biology *27*, 2650-2656.

Han, H.-S., Kang, G., Kim, J.S., Choi, B.H., and Koo, S.-H. (2016). Regulation of glucose metabolism from a liver-centric perspective. Experimental & Molecular Medicine *48*, e218.

Han, J., Wang, B., Xiao, Z., Gao, Y., Zhao, Y., Zhang, J., Chen, B., Wang, X., and Dai, J. (2008). Mammalian target of rapamycin (mTOR) is involved in the neuronal differentiation of neural progenitors induced by insulin. Molecular and Cellular Neuroscience *39*, 118-124.

Hanawa-Suetsugu, K., Kukimoto-Niino, M., Mishima-Tsumagari, C., Akasaka, R., Ohsawa, N., Sekine, S.-i., Ito, T., Tochio, N., Koshiba, S., Kigawa, T.*, et al.* (2012). Structural basis for mutual relief of the Rac guanine nucleotide exchange factor DOCK2 and its partner ELMO1 from their autoinhibited forms. Proceedings of the National Academy of Sciences *109*, 3305-3310.

Harada, Y., Tanaka, Y., Terasawa, M., Pieczyk, M., Habiro, K., Katakai, T., Hanawa-Suetsugu, K., Kukimoto-Niino, M., Nishizaki, T., Shirouzu, M.*, et al.* (2012). DOCK8 is a Cdc42 activator critical for interstitial dendritic cell migration during immune responses. Blood *119*, 4451-4461.

Hart, M.J., Eva, A., Evans, T., Aaronson, S.A., and Cerione, R.A. (1991). Catalysis of guanine nucleotide exchange on the CDC42Hs protein by the dbl oncogene product. Nature *354*, 311-314.

Heasman, S.J., and Ridley, A.J. (2008). Mammalian Rho GTPases: new insights into their functions from in vivo studies. Nature Reviews Molecular Cell Biology *9*, 690.

Heijboer, A.C., Donga, E., Voshol, P.J., Dang, Z.C., Havekes, L.M., Romijn, J.A., and Corssmit, E.P. (2005). Sixteen hours of fasting differentially affects hepatic and muscle insulin sensitivity in mice. Journal of Lipid Research *46*, 582-588.

Hernandez-Negrete, I., Carretero-Ortega, J., Rosenfeldt, H., Hernandez-Garcia, R., Calderon-Salinas, J.V., Reyes-Cruz, G., Gutkind, J.S., and Vazquez-Prado, J. (2007). P-Rex1 links mammalian target of rapamycin signaling to Rac activation and cell migration. The Journal of Biological Chemistry *282*, 23708-23715.

Herter, J.M., Rossaint, J., Block, H., Welch, H., and Zarbock, A. (2013). Integrin activation by P-Rex1 is required for selectin-mediated slow leukocyte rolling and intravascular crawling. Blood *121*, 2301-2310.

Herzig, S., Long, F., Jhala, U.S., Hedrick, S., Quinn, R., Bauer, A., Rudolph, D., Schutz, G., Yoon, C., Puigserver, P.*, et al.* (2001). CREB regulates hepatic gluconeogenesis through the coactivator PGC-1. Nature *413*, 179-183.

Hill, K., Krugmann, S., Andrews, S.R., Coadwell, W.J., Finan, P., Welch, H.C., Hawkins, P.T., and Stephens, L.R. (2005). Regulation of P-Rex1 by phosphatidylinositol (3,4,5)-trisphosphate and Gbetagamma subunits. The Journal of Biological Chemistry *280*, 4166-4173.

Hill, K., and Welch, H.C.E. (2006). Purification of P-Rex1 from Neutrophils and Nucleotide Exchange Assay. Methods in Enzymology *406*, 26-41.

Hodakoski, C., Hopkins, B.D., Barrows, D., Mense, S.M., Keniry, M., Anderson, K.E., Kern, P.A., Hawkins, P.T., Stephens, L.R., and Parsons, R. (2014). Regulation of PTEN inhibition by the pleckstrin homology domain of P-REX2 during insulin signaling and glucose homeostasis. Proceedings of the National Academy of Sciences of the United States of America *111*, 155-160.

Holland, W.L., Miller, R.A., Wang, Z.V., Sun, K., Barth, B.M., Bui, H.H., Davis, K.E., Bikman, B.T., Halberg, N., Rutkowski, J.M.*, et al.* (2011). Receptor-mediated activation of ceramidase activity initiates the pleiotropic actions of adiponectin. Nature Medicine *17*, 55-63.

Holst, J.J., Gribble, F., Horowitz, M., and Rayner, C.K. (2016). Roles of the Gut in Glucose Homeostasis. Diabetes Care *39*, 884-892.

Hornigold, K., Tsonou, E., Pantarelli, C., and Welch, H.C.E. (2018). P-Rex1. In Encyclopedia of Signaling Molecules, S. Choi, ed. (Cham: Springer International Publishing), pp. 4142-4154.

Horrigan, S.K., Courville, P., Sampey, D., Zhou, F., Cai, S., and Reproducibility Project: Cancer, B. (2017). Replication Study: Melanoma genome sequencing reveals frequent PREX2 mutations. Elife *6*, e21634.

Hotamisligil, G.S., and Erbay, E. (2008). Nutrient sensing and inflammation in metabolic diseases. Nature Reviews Immunology *8*, 923.

Huang-Doran, I., Tomlinson, P., Payne, F., Gast, A., Sleigh, A., Bottomley, W., Harris, J., Daly, A., Rocha, N., Rudge, S.*, et al.* (2016). Insulin resistance uncoupled from dyslipidemia due to C-terminal PIK3R1 mutations. JCI insight *1*, e88766-e88766.

Hughey, C.C., Wasserman, D.H., Lee-Young, R.S., and Lantier, L. (2014). Approach to assessing determinants of glucose homeostasis in the conscious mouse. Mammalian Genome *25*, 522-

538.

Innocenti, M., Tenca, P., Frittoli, E., Faretta, M., Tocchetti, A., Di Fiore, P.P., and Scita, G. (2002). Mechanisms through which Sos-1 coordinates the activation of Ras and Rac. Journal of Cell Biology *156*, 125-136.

Jackson, C., Welch, H.C., and Bellamy, T.C. (2010). Control of cerebellar long-term potentiation by P-Rex-family guanine-nucleotide exchange factors and phosphoinositide 3-kinase. PLOS One *5*, e11962-e11962.

Jackson, C.L., and Bouvet, S. (2014). Arfs at a Glance. Journal of cell science *127*, 4103-4109.

JeBailey, L., Rudich, A., Huang, X., Ciano-Oliveira, C.D., Kapus, A.s., and Klip, A. (2004). Skeletal Muscle Cells and Adipocytes Differ in Their Reliance on TC10 and Rac for Insulin-Induced Actin Remodeling. Molecular Endocrinology *18*, 359-372.

Jordan, P., Brazao, R., Boavida, M.G., Gespach, C., and Chastre, E. (1999). Cloning of a novel human Rac1b splice variant with increased expression in colorectal tumors. Oncogene *18*, 6835-6839.

Joshi, R.L., Lamothe, B., Cordonnier, N., Mesbah, K., Monthioux, E., Jami, J., and Bucchini, D. (1996). Targeted disruption of the insulin receptor gene in the mouse results in neonatal lethality. EMBO Journal *15*, 1542-1547.

Jungmichel, S., Sylvestersen, Kathrine B., Choudhary, C., Nguyen, S., Mann, M., and Nielsen, Michael L. (2014). Specificity and Commonality of the Phosphoinositide-Binding Proteome Analyzed by Quantitative Mass Spectrometry. Cell Reports *6*, 578-591.

Kadowaki, T., and Yamauchi, T. (2005). Adiponectin and Adiponectin Receptors. Endocrine Reviews *26*, 439-451.

Kamp, M.E., Liu, Y., and Kortholt, A. (2016). Function and Regulation of Heterotrimeric G Proteins during Chemotaxis. International Journal of Molecular Sciences *17*, 90.

Kanno, T., and Saito, A. (1976). The potentiating influences of insulin on pancreozymin-induced hyperpolarization and amylase release in the pancreatic acinar cell. The Journal of Physiology *261*, 505-521.

Kasper, B., Tidow, N., Grothues, D., and Welte, K. (2000). Differential expression and regulation of GTPases (RhoA and Rac2) and GDIs (LyGDI and RhoGDI) in neutrophils from patients with severe congenital neutropenia. Blood *95*, 2947-2953.

Kawamori, D., Kurpad, A.J., Hu, J., Liew, C.W., Shih, J.L., Ford, E.L., Herrera, P.L., Polonsky, K.S., McGuinness, O.P., and Kulkarni, R.N. (2009). Insulin signaling in alpha cells modulates glucagon secretion in vivo. Cell Metabolism *9*, 350-361.

Kazanietz, M.G., Barrio-Real, L., Casado-Medrano, V., Baker, M.J., and Lopez-Haber, C. (2018). The P-Rex1/Rac signaling pathway as a point of convergence for HER/ErbB receptor and GPCR responses. Small GTPases *9*, 297-303.

Keane, K.N., Calton, E.K., Carlessi, R., Hart, P.H., and Newsholme, P. (2017). The bioenergetics of inflammation: insights into obesity and type 2 diabetes. European Journal Of Clinical Nutrition *71*, 904.

Keane, K.N., Cruzat, V.F., Carlessi, R., de Bittencourt, P.I.H., and Newsholme, P. (2015). Molecular Events Linking Oxidative Stress and Inflammation to Insulin Resistance and β-Cell

Dysfunction. Oxidative Medicine and Cellular Longevity *2015*, 15.

Kelly, M., Keller, C., Avilucea, P.R., Keller, P., Luo, Z., Xiang, X., Giralt, M., Hidalgo, J., Saha, A.K., Pedersen, B.K.*, et al.* (2004). AMPK activity is diminished in tissues of IL-6 knockout mice: the effect of exercise. Biochemical and Biophysical Research Communications *320*, 449-454.

Kern, L., Mittenbühler, M.J., Vesting, A.J., Ostermann, A.L., Wunderlich, C.M., and Wunderlich, F.T. (2018). Obesity-Induced TNFα and IL-6 Signaling: The Missing Link between Obesity and Inflammation-Driven Liver and Colorectal Cancers. Cancers (Basel) *11*, 24.

Khayat, Z.A., Tong, P., Yaworsky, K., Bloch, R.J., and Klip, A. (2000). Insulin-induced actin filament remodeling colocalizes actin with phosphatidylinositol 3-kinase and GLUT4 in L6 myotubes. Journal of Cell Science *113*, 279-290.

Kieffer, T.J., and Habener, J.F. (2000). The adipoinsular axis: effects of leptin on pancreatic β-cells. American Journal of Physiology-Endocrinology and Metabolism *278*, E1-E14.

Kim, E.K., Yun, S.J., Ha, J.M., Kim, Y.W., Jin, I.H., Woo, D.H., Lee, H.S., Ha, H.K., and Bae, S.S. (2012). Synergistic induction of cancer cell migration regulated by Gbetagamma and phosphatidylinositol 3-kinase. Experimental & Molecular Medicine *44*, 483-491.

Kim, E.K., Yun, S.J., Ha, J.M., Kim, Y.W., Jin, I.H., Yun, J., Shin, H.K., Song, S.H., Kim, J.H., Lee, J.S.*, et al.* (2011a). Selective activation of Akt1 by mammalian target of rapamycin complex 2 regulates cancer cell migration, invasion, and metastasis. Oncogene *30*, 2954.

Kim, M.-S., Pak, Y.K., Jang, P.-G., Namkoong, C., Choi, Y.-S., Won, J.-C., Kim, K.-S., Kim, S.-W., Kim, H.-S., Park, J.-Y.*, et al.* (2006). Role of hypothalamic Foxo1 in the regulation of food intake and energy homeostasis. Nature Neuroscience *9*, 901-906.

Kim, S., Cho, B., Lee, H., Choi, K., Hwang, S.S., Kim, D., Kim, K., and Kwon, H. (2011b). Distribution of abdominal visceral and subcutaneous adipose tissue and metabolic syndrome in a Korean population. Diabetes Care *34*, 504-506.

Kiriyama, Y., and Nochi, H. (2018). Role and Cytotoxicity of Amylin and Protection of Pancreatic Islet β-Cells from Amylin Cytotoxicity. Cells *7*, 95.

Kjøbsted, R., Munk-Hansen, N., Birk, J.B., Foretz, M., Viollet, B., Björnholm, M., Zierath, J.R., Treebak, J.T., and Wojtaszewski, J.F.P. (2017). Enhanced Muscle Insulin Sensitivity After Contraction/Exercise Is Mediated by AMPK. Diabetes *66*, 598-612.

Koch, L., Wunderlich, F.T., Seibler, J., Könner, A.C., Hampel, B., Irlenbusch, S., Brabant, G., Kahn, C.R., Schwenk, F., and Brüning, J.C. (2008). Central insulin action regulates peripheral glucose and fat metabolism in mice. The Journal of Clinical Investigation *118*, 2132-2147.

Koren, D., and Palladino, A. (2016). Chapter 3 - Hypoglycemia. In Genetic Diagnosis of Endocrine Disorders (Second Edition), R.E. Weiss, and S. Refetoff, eds. (San Diego: Academic Press), pp. 31-75.

Kristelly, R., Earnest, B.T., Krishnamoorthy, L., and Tesmer, J.J. (2003). Preliminary structure analysis of the DH/PH domains of leukemia-associated RhoGEF. Acta Crystallographica Section D Biological Crystallography *59*, 1859-1862.

Krogh-Madsen, R., Thyfault, J.P., Broholm, C., Mortensen, O.H., Olsen, R.H., Mounier, R., Plomgaard, P., Hall, G.v., Booth, F.W., and Pedersen, B.K. (2010). A 2-wk reduction of ambulatory activity attenuates peripheral insulin sensitivity. Journal of Applied Physiology *108*, 1034-1040.

Kubota, N., Tobe, K., Terauchi, Y., Eto, K., Yamauchi, T., Suzuki, R., Tsubamoto, Y., Komeda, K., Nakano, R., Miki, H., *et al.* (2000). Disruption of insulin receptor substrate 2 causes type 2 diabetes because of liver insulin resistance and lack of compensatory beta-cell hyperplasia. Diabetes *49*, 1880-1889.

Kukimoto-Niino, M., Tsuda, K., Ihara, K., Mishima-Tsumagari, C., Honda, K., Ohsawa, N., and Shirouzu, M. (2019). Structural Basis for the Dual Substrate Specificity of DOCK7 Guanine Nucleotide Exchange Factor. Structure *27*, 741-748.e743.

Kulkarni, K., Yang, J., Zhang, Z., and Barford, D. (2011). Multiple Factors Confer Specific Cdc42 and Rac Protein Activation by Dedicator of Cytokinesis (DOCK) Nucleotide Exchange Factors. Journal of Biological Chemistry *286*, 25341-25351.

Kwon, H., Kim, D., and Kim, J.S. (2017). Body Fat Distribution and the Risk of Incident Metabolic Syndrome: A Longitudinal Cohort Study. Scientific Reports *7*, 10955.

Laurin, M., and Côté, J.-F. (2014). Insights into the biological functions of Dock family guanine nucleotide exchange factors. Genes & Development *28*, 533-547.

Lawson, C.D., Donald, S., Anderson, K.E., Patton, D.T., and Welch, H.C. (2011). P-Rex1 and Vav1 cooperate in the regulation of formyl-methionyl-leucyl-phenylalanine-dependent neutrophil responses. Journal of Immunology *186*, 1467-1476.

Lee, S.D., and Tontonoz, P. (2014). Eosinophils in fat: pink is the new brown. Cell *157*, 1249-1250.

Lemmon, M.A., Ferguson, K.M., O'Brien, R., Sigler, P.B., and Schlessinger, J. (1995). Specific and high-affinity binding of inositol phosphates to an isolated pleckstrin homology domain. Proceedings of the National Academy of Sciences *92*, 10472-10476.

Leto, D., and Saltiel, A.R. (2012). Regulation of glucose transport by insulin: traffic control of GLUT4. Nature Reviews Molecular Cell Biology *13*, 383.

Lewis, J.P., Palmer, N.D., Ellington, J.B., Divers, J., Ng, M.C., Lu, L., Langefeld, C.D., Freedman, B.I., and Bowden, D.W. (2010). Analysis of candidate genes on chromosome 20q12-13.1 reveals evidence for BMI mediated association of PREX1 with type 2 diabetes in European Americans. Genomics *96*, 211-219.

Li, B., Yu, H., Zheng, W., Voll, R., Na, S., Roberts, A.W., Williams, D.A., Davis, R.J., Ghosh, S., and Flavell, R.A. (2000). Role of the guanosine triphosphatase Rac2 in T helper 1 cell differentiation. Science *288*, 2219-2222.

Li, G., and Marlin, M.C. (2015). Rab family of GTPases. Methods in Molecular Biology *1298*, 1-15.

Li, J., Chai, A., Wang, L., Ma, Y., Wu, Z., Yu, H., Mei, L., Lu, L., Zhang, C., Yue, W., *et al.* (2015). Synaptic P-Rex1 signaling regulates hippocampal long-term depression and autism-like social behavior. Proceedings of the National Academy of Sciences *112*, E6964-E6972.

Li, Z., Paik, J.-H., Wang, Z., Hla, T., and Wu, D. (2005). Role of guanine nucleotide exchange factor P-Rex-2b in sphingosine 1-phosphate-induced Rac1 activation and cell migration in endothelial cells. Prostaglandins & Other Lipid Mediators *76*, 95-104.

Liang, Q., Cheng, N., Zhang, G., Liang, Y., Qian, F., Wu, D., and Ye, R.D. (2016). Identification of P-Rex1 as an anti-inflammatory and anti-fibrogenic target for pulmonary fibrosis. Scientific Reports *6*, 25785-25785.

Lim, G.E., Xu, M., Sun, J., Jin, T., and Brubaker, P.L. (2009). The Rho Guanosine 5′-Triphosphatase, Cell Division Cycle 42, Is Required for Insulin-Induced Actin Remodeling and Glucagon-Like Peptide-1 Secretion in the Intestinal Endocrine L Cell. Endocrinology *150*, 5249-5261.

Lin, E., Kuo, P.-H., Liu, Y.-L., Yu, Y.W.Y., Yang, A.C., and Tsai, S.-J. (2018). A Deep Learning Approach for Predicting Antidepressant Response in Major Depression Using Clinical and Genetic Biomarkers. Front Psychiatry *9*, 290-290.

Lindsay, C.R., Lawn, S., Campbell, A.D., Faller, W.J., Rambow, F., Mort, R.L., Timpson, P., Li, A., Cammareri, P., Ridgway, R.A.*, et al.* (2011). P-Rex1 is required for efficient melanoblast migration and melanoma metastasis. Nature Communications *2*, 555.

Lindsay, C.R., Li, A., Faller, W., Ozanne, B., Welch, H., Machesky, L.M., and Sansom, O.J. (2015). A Rac1-independent role for P-Rex1 in melanoblasts. Journal of Investigative Dermatology *135*, 314-318.

Lissanu Deribe, Y., Shi, Y., Rai, K., Nezi, L., Amin, S.B., Wu, C.-C., Akdemir, K.C., Mahdavi, M., Peng, Q., Chang, Q.E.*, et al.* (2016). Truncating PREX2 mutations activate its GEF activity and alter gene expression regulation in NRAS-mutant melanoma. Proceedings of the National Academy of Sciences *113*, E1296-E1305.

Liu, G.-M., and Zhang, Y.-M. (2018). Targeting FBPase is an emerging novel approach for cancer therapy. Cancer Cell International *18*, 36.

Liu, H.-J., Ooms, L.M., Srijakotre, N., Man, J., Vieusseux, J., Waters, J.E., Feng, Y., Bailey, C.G., Rasko, J.E.J., Price, J.T.*, et al.* (2016). PtdIns(3,4,5)P3-dependent Rac Exchanger 1 (PREX1) Rac-Guanine Nucleotide Exchange Factor (GEF) Activity Promotes Breast Cancer Cell Proliferation and Tumor Growth via Activation of Extracellular Signal-regulated Kinase 1/2 (ERK1/2) Signaling. The Journal of Biological Chemistry *291*, 17258-17270.

Liu, X., Rossmeisl, M., McClaine, J., Riachi, M., Harper, M.-E., and Kozak, L.P. (2003). Paradoxical resistance to diet-induced obesity in UCP1-deficient mice. Journal of Clinical Investigation *111*, 399-407.

Liu, X., Wang, H., Eberstadt, M., Schnuchel, A., Olejniczak, E.T., Meadows, R.P., Schkeryantz, J.M., Janowick, D.A., Harlan, J.E., Harris, E.A.*, et al.* (1998). NMR structure and mutagenesis of the N-terminal Dbl homology domain of the nucleotide exchange factor Trio. Cell *95*, 269-277.

Loh, K., Zhang, L., Brandon, A., Wang, Q., Begg, D., Qi, Y., Fu, M., Kulkarni, R., Teo, J., Baldock, P.*, et al.* (2017). Insulin controls food intake and energy balance via NPY neurons. Molecular Metabolism *6*, 574-584.

Lopez-Haber, C., Barrio-Real, L., Casado-Medrano, V., and Kazanietz, M.G. (2016). Heregulin/ErbB3 Signaling Enhances CXCR4-Driven Rac1 Activation and Breast Cancer Cell Motility via Hypoxia-Inducible Factor 1α. Molecular and Cellular Biology *36*, 2011-2026.

Lucato, C.M., Halls, M.L., Ooms, L.M., Liu, H.J., Mitchell, C.A., Whisstock, J.C., and Ellisdon, A.M. (2015). The Phosphatidylinositol (3,4,5)-Trisphosphate-dependent Rac Exchanger 1.Ras-related C3 Botulinum Toxin Substrate 1 (P-Rex1.Rac1) Complex Reveals the Basis of Rac1 Activation in Breast Cancer Cells. Journal of Biological Chemistry *290*, 20827-20840.

Mack, N.A., Whalley, H.J., Castillo-Lluva, S., and Malliri, A. (2011). The diverse roles of Rac signaling in tumorigenesis. Cell Cycle *10*, 1571-1581.

Marei, H., Carpy, A., Macek, B., and Malliri, A. (2016a). Proteomic analysis of Rac1 signaling regulation by guanine nucleotide exchange factors. Cell Cycle *15*, 1961-1974.

Marei, H., Carpy, A., Woroniuk, A., Vennin, C., White, G., Timpson, P., Macek, B., and Malliri, A. (2016b). Differential Rac1 signalling by guanine nucleotide exchange factors implicates FLII in regulating Rac1-driven cell migration. Nature Communications *7*, 10664.

Matos, P., Collard, J.G., and Jordan, P. (2003). Tumor-related Alternatively Spliced Rac1b Is Not Regulated by Rho-GDP Dissociation Inhibitors and Exhibits Selective Downstream Signaling. Journal of Biological Chemistry *278*, 50442-50448.

Mauvais-Jarvis, F., Clegg, D.J., and Hevener, A.L. (2013). The role of estrogens in control of energy balance and glucose homeostasis. Endocrine Reviews *34*, 309-338.

Mavrakis, K.J., McKinlay, K.J., Jones, P., and Sablitzky, F. (2004). DEF6, a novel PH-DH-like domain protein, is an upstream activator of the Rho GTPases Rac1, Cdc42, and RhoA. Experimental Cell Research *294*, 335-344.

Mayeenuddin, L.H., and Garrison, J.C. (2006). Phosphorylation of P-Rex1 by the cyclic AMP-dependent protein kinase inhibits the phosphatidylinositiol (3,4,5)-trisphosphate and Gbetagamma-mediated regulation of its activity. Journal of Biological Chemistry *281*, 1921-1928.

McGuinness, O.P., Ayala, J.E., Laughlin, M.R., and Wasserman, D.H. (2009). NIH experiment in centralized mouse phenotyping: the Vanderbilt experience and recommendations for evaluating glucose homeostasis in the mouse. American Journal of Physiology-Endocrinology and Metabolism *297*, E849-E855.

Meier, J.J., Gallwitz, B., Siepmann, N., Holst, J.J., Deacon, C.F., Schmidt, W.E., and Nauck, M.A. (2003). Gastric inhibitory polypeptide (GIP) dose-dependently stimulates glucagon secretion in healthy human subjects at euglycaemia. Diabetologia *46*, 798-801.

Menacho-Márquez, M., Nogueiras, R., Fabbiano, S., Sauzeau, V., Al-Massadi, O., Diéguez, C., and Bustelo, Xosé R. (2013). Chronic Sympathoexcitation through Loss of Vav3, a Rac1 Activator, Results in Divergent Effects on Metabolic Syndrome and Obesity Depending on Diet. Cell Metabolism *18*, 199-211.

Mense, S.M., Barrows, D., Hodakoski, C., Steinbach, N., Schoenfeld, D., Su, W., Hopkins, B.D., Su, T., Fine, B., Hibshoosh, H.*, et al.* (2015). PTEN inhibits PREX2-catalyzed activation of RAC1 to restrain tumor cell invasion. Science Signaling *8*, ra32.

Meyer, C., Dostou, J., Nadkarni, V., and Gerich, J. (1998). Effects of physiological hyperinsulinemia on systemic, renal, and hepatic substrate metabolism. American Journal of Physiology-Renal Physiology *275*, F915-F921.

Mighiu, P.I., Yue, J.T.Y., Filippi, B.M., Abraham, M.A., Chari, M., Lam, C.K.L., Yang, C.S., Christian, N.R., Charron, M.J., and Lam, T.K.T. (2013). Hypothalamic glucagon signaling inhibits hepatic glucose production. Nature Medicine *19*, 766.

Miller, T.B., Jr., and Larner, J. (1973). Mechanism of control of hepatic glycogenesis by insulin. Journal of Biological Chemistry *248*, 3483-3488.

Mitchell, J.S., Li, N., Weinhold, N., Försti, A., Ali, M., van Duin, M., Thorleifsson, G., Johnson, D.C., Chen, B., Halvarsson, B.-M.*, et al.* (2016). Genome-wide association study identifies multiple susceptibility loci for multiple myeloma. Nature Communications *7*, 12050-12050.

Montero, J.C., Seoane, S., García-Alonso, S., and Pandiella, A. (2016). Multisite phosphorylation of P-Rex1 by protein kinase C. Oncotarget *7*, 77937-77949.

Montero, J.C., Seoane, S., Ocaña, A., and Pandiella, A. (2010). P-Rex1 participates in Neuregulin-ErbB signal transduction and its expression correlates with patient outcome in breast cancer. Oncogene *30*, 1059.

Montero, J.C., Seoane, S., and Pandiella, A. (2013). Phosphorylation of P-Rex1 at serine 1169 participates in IGF-1R signaling in breast cancer cells. Cellular Signalling *25*, 2281-2289.

Moriya, H. (2015). Quantitative nature of overexpression experiments. Molecular Biology of the Cell *26*, 3932-3939.

Muoio, D.M., and Newgard, C.B. (2008). Mechanisms of disease:Molecular and metabolic mechanisms of insulin resistance and beta-cell failure in type 2 diabetes. Nature Reviews Molecular Cell Biology *9*, 193-205.

Murayama, K., Shirouzu, M., Kawasaki, Y., Kato-Murayama, M., Hanawa-Suetsugu, K., Sakamoto, A., Katsura, Y., Suenaga, A., Toyama, M., Terada, T.*, et al.* (2007). Crystal structure of the rac activator, Asef, reveals its autoinhibitory mechanism. Journal of Biological Chemistry *282*, 4238-4242.

Naikawadi Ram, P., Cheng, N., Vogel Stephen, M., Qian, F., Wu, D., Malik Asrar, B., and Ye Richard, D. (2012). A Critical Role for Phosphatidylinositol (3,4,5)-Trisphosphate–Dependent Rac Exchanger 1 in Endothelial Junction Disruption and Vascular Hyperpermeability. Circulation Research *111*, 1517-1527.

Nauck, M.A., Heimesaat, M.M., Behle, K., Holst, J.J., Nauck, M.S., Ritzel, R., Hüfner, M., and Schmiegel, W.H. (2002). Effects of Glucagon-Like Peptide 1 on Counterregulatory Hormone Responses, Cognitive Functions, and Insulin Secretion during Hyperinsulinemic, Stepped Hypoglycemic Clamp Experiments in Healthy Volunteers. The Journal of Clinical Endocrinology & Metabolism *87*, 1239-1246.

Nauck, M.A., Heimesaat, M.M., Orskov, C., Holst, J.J., Ebert, R., and Creutzfeldt, W. (1993). Preserved incretin activity of glucagon-like peptide 1 [7-36 amide] but not of synthetic human gastric inhibitory polypeptide in patients with type-2 diabetes mellitus. The Journal of Clinical Investigation *91*, 301-307.

Nauck, M.A., and Meier, J.J. (2018). Incretin hormones: Their role in health and disease. Diabetes, Obesity and Metabolism *20*, 5-21.

Neeland, I.J., Ayers, C.R., Rohatgi, A.K., Turer, A.T., Berry, J.D., Das, S.R., Vega, G.L., Khera, A., McGuire, D.K., Grundy, S.M.*, et al.* (2013). Associations of visceral and abdominal subcutaneous adipose tissue with markers of cardiac and metabolic risk in obese adults. Obesity (Silver Spring, Md) *21*, E439-447.

Newsholme, E.A., and Stanley, J.C. (1987). Substrate cycles: their role in control of metabolism with specific references to the liver. Diabetes/metabolism Research and Reviews *3*, 295-305.

Nizar, J.M., Shepard, B.D., Vo, V.T., and Bhalla, V. (2018). Renal tubule insulin receptor modestly promotes elevated blood pressure and markedly stimulates glucose reabsorption. JCI insight *3*.

Ogg, S., and Ruvkun, G. (1998). The C. elegans PTEN homolog, DAF-18, acts in the insulin receptor-like metabolic signaling pathway. Molecular Cell *2*, 887-893.

Oh, K.-J., Han, H.-S., Kim, M.-J., and Koo, S.-H. (2013). CREB and FoxO1: two transcription factors for the regulation of hepatic gluconeogenesis. BMB Rep *46*, 567-574.

Oldham, W.M., and Hamm, H.E. (2008). Heterotrimeric G protein activation by G-protein-coupled receptors. Nature Reviews Molecular Cell Biology *9*, 60.

Ortega-Molina, A., Efeyan, A., Lopez-Guadamillas, E., Muñoz-Martin, M., Gómez-López, G., Cañamero, M., Mulero, F., Pastor, J., Martinez, S., Romanos, E.*, et al.* (2012). Pten Positively Regulates Brown Adipose Function, Energy Expenditure, and Longevity. Cell Metabolism *15*, 382-394.

Pan, D., Amison, R.T., Riffo-Vasquez, Y., Spina, D., Cleary, S.J., Wakelam, M.J., Page, C.P., Pitchford, S.C., and Welch, H.C.E. (2015). P-Rex and Vav Rac-GEFs in platelets control leukocyte recruitment to sites of inflammation. Blood *125*, 1146-1158.

Pan, D., Barber, M.A., Hornigold, K., Baker, M.J., Toth, J.M., Oxley, D., and Welch, H.C.E. (2016). Norbin Stimulates the Catalytic Activity and Plasma Membrane Localization of the Guanine-Nucleotide Exchange Factor P-Rex1. The Journal of Biological Chemistry *291*, 6359-6375.

Pandiella, A., and Montero, J.C. (2013). Molecular pathways: P-Rex in cancer. Clinical Cancer Research *19*, 4564-4569.

Pantarelli, C., and Welch, H.C.E. (2018). Rac-GTPases and Rac-GEFs in neutrophil adhesion, migration and recruitment. Eur J Clin Invest *48 Suppl 2*, e12939.

Paranjape, S.A., Chan, O., Zhu, W., Horblitt, A.M., McNay, E.C., Cresswell, J.A., Bogan, J.S., McCrimmon, R.J., and Sherwin, R.S. (2010). Influence of insulin in the ventromedial hypothalamus on pancreatic glucagon secretion in vivo. Diabetes *59*, 1521-1527.

Parker, H.E., Reimann, F., and Gribble, F.M. (2010). Molecular mechanisms underlying nutrient-stimulated incretin secretion. Expert Reviews in Molecular Medicine *12*, e1.

Pennucci, R., Talpo, F., Astro, V., Montinaro, V., Morè, L., Cursi, M., Castoldi, V., Chiaretti, S., Bianchi, V., Marenna, S.*, et al.* (2016). Loss of Either Rac1 or Rac3 GTPase Differentially Affects the Behavior of Mutant Mice and the Development of Functional GABAergic Networks. Cerebral Cortex *26*, 873-890.

Perrin, C., Knauf, C., and Burcelin, R.m. (2004). Intracerebroventricular Infusion of Glucose, Insulin, and the Adenosine Monophosphate-Activated Kinase Activator, 5-Aminoimidazole-4-Carboxamide-1-β-d-Ribofuranoside, Controls Muscle Glycogen Synthesis. Endocrinology *145*, 4025-4033.

Petersen, M.C., and Shulman, G.I. (2018). Mechanisms of Insulin Action and Insulin Resistance. Physiological Reviews *98*, 2133-2223.

Pi-Sunyer, X. (2009). The medical risks of obesity. Postgrad Med *121*, 21-33.

Pierzynowska, K.G., Lozinska, L., Woliński, J., and Pierzynowski, S. (2018). The inverse relationship between blood amylase and insulin levels in pigs during development, bariatric surgery, and intravenous infusion of amylase. PLOS One *13*, e0198672.

Pierzynowski, S.G., Gregory, P.C., Filip, R., Woliński, J., and Pierzynowska, K.G. (2018). Glucose homeostasis dependency on acini–islet–acinar (AIA) axis communication: a new possible pathophysiological hypothesis regarding diabetes mellitus. Nutrition & Diabetes *8*, 55.

Pilkis, S.J., El-Maghrabi, M.R., McGrane, M., Pilkis, J., and Claus, T.H. (1982). Regulation by glucagon of hepatic pyruvate kinase, 6-phosphofructo 1-kinase, and fructose-1,6-bisphosphatase. Federation Proceedings *41*, 2623-2628.

Pitchford, S., Pan, D., and Welch, H.C. (2017). Platelets in neutrophil recruitment to sites of inflammation. Current Opinion in Hematology *24*, 23-31.

Pocai, A., Lam, T.K.T., Gutierrez-Juarez, R., Obici, S., Schwartz, G.J., Bryan, J., Aguilar-Bryan, L., and Rossetti, L. (2005). Hypothalamic KATP channels control hepatic glucose production. Nature *434*, 1026-1031.

Premkumar, L., Bobkov, A.A., Patel, M., Jaroszewski, L., Bankston, L.A., Stec, B., Vuori, K., Côté, J.-F., and Liddington, R.C. (2010). Structural Basis of Membrane Targeting by the Dock180 Family of Rho Family Guanine Exchange Factors (Rho-GEFs). Journal of Biological Chemistry *285*, 13211-13222.

Proud, C., Rylatt, D., Yeaman, S., Cohen, P., Proud, C., Rylatt, D., Yeaman, S., and Cohen, P. (1977). Amino acid sequences at the two sites on glycogen synthetase phosphorylated by cyclic AMP-dependent protein kinase and their dephosphorylation by protein phosphatase-III. FEBS letters *80*, 435-442.

Qi, L.S., Larson, M.H., Gilbert, L.A., Doudna, J.A., Weissman, J.S., Arkin, A.P., and Lim, W.A. (2013). Repurposing CRISPR as an RNA-guided platform for sequence-specific control of gene expression. Cell *152*, 1173-1183.

Qian, F., Le Breton, G.C., Chen, J., Deng, J., Christman, J.W., Wu, D., and Ye, R.D. (2012). Role for the guanine nucleotide exchange factor phosphatidylinositol-3,4,5-trisphosphate-dependent rac exchanger 1 in platelet secretion and aggregation. Arteriosclerosis, Thrombosis, and Vascular Biology *32*, 768-777.

Ramachandran, C., Goris, J., Waelkens, E., Merlevede, W., and Walsh, D.A. (1987). The interrelationship between cAMP-dependent alpha and beta subunit phosphorylation in the regulation of phosphorylase kinase activity. Studies using subunit specific phosphatases. The Journal of Biological Chemistry *262*, 3210-3218.

Ran, F.A., Hsu, P.D., Lin, C.Y., Gootenberg, J.S., Konermann, S., Trevino, A.E., Scott, D.A., Inoue, A., Matoba, S., Zhang, Y*., et al.* (2013a). Double nicking by RNA-guided CRISPR Cas9 for enhanced genome editing specificity. Cell *154*, 1380-1389.

Ran, F.A., Hsu, P.D., Wright, J., Agarwala, V., Scott, D.A., and Zhang, F. (2013b). Genome engineering using the CRISPR-Cas9 system. Nature Protocols *8*, 2281-2308.

Reiner, D.J., and Lundquist, E.A. (2018). Small GTPases. WormBook *2018*, 1-65.

Reynolds, T.H., Dalton, A., Calzini, L., Tuluca, A., Hoyte, D., and Ives, S.J. (2019). The impact of age and sex on body composition and glucose sensitivity in C57BL/6J mice. Physiological Reports *7*, e13995.

Richter, E.A., and Hargreaves, M. (2013). Exercise, GLUT4, and Skeletal Muscle Glucose Uptake. Physiological Reviews *93*, 993-1017.

Rider, M., Bertrand, L., Vertommen, D., Michels, P., Rousseau, G., Hue, L., Rider, M., Bertrand, L., Vertommen, D., Michels, P*., et al.* (2004). 6-phosphofructo-2-kinase/fructose-2,6-bisphosphatase: head-to-head with a bifunctional enzyme that controls glycolysis. Biochemical Journal *381*, 561-579.

Ridley, A.J., Paterson, H.F., Johnston, C.L., Diekmann, D., and Hall, A. (1992). The small GTP-binding protein rac regulates growth factor-induced membrane ruffling. Cell *70*, 401-410.

Roberts, A.W., Kim, C., Zhen, L., Lowe, J.B., Kapur, R., Petryniak, B., Spaetti, A., Pollock, J.D., Borneo, J.B., Bradford, G.B.*, et al.* (1999). Deficiency of the hematopoietic cell-specific Rho family GTPase Rac2 is characterized by abnormalities in neutrophil function and host defense. Immunity *10*, 183-196.

Röder, P.V., Wu, B., Liu, Y., and Han, W. (2016). Pancreatic regulation of glucose homeostasis. Experimental & Molecular Medicine *48*, e219.

Rodríguez-Fdez, S., and Bustelo, X.R. (2019). The Vav GEF Family: An Evolutionary and Functional Perspective. Cells *8*, 465.

Rosen, Evan D., and Spiegelman, Bruce M. (2014). What We Talk About When We Talk About Fat. Cell *156*, 20-44.

Rosenfeldt, H., Vazquez-Prado, J., and Gutkind, J.S. (2004). P-REX2, a novel PI-3-kinase sensitive Rac exchange factor. FEBS letters *572*, 167-171.

Rossman, K.L., Cheng, L., Mahon, G.M., Rojas, R.J., Snyder, J.T., Whitehead, I.P., and Sondek, J. (2003). Multifunctional Roles for the PH Domain of Dbs in Regulating Rho GTPase Activation. Journal of Biological Chemistry *278*, 18393-18400.

Rossman, K.L., Der, C.J., and Sondek, J. (2005). GEF means go: turning on RHO GTPases with guanine nucleotide-exchange factors. Nature Reviews Molecular Cell Biology *6*, 167-180.

Rossman, K.L., Worthylake, D.K., Snyder, J.T., Siderovski, D.P., Campbell, S.L., and Sondek, J. (2002). A crystallographic view of interactions between Dbs and Cdc42: PH domain-assisted guanine nucleotide exchange. EMBO J *21*, 1315-1326.

Routh, V.H., Hao, L., Santiago, A.M., Sheng, Z., and Zhou, C. (2014). Hypothalamic glucose sensing: making ends meet. Frontiers in Systems Neuroscience *8*.

Russo, C., Gao, Y., Mancini, P., Vanni, C., Porotto, M., Falasca, M., Torrisi, M.R., Zheng, Y., and Eva, A. (2001). Modulation of oncogenic DBL activity by phosphoinositol phosphate binding to pleckstrin homology domain. The Journal of Biological Chemistry *276*, 19524-19531.

Sacks, D.B. (2011). A1C Versus Glucose Testing: A Comparison. Diabetes Care *34*, 518-523.

Sadok, A., and Marshall, C.J. (2014). Rho GTPases: masters of cell migration. Small GTPases *5*, e29710-e29710.

Saltiel, A.R. (2016). Insulin Signaling in the Control of Glucose and Lipid Homeostasis. In Metabolic Control. Handbook of Experimental Pharmacology. 233, 51-71.

Saltiel, A.R., and Kahn, C.R. (2001). Insulin signalling and the regulation of glucose and lipid metabolism. Nature *414*, 799-806.

Saltiel, A.R., and Olefsky, J.M. (2017). Inflammatory mechanisms linking obesity and metabolic disease. Journal of Clinical Investigation *127*, 1-4.

Sandoval, D.A., Bagnol, D., Woods, S.C., D'Alessio, D.A., and Seeley, R.J. (2008). Arcuate glucagon-like peptide 1 receptors regulate glucose homeostasis but not food intake. Diabetes *57*, 2046-2054.

Sasaki, M., Sasako, T., Kubota, N., Sakurai, Y., Takamoto, I., Kubota, T., Inagi, R., Seki, G., Goto, M., Ueki, K.*, et al.* (2017). Dual Regulation of Gluconeogenesis by Insulin and Glucose in the Proximal Tubules of the Kidney. Diabetes *66*, 2339-2350.

Saveliev, A., Vanes, L., Ksionda, O., Rapley, J., Smerdon, S.J., Rittinger, K., and Tybulewicz, V.L. (2009). Function of the nucleotide exchange activity of vav1 in T cell development and activation. Science Signaling *2*, ra83.

Scherer, T., O'Hare, J., Diggs-Andrews, K., Schweiger, M., Cheng, B., Lindtner, C., Zielinski, E., Vempati, P., Su, K., Dighe, S.*, et al.* (2011). Brain insulin controls adipose tissue lipolysis and lipogenesis. Cell Metabolism *13*, 183-194.

Schnelzer, A., Prechtel, D., Knaus, U., Dehne, K., Gerhard, M., Graeff, H., Harbeck, N., Schmitt, M., and Lengyel, E. (2000). Rac1 in human breast cancer: overexpression, mutation analysis, and characterization of a new isoform, Rac1b. Oncogene *19*, 3013-3020.

Schwartz, M.W., Woods, S.C., Porte, D., Seeley, R.J., and Baskin, D.G. (2000). Central nervous system control of food intake. Nature *404*, 661-671.

Simanshu, D.K., Nissley, D.V., and McCormick, F. (2017). RAS Proteins and Their Regulators in Human Disease. Cell *170*, 17-33.

Singh, P., Schimenti, J.C., and Bolcun-Filas, E. (2015). A mouse geneticist's practical guide to CRISPR applications. Genetics *199*, 1-15.

Sjøberg, K.A., Frøsig, C., Kjøbsted, R., Sylow, L., Kleinert, M., Betik, A.C., Shaw, C.S., Kiens, B., Wojtaszewski, J.F.P., Rattigan, S.*, et al.* (2017). Exercise Increases Human Skeletal Muscle Insulin Sensitivity via Coordinated Increases in Microvascular Perfusion and Molecular Signaling. Diabetes *66*, 1501-1510.

Snyder, J.T., Rossman, K.L., Baumeister, M.A., Pruitt, W.M., Siderovski, D.P., Der, C.J., Lemmon, M.A., and Sondek, J. (2001). Quantitative Analysis of the Effect of Phosphoinositide Interactions on the Function of Dbl Family Proteins. Journal of Biological Chemistry *276*, 45868-45875.

Soisson, S.M., Nimnual, A.S., Uy, M., Bar-Sagi, D., and Kuriyan, J. (1998). Crystal structure of the Dbl and pleckstrin homology domains from the human Son of sevenless protein. Cell *95*, 259-268.

Song, G., Pacini, G., Ahrén, B., and D'Argenio, D.Z. (2017). Glucagon increases insulin levels by stimulating insulin secretion without effect on insulin clearance in mice. Peptides *88*, 74-79.

Sosa, M.S., Lopez-Haber, C., Yang, C., Wang, H., Lemmon, M.A., Busillo, J.M., Luo, J., Benovic, J.L., Klein-Szanto, A., Yagi, H.*, et al.* (2010). Identification of the Rac-GEF P-Rex1 as an essential mediator of ErbB signaling in breast cancer. Molecular Cell *40*, 877-892.

Statistics, N. (2018). Statistics on Obesity, Physical Activity and Diet - England, 2018 [PAS], NHS, ed.

Sugihara, K., Nakatsuji, N., Nakamura, K., Nakao, K., Hashimoto, R., Otani, H., Sakagami, H., Kondo, H., Nozawa, S., Aiba, A.*, et al.* (1998). Rac1 is required for the formation of three germ layers during gastrulation. Oncogene *17*, 3427-3433.

Suzuki, A., Mimaki, S., Yamane, Y., Kawase, A., Matsushima, K., Suzuki, M., Goto, K., Sugano, S., Esumi, H., Suzuki, Y.*, et al.* (2013). Identification and characterization of cancer mutations in Japanese lung adenocarcinoma without sequencing of normal tissue counterparts. PLOS One *8*, e73484-e73484.

Sylow, L., Jensen, T.E., Kleinert, M., Højlund, K., Kiens, B., Wojtaszewski, J., Prats, C., Schjerling, P., and Richter, E.A. (2013). Rac1 signaling is required for insulin-stimulated glucose uptake

and is dysregulated in insulin-resistant murine and human skeletal muscle. Diabetes *62*, 1865-1875.

Sylow, L., Kleinert, M., Pehmøller, C., Prats, C., Chiu, T.T., Klip, A., Richter, E.A., and Jensen, T.E. (2014). Akt and Rac1 signaling are jointly required for insulin-stimulated glucose uptake in skeletal muscle and downregulated in insulin resistance. Cellular Signalling *26*, 323-331.

Syrovatkina, V., and Huang, X.-Y. (2019). Signaling mechanisms and physiological functions of G-protein Gα13 in blood vessel formation, bone homeostasis, and cancer. Protein Science *28*, 305-312.

Szablewski, L. (2011). Glucose Homeostasis – Mechanism and Defects. In Diabetes - Damages and Treatments, E.C. Rigobelo, ed. (IntechOpen).

Takenaka, N., Araki, N., and Satoh, T. (2019). Involvement of the protein kinase Akt2 in insulin-stimulated Rac1 activation leading to glucose uptake in mouse skeletal muscle. PLOS One *14*, e0212219-e0212219.

Tamemoto, H., Kadowaki, T., Tobe, K., Yagi, T., Sakura, H., Hayakawa, T., Terauchi, Y., Ueki, K., Kaburagi, Y., Satoh, S.*, et al.* (1994). Insulin resistance and growth retardation in mice lacking insulin receptor substrate-1. Nature *372*, 182-186.

Tan, B.K., Adya, R., Farhatullah, S., Lewandowski, K.C., O'Hare, P., Lehnert, H., and Randeva, H.S. (2008). Omentin-1, a Novel Adipokine, Is Decreased in Overweight Insulin-Resistant Women With Polycystic Ovary Syndrome: ex vivo and in vivo regulation of omentin-1 by insulin and glucose. Diabetes 57(4), 801-808.

Ex Vivo and In Vivo Regulation of Omentin-1 by Insulin and Glucose. Diabetes *57*, 801-808.

Tchkonia, T., Thomou, T., Zhu, Y., Karagiannides, I., Pothoulakis, C., Jensen, Michael D., and Kirkland, James L. (2013). Mechanisms and Metabolic Implications of Regional Differences among Fat Depots. Cell Metabolism *17*, 644-656.

Terauchi, Y., Tsuji, Y., Satoh, S., Minoura, H., Murakami, K., Okuno, A., Inukai, K., Asano, T., Kaburagi, Y., Ueki, K.*, et al.* (1999). Increased insulin sensitivity and hypoglycaemia in mice lacking the p85α subunit of phosphoinositide 3–kinase. Nature Genetics *21*, 230-235.

Tiwari, S., Singh, R.S., Li, L., Tsukerman, S., Godbole, M., Pandey, G., and Ecelbarger, C.M. (2013). Deletion of the Insulin Receptor in the Proximal Tubule Promotes Hyperglycemia. Journal of the American Society of Nephrology *24*, 1209-1214.

Tokarz, V.L., MacDonald, P.E., and Klip, A. (2018). The cell biology of systemic insulin function. Journal of Cell Biology *217*, 2273-2289.

Tong, D., Zhao, L., He, K., Sun, H., Cai, D., Ni, L., Sun, R., Chang, S., Song, T., and Huang, C. (2016). MECP2 promotes the growth of gastric cancer cells by suppressing miR-338-mediated antiproliferative effect. Oncotarget *7*, 34845-34859.

transOMIC technologies (2012). CRISPR Cas9 for Genome Editing.

Trimble, E.R., Bruzzone, R., and Belin, D. (1986). Insulin resistance is accompanied by impairment of amylase-gene expression in the exocrine pancreas of the obese Zucker rat. Biochemical Journal *237*, 807-812.

Triplitt, C.L. (2012). Examining the mechanisms of glucose regulation. The American Journal of Managed Care *18*, S4-10.

Tsonou, E., Pantarelli, C., Hornigold, K., and Welch, H.C.E. (2018). P-Rex2. In Encyclopedia of Signaling Molecules, S. Choi, ed. (Cham: Springer International Publishing), pp. 4154-4164.

Tunduguru, R., Chiu, T.T., Ramalingam, L., Elmendorf, J.S., Klip, A., and Thurmond, D.C. (2014). Signaling of the p21-activated kinase (PAK1) coordinates insulin-stimulated actin remodeling and glucose uptake in skeletal muscle cells. Biochemical Pharmacology *92*, 380-388.

Turton, M.D., O'Shea, D., Gunn, I., Beak, S.A., Edwards, C.M., Meeran, K., Choi, S.J., Taylor, G.M., Heath, M.M., Lambert, P.D.*, et al.* (1996). A role for glucagon-like peptide-1 in the central regulation of feeding. Nature *379*, 69-72.

Ugi, S., Imamura, T., Maegawa, H., Egawa, K., Yoshizaki, T., Shi, K., Obata, T., Ebina, Y., Kashiwagi, A., and Olefsky, J.M. (2004). Protein phosphatase 2A negatively regulates insulin's metabolic signaling pathway by inhibiting Akt (protein kinase B) activity in 3T3-L1 adipocytes. Molecular and Cellular Biology *24*, 8778-8789.

Uhlén, M., Fagerberg, L., Hallström, B.M., Lindskog, C., Oksvold, P., Mardinoglu, A., Sivertsson, Å., Kampf, C., Sjöstedt, E., Asplund, A.*, et al.* (2015). Tissue-based map of the human proteome. Science *347*, 1260419.

Urano, D., Nakata, A., Mizuno, N., Tago, K., and Itoh, H. (2008). Domain-domain interaction of P-Rex1 is essential for the activation and inhibition by G protein betagamma subunits and PKA. Cellular Signalling *20*, 1545-1554.

van Greevenbroek, M.M., Schalkwijk, C.G., and Stehouwer, C.D. (2013). Obesity-associated low-grade inflammation in type 2 diabetes mellitus: causes and consequences. The Netherlands Journal of Medicine *71*, 174-187.

van Hooren, K.W.E.M., van Breevoort, D., Fernandez-Borja, M., Meijer, A.B., Eikenboom, J., Bierings, R., and Voorberg, J. (2014). Phosphatidylinositol-3,4,5-triphosphate-dependent Rac exchange factor 1 regulates epinephrine-induced exocytosis of Weibel–Palade bodies. Journal of Thrombosis and Haemostasis *12*, 273-281.

Veluthakal, R., Tunduguru, R., Arora, D.K., Sidarala, V., Syeda, K., Vlaar, C.P., Thurmond, D.C., and Kowluru, A. (2015). VAV2, a guanine nucleotide exchange factor for Rac1, regulates glucose-stimulated insulin secretion in pancreatic beta cells. Diabetologia *58*, 2573-2581.

Vetter, I.R., and Wittinghofer, A. (2001). The Guanine Nucleotide-Binding Switch in Three Dimensions. Science *294*, 1299-1304.

Vigorito, E., Bell, S., Hebeis, B.J., Reynolds, H., McAdam, S., Emson, P.C., McKenzie, A., and Turner, M. (2004). Immunological function in mice lacking the Rac-related GTPase RhoG. Molecular and Cellular Biology *24*, 719-729.

Villarroya, F., Cereijo, R., Villarroya, J., Gavalda-Navarro, A., and Giralt, M. (2018). Toward an Understanding of How Immune Cells Control Brown and Beige Adipobiology. Cell Metabolism *27*, 954-961.

Waddell, N., Pajic, M., Patch, A.-M., Chang, D.K., Kassahn, K.S., Bailey, P., Johns, A.L., Miller, D., Nones, K., Quek, K.*, et al.* (2015). Whole genomes redefine the mutational landscape of pancreatic cancer. Nature *518*, 495.

Wang, H., Nong, Y., Bazan, F., Greengard, P., and Flajolet, M. (2010). Norbin: A promising central nervous system regulator. Communicative & Integrative Biology *3*, 487-490.

Wang, J., Hirose, H., Du, G., Chong, K., Kiyohara, E., Witz, I.P., and Hoon, D.S.B. (2017). P-REX1 amplification promotes progression of cutaneous melanoma via the PAK1/P38/MMP-2 pathway. Cancer Letters *407*, 66-75.

Wang, Y., Li, G., Goode, J., Paz, J., Ouyang, K., Screaton, R., Fischer, W., Chen, J., Tabas, I., Montminy, M.*, et al.* (2012). Inositol-1,4,5-trisphosphate receptor regulates hepatic gluconeogenesis in fasting and diabetes. Nature *485*, 128-132.

Wang, Z., Dong, X., Li, Z., Smith, J.D., and Wu, D. (2008). Lack of a significant role of P-Rex1, a major regulator of macrophage Rac1 activation and chemotaxis, in atherogenesis. Prostaglandins & Other Lipid Mediators *87*, 9-13.

Waters, J.E., Astle, M.V., Ooms, L.M., Balamatsias, D., Gurung, R., and Mitchell, C.A. (2008). P-Rex1 - a multidomain protein that regulates neurite differentiation. Journal of Cell Science *121*, 2892-2903.

Welch, H., Eguinoa, A., Stephens, L.R., and Hawkins, P.T. (1998). Protein kinase B and rac are activated in parallel within a phosphatidylinositide 3OH-kinase-controlled signaling pathway. The Journal of Biological Chemistry *273*, 11248-11256.

Welch, H.C. (2015). Regulation and function of P-Rex family Rac-GEFs. Small GTPases *6*, 49-70.

Welch, H.C., Coadwell, W.J., Ellson, C.D., Ferguson, G.J., Andrews, S.R., Erdjument-Bromage, H., Tempst, P., Hawkins, P.T., and Stephens, L.R. (2002). P-Rex1, a PtdIns(3,4,5)P3- and Gbetagamma-regulated guanine-nucleotide exchange factor for Rac. Cell *108*, 809-821.

Welch, H.C., Condliffe, A.M., Milne, L.J., Ferguson, G.J., Hill, K., Webb, L.M., Okkenhaug, K., Coadwell, W.J., Andrews, S.R., Thelen, M.*, et al.* (2005). P-Rex1 regulates neutrophil function. Current Biology *15*, 1867-1873.

Welch, H.C.E., Coadwell, W.J., Stephens, L.R., and Hawkins, P.T. (2003). Phosphoinositide 3-kinase-dependent activation of Rac. FEBS letters *546*, 93-97.

Wennerberg, K., and Der, C.J. (2004). Rho-family GTPases: it's not only Rac and Rho (and I like it). Journal of Cell Science *117*, 1301-1312.

Wennerberg, K., Rossman, K.L., and Der, C.J. (2005). The Ras superfamily at a glance. Journal of Cell Science *118*, 843-846.

Wettschureck, N., and Offermanns, S. (2005). Mammalian G Proteins and Their Cell Type Specific Functions. Physiological Reviews *85*, 1159-1204.

Wijesekara, N., Krishnamurthy, M., Bhattacharjee, A., Suhail, A., Sweeney, G., and Wheeler, M.B. (2010). Adiponectin-induced ERK and Akt phosphorylation protects against pancreatic beta cell apoptosis and increases insulin gene expression and secretion. The Journal of Biological Chemistry *285*, 33623-33631.

Wilding, J.P.H. (2014). The role of the kidneys in glucose homeostasis in type 2 diabetes: Clinical implications and therapeutic significance through sodium glucose co-transporter 2 inhibitors. Metabolism *63*, 1228-1237.

Williams, D.A., Tao, W., Yang, F., Kim, C., Gu, Y., Mansfield, P., Levine, J.E., Petryniak, B., Derrow, C.W., Harris, C.*, et al.* (2000). Dominant negative mutation of the hematopoietic-specific Rho GTPase, Rac2, is associated with a human phagocyte immunodeficiency. Blood *96*, 1646-1654.

Withers, D.J., Gutierrez, J.S., Towery, H., Burks, D.J., Ren, J.-M., Previs, S., Zhang, Y., Bernal, D., Pons, S., Shulman, G.I.*, et al.* (1998). Disruption of IRS-2 causes type 2 diabetes in mice. Nature *391*, 900-904.

Wong, C.Y., Wuriyanghan, H., Xie, Y., Lin, M.F., Abel, P.W., and Tu, Y. (2011). Epigenetic regulation of phosphatidylinositol 3,4,5-triphosphate-dependent Rac exchanger 1 gene expression in prostate cancer cells. The Journal of Biological Chemistry *286*, 25813-25822.

Worthylake, D.K., Rossman, K.L., and Sondek, J. (2000). Crystal structure of Rac1 in complex with the guanine nucleotide exchange region of Tiam1. Nature *408*, 682-688.

Worzfeld, T., Wettschureck, N., and Offermanns, S. (2008). G(12)/G(13)-mediated signalling in mammalian physiology and disease. Trends in Pharmacological Sciences *29*, 582-589.

Xue, R., Lynes, M.D., Dreyfuss, J.M., Shamsi, F., Schulz, T.J., Zhang, H., Huang, T.L., Townsend, K.L., Li, Y., Takahashi, H.*, et al.* (2015). Clonal analyses and gene profiling identify genetic biomarkers of the thermogenic potential of human brown and white preadipocytes. Nature Medicine *21*, 760-768.

Yang, H., Wang, H., Shivalila, C.S., Cheng, A.W., Shi, L., and Jaenisch, R. (2013). One-step generation of mice carrying reporter and conditional alleles by CRISPR/Cas-mediated genome engineering. Cell *154*, 1370-1379.

Yang, J., Gong, X., Ouyang, L., He, W., Xiao, R., and Tan, L. (2016). PREX2 promotes the proliferation, invasion and migration of pancreatic cancer cells by modulating the PI3K signaling pathway. Oncology letters *12*, 1139-1143.

Yang, J., Zhang, Z., Roe, S.M., Marshall, C.J., and Barford, D. (2009). Activation of Rho GTPases by DOCK Exchange Factors Is Mediated by a Nucleotide Sensor. Science *325*, 1398-1402.

Yang, R.-Z., Lee, M.-J., Hu, H., Pray, J., Wu, H.-B., Hansen, B.C., Shuldiner, A.R., Fried, S.K., McLenithan, J.C., and Gong, D.-W. (2006). Identification of omentin as a novel depot-specific adipokine in human adipose tissue: possible role in modulating insulin action. American Journal of Physiology-Endocrinology and Metabolism *290*, E1253-E1261.

Ye, J. (2009). Emerging role of adipose tissue hypoxia in obesity and insulin resistance. International Journal of Obesity *33*, 54-66.

Yoshizawa, M., Kawauchi, T., Sone, M., Nishimura, Y.V., Terao, M., Chihama, K., Nabeshima, Y., and Hoshino, M. (2005). Involvement of a Rac activator,P-Rex1, in neurotrophin-derived signaling and neuronal migration. The Journal of Neuroscience *25*, 4406-4419.

You, G.Y., Lee, J.O., Kim, J.H., Kim, N., Lee, S.K., Moon, J.W., Jie, S., Lee, H.J., Kim, S.J., Park, S.H.*, et al.* (2013). Tiam-1, a GEF for Rac1, plays a critical role in metformin-mediated glucose uptake in C2C12 cells. Cellular Signalling *25*, 2558-2565.

Zhang, D., and Aravind, L. (2010). Identification of novel families and classification of the C2 domain superfamily elucidate the origin and evolution of membrane targeting activities in eukaryotes. Gene *469*, 18-30.

Zhao, F., Siu, J.J., Huang, W., Askwith, C., and Cao, L. (2019). Insulin Modulates Excitatory Synaptic Transmission and Synaptic Plasticity in the Mouse Hippocampus. Neuroscience *411*, 237-254.

Zhou, Y., Johnson, J.L., Cerione, R.A., and Erickson, J.W. (2013). Prenylation and Membrane Localization of Cdc42 Are Essential for Activation by DOCK7. Biochemistry *52*, 4354-4363.

Zmora, N., Bashiardes, S., Levy, M., and Elinav, E. (2017). The Role of the Immune System in Metabolic Health and Disease. Cell Metabolism *25*, 506-521.

Appendix A - Supplementary Material

Metabolic phenotype of Prex Wild Type mice

In order to better illustrate the metabolic phenotype of genetically modified mice, the responses of wild type mice are described here, using combined data from all cohorts of $Prex1^{+/+}$;$Prex2^{+/+}$ (Prex WT) mice that were tested throughout this PhD project. In summary, the mice were tested for fasting blood glucose levels, response to glucose tolerance test and response to insulin tolerance test, throughout ageing. Glucose tolerance tests were performed at 10 and 15 weeks, and at 6, 9 and 12 months of age. Insulin tolerance tests were done at 5 and 10 months of age. Both sexes were tested, and two diets were compared, normal chow diet and high fat (45%) diet. In addition, mice were assessed for body weight throughout ageing, tested in metabolic cages at 11 months of age, and their body composition was analysed post mortem at one year.

1. Metabolic phenotype of male Prex WT mice on chow diet

First, we will consider the responses of male Prex WT mice on chow diet. As seen in **Figures S1A and S2A**, the blood glucose levels in young males was 12 mM after 6 h of fasting, and rose steadily to 15 mM at one year of age, as expected (Reynolds et al., 2019). During glucose tolerance tests by i.p. administration of 2 g/kg glucose (20% glucose at 10 ml/kg), the blood glucose level reached a maximum of 25-30 mM at 15 min post injection and gradually returned towards basal level to around 15 mM after 90 min (**Figure S1B**). Normalisation of the glucose response by subtracting the basal blood glucose level for each mouse showed that glucose challenge triggers an average increase of blood glucose levels by 15 mM (**Figure S1C**). Both raw and normalised data showed that the glucose response of mice changed from the age of 6 months onwards, as their blood glucose levels remained elevated up to 30 min post injection rather than declining after 15 min as at younger age. The area under the curve of the normalised data was used to assess the total response to glucose challenge (dots represent individual mice) (**Figure S1D**). Overall, despite the increase in basal blood glucose level from 12 to 15 mM during ageing (**Figure S2A**), the total response to glucose challenge did not change significantly with age, although it fluctuated somewhat between 50 and 70 units

(**Figure S2B**). As expected, the mice gained weight in a steady way throughout ageing, starting from 26 g at 10 weeks and reaching 35 g at one year (**Figure S2C**).

For insulin tolerance tests, the mice were starved for 4 h prior to being challenged by s.c. administration of 0.75 IU/kg of human recombinant insulin at 0.15 IU/ml. As shown in **Figure S3A,** both at 5 and at 10 months the blood glucose level dropped from 13 to 7 mM at 45 min post injection and then returned gradually to around 10 mM, remaining at that level throughout the 3 h of testing (**Figure S3B**). Normalisation of glucose levels by subtracting the basal blood glucose level for each mouse showed that insulin challenge triggered an average decrease of blood glucose levels by 5 mM (**Figure S3C**). A small decrease was observed in the total insulin response between 5 and 10 months of age, from 25 to 20 units (**Figure S3D**), indicating that the mice developed a mild insulin resistance due to ageing. However, this decrease in insulin sensitivity did not reach statistical significance.

To further investigate the metabolic phenotype of Prex WT males, the mice were introduced to metabolic cages at 11 months of age. After habituation, the mice were group-housed in metabolic cages overnight for 16 h on 3 subsequent nights. Food and water were provided *ad libitum.* Prex WT males consumed on average 78 mg of water and 71 mg of food per gram of body weight per night, and they produced 34 mg of urine and 28 mg of faeces per gram of body weight per night (**Figure S4A-D**).

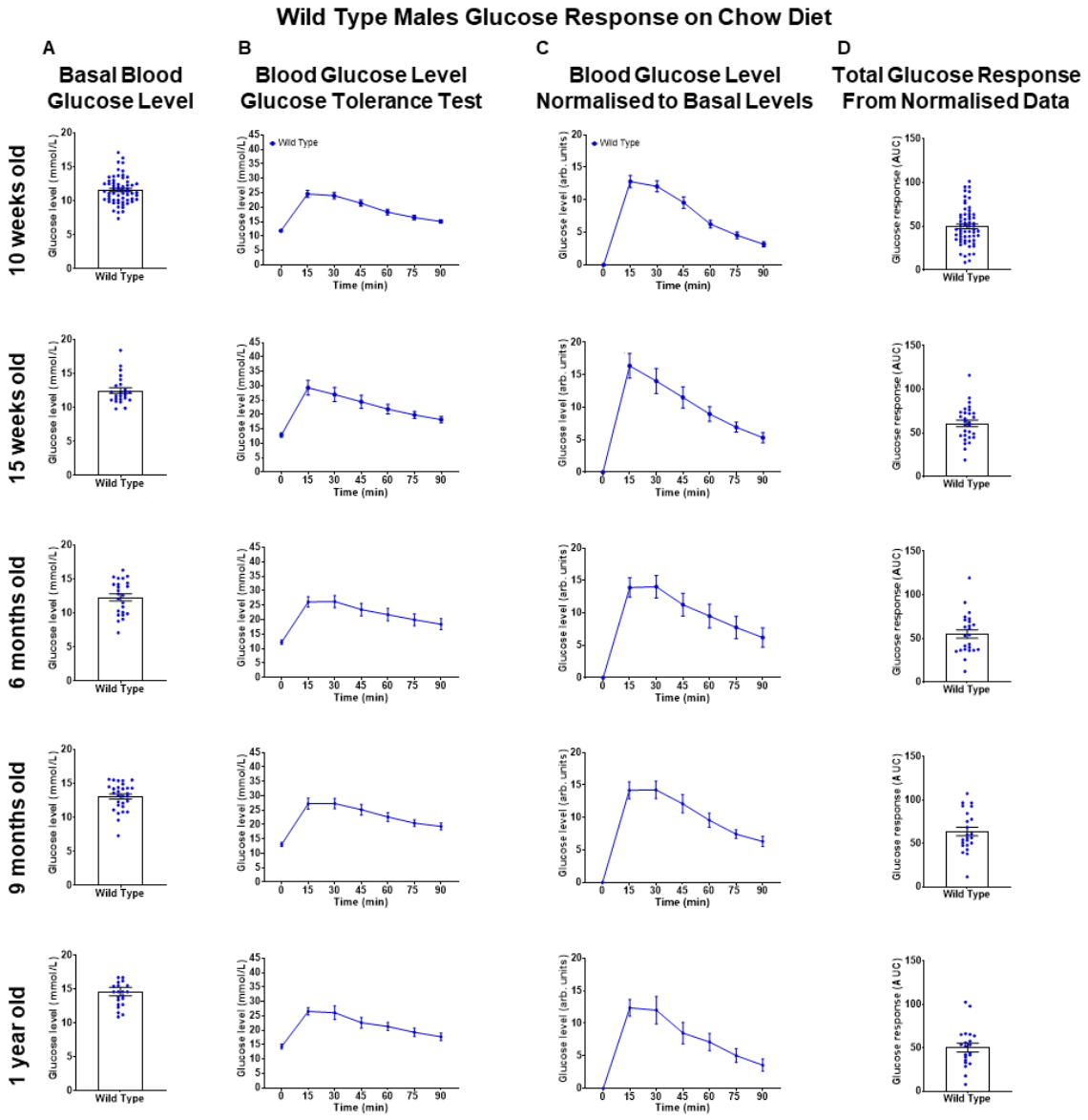

Figure S1: Fasting blood glucose level and response to glucose challenge of male Prex WT mice on chow diet.

Male *Prex1*$^{+/+}$;*Prex2*$^{+/+}$ (Prex WT) mice on chow diet were subjected to i.p. glucose tolerance test (IPGTT) at the ages of 10 and 15 weeks, 6, 9 and 12 months. Food was withdrawn 6 h prior to i.p. injection of 20% glucose at 10 ml/kg (final concentration 2 g/kg). Blood glucose levels were tested by tail bleed 15 min prior to the i.p. injection to determine the basal fasted blood glucose levels, and every 15 min after the glucose injection for 90 min, as indicated, to assess the response to glucose challenge. Data are pooled from 18 independent cohorts with 2-6 animals each, and presented as mean ± SEM. **(A)** Fasting blood glucose levels. **(B)** Blood glucose concentration during IPGTT. **(C)** Blood glucose levels during IPGTT, normalised by subtracting the basal blood glucose level from each mouse individually. **(D)** Total glucose response calculated as AUC of normalised data.

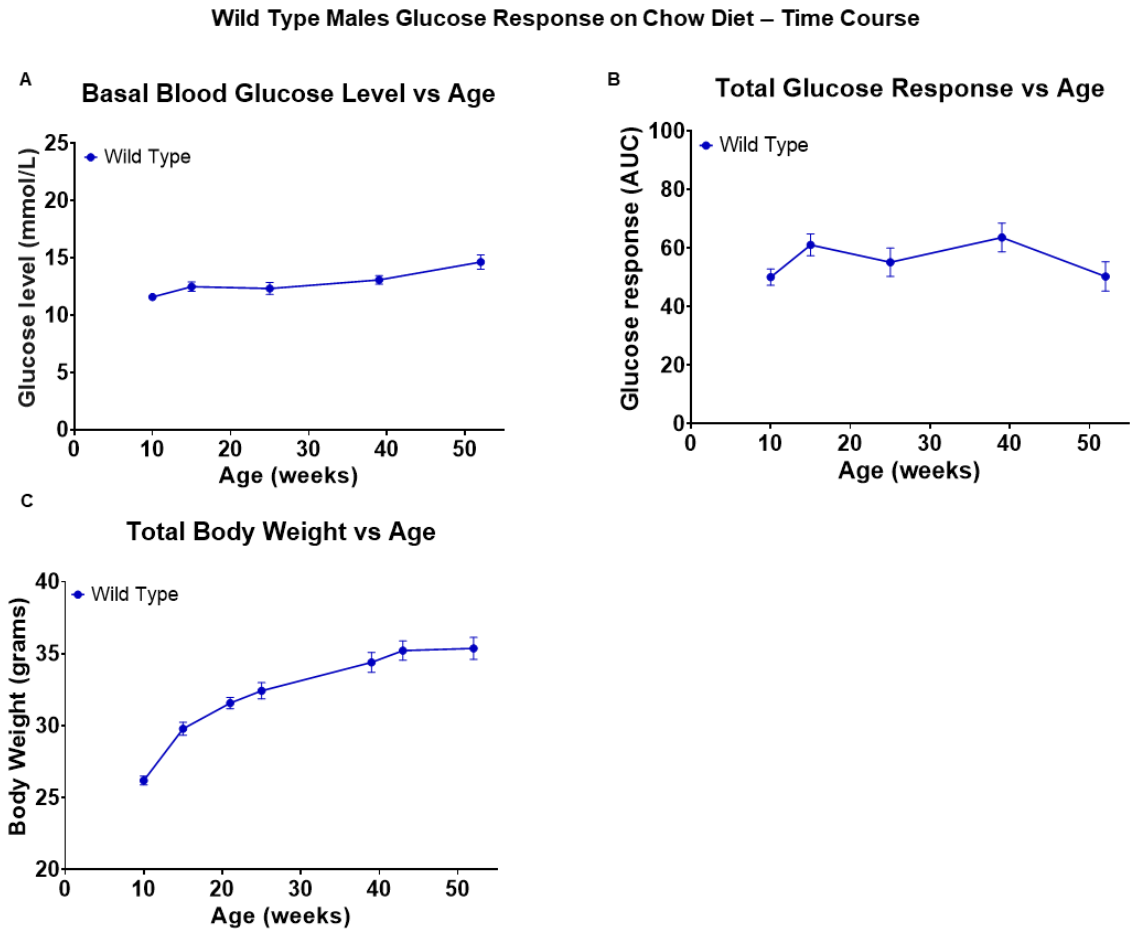

Figure S2: Effects of ageing on the response to glucose challenge, fasting blood glucose levels, and body weight of male Prex WT mice on chow diet.

The fasting blood glucose level, response to glucose challenge, and body weight of the male Prex WT mice in **Figure S1** are expressed as a function of age. Data are pooled from 18 independent cohorts with 2-6 animals each, and are presented as mean ± SEM. **(A)** Fasting blood glucose levels; data from column A in **Figure S1**. **(B)** Response to IPGTT; normalised data from column D in **Figure S1**. **(C)** Total body weight, measured after 6 and 4 h fasting, prior to glucose and insulin challenges, respectively.

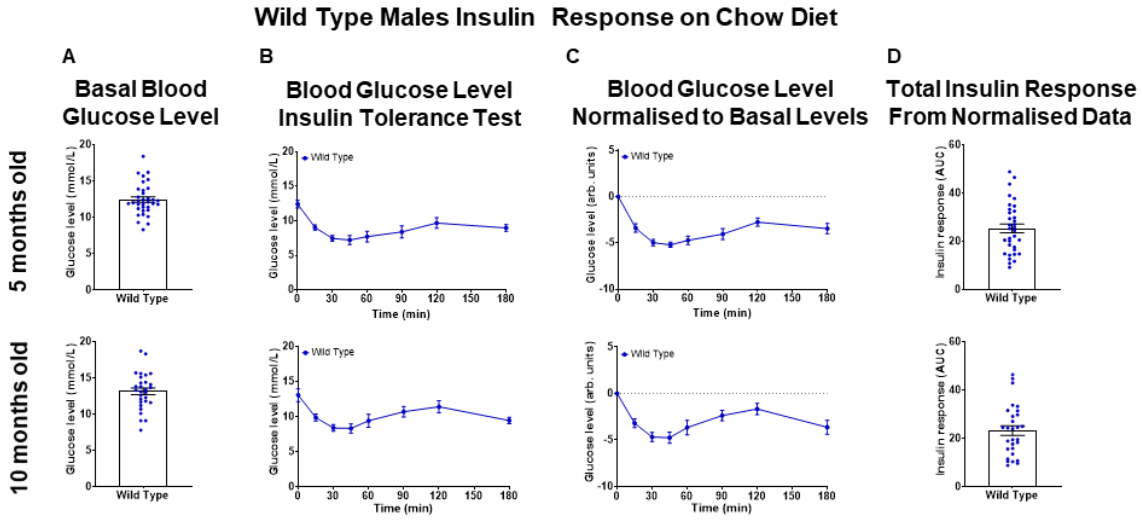

Figure S3: Response of male Prex WT mice on chow diet to insulin challenge at 5 months and 10 months of age.

The male Prex WT mice on chow diet shown in **Figure S1** were subjected to s.c. insulin tolerance test (SCITT) at the ages of 5 and 10 months. Food was withdrawn 4 h prior to s.c. injection of 0.75 IU/kg of human recombinant insulin at 0.15 IU/ml. Blood glucose levels were tested by tail bleed 15 min prior to the s.c. injection to determine basal blood glucose levels, as well as after the insulin injection at 15, 30, 45, 60, 90,120 and 180 min to assess the response to insulin. Data are pooled from 6 independent cohorts with 4-5 animals each, and are presented as mean ± SEM. **(A)** Fasting basal blood glucose levels. **(B)** Blood glucose levels during SCITT. **(C)** Glucose levels during SCITT, normalised by subtracting the fasting basal blood glucose level from each mouse individually. **(D)** Total insulin response, calculated as AUC of normalised data.

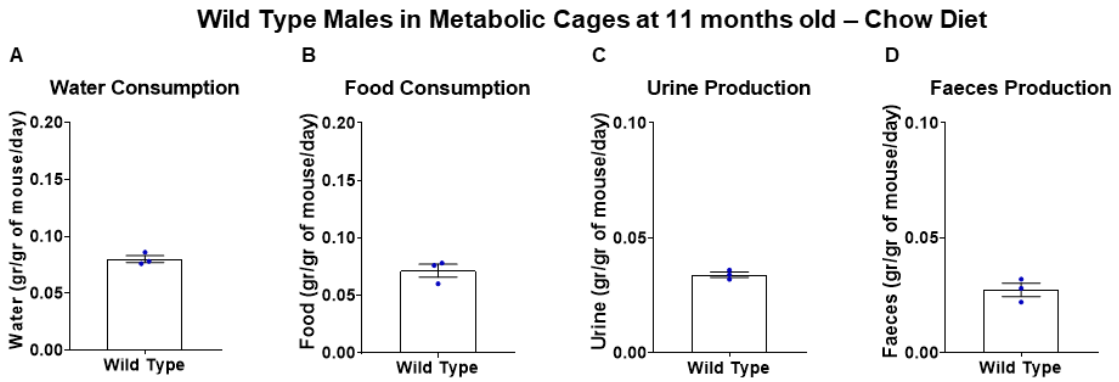

Figure S4: Male Prex WT mice water and food consumption as well as urine and faeces production in metabolic cages.

The male Prex WT mice from **Figure S1** were habituated to metabolic cages at 11 months of age as detailed in Materials and Methods, weighed and group-housed (up to 3) in metabolic cages overnight for 16 h on 3 subsequent nights with food and water provided *ad libitum*. Their **(A,E)** water consumption, **(B,F)** food consumption, **(C,G)** urine production, and **(D,H)** faeces production were measured after each night and were normalised to the combined body weights of the mice housed in each cage. Data are pooled from 6 independent cohorts with 4-5 animals each, and are presented as the mean ± SEM of each night (n=3).

2. Metabolic phenotype of male Prex WT mice on HFD

To investigate the effect of diet on glucose metabolism, male Prex WT mice were introduced to 45% HFD, after a “reference” glucose challenge at 10 weeks of age, and remained on this HFD throughout their life.

Figure S5A compares the basal blood glucose levels of mice on HFD (dark blue) to mice on chow diet (light blue). Overall, mice on HFD had elevated basal blood glucose levels, reaching 15 mM at 15 weeks, after only one month of HFD, compared to 12 mM for chow diet, and rising further to 18 mM, to diabetic level, at 6 months. IPGTT in 15-week old mice (that had been on HFD for one month) was performed under the same conditions as for mice on chow diet. This showed that the HFD had caused a rapid onset of glucose intolerance (**Figure S5B**). The blood glucose levels of HFD-fed mice kept increasing beyond the 15 min time point, reaching a dangerous level of 40 mM at 45 min and remaining above 30 mM within the 90 min of the test. These mice had to remain under observation for up to 2.5 h to ensure their blood glucose levels returned to 20 mM or below. Normalisation of the glucose response by subtracting the basal blood glucose level for each mouse showed that glucose challenge triggered an increase of blood glucose levels by 25 mM, 1.7 times more than for mice on chow diet (**Figure S5C-D**). As it was apparent that one month of HFD was sufficient to render the mice severely glucose intolerant, we reduced the dosage of glucose in IPGTTs at later ages to 0.5 g/kg (20% glucose at 2.5 ml/kg), one quarter of the original dose (data in ochre box), in order to prevent mice from going into hyperglycaemic shock. Under these conditions, blood glucose levels did not rise as much, but the duration of the response to IPGTT was similar to the test at 15-weeks, as it took again longer for blood glucose levels to return to normal.

The effects of ageing are summarised in **Figure S6**. As mentioned above, the HFD induced a rapid increase in fasting blood glucose levels. However, curiously, these basal blood glucose levels of HFD-fed mice improved again after the age of 6 months and were comparable to that of chow-fed mice (15 mM) by one year (**Figure S6A**). Due to the different amount of glucose used for IPGTTs, no direct comparison can be drawn regarding the total glucose response of HFD- and chow-fed mice, apart from the 15 weeks time point. Interestingly, just like for fasting

blood glucose levels, an improvement was also observed in the response of HFD-fed mice to IPGTT after the age of 6 months (**Figure S6B**).

Insulin tolerance tests showed that HFD also had complex effects on insulin sensitivity. Indeed, at 5 months of age, the insulin tolerance of mice on HFD was better than that of chow-fed mice. Although the diet had increased their fasting blood glucose level from 12 to 18 mM (**Figure S7A**), during insulin challenge (s.c. insulin at 0.75 IU/kg) blood glucose levels dropped to 8.5 mM at 45 min (**Figure S7B**). Normalising for basal blood glucose level showed that insulin challenge caused a drop by 8.5 mM in mice on HFD compared to 5 mM for mice on chow (**Figure S7C**). However, at 10 months of age, when basal blood glucose levels were similar between diets, the insulin response was also comparable. Hence, the insulin response of HFD-fed mice was lower at 10 months than at 5 months of age (**Figure S7D**), indicating that HFD rendered mice insulin intolerant with age, as expected.

Finally, also as expected, mice on HFD gained weight at a much higher rate than chow-fed mice, weighing roughly twice as much from the age of 9 months (**Figure S6C**). However, while housed in the metabolic cages, mice on HFD consumed half as much water and almost three times less food than their chow diet-fed counterparts (**Figure S8A-B**), and consequently also their urine and faeces production was decreased (**Figure S8C-D**).

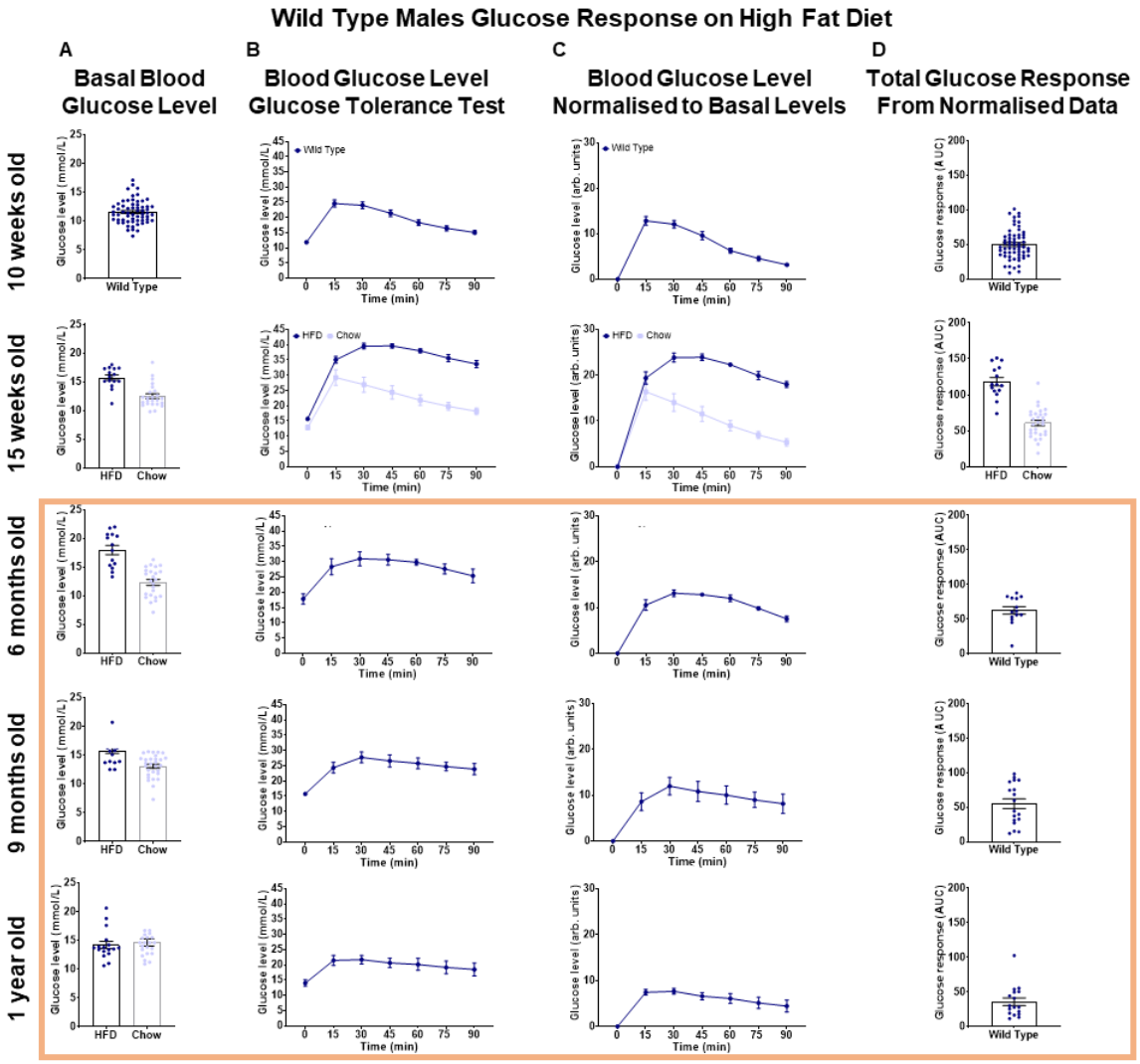

Figure S5: Fasting blood glucose level and response to glucose challenge of male Prex WT mice on HFD.

Male Prex WT mice on 45% HFD (dark blue) were subjected to IPGTT at the ages of 10 and 15 weeks, 6, 9 and 12 months. Food was withdrawn 6 h prior to i.p. injection of 20% glucose at 10 ml/kg (final concentration 2 g/kg) at 10 and 15 weeks old and at 2.5 ml/kg (final concentration 0.5g/kg) at 6, 9 and 12 months old - data in ochre box. Blood glucose levels were tested by tail bleed 15 min prior to the i.p. injection to determine the basal fasted blood glucose levels, and every 15 min after the glucose injection for 90 min, to assess the response to glucose challenge. Data are pooled from 4 independent cohorts with 4-5 animals each, and presented as mean ± SEM. In light blue are represented the male mice on chow diet from **Figure S1** for visual comparison, but no statistical analysis was performed, as these animals were not directly compared experimentally. **(A)** Fasting blood glucose levels. **(B)** Blood glucose concentration during IPGTT. **(C)** Blood glucose levels during IPGTT, normalised by subtracting the basal blood glucose level from each mouse individually. **(D)** Total glucose response calculated as AUC of normalised data.

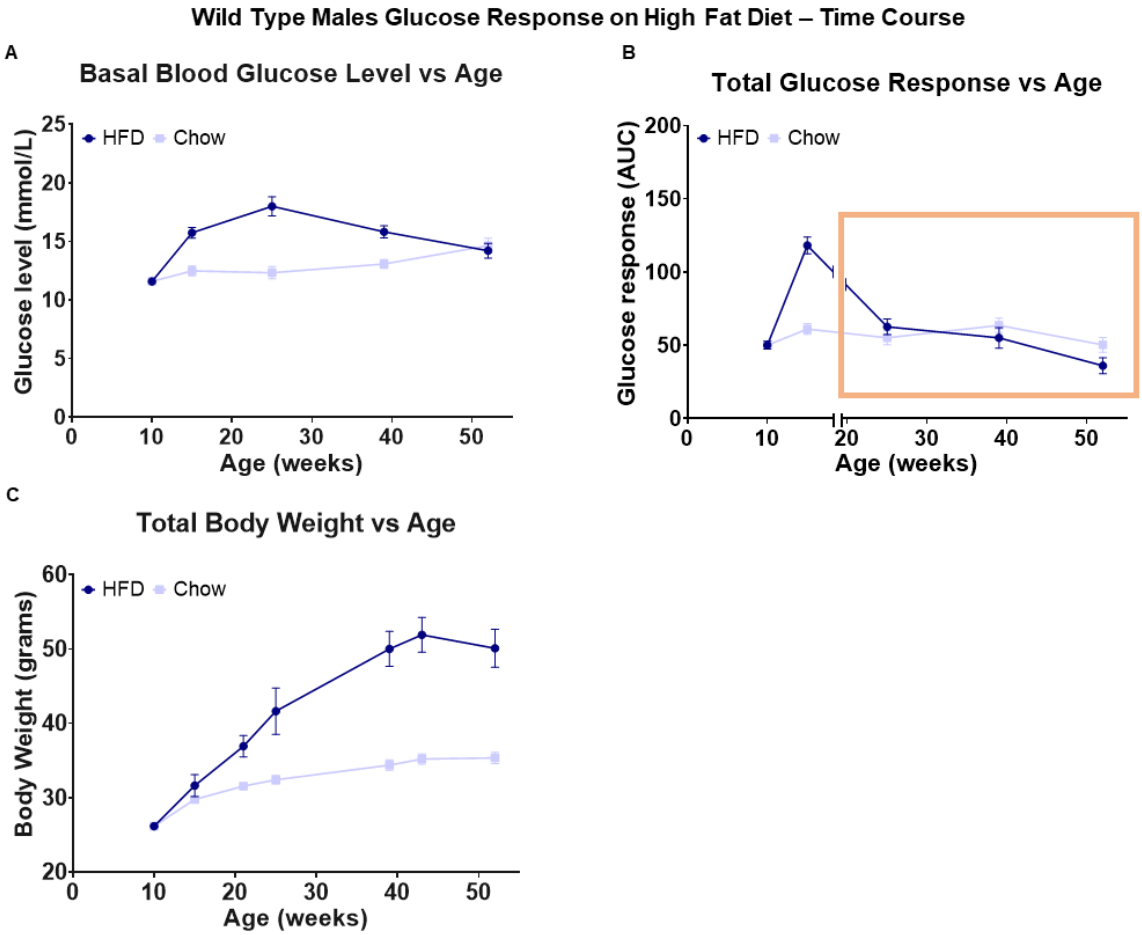

Figure S6: Effects of ageing on the fasting blood glucose levels, response to glucose challenge, and body weight of male Prex WT mice on HFD.

The fasting blood glucose level, response to glucose challenge, and body weight of the HFD-fed male Prex WT mice in **Figure S5** are expressed as a function of age (dark blue). Data are pooled from 4 independent cohorts with 4-5 animals each, and are presented as mean ± SEM. Note that the dose of glucose was reduced from 2 g/kg to 0.5 g/kg from the age of 6 months onwards (data in ochre box). In light blue are represented the male mice on chow diet from **Figure S2** for visual comparison, but no statistical analysis was performed, as these animals were not directly compared experimentally. **(A)** Fasting blood glucose levels; data from column A in **Figure S5**. **(B)** Response to IPGTT; normalised data from column D in **Figure S5**. Note that IPGTT was done with 2 g/kg at 10 and 15 weeks, but with 0.5 g/kg at later ages (ochre box). **(C)** Total body weight, measured after 6 and 4 h fasting, prior to glucose and insulin challenges, respectively.

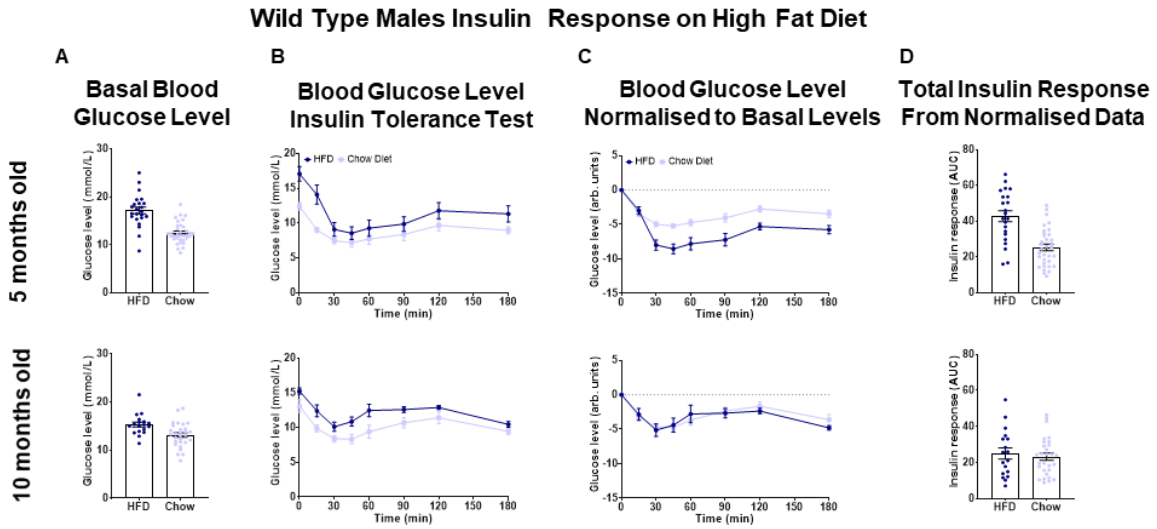

Figure S7: Response of male Prex WT mice on HFD to insulin challenge at 5 and 10 months of age.

The male Prex WT mice on 45% HFD shown in **Figure S5** were subjected to SCITT at the ages of 5 and 10 months (dark blue). Food was withdrawn 4 h prior to s.c. injection of 0.75 IU/kg of human recombinant insulin at 0.15 IU/ml. Blood glucose levels were tested by tail bleed 15 min prior to the s.c. injection to determine basal blood glucose levels, as well as after the insulin injection at 15, 30, 45, 60, 90,120 and 180 min to assess the response to insulin. Data are pooled from 6 independent cohorts with 4-5 animals each, and are presented as mean ± SEM. In light blue are represented the male mice on chow diet from **Figure S3** for visual comparison, but no statistical analysis was performed, as these animals were not directly compared experimentally. **(A)** Fasting basal blood glucose levels. **(B)** Blood glucose levels during SCITT. **(C)** Glucose levels during SCITT, normalised by subtracting the fasting basal blood glucose level from each mouse individually. **(D)** Total insulin response, calculated as AUC of normalised data.

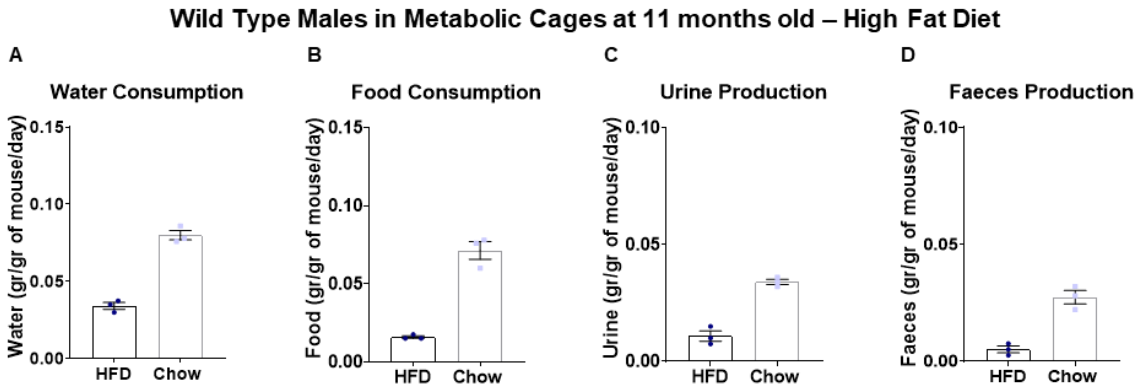

Figure S8: HFD-fed male Prex WT mice water and food consumption as well as urine and faeces production in metabolic cages.

The male Prex WT mice on HFD from **Figure S5** (dark blue) were habituated to metabolic cages at 11 months of age, as detailed in Materials and Methods, weighed and group-housed (up to 3) in metabolic cages overnight for 16 h on 3 subsequent nights with food and water provided *ad libitum*. In light blue are represented the male mice on chow diet from **Figure S4** for visual comparison, but no statistical analysis was performed, as these animals were not directly compared experimentally. Their **(A)** water consumption, **(B)** food consumption, **(C)** urine production, and **(D)** faeces production were measured after each night and were normalised to the combined body weights of the mice housed in each cage. Data are pooled from 6 independent cohorts with 4-5 animals each, and are presented as the mean ± SEM of each night (n=3).

3. Metabolic phenotype of female Prex WT mice on chow diet

After investigating males, I wanted to explore the possibility of sex differences. To this end, female Prex WT mice were tested on both chow and HFD, in a similar manner to the males. Again, data displayed are from all cohorts that were tested throughout this PhD project, comparing females (dark blue) with males (light blue).

As shown in **Figures S9A** and **S10A**, females had lower fasting blood glucose levels than males throughout ageing, around 10 mM at 10 weeks and 11 mM at one year, compared to 12-15 mM for males. During IPGTT (2 g/kg), blood glucose levels peaked at 20 mM 15 min after challenge in females and then decreased rapidly back to basal levels, at all ages tested, contrary to the higher maximal level and steadier decline seen in males (**Figure S9B**). During ageing, the total response of females to glucose challenge fluctuated somewhat, but did not change significantly (**Figure S10B**). Overall, therefore, females had better glucose tolerance than males throughout ageing (**Figure S9C, D**).

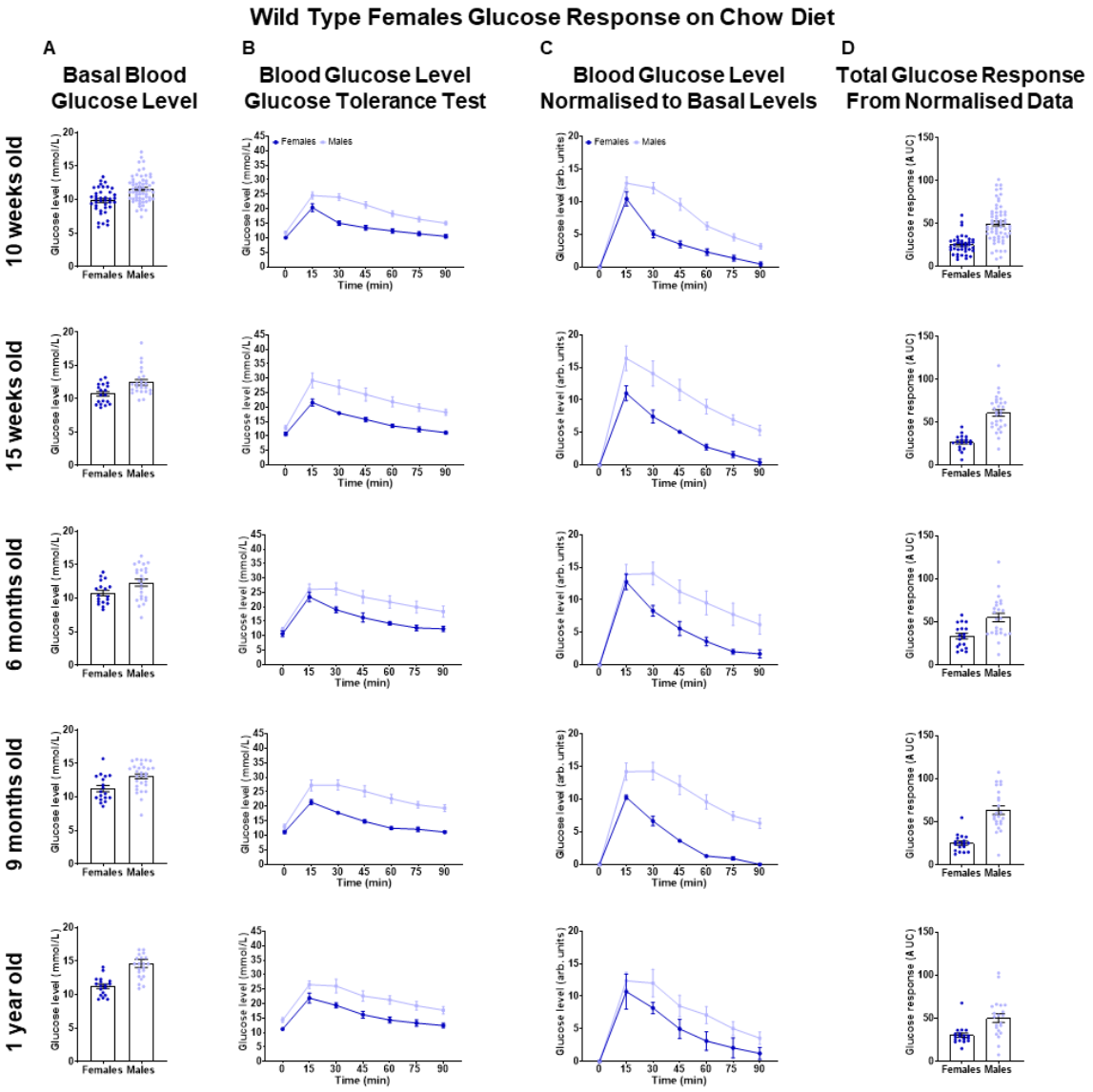

Figure S9: Fasting blood glucose level and response to glucose challenge of female Prex WT mice on chow diet.

Female Prex WT mice on chow diet (dark blue) were subjected to IPGTT at the ages of 10 and 15 weeks, 6, 9 and 12 months. Food was withdrawn 6 h prior to i.p. injection of 20% glucose at 10 ml/kg (final concentration 2 g/kg). Blood glucose levels were tested by tail bleed 15 min prior to the i.p. injection to determine the basal fasted blood glucose levels, and every 15 min after the glucose injection for 90 min, as indicated, to assess the response to glucose challenge. Data are pooled from 4 independent cohorts with 4-5 animals each, and presented as mean ± SEM. In light blue are represented the male mice on chow diet from **Figure S1** for visual comparison, but no statistical analysis was performed, as the animals were not directly compared experimentally. **(A)** Fasting blood glucose levels. **(B)** Blood glucose concentration during IPGTT. **(C)** Blood glucose levels during IPGTT, normalised by subtracting the basal blood glucose level from each mouse individually. **(D)** Total glucose response calculated as AUC of normalised data.

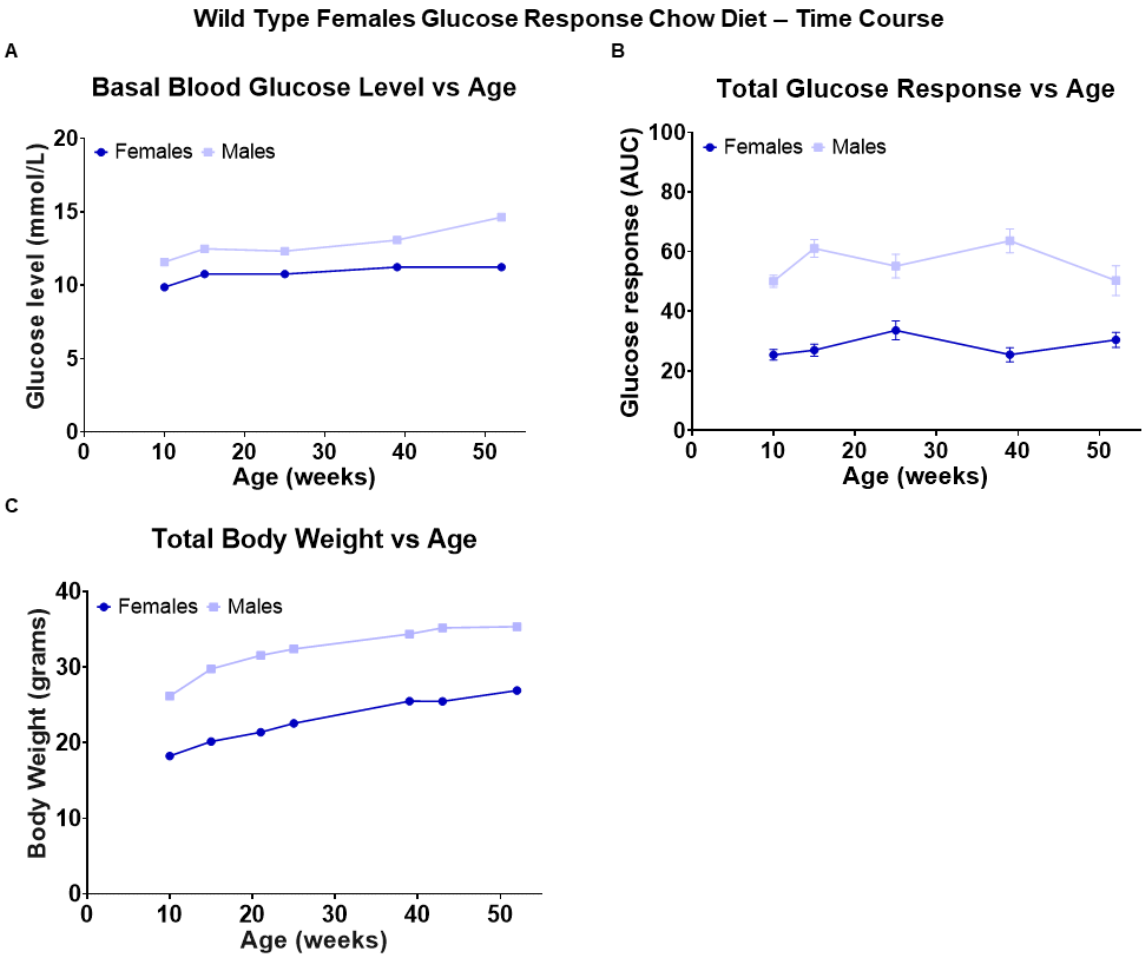

Figure S10: Effects of ageing on the fasting blood glucose levels, response to glucose challenge, and body weight of female Prex WT mice on chow diet.

The fasting blood glucose level, response to glucose challenge, and body weight of the female Prex WT mice in **Figure S9** (dark blue) are expressed as a function of age. Data are pooled from 4 independent cohorts with 4-5 animals each, and are presented as mean ± SEM. In light blue are represented the male mice on chow diet from **Figure S2** for visual comparison, but no statistical analysis was performed, as the animals were not directly compared experimentally. **A)** Fasting blood glucose levels; data from column A in **Figure S9**. **(B)** Response to IPGTT; normalised data from column D in **Figure S9**. **(C)** Total body weight, measured after 6 and 4 h fasting, prior to glucose and insulin challenges, respectively.

Upon insulin challenge, females demonstrated a slightly bigger response to insulin than the males. At 5 months of age, similarly to males, their blood glucose level dropped to its lowest level at 45 min post injection and returned to around 10 mM at 180 min (**Figure S11B**). However, the amplitude of the response was larger, as glucose levels dropped by 7 mM in females compared to 5 mM in males (**Figure S11C**). Interestingly, females retained similar insulin sensitivity at 10 months (30 units), unlike males which showed a slight reduction in their response, suggesting that females on chow diet do not develop age-related insulin resistance. In addition, the response to insulin was longer-lasting in females than males (**Figure S11D**).

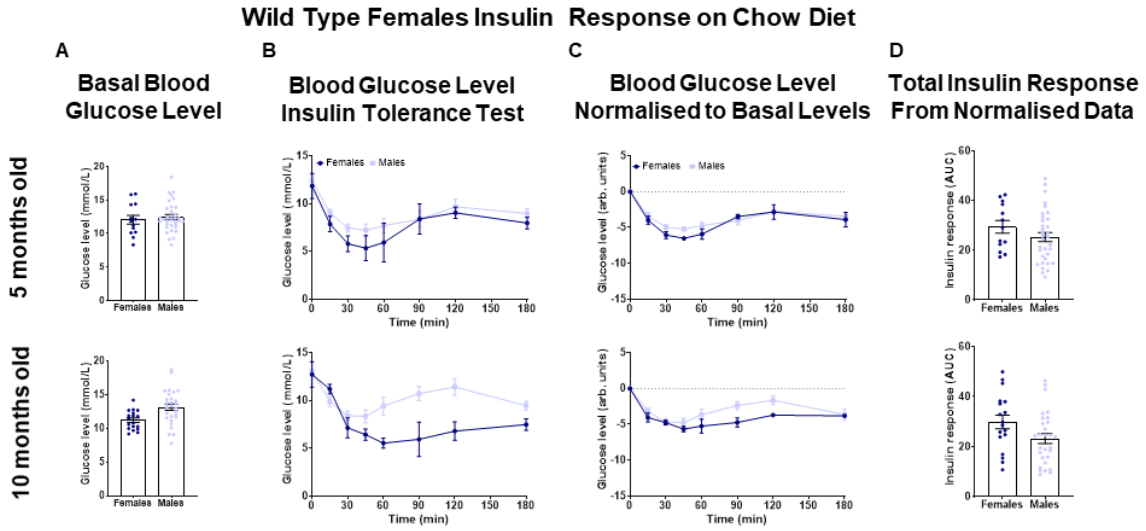

Figure S11: Response of female Prex WT mice on chow diet to insulin challenge.
The female Prex WT mice on chow diet shown in **Figure S9** (dark blue) were subjected to SCITT at the ages of 5 and 10 months. Food was withdrawn 4 h prior to s.c. injection of 0.75 IU/kg of human recombinant insulin at 0.15 IU/ml. Blood glucose levels were tested by tail bleed 15 min prior to the s.c. injection to determine basal blood glucose levels, as well as after the insulin injection at 15, 30, 45, 60, 90,120 and 180 min to assess the response to insulin. Data are pooled from 4 independent cohorts with 4-5 animals each, and are presented as mean ± SEM. In light blue are represented the male mice on chow diet from **Figure S3** for visual comparison, but no statistical analysis was performed, as these animals were not directly compared experimentally. **(A)** Fasting basal blood glucose levels. **(B)** Blood glucose levels during SCITT. **(C)** Glucose levels during SCITT, normalised by subtracting the fasting basal blood glucose level from each mouse individually. **(D)** Total insulin response, calculated as AUC of normalised data.

Finally, Prex WT females gained weight steadily throughout their lives, from

18 g at 10 weeks to 27 g at one year, but remained much lighter throughout than their male counterparts, as expected (**Figure S10C**). Hence, it was surprising to see from their housing in metabolic cages that they had higher water and food intake than the males at the same age. They consumed 0.1 g of water and 0.1 g of food per g of mouse per night, and they produced 0.04 g of urine and 0.04 g of faeces per g of mouse per night (**Figure S12A-D**).

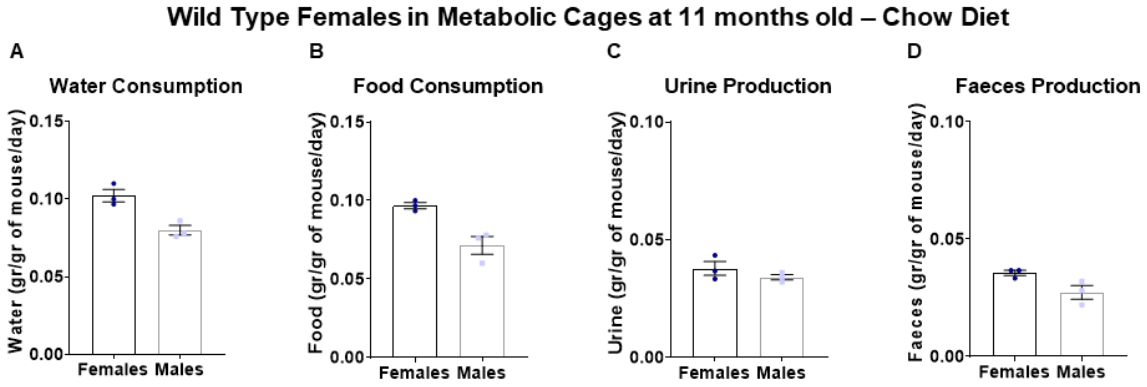

Figure S12: Female Prex WT mice water and food consumption as well as urine and faeces production in metabolic cages.

The female Prex WT mice in **Figure S9** (dark blue) were habituated to metabolic cages at 11 months of age, as detailed in Materials and Methods, weighed and group-housed (up to 3) in metabolic cages overnight for 16 h on 3 subsequent nights with food and water provided *ad libitum*. In light blue are represented the male mice on chow diet from **Figure S4** for visual comparison, but no statistical analysis was performed, as these animals were not directly compared experimentally. Their **(A)** water consumption, **(B)** food consumption, **(C)** urine production, and **(D)** faeces production were measured after each night and were normalised to the combined body weights of the mice housed in each cage. Data are pooled from 6 independent cohorts with 4-5 animals each, and are presented as the mean ± SEM of each night (n=3).

4. Metabolic phenotype of female Prex WT mice on HFD

Finally, Prex WT females were introduced to HFD after the 10-week glucose challenge. To elucidate the effect of diet, data for females on HFD (dark blue) are compared to those for females on chow diet (light blue).

Figure S13A shows that there was a slight increase in basal blood glucose level due to HFD, from 10 to 12 mM, but not as big as for the males (**Figure S6A**). In contrast, diet had a more striking effect on glucose tolerance (**Figure S13B, C**). At 15 weeks of age, IPGTT caused an increase in the glucose levels of females on HFD to 27 mM at 15 min post glucose injection and glucose levels remained high up to 30 min before returning to basal levels at 90 min. At 6 and 9 months, glucose challenge caused a similarly rapid increase, but glucose levels kept rising, reaching a high of 30 mM after 45 min, then declined, but did not return to baseline. Because the females showed worryingly high levels of blood glucose during IPGTT at 9 months of age, we reduced the dose at the 12 months test for some cohorts to half, 1 g/Kg. As previously seen in males, this milder dose reduced the amplitude of the response, but the slow return towards basal levels that is typical for glucose intolerance remained (**Figure S13B-D**). Altogether, the fasting blood glucose levels of females did not change significantly during ageing due to diet (**Figure S14A**), but the glucose tolerance of females on HFD was much worse than that of chow-fed females (**Figure S14B**).

Due to the increased response of females to IPGTT compared to males, we feared that females might also be more sensitive to insulin. In order to avoid causing hypoglycaemic shock, we therefore initially challenged some cohorts of females with a lower dose of insulin (0.5 IU/kg compared to 0.75 IU/kg for males). However, there was no significant drop in glucose levels under these conditions (**Figure S15A-D**). In contrast, insulin challenge at the standard dose of 0.75 IU/kg caused blood glucose levels in 5-month old females on HFD to drop lower than in females on chow diet, reaching a low of 4 mM after 45 min before steadily returning to ~10 mM at 120 min and remaining there until the end of the test (**Figure S15B-D**). At 10 months of age, the insulin sensitivity of HFD fed mice was similar to that of females on chow diet, and their response to insulin was longer-lasting, with blood glucose levels remaining below 10 mM throughout. Hence, as previously seen in males, HFD

caused an increase in insulin sensitivity in both sexes, which we had not expected. However, in males, this improved insulin sensitivity did not persist into old age, whereas it did in females. This resulted in similar blood glucose levels upon insulin challenge despite increased fasting blood sugar levels in female mice on HFD, indicating the existence of robust homeostatic mechanisms of regulation that were not overcome by the HFD.

As expected, females on HFD also gained more weight throughout their lifetime than females on chow diet; however, the effect was not as large as in males, where the difference had been two-fold (**Figure S14C**). Similarly to the males though, females on HFD consumed less water and food and produced less urine and faeces compared to their chow-fed counterparts (**Figure S16A-D**).

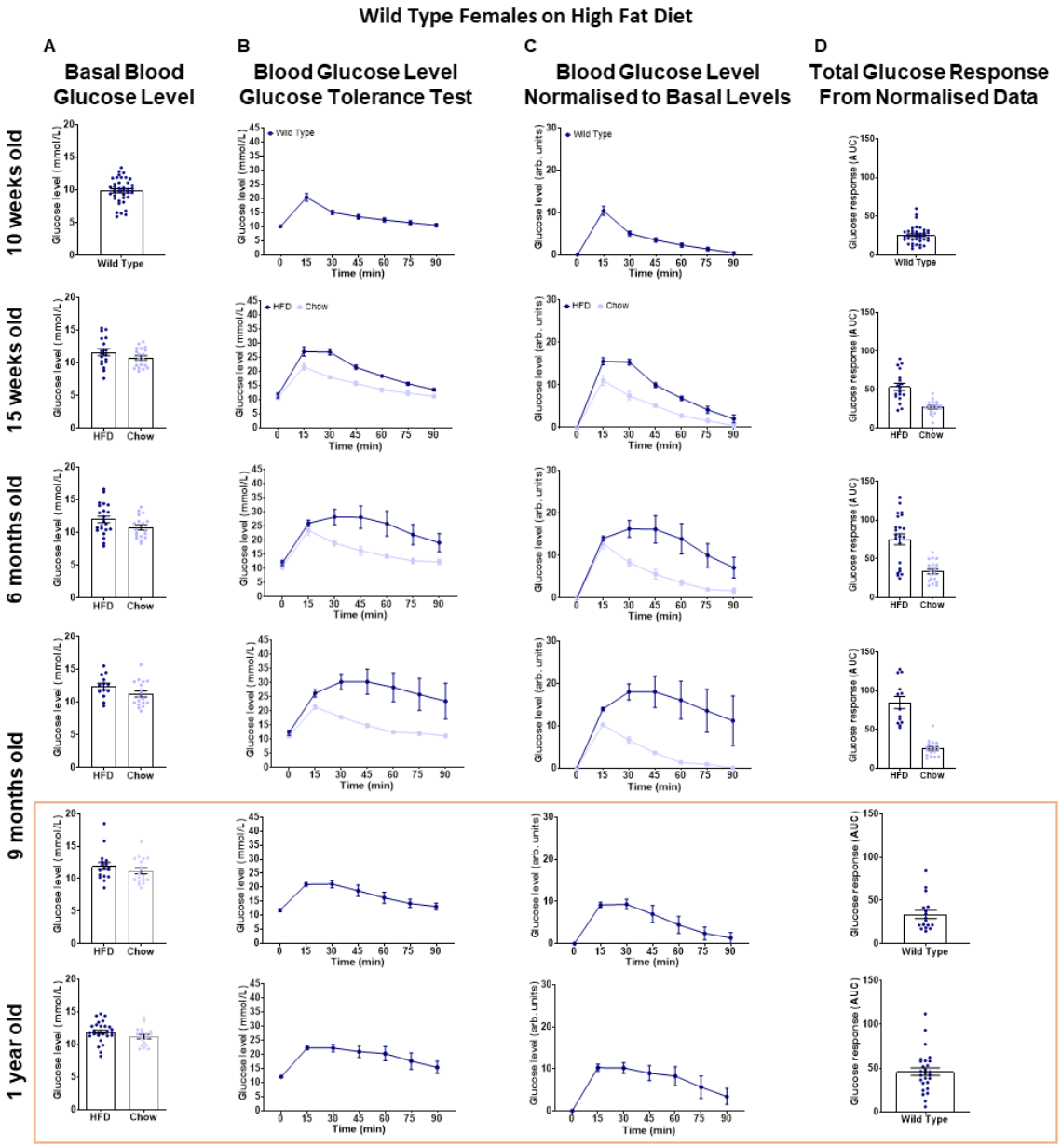

Figure S13: Fasting blood glucose level and response to glucose challenge of female Prex WT mice on HFD.

Female Prex WT mice on 45% HFD (dark blue) were subjected to IPGTT at the ages of 10 and 15 weeks, 6, 9 and 12 months old. Food was withdrawn 6 h prior to i.p. injection of 20% glucose at 10 ml/kg (final concentration 2 g/kg) at 10, 15 weeks, 6, and 9 months old and at 1 g/kg (20% glucose at 5 ml/kg) at 9 and 12 months old – data in ochre box. Blood glucose levels were tested by tail bleed 15 min prior to the i.p. injection to determine the basal fasted blood glucose levels, and every 15 min after the glucose injection for 90 min, to assess the response to glucose challenge. Data are pooled from 7 independent cohorts with 4-5 animals each, and presented as mean ± SEM. In light blue are represented the female mice on chow diet from **Figure S9** for visual comparison, but no statistical analysis was performed, as these animals were not directly compared experimentally. **(A)** Fasting blood glucose levels. **(B)** Blood glucose concentration during IPGTT. **(C)** Blood glucose levels during IPGTT, normalised by subtracting the basal blood glucose level from each mouse individually. **(D)** Total glucose response calculated as AUC of normalised data.

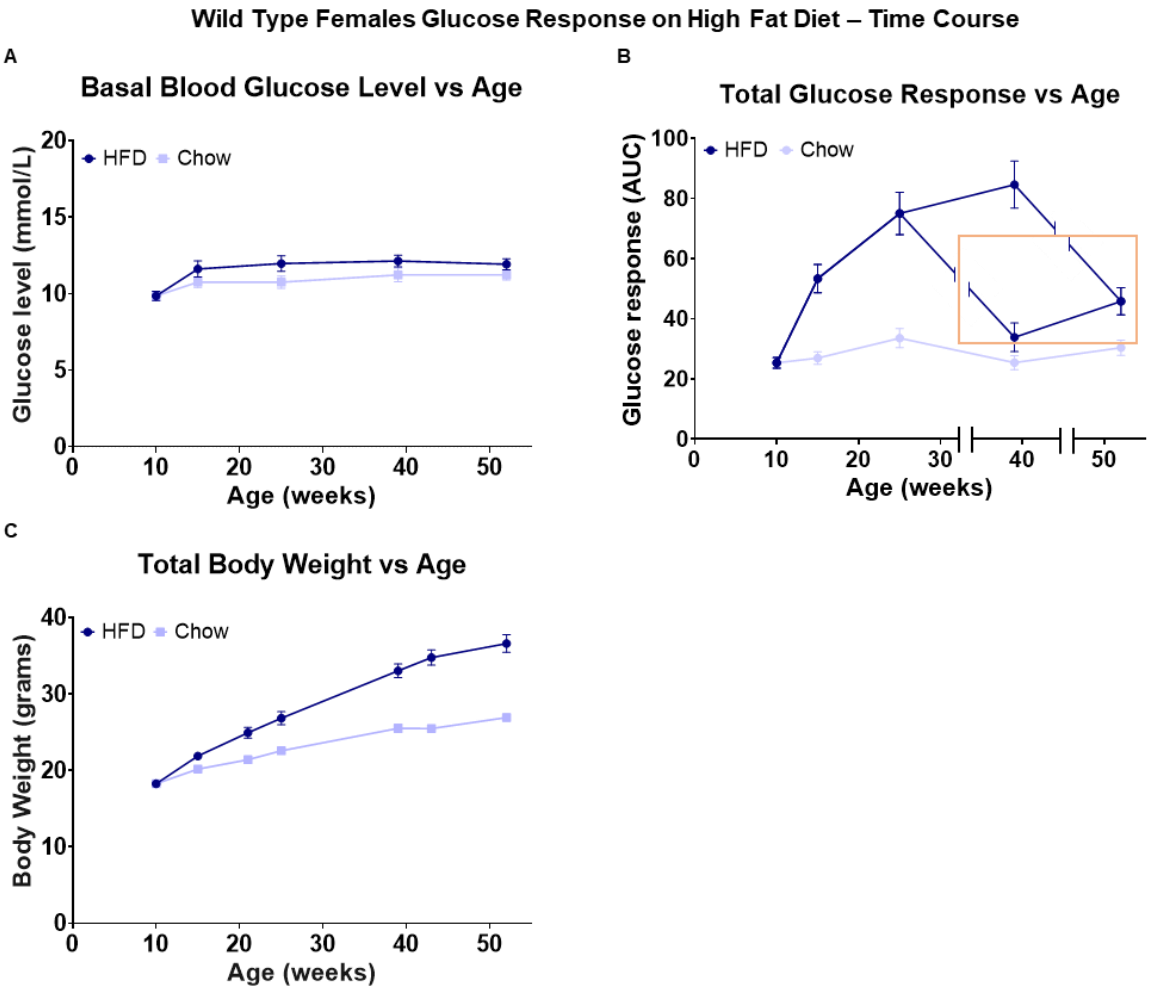

Figure S14: Effects of ageing on the fasting blood glucose levels, response to glucose challenge, and body weight of female Prex WT mice on HFD.

The fasting blood glucose level, response to glucose challenge, and body weight of the female Prex WT mice on HFD from **Figure S13** (dark blue) are expressed as a function of age. Data are pooled from 7 independent cohorts with 4-5 animals each, and are presented as mean ± SEM. Note that the dose of glucose was reduced from 2 g/kg to 0.5 g/kg from the age of 6 months onwards (data in ochre box). In light blue are represented the female mice on chow diet from **Figure S10** for visual comparison, but no statistical analysis was performed, as these animals were not directly compared experimentally. **(A)** Response to IPGTT; normalised data from columns B and C in **Figure S13**. **(B)** Fasting blood glucose levels; data from column D in **Figure S13**. Note that IPGTT was done with 2 g/kg at 10 and 15 weeks as well as 6 and 9 months, but with 1 g/kg at later ages (ochre box). **(C)** Total body weight, measured after 6 and 4 h fasting, prior to glucose and insulin challenges, respectively.

Figure S15: Response of female Prex WT mice on HFD to insulin challenge at 5 months and 10 months of age.

The female Prex WT mice on 45% HFD shown in **Figure S13** (dark blue) were subjected to SCITT at the ages of 5 and 10 months. Food was withdrawn 4 h prior to s.c. injection of 0.15 IU/ml of human recombinant insulin at 0.5 IU/kg (data in green box) or 0.75 IU/kg, as indicated in the figure. Blood glucose levels were tested by tail bleed 15 min prior to the s.c. injection to determine basal blood glucose levels, as well as after the insulin injection at 15, 30, 45, 60, 90,120 and 180 min to assess the response to insulin. Data are pooled from 7 independent cohorts with 4-5 animals each, and are presented as mean ± SEM. In light blue are represented the female mice on chow diet from **Figure S11** for visual comparison, but no statistical analysis was performed, as these animals were not directly compared experimentally. **(A)** Fasting basal blood glucose levels. **(B)** Blood glucose levels during SCITT. **(C)** Glucose levels during SCITT, normalised by subtracting the fasting basal blood glucose level from each mouse individually. **(D)** Total insulin response, calculated as AUC of normalised data.

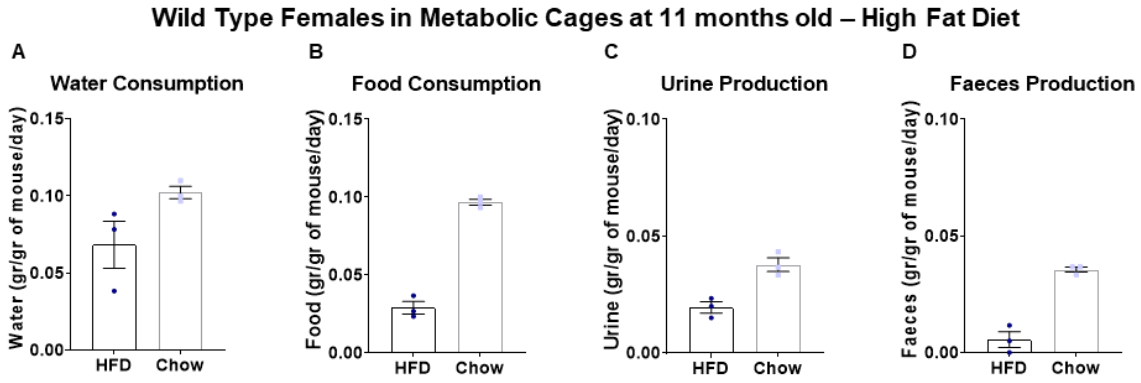

Figure S16: HFD-fed female Prex WT mice water and food consumption as well as urine and faeces production in metabolic cages.

The female Prex WT mice on HFD in **Figure S13** (dark blue) were habituated to metabolic cages at 11 months of age, as detailed in Materials and Methods, weighed and group-housed (up to 3) in metabolic cages overnight for 16 h on 3 subsequent nights with food and water provided *ad libitum*. In light blue are represented the female mice on chow diet from **Figure S12** for visual comparison, but no statistical analysis was performed, as these animals were not directly compared experimentally. Their **(A)** water consumption, **(B)** food consumption, **(C)** urine production, and **(D)** faeces production were measured after each night and were normalised to the combined body weights of the mice housed in each cage. Data are pooled from 7 independent cohorts with 4-5 animals each, and are presented as the mean ± SEM on each night (n=3).

Appendix B - Publications

Sangdun Choi
Editor

Encyclopedia of Signaling Molecules

Second Edition

With 1893 Figures and 247 Tables

Editor
Sangdun Choi
Department of Molecular Science and Technology
Ajou University
Suwon, Korea

ISBN 978-3-319-67198-7 ISBN 978-3-319-67199-4 (eBook)
ISBN 978-3-319-67200-7 (print and electronic bundle)
https://doi.org/10.1007/978-3-319-67199-4

Library of Congress Control Number: 2017951593

Printed on acid-free paper

This Springer imprint is published by Springer Nature
The registered company is Springer International Publishing AG
The registered company address is: Gewerbestrasse 11, 6330 Cham, Switzerland

macrophage Rac1 activation and chemotaxis, in atherogenesis. Prostaglandins Other Lipid Mediat. 2008;87:9–13.
Welch HC. Regulation and function of P-Rex family Rac-GEFs. Small GTPases. 2015;6:49–70.
Welch HC, Coadwell WJ, Ellson CD, Ferguson GJ, Andrews SR, Erdjument-Bromage H, et al. P-Rex1, a PtdIns(3,4,5)P3- and Gbetagamma-regulated guanine-nucleotide exchange factor for Rac. Cell. 2002;108:809–21.
Welch HC, Condliffe AM, Milne LJ, Ferguson GJ, Hill K, Webb LM, et al. P-Rex1 regulates neutrophil function. Curr Biol. 2005;15:1867–73.
Yoshizawa M, Kawauchi T, Sone M, Nishimura YV, Terao M, Chihama K, et al. Involvement of a Rac activator, P-Rex1, in neurotrophin-derived signaling and neuronal migration. J Neurosci. 2005;25:4406–19.

PREX1

- P-Rex
- P-Rex1

P-Rex1

Kirsti Hornigold, Elpida Tsonou,
Chiara Pantarelli and Heidi C. E. Welch
Signalling Programme, Babraham Institute,
Cambridge, UK

Synonyms

G630042G04; KIAA1415; mKIAA1415; NM_020820 (NCBI reference sequence for homo sapiens Prex1 cDNA) / NM_177782 (NCBI reference sequence for mus musculus Prex1 cDNA); Phosphatidylinositol (3,4,5)-trisphosphate-dependent Rac exchanger; PREX1; Prex1

Historical Background

P-Rex1 (PIP_3-dependent Rac exchanger 1, PREX1) is a Dbl-type guanine-nucleotide exchange factor (GEF) that activates Rac-like small G proteins (small GTPases). P-Rex1 was discovered in 2002, during a search for targets of the lipid second messenger phosphatidyl inositol (3,4,5)-trisphosphate (PIP_3) which is generated by phosphoinositide 3-kinase (PI3K) (Welch et al. 2002). At the time, it was known that PI3K can activate Rac and that this activation must occur indirectly, through unknown mediators. P-Rex1 was purified on the basis of its ability to activate recombinant Rac1 in the presence of PIP_3 (Welch et al. 2002). The Gbg subunits of heterotrimeric G proteins, which are released upon the activation of G protein-coupled receptors (GPCRs), were also known to be powerful but indirect activators of Rac in neutrophils. This led to the discovery that P-Rex1 can be also activated by Gbg subunits and that PIP_3 and Gbgs can activate P-Rex1 synergistically, making this Rac-GEF a coincidence detector for cell signaling through PI3K-coupled receptors and GPCRs (Welch et al. 2002).

Since these early discoveries, several other mechanisms of P-Rex1 regulation have been discovered. Knockdown, knockout, and mutational strategies have served to elucidate the varied physiological roles of P-Rex1 in leukocytes, platelets, and endothelial cells during the inflammatory response, in the migration of melanoblasts during development, in the thermogenic potential of adipose tissue, and in social recognition. The evaluation of cancer patients and of murine tumor models has shown that deregulation of P-Rex1 expression occurs in many types of cancer and promotes tumor growth and metastasis. Several detailed reviews have described these discoveries, including our own recent review (Welch 2015). Please refer to this review for all original papers and reviews of the P-Rex literature published up to mid-2014. This allows us to focus here on the most recent discoveries.

Gene and Protein

Structure and Function

The P-Rex1 gene is conserved throughout vertebrates. In the human genome, *PREX1* (NM_020820) is located on chromosome 20q13.13, near a region associated with type 2 diabetes.

PREX1 encodes the 185 kDa protein P-Rex1 (NP_065871). The possibility of splice variants has been proposed but requires further corroboration. The P-Rex1 gene has one homologue, P-Rex2, and both are found throughout the vertebrate kingdom.

The P-Rex1 protein consists of an N-terminal Dbl homology (DH) domain that confers catalytic Rac-GEF activity, in tandem with a pleckstrin homology (PH) domain, followed by two DEP and two PDZ protein interaction domains and homology over its C-terminal half to inositol polyphosphate 4-phosphatase (IP4P) (Fig. 1a). The IP4P domain does not seem to harbor any catalytic phosphatase activity.

Lucato et al. recently reported the first crystal structure of the P-Rex1 DHPH domain tandem in complex with constitutively active Rac1, at a resolution of 1.95 Å (Lucato et al. 2015). The P-Rex1 DH domain is composed of six main a-helices, arranged into an elongated bundle, as is typical of Dbl-family Rho-GEFs. The extended helix a6 bridges both the DH and PH domains and allows significant flexibility between these domains, which is also common in Dbl-family Rho-GEFs. This arrangement effectively orientates the PH domain away from the DH domain. Similar structures were recently reported by Cash et al., who also crystalized the P-Rex1 DHPH domain tandem in complex with nucleotide-free Rac1 or Cdc42, at a resolution of 3.3 Å and 3.2 Å, respectively (Cash et al. 2016) (Fig. 1b).

These crystal structures showed that the P-Rex1 DH domain alone confers Rac1 activation (Lucato et al. 2015; Cash et al. 2016). The DH domain makes multiple contacts with Rac1, whereas the PH domain makes none. Among three highly conserved regions of the P-Rex1 DH domain (CR1–3), CR1 and CR3 make extensive contacts with both the switch 1 and switch 2 regions of Rac1. Interactions with switch 1 are formed by Glu56 in CR1 and by Gln197 in CR3, both of which are highly conserved. Interactions with switch 2 are formed by Lys201, Asn238, and Arg242. No contacts occur between P-Rex1 and the Rac1 P-loop, which is consistent with the catalytic domain structures of other Rac-GEFs. Furthermore, Glu56 and Asn238 were confirmed to be essential for catalytic activity and Rac1 binding (Fig. 1b). These residues had previously been predicted to be important, and Glu56/Asn238 mutants are thus already in widespread use as "GEF-dead" forms of P-Rex1.

Through its catalytic GEF activity, P-Rex1 promotes the release of GDP from Rac, allowing excess free cellular GTP to bind and thus inducing the active conformation of Rac that is able to engage its downstream target proteins. In this manner, P-Rex1 controls a wide range of Rac-dependent cellular functions, including responses that depend on the structure of the actomyosin cytoskeleton, such as cell adhesion and migration, but also reactive oxygen species (ROS) production and gene expression (Welch 2015).

P-Rex1 can activate all Rac-like small G proteins (the ubiquitous Rac1, hematopoietic Rac2, neuronal Rac3, and widely expressed RhoG). P-Rex1 can also activate Cdc42-like GTPases in vitro, but not other Rho-family GTPases. (Please see references in Welch (2015) for further reading on substrate specificity). The recent crystal structures of the P-Rex1 DHPH domains in complex with Rac1 or Cdc42 showed that P-Rex can accommodate both these GTPases in vitro. Thus, it remains unclear why P-Rex1-dependent activation of Cdc42 has not yet been seen in vivo. In contrast, modeling of P-Rex1 and RhoA suggested that steric hindrance would not allow RhoA binding, which explains why P-Rex1 cannot activate this GTPase (Cash et al. 2016).

Regulation of Expression

The original purification of P-Rex1 showed that the Rac-GEF is highly abundant in neutrophils, where it makes up 0.1% of the cytosolic protein (Welch et al. 2002). P-Rex1 is also expressed in other types of leukocytes as well as in platelets, endothelial cells, and neurons and at lower levels in many other cell types. Tissue-wise, P-Rex1 is expressed widely throughout the brain and is also present in bone marrow, thymus, spleen, lymph nodes, and lung.

The Tu lab showed in 2011 that P-Rex1 expression can be driven by the binding of transcription factor Sp1 to the *PREX1* promoter, which is situated 190–198 base pairs 5^{0} of the

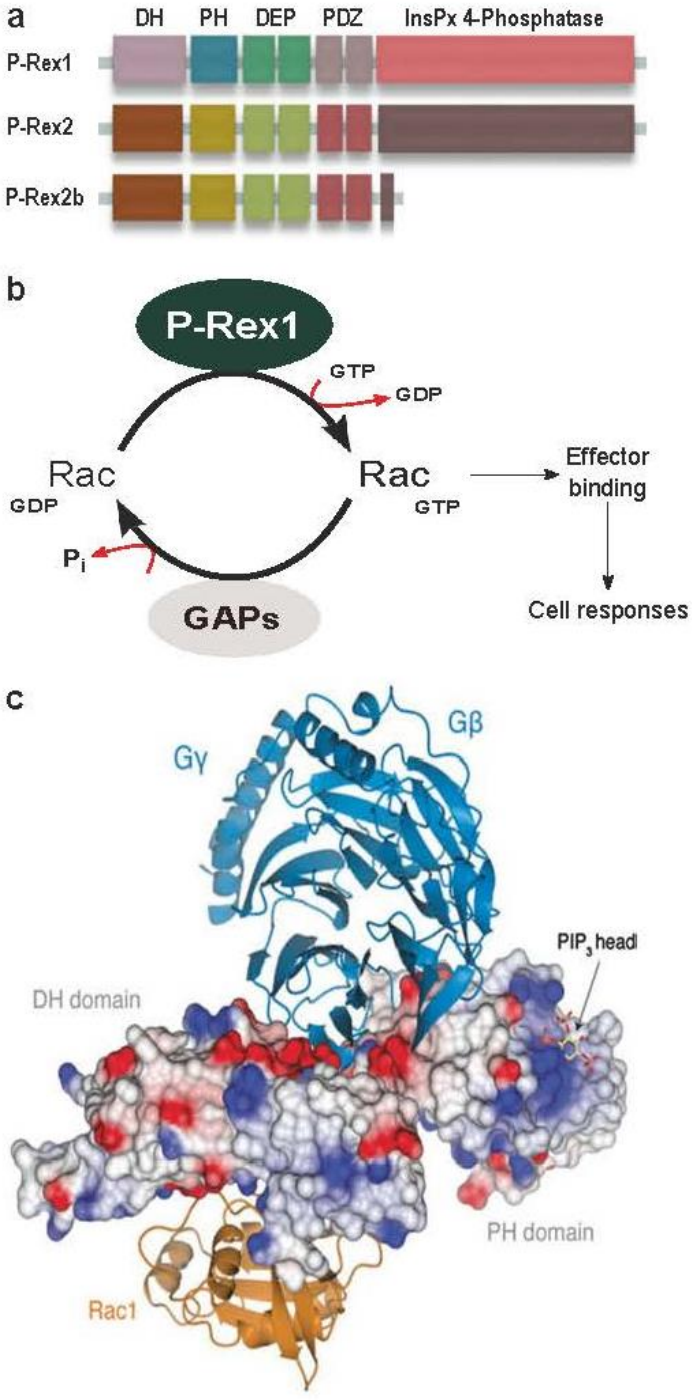

P-Rex1, Fig. 1 P-Rex1 (a) Domain structure: P-Rex family proteins (P-Rex1, P-Rex2, and the splice variant P-Rex2b) are Dbl-type Rho-GEFs that activate the Rac subclass of Rho-family small GTPases. P-Rex Rac-GEFs have an N-terminal catalytic DH domain that confers Rac-GEF activity, in tandem with a PH domain, followed by two DEP and two PDZ protein interaction domains and homology over their C-terminal halves to inositol polyphosphate 4-phosphatase (IP4P). The IP4P domain does not seem to have phosphatase activity and is not present in P-Rex2b. (b) Rac-GEF activity: P-Rex1 can activate all Rac-like small G proteins, the ubiquitous Rac1, hematopoietic Rac2, neuronal Rac3, and widely expressed Rho-G. Binding of Rac to the catalytic DH domain of P-Rex1 promotes the release of GDP from Rac, thus enabling excess free cellular GTP to bind. This induces the active conformation of Rac that engages downstream targets and stimulates cell responses such as ROS production,

coding region. In normal prostate epithelial cells, this transcription was repressed epigenetically by the binding of histone deacetylases (HDACs) to the promoter and the deacetylation of promoter-associated histone H4. In metastatic prostate cancer cells, this HDAC-mediated repression was lost, thus resulting in increased H4 acetylation and deregulated P-Rex1 expression. It was proposed that a locus-specific increase in H4 acetylation induces an open chromatin conformation which favors *PREX1* transcription. It remains to be shown how the association of Sp1 and HDACs with the locus is controlled. A further mechanism of P-Rex1 expression was recently discovered that causally links P-Rex1 deregulation to drug resistance of prostate carcinoma cells. In drug-resistant cells, the transcription factor Myc was upregulated, and binding of Myc to a consensus site in the *PREX1* promoter induced *PREX1* transcription (see also section 5) (Goel et al. 2016).

A recent study by the Kazanietz lab identified hypermethylation of CpG islands in the promoter and transcriptional start regions of *PREX1* as a major mechanism to suppress P-Rex1 expression in normal breast epithelial cells, together with regulation by HDACs (Barrio-Real et al. 2014). Treatment of mammary epithelial cells with a demethylating agent and HDAC inhibitors was sufficient to drive P-Rex1 expression. *PREX1* promoter methylation was found to be reduced in luminal breast tumors and was associated with ER-positive status. Importantly, hypomethylation was also correlated with high P-Rex1 expression and with poor long-term survival of breast cancer patients (Barrio-Real et al. 2014).

Regulation

Full-length P-Rex1 has a low basal catalytic Rac-GEF activity and is activated by through the release of intramolecular inhibition, which can be brought about by several mechanisms in response to cell stimulation. This mode of activation was first proposed in a P-Rex1 mutagenesis study by Hill et al. in 2005 and was supported by the recent crystal structures of the DHPH domain tandem (Lucato et al. 2015; Cash et al. 2016). Please also see reference (Welch 2015) for a detailed review and citations of the original literature up to 2014 on the mechanisms that regulate the catalytic activity and subcellular localization of P-Rex1.

PIP_3 and Gbg

P-Rex1 can be directly activated by PIP_3 and Gbg, either independently or synergistically. Synergistic activation allows for coincidence detection of signaling through PI3K-coupled receptors and GPCRs, a unique feature of the P-Rex family that enables the integration of highly complex signaling pathways. P-Rex1 Rac-GEF activity is stimulated more than 30-fold by PIP_3 (EC_{50} 1.5 mM) and with similar efficacy by Gbg subunits, which bind full-length P-Rex1 at 1:1 stoichiometry (K_D 0.3 mM).

Hill et al. first showed that PIP_3 binds to the PH domain of P-Rex1. This was confirmed by a crystal structure of the P-Rex1 PH domain, which was solved in complex with the soluble PIP_3 analogue inositol-1,3,4,5-tetraphosphate (IP_4) at a resolution of 2 Å (Cash et al. 2016). The PH domain was shown to form a seven-stranded antiparallel

P-Rex1, Fig. 1 (continued) migration, and gene expression. (c) Crystal structure of the catalytic core: Crystal structure of the DHPH domain tandem of P-Rex1 (electrostatic surface view) in complex with Rac1, shown alongside modeling of Gbg and PIP_3 binding. This research was originally published in the Journal of Biological Chemistry (Lucato et al. 2015 # the American Society for Biochemistry and Molecular Biology) and is reproduced here with kind permission from the authors. The crystal structure confirmed that residues Glu56 and Asn238 in the P-Rex1 DH domain are crucial for Rac1 binding, and that the DH domain is sufficient for catalysis. The modeling suggested furthermore that PIP_3 and Gbg binding sites are likely situated away from the Rac1 binding site and that Gbg might contact both the P-Rex1 DH and PH domains. Cash et al. (2016) reported a similar structure and also crystalized the PH domain in complex with the soluble PIP_3 analog IP_4, which revealed that Lys280, Arg289, and Lys368 in the PH domain are required for PIP_3 binding

b-sandwich, capped at one end by a C-terminal a-helix, whereas the other end is open and features loops that are typically involved in ligand binding or membrane interactions. IP_4 bound within the open end of the b-sandwich, in a pocket lined with basic residues that tightly coordinate the 3- and 4-phosphates of the inositol ring. Deep within the binding pocket, Lys280 interacted with the 3- and 4-phosphates, Arg289 with the 3-phosphate, and Lys368 with the 4- and 5-phosphates of IP_4. Accordingly, mutations of Lys280, Arg289, and Lys368 all reduced IP_4 binding (Cash et al. 2016). The affinity of IP_4 for the PH domain was K_D 0.4 mM, whereas a soluble analog of phosphatidyl inositol (3,4)-bisphosphate ($PI(3,4)P_2$) bound to a lesser extent (Cash et al. 2016). This confirmed the previous observation that although P-Rex1 can bind both PIP_3 and $PI(3,4)P_2$, only PIP_3 can stimulate the GEF activity (Welch et al. 2002).

A study by the Garrison lab in 2006 showed that a range of different Gb and Gg protein dimers can stimulate P-Rex1 Rac-GEF activity, with the exception of Gb_5g_2. The potency with which the various Gbg combinations could activate P-Rex1 matched their effects on another Gbg effector, PI3Kg. We showed that Gbgs activate P-Rex1 primarily through the DH domain in vitro, and the Itoh lab found that other P-Rex1 domains contribute to Gbg binding in vivo (Welch 2015). The Gbg binding site was recently modeled on the crystal structures of P-Rex1:Rac1 and GRK2:Gbg complexes, which suggested that a negatively charged surface patch of P-Rex1 could accommodate Gbg with few steric clashes (Lucato et al. 2015). In this model, Gbg would contact both the DH and PH domains, sit on the opposite side of P-Rex1 to Rac1, and not make any contacts with the GTPase (Fig. 1b).

Phosphorylation

Barber et al. reported in 2012 that P-Rex1 can bind the serine phosphatase PP1a through an RVxF motif in its IP4P domain. PP1a (and to a lesser extent also PP1b) could stimulate the Rac-GEF activity of P-Rex1 directly, around two-fold, by dephosphorylating several residues in the C-terminal half. Ser1165 was identified as the major target site, and a S1165A mutation was sufficient for P-Rex1 activation (Fig. 2). In addition, a recent study showed that stimulation of hippocampal neurons through the ionotropic glutamate receptor NMDAR leads to increased binding of PP1a to P-Rex1 (Li et al. 2015). It remains to be shown which kinase(s) phosphorylate the PP1a target sites.

The Garrison lab first showed in 2006 that cAMP-dependent kinase (PKA) inhibits P-Rex1 by blocking Gbg binding and the activation by PIP_3. A recent study identified the PKA binding site and one of the PKA target sites (Fig. 2). The regulatory subunit of PKA was shown to interact with the PDZ1 domain of P-Rex1 through its C-terminal cAMP-binding domain, and the catalytic domain of PKA was found to phosphorylate Ser436 in the DEP1 domain (Chavez-Vargas et al. 2016). In endothelial cells, PKA inhibited P-Rex1-dependent Rac1 activity and cell migration, whereas an S436A mutant of P-Rex1 was insensitive to PKA inhibition (Chavez-Vargas et al. 2016). Furthermore, the DEP1 domain of P-Rex1 was shown to interact with the isolated DHPH domain tandem, whereas a DEP1-S436A mutant could not, suggesting that PKA-dependent phosphorylation of Ser436 confers an inhibitory intramolecular interaction. Similarly, PKA also strengthened the inhibition of the DHPH core by the C-terminal half of P-Rex1, indicating that additional PKA target residues may lie in the C-terminus (Fig. 2). Interestingly, phosphorylation of Ser436 did not affect the interaction of P-Rex1 with Gbl (or mTOR) (Chavez-Vargas et al. 2016), suggesting that PKA regulates Gbg binding through a separate mechanism. Finally, it is unlikely that PKA is the kinase which counteracts the activation of P-Rex1 by PP1a, because the main PP1a target residue, Ser1165, does not lie within a PKA consensus sequence.

Recent work identified phosphorylation by p21-activated kinase (PAK) as a further mechanism to inhibit P-Rex1 (Barrows et al. 2016). PAKs were shown to phosphorylate P-Rex1 in response to stimulation of receptor tyrosine kinases (RTKs), PAK2 could phosphorylate P-Rex1 directly in vitro, and phosphorylation by PAK1 reduced the PIP_3-stimulated Rac-GEF activity of P-Rex1

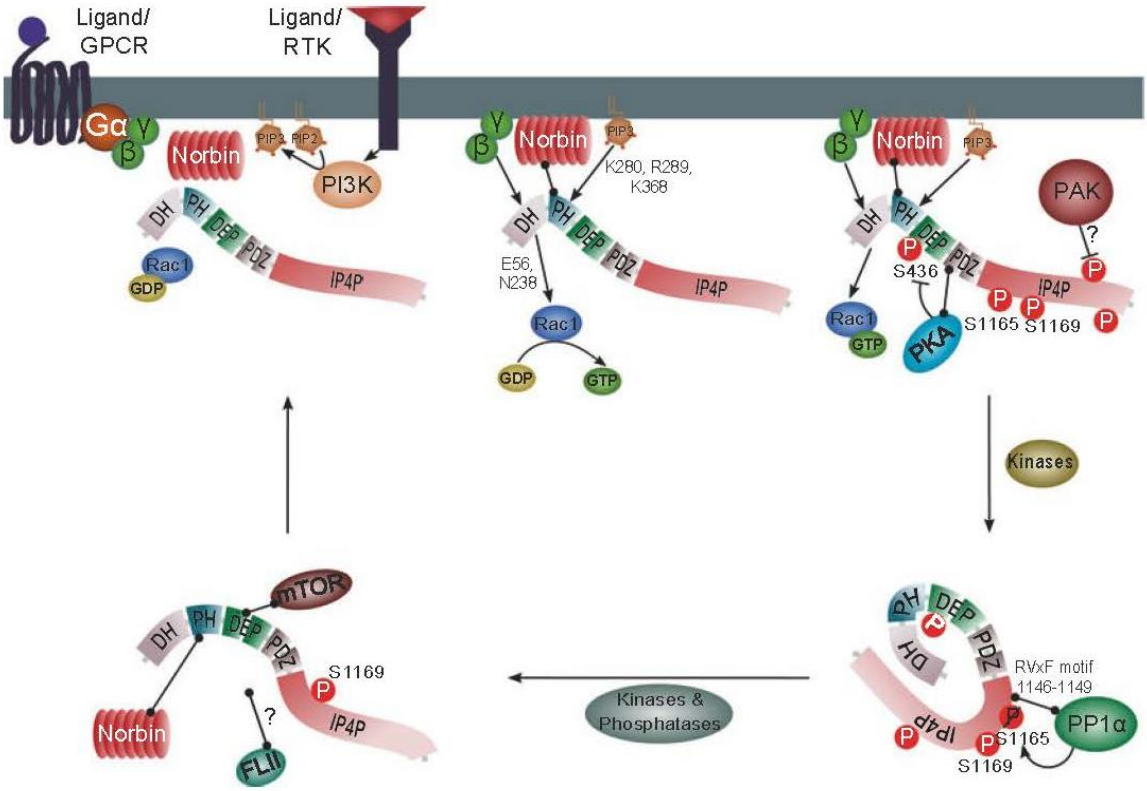

P-Rex1, Fig. 2 P-Rex1 regulation and binding partners. Depicted are direct interactions of P-Rex1 with its regulators, substrate, and binding proteins. *Arrows* denote activation, *blunt ends* show inhibition, and *bobble-ends* show direct binding. In basal cells: P-Rex1 is largely cytosolic and has low basal Rac-GEF activity, due to intramolecular inhibition. In the cytosol, P-Rex1 binds constitutively to the serine phosphatase PP1a, the GPCR adaptor protein Norbin, the protein kinases PKA and mTOR and the gelsolin superfamily adaptor protein FLII. PP1a binds to the RVXF motif (residues 1146–1149) of P-Rex1 and dephosphorylates Ser1165, which is sufficient to weakly stimulate P-Rex1 Rac-GEF activity. This interaction between PP1a and P-Rex1 was recently shown to increase in neurons upon NMDAR stimulation. Norbin binds to the PH domain, induces a robust membrane translocation of P-Rex1 and also weakly stimulates Rac-GEF activity. FLII binds P-Rex1 constitutively (at an unknown site), and P-Rex1 mediates an interaction of FLII with Rac1-GTP that promotes cell migration and contraction. In addition, P-Rex1 binds constitutively to mTOR through its DEP domains and forms part of TORC1 and TORC2. P-Rex1 affects mTOR responses (and likely also vice versa), but the underlying mechanisms remain to be elucidated. It also remains to be shown if the interactions of P-Rex1 with Norbin, FLII and mTOR are affected by cell stimulation. Upon cell stimulation: Both the membrane association and the catalytic activity of P-Rex1 are increased upon cell stimulation, through various mechanisms that cause release of intramolecular inhibition. P-Rex1 is directly activated by the lipid second messenger PIP_3, which is generated by PI3K, and by the Gbg subunits of heterotrimeric G proteins. PIP_3 binds to the PH domain, and activation by Gbg occurs through the DH domain, although further domains are involved in Gbg binding in vivo. PIP_3 and Gbg can activate P-Rex1 independently, but also synergistically. This synergistic activation makes P-Rex1 a coincidence detector for the concomitant stimulation of PI3K-coupled receptors and GPCRs. As well as Rac-GEF activity, PIP_3, and Gbg also synergistically stimulate the membrane localization of P-Rex1. Other mechanisms of P-Rex1 activation include Norbin binding and dephosphorylation by PP1a (as described here-above), as well as the phosphorylation of Ser1169 by unidentified serine kinases. Interestingly, the equivalent site in P-Rex2 (Ser1107) is phosphorylated by PAK, an inhibitor of P-Rex Rac-GEFs. Negative regulation: PKA binds to the PDZ1 domain and inactivates P-Rex1 by phosphorylating Ser436 in the DEP1 domain, which promotes an inhibitory intramolecular interaction with the catalytic core. In addition, PKA also regulates (possibly indirectly) an intramolecular interaction of the C-terminal half with the catalytic core. The Rac1-GTP-dependent kinase PAK can also phosphorylate P-Rex1 directly (at unknown sites) and inhibits P-Rex1 activity (possibly indirectly) within cells, which led to the proposal of a negative feedback loop involving P-Rex1, Rac1, and PAK to limit P-Rex1 signaling

in a broken-cell assay (Barrows et al. 2016). As PAKs are activated by Rac1-GTP, the existence of a negative feedback loop to limit P-Rex1 activity was proposed (Barrows et al. 2016). The PAK target residue in P-Rex1 remains to be identified, but the Parsons lab recently found Ser1107 in the P-Rex1 homologue P-Rex2 to be phosphorylated by PAK. Interestingly, the Pandiella lab had previously demonstrated that phosphorylation of the equivalent site in P-Rex1, Ser1169, by unknown kinases in breast cancer cells is associated with activation rather than inhibition.

The Pandiella lab had also identified that phosphorylation of Ser313 limits P-Rex1 Rac-GEF activity. Interestingly, the crystal structure of the P-Rex1 DHPH domain revealed that Ser313 lies within the b3/b4 loop of the PH domain, which is thought to be highly mobile. On this basis, Lucato et al suggested that phosphorylation of Ser313 might enable the b3/b4 loop to interact with the DH domain to sterically inhibit Rac1 binding (Lucato et al. 2015). Apart from PAK, further kinases and phosphatases that modulate P-Rex1 phosphorylation in response to RTK stimulation remain to be identified. mTOR was investigated by the Pandiella lab as a possible candidate in breast cancer cells and was largely ruled out. Furthermore, PKCd and Akt were shown by the Ye and Bae labs to activate P-Rex1 in various cell systems, but it is unknown if the effects of these kinases are direct. In addition, various reports suggested that Akt can be a downstream target as well as an upstream regulator of P-Rex1 (e.g., in breast cancer).

Subcellular Localization

P-Rex1 is largely cytosolic in basal cells and must translocate to the plasma membrane in order to activate Rac upon cell stimulation. PIP_3 and Gbg are both membrane-bound signals. Early studies by us and by the Bokoch lab showed that these signals synergistically mediate the membrane translocation of P-Rex1, as well as its activation, although PIP_3 alone appears to be sufficient in some situations (Fig. 2). Barber et al. showed that membrane-derived purified P-Rex1 is more active than the cytosolic protein. Furthermore, membrane-derived P-Rex1 exhibits different mobility on gels compared to the cytosolic protein. As similar gel mobility shifts are seen upon phosphatase treatment, this suggested that P-Rex1 phosphorylation may contribute to subcellular localization. Finally, we recently identified the GPCR adaptor protein Norbin as a further regulator of P-Rex1 subcellular localization. Norbin could bind and stimulate the Rac-GEF activity of P-Rex1 directly, but the biggest effect of co-expressing the two proteins was a robust membrane translocation of both. We proposed that Norbin-dependent membrane translocation brings P-Rex1 into closer proximity with its activators PIP_3 and Gbg, thus stimulating the GEF activity (Pan et al. 2016).

Binding Proteins

Apart from Rac and the regulators described above, few binding proteins of P-Rex1 have been identified. Only proteins known to bind P-Rex1 directly are considered here. For further reading on P-Rex1 interactions, please see reference (Welch 2015).

mTOR

The Vazquez-Prado lab identified in 2007 that the serine kinase mTOR binds P-Rex1 directly, through the DEP domains. P-Rex1 interacts with both mTOR-containing protein complexes, TORC1, which is central in cell growth, and TORC2 (also known as PDK2), which controls cell morphology and migration (Fig. 2). More research is required to elucidate if P-Rex1 can regulate both TORC1- and TORC2-dependent cellular processes and to build on evidence by the Vazquez-Prado and Bae labs, which suggests that P-Rex1 can signal both upstream and downstream of mTOR.

FLII

The Malliri lab recently performed a SILAC screen to identify proteins that interact with Rac1 specifically in the presence of P-Rex1. This identified the actin remodeling protein FLII (flightless-1 homolog), a member of the gelsolin superfamily, as a P-Rex1 binding protein

(Marei et al. 2016a). P-Rex1 bound directly to FLII, independently of its Rac-GEF activity. P-Rex1 interacted with the C-terminal GEL domain of FLII, whereas Rac1 bound to the N-terminal LRR domain of FLII. In addition, the actin capping protein TMOD3 was shown to bind Rac1 and FLII more strongly in the presence of P-Rex1 (Marei et al. 2016b). Importantly, P-Rex1 enabled the interaction between Rac1 and FLII in fibroblasts preferentially when Rac1 was GTP-loaded, and the ability of P-Rex1 to induce cell migration and myosin contractility required FLII. Based on these findings, a model was proposed where P-Rex1 activates Rac1 and acts as a scaffold that enables FLII to interact with this active Rac1, thus inducing cell responses that require both Rac1-GTP and FLII (Marei et al. 2016a).

Physiological Roles

Leukocytes, Platelets, and Inflammation

Knockdown of P-Rex1 in neutrophil-like NB4 cells provided the first evidence that P-Rex1 is important for myeloid cell function (Welch et al. 2002), and this was corroborated later in *Prex1*$^{-/-}$ mouse strains generated by us and by the Wu lab (please see also review Welch 2015). *Prex1*$^{-/-}$ neutrophils have defects in toll-like receptor 4 (TLR4)-dependent priming and in GPCR-dependent Rac2 and RhoG activity, ROS production, F-actin polymerization, polarity, and migration. The migration defect comes from a reduction in cell speed (chemokinesis), whereas the directionality of migration (chemotaxis) is normal. The Zarbock lab showed that P-Rex1 mediates the E-selectin-dependent activation of the neutrophil integrin LFA1 under flow conditions, thus controlling the slow rolling of neutrophils along the endothelial vessel wall, as well as the activation of the integrin Mac1, to regulate neutrophil crawling along the vessel wall. In vivo, *Prex1*$^{-/-}$ mice show impaired neutrophil and macrophage recruitment during sterile and septic inflammation (please see references in Welch (2015) for more details).

Neutrophils from mice deficient both in P-Rex1 and the Vav-family Rac-GEF Vav1 have more profound defects in GPCR-dependent Rac activity, ROS formation, adhesion, and migration than cells which lack either the whole P-Rex or the whole Vav family. This suggested that P-Rex1 and Vav1 can cooperate to generate robust levels of Rac activity in neutrophils. We showed recently that *Prex1*$^{-/-}$*Vav1*$^{-/-}$ and *Prex1*$^{-/-}$*Vav3*$^{-/-}$ mice also have more profound impairments in neutrophil recruitment than mice lacking either GEF family (Pan et al. 2015). Intravital imaging revealed that this recruitment defect is caused by the loss of L-selectin- and E-selectin-dependent neutrophil adhesion to the postcapillary endothelial microvasculature prior to extravasation. Surprisingly, this adhesion defect was largely caused by platelets, as P-Rex1/Vav deficiency in platelets was sufficient to block neutrophil adhesion to the vessel wall. *Prex1*$^{-/-}$*Vav1*$^{-/-}$ and *Prex1*$^{-/-}$*Vav3*$^{-/-}$ platelets had low surface levels of the selectin-ligand PSGL-1, and the mice showed a reduced occurrence of platelet-neutrophil adhesion in the circulation, which is prerequisite for leukocyte extravasation (Pan et al. 2015). Furthermore, platelet P-Rex1 and Vav were also important for the recruitment of other types of inflammatory cells. During allergic inflammation, the pulmonary recruitment of eosinophils, monocytes and lymphocytes was compromised by *Prex1*$^{-/-}$*Vav1*$^{-/-}$ or *Prex1*$^{-/-}$*Vav3*$^{-/-}$ platelets, and airway inflammation was essentially abolished in *Prex1*$^{-/-}$*Vav1*$^{-/-}$ and *Prex1*$^{-/-}$*Vav3*$^{-/-}$ mice, resulting in improved airway responsiveness (Pan et al. 2015). In contrast work by the Ye lab in 2012 showed that *Prex1*$^{-/-}$ mice only have a mild defect in blood clotting, and *Prex1*$^{-/-}$ platelets show partial impairments in GPCR-dependent aggregation and dense granule secretion. Together, these studies suggest therefore that P-Rex1 plays a preferential role in inflammatory rather than hemostatic platelet functions.

Recently, the Ye lab showed P-Rex1 to be required for pulmonary fibrosis, a late phase of pulmonary inflammation which can result in loss of lung function. In a model of pulmonary fibrosis, both early leukocyte infiltration and the development of fibrosis were reduced in *Prex1*$^{-/-}$ mice, which drastically increased survival (Liang et al. 2016). The lungs of *Prex1*$^{-/-}$ mice showed

reduced accumulation of extracellular matrix proteins and other markers of fibrosis, as well as impaired production of the cytokine TGFb1, which is required for disease development. Finally, primary fibroblasts isolated from the lungs of *Prex1*$^{-/-}$ mice showed reduced TGFb1-induced signaling and cell migration (Liang et al. 2016).

In summary, P-Rex1 plays many different roles in inflammation. An important question for future inflammation research is whether deregulation of P-Rex1 expression occurs in human immune-deficiencies or inflammatory conditions.

Endothelial Cells and Vascular Biology

Control of endothelial cell function by P-Rex1 was first demonstrated in 2010 by the Vázquez-Prado lab who showed that knockdown in human microvascular endothelial cells (HMEC) inhibits SDF1-stimulated Rac1 activity, chemotaxis and in vitro angiogenesis. Since then, the Ye lab found that P-Rex1 also contributes to the temporary decrease in barrier function that the vascular endothelium undergoes under inflammatory conditions. This was demonstrated by P-Rex1 knockdown in human lung microvascular endothelial cells (HLMVEC), which increased endothelial barrier function through effects on Rac1 activity, VE-cadherin phosphorylation and ROS formation. TNFa-stimulated "transmigration" of neutrophils across HLMVEC monolayers with P-Rex1 depletion suggested that endothelial P-Rex1 may regulate leukocyte recruitment. In addition, the Voorberg lab showed in primary human umbilical vein endothelial cells (HUVECs) that endothelial P-Rex1 can also mediate Weibel-Palade body secretion, a process required for the upregulation of P-selectin on the endothelium and for the capture of leukocytes from the blood stream during inflammation. Thus, endothelial P-Rex1 appears to have roles in inflammation and angiogenesis that merit further study in vivo.

Neurons and Behavior

P-Rex1 is widely expressed throughout the nervous system. Its functional roles in neurons were first investigated in 2005 by the Hoshino lab, who used knockdown and a dominant-negative DDH mutant of P-Rex1 in PC12 cells to inhibit NGF-stimulated Rac1 activity, lamellipodia formation, membrane ruffling, cell spreading and migration. More recently, the Vanderhaeghen lab used ectopic expression of a DDH mutant in mouse embryos to suggest that P-Rex1 controls the ephrin-B1 dependent migration of pyramidal neurons within the cortex during development. However, it should be emphasized that *Prex1*$^{-/-}$ mice show no overt defects in cerebral development. We also reported in 2008 that *Prex1*$^{-/-}$ mice have normal cerebellar morphology and synaptic plasticity, as well as normal motor behavior. However, our studies did show that P-Rex1 contributes to the plasticity of Purkinje neurons, as *Prex1*$^{-/-}$*Prex2*$^{-/-}$ mice have an exacerbated impairment in cerebellar long-term potentiation and motor coordination compared to *Prex2*$^{-/-}$ mice. Please see (Welch 2015) for further reading.

An extraordinary recent study found SNPs, copy number deletions and reduced mRNA levels of P-Rex1 in children with autism spectrum disorders (Li et al. 2015). Evaluation of *Prex1*$^{-/-}$ mice in behavioral models of autism revealed deficits in social recognition, reversal learning and fear extinction. Acute knockdown of P-Rex1 in the hippocampal CA1 region of young wild-type mice resulted in similar behavioral defects as seen in *Prex1*$^{-/-}$ mice, suggesting that P-Rex1 expression in the hippocampus is required for social interaction and flexible behaviors (Li et al. 2015). Furthermore, NMDAR-induced long term depression (LTD) was shown to be impaired in in the hippocampal CA1 region of *Prex1*$^{-/-}$ mice.

Remarkably, the impairments in NMDAR-dependent hippocampal LTD, social recognition and behavioral flexibility seen in *Prex1*$^{-/-}$ mice could be rescued by the overexpression of P-Rex1 in pyramidal neurons of the CA1 region of the hippocampus (Li et al. 2015).

This study also provided important mechanistic insight: PPI phosphatases are important mediators of NMDA-stimulated hippocampal LTP, and as PP1a can activate P-Rex1 directly (see above), the interaction of PP1a with P-Rex1 in the hippocampus was investigated. Indeed, NMDA stimulation was found to increase the interaction of PP1a with P-Rex1 in hippocampal slices from the CA1 region (Li et al. 2015). Furthermore,

hippocampal plasticity requires the internalization of the glutamate receptor GluR2 following NMDA stimulation. Hence, the subcellular localization of GluR2 was assessed in NMDA-treated hippocampal neurons, and P-Rex1 deficiency was found to impair the internalization of GluR2. This internalization could be rescued by the re-expression of wild-type P-Rex1 or Rac1, but neither by a P-Rex1 mutant that cannot interact with PP1a (VAFA mutant), nor by catalytically inactive P-Rex1. Thus, the following model was proposed: NMDAR stimulation induces Ca^{2+} influx into neurons, which activates PP1a to dephosphorylate and activate P-Rex1. P-Rex1 then activates Rac1 to mediate both AMPAR endocytosis and the large-scale actin cytoskeletal remodeling required for LTD. Together, the results of this important study have suggested that approaches to restore P-Rex1 function in hippocampal neurons may prove beneficial in the future in the treatment of autism spectrum disorders.

Melanocytes and Pigmentation

The Sansom lab showed in 2011 that *Prex1*$^{-/-}$ mice on C57Bl6 genetic background have the expected black fur but white bellies, feet and tail tips, due to impaired melanoblast migration during development. This migration defect becomes relevant in melanoma, where melanocytes are transformed into melanoma cells. P-Rex1 expression is deregulated in melanoma cells and is critical for melanoma metastasis. A recent follow-on paper from the same lab described *Prex1*$^{-/-}$ mice with an additional melanocyte-specific deletion of Rac1. These mice showed impaired melanoblast proliferation as well as the melanoblast migration defect (the mice had mostly white fur). This showed that P-Rex1 controls melanocyte development not only through Rac1 but possibly also through other Rac-GTPases, such as RhoG. Another possibility is that unknown GEF-independent adaptor functions of P-Rex1 are involved.

Adipocytes and Metabolism

The Mitchell lab showed in 2011 that P-Rex1 is expressed in 3T3-L1 adipocytes, where it controls insulin-stimulated trafficking of the glucose transporter Glut4 and glucose uptake. This is likely to be mediated by the Rac1-GEF activity of P-Rex1, as a dominant-negative Rac1 mutant could block the P-Rex1 dependent membrane localization of Glut4. The Bowden lab also found potential links of P-Rex1 to metabolism, through the identification of SNPs in the 3′ perigenic region of *PREX1* associated with an increased risk of obesity developing into type-2 diabetes. However, it remains to be seen if these SNPs affect P-Rex1 expression or function.

P-Rex1 has also recently been identified as a biomarker of the thermogenic potential of human brown adipocytes (Xue et al. 2015). Immortalized preadipocytes were established from human brown and white adipose tissue, and were screened by microarray profiling for molecular determinants of thermogenic potential. This identified that P-Rex1 expression in preadipocytes correlates with the presence of the brown fat marker UCP1 in differentiated cells. CRISPR-mediated knockout of P-Rex1 in brown adipose precursors showed that the GEF has no effect on the ability of preadipocytes to differentiate into adipocytes. However, P-Rex1 deficiency significantly decreased the expression of UCP1 and other brown fat markers, as well as reducing the basal respiration, proton leak and maximal respiration capacity of differentiated adipocytes. Therefore, P-Rex1 is required for the development of the thermogenic potential of brown adipose cells (Xue et al. 2015). The mechanism through which P-Rex1 regulates gene expression in adipocytes, and its significance for the function of brown adipose tissue in vivo, remain to be investigated.

Zebrafish Development

During zebrafish development, endoderm and mesoderm formation is regulated by the TGF- b-like cytokine Nodal. In 2012, the Stainier lab used morpholino knockdown to show that P-Rex1 controls the persistence and speed of endodermal cell migration. Overexpression of P-Rex1 could partially rescue the migration defect caused by Nodal inhibition. The recent study by the Ye lab on the role of P-Rex1 in pulmonary fibrosis in mice suggests furthermore that this role of

P-Rex1 in TGFb-dependent zebrafish embryonic development be transformed into into a functional role in inflammatory TGFb signaling in mammals (Liang et al. 2016).

Cancer

Overexpression and Mutation

Deregulated P-Rex1 expression is seen in many types of cancer, including melanoma, breast, prostate, kidney, thyroid and colon cancer. P-Rex1 deregulation is sufficient to drive the growth of breast tumors and the metastasis of prostate cancer and melanoma. Many excellent reviews on the roles of P-Rex1 in cancer have recently been published, please see reference (Welch 2015) for citations of these reviews and for an overview. We will focus here on the most recent reports.

Overexpression of P-Rex1 can occur through amplification of the *PREX1* gene, as was first discovered in breast cancer by the Kazanietz lab, or through loss of epigenetic repression in breast and prostate cancer, as described above. In contrast, somatic mutations of P-Rex1 in cancer are rare, although the Tsuchihara lab reported in 2013 mutations in the coding region to occur in lung carcinomas with a frequency of 5%. It remains to be shown if such mutations affect the function of the P-Rex1 in a manner that could promote the growth or spread of lung cancer. Finally, a SNP in the third intron of *PREX1* (rs6066835) was recently identified in a GWAS study to be associated with multiple myeloma and with increased P-Rex1 expression in multiple myeloma plasma cells (Mitchell et al. 2016).

Breast Cancer

The Pandiella and Kazanietz labs first showed in 2010 that, although P-Rex1 is not detected in normal breast tissue, it is expressed in 58% of human breast tumors, particularly the luminal B subtype. Highest levels were reported in advanced tumors and metastases, correlated with estrogen receptor and ErbB2 expression. Disease-free survival of breast cancer patients with high levels of P-Rex1 was significantly reduced. P-Rex1 promoted the viability, proliferation and motility of breast cancer cells, in a Rac-GEF activity dependent manner, within a range of RTK-dependent pathways. Downregulation of P-Rex1 reduced tumor growth in xenograft mouse models of breast cancer.

Sosa et al. reported in 2010 that stimulation of breast cancer cells through the RTK ErbB3 leads to P-Rex1 activation via transactivation of the GPCR CXCR4 (SDF1 receptor), resulting in increased cell growth and migration. Recent follow-on studies by the same lab showed that Hypoxia-Inducible Factor 1a (HIF-1a) upregulates CXCR4 upon ErbB3 activation, and this likely contributes to the aberrant P-Rex1 signaling in breast cancer cells (Lopez-Haber et al. 2016). Furthermore, P-Rex1 expression led to the deregulation of 89 genes in these cells, including the prometastatic metalloproteinase MMP10 which is associated with poor prognosis.

The Engelman lab proposed in 2013 that activating PI3K mutations and ErbB2 amplification in breast cancer cells involve P-Rex1/Rac1 signaling through the Raf/Mek/Erk pathway, and two recent studies found similar pathways (Dillon et al. 2015; Liu et al. 2016). These studies showed furthermore that P-Rex1 affects the expression of the cell cycle regulators Cyclin D1 and $p21^{Cip1}$ (Liu et al. 2016), and that PI3K pathway activity regulates P-Rex1 protein levels in breast cancer cells (Dillon et al. 2015).

Melanoma

The Sansom lab reported in 2011 that, although P-Rex1 is not detectable in adult human skin, it is expressed in 80% of melanomas. Highest expression was found in advanced melanoma and metastases, correlating with invasiveness rather than with N-Ras or B-Raf status. Knockdown of P-Rex1 in human melanoma cells reduced invasiveness, and $Prex1^{-/-}$ mice exhibited a drastic reduction in melanoma metastasis and a significant improvement in survival. Furthermore, the metastasis-promoting role of P-Rex1 was dependent on its Rac1-GEF activity. In addition, a recent study showed that P-Rex1 expression in melanoma cells correlates with high ERK activity, and pharmacological inhibition of MEK or ERK

reduced P-Rex1 expression in these cells (Ryan et al. 2016).

Prostate Cancer

The Tu lab first reported in 2009 that P-Rex1 expression is low in normal human prostate and in primary prostate tumors, but high in advanced tumors and metastases. Knockdown of P-Rex1 in human metastatic prostate cancer cells reduced invasiveness, whereas overexpression induced metastasis of xenografts in immune-deficient mice in a GEF-activity dependent manner. A recent study also implicated P-Rex1 in drug resistance of prostate cancer. Drugs that target vascular endothelial growth factor (VEGF) or its receptor are used to treat prostate cancer, but drug resistance is common. VEGF signaling through the RTK NRP2 and Rac1 was shown to be important for the development of drug resistance by a subpopulation of stem-cell like cancer cells. Expression analysis revealed upregulation of P-Rex1 and the transcription factor Myc in this subpopulation (Goel et al. 2016). Myc was shown to regulate the transcription of P-Rex1 in the drug resistant prostate cancer cells by binding to a consensus site in the *PREX1* promoter 246 bp 5^0 of the transcriptional start. Importantly, downregulation of P-Rex1 restored drug sensitivity, and it increased the survival of mice in xenograft models and in a prostate cancer model driven by transgenic expression of Myc (Goel et al. 2016).

Summary

The biggest progress in P-Rex1 research over the past couple of year arguably came from the availability of structural information of P-Rex1 (Lucato et al. 2015; Cash et al. 2016). Other important contributions were the identification of new functional roles in thermogenic capacity and in social interactions, as well as new roles of P-Rex1 in inflammation, new P-Rex1 binding partners and new mechanisms of regulation. Future directions should include investigations into potential adaptor functions of P-Rex1, and into the possibility of P-Rex1 deregulation in human inflammatory disorders, immune-deficiencies and metabolic syndrome.

The roles of P-Rex1 in tumor growth and metastasis make this Rac-GEF an attractive target for cancer therapy. However, targeting Rac-GEFs is not trivial, because it entails (b)locking the interaction with Rac, which is difficult to achieve with high specificity and efficacy. The development of small-molecule inhibitors for Rac-GEFs is currently widely pursued, but compounds with particular efficacy or specificity for P-Rex1 have not been reported to date. One promising avenue for targeting P-Rex1 could be to inhibit its activation by phosphorylation. Among these phosphorylation events, effective and specific blockade of the kinase that phosphorylates Ser1169 may be a promising path to pursue.

Funding This review was funded by Institute Strategic Programme Grant BB/J004456/1 from the Biotechnology and Biological Sciences Research Council (BBSRC) to the Babraham Institute Signalling Programme. CP is funded by a Targeted PhD studentship from the BBSRC Doctoral Training Programme. ET is funded by a CASE PhD studentship from the BBSRC in collaboration with the Cardiovascular and Metabolic Disease unit of MedImmune, Cambridge.

See Also

► P-Rex

References

Barrio-Real L, Benedetti LG, Engel N, Tu Y, Cho S, Sukumar S, et al. Subtype-specific overexpression of the Rac-GEF P-REX1 in breast cancer is associated with promoter hypomethylation. Breast Cancer Res. 2014;16:441.

Barrows D, He JZ, Parsons R. PREX1 protein function is negatively regulated downstream of receptor tyrosine kinase activation by p21-activated Kinases (PAKs). J Biol Chem. 2016;291:20042–54.

Cash JN, Davis EM, Tesmer JJ. Structural and biochemical characterization of the catalytic core of the metastatic factor P-Rex1 and its regulation by PtdIns(3,4,5)P3. Structure. 2016;24:730–40.

Chavez-Vargas L, Adame-Garcia SR, Cervantes-Villagrana RD, Castillo-Kauil A, Bruystens JG, Fukuhara S, et al. Protein Kinase A (PKA) Type I interacts with P-Rex1, a Rac Guanine Nucleotide Exchange Factor: effect on PKA localization and P-Rex1 signaling. J Biol Chem. 2016;291:6182–99.

Dillon LM, Bean JR, Yang W, Shee K, Symonds LK, Balko JM, et al. P-REX1 creates a positive feedback loop to activate growth factor receptor, PI3K/AKT and MEK/ERK signaling in breast cancer. Oncogene. 2015;34:3968–76.

Goel HL, Pursell B, Shultz LD, Greiner DL, Brekken RA, Vander Kooi CW, et al. P-Rex1 promotes resistance to VEGF/VEGFR-targeted therapy in prostate cancer. Cell Rep. 2016;14:2193–208.

Li J, Chai A, Wang L, Ma Y, Wu Z, Yu H, et al. Synaptic P-Rex1 signaling regulates hippocampal long-term depression and autism-like social behavior. Proc Natl Acad Sci U S A. 2015;112:E6964–72.

Liang Q, Cheng N, Zhang G, Liang Y, Qian F, Wu D, et al. Identification of P-Rex1 as an anti-inflammatory and anti-fibrogenic target for pulmonary fibrosis. Sci Rep. 2016;6:25785.

Liu HJ, Ooms LM, Srijakotre N, Man J, Vieusseux J, Waters JE, et al. PtdIns(3,4,5)P3-dependent Rac Exchanger 1 (PREX1) Rac-Guanine Nucleotide Exchange Factor (GEF) activity promotes breast cancer cell proliferation and tumor growth via activation of Extracellular Signal-Regulated Kinase 1/2 (ERK1/2) Signaling. J Biol Chem. 2016;291:17258–70.

Lopez-Haber C, Barrio-Real L, Casado-Medrano V, Kazanietz MG. Heregulin/ErbB3 signaling enhances CXCR4-driven Rac1 activation and breast cancer cell motility via Hypoxia-Inducible Factor 1alpha. Mol Cell Biol. 2016;36:2011–26.

Lucato CM, Halls ML, Ooms LM, Liu HJ, Mitchell CA, Whisstock JC, et al. The Phosphatidylinositol (3,4,5)-trisphosphate-dependent Rac Exchanger 1:Ras-related C3 Botulinum Toxin Substrate 1 (P-Rex1:Rac1) complex reveals the basis of Rac1 activation in breast cancer cells. J Biol Chem. 2015;290:20827–40.

Marei H, Carpy A, Woroniuk A, Vennin C, White G, Timpson P, et al. Differential Rac1 signalling by guanine nucleotide exchange factors implicates FLII in regulating Rac1-driven cell migration. Nat Commun. 2016a;7:10664.

Marei H, Carpy A, Macek B, Malliri A. Proteomic analysis of Rac1 signaling regulation by guanine nucleotide exchange factors. Cell Cycle. 2016b;15:1961–74.

Mitchell JS, Li N, Weinhold N, Forsti A, Ali M, van Duin M, et al. Genome-wide association study identifies multiple susceptibility loci for multiple myeloma. Nat Commun. 2016;7:12050.

Pan D, Amison RT, Riffo-Vasquez Y, Spina D, Cleary SJ, Wakelam MJ, et al. P-Rex and Vav Rac-GEFs in platelets control leukocyte recruitment to sites of inflammation. Blood. 2015;125:1146–58.

Pan D, Barber MA, Hornigold K, Baker MJ, Toth JM, Oxley D, et al. Norbin stimulates the catalytic activity and plasma membrane localization of the Guanine-Nucleotide Exchange Factor P-Rex1. J Biol Chem. 2016;291:6359–75.

Ryan MB, Finn AJ, Pedone KH, Thomas NE, Der CJ, Cox AD. ERK/MAPK signaling drives overexpression of the Rac-GEF, PREX1, in BRAF- and NRAS-mutant melanoma. Mol Cancer Res. 2016;14:1009–18.

Welch HC. Regulation and function of P-Rex family Rac-GEFs. Small GTPases. 2015;6:1–11.

Welch HC, Coadwell WJ, Ellson CD, Ferguson GJ, Andrews SR, Erdjument-Bromage H, et al. P-Rex1, a PtdIns(3,4,5)P_3- and Gbg-regulated guanine-nucleotide exchange factor for Rac. Cell. 2002;108:809–21.

Xue R, Lynes MD, Dreyfuss JM, Shamsi F, Schulz TJ, Zhang H, et al. Clonal analyses and gene profiling identify genetic biomarkers of the thermogenic potential of human brown and white preadipocytes. Nat Med. 2015;21:760–8.

PREX2

▶ P-Rex
▶ P-Rex2

P-Rex2

Elpida Tsonou, Chiara Pantarelli, Kirsti Hornigold and Heidi C. E. Welch
Signalling Programme, Babraham Institute, Cambridge, UK

Synonyms

DEP domain containing 2; Depdc2; Phosphatidylinositol 3,4,5-trisphosphate-dependent RAC exchanger 2; PREX2; Prex2; PtdIns(3,4,5)-dependent Rac exchanger 2

Historical Background

P-Rex2 (PIP_3-dependent Rac exchanger 2, PREX2) is a Dbl-type guanine-nucleotide

exchange factor (GEF) that activates the small G protein (small GTPase) Rac1, a member of the Rho family. P-Rex2 was discovered in 2004 on the basis of its homology to P-Rex1 (Donald et al. 2004; Rosenfeldt et al. 2004). Like P-Rex1, P-Rex2 is synergistically activated by the lipid second messenger phosphatidyl inositol (3,4,5)-trisphosphate (PIP_3), which is generated by phosphoinositide 3-kinase (PI3K), and by the Gbg subunits of heterotrimeric G proteins, which are released upon the activation of G protein-coupled receptors (GPCRs) (Donald et al. 2004; Li et al. 2005). Studies using genetically modified mice showed that P-Rex2 controls the dendrite morphology and synaptic plasticity of cerebellar Purkinje neurons and thus plays a role in motor coordination (Donald et al. 2008; Jackson et al. 2010). A more recent study in mice revealed that P-Rex2 is also important for glucose homeostasis and insulin sensitivity (Hodakoski et al. 2014). This is likely to be relevant in humans, as reduced levels of P-Rex2 are observed in adipose tissue of insulin-resistant patients (Hodakoski et al. 2014).

Whereas our understanding of the physiological roles of P-Rex2 is still relatively limited, P-Rex2 is widely recognized for its roles in cancer progression. P-Rex2 is the most frequently mutated Rho-GEF in cancer, particularly in melanoma and pancreatic cancer. Deregulatedexpression of P-Rex2 is also seen in many types of cancer (Berger et al. 2012; Waddell et al. 2015). Furthermore, P-Rex2 is a negative regulator of the tumor suppressor PTEN, independently of its Rac-GEF activity (Fine et al. 2009). Through deregulation of its expression and activity, P-Rex2 can promote the growth and invasive migration of cancer cells in vitro and accelerate tumor growth in vivo.

Several reviews have recently evaluated the P-Rex2 literature, including reference (Welch 2015). This allows us to focus here on the newest developments, such as the elucidation of novel mechanisms of P-Rex2 regulation and the discovery that cancer-associated P-Rex2 mutations render the GEF insensitive to negative regulation by PTEN.

Gene and Proteins

The human P-Rex2 gene (*PREX2*; NM_024870) is located on chromosome 8 (8q13.2) in a region linked to aggressive cancers and metastasis. *PREX2* encodes two proteins, the 183 kDa full-length P-Rex2 (PREX2, also known as P-Rex2a; NP_079146) and the 112 kDa splice variant P-Rex2b (NP_079446) (Fig. 1a) (Donald et al. 2004; Rosenfeldt et al. 2004). The possibility of a third 120 kDa isoform, P-Rex2c, has also been proposed (Hodakoski et al. 2014) but requires further corroboration. The P-Rex2 gene and P-Rex2b splice site are conserved throughout vertebrates (Donald et al. 2004).

The P-Rex2 protein has the same domain structure as P-Rex1, consisting of an N-terminal Dbl homology (DH) domain, which harbors the catalytic Rac-GEF activity, in tandem with a pleckstrin homology (PH) domain, followed by two DEP and two PDZ protein interaction domains, and weak homology over the C-terminal half to inositol polyphosphate 4-phosphatase (IP4P). This IP4P domain is not present in the P-Rex2b splice variant and is thought to be devoid of phosphatase activity (Fig. 1a).

P-Rex2 and P-Rex2b activate the small G protein (GTPase) Rac1 (Donald et al. 2004; Joseph and Norris 2005) and possibly also other Rac isoforms, although this remains to be investigated. In vivo, P-Rex2 and P-Rex2b were shown to activate Rac1 but not the other principal Rho family GTPases Cdc42 and RhoA (Donald et al. 2004; Rosenfeldt et al. 2004). P-Rex2 promotes the release of GDP from Rac1, allowing excess free cellular GTP to bind to the GTPase and thus inducing the active Rac1 conformation that is able to engage downstream target proteins (Donald et al. 2004; Rosenfeldt et al. 2004) (Fig. 1b). Through this Rac-GEF activity, P-Rex2 controls a wide range of cellular functions, including responses that depend on the structure of the actomyosin cytoskeleton, such as cell adhesion and migration, but also others such as gene expression. In addition, P-Rex2 serves as a positive regulator of PI3K signaling, through its ability to inhibit the tumor suppressor PTEN

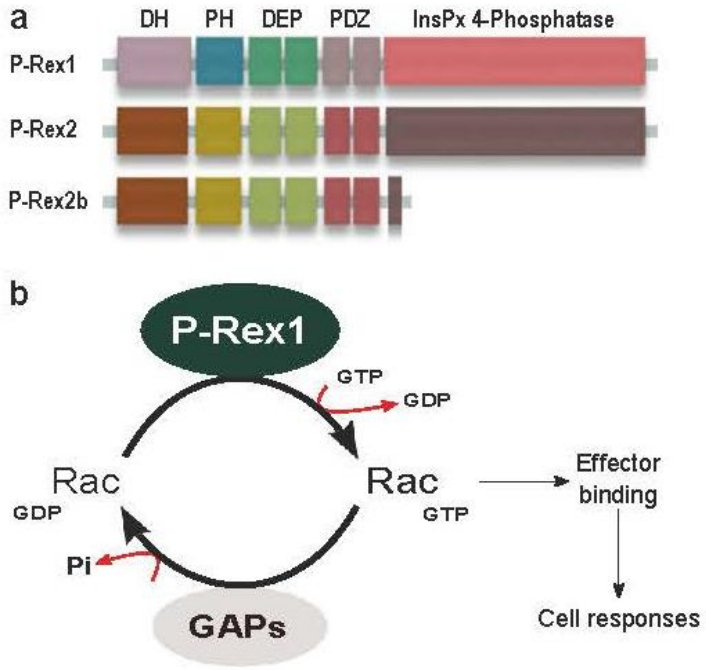

P-Rex2, Fig. 1 (a) Domain structure: P-Rex2 is a typical Dbl-type Rho-GEF that activates the small G protein Rac1. P-Rex2 has the same domain structure as its homologue P-Rex1. Its N-terminal DH domain, which confers Rac1-GEF activity, is followed by a PH domain, two DEP and two PDZ protein interaction domains and weak homology over the C-terminal half to inositol polyphosphate 4-phosphatase (IP4P). P-Rex2b is a splice variant that lacks the IP4P domain. (b) GEF activity: P-Rex2 catalyzes the release of GDP from Rac1, thus allowing excess free cellular GTP to bind and inducing the active Rac1 conformation that is able to engage downstream target proteins. Through this Rac-GEF activity, P-Rex2 controls a wide range of cellular functions, including responses that depend on the structure of the actomyosin cytoskeleton, such as cell migration and synaptic plasticity, but also other responses such as gene expression

(Fine et al. 2009). This inhibition of PTEN is an adaptor function of P-Rex2 that is independent of the catalytic Rac-GEF activity (see below). A catalytically inactive P-Rex2 mutant (E30A/N212A, GEF-dead) was recently developed (Mense et al. 2015) that will help to dissect GEF-activity dependent and independent functions in the future.

P-Rex2 mRNA is detectable in many tissues (Donald et al. 2004). However, the tissue distribution of the P-Rex2 protein is more restricted, being highest in brain (particularly the cerebellum) and lung (Donald et al. 2004; Donald et al. 2008). Notably, P-Rex2 is absent from leukocytes, in contrast to P-Rex1. The splice variant P-Rex2b is found in endothelial cells and in heart (Rosenfeldt et al. 2004; Li et al. 2005). One mechanism that could explain why P-Rex2 mRNA, but not P-Rex2 protein, can be seen in some tissues is through post-transcriptional control by micro-RNAs (miRs). P-Rex2 expression was found to be regulated by the binding of miR-338-3p to the 3^0 UTR of its mRNA, which limited protein production. This repression was lost in human neuroblastoma and gastric cancer cells, resulting in the upregulation of P-Rex2 (Chen et al. 2013; Guo et al. 2014). In neuroblastoma cells, this mechanism was sufficient to induce anchorage-independent cell growth and invasiveness (Chen et al. 2013). Similarly, in gastric cancer cells, blockade of the miR-338 promoter by the transcriptional suppressor MECP2 was sufficient to induce P-Rex2 expression, cell growth, and proliferation (Tong et al. 2016).

Regulators and Binding Partners

As is typical for Rho-GEFs, P-Rex2 and P-Rex2b have low basal catalytic Rac-GEF activity that is

increased upon cell stimulation, through the release of intramolecular inhibition (Fig. 2). Indeed, the isolated catalytic core of P-Rex2 (DHPH domain tandem) is constitutively active compared to the full-length protein (Lissanu Deribe et al. 2016).

PIP_3 and G*bg*

As mentioned above, P-Rex2 and P-Rex2b can be activated by PIP_3 and G**bg**, both in vitro and in vivo (Donald et al. 2004; Rosenfeldt et al. 2004; Li et al. 2005). Furthermore, PIP_3 and G**bg** can activate P-Rex2 either independently or synergistically (Donald et al. 2004). This synergistic mode of activation is unique to the P-Rex family and enables the GEFs to act as coincidence detectors for concomitant signaling through PI3K-coupled receptors and GPCRs.

Recently, the isolated DH domain of P-Rex2 was shown to be sufficient for the G**bg**-mediated stimulation of Rac-GEF activity in vitro, similar to previous findings for P-Rex1 (Welch 2015), and modeling was used to predict that residues Lys254 and Arg263 in the P-Rex2 PH domain are critical for the interaction with PIP_3. Indeed, K254E and R263E mutations were shown to be sufficient to inhibit PIP_3 binding and the PIP_3 mediated stimulation of Rac-GEF activity (Barrows et al. 2015) (Fig. 2). Likewise, the equivalent residues in P-Rex1, Lys280 and Arg289, were shown by Cash et al. to be required for PIP_3 binding (see P-Rex1 chapter). An intriguing early study had proposed that the PH domain of P-Rex2 may also contribute to Rac1 binding (Joseph and Norris 2005). If confirmed, this would suggest a very different mechanism of catalysis for P-Rex2 compared to P-Rex1, given the recent crystal structures of P-Rex1 which showed that the PH domain does not make contact with Rac1. However, as the DH/PH domains of P-Rex1 and P-Rex2 are quite similar, this seems unlikely.

Finally, P-Rex2 is mainly cytosolic under basal conditions, but must translocate to the cell membrane in order to activate Rac1 (Donald et al. 2004). For P-Rex1, it is known that PIP_3 and G**bg** can synergistically stimulate membrane translocation as well as Rac-GEF activity. It seems likely that the same mechanism regulates the subcellular localization of P-Rex2, but this remains to be investigated.

Pten

P-Rex2 binds directly to the tumor suppressor PTEN that blocks PI3K signaling by converting the PI3K product PIP_3 back to $PI(4,5)P_2$ (Fine et al. 2009). This interaction between P-Rex2 and PTEN is conferred by binding of the P-Rex2 PH domain to the catalytic and C2 domains of PTEN and through additional contacts of the P-Rex2 IP4P domain with the C-terminal PDZ-binding domain of PTEN (Fine et al. 2009; Hodakoski et al. 2014) (Fig. 2). The interaction is specific to P-Rex2, as P-Rex1 does not bind PTEN. Importantly, P-Rex2 inhibits the phosphatase activity of PTEN, independently of its Rac-GEF activity. In consequence, P-Rex2 deficiency leads to increased PTEN activity and a suppression of PIP_3 levels and PI3K pathway activity (see below) (Hodakoski et al. 2014). The inhibition of PTEN by P-Rex2 requires phosphorylation of the PTEN tail. However, this phosphorylation seems to occur constitutively, to maintain PTEN stability. Moreover, in mouse embryonic fibroblasts, the P-Rex2 mediated inhibition of PTEN was only seen upon insulin stimulation, whereas in the liver, it occurred constitutively (Hodakoski et al. 2014). Further research is therefore required to determine under which physiological conditions P-Rex2 can inhibit PTEN.

A recent study demonstrated that P-Rex2 not only inhibits PTEN, but inversely, PTEN also regulates P-Rex2 (Mense et al. 2015). PTEN attenuated the P-Rex2-dependent invasive migration of breast cancer cells, independently of its lipid- and protein-phosphatase activities. This suggested that PTEN has an adaptor role, which blocks P-Rex2 function. Indeed, PTEN reduced the Rac1-GEF activity of P-Rex2, both in vitro and upon expression in HEK293 cells, independently of its own catalytic activities (Fig. 3a). Mutational analysis identified furthermore that the most C-terminal amino acids of PTEN are required for the inhibition of P-Rex2-dependent invasive cell migration (Mense et al. 2015). Importantly, P-Rex2 mutants that are frequently

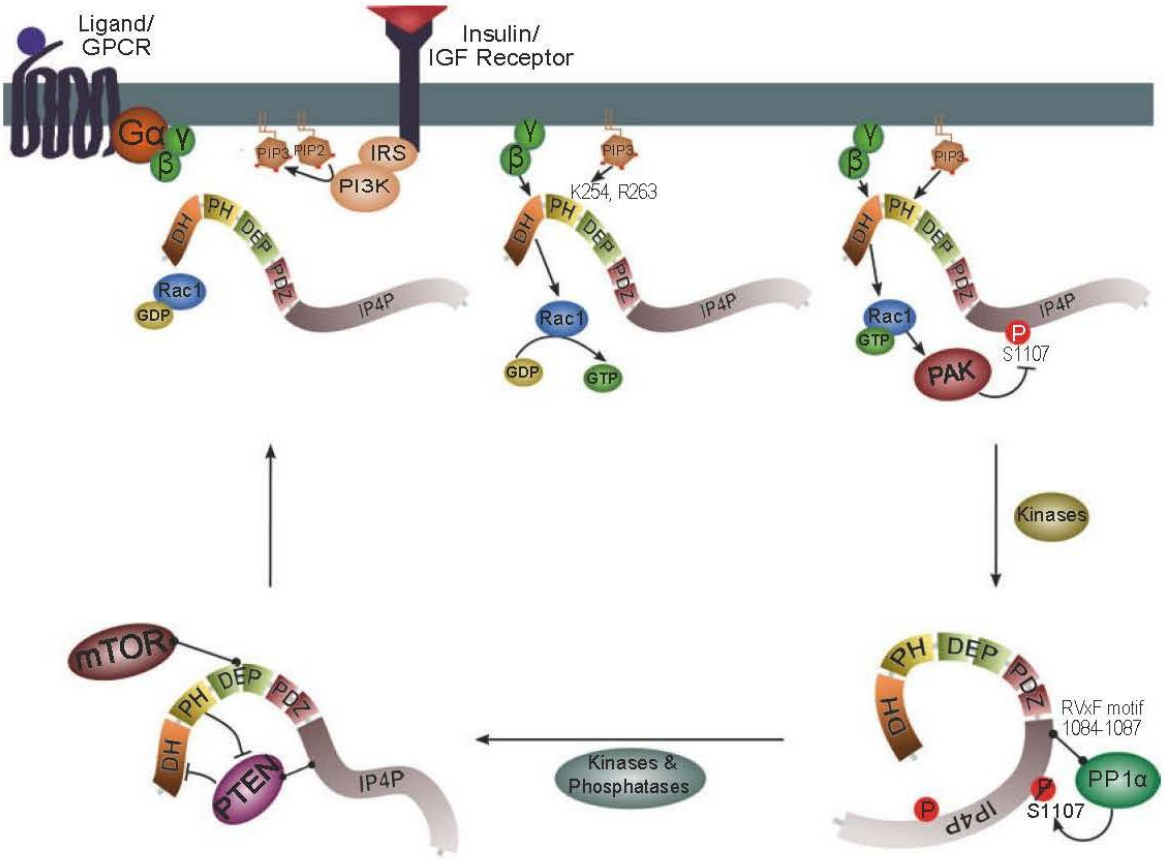

P-Rex2, Fig. 2 Regulation and interacting proteins. *In basal cells*: P-Rex2 is largely cytosolic and has low basal Rac-GEF activity, through intramolecular inhibition. In the cytosol, P-Rex2 constitutively interacts with the tumor suppressor PTEN, the serine phosphatase PP1a, and the serine kinase mTOR. P-Rex2 and PTEN can inhibit each other, independently of their respective catalytic activities (see also Fig. 3). PP1a binds to the RVxF motif (residues 1084–1087) and dephosphorylates Ser1107 of P-Rex2, and possibly other residues. It is likely that PP1a activates P-Rex2, similar to P-Rex1. The consequences of the interaction with mTOR are unknown. *Upon cell stimulation*: P-Rex2 is activated by the lipid second messenger PIP_3, which is generated by PI3K, and by the Gbg subunits of heterotrimeric G proteins, which are released upon stimulation of GPCRs. PIP_3 and Gbg can activate P-Rex2 either individually or synergistically. The DH domain is sufficient for activation by Gbg, whereas Lys254 and Arg263 in the PH domain are required for activation by PIP_3. In order to activate Rac1, P-Rex2 must be recruited to the cell membrane. By analogy with P-Rex1, it seems likely that PIP_3 and Gbg not only activate the Rac-GEF, but also induce its membrane translocation in a synergistic manner. *Negative regulation*: One of the effector proteins of active Rac1 (Rac1-GTP) is the serine kinase PAK. Active PAK can phosphorylate P-Rex2 directly and inhibit P-Rex2 Rac-GEF activity in broken-cell assays. Thus, active P-Rex2 can generate a negative feedback loop from P-Rex2/Rac1/PAK for PAK-mediated inhibition of its own Rac-GEF activity. PAK phosphorylates Ser1107 of P-Rex2, among other residues, but it is unknown if phosphorylation of Ser1107 is sufficient for inhibition

found in cancer were able to escape the inhibition by PTEN, both in vitro and in assays of invasive migration. The P-Rex2 V432M and P948S mutants (which are seen in melanoma and pancreatic cancer, respectively) showed normal binding to PTEN, but the ability of PTEN to inhibit their Rac-GEF activity was reduced (Fig. 3b). In contrast, the melanoma-associated P-Rex2 G844D mutant evaded PTEN inhibition through reduced binding (Mense et al. 2015) (Fig. 3c). It remains to be shown why PTEN could not inhibit the former two P-Rex2 mutants. However, it appears that these mutants retained their ability to inhibit PTEN, as PTEN was unable to suppress Akt phosphorylation in glioblastoma cells expressing the mutants (Mense et al. 2015). In summary,

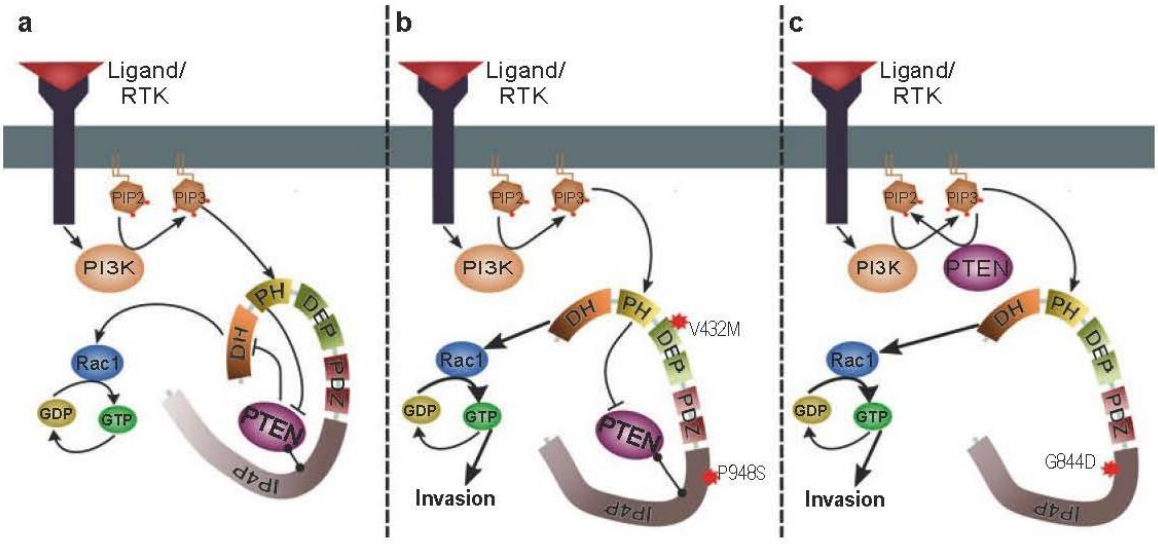

P-Rex2, Fig. 3 Cancer-associated P-Rex2 mutants escape negative regulation by PTEN. (a) *Wild-type P-Rex2*: P-Rex2 binds to the tumor suppressor PTEN through its PH and IP4P domains and inhibits PTEN phosphatase activity, independently of its Rac-GEF activity. This leads to increased PI3K pathway activity. Inversely, PTEN also inhibits P-Rex2 Rac-GEF activity, thus limiting cell migration. It remains to be investigated under which physiological conditions PTEN can inhibit P-Rex2, and vice versa. (b) *Cancer-associated P-Rex2 mutations V432M and P948S*: The melanoma-associated P-Rex2 mutant V432M and the pancreatic cancer-associated mutant P948S escape inhibition by PTEN. These mutants bind PTEN normally, but their Rac-GEF activity is less sensitive to PTEN. It is likely that these P-Rex2 mutants retain their ability to inhibit PTEN, however. Cancer cells carrying these P-Rex2 mutations show increased invasive migration. (c) *Cancer-associated P-Rex2 mutation G844D*: The melanoma-associated P-Rex2 mutant G844D escapes inhibition by PTEN through reduced PTEN binding. Cancer cells carrying this P-Rex2 mutation show increased invasive migration. Due to the reduced interaction, this P-Rex2 mutant should also not be able to inhibit PTEN. This may lead to a suppression of PI3K signaling in cells expressing Prex2 G844D, which requires further investigation

PTEN is a negative regulator of P-Rex2, and loss of this inhibition in cancer cells promotes invasive migration. Future work will need to elucidate the effects of PTEN on physiological roles of P-Rex2.

PAK

A recent study showed that treatment of HEK293 cells with phosphatase inhibitors reduces the sensitivity of P-Rex2 activity to PIP_3 and Gbg upon isolation of the GEF (Barrows et al. 2015), suggesting that globally high P-Rex2 phosphorylation levels are associated with low activity. Mass spectrometric analysis revealed that multiple serine and threonine residues of P-Rex2 were phosphorylated, both in basal and insulin-stimulated HEK293 cells. Among these sites, Ser1107 was phosphorylated specifically in insulin-stimulated cells and was therefore investigated further. Use of PH domain mutants and of the GEF-dead E30A/N212A mutant revealed that phosphorylation of Ser1107 depends on PIP_3 binding to P-Rex2, and on its Rac-GEF activity. Hence, phosphorylation of Ser1107 occurred downstream of the P-Rex2-mediated activation of Rac1, within the PI3K signaling pathway. This led to the discovery of the Rac-GTP effector p21-activated kinase (PAK) as the kinase responsible (Barrows et al. 2015) (Fig. 2). PAK2 could phosphorylate P-Rex2 directly in vitro, and Ser1107 was identified as one of its target residues (although not the only one). Importantly, coexpression with wild-type but not kinase-dead PAK1 inhibited the Rac-GEF activity of P-Rex2 in broken-cell assays (Barrows et al. 2015). Therefore, it appears that P-Rex2 is able to catalyze its own inactivation through a Rac1/PAK-dependent negative feedback loop (Fig. 2). However, it is still unknown if phosphorylation of Ser1107 by PAK is

sufficient to inhibit P-Rex2. Intriguingly, phosphorylation of the equivalent residue in P-Rex1 (Ser1169) by unknown kinases is associated with increased Rac-GEF activity (see P-Rex1 chapter). It also remains to be shown whether other pathways affect the PAK-dependent inhibition of P-Rex2 during PI3K signaling.

PP1*a*

The serine phosphatase PP1**a** binds directly and constitutively to P-Rex2, through an RVxF motif (residues 1084-1087) in the C-terminal half of the GEF (Barber et al. 2012). P-Rex1 also binds PP1**a** and is activated by PP1**a**-mediated dephosphorylation of Ser1165 (Barber et al. 2012). However, it remains unknown whether PP1**a** can dephosphorylate the equivalent residue in P-Rex2, Ser1103. Instead, Ser1107 of P-Rex2 was recently identified as one of the target residues of PP1**a** (and to a lesser extent of PP2A), whereas the phosphorylation of that residue was mediated by the negative regulator PAK (Barrows et al. 2015) (Fig. 2). Altogether, it therefore seems likely that P-Rex2 activity is regulated by PP1**a**, but it this remains to be investigated further, particularly on the endogenous level. A P-Rex2 mutant with an RvXF motif unable to bind PP1**a** (V1085A/F1087A, "VAFA") was recently generated (Barrows et al. 2015) that will enable future investigation of PP1-**a**-dependent P-Rex2 functions. It should also be noted that, in contrast to full-length P-Rex2, the splice variant P-Rex2b does not contain the consensus RVxF motif for PP1**a** binding, so P-Rex2b is unlikely to be regulated PP1**a**.

Finally, P-Rex2 migrates on gels as two distinct bands, and the mobility of these bands can be affected by phosphorylation. Cell fractionation was used to show that the lower-migrating band, which reflects an overall dephosphorylated state, is found preferentially in the membrane fraction, whereas the upper band was seen only in the cytosolic fraction (Barrows et al. 2015). This suggested that phosphorylation of P-Rex2 not only regulates Rac-GEF activity, but might also contribute to the control of subcellular localization. This possibility also requires further study. In general, the mechanisms that regulate P-Rex2 membrane translocation remain to be elucidated.

mTOR

Like P-Rex1, P-Rex2 and P-Rex2b also directly interact with the serine kinase mTOR, a key regulator of cell growth and of a plethora of other cell responses (Hernández-Negrete et al. 2007). However, it is unknown if P-Rex2 and P-Rex2b can modulate mTOR signaling or vice versa (Fig. 2).

Physiological Functions

Neurons and Behavior

P-Rex2 is highly expressed in cerebellar Purkinje neurons, which control motor coordination (Donald et al. 2008). Dendrite morphology was shown to be altered in Purkinje neurons of *Prex2*$^{-/-}$ mice, and the mice developed a motor coordination defect that worsens with age, particularly in females (Donald et al. 2008). *Prex1*$^{-/-}$*Prex2*$^{-/-}$ double-deficient mice showed an exacerbated phenotype, with a more severe impairment of motor activity, as well as posture and gait defects. These impairments were consistent with cerebellar dysfunction and were evident in both males and females from a young age (Donald et al. 2008). Furthermore, patch clamp electrophysiology showed that *Prex1*$^{-/-}$*Prex2*$^{-/-}$ Purkinje neurons compensate well for the dendrite morphology defect, as their passive membrane properties and basal synaptic transmission were normal. However, these neurons had impaired synaptic plasticity, as they were unable to maintain long-term potentiation, which is required for learned motor coordination skills (Jackson et al. 2010).

Glucose Homeostasis and Insulin Sensitivity

P-Rex2 controls glucose homeostasis and insulin sensitivity. This was first demonstrated in *Prex2*$^{-/-}$ mice, which showed an impaired ability to control blood glucose levels upon glucose or insulin challenge (Hodakoski et al. 2014). PIP_3 levels and the activities of several insulin pathway components were suppressed in the adipose tissue

and liver of *Prex2*$^{-/-}$ mice, whereas PTEN activity was elevated (Hodakoski et al. 2014). Therefore, it was proposed that P-Rex2 controls insulin signaling, at least in part, through its inhibition of PTEN. However, the relative contribution of GEF-dependent and -independent functions of P-Rex2 to insulin signaling and glucose homeostasis remains to be elucidated. Importantly, the role of P-Rex2 in glucose homeostasis seems to be relevant in humans, as P-Rex2 protein levels were shown to be reduced in adipose tissue of insulin-resistant patients (Hodakoski et al. 2014). As insulin resistance can develop into type 2 diabetes, it seems possible that reduced P-Rex2 expression may be involved in the development of metabolic syndrome, although this remains to be investigated.

Endothelial Cells

Knockdown of P-Rex2b in human umbilical vein endothelial cells (HUVECs) showed that this Rac-GEF is required for the sphingosine 1-phosphate stimulated migration of endothelial cells (Li et al. 2005). Moreover, a recent study, which employed an shRNA knockdown screen in HUVECs, identified P-Rex2 as a potential regulator of mechanical-force-induced orientation of endothelial cells, a response which is relevant in vivo for the integrity of blood vessel walls (Abiko et al. 2015). Therefore, P-Rex2 and P-Rex2b appear to control endothelial cell function, but a full characterization of the physiological roles of these Rac-GEFs in vascular biology remains to be done.

Cancer

The roles of P-Rex2 in cancer have recently been widely reviewed elsewhere; please see reference (Welch 2015) for citations of detailed reviews. Here we provide largely an update.

The human *PREX2* locus lies in a genomic region that is often amplified in melanoma, breast, prostate, and colorectal cancers (Fine et al. 2009; Berger et al. 2012). In melanoma, the locus also undergoes frequent chromosomal translocations and rearrangements (Berger et al. 2012). Hence, multiple mechanisms seem to contribute to the deregulation of P-Rex2 expression in cancer. Furthermore, although it is very unusual for Rho-GEFs to be mutated, P-Rex2 mutations are frequently observed in cancer, particularly in melanoma, where the Rac-GEF is mutated in 14% of cases (Berger et al. 2012), and in pancreatic ductal adenocarcinomas (PDACs; 10%) (Waddell et al. 2015). Both the deregulated expression and mutations of P-Rex2 have been shown to promote tumor growth.

Breast Cancer

In breast cancer, P-Rex2 expression is correlated with wild-type PTEN status and with activating PI3K mutations (Fine et al. 2009). Knockdown of P-Rex2 in breast cancer cells, which have normal PTEN levels (e.g. MCF7), showed that the Rac-GEF is required for Akt activation, as well as for cell growth (Fine et al. 2009). Furthermore, comparison of various breast cancer cell lines that either do or do not express PTEN suggested that P-Rex2 may control cell growth at least in part through its inhibition of PTEN (Fine et al. 2009). Finally, aberrant tyrosine phosphorylation of P-Rex2 was recently proposed as another mechanism through which the Rac-GEF might promote breast cancer, from a phospho-proteome screen of murine mammary tumors driven by loss of the tumor suppressor p53 (Ali et al. 2014).

Melanoma

Many different P-Rex2 mutations are seen in human melanomas. These mutations include truncations and missense mutations that are distributed throughout the length of the coding region (Berger et al. 2012). Several of these mutations have been evaluated in murine xenograft and transgenic models of melanoma. Expression of the P-Rex2 mutants K278*, E824*, G844D, or Q1430* in melanocytes that also bore an activating N-Ras mutation accelerated the tumor growth of xenografts and reduced tumor-free survival (Berger et al. 2012). Similarly, reduced

tumor-free survival was seen in a transgenic mouse strain with melanocytes that inducibly expressed the P-Rex2 mutant E824* as well as an activating N-Ras mutation, and tumors from this mouse exhibited increased cell proliferation (Lissanu Deribe et al. 2016). Tumors from the xenograft and transgenic models also showed decreased levels of the cell cycle inhibitors CdcN1C (Kip2) and CdcN1B (Kip1), respectively (Lissanu Deribe et al. 2016). Furthermore, increased levels of Rac1-GTP and Akt phosphorylation were observed in melanocytes that expressed the P-Rex2 mutants K278*, E824* or Q1430* in combination with an activating N-Ras mutation (Lissanu Deribe et al. 2016). Such increased Rac1-GTP levels could either be caused by lost intramolecular inhibition of P-Rex2, or through loss of inhibition by PTEN. As described above, the P-Rex2 G844D mutant evaded PTEN inhibition through reduced binding, and the Rac-GEF activity of the P-Rex2 V432M mutant was insensitive to PTEN (Mense et al. 2015) (Fig. 3). Inversely, the increased levels of Akt phosphorylation were thought be a consequence of continued PTEN inhibition by P-Rex2 mutants. However, the K278* mutant (which is essentially an isolated DH domain and thus should not be able to bind and inhibit PTEN) still increased Akt phosphorylation (Lissanu Deribe et al. 2016), suggesting that P-Rex2 can increase PI3K signaling in melanoma also independently of PTEN. Altogether, it appears that P-Rex2 mutations can promote melanoma growth through a combination of mechanisms which need to be delineated further in the future.

Pancreatic Cancer

A recent study that used whole-genome sequencing and copy number variation analysis of 100 PDACs identified P-Rex2 as a new candidate driver of pancreatic cancer (Waddell et al. 2015). P-Rex2 was found to be mutated in 10% of PDAC patients, and these mutations included frame shift, splice site, and missense mutations. As described above, the Parsons lab recently investigated one of these pancreatic cancer-associated mutants, P-Rex2 P948S, which showed reduced sensitivity to inhibition by PTEN in vitro and caused increased invasive cell migration (Mense et al. 2015) (Fig. 3b). Furthermore, another recent study showed that overexpression of P-Rex2 also occurs in pancreatic cancer and that P-Rex2 is required for the growth and invasive migration of pancreatic cancer cells (Yang et al. 2016). P-Rex2 thus seems to be emerging as an important factor in pancreatic cancer progression. However, the effects of deregulated expression and mutation of P-Rex2 on pancreatic cancer growth and metastasis require extensive future study.

Other Cancers

P-Rex2 is also overexpressed in several other types of cancers. As described above, expression of P-Rex2 in gastric cancer and neuroblastoma is caused through loss of repression by miR-338-3p, driving the growth of gastric cancer cells (Guo et al. 2014; Tong et al. 2016) and the growth and invasive migration of neuroblastoma cells (Chen et al. 2013). In liver cancer, overexpression of P-Rex2 is correlated with hepatitis-B virus status and stimulated by the chemokine CXCL9. Relevantly, P-Rex2 is required for invasive migration of hepatocellular carcinoma cells (Lan et al. 2014; He et al. 2016). Furthermore, a recent transcriptomic analysis of acute myeloid leukemias revealed upregulation of P-Rex2 mRNA in a subset of these cancers that features rearrangements in the gene for the transcription factor EVI1. It will be interesting to learn if P-Rex2 protein is produced in these leukemias, as P-Rex2 is not normally detected in leukocytes (Lavallee et al. 2015). Finally, a SNP (rs4512367) in *PREX2* that causes a homozygous intronic variant was recently found to be strongly associated with the risk of tobacco habitues developing oral squamous cell carcinoma. This risk was increased further when the P-Rex2 SNP was co-inherited with SNPs in the Ras-GEF RASGRP3 and the glutamate receptor GRIK2 (Multani et al. 2016). In conclusion, P-Rex2 appears to drive the growth and invasive migration of cells from many different types of cancers, although for most of these cancers, a causal role for! P-Rex2 still remains to be evaluated in vivo.

Summary

Important recent discoveries in P-Rex2 research were the description of negative P-Rex2 regulation by PAK and PTEN, the molecular characterization of cancer-associated P-Rex2 mutations, and the discovery that cancer-associated P-Rex2 mutants can escape from PTEN inhibition. Many fundamental aspects of P-Rex2 biology are still unknown, however. Future research should include an elucidation of the precise substrate specificity and the regulation of subcellular localization, as well as structural analysis. Searches should be conducted to identify further P-Rex2 interacting proteins for evaluation as potential regulators or effectors. It will also be interesting to discover new physiological roles of P-Rex2 and to define specific functions for P-Rex2b, for example the respective roles of the two P-Rex2 isoforms in vascular biology. Furthermore, it will be important to elucidate the contribution of Rac-GEF activity dependent and independent roles of P-Rex2, both in cancer and elsewhere, and to explore further the importance of the P-Rex2 interaction with PTEN for the functions of both proteins. More research with insulin resistant and type-2 diabetic patients is also required to elucidate the possibility that deregulation of P-Rex2 contributes to the development of metabolic syndrome.

The importance of P-Rex2 in cancer makes the Rac-GEF a valid therapeutic target. However, the catalytic activity of Rac-GEFs is not easily targetable. For P-Rex2, alternative opportunities might be found in the development of small-molecule compounds that mimic the negative regulation of P-Rex2 by PAK or PTEN. In the development of such drugs, one would have to be mindful, however, to control also the P-Rex2-dependent inhibition of PTEN, in order to preserve the ability of the tumor suppressor to downregulate pro-survival PI3K signaling.

See Also

► P-Rex

References

Abiko H, Fujiwara S, Ohashi K, Hiatari R, Mashiko T, Sakamoto N, et al. Rho guanine nucleotide exchange factors involved in cyclic-stretch-induced reorientation of vascular endothelial cells. J Cell Sci. 2015;128:1683–95.

Ali NA, Wu J, Hochgrafe F, Chan H, Nair R, Ye S, et al. Profiling the tyrosine phosphoproteome of different mouse mammary tumour models reveals distinct, model-specific signalling networks and conserved oncogenic pathways. Breast Cancer Res. 2014;16:437.

Barber MA, Hendrickx A, Beullens M, Ceulemans H, Oxley D, Thelen S, et al. The guanine-nucleotide-exchange factor P-Rex1 is activated by protein phosphatase 1alpha. Biochem J. 2012;443:173–83.

Barrows D, Schoenfeld SM, Hodakoski C, Silkov A, Honig B, Couvillon A, et al. p21-activated kinases (PAKs) mediate the phosphorylation of PREX2 protein to initiate feedback inhibition of Rac1 GTPase. J Biol Chem. 2015;290:28915–31.

Berger MF, Hodis E, Heffernan TP, Deribe YL, Lawrence MS, Protopopov A, et al. Melanoma genome sequencing reveals frequent PREX2 mutations. Nature. 2012;485:502–6.

Chen X, Pan M, Han L, Lu H, Hao X, Dong Q. miR-338-3p suppresses neuroblastoma proliferation, invasion and migration through targeting PREX2a. FEBS Letts. 2013;587:3729–37.

Donald S, Hill K, Lecureuil C, Barnouin R, Krugmann S, John Coadwell W, et al. P-Rex2, a new guanine-nucleotide exchange factor for Rac. FEBS Letts. 2004;572:172–6.

Donald S, Humby T, Fyfe I, Segonds-Pichon A, Walker SA, Andrews SR, et al. P-Rex2 regulates Purkinje cell dendrite morphology and motor coordination. Proc Natl Acad Sci USA. 2008;105:4483–8.

Fine B, Hodakoski C, Koujak S, Su T, Saal LH, Maurer M, et al. Activation of the PI3K pathway in cancer through inhibition of PTEN by exchange factor P-Rex2a. Science. 2009;325:1261–5.

Guo B, Liu L, Yao J, Ma R, Chang D, Li Z, et al. miR-338-3p suppresses gastric cancer progression through a PTEN-AKT axis by targeting P-REX2a. Mol Cancer Res. 2014;12:313–21.

He S, Lin J, Yu S, Sun S. Upregulation of PREX2 promotes the proliferation and migration of hepatocellular carcinoma cells via PTEN-AKT signaling. Oncol Lett. 2016;11:2223–8.

Hernández-Negrete I, Carretero-Ortega J, Rosenfeldt H, Hernández-García R, Calderón-Salinas JV, Reyes-Cruz G, et al. P-Rex1 links mammalian target of rapamycin signaling to Rac activation and cell migration. J Biol Chem. 2007;282:23708–15.

Hodakoski C, Hopkins BD, Barrows D, Mense SM, Keniry M, Anderson KE, et al. Regulation of PTEN inhibition by the pleckstrin homology domain of

P-REX2 during insulin signaling and glucose homeostasis. Proc Natl Acad Sci USA. 2014;111:155–60.
Jackson C, Welch HC, Bellamy TC. Control of cerebellar long-term potentiation by P-Rex-family guanine-nucleotide exchange factors and phosphoinositide 3-kinase. PLoS One. 2010;5:e11962.
Joseph RE, Norris FA. Substrate specificity and recognition is conferred by the pleckstrin homology domain of the Dbl family guanine nucleotide exchange factor P-Rex2. J Biol Chem. 2005;280:27508–12.
Lan X, Xiao F, Ding Q, Liu J, Liu J, Li J, et al. The effect of CXCL9 on the invasion ability of hepatocellular carcinoma through up-regulation of PREX2. J Mol Histol. 2014;45:689–96.
Lavallee VP, Gendron P, Lemieux S, D'Angelo G, Hebert J, Sauvageau G. EVI1-rearranged acute myeloid leukemias are characterized by distinct molecular alterations. Blood. 2015;125:140–3.
Li Z, Paik JH, Wang Z, Hla T, Wu D. Role of guanine nucleotide exchange factor P-Rex2b in sphingosine 1-phosphate-induced Rac1 activation and cell migration in endothelial cells. Prostaglandins Other Lipid Mediat. 2005;76:95–104.
Lissanu Deribe Y, Shi Y, Rai K, Nezi L, Amin SB, Wu CC, et al. Truncating PREX2 mutations activate its GEF activity and alter gene expression regulation in NRAS-mutant melanoma. Proc Natl Acad Sci USA. 2016;113(9):E1296–305.
Mense SM, Barrows D, Hodakoski C, Steinbach N, Schoenfeld D, Su W, et al. PTEN inhibits PREX2-catalyzed activation of RAC1 to restrain tumor cell invasion. Sci Signal. 2015;8:ra32.
Multani S, Pradhan S, Saranath D. Gene polymorphisms and oral cancer risk in tobacco habitues. Tumour Biol. 2016;37:6169–76.
Rosenfeldt H, Vazquez-Prado J, Gutkind JS. P-Rex2, a novel PI-3-kinase sensitive Rac exchange factor. FEBS Letts. 2004;572:167–71.
Tong D, Zhao L, He K, Sun H, Cai D, Ni L, et al. MECP2 promotes the growth of gastric cancer cells by suppressing miR-338-mediated antiproliferative effect. Oncotarget. 2016;7:34845–59.
Waddell N, Pajic M, Patch AM, Chang DK, Kassahn KS, Bailey P, et al. Whole genomes redefine the mutational landscape of pancreatic cancer. Nature. 2015;518:495–501.
Welch HC. Regulation and function of P-Rex family Rac-GEFs. Small GTPases. 2015;6:1–11.
Yang J, Gong X, Ouyang L, He W, Xiao R, Tan L. PREX2 promotes the proliferation, invasion and migration of pancreatic cancer cells by modulating the PI3K signaling pathway. Oncol Lett. 2016;12:1139–43.